

NAT'L INST. OF STAND & TECH R.I.C.



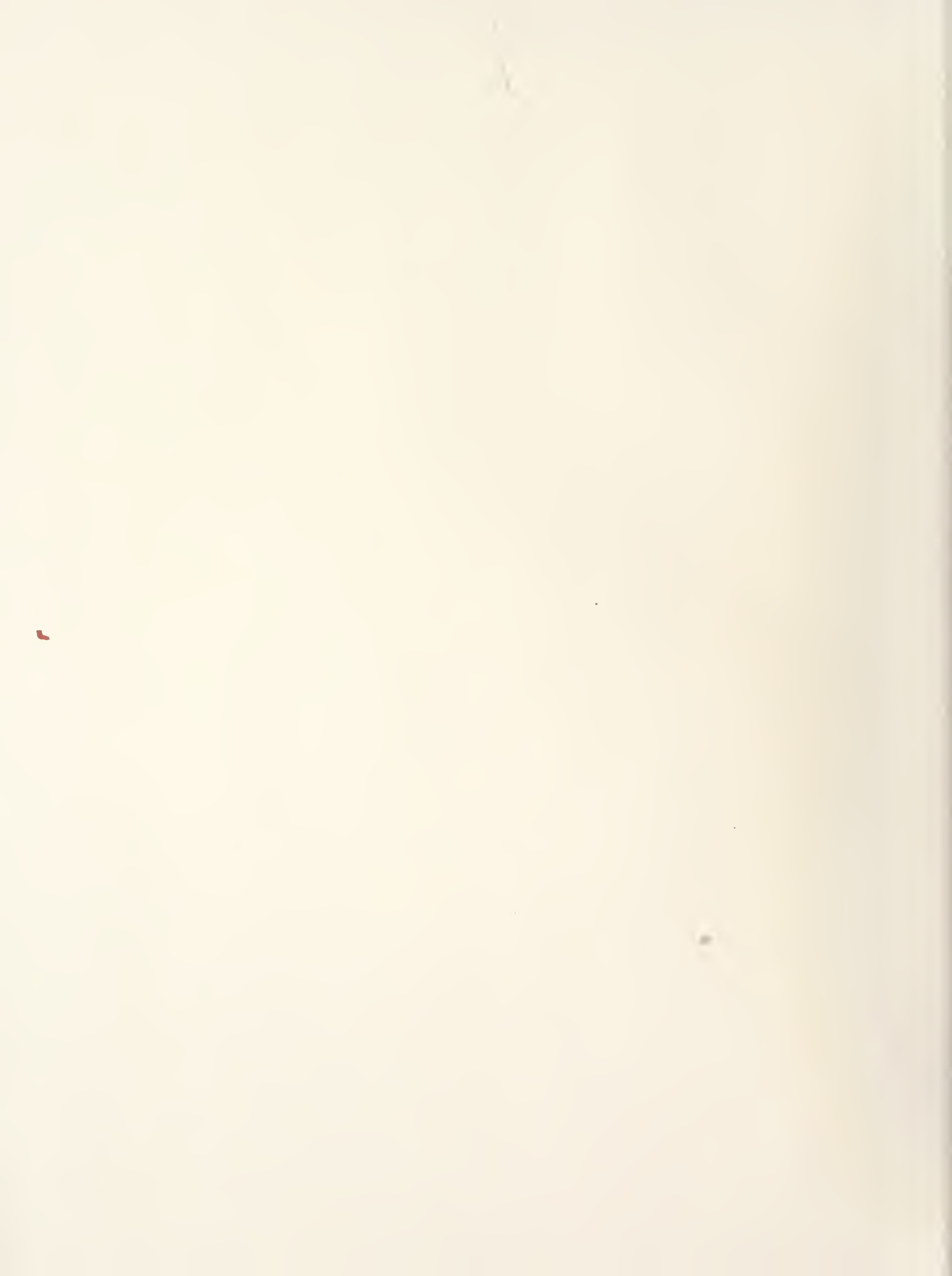
A11105 652420

NIST

PUBLICATIONS







191048

92
100
1157

Volume 1



NATIONAL BUREAU OF STANDARDS

The National Bureau of Standards¹ was established by an act of Congress March 3, 1901. The Bureau's overall goal is to strengthen and advance the Nation's science and technology and facilitate their effective application for public benefit. To this end, the Bureau conducts research and provides: (1) a basis for the Nation's physical measurement system, (2) scientific and technological services for industry and government, (3) a technical basis for equity in trade, and (4) technical services to promote public safety. The Bureau consists of the Institute for Basic Standards, the Institute for Materials Research, the Institute for Applied Technology, the Institute for Computer Sciences and Technology, the Office for Information Programs, and the Office of Experimental Technology Incentives Program.

THE INSTITUTE FOR BASIC STANDARDS provides the central basis within the United States of a complete and consistent system of physical measurement; coordinates that system with measurement systems of other nations; and furnishes essential services leading to accurate and uniform physical measurements throughout the Nation's scientific community, industry, and commerce. The Institute consists of the Office of Measurement Services, and the following center and divisions:

Applied Mathematics — Electricity — Mechanics — Heat — Optical Physics — Center for Radiation Research — Laboratory Astrophysics² — Cryogenics² — Electromagnetics² — Time and Frequency².

THE INSTITUTE FOR MATERIALS RESEARCH conducts materials research leading to improved methods of measurement, standards, and data on the properties of well-characterized materials needed by industry, commerce, educational institutions, and Government; provides advisory and research services to other Government agencies; and develops, produces, and distributes standard reference materials. The Institute consists of the Office of Standard Reference Materials, the Office of Air and Water Measurement, and the following divisions:

Analytical Chemistry — Polymers — Metallurgy — Inorganic Materials — Reactor Radiation — Physical Chemistry.

THE INSTITUTE FOR APPLIED TECHNOLOGY provides technical services developing and promoting the use of available technology; cooperates with public and private organizations in developing technological standards, codes, and test methods; and provides technical advice services, and information to Government agencies and the public. The Institute consists of the following divisions and centers:

Standards Application and Analysis — Electronic Technology — Center for Consumer Product Technology: Product Systems Analysis; Product Engineering — Center for Building Technology: Structures, Materials, and Safety; Building Environment; Technical Evaluation and Application — Center for Fire Research: Fire Science; Fire Safety Engineering.

THE INSTITUTE FOR COMPUTER SCIENCES AND TECHNOLOGY conducts research and provides technical services designed to aid Government agencies in improving cost effectiveness in the conduct of their programs through the selection, acquisition, and effective utilization of automatic data processing equipment; and serves as the principal focus within the executive branch for the development of Federal standards for automatic data processing equipment, techniques, and computer languages. The Institute consist of the following divisions:

Computer Services — Systems and Software — Computer Systems Engineering — Information Technology.

THE OFFICE OF EXPERIMENTAL TECHNOLOGY INCENTIVES PROGRAM seeks to affect public policy and process to facilitate technological change in the private sector by examining and experimenting with Government policies and practices in order to identify and remove Government-related barriers and to correct inherent market imperfections that impede the innovation process.

THE OFFICE FOR INFORMATION PROGRAMS promotes optimum dissemination and accessibility of scientific information generated within NBS; promotes the development of the National Standard Reference Data System and a system of information analysis centers dealing with the broader aspects of the National Measurement System; provides appropriate services to ensure that the NBS staff has optimum accessibility to the scientific information of the world. The Office consists of the following organizational units:

Office of Standard Reference Data — Office of Information Activities — Office of Technical Publications — Library — Office of International Standards — Office of International Relations.

¹ Headquarters and Laboratories at Gaithersburg, Maryland, unless otherwise noted; mailing address Washington, D.C. 20234.

² Located at Boulder, Colorado 80302.

NOV 8 1977

not acc

SC100

057

0 484

V.1

977

2

Flow Measurement in Open Channels and Closed Conduits

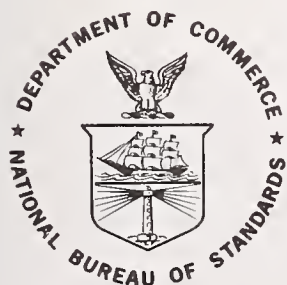
Volume 1

Spectral publication no. 484, V

Proceedings of the Symposium on Flow Measurement
in Open Channels and Closed Conduits held at the
National Bureau of Standards in Gaithersburg,
Maryland on February 23-25, 1977

Lafayette K. Irwin, Editor

Mechanics Division
Institute for Basic Standards
National Bureau of Standards
Washington, D.C. 20234



U.S. DEPARTMENT OF COMMERCE, Juanita M. Kreps, Secretary

Dr. Sidney Harman, Under Secretary
Jordan J. Baruch, Assistant Secretary for Science and Technology

U.S. NATIONAL BUREAU OF STANDARDS, Ernest Ambler, Acting Director

Issued October 1977

Library of Congress Cataloging in Publication Data

Symposium on Flow Measurement in Open Channels and Closed
Conduits, National Bureau of Standards, 1977.

Flow measurement in open channels and closed conduits.

(National Bureau of Standards special publication ; 484)

Includes index.

Supt. of Docs. no.: C13.10:484

I. Flow meters--Congresses. I. Irwin, Lafayette K. II. Title. III.

Series: United States. National Bureau of Standards. Special publica-
tion ; 484.

QC100.U57 no. 484 [TC177] 602'.1s [6a0.1'064] 77-14243

National Bureau of Standards Special Publication 484/1

Nat. Bur. Stand. (U.S.), Spec. Publ. 484/1, 479 pages (Oct. 1977)

CODEN: XNBSAV

U.S. GOVERNMENT PRINTING OFFICE
WASHINGTON: 1977

For sale by the Superintendent of Documents, U.S. Government Printing Office
Washington, D.C. 20402 - Price \$12.25 per 2 part set ; sold in sets only

Stock No. 003-003-01845-7

PREFACE

These Proceedings include most of the papers presented at the three-day symposium on fluid flow measurements held at the National Bureau of Standards, Gaithersburg, Maryland, on February 23, 24, and 25, 1977. The papers dealt with flow in open channels and closed conduits and a special related session on international standards.

The impetus to hold the symposium came from several sources. These included (1) continuing requests for the information presented at the 1974 Flow Measurement Conference held to establish connections between flow measurement and national needs (conference presentations not published), (2) increasing use of measurement technology by regulators to monitor or enforce the effects of their rule making, and (3) rising awareness of the importance of international standards to this nation, particularly, for quantifying energy-related fluids. The purpose of the symposium was to bring together a significant group of the producers and users of flow measurement technology, to provide a forum for presenting and discussing both the new and the proven ideas for making useful flow measurements, and to assemble and disseminate the resulting information.

Initially, the theme was to emphasize identification and assessment of sources of errors, formulation of error analysis techniques and recommendations for resolving the uncertainties for flow measurement. The strong interests of investigators in presenting related research, of instrument developers in describing the performance of flow measurement devices and systems, and of users in discussing applications resulted in a broader spectrum and larger number of papers than was envisioned. An optimum ordering of papers in the resulting two volumes has not evolved.

Lafayette K. Irwin, Editor

Conversions for Customary to International System (SI) Units*

Reflecting the transitional stage of the measurement units in this technological area, both U. S. customary and SI units of measurement are used in different papers of these Proceedings. The U.S.A. is a member of the General Conference on Weights and Measures which gave official status to the SI metric units in 1960. Conversion factors for selected units in these Proceedings are:

<u>Quantity</u>	<u>Conversion customary to SI</u>	<u>Factor, approximate</u>
Length	inch (in) to meter (m)	0.0254 [†]
	foot (ft) to meter (m)	0.3048 [†]
Area	inch ² (in ²) to meter ² (m ²)	0.0006452
	foot ² (ft ²) to meter ² (m ²)	0.09290
Volume	inch ³ (in ³) to meter ³ (m ³)	0.00001639
	foot ³ (ft ³) to meter ³ (m ³)	0.02832
	gallon ^{††} (gal) to meter ³ (m ³)	0.003785
Mass	pound, avoirdupois (lb) to kilogram (kg)	0.4536
Force	pound (lbf) to newton (N)	4.448
	kilogram (kgf) to newton (N)	9.807
Pressure, or Stress	pound/inch ² (psi) to newton/meter ² (N/m ²)	6895
	inch of mercury, 60 °F (inHg) to newton/meter ² (N/m ²)	3377
	inch of water, 60 °F (inH ₂ O) to newton/meter ² (N/m ²)	248.8
	millimeter of mercury, 0 °C (mmHg) to newton/meter ² (N/m ²)	133.3
Velocity	inch/second (in/s) to meter/second (m/s)	0.0254 [†]
	foot/second (ft/s) to meter/second (m/s)	0.3048 [†]
Acceleration	foot/second ² (ft/s ²) to meter/second ² (m/s ²)	0.3048 [†]
	free fall, standard (g) to meter/second ² (m/s ²)	9.807
Density	pound/foot ³ (lb/ft ³) to kilogram/meter ³ (kg/m ³)	16.02
	pound/gallon ^{††} (lb/gal) to kilogram/meter ³ (kg/m ³)	119.8
Flow	foot ³ /second (ft ³ /s) to meter ³ /second (m ³ /s)	0.02832
	foot ³ /minute (ft ³ /min) to meter ³ /second (m ³ /s)	0.0004719
	gallon ^{††} /minute (gal/min) to meter ³ /second (m ³ /s)	0.00006309
	pound/second (lb/s) to kilogram/second (kg/s)	0.4536
Temperature	degree Fahrenheit to degree Celsius	$t_{°C} = (t_{°F} - 32) 1.8$

* See NBS SP330, 1977 ed., The International System of Units (SI) and ASTM E380-76, Metric Practice Guide for more complete information.

† Exact

†† U. S. liquid

TABLE OF CONTENTS- Volume 1

PREFACE	iii
Conversions for Customary to International (SI) Units	iv
ABSTRACT	ix
Measuring the Repeatability of Flowmeters	1
A. T. J. Hayward	
The Navy Liquid Flow Correlation Program	25
J. H. Tabler and C. G. Kullman	
A Laboratory Study of Turbine Meter Uncertainty	33
G. Mattingly, P. Pontius, H. Allion, and E. Moore	
Evolution of a Modern Petroleum Measurement Manual	55
L. M. Davis	
Building Blocks Towards Flowmeter Reliability	61
Dezsoe Halmi	
Open Channel Flow Monitoring or Metering, That is the Question ...	83
Kenneth W. Martig, Jr.	
Instrument Errors in Open Channel Flow Measurement Systems	91
D. M. Grant	
Marine Dynamics and Its Effects on Current Measuring Transducers .	109
Thomas Mero, Gerald Appell, and Raul S. McQuivey	
Some Error Sources in Price and Pygmy Current Meter Traverses	123
G. Kulin	
Flow Measurements in the Canals of Power Plant Closed Loop Cooling Systems	145
Joseph F. O'Brien, James Skridulis, John Annett, G. Wayne Singley and Harold L. Koenig	
Errors in Flow Measurement and Their Importance in Infiltration/ Inflow Analysis	173
D. L. Guthrie, D. R. Washington and C. Vincenty	
Rating Broad-Crested V-Notch Weirs with Narrow, Sloping Approach Channels and Sediment Deposits	187
James F. Ruff, Keith Saxton and Clement Dang	
Compensating for Construction Errors in Critical-Flow Flumes and Broad-Crested Weirs	201
John A. Replogle	

Table of Contents - Volume 1 (Continued)

Numerical Modeling of Two-Dimensional Flumes	219
Ronald W. Davis	
The Design of Open Channel Acoustic Flowmeters for Specified Accuracy: Sources of Error and Calibration Test Results	243
Francis C. Lowell, Jr.	
Application Considerations & Performance Capability of the Time Differential Clamp-On Ultrasonic Flowmeter	267
J. Baumoel	
Theoretical and Experimental Assessment of Uncertainties in Non- Intrusive, Ultrasonic Flow Measurement	277
Ronald F. Bruner	
A New Ultrasonic Flowmeter for the Natural Gas Industry	293
N. E. Pedersen, J. E. Bradshaw, L. C. Lynnworth and P. F. Morel	
A New Non-Intrusive Flowmeter	319
R. S. Flemons	
Reconstructing Three-Dimensional Fluid Velocity Vector and Tempera- ture Fields from Acoustic Transmission Measurements	335
S. A. Johnson, J. F. Greenleaf, M. Tanaka, and G. Flandro	
Validation of Use of Dye-Dilution Method for Flow Measurement in Large Open and Closed Channel Flows	361
W. H. Morgan, D. Kempf, R. E. Phillips	
Dilution Method of Discharge Measurement in Pipes	395
E. R. Holley	
Application of a Fluorescence Technique to Dye-Concentration Measure- ments in a Turbulent Jet	423
Hsien-Ta Liu, Jung-Tai Lin, Donald P. Delisi and Frank A. Robben	
The Application of Monte Carlo and Bayesian Probability Techniques to Flow Prediction and Determination	447
Frank J. Berté	
Author Index	470-A

TABLE OF CONTENTS - Volume 2

Laser Doppler Anemometry for Flow Measurement	471
William W. Durgin and Lawrence C. Neale	
On Improving the Pitot-Tube Determination of Flows in Large Pipes.	479
J. M. Robertson and M. E. Clark	
Numerical Modeling and Turbulent Flow Through Thin Orifice Plates.	491
R. W. Davis and G. E. Mattingly	

Table of Contents - Volume 2 (Continued)

Studies of Pulsating Incompressible Flow Through Orifice Meters ..	523
R. A. Bajura and M. T. Pellegrin	
A Vortex Flowmeter - Calibration Results and Application Experiences	549
R. W. Miller, J. P. DeCarlo, and J. T. Cullen	
Temperature Field Measurements in Turbulent Thermals	571
Mohamed Gad-el-Hak	
Flow Measurement Up-Date	597
Robert B. Suhoke	
Near Wall Velocity Measurements for Wall Shear Inference in Turbulent Flows	621
F. J. Pierce and D. S. Gold	
On Reduction of Errors Arising in Hot-Wire Anemometry of Thin Turbulent Shear Layers	649
J. Gaviglio and J. P. Dussauge	
Probe and Method for Simultaneous Measurements of 'True' Instantaneous Temperature and Three Velocity Components in Turbulent Flow	659
Gracio Fabris	
Measurement of Boundary Layer Transition Using Acoustic Techniques	687
Donald C. Sachs, Thomas F. V. Meagher, and Vernon D. Peckham	
Measurement of Recirculating Flow Behind a Cylinder with Spray Cooling	705
R. S. Rudland	
A New Type of Velocity Probe	719
W. B. Brower, Jr. and Alan Servoz	
The Influence of Turbulence on Static and Total Pressure Probes ..	737
V. E. Scottron	
Determination and Elimination of Errors in Velocity Readings at Ventilation Tubing Inlets	755
Robert A. Haney	
Indirect Two-Phase Flow Measurement: Analysis and Reduction of Methods Errors	765
N. N. Kondic	

Table of Contents - Volume 2 (Continued)

Measurements of Density and Density Gradient With an Oscillating Conductivity Probe	783
Donald P. Delisi and Robert H. Kirchhoff	
New Techniques for Automotive Fuel Flow Measurements	803
Milton Baker	
A New Digital Technique for Temperature and Viscosity Compensation of Turbine and Positive-Displacement Flow Transducers	821
Roger Jennings	
Viscosity Effects on the Turbine Flowmeter	847
John M. Ball	
Turbine Meters for the Measurement of Gaseous Hydrocarbons	871
Paul J. LaNasa	
On a New Method of Gas Flow Measurement Using Cryogenic Techniques	881
D. B. Mann and J. A. Brennan	
An Anatomy of the International Standards Producing System - Flow Measurement	895
L. K. Irwin	
OIML and EEC, Their Impact on the International Standards Producing System	921
D. E. Edgerly	
The Interface Between Industrial, National and International Standards	929
Wallace N. Seward	
The Adequacy of the Data Bases Available for Promulgating International Standards	935
H. H. Dijstelbergen	
Equitable Implementation of National and International Allocation Programs - Summary of Remarks	945
James A. West	
Of Form and Substance for Effective Standards	947
E. A. Spencer	
Comments On: Role of International Standards in Measuring and Allocating Hydrocarbons - A Program for Solution of our Present Problems	957
F. H. Abernathy	
Author Index	960

The wide range and complexity of problems and potential solutions that must be considered for useful flow measurements are emphasized by the papers contained in these proceedings. Fifty-three presentations cover: characteristics of new and improved instruments; applications of traditional and new measuring devices in field environments; procedures for identifying and analyzing errors or uncertainties in data under specific conditions; uses of physical and numerical models; politico-economic changes that affect international standards for flow measurement; and philosophical bases for making measurements. The fluids of most interest are water and waste water, petroleum and related refined products, air, natural gas and stack gas.

Experimental and analytical investigations on instrument performance and interpretation of results include innovative applications of traditional and new flow measurement techniques to fluid flows in open channels and closed conduits. The traditional devices or techniques include weirs, flumes, current meters, orifice plates, turbines, hot-wires, pitot-static tubes, velocity traverses, dye-dilution, and others. More recent instrumentation developments and procedures such as laser doppler anemometry, acoustic and thermal imaging, acoustic pulse velocity and doppler anemometry, numerical modeling, vortex shedding and digital computation are covered for particular measurement purposes.

The most significant trend reflected in these presentations is the general awareness that uncertainties in measured quantities at the lowest point in the measurement chain, i.e., in the field or plant, are more important than accuracy statements derived from controlled laboratory studies. Other trends in evidence are the rising importance of turbine meters for use as transfer standards and in-line measurements of liquids and gases in filled pipes and the increasing number of applications for acoustics and laser technology for flow measurements in both open channels and closed conduits.

Key Words: Acoustic flow meters; closed conduit flows; current meters; dye-dilution methods; errors in flow measurement; flow measurement; fluid flow modeling; fluid velocity; flumes; gas flow standard; hot-wire anemometry; international flow standards; laser anemometry; open channel flows; orifice meters; pitot-static meters; turbine meters; weirs.

DISCLAIMER:

Certain trade names and company products are identified in order to adequately specify the experimental procedure. In no case does such identification imply recommendation or endorsement by the National Bureau of Standards, nor does it imply that the products are necessarily the best available for the purpose.

MEASURING THE REPEATABILITY OF FLOWMETERS

A. T. J. Hayward

National Engineering Laboratory
East Kilbride, Glasgow, Scotland

A technique for measuring the repeatability of flowmeters has been investigated in an extensive series of tests. The technique involves installing a pair of nominally identical flowmeters in series and comparing their readings in a batch of repeat tests; the repeatability is then given by $t\sigma/\sqrt{2}$, where σ is the standard deviation of the ratio of the simultaneous readings of the two meters and t is Student's t .

The method shows great promise, and has revealed small but significant drift (sometimes as low as a few parts per million over a short series of tests) in meters where drift had not previously been suspected. Extensions of the method have also been used successfully to determine the repeatability of a flowmeter calibration system, and to measure the intra-rotational linearity of a positive displacement meter.

1. Introduction

Although repeatability is a very important property of a flowmeter, and is glibly referred to very frequently by manufacturers and users alike, there is as yet no recognized method of measuring it. The reason for this is fairly obvious. There is no particular difficulty in determining the repeatability of an instrument that measures some fixed quantity - for example, the mass, the length, or the elastic modulus of a solid specimen - and standard methods for determining repeatability in the case of measurements such as these are either in existence or under preparation by ISO/TC69 and related national standardization committees. It is only under identical test conditions, and the results can be analysed statistically to yield a repeatability value.

Unfortunately this method does not work with instruments that measure transient quantities, since these never remain absolutely constant with time. Many important industrial instruments fall into this category, including flowmeters, ammeters, radiation meters, accelerometers, and a host of others. Any attempt to measure the repeatability of a flowmeter by the technique mentioned above would yield a result that was adversely affected by the unsteadiness of the flow being repeatedly measured, since it is a physical impossibility to produce a perfectly steady flow.

There is clearly a need for a standard technique for determining the repeatability of instruments measuring transient quantities. Indeed, proposals for such a standard method have been developed at the National Engineering Laboratory and will be published shortly [1]. This paper describes the experiments carried out at the Laboratory during the past year to investigate the validity of the proposed method and to obtain information about the repeatability of various measuring instruments, including several flowmeters.

2. Basis of the method

The theoretical basis for the method is described in detail in Reference 1*. It is based upon the fact that the repeatability of a measuring instrument depends upon the random uncertainties relating to it, and the assumption that these follow a Gaussian distribution. Probability theory indicates that where uncertainties are Gaussian they can be added in quadrature, which means that they can be added by squaring the individual quantities, adding the squares, and taking the square root of their sum.

If two flowmeters are installed in series in a pipe and a number of simultaneous readings of both flowmeters, M_1 and M_2 , are made, the variation of the difference of the two readings ($M_1 - M_2$), or of their ratio (M_1/M_2), will indicate the combined repeatability of the two flowmeters. Minor fluctuations in flowrate between measurements will be of no consequence, since they will presumably affect both flowmeters in exactly the same manner.

Assuming Gaussian distribution as mentioned above, it follows that if R_{12} is the measured repeatability of the combination of the two flowmeters and R_1 and R_2 are the individual repeatabilities of the two flowmeters, then

$$R_{12}^2 = R_1^2 + R_2^2. \quad (1)$$

If it is also assumed that the two flowmeters are identical, then it follows from eq. (1) that

$$R_1 = R_2 = \frac{R_{12}}{\sqrt{2}}. \quad (2)$$

Employing this principle, the following procedure can be used to obtain the repeatability of a flowmeter.

a Instal two nominally identical flowmeters in the same pipe in such a way that the wake from the upstream flowmeter cannot significantly affect the performance of the downstream flowmeter. (This generally necessitates either having a long length of straight pipe separating the flowmeters, or using a flow straightener.)

b Pass flow through the two flowmeters for a period, during which the flowrate should be as nearly constant and steady as is practicable.

* References are listed at the end of this paper on page 13.

c Take a number of simultaneous readings (at NEL we have generally used either 10 or 20 readings in a batch) of the two meters, and evaluate the standard deviation, σ , of the ratios of the readings of the two flowmeters.

d The repeatability of each flowmeter is then given by the expression

$$R = \frac{t\sigma}{\sqrt{2}} \quad (3)$$

where t is the value of Student's t for the appropriate batch size and a probability of 95 per cent.

The method requires the flow passing through both meters to be identical at any instant when a reading is taken. For incompressible flow this is necessarily so, but it may not prove easy to achieve this with gas flow. So far experiments have been confined to liquid flows, although it is hoped to investigate the method with gas flow later. The method can be applied equally well to flowrate meters and to totalizing meters used for measuring total volumes passed, although it so happens that most of the tests described in this paper have been carried out with the latter.

3. Repeatability tests on positive displacement meters

The largest series of tests has been carried out on a vane-type PD meter, employing three alternative methods of readout and a number of variations in test method. These are described in detail below. A 5 cSt oil was used as the test fluid throughout.

3.1 Mechanical readout, standing-start-and-finish tests

The first tests were carried out with a vane-type PD meter fitted with a mechanical readout, in the form of a Veeder-Root head and a sandwich drum enabling volumes to be read to the nearest 10 millilitres. This form of readout necessitated the use of a standing-start-and-finish method. In this, both meters were set to zero, then flow was started by the sudden opening of a downstream valve and allowed to continue until approximately 1000 litres had been passed by the meters, when flow was stopped by the sudden closing of the valve, and a final reading of both meters was then made.

It is important to ensure, in tests of this kind, that the discrimination of the meter in relation to the total volume being passed is small compared with the repeatability values being measured. In this particular case the requirement was fulfilled, since the discrimination of 10 millilitres in a run of 1000 litres represents 10 parts per million, which is very much less than the lowest repeatability value measured in this experiment.

The results of these tests are given in Table 1. Five complete tests, each involving at least 10 runs, were made at the maximum flowrate of the meter, and three tests at each of two lower flowrates. The repeatabilities found varied widely from test to test, over a range from 60 to 250 parts per million; the variation in results appears to be random and not related

to flowrate. Part of the variation in the test results is probably due to the variations imposed by the standing-start-and-finish method of test which is inherently less consistent than a flying-start-and-finish method. Even so, however, it was obvious from these first tests that the repeatability of a flowmeter is a rather variable quantity which is liable to change significantly from day to day - a conclusion which, as will be seen later, is borne out by every other test made.

3.2 Photocell pulse-generator readout, flying-start-and-finish tests

In the next series of experiments the same two meters were fitted with electrical pulse generators of the photocell type supplied by the manufacturers and having a discrimination of 10 millilitres per pulse. The addition of the electrical readout enabled a flying-start-and-finish test, again of 1000 litres duration, to be employed. In this method the flow was allowed to pass at a constant rate throughout each batch of test runs, and the output from one meter was passed into a preset counter which automatically gated the counts from the other meter after every hundred thousand counts. (In anthropomorphic terms, one meter was made to say to the other meter, 'I have just registered my hundred-thousandth pulse; how many pulses have you generated in the same period?'). By using two sets of counters and zeroing one set while the other set is counting, it is possible to carry out continuous testing without any break between the runs of one hundred thousand counts. Generally about 20 runs were made in each batch in this part of the experiment.

The results of this series of tests revealed an interesting and hitherto unsuspected aspect of the behaviour of this type of meter. The individual results of three typical batches are shown in figure 1, where the difference between the meters ($M_1 - M_2$) is shown plotted for each individual run in a batch. For the sake of uniformity $M_1 - M_2$ is expressed in parts per million - in other words, the difference between the two pulse counts was multiplied by 10. The type of result which had been expected, and which in fact was frequently obtained, is that shown in figure 1(a); here, the results of successive runs are randomly distributed about a mean value. This value would have been zero if the meter factors of the two meters had been identical, but since the two meter factors were slightly different the mean value of $M_1 - M_2$ is approximately 1850 parts per million.

Sometimes, however, the value of $M_1 - M_2$ was found to drift steadily upwards or downwards during the course of a test. A typical result of a test in which steady drift of this kind occurred is shown in figure 1(b).

More rarely, a sudden change in the value of $M_1 - M_2$ occurred part way through a test. An example of a stepwise change of this character is given in figure 1(c).

It is arguable whether this phenomenon of drift should be considered separately from repeatability, or whether it should be ignored and its effect should merely be allowed to increase the repeatability values obtained from any one run. My own view is that the drift which has been observed is a distinct phenomenon which deserves recognition in its own

right, and that it needs separate study with a view to ascertaining its cause and preventing its occurrence in future flowmeters.

Consequently, in presenting the results in this part of the experiment I have as far as possible tried to allow for the effect of drift. In the case of a stepwise change as in figure 1(c) the only way to do this is to continue the series of runs until 20 consecutive tests have given a line without a step in it - and preferably a horizontal line. In the case of steady drift as exemplified in figure 1(b) it is possible to allow for the effect of drift by fitting a least-squares line to the experimental points and calculating the standard deviation about this line instead of the standard deviation about a mean value; this inevitably gives a smaller value of standard deviation. The results of the tests are given in figure 2, where repeatability is plotted against flowrate. Those points in this figure which are based on batches of runs where steady drift occurred are denoted by the presence of figures in brackets; these indicate the number of parts per million by which the ordinate of each point should be increased if it is desired to ignore drift. Thus the figures in brackets denote the amount by which the repeatability value has been reduced by basing the standard deviation on the least squares line through the test results rather than on a simple mean value.

These results show that, provided corrections for drift are made in those tests where it appeared, the repeatability of this type of flowmeter tested in the flying-start-and-finish mode is between 30 and 70 parts per million. Even if corrections for drift are not made, all but two of the results fall below 70 parts per million and these two fall below 100 parts per million. This means that there is an approximately three-fold increase in repeatability over the previous tests with the same basic meters. The improvement is probably due more to the change from standing to flying-start-and-finish testing than the change in readout method, since the electronic readout used this time was superimposed upon the mechanical head used in the previous tests.

3.3 Shaft-encoder pulse-generator readout, flying-start-and-finish

In the next series of tests the same two basic meters were used, but all the gearing associated with the method of readout used in the two previous series was removed and an interferometric shaft encoder was fastened directly to the main shaft of the PD meter. Since the particular shaft encoders used generate 2540 pulses per revolution the result was a meter with extraordinarily high discrimination, which was found by calibration to be approximately 0.9 millilitres per pulse. In this series the preset counter was set to work on counts of one million pulses, and consequently the throughput per run was approximately 900 litres. As in the previous test all the runs were made in immediate succession, but in some of the tests in this series an additional refinement was introduced. The data from the counters were fed through a suitable interface into a programmable calculator, which stored the test data and calculated the repeatabilities obtained from each batch of tests. When this system is used the testing is carried out almost automatically and the operator has very little to do except to set the flowrate at the start of each batch of tests and then press the starting button.

Typical results obtained from three tests in this series are shown in figure 3. When the meters were free from drift, as in the test illustrated in figure 3(a), exceptionally high repeatabilities were obtained - usually below 10 parts per million. Sometimes a small amount of drift was present, as illustrated in the test reported in figure 3(b), but, even if this drift is not allowed for, the repeatabilities in such tests usually were still not much more than 10 parts per million. At flowrates below about 5 litres per second, that is, below about 25 per cent of the rated maximum for the meter, drift became a very serious problem. Sometimes it took the form of severe steady drift as shown in figure 3(c), and sometimes it took the form of very severe stepwise drift. On one occasion the value of $M_1 - M_2$ was observed to change by more than 1000 parts per million between the last batch of runs carried out one afternoon and the first batch carried out the next morning. In general, the results of tests at these lower flowrates were so unrepresentative that they have not been plotted along with the other test results. Since no corresponding deterioration of performance was obtained at lower flowrates in the previous experiment with this meter, this erratic behaviour is believed to emanate from the shaft-encoder employed and is the subject of further investigation at the time of writing.

The results of this part of the experiment are shown in figure 4, from which several interesting conclusions immediately appear. First, if the problem of severe drift at low flowrates can be overcome, this form of flowmeter has great potential as a tool for standards laboratories, since its repeatability is better than that of the same flowmeter with a conventional readout: under favourable conditions repeatabilities as good as 10 parts per million appear to be easily attainable. Secondly, the repeatability of this instrument appears to be flowrate dependent: between 5 and 11 litres per second, and again between 14 and 19 litres per second, repeatability is below 10 parts per million, but between 11 and 14 litres per second the repeatability deteriorates to values around 20 parts per million. Further investigation is needed to ascertain whether this deterioration in the middle flowrate range is related to the meter capsule itself or to the behaviour of the shaft encoder.

4. Repeatability tests on turbine meters

The work at NEL on the repeatability of turbine meters is still in its early stages. At the time of writing the only tests that have been completed are a series on a pair of 75 millimetre (3 in) turbine meters installed in a calibration line supplied with water from a constant-head tank at flowrates up to 30 litres per second. These meters had been used extensively before the present experiment took place, and one object of the work was to assess the improvement in repeatability that could be obtained by fitting new bearings. The meters were therefore tested over a range of flowrates in their original condition and then re-tested after the bearings had been replaced with new ones.

This experiment brought to light one practical problem in repeatability testing of turbine meters. The pulse generation rate of a turbine meter is rather low, especially at the lower flowrates, and since one repeatability measurement necessitates making at least 10 runs and preferably 20,

it becomes prohibitively time-consuming to take more than ten thousand pulse counts during one run. Unfortunately this introduces a random rounding-off uncertainty which may be as large as 200 parts per million, and this is so large that it almost obscures the true repeatability of the turbine meter.

This point is brought out in figure 5 where the results of this preliminary experiment are plotted. There does appear to be a distinct improvement in repeatability as a result of renewing the bearings of these meters, but the improvement is only large enough to be clearly visible at the lowest flowrate, where bearing friction is at its most significant. At the higher flowrates the effect of the new bearings on repeatability is largely masked by the effect of the rounding-off error on the repeatability values obtained. Further experiments are now in hand with 50 millimetre turbine meters where the pulse generation rate is higher, and where an electronic pulse multiplier is being used, which should reduce the rounding-off error by a factor of 10.

5. Tests on a proprietary flowmeter calibrator

A proprietary device used for dynamically measuring flow, and hence for calibrating flowmeters, has also been tested extensively in the author's laboratory by the methods of this paper, and has thrown additional light on the problem of drift.

It is a matter of common knowledge that the short-term repeatability of practically any measuring instrument is substantially better than the long-term repeatability of the same instrument. Many writers have commented in qualitative terms on this fact. For example, Ascough [2] speaks of three classes of errors: Class I errors, which are associated with the repeatability obtained during a single test period; Class II errors, which are constant during one test period but vary between batches of tests, and consequently cause increases in the values of repeatability measured over a long period of time; and Class III errors, which are fixed systematic errors. The techniques described in the present paper may eventually make it possible to assign quantitative values to Ascough's first two classes of error. In particular, the stepwise form of drift mentioned above is clearly identifiable as one of Ascough's Class II errors.

The steady form of drift is more difficult to analyse since it undoubtedly affects both Class I and Class II errors. Some tests on a pair of ultrasonic flowmeters by a method very similar to that described in this paper have recently been reported [3] and it is interesting to note that one of the seven sets of results published there (batch number 118) clearly reveals steady drift.

Stepwise drift between batches of tests is very evident in figure 6, which shows the results of tests on the proprietary flowmeter-calibrating device, which was specially fitted with dual sets of measuring instruments, so that two simultaneous measurements of volume passed could be made. Runs were made in batches of 20 in rapid succession, at each of a number of velocities. For each batch of 20 repeat readings the mean of the difference between the two parallel sets of instruments ($I_1 - I_2$) was evaluated, as was

the standard deviation of $(I_1 - I_2)$, namely, σ . The results of these tests at different velocities are shown in figure 6, where $(I_1 - I_2)$ is plotted against velocity. Each cross on this graph represents the results of one batch of 20 runs: the centre of the cross is the mean value of $(I_1 - I_2)$, and the overall height of the cross represents the effective range (2σ) of the batch.

It is immediately apparent from this graph that the variations between batches of runs are often much greater than the variation within any one batch. In other words, using Ascough's terminology, when this device is used under these conditions, Class II errors are much greater than Class I errors; or using my terminology, its long-term repeatability is much worse than its short-term repeatability. It is worth noting in passing that the device's repeatability is obviously not a function of velocity.

In the tests reported in figure 6 the runs within one batch were carried out in continuous succession, using automatic data collection and a dedicated computer. But it was necessary to shut the apparatus down for a few minutes after each batch, in order to change the velocity of operation and to make other necessary adjustments in readiness for the next batch of runs. In a further experiment, the results of which are given in figure 7, the apparatus was allowed to run continuously at a velocity of 2.5 m/s, with no interruption whatever between batches of runs except for three overnight breaks.

The contrast between these results obtained when the apparatus was running in this continuous fashion (figure 7) and the results already described when it was being operated intermittently (figure 6) are most striking. Whenever the equipment was running continuously the between-batch variations were very small, and were commensurate with the variations within the batches. The only occasions when a significant between-batch shift occurred were overnight between 8 and 9 November, and again overnight between 9 and 10 November. Taken together, figures 6 and 7 provide very convincing proof that this particular device gives highly repeatable results as long as it is in continuous operation, but that its performance is liable to deteriorate markedly whenever it is allowed to rest for even a brief period.

6. Extensions of the test method

These methods can be adapted to meet a number of other needs in the field of instrument technology. We have already applied them to two other flow measurement problems which are discussed below.

6.1 Measuring the repeatability of a flowmeter calibration system

The method of this paper cannot generally be used to measure the repeatability of a complex flowmeter calibration system directly, because such systems are generally unique, and even when two identical systems exist it is usually not practicable to connect them in series and compare their readings. To measure the repeatability of a flowmeter calibrator it is therefore usually necessary to connect two identical flowmeters in series with each other and with the calibrator, as shown schematically in figure 8. However, by taking simultaneous readings of both instruments and the

calibrator it is then possible to use the method to derive three 'combined repeatabilities', namely, the repeatability of instrument 1 against the calibrator, R_{1C} , the repeatability of instrument 2 against the calibrator, R_{2C} , and the repeatability of instrument 1 against instrument 2, R_{12} . Then, provided that the repeatabilities of the flowmeters are not greatly inferior to that of the calibrator, it can be shown [1] that the repeatability of the calibrator, R_C , is given by

$$R_C = \{\frac{1}{2}(R_{1C}^2 + R_{2C}^2 - R_{12}^2)\}^{\frac{1}{2}}. \quad (4)$$

The technique has been used to determine the repeatability at a number of flowrates of a gravimetric standing-start-and-finish calibrator, operating with 5 cSt mineral oil. The same positive displacement meters as were used in the experiment described in Section 3.1, above, were used in this experiment also.

The results of tests at flowrates of 4, 11 and 16.5 litres per second are given in Table 2. The repeatability of the calibrator was found to be between 80 and 220 parts per million during these tests, with a small but probably significant tendency to better repeatabilities at the lowest flowrate; this can be attributed to the increased uncertainty imposed by the periods of acceleration and deceleration in a standing-start-and-finish test at the higher flowrates. There has not yet been opportunity to try the method with a flying-start-and-finish calibrator, but there seems no reason why it should not prove equally successful when used in that way.

6.2 Measuring the intra-rotational linearity of a rotary PD meter

The PD meter fitted with a shaft encoder, as described in Section 3.3 above, has been developed for use as a high-precision laboratory tool. It is intended that it should be used to study the performance, under flying-start-and-finish conditions, of other devices used in flow measurement, such as flowmeter calibrators and meter provers. In such experiments it will be read to the nearest pulse, that is, with a discrimination of 0.9 millilitres. Since it emits 2540 pulses per revolution, this means that it will be read to the nearest $1/2540$ of a revolution. Calibration has shown that, on average, each pulse represents 0.9 millilitres, but it is necessary to know whether the instrument is linear within one revolution - that is to say, whether each pulse represents almost exactly 0.9 millilitres, or whether at some part of a revolution a pulse represents much less than 0.9 millilitres and at other parts of a revolution a pulse represents much more than this.

This question has been resolved by the use of a technique whose principle is illustrated in figure 9. A PD meter can be visualised as being essentially a piston moving in a cylinder, where the distance travelled by the piston is used as an indicator of the amount of liquid passing through the meter. In Case 1 of figure 9 a situation is envisaged in which there are two perfectly regular and identical cylinders connected in series, with the same volume of liquid passing in succession through both cylinders. Under these conditions the piston in cylinder A keeps perfectly in line with the piston in cylinder B: thus at the start of the

run A1 is immediately over B1, half way through the run A2 is immediately over B2, and at the end, A3 is immediately over B3.

In Case 2 of figure 9 the situation is considered where there are identical bulges in both cylinders, and where these bulges are in corresponding positions. In this case also the two pistons keep exactly in line throughout the stroke. At the start, A1 is immediately above B1; when half the volume of liquid has been passed, A2 is still exactly over B2, but in this case the distance travelled by both pistons is significantly less than the distance travelled by the pistons in the first case; and again, at the end of the stroke A3 is in line with B3.

In Case 3 of figure 9, both cylinders have identical bulges, but the bulge in A is near to its beginning and the bulge in B is near to its end. In this case, the fact that the bulges are out of phase means that, although the pistons are in line in positions 1 and 3, they become out of line in position 2, where piston A has passed its bulge but piston B has not yet reached its bulge.

These bulges in figure 9 are an idealized way of representing the non-linearity within one revolution that might be expected to occur within a PD meter. If two such meters of nominally identical pattern are connected in series and their readings compared over less than one revolution, their readings may or may not be found to be in close agreement. If they are not in close agreement, it may mean that one or both meters contain some intra-rotational non-linearity, or it may merely mean that their meter factors are significantly different. The meter-factor question can be quickly resolved by means of a calibration, and if the reading of one of the meters is multiplied by the ratio of the two meter factors, this procedure (known as 'normalizing') will eliminate the effect of differing meter factors. If, after normalizing, the two meter readings still disagree, this proves that one or both meters must have a significant degree of intra-rotational non-linearity.

On the other hand, if the two meter readings after normalizing are in good agreement, this does not necessarily mean that both meters have perfect intra-rotational linearity, as in Case 1 of figure 9; it could equally well mean that they both have a severe non-linearity, but that the two linearities are in phase, as shown in Case 2 of figure 9. To ascertain whether this is so it is therefore necessary to make a number of comparative measurements between the two meters in series, with the two meters in a number of different phase positions relative to each other. This can easily be achieved in practice by inserting a bleed tapping between the two meters and drawing off a small quantity of the test liquid, so causing one meter to rotate through the required angle while the other meter remains stationary.

In an experiment of this kind, where each test run occupies considerably less than one second, the use of fully automatic data collection and recording is essential. It was arbitrarily decided to set the preset counters to collect totals of 2386 pulses, which corresponds to 2386/2540 of a revolution (approximately 338 degrees) and to make 500 runs in immediate succession in each batch. Figure 10 illustrates

diagrammatically how, in this method of test, where the end of one run signifies the beginning of the next run, the initial position of the meter shaft was caused to precess backwards by about 22 degrees in each test run. Not only did the starting point change in each test, but, because the meter factors of the two meters were not identical, there was also a progressive increase in phase angle throughout the duration of the test; consequently in a test of 500 runs a practically random assortment of starting positions and phase differences was encountered.

The results from a typical batch of 500 runs are given in histogram form in figure 11. The normalized discrepancy between the two meters is remarkably small, being never more than 8 pulses out of 2386 pulses in any one of these 500 runs. Moreover, the shape of the distribution curve is not far removed from being Gaussian, which shows that the initial assumption of randomness was not far from the truth. Consequently it is reasonable to apply the principle of the method used throughout this paper to derive a non-linearity constant, N , given by

$$N = \frac{t\sigma}{\sqrt{2}} \quad (5)$$

where σ is the standard deviation of the normalized discrepancy between the two meters over the batch of 500 runs.

In physical terms, this constant N has the following meaning. If the operator uses one of the meters that has been tested to measure the quantity of liquid passed during part of a revolution, and assumes perfect intra-rotational linearity for the meter, the error introduced through this assumption will be less than or equal to N in 95 cases out of 100. (This non-linearity error, N , is, of course, additional to all the other errors arising from random uncertainties and systematic uncertainties that are involved in using any measuring instrument.)

The results of non-linearity measurements at a number of different flowrates are given in Table 3. As an additional check on the assumption that the phase difference between the two meters would randomise itself over a period of 500 runs, the initial phase angle between the meters was varied in successive tests. That is to say, at each flowrate one batch of 500 runs was carried out with the two flowmeters in a given initial phase position; in the next batch one of the meters was advanced by 90 degrees from the initial position of the previous batch before starting the second batch; in the next batch the initial phase difference was 180 degrees; and in the final batch 270 degrees. As will be seen from Table 3 this variation in phase angle at the start of the tests had no detectable effect - an observation which confirms the assumption of randomness. It is worthy of note that the values of N determined in this experiment by successive tests at the same flowrate are in much better agreement than the values of R obtained in successive repeatability tests on the same instrument. It is evident that non-linearity is a property that can be measured more precisely than repeatability, even though similar statistical methods are used for its determination. This conclusion is reassuring but not unexpected.

It also appears from Table 3 that the intra-rotational non-linearity of this meter is to some extent dependent upon flowrate. At 17 litres per second, which is close to the maximum rated capacity of this meter, the non-linearity approximately doubles. This may mean that some form of vibration within the meter begins at these high speeds.

Despite this slight increase in non-linearity at the highest flowrate, the values obtained are remarkably good. They mean that the assumption of linearity within one revolution of the meter will very rarely introduce an error of more than 4 millilitres, and at flowrates well below the maximum capacity of the meter the error is unlikely to exceed 2 millilitres.

7. Conclusions

a The technique of coupling two liquid flowmeters in series and comparing their readings in a large number of repeat tests is an effective method of obtaining a numerical value for the repeatability of a flowmeter of a given pattern. With meters of sufficiently high discrimination it becomes an exceedingly sensitive method of assessing the performance of the meter, and enables effects to be studied that have not previously been detected by the conventional method of calibrating a flowmeter against a calibration standard.

b There appears to be no reason why the method should be restricted to flowmeters, since it would appear to be suitable for use with almost any type of instrument for measuring transient quantities. Depending upon the nature of the instruments it will sometimes be necessary to couple them in parallel rather than in series.

c Extensions of the basic method have been successfully applied to the determination of the repeatability of a flowmeter calibration system, and to the determination of the intra-rotational linearity of a flowmeter with an extremely high pulse-generation rate.

d The method can be applied to instruments with manual readout, but it then becomes rather time-consuming. For instruments with an electrical readout the tests can be carried out at great speed and with little effort by the use of fully automatic data collection and processing facilities incorporating a dedicated computer.

e Using this method has led to the discovery of drift, which sometimes takes a steady form and sometimes the form of abrupt change, in several types of instrument. In one case the drift was only a few parts per million and would have remained undetected but for the present technique. The existence of unsuspected drift would appear to explain the well-known fact that nearly all instruments have a much better short-term repeatability than long-term repeatability. The use of this method to detect and study this phenomenon of drift might enable manufacturers and users to ascertain its cause in particular cases, and hence to reduce the severity of drift and thus improve the long-term repeatability of instruments.

f The combination of a positive displacement meter capsule and a shaft encoder of the interferometric type yields a promising tool for use in standards laboratories, since repeatabilities of better than 10 parts per million seem attainable provided that the problem of drift (which probably arises from the shaft encoder rather than the meter capsule) can be solved.

g The particular vane-type PD meter used in this experiment appears to be especially suitable for standards laboratory work of this kind, since its intra-rotational linearity has been found to be extremely good also.

Acknowledgements

I am indebted to my colleagues J. C. Foot, J. S. Humphreys, K. I. Jespersen, W. C. Pursley and B. Reed, for this assistance with the experiments reported in this paper. This paper is presented by permission of the Director, National Engineering Laboratory, Department of Industry. It is Crown copyright.

References

- [1] Hayward, A. T. J. Repeatability and accuracy, Mechanical Engineering Publications, London and New York, 1977. (In press)
- [2] Ascough, J. C. The accuracy of thrust in flight from engine calibrations in an altitude test facility. Paper presented at Tenth International Council of the Aeronautical Sciences Congress, Ottawa, October 1976.
- [3] Westinghouse LEFM May 1976 tests, Westinghouse Electric Corporation, Annapolis, 1976.

T A B L E 1

RESULTS OF REPEATABILITY TESTS ON PD METERS WITH MECHANICAL
READOUT (STANDING-START-AND-FINISH TESTS)

Flowrate ℓ/s	Repeatability p.p.m.
4	130
4	90
4	170
11	140
11	110
11	180
16.5	200
16.5	250
16.5	120
16.5	60
16.5	110

T A B L E 2

RESULTS OF REPEATABILITY TESTS ON A GRAVIMETRIC FLOWMETER
CALIBRATOR OF THE STANDING-START-AND-FINISH TYPE

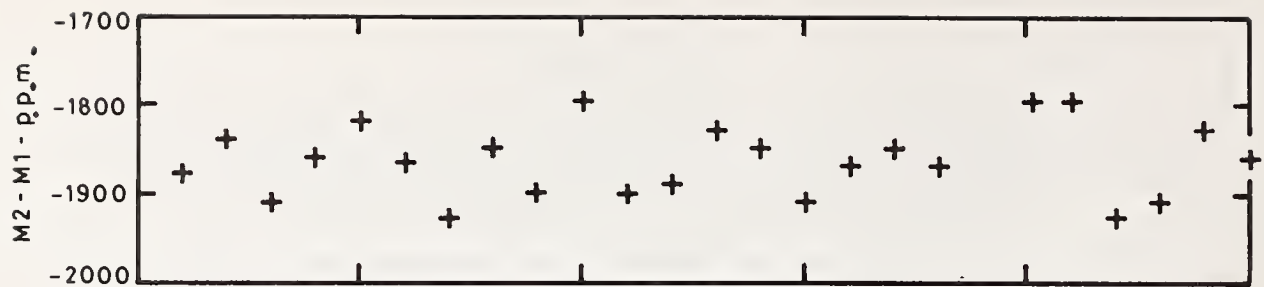
Flowrate ℓ/s	Repeatabilities - p.p.m.			
	R _{1C}	R _{2C}	R ₁₂	Calibrator
4	350	180	380	80
4	480	190	490	140
4	450	260	490	130
11	220	200	130	190
11	210	130	180	130
11	180	160	130	180
16.5	290	210	220	200
16.5	230	230	150	200
16.5	250	240	170	210

T A B L E 3

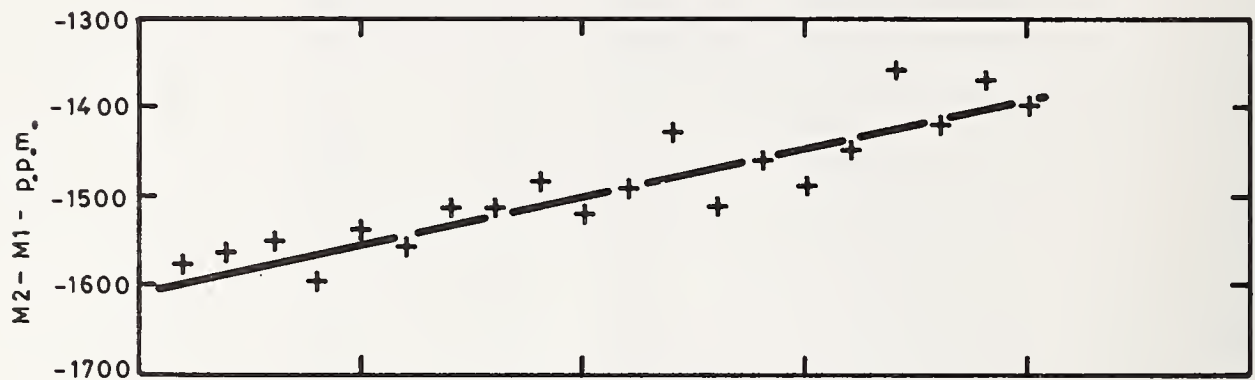
RESULTS OF INTRA-ROTATIONAL NON-LINEARITY TESTS

Flowrate ℓ/s	Initial phase angle degrees	Non-linearity, N pulses
4.5	0	1.95
4.5	90	1.98
4.5	180	1.91
4.5	270	1.87
9.4	0	1.45
9.4	90	1.46
9.4	180	1.47
9.4	270	1.57
9.4	0	1.54
9.4	90	1.54
9.4	180	1.46
9.4	270	1.54
14.0	0	1.60
14.0	90	1.49
14.0	180	1.50
14.0	270	1.57
17.1	0	4.00
17.1	90	2.90
17.1	180	3.11
17.1	270	3.22
17.1	0	3.96
17.1	90	3.25
17.1	180	4.02
17.1	270	3.72

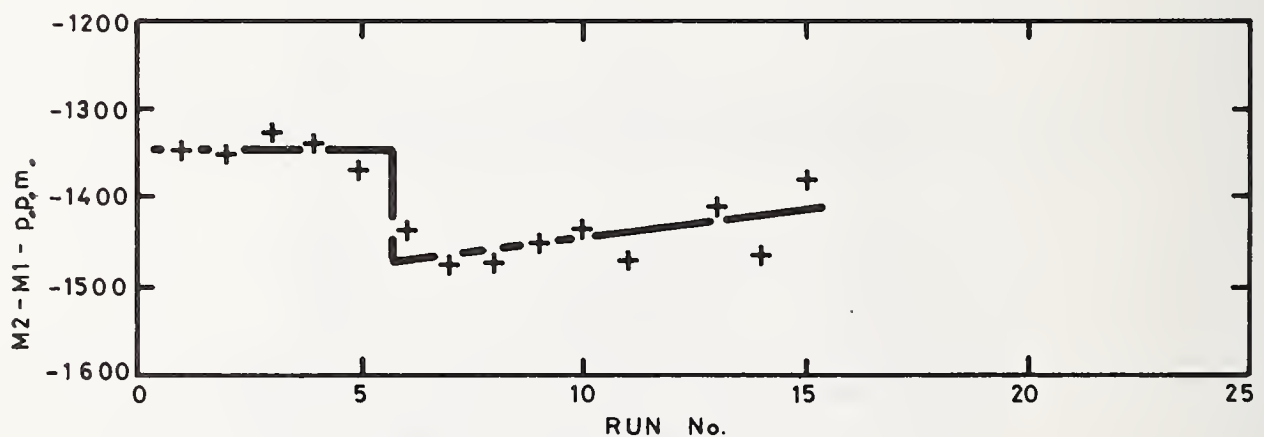
Each value is based on 500 flying counts of $M_1 - M_2$ in immediate succession, in each of which M_1 was 2386 pulses, which is equivalent to approximately 338 degrees rotation.



a) EXAMPLE OF TEST FREE FROM DRIFT



b) EXAMPLE OF TEST SHOWING STEADY DRIFT



c) EXAMPLE OF TEST SHOWING STEPWISE DRIFT

FIG 1 TYPICAL TEST RESULTS FOR P.D. METERS WITH
PHOTOCELL-TYPE PULSE GENERATORS (BASED
ON 100,000 PULSE COUNTS PER RUN)

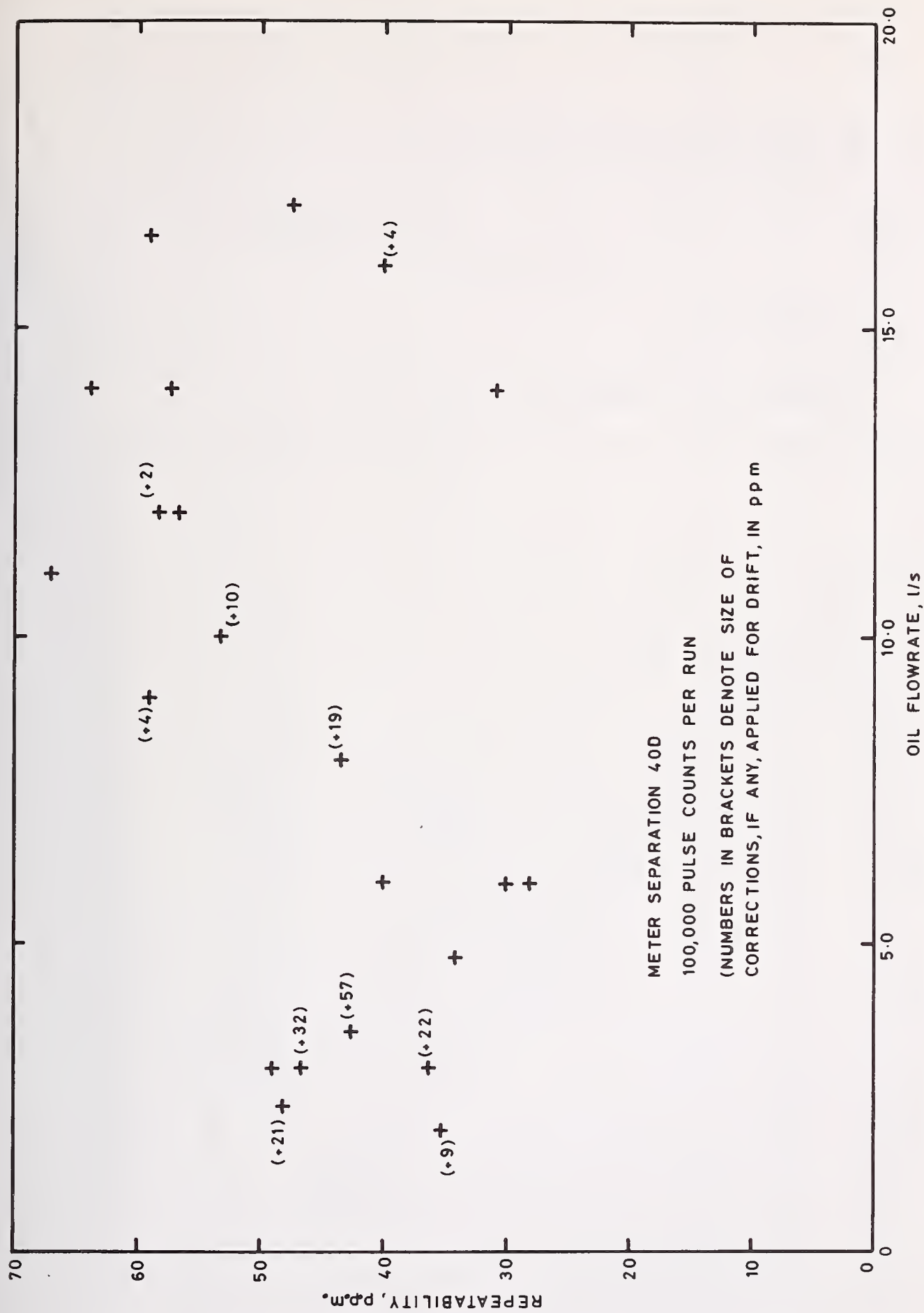
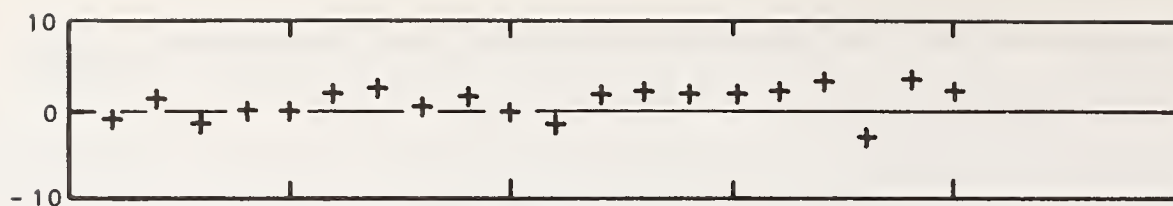
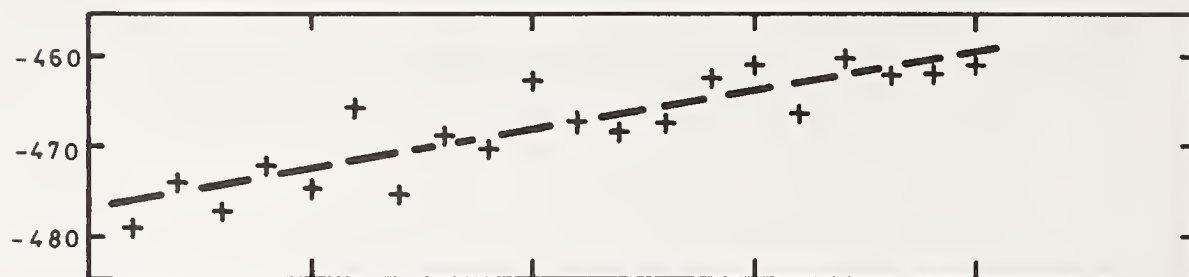


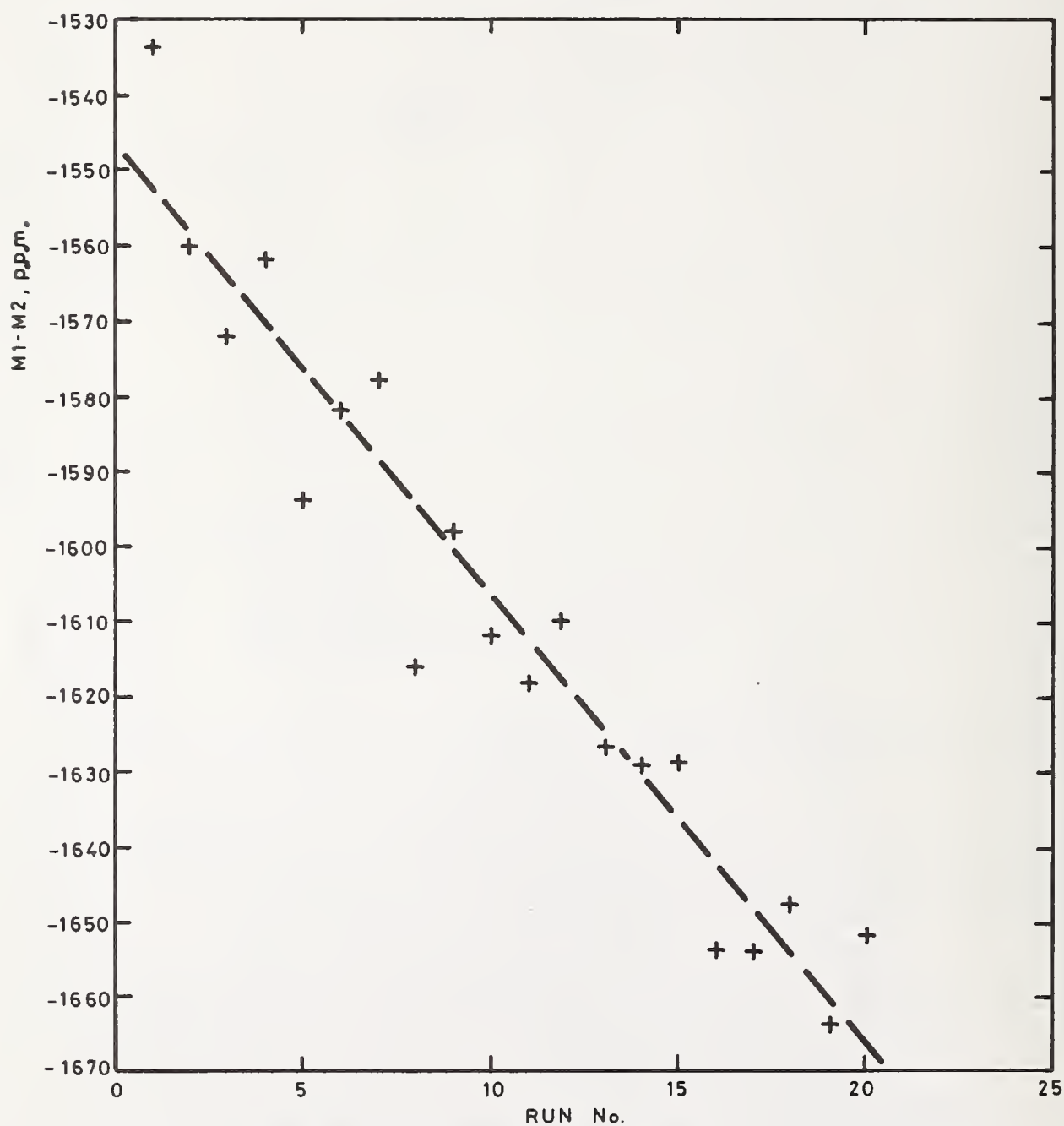
FIG 2 RESULTS OF REPEATABILITY TESTS ON PD. METERS WITH PHOTOCCELL-TYPE PULSE GENERATORS



a) EXAMPLE OF TEST FREE FROM DRIFT



b) EXAMPLE OF TEST SHOWING SLIGHT DRIFT



c) EXAMPLE OF TEST SHOWING SEVERE DRIFT

FIG 3 TYPICAL TEST RESULTS ON P.D. METERS FITTED WITH SHAFT ENCODERS (BASED ON 1,000 000 PULSE COUNTS PER RUN)

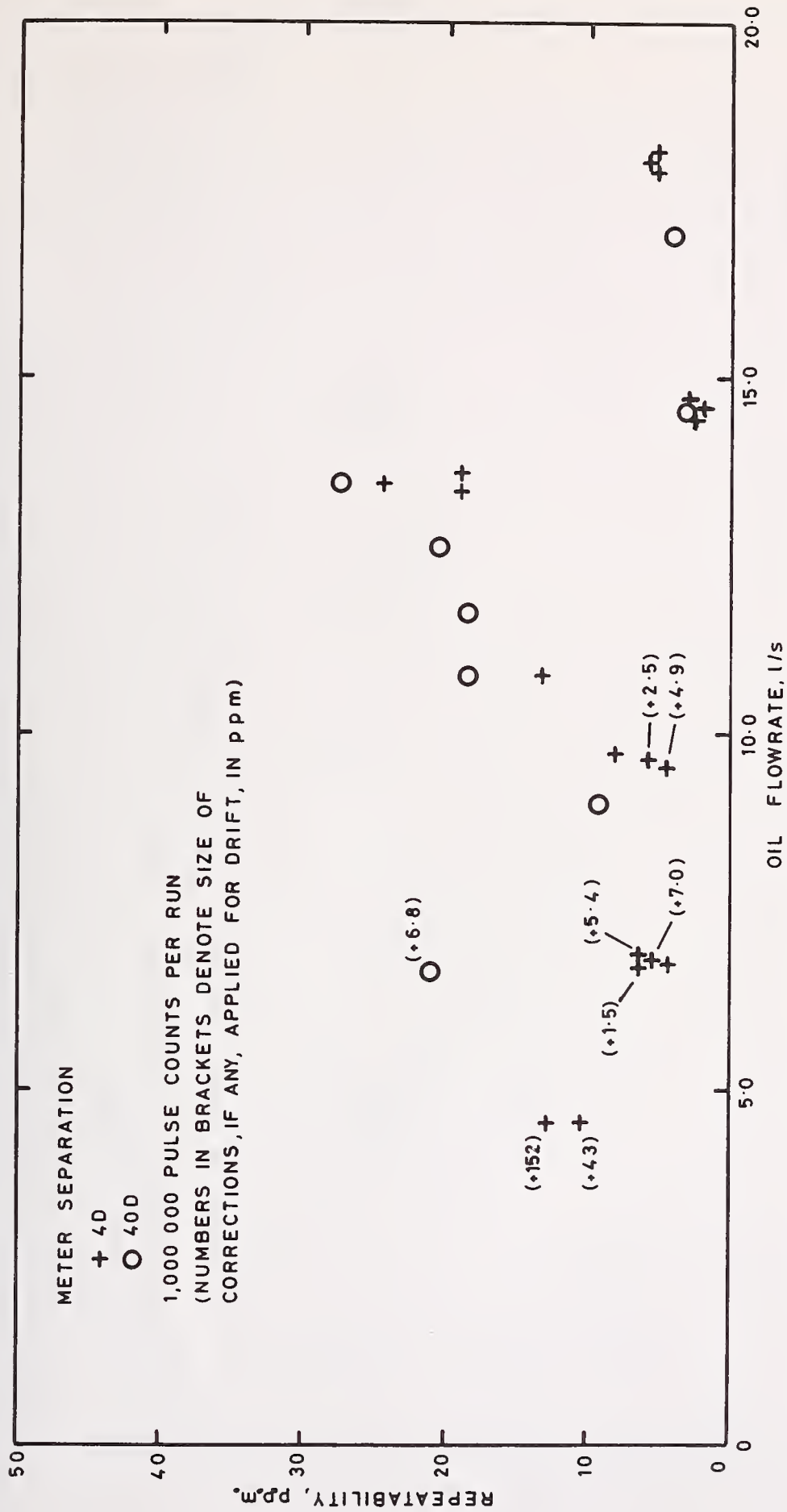


FIG 4 RESULTS OF REPEATABILITY TESTS ON P.D. METERS FITTED WITH SHAFT ENCODERS

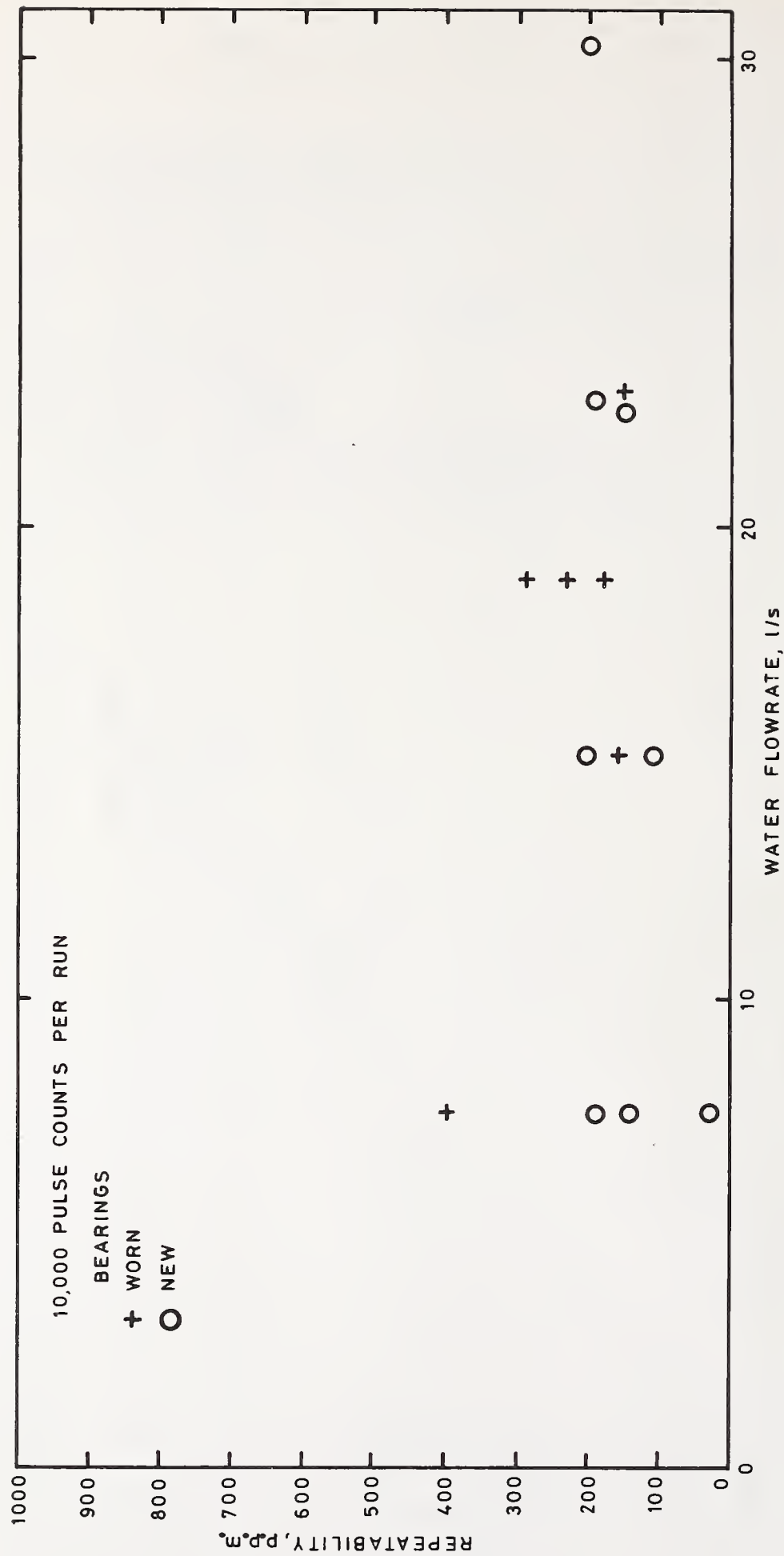


FIG 5 THE EFFECT OF BEARING WEAR ON THE REPEATABILITY OF 75mm (3in) TURBINE METERS

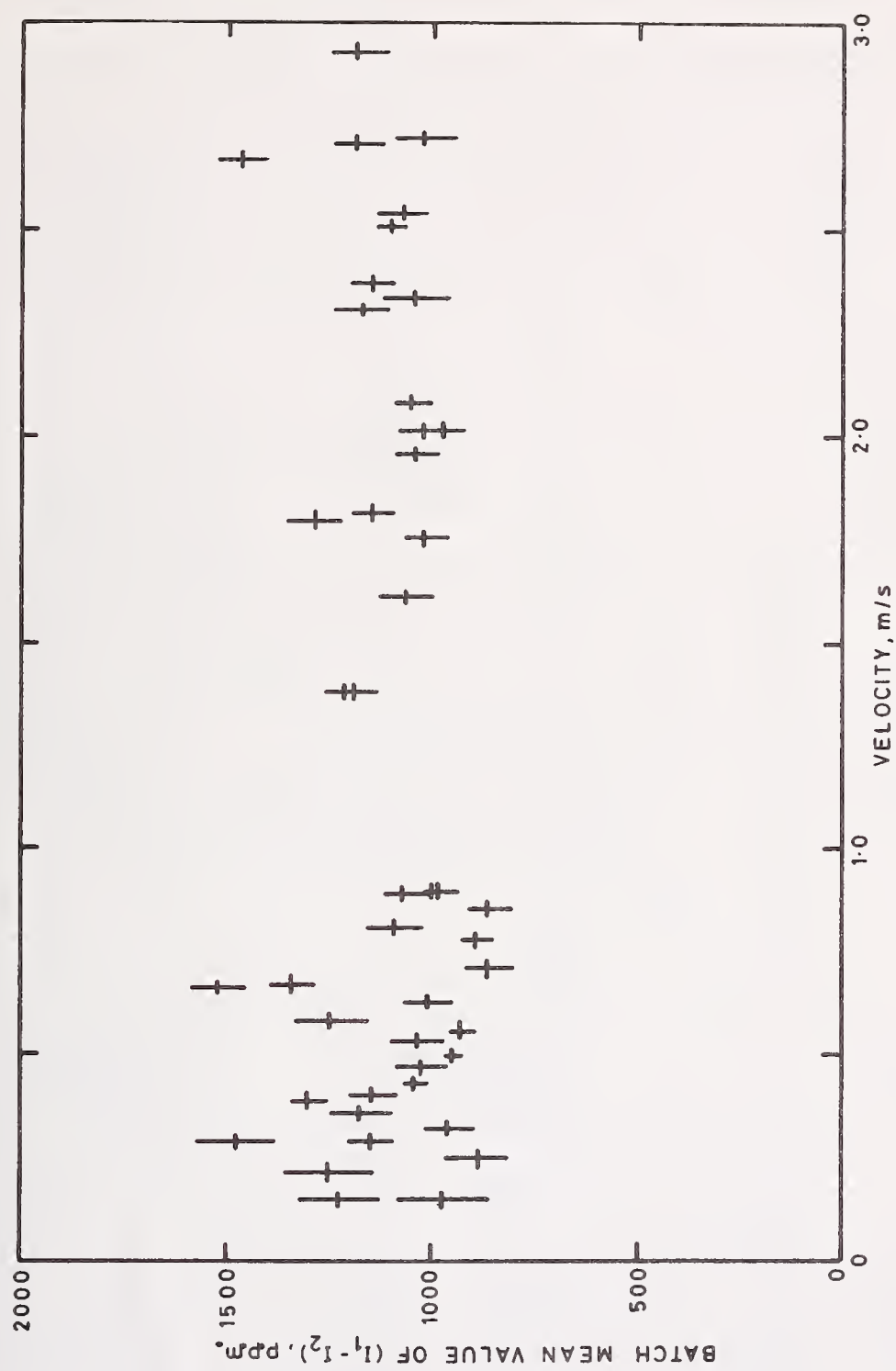


FIG 6 RESULTS OF REPEATABILITY TESTS ON A PROPRIETARY FLOWMETER-CALIBRATION DEVICE, WITH PAUSES BETWEEN BATCHES OF RUNS (DIFFERENT VELOCITIES)



FIG 7 RESULTS OF REPEATABILITY TESTS ON A PROPRIETARY FLOWMETER-CALIBRATION DEVICE WITH NO PAUSES BETWEEN BATCHES OF RUNS (EXCEPT OVERNIGHT)

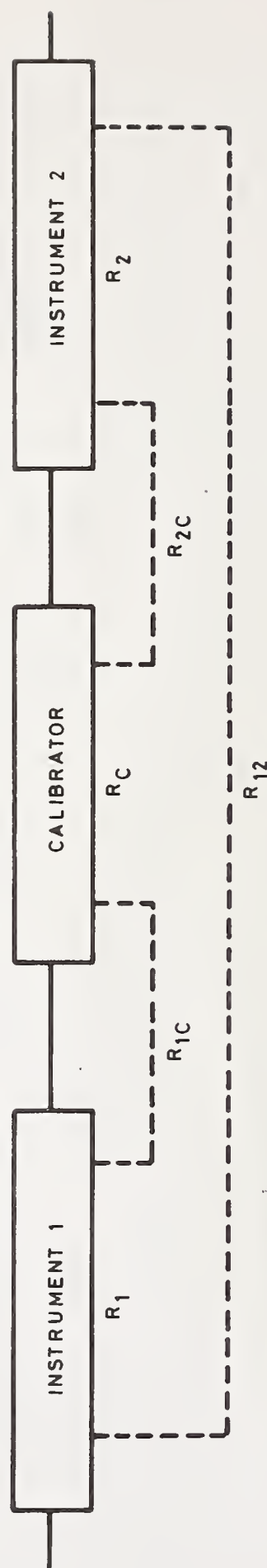
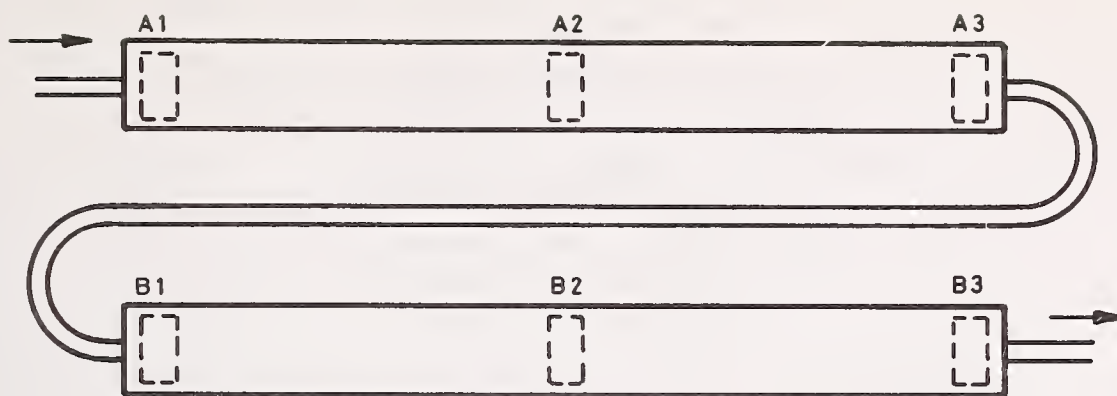
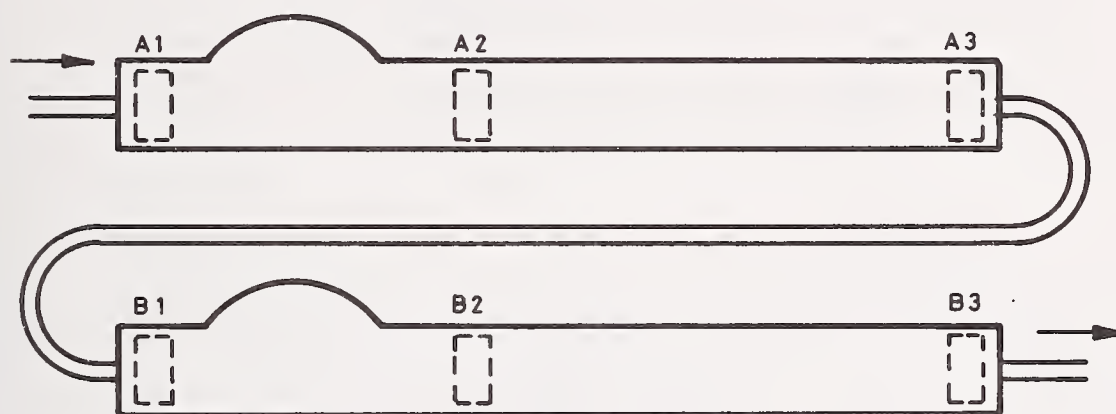


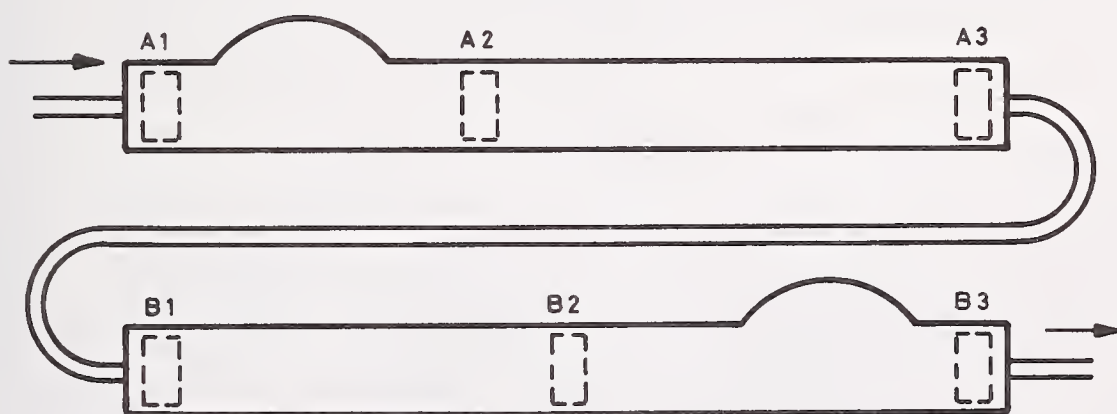
FIG 8 ARRANGEMENT FOR MEASURING THE REPEATABILITY OF A CALIBRATOR, R_C



CASE 1. PERFECT LINEARITY



CASE 2. BULGES IN PHASE



CASE 3. BULGES OUT OF PHASE

FIG 9 PRINCIPLE OF METHOD FOR MEASURING
INTRA-ROTATIONAL LINEARITY OF P.D. METERS

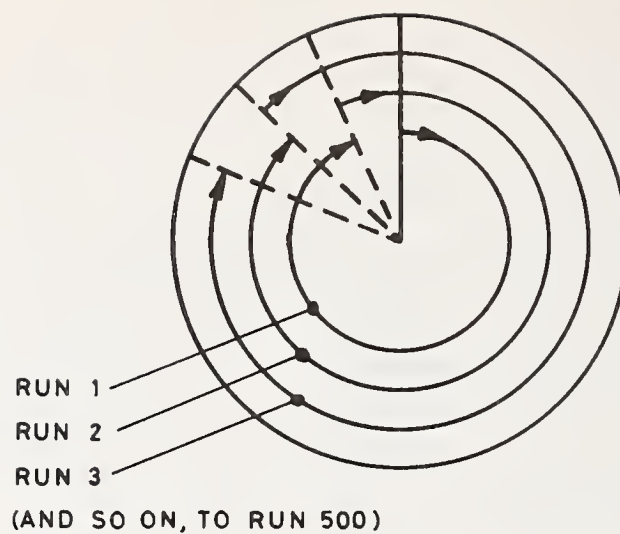


FIG 10 MODE OF ANGULAR ROTATION OF
ROTARY P.D. METER IN EACH OF
500 CONSECUTIVE FLYING-START-
AND-FINISH TEST RUNS

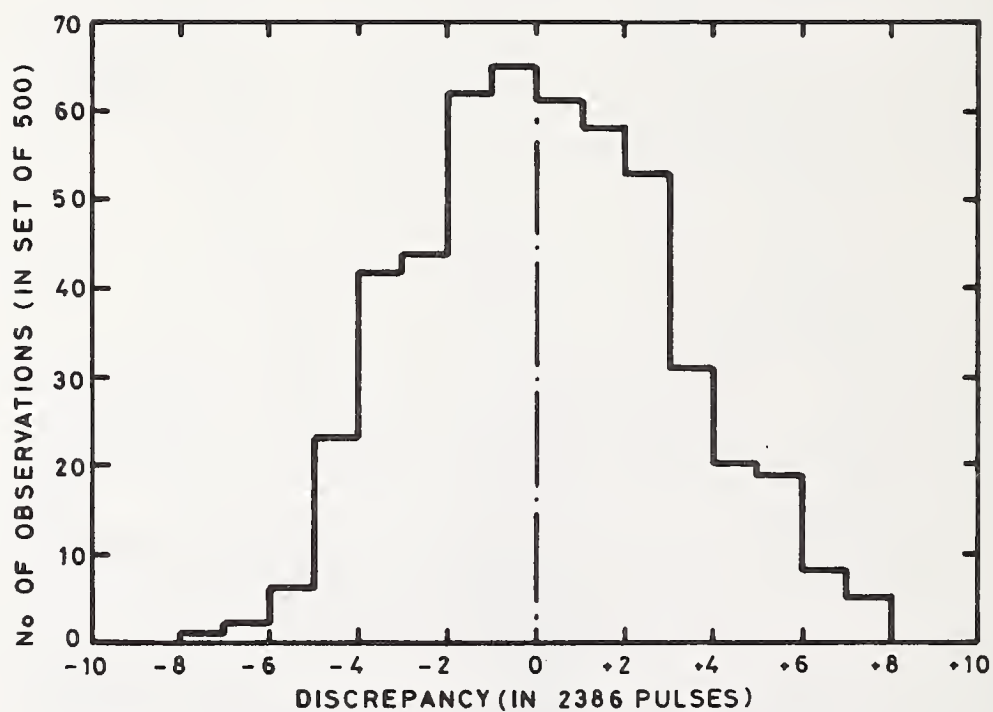


FIG 11 DISTRIBUTION OF NORMALIZED
DISCREPANCY BETWEEN METERS
AFTER ROTATING 338°

THE NAVY LIQUID FLOW CORRELATION PROGRAM

J. H. Tabler and C. G. Kullmann
Navy Type I Standards Laboratory
Naval Air Station, North Island
San Diego, California 92135

. A brief history of the Navy Flow Correlation Program is described. The present flow correlation program is outlined in detail. The object of the on-going program is to assure compatibility of all primary liquid flow stands in the Navy Metrology System to within $\pm 0.15\%$. This is accomplished by first assuring that the primary weigh/time dynamic liquid flow stands at the Navy Type I Laboratory are in agreement with those at the National Bureau of Standards. The method of maintaining compatibility of the four flow provers at the Type I Laboratory is discussed. Application of process control charts is described.

Approximately 15 primary volumetric and dynamic weighing flow stands are located at various Navy Metrology Laboratories and Test Centers throughout the Continental U. S. The technique used to maintain control is the use of turbine type flowmeters at discrete frequencies and the use of a common very stable calibrating fluid. The excellent short term repeatability of these transfer devices lends itself to this type of correlation program. The Type I Laboratory calibrates the turbine meters before and after a participating laboratory calibration is performed. The report issued to participating laboratories is described.

1. Introduction

In the mid 1950's there was a requirement to improve flow measurements throughout the Navy. This was brought about by the relatively close flow tolerance on jet engine fuel controls. In 1955, the Navy Bureau of Aeronautics purchased eleven of the Cox Instruments model 311 Primary Fuel Flow Calibrators. One of these went to the National Bureau of Standards (NBS) and the others were sent to Navy Overhaul and Repair Activities and Test Centers located throughout the U. S. In 1960, under the sponsorship of the Bureau of Aeronautics, the National Bureau of Standards and the Navy Metrology Engineering Center (MEC) were engaged to conduct a program to determine the degree of correlation between the calibrator at the NBS and those at the Navy Activities. The transfer devices used were sharp-edged orifices, a positive displacement meter and turbine meters. Results of this correlation lead to modifications and improvements in these stands and in standardization

of test fluids. The objection to the use of orifice plates was the narrow range of flow with each orifice plate and the rather stringent data reduction requirements. Most of the fluid measurements being made by personnel at Naval Aviation activities were with turbine type flowmeters or the variable area float type meters. Because of the performance characteristics, high resolution and the small size which makes shipping easy, turbine meters have been used for all subsequent correlation programs. In 1964, the Navy Western Standards Laboratory (WSL) was assigned the responsibility of maintaining compatibility of flow measurements in the Navy Metrology System and assuring traceability to the National Bureau of Standards. A second correlation program was initiated at this time. Knowledge and experience gained from these programs and others that followed have resulted in corresponding improvements in the compatibility of flow measurements in the Navy system. Today an on-going correlation program is conducted, and compatibility between approximately fifteen of the primary flow calibrators in the Navy is routinely within $\pm 0.15\%$.

2. Primary Liquid Flow Provers at the Western Standards Laboratory

The WSL has four primary liquid flow provers. Three of these stands are Cox 311-AT flow stands containing calibrating fluids of varying viscosities in order to calibrate flowmeters over a large range of viscosities without the need to change fluids. One stand contains MIL-C-7024B Type II, another stand contains MIL-H-5606C and the third stand contains a blend of the two fluids. By using three stands with different fluids, flow calibrations can be performed to 200 gal/min over a viscosity range of 1 to 20 centistokes. The Cox 311-AT flow stands have two complete flow circuits, a low flow system (0.014 to 2.8 gal/min) and a high flow system (1.4 to 200 gal/min). Each system has its own pumps, valves, filters, heat exchangers, temperature controls, gages and weighing systems. The frequency meter, electronic counter and timer are common to both systems and are triggered by proximity type switches which are operated by the weigh beams. The principle of operation is that of measuring the time interval to collect a predetermined weight of liquid that has passed through the test flowmeter. The weigh tanks of each system are supported on weigh beams. The low range system has a one to one beam ratio and the high range system has a 50 to 1 beam ratio.

The fourth flow prover is a Flow Technology Ballistics Flow Calibrator. This is also a self-contained instrument with two complete flow systems. (A high flow section with a 4" ID flow tube and a low flow section with a 1" ID flow tube.) This stainless steel volumetric flow prover is designed to calibrate turbine flowmeters up to 1000 gal/min using any liquid with viscosities up to 500 centistokes. Pickoffs are positioned externally on the flow tubes. A free moving piston actuated by compressed air pushes fluid down the tubes. As the piston passes each pickoff point an electrical pulse is generated. The time between pulses is displayed indicating the time required to displace a known amount of fluid.

3. Correlation of the WSL Flow Stands

In order to perform the correlation of the three Cox 311 stands the following procedure is used. The fluids in the low flow system of all three stands are drained and replaced with MIL-C-7024B Type II. This fluid has been accurately measured for density and viscosity beforehand by WSL. Two turbine flowmeters are then calibrated on the low system of each stand at 80°F and at the same nominal flow rates. Opening and closing measurements are made on the one stand which normally contains the Type II fluid. Closing measurements are taken to verify that no shift has occurred in the turbine meters and to determine the short time repeatability of the calibrator. The stand which normally contains the Type II fluid is used as the reference because it is the calibrator used in periodic correlations with the National Bureau of Standards.

When the low flow systems are in correlation the original fluids are replaced in each stand and the two turbine meters calibrated to their maximum flow rate of five gallons per minute. This calibration provides correlation information between the high and low flow systems of the flow stands. "Crossovers" between the high and low system are normally within $\pm 0.05\%$. Whenever a customer flowmeter is calibrated using both flow systems, the compatibility between these systems is determined.

Two higher range flowmeters of 50 GPM capacity are calibrated on the high range system up to their rated capacity. The pulses per gallon ("K" factors) obtained for the flowmeters on both flow systems are used as reference points for control charts maintained for the flow stands.

The ballistics prover is correlated to the 311 stand using these same four turbine meters. The ballistics prover at the WSL does not presently have temperature control and the flow rate cannot be set precisely, therefore, the 311 stand is set up to match the frequency and temperature data obtained on the ballistics prover.

The turbine meters used for the correlation of the WSL flow stands are used only for this purpose. These correlations are done periodically and process control charts are maintained. A complete discussion and test results of the first in-house correlation at the WSL is given in [1]¹. Figure 1 shows a typical process control chart being maintained at the WSL. The chart includes all values over the range of frequencies investigated and "crossover" information between the two systems. Since the turbine type meter has its best performance over the upper 50% of the range, this data has more significance when comparing results. Use of process control charts will not eliminate the requirement to periodically calibrate individual components of each flow system. However, confidence in the total measurement system is greatly improved through the use of these charts.

¹Figures in brackets indicate the literature references at the end of this paper.

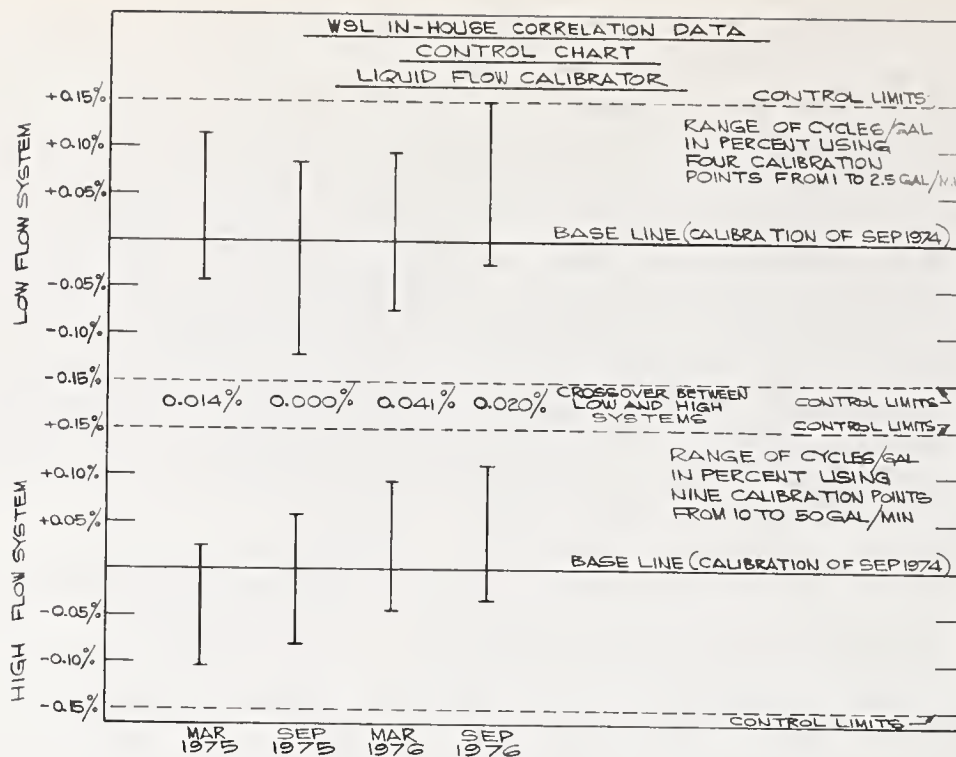


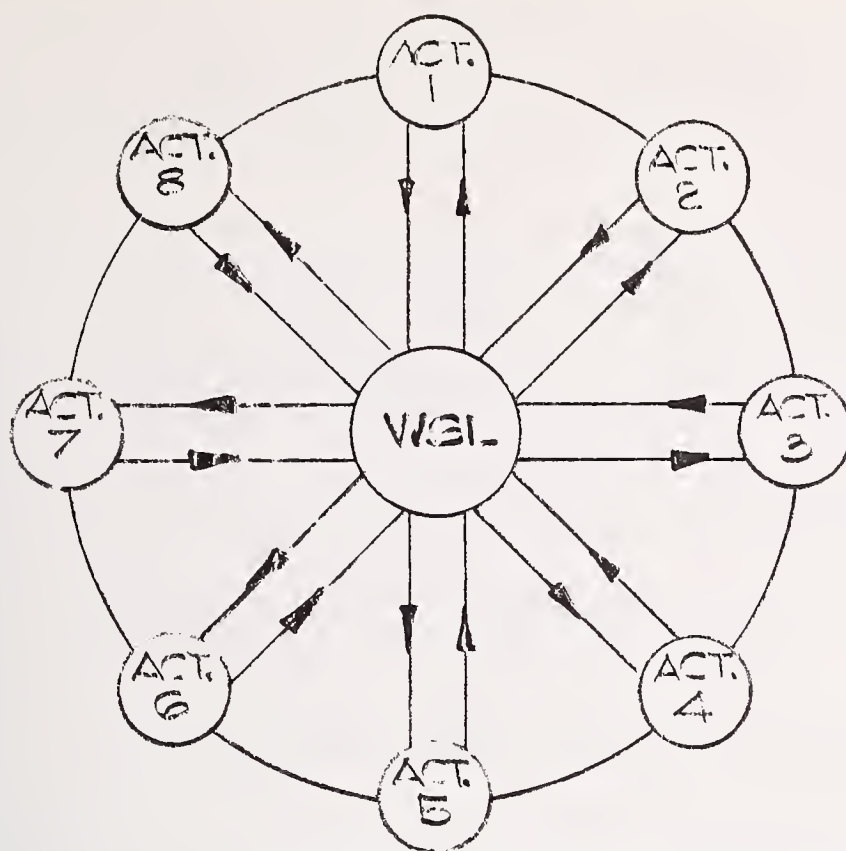
Figure 1. MEASUREMENT PROCESS CONTROL CHART FOR WSL FLOW STAND CORRELATIONS

4. Correlations with Other Navy Flow Stands

The objectives of the program are:

1. Determine if the primary flow stands in the Navy are performing within specifications.
2. Determine from the test data such factors as repeatability, correlation agreement, and determine any corrective adjustment or repairs required.
3. Appraise the knowledge and ability of the operators of participating laboratories in the field of fluid mechanics, so training can be provided if required.

At present WSL is using three turbine meters of different ranges for correlations with other Navy activities. Closing measurements are made at WSL after the meters are returned from each activity. These closing measurements are used as opening data for the next activity. See Figure 2. This "spoked-wheel" scheme has some major advantages for correlation programs of this type. A shift in the meter coefficient can be detected immediately and the meter replaced before another customer is sent the correlation. Each loop is a complete correlation in itself and does not directly depend on all other participants for statistical data. These meters were selected to measure flow stand performance over a large portion of each flow system. One of the meters was selected to be calibrated at the same flow rate on both the high and low flow systems of the 311 flow stands and provide a measure of the compatibility between the two systems.



ACT = NAVAL CALIBRATION
ACTIVITY

Figure 2. SPOKED WHEEL CORRELATION SCHEME

The fluid specified for the correlation is MIL-C-7024B Type II at $80^{\circ} \pm 1^{\circ}\text{F}$. In addition, the nominal pulses per second and the weight of the fluid to collect in the flow stand weigh tank is specified for each flow rate. A minimum of three runs is made at each setting to determine repeatability.

After closing measurements are made at the WSL, the activity is informed by telephone of the results. A formal report is then provided comparing the customer and WSL results. This report includes a graph (see figure 3) which is divided into two sections. The upper portion of the graph shows possible systematic errors as a function of flow rate, flowmeter and weigh system. The lower portion summarizes precision or repeatability. Each plotted point on the lower portion of the graph is the percent spread of three repeated observations. This graph suggested to WSL by the Fluid Meters Section of NBS contains on a single page the following:

- a. Flow range investigated
- b. Overlap between reference meters
- c. Overlap between large and small weigh systems
- d. Systematic error as a function of flow rates
- e. Repeatability as a function of flow rates and reference meter.

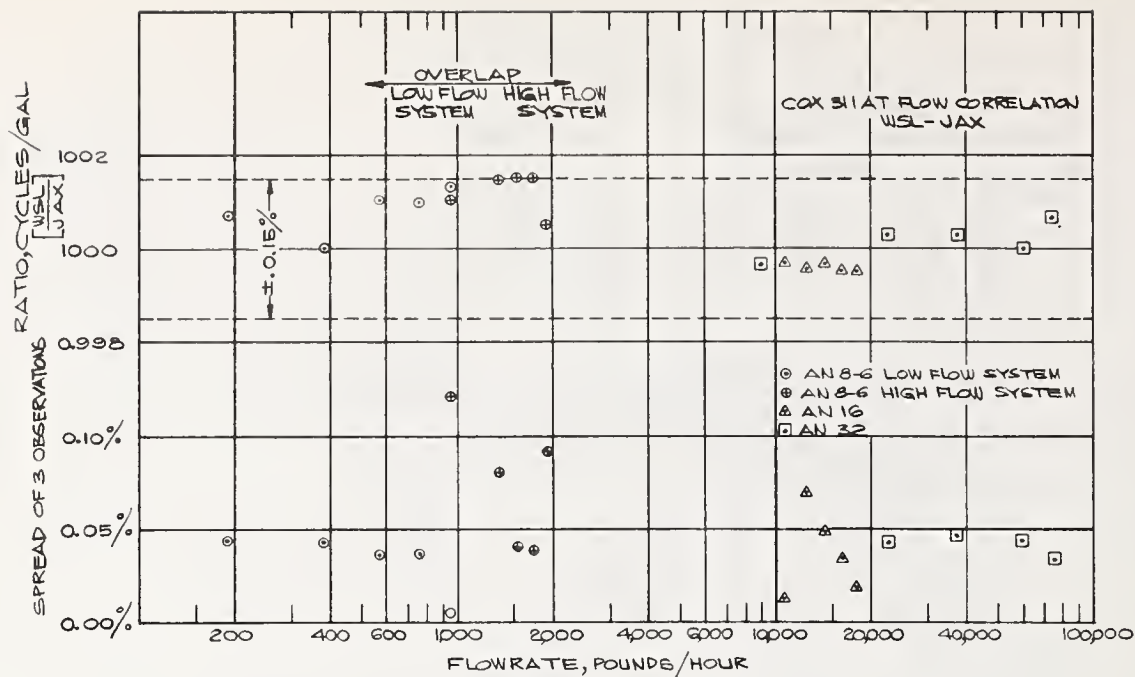


Figure 3. EXAMPLE OF WSL CORRELATION WITH ANOTHER ACTIVITY.

The formal report gives suggestions for corrective actions if any are required. Some typical causes of systematic error that have been reported are:

- a. Errors in measurement of fluid density
- b. Beam ratio incorrect
- c. Errors in temperature measurements. (Temperature at the stand can be as much as 5° different from temperature at the turbine meter.)

Some of the causes of poor repeatability have been:

- a. Low sensitivity of weigh system
- b. Leaking dump valve sealing gasket
- c. Insufficient tare time
- d. Empty or leaking vapor seal on weigh tanks

5. Conclusion

The present flow correlation has been very successful. It has been possible to correlate the Navy primary flow stands to within $\pm 0.15\%$. This uncertainty is near that of the National Bureau of Standards whose possible systematic uncertainty on dynamic weigh stands is given as $\pm 0.10\%$ with allowance of $\pm 0.03\%$ for random error based on a standard error of $\pm 0.01\%$ for a total estimated uncertainty of $\pm 0.13\%$ [2]. No attempt has been made to discuss the technical aspects of flow measurement in this paper, but references [3] through [5] discuss flow stand correlation techniques, uncertainties in flow measurements and standardization requirements.

Sending three meters of different ranges has caused no problems. The closing and opening measurements at WSL normally repeat within the turbine meters random uncertainty. Also, a shift in a meter can be detected immediately and the meter replaced before another customer is sent the correlation package.

In the past, pairs of turbine meters were calibrated at WSL and then circulated through a large number of customers before the closing measurements were made at WSL. A report with a Youden plot (see figure 4) was then sent to the participants. This method of plotting is given in [6]. Although this reporting method had advantages, the "round-robin" routing of the standards resulted in some distinct disadvantages.

- a. There is a longer period of time before the customer receives a report on whether or not his flow stand is within tolerance.
- b. There can be long holdups in the cycle if a customer is not ready for the correlation package.
- c. If a turbine meter should shift, WSL might not find out until other participants have used it for measurements.

We have found the present correlation method successful and in addition to such factors as repeatability and correlation with WSL, the program appraises the knowledge and ability of the participating laboratory operators in the field of fluid mechanics and the measurements of viscosity and density.

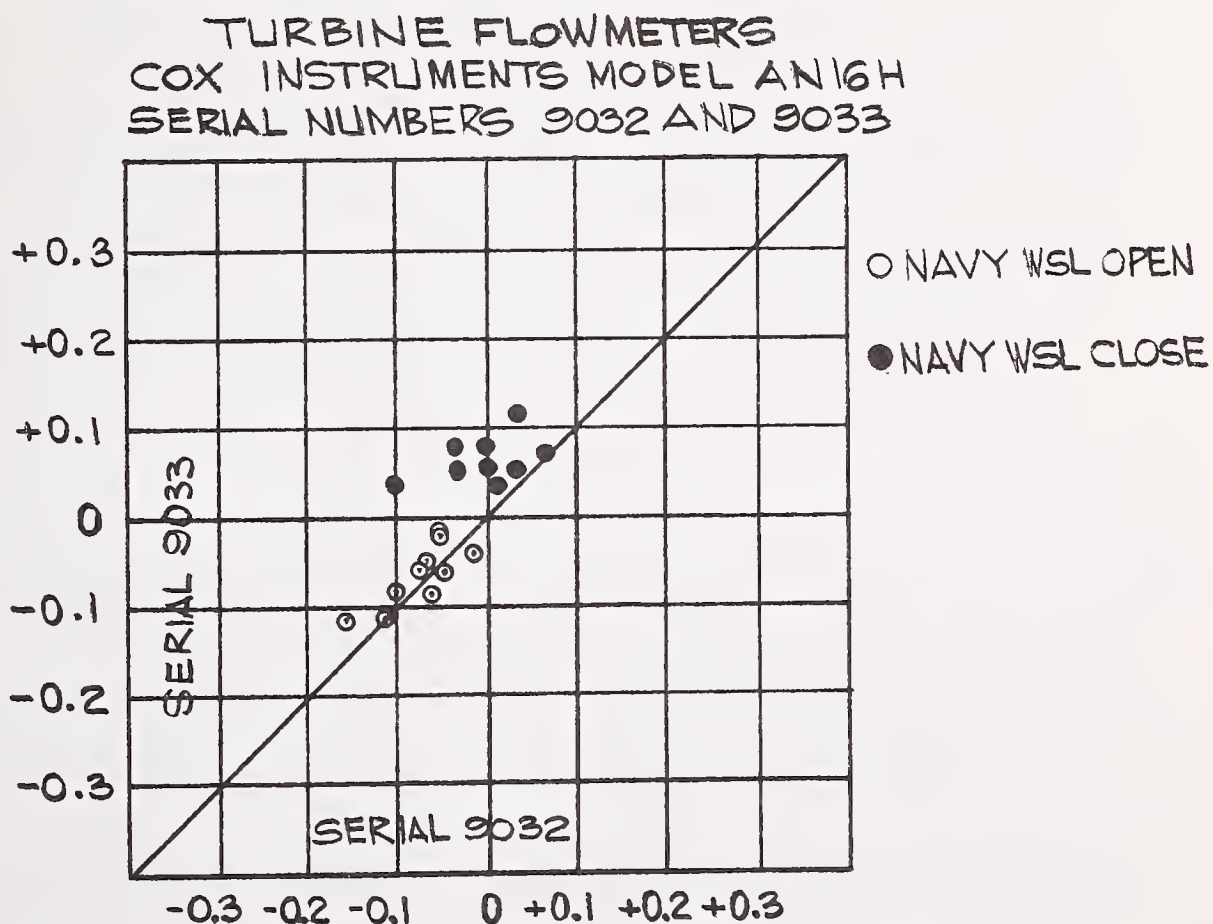


Figure 4. YODEN PLOT, "K" FACTOR DIFFERENCES FROM NBS (%), TEST RANGE 5.0 to 50 GPM

- [1] Kullmann, C. G., "In-House" correlation of the liquid flowmeter calibrations at the Western Standards Laboratory, Engineering Report 6-72 of 18 August 1972.
- [2] Filban, T. J. and Shafer, M. R., Flow measurement standardization, 19th annual ISA conference and exhibit, 12-15 October 1964, New York.
- [3] Shafer, M. R., Test stand correlation techniques, 23 February 1956.
- [4] Shafer, M. R. and Ruegg, F. W., Liquid flowmeter calibration techniques, transactions of the ASMG for October 1958.
- [5] Bean, H. S., Comments on how good are good flow measurements, GAS, November 1961.
- [6] Youden, W. J., The sample, the procedure, and the laboratory, Analytical Chemistry, December 1960.

A LABORATORY STUDY OF TURBINE METER UNCERTAINTY

G. E. Mattingly, P. E. Pontius, H. H. Allion
and E. F. Moore

Mechanics Division, IBS
National Bureau of Standards
Department of Commerce
Washington, D.C. 20234

A series of laboratory tests are conducted to assess, quantitatively, the uncertainties produced in making fluid flow measurements using turbine meters. The patterns of uncertainty are analyzed statistically and remedial modifications are described and evaluated.

Using a tandemly connected pair of conventional turbine meters with recommended meter tubes and straightening vane sections, calibration procedures are performed with a weigh-time reference for the liquid flow. The calibration data are analyzed using a variety of techniques. The results indicate that turbine meter performance can, within the realm of "normal" operating conditions, be perturbed to exceed specified values. Modifications, both to hardware and conventional testing procedures, are described which enhance metering assurance.

Key Words: Accuracy; calibration; flow conditioning; meter performance; perturbations; precision; turbine meter; uncertainty.

1. Introduction

A concerted effort at the National Bureau of Standards (NBS) has been recently directed toward the establishment of Measurement Assurance Programs (MAPs) for flow. The objective of a flow MAP is to quantitatively characterize the flow measurement process. It is not to force everyone into state-of-the-art measurements but rather to establish techniques and procedures which will provide assurance, at all levels of measurement, that the results are adequate for the intended purpose [1,2,3,4]¹.

¹Figures in brackets indicate the literature references at the end of this paper.

Throughout the flow metering industry and practice, turbine meters have earned a considerable reputation for their precision and reliability. The advantages and disadvantages of using turbine meters to measure fluid flow are widely known and well documented [5,6,7,8,9,10,11,12].

The advantages include:

- (1) A characteristic performance which exhibits a small range of variability over wide flow rate ranges. For normal fluids, this characteristic can be reduced to a single descriptor using dimensionless parameters.
- (2) A pulsed output which is readily digitized. The resolution is limited only by the least count.
- (3) Rotor bearing designs which have evolved to enable reliable performance over extended periods.
- (4) Relative insensitivity to minor variations in streamwise velocity profile, due to the fact that the multi-bladed rotor and hub completely fill the flow cross-sectional area.
- (5) Very rapid response characteristics.

In light of these advantages, turbine meters are widely used in aircraft applications, petroleum metering and other industrial areas where the user's flow measurement needs are critical. Turbine meters are not without their disadvantages, however. For example:

- (1) The flowing fluid and any materials in it must not impair the rotor bearing or the rotor and blade geometry.
- (2) The meter is susceptible to the effects of swirl in the inlet pipe flow and radical variations in the streamwise velocity profile have been known to cause variations in performance characteristics.

In view of these respective advantages and disadvantages, turbine meters have been selected for the initial phases of the flow MAP program. The present tests focus on turbine meter performance in water flows in medium pipe sizes.

2. Experimental Study

The experiments were carried out in the large, water calibration facilities of the Fluid Meters Section of the National Bureau of Standards. Shown in Figure 1, these facilities consist of a 60,000 gal. ($\sim 230\text{m}^3$) sump from which water is pumped by means of one or more submerged pumps. For the present tests, the water then flows through

filters and straight lengths of PVC pipe to the test sections where the meters under test are located. The flow is either bypassed to the sump or diverted into a collection tank positioned on a scale. The correspondence between the meter indication and the collected volume of water is determined from a static weighing of the water delivered in a measured time interval. More details on this system and procedure can be found in [13].

In the present experiments, pairs of turbine meters are tested in tandem. These turbine meters are commercially available, 4 in. (~ 10 cm) internal diameter meters, each of which is equipped with a matched meter tube. These meter tubes have both upstream and downstream sections. The upstream sections are fitted with flow straighteners consisting of tube bundles sized and located according to AGA/ASME recommendations [6-7]. This upstream meter tube section is bolted to its respective meter by means of pinned flanges to assure repeatable, aligned joints. The assembled meter and matched meter tube sections shall be referred to, in what follows, as a matched unit.

The present tests were confined to measurements at two flow rates set to achieve Reynolds numbers of 1.2×10^5 and 6.0×10^5 based on pipe diameter and water temperature. At each flow rate, respectively, given that a certain meter performance criterion (the ratio of meter responses) is satisfied, repeated water collections are performed and the so called "turbine meter constants" are determined in pulses per gallon corrected to 20°C . Initially, five such runs were made at each flow rate. The run-to-run variation obtained indicated that three such collections were adequate, and this change in the test procedure was implemented halfway through the test program.

The meter performance criterion used in this test is based upon a particular ratio of the two turbine meter responses. When this ratio closely approximates an expected value (formulated via averages from many previous tests), it is assumed that both meters are performing "properly" and the test results can be considered credible. Should the ratio criterion not be satisfied, it is assumed that something has impaired the meters - such as an anomalous deposit on a turbine blade. It is assumed that the probability of simultaneous and identical occurrences in both meters affecting each meter's performance in the same manner is negligibly small. Given repeatability of the ratio to within a specified tolerance of the expected value, the test procedure is continued. Otherwise, the meters are back flushed to remove anomalous deposits or the flow is stopped, and the pipeline drained and opened so that the meters can be inspected and cleaned by flushing with alcohol. To date, it has been possible at NBS to return this ratio to an acceptable value with one of these remedies.*

*In view of what follows, the actual value of the ratio may be a characteristic of a given test facility.

The specific procedures used to test the meters are given in Appendix 1. The data produced using this procedure will be referred to as "conventional." With a conventional data base determined, study consists of devising and evaluating a variety of schemes that perturb the meter performance from the conventional values. Once the perturbation effects have been determined, remedial procedures are devised and evaluated which are intended to re-establish conventional meter performance in the presence of perturbations.

The perturbation schemes devised include: (1) vibration effects, (2) radically changing the streamwise velocity profile entering the stream meter tube, and (3) inserting various levels of "swirl" in the inflow to the meter tube. It will be shown below that all of these have some effect on conventional meter performance. Of the three types of perturbations, swirl exerts the most significant perturbation effect.

The types of remedial procedures devised to re-establish conventional meter performance have included: (1) using a third turbine meter, installed upstream of the meters under test, (2) a particular "flow conditioner" installed upstream of the meters under test, and (3) flow conditioner installed ahead of the upstream section of the matched units.

To facilitate interpretation of the results of the present experiment, a list of symbols, shown in Figure 2, has been prepared. Using this list, particular piping configurations are efficiently described in the graphs that follow. It should be noted that the meter tube symbolized denotes both upstream and downstream sections. Thus, the connection of the meter tube with flow straightener and turbine meter symbols from Figure 2 denote the matched unit described above.

The flow straightener is of the tube bundle type containing nineteen tubes having OD = $3/4$ in. (1.9 cm), wall thickness 0.049 in. (1.24 mm), and length 10 in. (25.4 cm). The tubes in this bundle are arranged in the scallop pattern and the bundle is centered in the tube by means of spacer lugs. The turbine meters symbolized by the squares are those under test. The different meters are designated by the numbers 1 and 2 placed in the proper square symbol.

The flow conditioner used in these tests is a radial flow filter. As a flow conditioner it is unusual in that it contorts the flow through four right angle turns. Three such turns produce a flow radially toward the pipe centerline. This radial flow is then turned again so that it flows axially out of the device. During the radially inward flow, the fluid passes through a porous element. Although the details of the conditioning mechanisms in this device are presently unknown, it will be seen, in what follows, that they are effective.

The third turbine meter, denoted by the propeller symbol is of the same line size as the meters under test. It has approximately the same angular speed as the test meters.

The swirler consists of a semicircular shaped vane. This is positioned in the pipeline so that its diameter is aligned with the pipe centerline when the vane is parallel to the pipe. The angular position of the vane is adjusted from outside the pipe and can impart swirl to increase or decrease, respectively.

The "out of plane elbows" configuration was specially prepared for this test. It consists of seven straight 4 in. (~ 10 cm) diameter pipe lengths that are 6 diameters long and six elbows, and represent a "worst case" elbow configuration.

The 2:1 contraction, based upon diameters, was used when the meters were tested in the 8 in. (~ 20 cm) diameter pipeline. This contraction is produced by two reducers, one 8 in. (~ 20 cm) to 6 in. (~ 15 cm) and one 6 in. (~ 15 cm) to 4 in. (~ 10 cm).

3. Results for the Low Flow Rate

3.1 Conventional Configuration

A control chart for the performance characteristics of meter 2 for the low flow rate is presented in Figure 3. The piping configuration is symbolically shown as the conventional one having a long, straight pipe length upstream of the tested meter 2. In this figure the error bars shown on either side of the round, darkened circles refer to the ± 3 standard deviation spread from the averages of one set of meter constants. The center of the bars is the average of the set. On the other side of the large, darkened circle is the repeat set performed after the pump is turned off and on again. The large darkened circle is the average of the two set averages. In what follows, the term "repeatability" is used in several ways. By repeatability is meant the percentage within which a subsequent determination of meter constant reproduces a previously determined value. Accordingly, switch off-switch on repeatability refers to two values which are averages of from three to five individual runs that are obtained from performing the presently described test procedure once. As noted from the test procedure, the meter connections to the pipeline remain untouched between these repeated tests thus excluding from causes of variation the alignment of the meter in the pipeline. Analogously, day-to-day repeatability refers, here, to the percentage within which the meter constant averages of all runs performed for a single flow rate and meter position on one particular day are reproduced on another day. Hence, Figure 3 exhibits the degree of switch off-switch on repeatability via the centers of error brackets for a single day as well as that from day-to-day via the differences between the large darkened circles for any two days. The 3σ limits indicated for all the points are obtained from taking the average and standard deviation of the nine (9) ordinates given by the large, darkened circles. These values are given along the ordinate scale with the standard deviation given in parentheses under the average. It will be with these "conventional" values that the perturbation and remedial effects are compared.

Figure 4 presents the control chart for the ratio values corresponding to the results presented in Figure 3. This ratio is that of meter 2 divided by meter 1 and the graphical notation is identical to that used in Figure 2.

3.2 Perturbation and Remedial Effects

To examine the effects of pipeline vibration on turbine meter performance a controlled vibration source was attached directly to the pipeline. This source imparted a radial oscillation to the upstream section of the meter tube near the inlet. Vibration amplitude and frequency were controlled independently with this source.

The results of the vibration effects are shown in Figure 5. Here, on the left ordinate are the meter constant results plotted as a function of vibration frequency for constant amplitude as shown. The conventional mean results from Figure 3 are shown with 3σ brackets. The nominal background levels of vibration experienced by the pipeline at these flow rates is 0.010 to 0.020 in. (0.25 to .5 mm) peak-to-peak. On the right ordinate are the corresponding ratio results. These results indicate that, while this imposed vibration causes a decreasing trend in meter constants at the higher frequencies, the variations are well contained within the 3σ limits about the conventional mean. Similarly, the ratio values obtained show neither a systematic variation with frequency nor any excursion beyond the 3σ limits. It appears that this particular type of vibration does not significantly influence the performance of these turbine meters at low flow rates.

The range of perturbations imposed by various elements which alter the flow into the meters is shown in the modified Youden Plots⁴ presented in Figure 6. Here, the meter constant for upstream meter 2 under test is compared with downstream meter 1. All points for meter 2 include 3σ bars. Along the right side of the graph is the legend indicating the corresponding piping configurations. It is found that an out of plane elbow configuration produces a small decrease in meter constant. Combinations of elements such as the flow conditioner described earlier and the third turbine meter or the 2:1 contraction and the third meter tend to increase the turbine constant slightly. Each of these perturbations, however, does not cause the turbine constant to deviate beyond the 3σ limit about the conventional mean value. The effect of the third meter placed upstream of the meters under test is shown to cause an increase in meter constant of about 0.3 percent. The effect of swirl induced by the vane is shown by the extreme values in Figure 6. When the vane induced swirl is in the same direction as turbine rotor rotation, the overspinning effect causes the meter constant to increase 0.4 percent. This demonstrates that a considerable amount of swirl passes through the straightening vane in the meter tube. Reversing the swirl direction is shown to decrease the turbine constant about 0.3 percent. The distribution of vorticity across the flow section was not measured.

Figure 6 can be used to determine the corresponding data for the ratio of meter responses. For any value plotted, dividing the ordinate by the abscissa gives the desired ratio. Therefore, the percentage changes specified above for the meter constants also pertain, nominally, to the ratio values. Also evident from Figure 6 is that the downstream meter unit is relatively unaffected by the perturbations imposed ahead of the upstream meter unit. In fact, for all these perturbations, the variation sustained by the downstream meter is about 0.1 percent. This suggests that the upstream meter unit with its adjacent straightening tubes forms a rather effective flow conditioner. From the range of perturbations imposed on the flow into the test meters, the extreme values, namely those due to vane induced swirl, will now be selected as the basis for evaluating the various remedial schemes devised to reduce the perturbation effects.

In Figure 7 are presented the results obtained when the flow conditioner replaces the upstream section of the matched meter tube. The results plotted refer to three piping configurations: (1) the extreme perturbation effects denoted by the square symbols, (2) the flow conditioner installed with no perturbing effects present, and (3) the conditioner installed in the presence of perturbations. The meter constants, as determined with the conditioner and no perturbations, are found to be lowered approximately 0.15 percent from the conventional mean. This change exceeds the 3σ limits which correspond to about 0.1 percent. Although not presented here, the velocity profiles at the conditioner exit were measured and found to be more uniform than the "normal" turbulent profile found in these pipes. It is to this alteration in the velocity profile that the shift in meter constant is attributed. In the presence of positive swirl, the flow conditioner is found to dramatically lower the perturbed values which, it is recalled, exceeded the conventional mean by 0.4 percent. For the case of swirl opposite to turbine rotor rotation, the flow conditioned results are found to be highly scattered. Although the details are, as yet, unclear, these results suggest that the outlet flow from this conditioner which directly enters the meters produces unstable performance.

Figure 8 presents results for the remedial effects obtained with the flow conditioner directly upstream of the conventional piping configuration. With flow conditioning, the averaged meter constants with and without the extreme perturbation case of positive swirl are within 0.1 percent of each other. The 3σ limits are nominally the same with and without perturbations. In view of this set of results, it is concluded that the flow conditioner installed upstream of the conventional meter unit produces the most satisfactory arrangement of the presently devised schemes.

4. Results for the High Flow Rate

The control chart for the No. 2 meter at the high flow rate is shown in Figure 9 where the notation corresponds to that of Figure 3. It is noted in Figure 9, that the switch off-switch on repeatability can be as much as 0.06 percent. The day-to-day repeatability can be

as much as 0.12 percent. The ratio of meter responses at the high flow are given in the control chart presented in Figure 10. It is evident from this figure that before precise expected values can be chosen for a flow rate an extensive amount of data must be taken.

The effects of vibration on meter performance at the high flow rate are shown in Figure 11. Here again, as seen above in the results for the low flow, no significant variation is produced by this type of vibration.

The remedial effects produced by the flow conditioner bolted upstream of the conventional piping configuration are shown in Figure 12. Only the extreme perturbation effects due to vane induced swirl in the direction of turbine rotation are shown. This swirl increased meter constants 0.4 percent above conventional values. Vane induced swirl in the opposite direction produced reductions in meter constants which plot off this graph.

The meter constants obtained with the flow conditioner in place, without perturbing effects, indicate that the meter constants are reduced slightly (0.06 percent) in comparison with conventional values. In the presence of vane induced swirl, the flow conditioner was found to eliminate the swirl effects.

5. Conclusions

On the basis of this tightly controlled series of tests at two flow rates, day-to-day repeatability for turbine meter constants over a 10 month period ranges from ± 0.07 to ± 0.12 percent based upon averages of at least six runs. The repeatability obtained during a single day's test when the flow is switched off and then on again ranges from ± 0.03 percent at the low flow to ± 0.06 percent at the high flow rate. The results for the ratio criterion for "proper" meter performance indicate that a 3σ tolerance is ± 0.1 percent for the low flow and ± 0.18 percent for the high flow. The characteristics of these meters thus enable the investigation of the effects of flow phenomena beyond the "simple" questions of precision and accuracy of weighing, counting, timing, and temperature measurements which comprise overall accuracy estimates.

The effects of various levels of swirl, however, were found to produce the most significant changes in meter constants. These ranged from -0.3 percent to + 0.4 percent. For selected types of perturbations on conventional meter performance, those due to vibration and limited alterations to the streamwise velocity profiles entering the meters produced no significant changes in the values for the meter constants.

Of the various schemes devised to remedy the perturbing effects on meter constants, the most successful was a radial flow conditioner. In the absence of perturbations, this device produced a slight decrease in meter constants which was expected in view of the velocity profile at the exit of the conditioner. In the presence of the most severe perturbations, the flow conditioner was successful in restoring the meter

performance to within the 3σ limits of average conventional values.

Acknowledgment

Several persons in the Fluid Meters Section are to be acknowledged for their continued patience, attention to detail, and suggestions during this study. These are Messrs. K. R. Benson, J. D. Melvin, and V. Brame who conducted the tests and assisted with the preparation of the results. Mr. L. K. Irwin is acknowledged for his continued support and participation. Messrs. John B. Houser and John Heine are gratefully acknowledged for their contributions in conducting tests and preparing results. The secretarial assistance provided by P. Beall, and P. Gurewitz, and K. Durant is greatly appreciated. Last, but certainly not least, it is pertinent to acknowledge certain individuals from several of the laboratories where NBS is conducting the MAP tests. These individuals who, by agreement, shall remain anonymous have contributed significantly to the design of the test procedure used in the present tests.

References

- [1] Pontius, P. E., Notes on the Fundamentals of Measurement and Measurement as a Production Process, *NBSIR 74-545*, Sept, 1974.
- [2] Pontius, P. E., Measurement Assurance Programs - A Case Study: Length Measurements. Part I Long Gage Blocks (5 in. to 20 in.) *NBS Monograph 149*, Nov. 1975.
- [3] Pontius, P. E. and Cameron, J. M., Realistic Uncertainties and Mass Measurement Process: An Illustrated Review, *NBS Monograph 103*, Aug. 1967.
- [4] Youden, W. J. Graphical Diagnosis of Interlaboratory Test Results, *Industrial Quality Control*, Vol. XV, No. 11, May 1959.
- [5] Shafer, M. R., Baker, D. W., and Benson, K. R., The Calibration and Performance of Turbine Type Flow Transducers Operating at Pressure Levels Up to 1400 psig, *NBS Report 9088*, Apr. 1966.
- [6] American Gas Association, Report No. 3. *Orifice Metering of Natural Gas*, Arlington, Va, 1972.
- [7] Bean, H. S., ed, *Fluid Meters - Their Theory and Application*, ASME, New York, 1971.
- [8] Strohmeier, W. O., Turbine Flowmeters, Past, Present, and Future, *Symposium Proceedings: Flow - Its Measurement and Control in Science and Industry*, Vol. I, Part II, Flow Measuring Devices, ISA 1974, pp. 687-693.
- [9] Thompson, R. E. and Grey, J., Turbine Flowmeter Performance Model, *Trans ASME*, Dec. 1970, pp. 712-723.
- [10] Spencer, E. A., private communication; National Engineering Laboratory, East Kilbride, Glasgow, Great Britain, 1976.
- [11] Bellinga, H. and Stronk, H., The Practical Application of Flow Straighteners With Turbine Flow Meters for Gas. *British Fluids Laboratory paper No. 242*.

- [12] Rubin, M. Miller, R. W., and Fox, W. G., Driving Torques in a Theoretical Model of a Turbine Meter, *Trans ASME Journal of Basic Engineering*, 1964, Paper No. 64-WA/FM-2
- [13] Shafer, M. R. and Ruegg, F., Liquid-Flowmeter Calibration Techniques, *Trans ASME*, Oct. 1958, pp. 1369-1379.

Appendix 1 Test Procedure

1. The meters are bolted to their respective meter tubes with a new gasket inserted in the upstream flange joint of the meter.
2. The meters, with meter tubes, are bolted in tandem with a specified meter (No. 2) in the upstream position: the tandem pair of meters are then bolted into the test section of the pipeline.
3. A "run-in" flow is produced in the pipeline. This flow rate is the higher of the two test flow rates. It is continued for fifteen (15) minutes, during which time the ratio of meter responses is monitored and compared with the expected value.
4. The lower of the two test flow rates is produced in the pipeline. This flow is valved according to a Reynolds number criterion, i.e., a specified ratio of upstream turbine meter frequency in cyc/sec divided by the (temperature dependent) kinematic viscosity of the water in centistokes. The tolerance on the turbine meter frequency is nominally 2 cyc/sec.
5. The ratio of turbine meter frequencies, i.e., that of No. 2 divided by that of No. 1 is monitored. When this is within 0.05 percent of the expected value, the test may proceed. Should this ratio criterion not be satisfied, the following sequence of remedial procedures is suggested. The flow in the pipeline can be increased and decreased repeatedly. If possible a reversed flow in the pipeline, is produced to dislodge particles from the turbine blades. The meters are removed from the pipeline inspected for anomalous deposits or adherents to the internal components, cleaned via a flushing with alcohol and returned to the pipeline.
6. Repeated diversions of the flow into the collection system are performed and the data is processed to produce turbine constants in pulses per gallon corrected to 20°C. Five such "runs" are done.
7. The higher flow rate is produced according to a specified upstream turbine frequency-to-centistoke ratio; the ratio of meter frequencies is monitored. When satisfactory agreement with the expected value is obtained, repeated determinations of meter constants are done.
8. After the high flow meter constants are determined the flow is stopped and the pumps are turned off. After five (5) minutes, the pumps are switched on and the tests at both flow rates are repeated as per steps 4 through 7.
9. When this has been completed, the flow is again stopped, the pumps switched off, the line drained, and the positions of the meters with their matched meter tubes are reversed in the pipelines.
10. Steps 3 through 8 are repeated for this tandem configuration of the meters.

TURBINE METERS

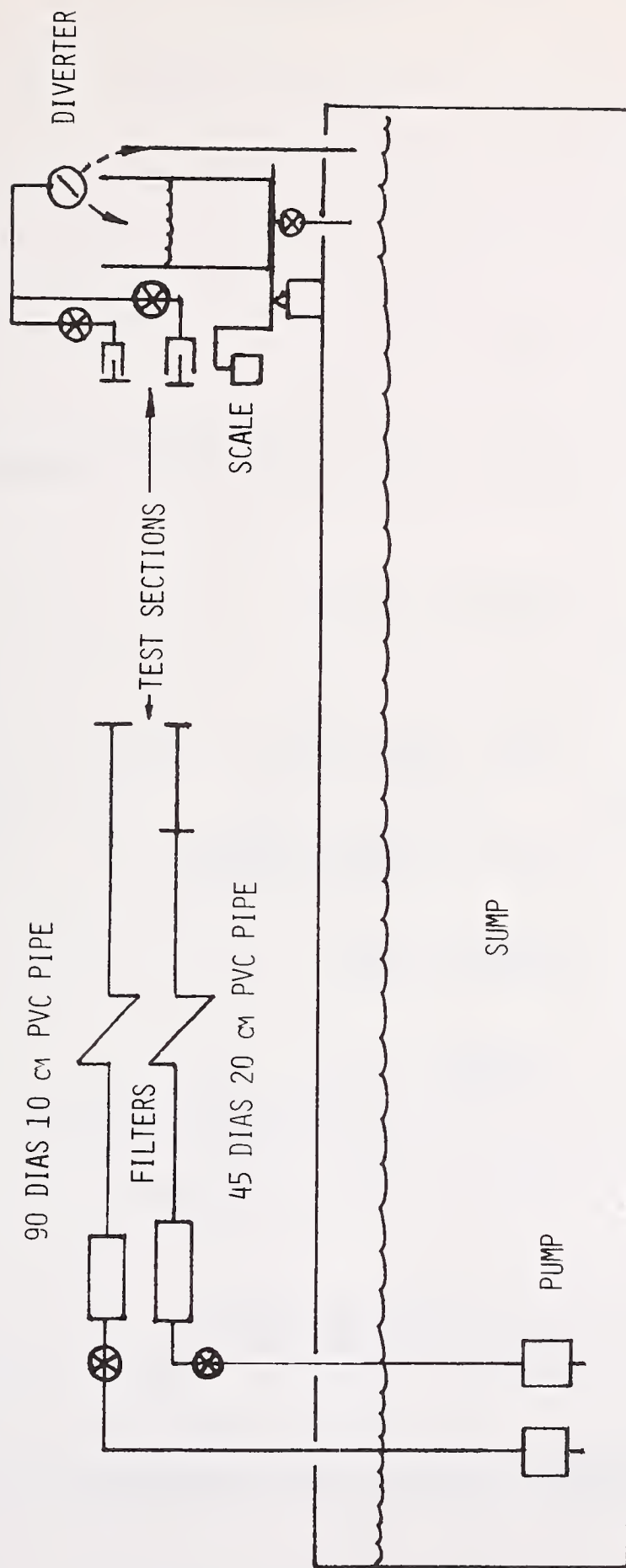


Figure 1. Sketch of Calibration Facilities.

LIST OF SYMBOLS










	PIPE
	METER TUBE WITH FLOW STRAIGHTENER
	TURBINE METER
	FLOW CONDITIONER
	OTHER TURBINE METER
	SWIRLER (+)
	SWIRLER (-)
	OUT OF PLANE ELBOWS
	2 : 1 CONTRACTION

Figure 2. List of Symbols.

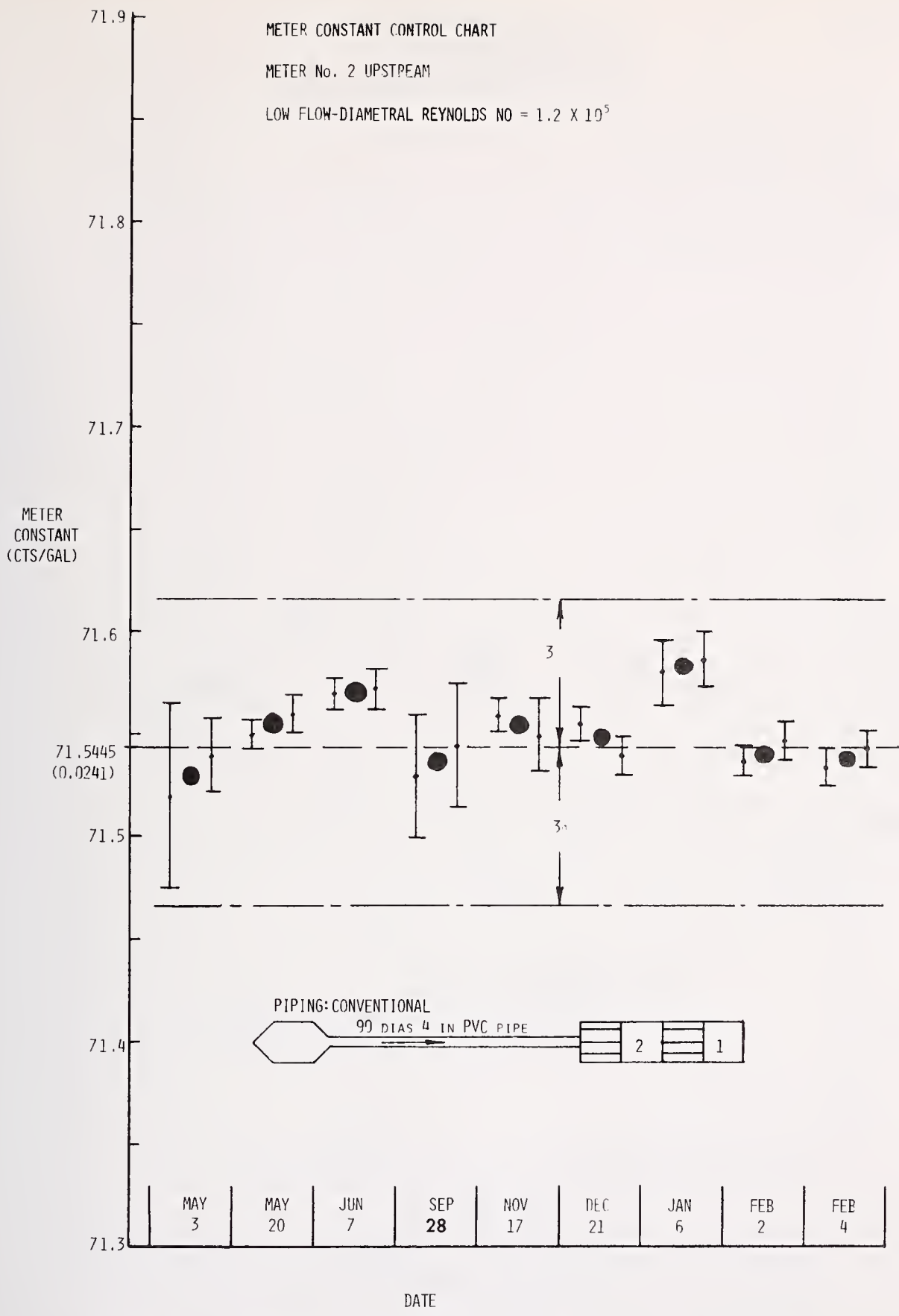


Figure 3. Control Chart for Meter No. 2. Low Flow.

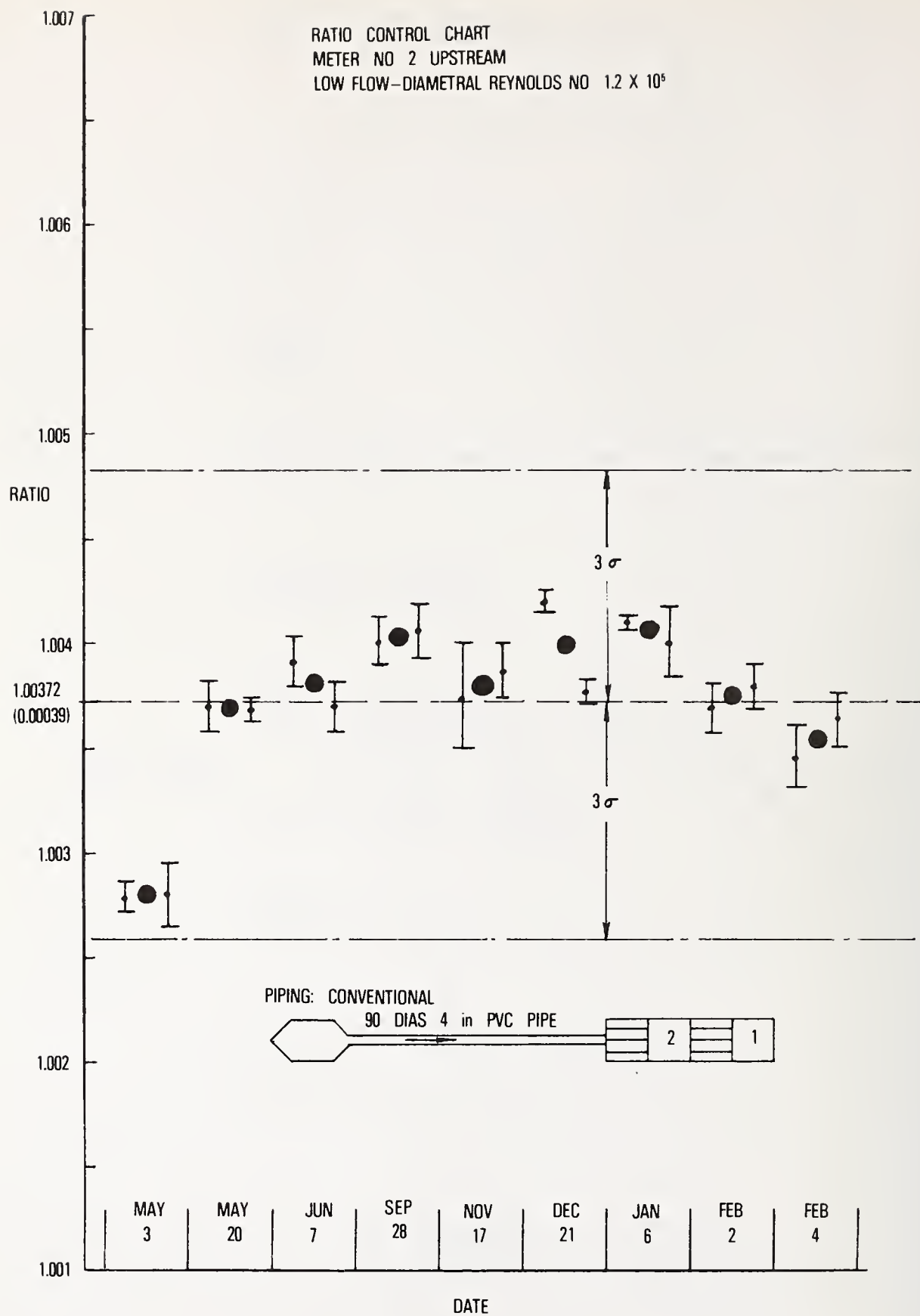


Figure 4. Control Chart for Ratio of Meter Constants. Low Flow.

VIBRATION EFFECTS
METER NO 2 UPSTREAM
LOW FLOW-DIAMETRAL REYNOLDS NO = 1.2×10^5

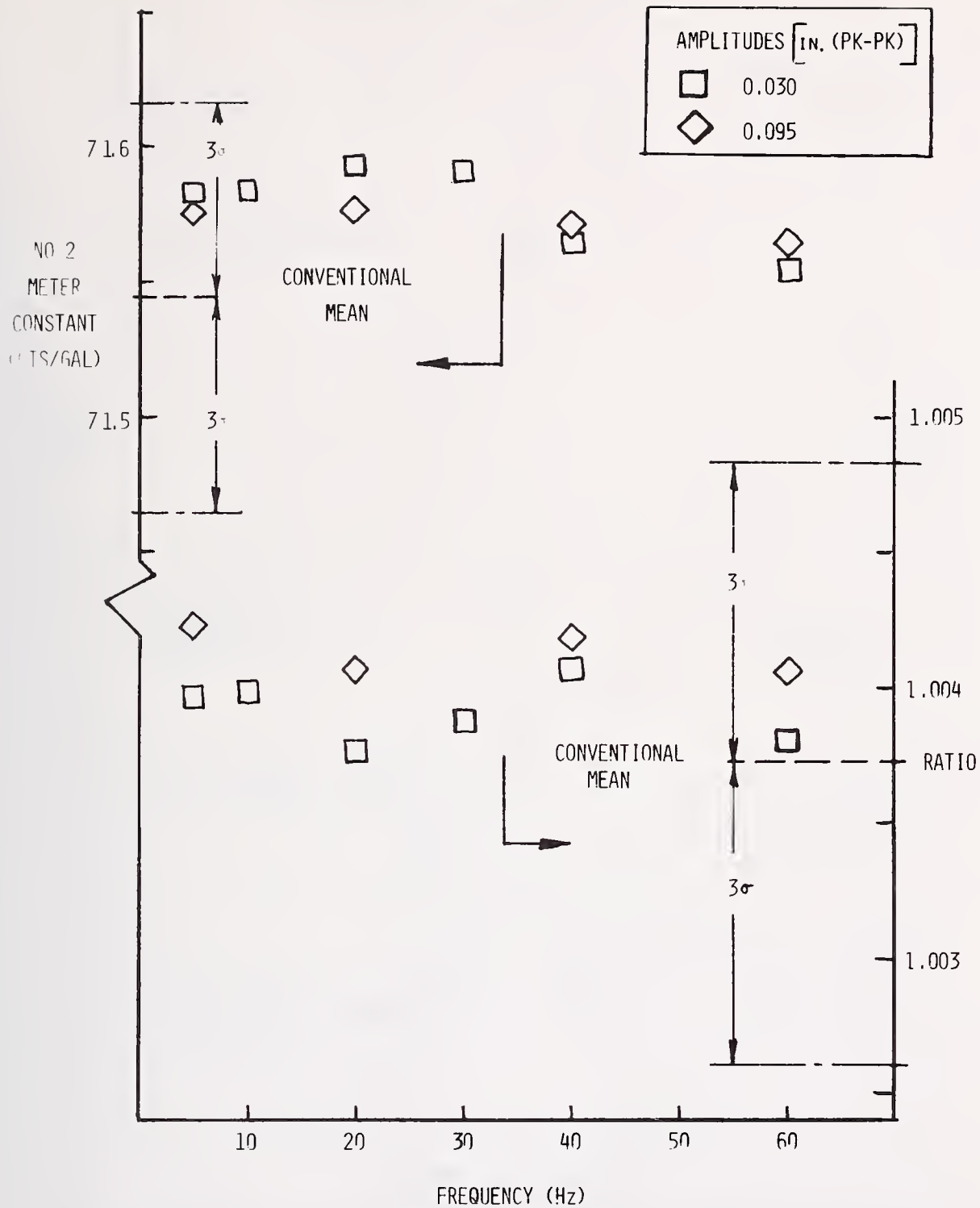
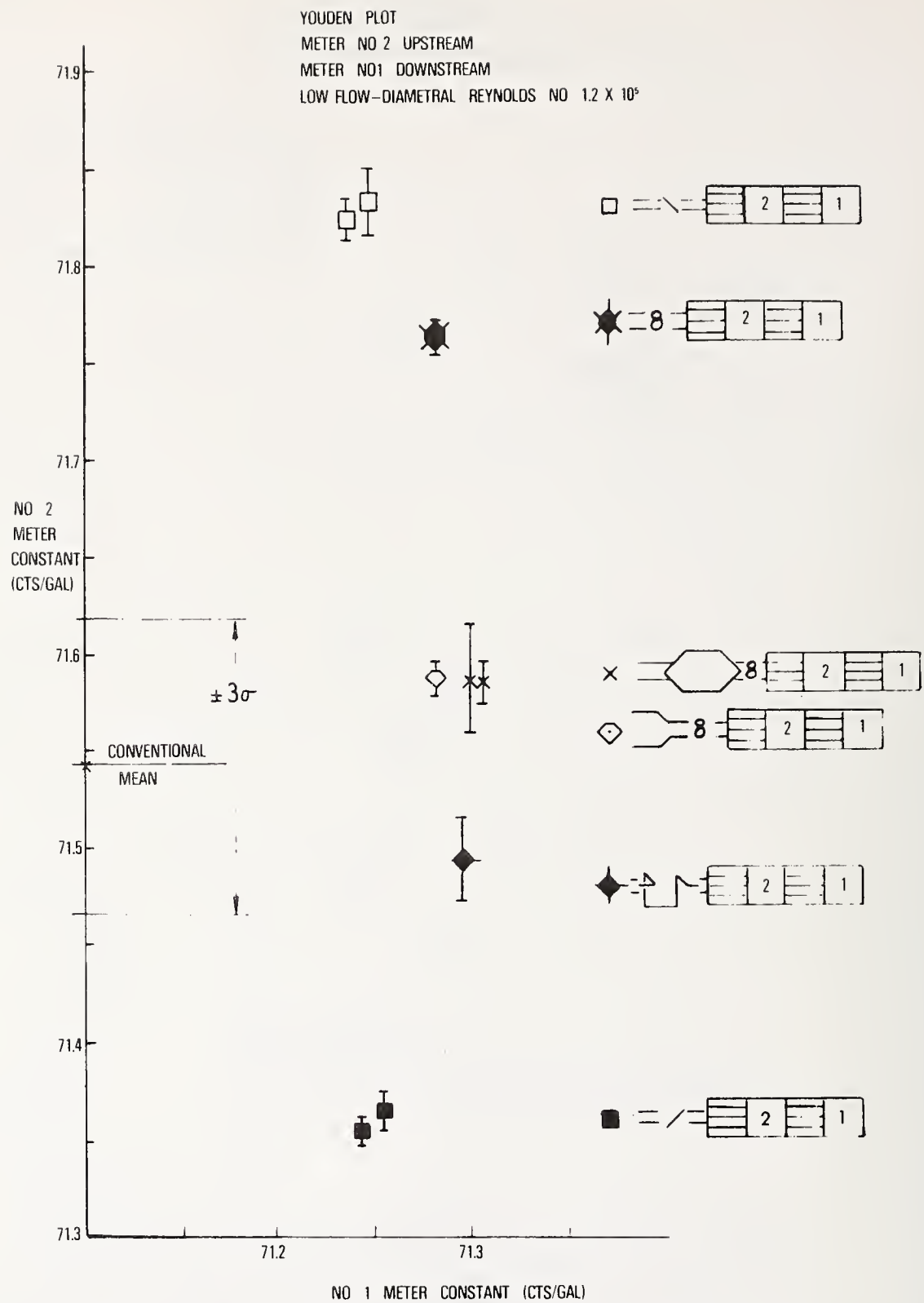


Figure 5. Vibration Effects on Meter No. 2. Low Flow.



**Figure 6. Modified Youden Plot for Perturbation Effects.
 Low Flow.**

YOUNG PLOT - REDUCTION OF VARIATION
 METER NO 2 UPSTREAM
 METER NO 1 DOWNSTREAM
 LOW FLOW-DIAMETRAL REYNOLDS NO 1.2×10^5

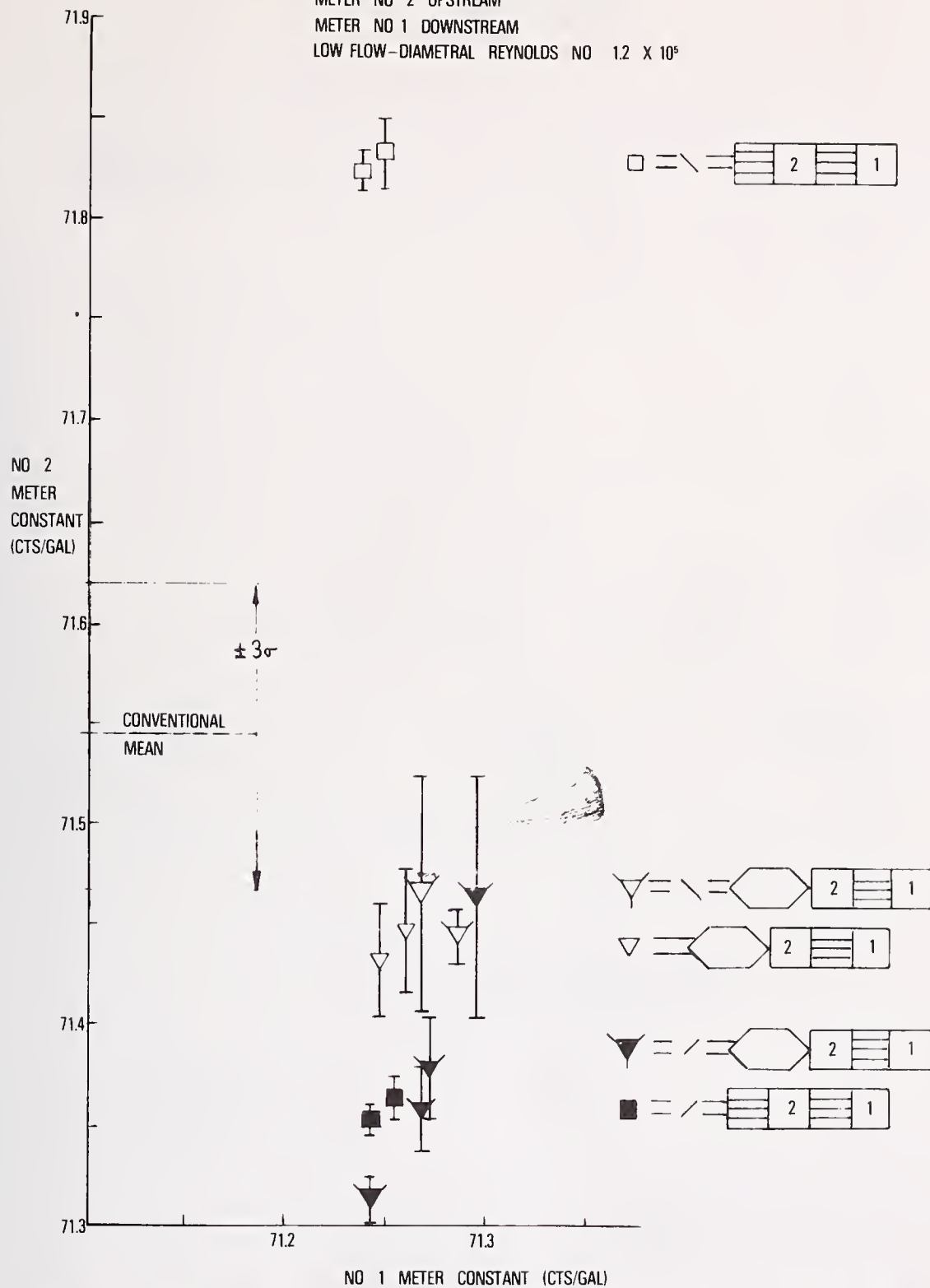


Figure 7. Modified Youden Plot for Remedial Effects Consisting of the Flow Conditioner Bolted Directly to the Meter. Low Flow.

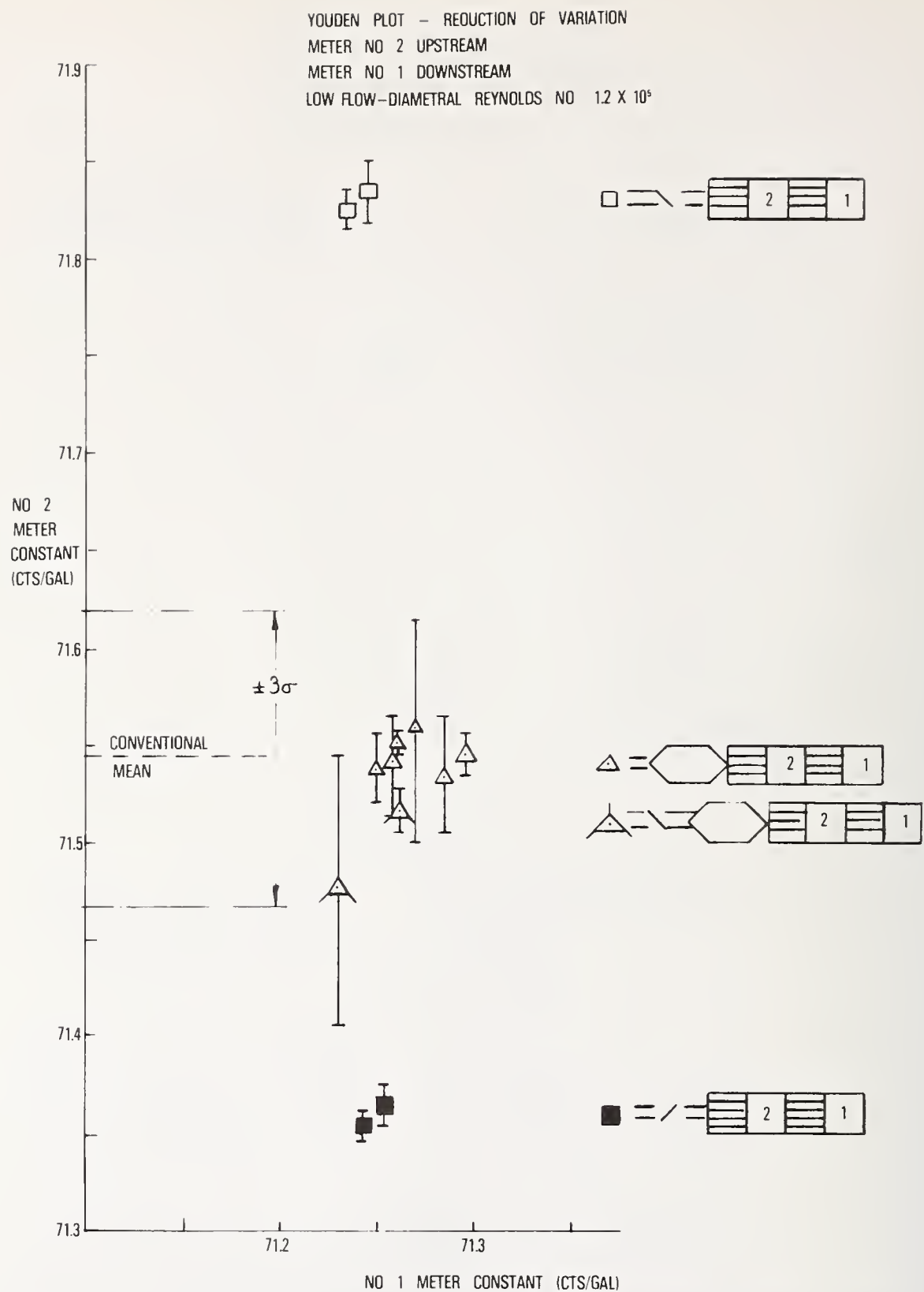


Figure 8. Modified Youden Plot for Remedial Effects Consisting of the Flow Conditioner Bolted Upstream of the Meter Tube Assembly. Low Flow.

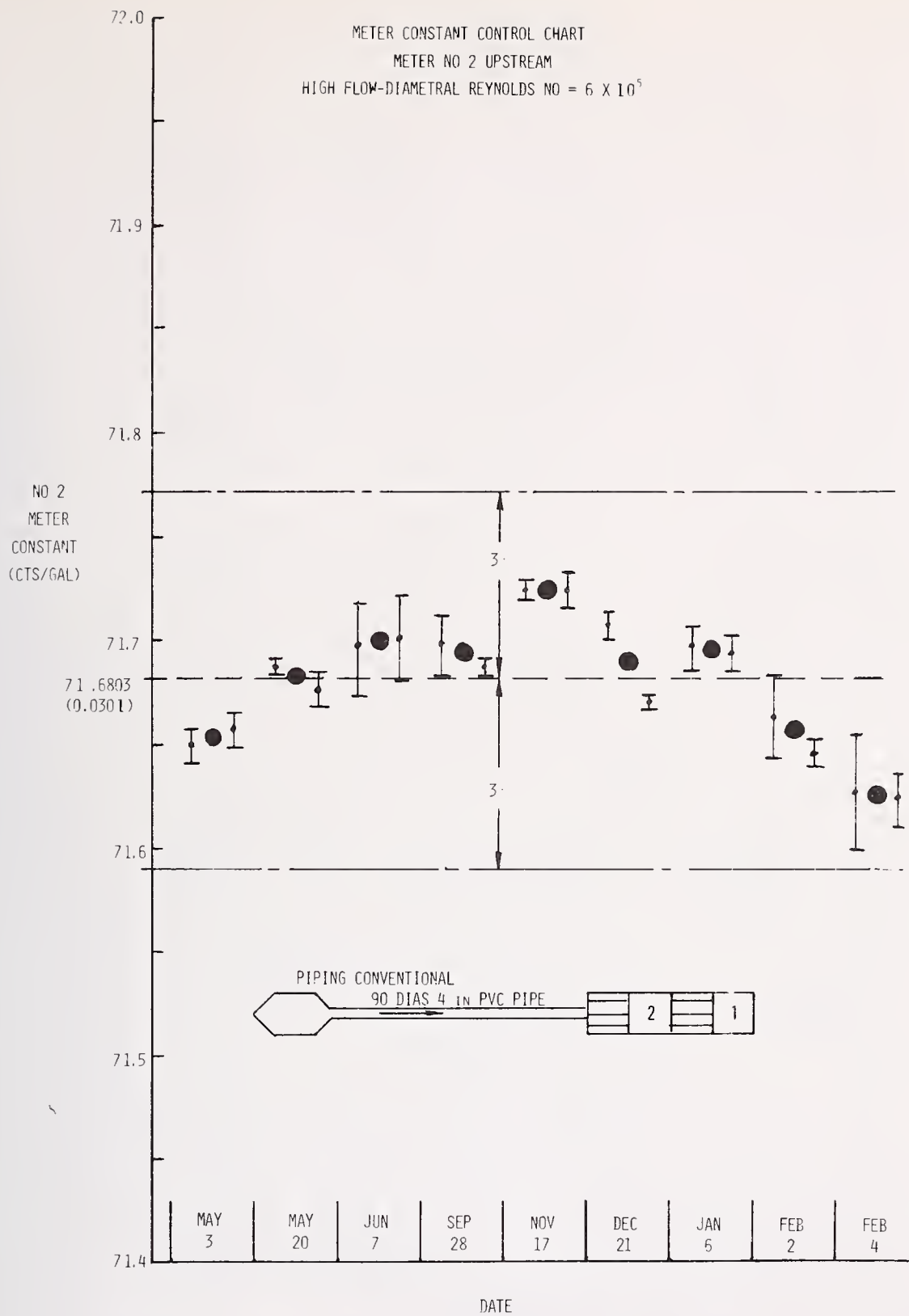


Figure 9. Control Chart for Meter No. 2. High Flow.

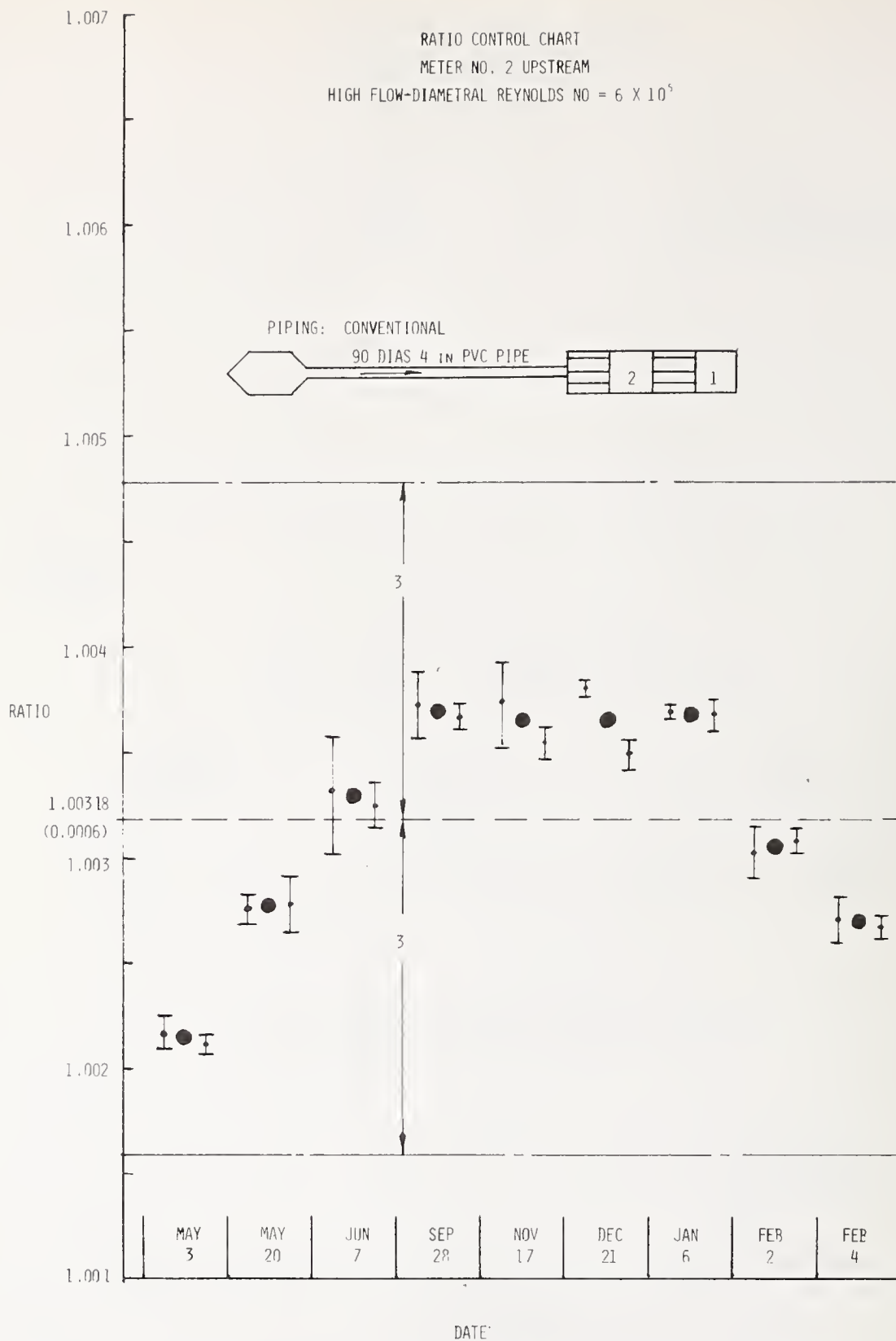


Figure 10. Control Chart for Ratio of Meter Constants. High Flow.

VIBRATION EFFECTS
METER NO 2 UPSTREAM
HIGH FLOW-DIAMETRAL REYNOLDS NO = 6×10^5

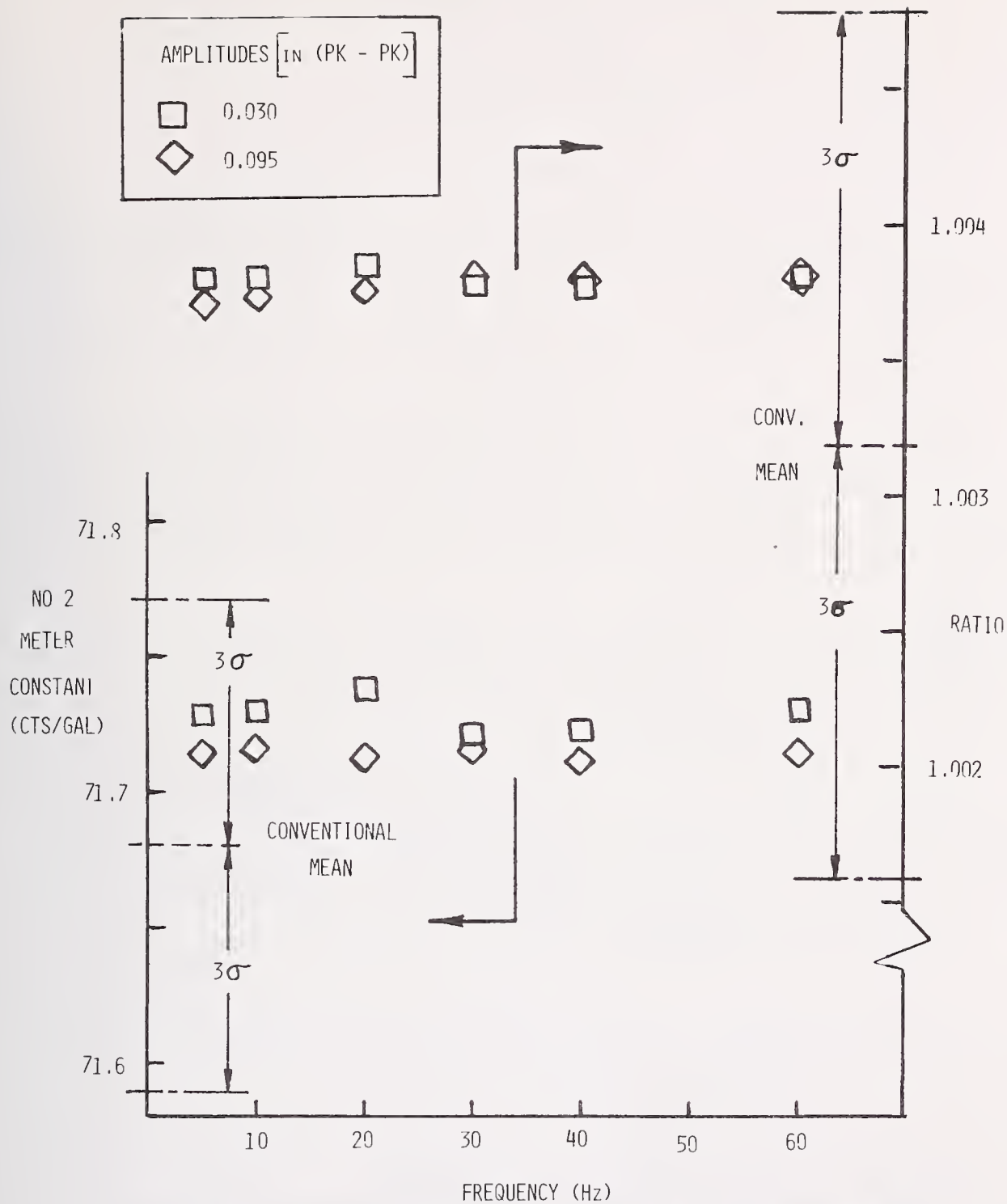


Figure 11. Vibration Effects on Meter No. 2. High Flow.

YOUTDEN PLOT-REDUCTION OF VARIATION

METER NO 2 UPSTREAM

METER NO 1 DOWNSTREAM

HIGH FLOW-DIAMETRAL REYNOLDS NO = 6×10^5

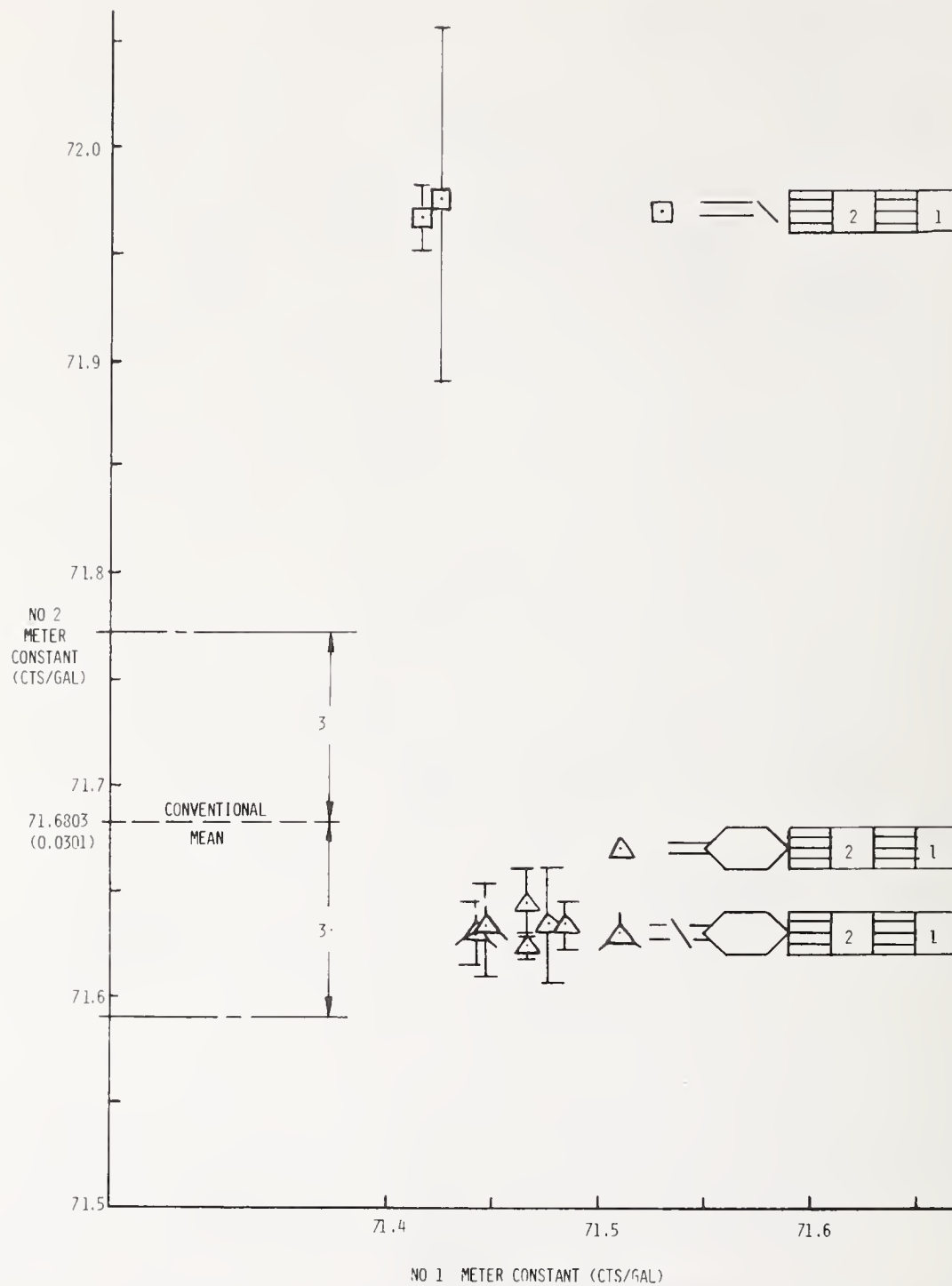


Figure 12. Modified Youden Plot for Remedial Effects Consisting of the Flow Conditioner Bolted Upstream of the Meter Tube Assembly. High Flow.

EVOLUTION OF A MODERN PETROLEUM MEASUREMENT MANUAL

L. M. Davis
Oil Measurement Consultant
Peterborough, Ontario

Abstract

Progress from early applications of positive displacement meters to modern measurement practices are reviewed with particular attention to liquid petroleum metering. Comments on some advantages of metering vs tank gaging are made. The realism of the new API Measurement Manual is discussed and an outline of its contents provided.

1. Background

The petroleum industry has for years measured the liquids it handles largely by meter; and it measures the liquids several times over; as it leaves the oil fields, then into and out of pipelines, into the refineries, then to the marketing terminals, and finally at the retail level. Each day in North America alone about 100 million barrels are measured.

The advantages of meter measurement are considerable, even though metering has by no means completely superseded tank gaging. The advantages are spelled out briefly in Chapter 5 Section 1 of the projected American Petroleum Institute Manual of Petroleum Measurement Standards (API Measurement Manual) -- of which more anon -- as follows:

The principal advantages of metering are:

- a) by being a continuous process it can increase the availability of tankage since no tank need be isolated for measurement alone;
- b) it lends itself to the calculation, indication or display of instantaneous flow rates, and of a volume up to the moment required;
- c) measured volumes can be printed either at the meter or at a distance from the meter, and the meter's coded identity can be part of the print-out on a measurement ticket;
- d) it is labor saving;
- e) it can deliver a measured volume taken from several sources at the same time into a single receiver; or from a single source into several receivers;
- f) buyers, sellers and fiscal authorities, and others, can witness all the basic steps of dynamic measurement and so be sure that their interests and those of the public are being safeguarded.

There are of course even more advantages to dynamic measurement compared with static measurement than those above cited, but a short list is enough to explain why metering is popular. It is also efficient and accurate; and its requirements have been set forth in a number of API Standards, the longest and oldest of which is API.1101. About 30 years ago, the American Society of Mechanical Engineers (ASME) and API published what was then called ASME-API Code 1101, and since that time it has been widely used by all measurement practitioners in the oil business. It consists of some 100 pages and deals with what was then the only type of meter in general use, the so-called positive displacement or P.D. meter. It covers installation, meter provers and their calibration, meter proving, meter performance, and the operation and maintenance of metering systems, as well as calculations, tables of correction factors, diagrams and definitions. It was revised in 1952 and again in 1960.

In this granddaddy of oil measurement documents now called API Standard 1101, a critical observer will detect not only the background but also what might be called the backdrop. If a backdrop is usually a pretty scene of trees, flowers and perhaps a fairy castle, installed to set the mood for a well drilled ballet, and at the same time to conveniently cover up the stage hands, electricians, and inevitable ropes and pulleys, then 'backdrop' is the right word. For the picture on the backdrop has a slightly archaic aspect, namely the time when water meters were the principal application to large scale measurement, and the hidden ropes and pulleys were the then warranted assumption that a meter could be calibrated and adjusted mechanically to read out correctly for a long period subject only to a tolerable uncertainty.

Archaic expressions which survive in API.1101 are "accuracy curve" and "positive displacement meter". They are analogous to the sylvan setting of flowers and a castle on the backdrop. They are archaic because oil is not measured on the assumption that a meter can be calibrated once and for all, and will thenceforward retain its calibration. Nor is any P.D. meter capable of effecting positive displacement. There is always some slippage, and slippage is variable according to rate, viscosity, temperature and so on.

What happened when the oil business started using meters, was that it decided also to modify the water measurement procedures because a single meter could be used to measure a wide variety of petroleum liquids. It was not possible to attain the accuracy required in oil measurement by pretending that a meter had an accuracy curve, determined by a set of calibrations, and that this curve would hold good for a long time. It was fully expected that its meter factor would change with every change in liquid, and with rate. So instead of pretending to "calibrate" a meter, with the implied belief that it would hold its calibration, the expression "to prove" a meter came into common usage. But words die hard. Some people still talk of 'calibrating' a meter, just as we still talk of 'shipping' oil by pipeline, with no ships for miles around.

About six years ago API's Committee on Petroleum Measurement (COPM) decided it had to update and reorganize all its measurement Standards. It soon

became apparent that the only possible way to do this was to start all over again. It was not practical business to patch up the existing Standards. There might then be more patches than whole cloth. So the best way to go about it was to start writing a comprehensive oil measurement Manual divided into Chapters. Chapter 1 is called Vocabulary. In compiling a vocabulary certain archaic expressions could be dropped, or at least played down. For example a P.D. meter is now called simply a displacement meter. There are now just two kinds of provers - tank provers and pipe provers. "Volumetric prover" has been dropped because all provers are volumetric, except gravimetric provers and these are museum pieces; they have no place in the projected API Measurement Manual. The expression "accuracy curve" survives but in an anaemic condition; "meter factor curve" is a more suitable term, although of course there has to be such a curve (as a function of rate) for each and every type of liquid, or grade of crude oil.

2. A Sense of Realism

What must distinguish the API Measurement Manual is a sense of realism, and not only in its vocabulary. Its underlying purposes and emphasis is to get the right answer, not to standardize the hardware. Even to get the same answer from the same data, however, does require that the software be standardized, something which the several API Standards had not really tackled before.

The sense of realism can perhaps be summarized as follows:

(i) A petroleum liquid meter is not and cannot be a sort of solid gold water meter. Petroleum liquids differ widely in physical properties, unlike water, and the rates are forever changing.

(ii) Petroleum is much more costly than water, so it is necessary to re-confirm the industry's established practice of reproving a meter and obtaining a new meter factor every time operating conditions change significantly.

(iii) It is not only desirable but necessary to use the same meter, but not the same meter factor, for each successive batch of petroleum liquid to be measured.

(iv) It is necessary to have a fixed or portable prover available as needed for fairly frequent meter proving.

(v) It is desirable to have a standard procedure (i.e., standard software) for computing the four values that collectively make possible good measurement. These are:

- a) base volume of a prover;
- b) meter factor;
- c) measurement ticket;

and, d) changes in line inventory for pipeline measurement.

The absence, so far, of standard procedures for computing the above values has led to tears, sweat and some loss of hair among measurement practitioners. A sense of realism must admit that $a \times b \times c$ does not necessarily have the identical same value as $c \times a \times b$ or $b \times c \times a$, unless rules for rounding and truncating are spelled out and uniformly observed. A realist knows that thousands of dollars are spent each day, in time and long distance calls, in the attempt to find out why $a \times b \times c$ does not always equal $c \times a \times b$. So Chapter 12 of the API Manual will attempt to establish standard calculating procedures for oil quantities. This is especially necessary today when different persons calculate meter factors, and a computer calculates measurement tickets, and sometimes no one told the man who programmed the computer exactly at what step to round or truncate numbers. The idea is to get the same answer from the same data, regardless of who or what does the computing.

(vi) Sixth and last in the list of items which a realist must keep in mind is records. Today measurement of oil affects not only the buyer and seller and the temporary custodian of oil, but many levels of government. Therefore records of measurement should be open and understandable to all concerned. If something goes wrong, all interested parties should have access to the records. Happily this is pretty well established, and no one yet has come up with a wonderful idea to build pipeline-custom-houses at every point where a pipeline crosses the US-Canadian border, for example. If something appears to get out of whack in terms of measurement, a systematic examination of all relevant meter station records, particularly of the meter factor control charts, is usually sufficient to find the causes of the trouble. But even here, a sense of realism must govern so as to prevent looking for trouble that does not exist, or not looking for trouble that does exist.

3. The API Measurement Manual

We have so far considered the background to existing API measurement standards and the need for starting all over again, rather than patching them up. It is hoped that the projected API Manual of Measurement Standards will be a comprehensive loose-leaf book in which the main topics are sorted out into Chapters*, and each Chapter of which will have as many separately printed Sections as it may require. For example as new or extended compressibility data becomes available, it can be printed and fitted into its slot without upsetting or intruding into an established publication. The Chapter subjects are as follows:

CHAPTER 1	- Vocabulary
2	- Tank calibration
3	- Tank gaging
4	- Proving systems

*Manual of Petroleum Measurement Standards, Chapter Introductions and Scopes, available from American Petroleum Institute, 2101 L Street, NW, Washington, D. C. 20032

CHAPTER 5	- Metering
6	- Metering systems
7	- Temperature determination
8	- Sampling
CHAPTER 9	- Density determination
10	- Sediment and water determination
11	- Physical property data
12	- Calculation of petroleum quantities
CHAPTER 13	- Application of statistical methods
14	- Natural gas fluids
15	- Metrication
16	- Measurement by weighing

Some chapters are already completed; more are now being written by working groups, which drafts will then be balloted through the committees. Some should be available this year.

One of the difficulties of the period between the virtual completion of the new book and the phasing out of the old standards is that there has to be a sort of minimum critical mass of new publications before they become useful. To have the metering chapter before the proving chapter, or the two of them without the calculation chapter, is not very practical.

Chapter 5 deals with metering and covers displacement meters, turbine meters and an assortment of accessory equipment. Chapter 6 deals with metering systems; each section of Chapter 6 being devoted to a specialized assembly for measurement, such as LACT, aviation hydrant fueling, pipeline metering systems and so on.

Primary units will be in SI, that is of course cubic meters, m^3 , for volumes, Kelvin, K, for temperature, Pascals, Pa, for pressure; with customary units (bbls., °F, psi) given parenthetically.

4. Hardware

The API Manual consists of performance standards, not hardware standards. The whole idea is to get the right answer, and the publications tell you how to go about it. For example, central proving of meters, not being a realistic proposition, is not covered. But a central prover-calibrating facility might well be a very practical proposition. Water drawing a prover in the field is a tricky business at best, and in the Arctic or on an offshore platform it becomes virtually impossible. So a portable central-proving facility consisting of a small prover and a transfer meter is a likely looking candidate for minimizing current problems. In the natural hierarchy of accuracies in oil measurement, provers are at the top, meter factors are next, and measurement tickets follow. If the uncertainty at the top of the hierarchy can be squeezed down or made more consistent, this advantage will have beneficial effects further down the pyramid.

Of course, NBS calibrated cans and small prover tanks will still be necessary to the oil industry, and in this regard a passing tribute

to NBS publication 105-3* should be made. It is a hardware document on field standards and industry has been consulted and asked for comments, which is widely appreciated.

5. Software

In addition to the software aspects of calculation referred to previously under remarks about Chapter 12, the whole API Measurement Manual has software aspects because it is primarily a lesson book in oil measurement. API's Committee on Petroleum Measurement has a subcommittee on Personnel Training which promotes a school held in Baytown, Texas, twice per year; and also the yearly short course held in Norman, Oklahoma.

API is also financing the important work being carried out at present by NBS on the thermal coefficients of expansion of crude oils and petroleum products.

And last but not least, API continues to encourage all measurement education, in-house training programs and the free flow of ideas such as is exemplified by its NBS Symposium.

*NBS Handbook 105-3, Specifications and Tolerance for Metal Volumetric Field Standards, May 1971 (under revision)

Footnote:

Some of you are old enough to remember Fred Allen's weekly radio program, in which he always managed to sum up in a bizarre way what he was trying to get across with what he called "a poem". Taking this cue I too have written a poem called "The Meter Man", which some of you will realize I lifted from a work of John Keats. It goes as follows:

O what can ail thee meter-man,
Alone and palely loitering?
The rate and temperature have changed,
And no birds sing.

O what can ail thee, meter-man,
So haggard and so woe-begone?
The floating roof tank's full -
And the tender not yet done.

I met a meter in the ads,
Full beautiful - a faery's child.
It measured everything in sight -
It's factors never wild.

It took me to its elfin grot
Showed me its bearings, flanges, seal.
If it was truly all that good --
It weren't for real!

So this is why I sojourn here
Alone and palely loitering.
The pipeline's full of scraper dirt --
The gol-darn thing!

BUILDING BLOCKS TOWARDS FLOWMETER RELIABILITY

Dezsoe Halmi
Senior Principal Engineer
B I F

A Unit of General Signal Corporation
West Warwick, R. I. 02893

The need to analyze the question of flow measurement reliability as a special subject is pointed out. Attempt is made to give a definition to flow measurement reliability, review its types, and uncover the means by which it can be attained, in terms of "building blocks" which may be found in the nature of a meter, or in the method of its flow metering performance investigation.

INTRODUCTION

The first announcement and call for papers for this flow measurement symposium begins its statement "about the symposium" thus:

"Reliable and accurate flow measurements are becoming increasingly important..."

While accuracy is a well-known and extensively analyzed subject in flow meter literature, author was unable to find any direct discussion of the subject of flow measurement reliability, namely, what it is, and how it can be attained.

Due to this lack of information and the importance of the subject, it is attempted through this paper to place the subject of flow measurement reliability in the focus of general interest it requires and deserves, by endeavoring to define what is meant by it, explore its types, and discuss some of the more important building blocks of which it can be constructed.

DEFINITION OF RELIABILITY

In the lack of anything more directly related to flow metering, author takes the definition of reliability from the American College Dictionary:

"The person who or that which is reliable can be relied upon; from such a one, satisfactory performance may be expected with complete confidence (it may also have the suggestion of honesty)..."

To see how to apply this definition of reliability for flow measurement, it helps to realize, that, basically a flow measurement consists of the following elements:

- The flowing fluid and its properties; or fluid properties like: density, viscosity, temperature, pressure, compressibility, contamination, conductivity, etc.
- The physical phenomenon of fluid flow; or flow properties like: velocity, Reynolds number, flow pattern (upstream and downstream piping effect on metering), flow pulsation, fluctuation, etc.
- The primary part or function of the meter which generates the flow signal as fluid passes through it by some signal-generating flow mechanism.
- Secondary part or function of the meter that converts the flow signal into flow indication.
- Accuracy statement that pertains to the flow indication and is provided by the originator of the meter like: manufacturers, codes, standards, etc.

Since this is the case, the subject of reliability shall deal with forming answers to two basic questions:

- Why should one believe the flow indication to the meter?
- Why should one believe the accuracy statement to the originator of the meter?

Now, since perfect honesty is assumed, the answers to above questions shall have the task to gage the difference between the way the series of physical phenomena--that connects fluid flow to its indication--actually happen, to the level of their (possible) understanding from the part of the originator of the meter. Thus the level of reliability can be defined by qualitative equations, like:

$$\begin{array}{rclcl}
 \text{Full} & & & & \text{Zero} \\
 \text{Reliability} & = & \text{Actual} & - & \text{Lack of} \\
 & & \text{Happenings} & - & \text{Understanding} \\
 & & \text{Full Level} & - & \\
 & & \text{of Understanding} & = &
 \end{array}$$

$$\begin{array}{rclcl}
 \text{Zero} & & & & \text{Full} \\
 \text{Reliability} & = & \text{Actual} & - & \text{Lack of} \\
 & & \text{Happenings} & - & \text{Understanding} \\
 & & \text{Zero Level} & - & \\
 & & \text{of Understanding} & = &
 \end{array}$$

Since different types of meters may earn different placements between the full and zero reliability categories depending on how and where they are applied--as the next step toward the goal; the possible types of measurement reliabilities shall be explored.

TYPES OF MEASUREMENT RELIABILITIES

Since in the final analysis the metering performance of any meter can be only, thus must be verified by flow calibrations (which may be direct or indirect as becomes evident through the paper) where the "actual" flow is determined by weight or volume and time measurement; and since meters are used to measure flow for other fluids and at different fluid and flow properties than those encountered at their calibrations; different flow measurements may have different levels of reliabilities typical to the application; consequently, it becomes necessary to recognize different types of measurement reliabilities like:

- Reliability of Flow Measurement in the Calibrating Facility

Here the question is how the accuracy can be verified attributed to the flow determination at calibration.

- In Place Flow Measurement Reliability

This case is encountered when a meter is used for flow measurement in the same location, and without a change in installation, where its flow indication was derived by calibration (by any means).

- Physically Transferred Reliability

This case is encountered when a meter is used at a different locality, or in different installation at the same locality than at which its flow indication was derived by calibration (by any means).

- Meteringly Direct Reliability

This case is encountered when a meter is used to measure flow for the same fluid and flow properties as applied at its flow calibration.

- Meteringly Transferred Reliability

This case is encountered when the flow indication is assigned to a meter--which itself was not flow calibrated--based on metering sameness (par. 2.5) as ascertained by "bench inspection" (par 2.3); and the meter is used to measure flow for flow and fluid properties the same at which those "meteringly same" devices have been flow calibrated whose flow indication is transferred to the device in question.

- Meteringly Interpolated Reliability

This case is encountered when flow measurement is performed so that the device parameters, and/or fluid, and/or flow properties of the application have not been directly encountered by flow calibration of meteringly similar devices

(par. 2.6) but are bounded by them, thus their metering performance is interpolated to the condition of application once "metering similitude" of the device in question has been ascertained by "bench inspection."

Meteringly Extrapolated Reliability

This case is encountered when flow measurement is performed so that device parameters, and/or fluid, and/or flow properties of the application are beyond the parameters encountered at the flow calibration of "meteringly same" and/or "similar" devices whose metering performance is extrapolated to the conditions of application, once "metering sameness" or "similitude" of the device in question has been ascertained by "bench inspection."

Time Extrapolated Reliability

Here the question is: How does time affect the metering performance of a device; where time is considered a possibility that allows: The device to age (aging of components); all surfaces (that of devices and pipes) exposed to flow to corrode, erode, get coated causing change in diameters, surface finishes which in turn shall cause flow pattern change.

Having explored the different types of possible reliability categories, now we shall attempt to find building blocks that may raise the reliability of flow measurement to the required level.

BUILDING BLOCKS TOWARDS FLOWMETER RELIABILITY

1. FLOW CALIBRATION

Basically the flow indication of all meters is derived either by flow calibration of the device itself or by (metering) transfer, inter-, and/or extrapolation of the metering performance of calibrated devices by the help of "metering sameness" and "metering similitude."

While the accuracy of the calibration depends on the ability of the calibrating facility to measure the actual flow during calibration and the flow signal (or indication) generated by the meter as flow passes through it; thus can be known (calculated) and controlled; to assure that this known accuracy is truly present at all times during calibrations is a question to which the calibrating facility itself is unable to give continuous answer due to obvious handicaps inherent in the nature of the work. As a result, the paradoxical statement seems to be valid; that no matter how accurately can a facility flow calibrate devices, the reliability of any calibration--in its ultimate sense--can never be assured by the facility itself.

Flow calibration reliability can be achieved, however, in the facility and continuously if the metering performance of the device to be calibrated was already known before the calibration within some tolerance band. In such a case the calibration may improve the accuracy of the meter, while the facility and the device shall mutually support each other's reliability to the extent of the tolerance band warranted by the background knowledge about the metering performance of the device under calibration. Consequently, as Table 1 indicates, flow calibration helps to achieve all types of reliabilities except its own.

2. DEVICE CHARACTERISTICS

2.1 Signal is Assigned to the Device by Flow Calibration

Description: A device has this characteristic if its flow indication is not fixed in its design but can be adjusted and is intended to be assigned to the device by flow calibration.

Typical Examples: Magnetic and some ultrasonic flow meters.

Main effects on reliability: Devices with this characteristic ought to be called signal generators rather than true meters due to limits, inherent in their nature that may hinder them to achieve reliability in flow measurement. Since background knowledge about their flow indication cannot be "tied" to them, they are unable to help to improve the reliability of the flow calibration; since their set signal may get offset during operation or movement of the device, they cannot assure direct and time extrapolated reliabilities with in-place or physically transferred applications; also their nature prohibits their use for any other flow and fluid properties but the ones for which they have been directly calibrated. (See Table 1)

2.2 Signal Belongs to Device

Description: Such devices belong in this category whose flow signal is fixed in their "visible" design, but the flow value indicated by the flow signal is not known, thus must be assigned to each device by flow calibration.

Typical Examples: Differential producers made without background knowledge about their metering performance.

Main effect on reliability: This characteristic lifts typical signal generators one step upward on the ladder leading to reliable flow measurement. Since, by definition, devices possessing this characteristic should not change their flow signal unless their signal-generating shape was visibly changed by damage, corrosion, erosion or coating, they can attain direct and

time transferred reliabilities but are unable to help flow calibration reliability and prohibit all types of metering transfer, inter- and extrapolations. (Table 1)

2.3 Bench Predictability of Flow Indication

Description: This characteristic is possessed by a device if its flow indication can be assigned to it--not by its direct flow calibration--but based on bench inspection of its parameters that generate the flow signal and through a full knowledge about the metering performance of the device. In its purest sense to claim this characteristic would require a full, accurate and limitless knowledge and/or understanding of:

- The fluid properties encountered at the measurement.
- The properties of the fluid flow.
- The signal-generating flow mechanism utilized by the device and its interaction with the encountered fluid and flow properties.
- The operation of the secondary mechanism by which the flow signal is converted into flow indication by the device.
- The extent to which the full and exact understanding is approximated by the actual device operation, because the level of this approximation shall determine the accuracy of the flow measurement.

Typical Examples: While no device can claim full possession of this characteristic, true Venturi tubes and nozzles are examples that approximate several of its aspects.

Main Effects on Reliability: The most important single characteristic that can raise a mere signal generator to the level of a reliable flow meter is the bench predictability of its flow indication. This feature enables the device to check the validity of flow calibration thus raising its reliability level, also--and obviously--allows and helps to measure flow reliably under any type of application.

2.4 "Distance" Between the Fluid Flow and Its Indication

Description: Here the extent, complexity, sensitivity to defects and environment and the inspectability of the instrumentation is meant that composes the meter and by which the device converts flow into flow indication. The more complex, sensitive and the less inspectable is the instrumentation, the longer is the "distance."

Typical Example: For shorter distance: A differential producer that measures water flow and where flow is calculated based on the differential as read on a nearby water manometer.

2.5 Metering Sameness

Description: Devices are meteringly same if they have the same metering performance when their physical parameters generating the flow indication and "visible on the bench" appear to be the same.

Typical Example: True Venturi tubes, orifice plates, etc.

Effect on Reliability: As Table 1 shows, this characteristic--if available--helps to attain all types of reliabilities; if not available, prohibits meteringly transferred, interpolated and extrapolated application of a device.

2.6 Metering Similitude

Description: Devices are meteringly similar if they have the same metering performance when their physical parameters generating the flow indication and "visible on the bench" differ from each other, but according to a precisely defined, meteringly meaningful physical law that assures the same metering performance.

Typical Example: True Venturi tubes.

Effect on Reliability: As Table 1 shows, this characteristic--if available--helps to attain all types of reliabilities except the time extrapolated ones; if not available, prohibits the meteringly interpolated and extrapolated use of a device.

An immensely important fact in connection with metering sameness and similitude must be emphasized, namely: To utilize simulated tests for establishing installation effects (flow pattern effects) is impossible for types of devices that do not possess metering sameness and similitude. In other words, there is no way to transfer, inter- and extrapolate up and downstream piping effects as found with a given unit to other units of the same or different line sizes; leaving the question of--how to handle installation effects for all types of installations--without a reliable answer.

2.7 Metering Work

Description: A device performs metering work if it is intended to cause some change in the flow and/or fluid

properties of the entire body of the flow and utilizes the results of its own effect on the passing fluid to produce flow indication (on flow signal).

Typical Example: The classical Venturi tube or rather the Venturi metering principle seems to be the most suitable example. To explain it in scientific terms (Ref. 1) here would be a waste of space because it is widely known; but--for this very reason--it may be useful to restate it in terms less scientific but more pointedly enlightening the subject of the paper to recognize some very important characteristics of this metering method that has not been properly appreciated so far in flow metering literature. Thus the author takes the liberty to speak as follows:

The true Venturi tube receives the fluid from the upstream pipe in its own inlet (pipe) section. This inlet section leads the flow to the cross section where the inlet tap "looks" at the flow and registers its static pressure. From here its transition section accelerates the flow feeding it to the throat section designed so that the throat tap "sees" and registers true static pressure. The recovery cone captures now the high velocity throat jet, tries to slow it down and expand it to the pipe wall. The acceleration-deceleration process consumes energy, and the greater the acceleration, the larger is this well-known energy loss. The little appreciated yet very important fact about this lost energy is that it is consumed by the device to do "metering work" that may become beneficial for the user to improve measurement reliability.

Effect on Reliability: To illustrate the point, the following chain of thoughts is presented:

Due to its essence, volume flow rate is composed of area times velocity:

$$Q_a = A \times V; \quad (1)$$

which when applied for a meter:

Q_a = Actual Rate of Flow

A = Some area in the meter known from "bench inspection"

V = Velocity through area "A" estimated from the flow signal generated by the meter

The mathematical image used to calculate flow rate for Venturi tubes solves Eq. 1 (Ref. 1):

$$Q_a = C_a \frac{\sqrt{2g\Delta H}}{\sqrt{1-\beta^4}} \quad (2)$$

where

$$C = \text{Coefficient of discharge} = \frac{\text{Actual Rate of Flow}}{\text{Ideal Rate of Flow}} =$$

$$= \frac{\text{Actual Metering Phenomenon}}{\text{Ideal Phenomenon as Described by the Mathematical Image}}$$

a = Throat Area, measured on bench

ΔH = Differential Pressure indicated by the device as flow passes through it

g = Acceleration due to gravity

$$\beta = \frac{d}{D}$$

d = Throat diameter, measured on bench

D = Inlet diameter, measured on bench

To simplify the discussion, it is assumed that the actual physical phenomenon is fully described by its mathematical image, consequently

$$Q_a = a V_d = a \frac{\sqrt{2g\Delta H}}{\sqrt{1-\beta^4}} \quad (3)$$

where

$$\Delta H = P_D - P_d = \frac{V_d^2}{2g} - \frac{V_D^2}{2g} = \frac{V_D^2}{2g\beta^4} - \frac{V_D^2}{2g} \quad (4)$$

Where

p_D = Inlet static pressure

P_d = Throat static pressure

V_D = Average inlet velocity = inlet local velocities (because perfectly blunt velocity profile is assumed)

V_d = Average throat velocity = throat local velocities (perfectly blunt velocity profile is assumed)

Eqs. 3 and 4 clearly show the drastaic growth in ΔH , thus energy loss (which is about 10-20% of the differential) as the Beta ratio of a device is decreased (at a given flow rate); what it fails to reveal is the benefit in installed metering accuracy and reliability the metering work earns for the user at the expense of this energy loss.

To indicate this simply but with practical effectiveness, we further assume that all metering errors due to installation effects are caused by "wrong" kinetic energy content of the flow at the inlet tap cross section of the tube, consequently, the hydraulic shape of the tube is supposed to normalize the flow before it reaches the throat tap cross section, so that the throat flow does not contribute to the error. Now if " E_D " signifies the amount of this "wrong" kinetic energy content at the inlet tap in part of the ideal or correct one, then:

$$\frac{\Delta H_a}{\Delta H_I} = \frac{\frac{v_d^2}{2g} - \left(\frac{v_D^2}{2g} + E_D \frac{v_D^2}{2g} \right)}{\frac{v_D^2}{2g} - \frac{v_D^2}{2g}} \quad (5)$$

Where

ΔH_a = Actual differential

ΔH_I = Ideal or "correct" differential

E_D = Inlet kinetic head error, part of ideal or "correct" kinetic head

Since

$$v_d^2 = \frac{v_D^2}{\beta^4}$$

Eq. (5) can be reduced to:

$$\frac{\Delta H_a}{\Delta H_I} = 1 - \frac{E_D \beta^4}{1 - \beta^4} \quad (6)$$

and since:

$$Q \approx \sqrt{\Delta H};$$

$$\frac{Q_{IND}}{Q_I} \approx \sqrt{\frac{\Delta H_a}{\Delta H_I}} = \sqrt{1 - \frac{E_D \beta^4}{1 - \beta^4}} \quad (7)$$

Where

Q_{IND} = Indicated rate of flow

Consequently the error in % of flow

$$Eq = \left(\sqrt{1 - \frac{E_D \beta^4}{1 - \beta^4}} - 1 \right) \times 100 \quad (8)$$

Table 2 gives a feel of the mechanism Eq. (8) describes. It also lists actual installation effects as found by tests (Ref. 2) with classical Venturi tubes, to enable judgement about the validity of the thoughts presented in this paragraph. Fig. 1 illustrates some of the data from Table 2.

Once the meaning of the term "metering work" is fully understood and the fact is realized that the "same flow" almost never reaches a meter with "the same flow pattern" at different installations; or possibly on the same installation from time to time, it becomes a question of paramount importance from the point of view of measurement reliability--how does the meter estimate "V" for Eq. (1); namely, just by "looking" at the flow and accepting what is there, like: Velocity at a point, along a line (diameter), along several lines, in a volume (magnetic meters); or it performs metering work thus does something to the full body of the flow and uses its own effect for flow indication. But why should a difference be suspected in measurement reliability between devices where one just looks at the flow and accepts what is there, as opposed to another that works on the flow, observes its own influence and utilizes this influence to develop flow indication? The answer lies in the definition of the ideal meter (from the point of view of installation sensitivity) which, no doubt, would be the one that indicated the correct flow disregarding the patterns with which it reached the meter. From this definition follows that the reliability of devices should improve as in their flow indication or flow signal the portion generated by the influence of the device on the flow grows, while the part caused by the influence of the flow pattern on the signal generation diminishes. In view of these thoughts the data presented in Fig. 1 and Table 2 should obtain new significance, because it shows much desired benefits which devices doing metering work cannot but assure, while devices that just look at the flow deny, namely:

- Very large pipe flow pattern defects in terms of erroneous local velocities, line velocities and/or total kinetic energy content can be cut down to comparatively small flow indication errors just by selecting suitable Beta ratios.
- Installation effects as obtained by simulated tests can be summarized meaningfully so that the data can be used to control installation effects at the time of designing meter installations.
- The laying length of metering sections can be cut in "tight" situations by selecting smaller Beta ratios.

3. METHODS OF INVESTIGATION

Since the metering device is only one part of a flow measurement, the other, equally important part, being the knowledge about its metering performance possessed by the originator; and since this knowledge can be obtained by different research methods, it is useful to look at the difference of reliability levels that may belong to the different methods of the research.

3.1 Empirical Determination of the Flow Indication

Description: The flow indication is empirically derived for a device if:

- A) The device itself was flow calibrated, or if
- B) The flow indication of meteringly same or similar devices--as found by flow calibration--is transferred, inter-, or extrapolated for the device in question.

Typical Example: For case A) any meter; for case B) orifice plates.

3.2 Physical Determination of the Flow Indication

Description: If the flow indication is derived for a device based on its bench inspection and through the full understanding of the fluid and flow properties encountered at the measurement and of the way the device converts those into flow indication, then the flow indication is called physically determined.

Typical Example: Have been achieved to a certain extent for Venturi tubes and true nozzles.

3.3 Combined Determination of the Flow Indication

Description: This case is encountered when the flow indication of a device was derived by both methods: empirical and physical.

Typical Example: Venturi tubes and Venturi nozzles to a certain extent.

Effect on Reliability: The smaller the difference between the empirically and physically determined flow indications, the greater is the reliability of the flow measurement. It is important to recognize the benefit of this two-pronged method because it can powerfully raise the level of reliability of the flow measurement if it arrives to the same flow indication from sources of derivation located so far apart (flow calibration vs full understanding of the physical phenomenon involved).

3.4 Statistical Determination of the Accuracy of the Flow Indication

Description: Accepting the definition of accuracy as:

$$\text{Accuracy} = \frac{\text{Actual Flow}}{\text{Flow Indication of the Device}} - 1; \quad (9)$$

a statistical estimate of this accuracy can be developed:

- A) For flow calibrated devices; by combining the tolerances of the equipment used at calibration with tolerances incurred by the way the calibration work was performed.
- B) For devices not directly flow calibrated; by calculating the standard deviation of flow indications of metering same and/or similar devices which were flow calibrated and whose mean flow indication was assigned to the device in question. Once the standard deviation is known, the accuracy can be estimated with the required confidence level.

Typical Example: For Case A) any device; for case B) Venturi tubes, orifice plates. (Ref. 3)

3.5 Physical Determination of the Accuracy of Flow Indication

Description: If full knowledge of all physical sources of measurement inaccuracies and their magnitudes applicable to a given flow measurement are available, flow indication accuracy can be estimated based on the following definition:

$$\text{Accuracy} = \frac{\text{Actual Flow (= Full Knowledge)}}{\text{The extent to which the full knowledge was decided to be represented by the flow indication}} \quad (10)$$

Typical Example: A partial effort can be found in Ref. 4.

3.6 Combined Determination of the Accuracy of Flow Indication

Description: This case is encountered when the accuracy of the flow indication of a device was determined by both: statistical and physical methods.

Typical Example: Partial effort can be found in Ref. 4.

Effect on Reliability: The least recognized--yet in author's opinion--the most important single requisite

to secure flow measurement accuracy reliably is the combined, two-pronged method in the accuracy determination. One may say--just by common sense--that due to the nature of the subject, purely statistically or purely physically determined accuracies should never be relied upon. The truth in this statement is well substantiated by ASME literature (Ref. 1 and 5) which drastically changed--from 1959 to 1971--the accuracies on the uncalibrated discharge coefficients of orifice plates and ASME nozzles, and whose present accuracies are still questioned, for the single reason that the combined method has never been applied in their determination.

3.7 The Value, Behavior, Uncertainty Method

Description: Once a meter is built thus its "nature" gets fixed, it becomes a task of paramount importance to find out what this "nature" is; namely, how the ratio of:

$$\frac{\text{Actual Flow}}{\text{Indicated Flow}} ;$$

changed as evidenced by flow tests, or expected to change as determined by physical methods when the meter gets exposed to different aspects of the total task of flow measurement; namely, to different flow and fluid properties or the metering principle is used to design different line size devices. Since the value of above ratio may change in a certain, characteristic fashion as the device is exposed to the total task, it is helpful to consider this characteristic change as the behavior of the device and search it as such. Furthermore, since this search cannot "see" beyond the uncertainties of the available information, decision making must be controlled by these uncertainties. For this reason author recommends the use of the "value, behavior, uncertainty" method in flow metering performance analysis. This method tries to find the true "nature" of a meter, type of meters or metering methods by balancing the uncertainty of the understanding of the physical phenomenon used for flow measurement with the uncertainty of the data that tries to describe that phenomenon. (Ref. 6)

Typical Example: See Par. 3.8.

Effect on reliability: See Par. 3.8.

3.8 Specifically Organized Tests

Description: Since the only and final proof to the proper understanding of any physical phenomenon is

success in tests, but since in case of flow measurement testing facilities may not be accurate enough to reveal the true nature of all line size devices, under all fluid and flow properties, it becomes a powerful tool in the hands of the investigator--as well as his obligation--to organize tests so that their accuracy is sufficient to uncover the specific aspect of device nature under investigation. (Ref. 6)

Typical Example for parts 3.7 and 3.8: An interesting example showing the usefulness of the "value-behavior-uncertainty" method as it points at the need and importance of specifically organized tests can be found in Ref. 7. One of the purposes of this paper is to substantiate through flow tests a slight slope of the discharge coefficient (C) in the function of throat Reynolds number (Behavior of C) as determined by physical methods. The most enlightening data which is part of Fig. 1 in Ref. 7 is reproduced on Fig. 2 in this paper. The continuous line of Fig. 2 shows the value and "shape" (behavior) of the C as determined by the physical method; the circles are single flow calibration points; while the dashed line is supposed to be the best fit of the calibration points. A quick review of this data clearly shows that while the single point accuracies of the flow calibration were sufficient to support--within a small tolerance--the correctness of the physical understanding that led to the calculation of the value of C , but it proved to be entirely impotent to verify the slight slope of C indicated by the physical determination of C behavior. This is the typical case when by the value-behavior-uncertainty method limits and possibilities inherent in the available means to investigate must be uncovered, and the need of specifically organized tests recognized, with single point accuracies sufficient to reveal a slight slope.

Effect on reliability (for Par. 3.7 and 3.8): A beautiful example on how flow measurement reliability can be improved by the thoughts presented in Par. 3.7 and 3.8 can be composed by reviewing, under the light of these thoughts, what is stated about transition region in Ref. 8 pertaining to ASME throat tap nozzles and what flow calibration data shows about the same subject in Ref. 8. Quote from Par. 4.33 in Ref. 8:

"At throat Reynolds numbers below 800,000 the nozzle boundary layer is laminar; at high throat Reynolds numbers it is turbulent. In between these two regions is a zone called the transition region. This transition region should be established during calibration and should be avoided during test. Flow coefficients for the nozzles described in this code have been found to be influenced by transition region at throat Reynolds numbers from 2.0 million to 3.5 million."

Now reviewing Fig. 1 in Ref. 7, one's first impression would be that above statement about the occurrence of transition region is substantiated by the flow calibrations, because they reveal the largest single point scatter between 2×10^6 to 3.5×10^6 throat Reynolds numbers. Unfortunately, the fact that prohibits the drawing of such conclusion is somewhat hidden, namely, that in the "transition region" calibration points taken with colder water flows at the highest differential pressures (best single point accuracy) and with warmer water flows at the lowest differentials (poorest single point accuracy) overlap. Consequently, due to their inherent inaccuracy--while good enough to verify the value of C--they are unable to identify the effect of boundary layer transition on C, i.e., its behavior. Obviously to identify boundary layer transition through C change specifically organized tests are required that assure single calibration point accuracies with magnitudes a fraction of the expected C effect of boundary layer transition. The immense practical importance of what has been said so far becomes evident if one imagines a coded job (according to Ref. 8) where a properly built test section goes under flow calibration in a facility where water at one single sump temperature is used. One may wonder how boundary layer transition "established" in this facility would compare to another as "established" by a different facility that used colder and warmer water to cover the same Reynolds number range, also what the revealed single point scatter would have to do with the sought for transition region.

4. CONCLUSION

Author hopes that the paper has achieved the following:

- To point out that flow measurement reliability is--in fact--a new subject that has never been directly and systematically analyzed in flow measurement literature, yet should be done.
- To make a first effort toward developing a vocabulary that helps to discuss this new subject.
- To define what reliability in flow measurement may or should mean.
- To uncover some of the building blocks of which flow measurement reliability may be constructed.
- To make it clear that accuracy and reliability are utterly different characteristics of a meter which difference becomes obvious when one thinks about the difference in means that should be and/or can be utilized to achieve accuracy as opposed to the ones that assure reliability.

- To throw light on the fact that different devices that may yield equal accuracies in flow measurement may be drastically different in providing it reliably.
- To provide help to improve the efficiency and reliability of flow measurement research work by:
 - Emphasizing the total task of flow measurement thus enabling the researcher to measure up realistically the required effort to cover the total task; or to address the research effort to the desired or possible portion of the total task and keep conclusions within the selected boundaries.
 - Showing methods by which the accuracy and reliability of data analysis can be improved.
 - Showing means by which meter reliability can be improved.
- To help users to select the device suitable to their reliability requirements.
- To provide a frame within which the subject of reliability can be treated in:
 - Scientific papers
 - Flow meter standards
 - Sales literature
- To uncover the fact that certain types of devices due to their nature cannot provide reliable flow measurement for certain types of applications.

REFERENCES

1. ASME, Fluid Meters, Sixth Edition, 1971.
2. Pardoe, W. S., "The Effect of Installation on the Coefficient of Venturi Meters," presented at the ASME Annual Meeting in 1942.
3. Dowdell, R. B. and Che, You-lin, "A Statistical Approach to the Prediction of Discharge Coefficients for Concentric Orifice Plates," ASME Paper No. 69-WA/FM-6.
4. Halmi, D., "Metering Performance Investigation and Substantiation of the Universal Venturi Tube (UVT)," ASME Papers Nos. 73-WA/FM-3 and 73-WA/FM-4,
5. ASME, Fluid Meters, Fifth Edition, 1959,
6. Halmi, D. "'C' Evaluation - Differences Between 'Mathematical' and 'Physical' Possibilities," ASME Paper No. 74-WA/FM-2.
7. Cotton, Schofield and Carcich, "Experience with Throat Tap Nozzles for Accurate Flow Measurement," Journal of Engineering for Power, Trans. ASME, Series A, Vol. 94, No. 2, Apr. 1972, pp 133-141.
8. ASME Power Test Codes, Steam Turbines, PTC 6-1976.

TABLE 1

STRUCTURE OF RELIABILITY

"BUILDING BLOCKS"		TYPES OF RELIABILITIES										
		Flow Calibration	In Place				Physically Transferred					
			Meteringly				Time Extrapol.	Meteringly				Time Extrapol.
			Direct	Transf.	Int.Pol.	Ext.Pol.		Direct	Transf.	Int.Pol.	Ext.Pol.	
1. Flow Calibration	N	H	H	H	H	H	H	H	H	H	H	
2. Device Characteristics:												
2.1 "Signal" Assigned to Device:	N	N	P	P	P	N	N/P	P	P	P	N	
2.2 Signal Belongs to Device:	N	H	P	P	H	H	H	P	P	H	H	
2.3 Bench Predictability	H	H	H	H	N	H	H	H	N	N	H	
2.4 "Distance" if Short	H	H	H	N	N	H	H	H	N	N	H	
2.5 Metering Available	H	H	H	N	N	H	H	H	N	N	H	
2.5 Metering Not Avail.	N	N	P	P	P	N	N	P	P	P	N	
2.6 Metering Available	H	H	H	H	H	H	H	H	H	H	H	
2.6 Similitude Not Avail.	N	N	N	P	P	N	N	N	P	P	N	
2.7 Metering Work	H	H	H	H	H	H	H	H	H	H	H	
3. Methods of Investigation:												
3.3 Combined Flow Ind.	H	H	H	H	H	N	H	H	H	H	N	
3.6 Combined Accuracy	N	N	N	P	P	N	N	N	P	P	N	
3.7 Value-Behavior-Uncertainty Method	H	H	H	H	H	H	H	H	H	H	H	
3.8 Special Tests	H	H	H	H	H	H	H	H	H	H	H	
H = Helps												
N = Does not Help												
P = Prohibits												

TABLE 2 EFFECT OF "METERING WORK" ON
INSTALLATION SENSITIVITY OF CLASSICAL VENTURI TUBES

Beta Ratios	Eq (Flow Errors) % of Flow Caused By			Flow Errors Found in Ref. 2 % of Flow		
	ED = +1 (+100% Error)	ED = +0.5 (+50% Error)	ED = +0.1 (+10% Error)	Tube Direct Coupled to		
				Decreaser	Increaser	Single Elbow
0.4	1.3	0.7	0.1	0.1	0.4	0.05
0.5	3.4	1.7	0.3	0.2	1.2	0.2
0.6	7.7	3.8	0.7	0.5	2.3	0.6
0.7	17.3	8.2	1.6	0.7	5.1	1.2
0.8	44.6	19.2	3.5	1.3	12.0	2.5

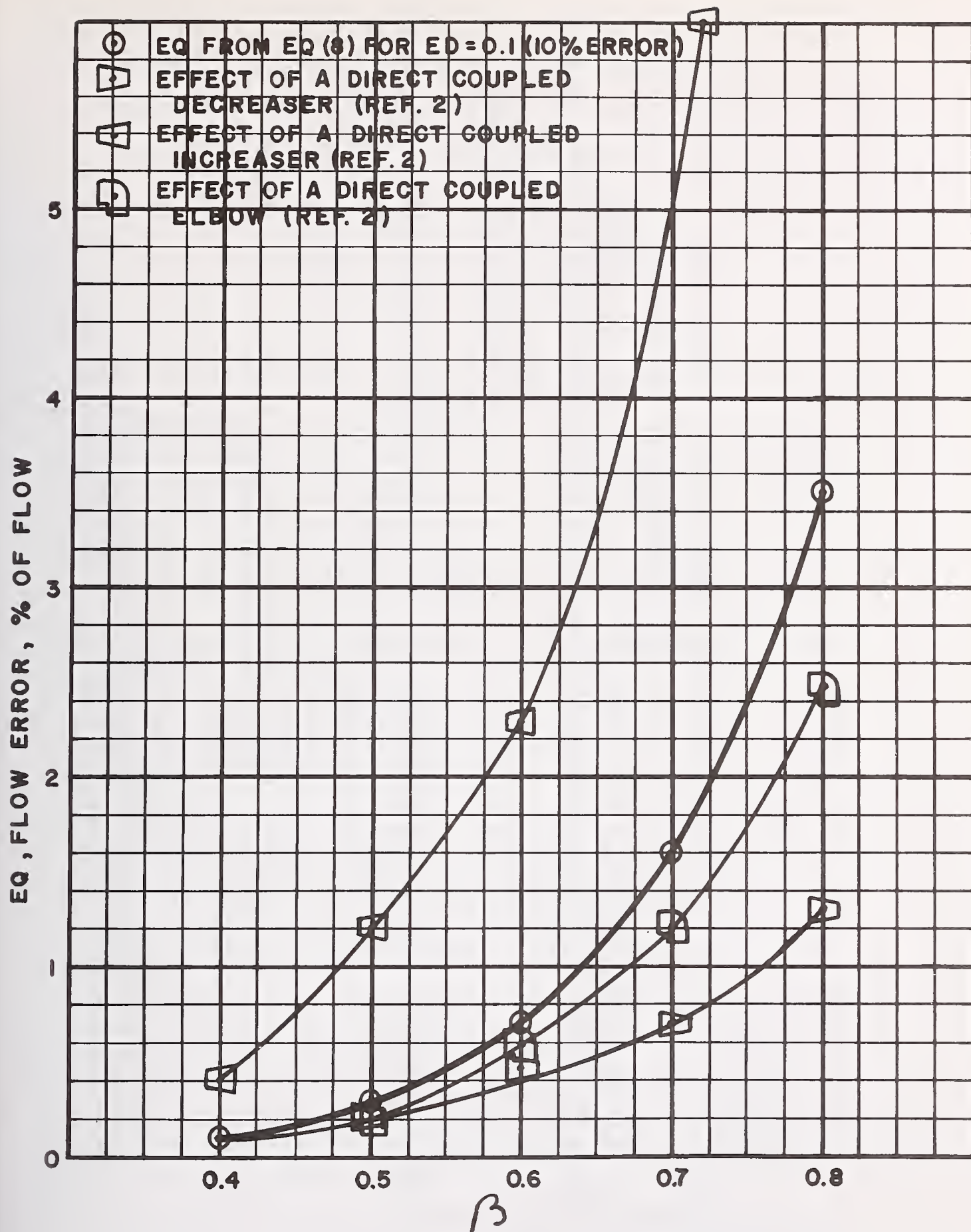


FIG. 1 EFFECT OF "METERING WORK"
ON INSTALLATION SENSITIVITY OF
CLASSICAL VENTURI TUBES

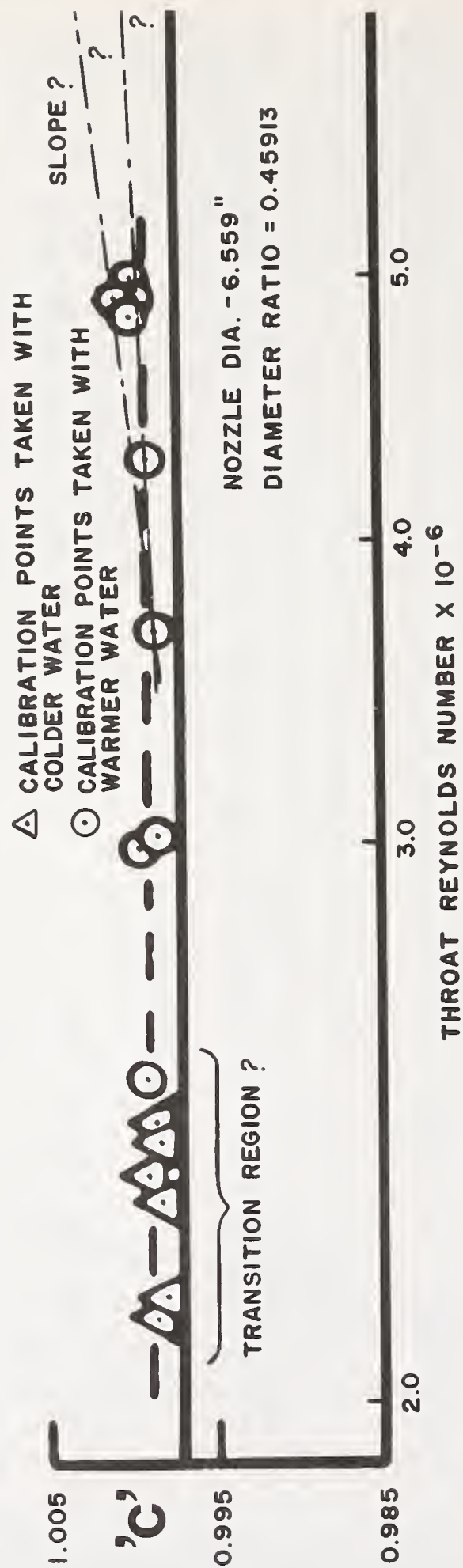


FIG. 2 DATA FROM FIG. 1 IN REF. 7

OPEN CHANNEL FLOW MONITORING OR METERING, THAT IS THE QUESTION

Kenneth W. Martig, Jr., P.E.

President, The Martig Bub-L-Air
and Senior Engineer Group Leader
in Hydraulic & Sanitary Systems with
Arvid Grant & Associates, Inc.
1600 East Fourth Avenue
Olympia, Washington 98506

For generations we have accurately MEASURED clean fluid flow conveyed in closed conduits employing precise, reliable flow meters. Clean fluids, historically, have had "Value". This "Value" has motivated precise METERING to apportion, buy, and sell said "Value". In contrast, most open channel conveyed fluids have by nature been low "value", liability "Value" or waste liquids containing debris. Therefore, there has been no incentive to MEASURE open channel flow. We simply have ignored or only applied loose MONITORING practices to these flows.

The advent of P.L. 92-500 in late 1972, has provided an instant incentive to MEASURE open channel flow more accurately, using METERING practices instead of less accurate MONITORING practices.

Instrumentation state-of-the-art does not lend itself to producing reliable, precise, cost effective METERING equipment to replace previously employed MONITORING equipment for use in existing systems. Recognizing this point is a significant step toward advancing open channel flow MEASURING technology and reducing the costly mistakes continuously being made by those who believe as gospel, the output from many new open channel flow devices being marketed and employed today.

In summary, our instant incentive to accurately MEASURE open channel flow has placed emphasis on equipment output means, assuming that technology exists to produce it. Users have not fully realized that measuring equipment presently available for use in existing sewers cannot supply METERING quality data, only MONITORING quality data. OPEN CHANNEL FLOW MONITORING OR METERING, THAT IS THE QUESTION. The answer is to provide society with a better understanding of what is actually possible in terms of open channel wastewater flow measurement so that "regulations" and required "measuring equipment" supplied can truly work together to solve our water pollution problems.

Key Words: Closed conduit flow; instrumentation; measuring flow; metering flow; monitoring flow; open channel flow; public law 92-500; sewerage flow, wastewater flow

1 Flow Measurement History

Open channel (gravity) conduits and closed (pressure) conduits have been used for generations to convey fluids from one point to another. Most clean fluids such as oil (black gold), petroleum products, milk, and water have economic value and are conveyed in closed conduits to keep them from evaporating or becoming contaminated. In order to apportion, buy, and sell these valuable clean fluids, precise reliable flow rate and totalized flow volume measurements are required. These measurement requirements have motivated the evolutionary development of precise, reliable, compact, easily installable, and relatively inexpensive closed conduit flow measuring apparatus called flow meters for METERING these flows.

Although water is sometimes conveyed in open channel conduits, most fluids conveyed in them have, by nature, been wastewaters or dirty fluids with low or negative economic value. Therefore, there has been little or no incentive for society to develop open channel fluid flow measuring meters of the same caliber as the meters developed to measure flow in closed conduits. In fact, society has historically demanded only occasional loose checking, watching, or MONITORING of these flows.

The advent of Public Law 92-500 in the fall of 1972 has provided an instant incentive to measure open channel flow, particularly wastewater flow in sewers while paying at least 75% of the cost through Federal Grant monies. Pursuit of this instant incentive has created problems typical of those experienced in the past when society takes too large a first step towards fulfilling a defined objective. The failure of the Teton Dam in Idaho is a recent example of how haste fosters waste and confusion.

2 Water Pollution Abatement Program Goals

During the late 1960's and early 1970's the impact of applying the age old philosophy that "Dilution is the Solution to Water Pollution" to wastewater discharges became quite apparent. Rivers, lakes, water courses, and even underground aquifers that once could be used for domestic water supplies, for water contact recreation activities and for supporting natural fish and aquatic ecosystems had literally become open sewers of liability value to society in and about heavily populated areas. To reverse this process and recover these waters dictated that wastewater discharges be MEASURED in terms of quantity and quality. Once the knowledge of quantity and quality of wastewater discharges could be determined, treatment processes could be properly and rationally prescribed to eliminate the discharge of the wastes that had polluted society's water resources. Obtaining this knowledge required that equipment for measuring both flow and water quality parameters be employed within tens of thousands of old, but still functional, existing open channel sewer systems. These systems had been designed and installed without provisions for accomodating measurements of any kind. However,

equipment for accomplishing measurements in existing systems had not yet been developed prior to about 1970, because such equipment had not been in demand.

The main goal of flow measuring is aimed toward prescribing adequate treatment of wastewater before discharge. Several other interim goals are:

- a) The evaluation of groundwater infiltration and storm water inflow quantities into existing sanitary sewers,
- b) The evaluation of domestic, commercial and industrial waste discharges for the proper development of user charges and industrial cost recovery systems, and
- c) The evaluation of wastewater flow twenty-four hour peaking curves.

Since most pollution sources are identifiable open channel sewer wastewater discharges from existing systems, flow measurement requirements at the respective discharge points, have also been incorporated into the regulations stemming from Public Law 92-500. These measurements satisfy one requirement of the N.P.D.E.S. (National Pollution Discharge Elimination System) discharge permit. These permits are required at all identifiable wastewater discharge points.

Early results of open channel flow measurement efforts indicate that our flow measuring program in older existing systems as imagined and requested by society is costing more than it should and is not supplying adequate data to cost effectively or environmentally evaluate water pollution control objectives required by law.

The main obstacle, then, in pursuing the achievement of pollution abatement goals appears to be the employment of equipment in existing sewers (both public and private) that will adequately measure and record the flow of wastewater within these open channel conduits and that will properly extract wastewater samples from these conduits for quality analysis.

3 Measurement, Both Monitoring and Metering

It is obvious today that considerable confusion exists in the field of flow measurement. Most of this confusion stems from the fact that the terms MONITORING and METERING have become used interchangeably with the word MEASURING. However, monitoring and metering represent two completely different measuring processes and instrumentation abilities. A correct understanding of these differences will substantially reduce the problems that have been created out of the misuse of these terms while trying to accomplish the goals and objectives of flow measurement in water pollution abatement regulations.

The term MONITORING means the process of watching, checking, or observing. Open channel flow MEASURING employs observed or empirically derived formulae to convert measured depth of flow to flow rate or totalized flow volume. Therefore, the association of the term MONITORING with equipment used to measure and record flow through open channels is natural, even though it is rarely experienced by most people.

The term METERING means the process of employing a meter. Most meters employed in flow measurement instrumentation are devices that can directly output flow rate or totalized flow volume while MEASURING either the positive displacement of flow during flow through the meter or the average velocity of flow during flow through a known constant area within the meter. The only restrictions on the use of these devices is that the flow must continuously fill meter constant area sections and the flow must not contain particulate matter or debris that would (i) interfere with positive displacement gears, buckets, etc., or (ii) interfere with propellers, pitot tubes, etc.. Meters are commonly used to measure the volume of domestic water and natural gas flowing into homes, businesses and industries. Their use is also observed daily at service stations by people fueling their automobiles. Therefore, the association of the term METERING with equipment used to measure and record pressure flow of clean fluids through closed conduits is natural and commonly experienced by most people.

Unlike hydraulic engineers and technicians, most people know very little about flow measurement. They do not know or appreciate the difference between pressure flow in closed conduits and gravity flow in open channels. However, these are the people making decisions on a day-to-day basis. The decisions they make are based upon what they know or what they have been directly associated with or exposed to. Therefore, the common concept that society has, in general, regarding flow measurement is METERING. They envision a precise, compact, reliable, mechanical device that can be easily installed directly into the closed conduit pipeline at a relatively low cost. Because they lack knowledge of open channel flow and have seldom been directly associated with or exposed to open channel flow measurement, they automatically but erroneously extrapolate their image of METERING into the field where MONITORING really applies. This erroneous extrapolation has fostered problems and costly errors by those responsible for dealing with regulation compliance whether they be the regulator or discharger (the regulatee).

4 Open Channel Flow Measurement

The rapid evolution of flow measurement in existing open channel conduits primarily began with the requirements associated with infiltration and inflow quantity assessments in the spring of 1973. These requirements specifically addressed sewers conveying wastewaters requiring treatment.

The use of Palmer Bowlus flume pipe inserts and 90° V-Notch weirs, although used in prior years, was not popular in the 1970's for several

reasons: They were difficult to install; they had flow rangeability problems and reliability problems that when coupled with normal flow debris, induced significant errors in their measurement output; and our concern for safety of personnel conducting the measuring, coupled with the high labor cost of larger crews suggested strongly that the measurements should be made without entering the manhole. Therefore, initial spot flow measurements were made using long sticks, rods, or plumb bobs on measuring tapes without entering the manhole.

The first modern piece of equipment designed to continuously measure flow in existing sewers was designed to be installed in a manhole, just under the lid. It produced a continuous recording of flow depth versus time and was supplied with a table for converting the recorded depths to flow rates, developed using the Manning Formula. This flow monitor did not fit the image society had of flow measuring, namely METERING, because it did not automatically produce an integrated total flow volume. Realizing this, the device was immediately modified to include an electronic calculator that would convert the measured depths to flow rates (employing the Manning Formula) so that the device would output a recording of flow rate instead of depth and so it could output a totalized flow volume.

This triggered the start of a race by instrumentation manufacturers to provide equipment designed primarily to provide the output format requested by regulators (and therefore desired by regulatees) because all parties envisioned sewer flow MEASURING to be METERING instead of MONITORING. The race produced high cost equipment called open channel flow meters that outputted data with significant errors. These errors were the direct result of society placing too much emphasis on the output format. The most important MONITORING/METERING component is the primary sensor, what it senses, its location in the channel, and its rangeability. The next most important component is the internal mechanisms dictating the output. Although the output readability must be accurate, the actual output format is of least importance as long as it allows the best use of the chosen empirical relationship for ultimately deriving actual flow. Too many users concern themselves only with the output format (totalized volume) without considering the absolute ability of all integral components of the device to produce that format.

Manufacturers are now looking for ways to produce equipment that will provide accurate flow output. This can be done, but not on a universal basis. Too many variations are inherent in the hundreds of thousands of miles of existing sewers that require flow measuring. Also, the variations in wastewater quality and flow rangeability logically dictate different degrees of accuracy of measurements and frequency of measurements when compared to the goals and objectives of water pollution abatement programs. Wastewater with critical pollutants such as heavy metals or cyanide must be more accurately measured than cooling water from ice plants or domestic sewage discharged from homes.

Also ignored in our haste to meet open channel flow measuring

requirements was the fact that two levels of flow measurement exist. The first level (the level neglected in many cases) is the initial learning level. It employs the use of relatively inexpensive temporary portable equipment to determine for the first time what historical flow rates have actually been. With this information, the sewer system can be properly evaluated to optimize its use, both economically and environmentally. Then and only then should larger amounts of money be expended to provide the second level of measurement. The second level involves the installation of permanent flow measuring stations to provide system control and to meet the flow measurement requirement normally contained in most N.P.D.E.S. discharge permits. Even at this level of measurement, flow MONITORING equipment may prove adequate instead of the more costly, but more accurate, METERING equipment.

5 Recommended Revisions To The Pollution Abatement Process

The purpose of the above four sections is to define the confusion and lack of knowledge that exists in society today regarding flow measurement and to show how costly mistakes have been fostered while hastily attempting to meet required wastewater flow measuring goals without due regard to the state-of-the-art and understanding in existence at the time.

Even today, February 24, 1977, regulators preparing N.P.D.E.S. discharge permits, dischargers purchasing and installing equipment in compliance with their permits, and manufacturers supplying the equipment that will be used do not completely understand what can and what cannot practically be accomplished regarding open channel flow measurement. OPEN CHANNEL FLOW MONITORING OR METERING, THAT IS THE QUESTION. The answer lies within the ability of hydraulic and environmental engineers to work together with congressmen, legislators, regulators, discharges, and manufacturers to re-evaluate and upgrade the requirements within individual N.P.D.E.S. discharge permits and to modify the process of compliance with the permits consistent with existing technology.

In conclusion, the following suggested water pollution abatement process is offered.

SUGGESTED WATER POLLUTION ABATEMENT PROCESS

Step 1 - The State Sets Preliminary Discharge Standards

The state evaluates the water resource where treated or untreated wastewater is released by the discharger. This evaluation sets preliminary standards for acceptable discharge quantities (as related to quality) based upon the small amount of initially available data.

Step 2 - The Discharger Conducts Preliminary Measuring Study

The discharger conducts a preliminary study, employing

portable temporary flow MONITORING and wastewater sampling equipment that can provide accurate data when properly calibrated for each specific monitoring site employed.

Step 3 - The Discharger Evaluates and Optimizes The Use of His System

The discharger evaluates the effective use of his system by identifying all significant components of the total discharge. Cost effective evaluations considering wastewater pretreatment, wastewater flow removal and process modifications consistent with state preliminary water quality standards would be conducted in this step to minimize the impact of the discharge.

Step 4 - The Discharger Obtains Final Measuring Study

After the discharger optimizes the use of his sewerage, consistent with economic principals but compatible with state defined environmental quality at the point of discharge, the discharger again uses portable flow MONITORING and wastewater sampling equipment to accurately define the impact of his optimized discharge.

Step 5 - The State Sets Discharge Permit Requirements Using Step 4 Data

The state reviews the data supplied them at the end of Step 4 and uses it to prepare the discharger's initial N.P.D.E.S. discharge permit. The resulting permit requirements can be based upon actual discharge characteristics and thus will be more rational and consistent with pollution abatement goals.

Step 6 - The Discharger Installs Permanent Measuring Equipment

At this point, the discharger can install pretreatment processes if necessary, and permanent flow MEASURING equipment (either METERING OR MONITORING) and wastewater sampling equipment as necessary for compliance with his permit requirements.

Step 7 - The State Reviews Its Program Effectiveness

When all dischargers to a given water resource complete Step 6, the state can evaluate the effectiveness of the implemented water pollution abatement program and make permit changes as necessary so that the best interest of society can be served.

INSTRUMENT ERRORS IN OPEN CHANNEL
FLOW MEASUREMENT SYSTEMS

D. M. Grant

Instrumentation Specialties Co.
P. O. Box 5437
Lincoln, Nebraska 68505

Certain aspects of open channel flow measurement systems are briefly discussed, including primary and secondary measuring devices. The two functions of a secondary measuring device (open channel flow meter) are discussed: level measurement and level-to-flow rate conversion. Some of the common methodologies used to accomplish each of the two functions of a secondary device are described, and the possible sources and magnitudes of errors associated with each of these methodologies are analyzed. Level measurement methods discussed are: float, electrical, ultrasonic, bubbler, and dipping probe. Level-to-flow rate conversion methods discussed are: mechanical cam, electronic analog function generator, electronic memory device, and opto-electronic function generator. In the interest of promoting a uniformity of specifications, a standard general format for open channel flow meters is proposed.

Key Words: Flow measurement, water; flow meters; instruments, flow measurement; level measurement; level-to-flow rate conversion; liquid flow; open channel flow measurement; secondary measuring device.

1. Introduction

The measurement of the quantity of flow in open channels, often in conjunction with sampling to determine the quality of the flow, is essential to nearly all aspects of water pollution monitoring and control. In order to fully characterize the nature of the liquid source, it is vital to know both the quality and the quantity of flow of the source.

This paper will be mainly concerned with one aspect of the flow measurement process, namely the secondary measuring devices, (commonly referred to as open channel flow meters) that constitute the "instrumentation" portion of an open channel flow measurement system. The majority of this paper will deal with the methodologies used in various types of

flow meters, and will analyze the possible sources and magnitudes of errors associated with each of these methodologies. A standard format for open channel flow meter accuracy specifications will also be proposed.

2. Open Channel Flow Measurement Systems

Open channel flow is defined to be flow in any channel in which the liquid flows with a free surface. Certain closed channels, such as sewers and tunnels when flowing partially full, and not under pressure, are also classified as open channels.

Flow in an open channel is normally measured through the use of a calibrated restriction inserted into the channel, which raises the level of the liquid upstream from the restriction. The rate of flow through or over the restriction is related to the liquid level upstream from the restriction by a known function. The restricting structures used to measure flow in open channels are known as primary measuring devices (see Figure 1) and may be divided into two broad categories: weirs and flumes. A weir is essentially a dam built across an open channel over which the liquid flows, while a flume is a specially shaped open channel flow section providing a restriction in the channel area. Both types of primary devices result in an increased upstream liquid level which is related to the flow rate of the channel by either test data (calibration curves) or by an empirically derived formula. [1] 1

A secondary measuring device (commonly referred to as an open channel flow meter) is used in conjunction with a primary measuring device to measure the rate of liquid flow in an open channel. The purpose of a secondary measuring device is two-fold: 1) to measure the liquid level in the primary measuring device, and 2) to convert this liquid level into an appropriate flow rate according to the known liquid level-flow rate relationship of the primary measuring device. This flow rate may then be directly displayed, integrated with time to obtain a totalized flow volume, transmitted to a recording device to be recorded as flow rate or totalized flow, and/or used to pace an automatic sampler in a flow proportional mode.

3. Sources Of Errors In Open Channel Flow Measurement Systems

When evaluating the possible sources of errors in an open channel flow measurement system, both of the integral subsystems of the total system must be considered: the primary measuring device and the secondary measuring device. The errors associated with a primary measuring device may originate with any or all of several factors, including: uncertainties associated with the basic level-flow rate relationship of the device;

¹Figures in brackets indicate the literature references at the end of this paper.

faulty installation and/or construction of the primary device; and improper maintenance of the primary device. A fairly large body of literature exists concerning the inaccuracies associated with the various primary measuring devices, [2,3] and these inaccuracies will not be further discussed here.

Unlike primary device errors, secondary measuring device errors have not been widely treated in the literature. The errors associated with secondary devices may be divided into two classifications: set-up or "zero" errors and instrument errors. The latter, instrument errors, originate with inaccuracies related to the two basic functions of a secondary device: level measurement and level-to-flow rate conversion. These errors will be discussed at length in the remainder of the paper. The former, set-up or "zero" errors, originate from improper instrument installation and/or failure to accurately adjust the flow meter's indicated liquid level with the actual liquid level in the open channel, and will be discussed briefly.

It is imperative that the flow meter be properly "zeroed" with the zero reference level in the primary measuring device. If this is not accurately done, a systematic level offset error will be introduced, resulting from the fact that the liquid level indicated by the flow meter will not correspond to the level actually existing in the primary measuring device. [4] Due to the non-linear level-flow rate relationship of most primary measuring devices, this will result in a flow rate error which becomes increasingly more significant at increased liquid levels, as shown in Figure 2.

A properly constructed flow meter can greatly aid in minimizing set-up or "zero" errors. The flow meter should have some type of accurate visual indication of the instrument liquid level, and the resolution of this level should be of at least the same order of magnitude as the readability of the level in the primary device. The flow meter should also have a mechanical or electronic control which easily allows the adjustment of the indicated liquid level.

4. Level Measurement Methodologies- Description And Error Analysis

The first of the two functions which a secondary measuring device must perform is that of the measurement of level in a primary measuring device. Some of the more commonly used methods of measuring liquid level are: float, electrical, ultrasonic, bubbler, and dipping probe.

Float-A float operated system is undoubtedly the oldest method of level measurement in existence. Basically, it consists of a float which moves in conjunction with the level of liquid in a primary device. The float either may be located in a stilling well adjacent to the weir or flume (float-in-well), or may ride directly on the actual surface of the

flow (float in-flow). See Figure 3. The float is connected by a cable or arm to a rotating member. As the liquid level in the primary device changes, the float will rise or fall correspondingly and the cable or arm will cause the rotating member to be angularly positioned proportional to the level of the liquid in the primary device.

There are several possible sources of errors in a float operated level measurement system. By far, the most significant error is that of "float lag" or hysteresis. In any type of float system, the float is required to perform a certain amount of mechanical work, arising from the operation of related mechanical devices by the rotating member and/or frictional losses in the rotating member. These mechanical losses result in the float not correctly following ("lagging") a changing liquid level, in a phenomenon basically analogous to backlash between two gears. The error caused by these hysteresis losses varies directly with the force required to move the flow meter rotating mechanism and inversely with the square of the float diameter. This type of error can never be eliminated from a float system, but can be minimized by reducing the amount of mechanical work required of the float and/or by making the float diameter as large as possible. Any additional play or backlash in the rotating mechanism (e.g., gear reduction systems) will add to errors of this type.

A cable operated float system can also suffer from temperature and humidity related errors. A change in ambient temperature will cause the float cable to expand or contract, resulting in a corresponding shift in the indicated level. For hygroscopic cable materials, a change in humidity will have a similar effect. However, proper choice of cable material can minimize these effects, and except for extremely long cable lengths, the errors involved are usually so small as to be negligible.

Manufacturing tolerances in a cable pulley or related mechanical systems can also lead to errors. If the cable pulley is not manufactured to the correct diameter, the instrument will not track a changing level correctly. That is, the level indication will be correct at the set point, but as the actual liquid level in the primary device changes, the indicated level will become increasingly less reflective of the actual level. A similar error will also result from inaccuracies in associated gear reduction or mechanical linkage systems.

Manufacturer's claims of accuracy for float operated level measuring devices range from ± 0.005 ft. to ± 0.020 ft. For a well constructed float operated device, accuracies of at least ± 0.010 ft. should be attainable. It should be recognized, though, that the accuracy of any float operated device can be increased by increasing the float diameter; there is, however, usually a maximum possible float diameter dictated by installation conditions.

Electrical-This type of level measurement system utilizes some sort of change in an electrical circuit caused by a changing level in order to

indicate the liquid level. In most designs, a probe or some similar sensor is immersed in the flow stream. The probe functions as an element in an electrical circuit, and its behavior in the circuit is a function of the amount of its immersion in the stream. [2] Changes in any electrical property can be used to sense liquid depth; capacitance appears to be the property most often used. A capacitive type probe consists of two conductive plates separated by a non-conductive material. The liquid surrounding the probe functions as a dielectric material, and the capacitance of the system changes as the degree of immersion of the probe changes. The capacitance of the probe, then, is a measure of the level in the primary device.

The first source of error in this type of level measuring device lies with the instrumentation used to measure the changing electrical property. Modern electronic techniques should allow the property in question to be measured with almost any desired degree of accuracy. Therefore, the size of this type of error can be controlled by the cleverness and/or design objectives of the circuit designer, and should be stated by the manufacturer. The probe itself is a second possible source of error in the system. Appreciable foam or floating oil and grease in the flow stream may build up on the probe, and could cause serious errors in most designs. This type of error can be minimized only by frequent maintenance. A probe in the flow stream can also cause disturbances to the flow which could affect the basic level-to-flow rate relationship of the primary device, in addition to being an attractive depository for all types of debris, which compounds this problem. Errors of this type can be overcome by placing the probe in a stilling well or by using a sensor which is an integral portion of the primary device.

Also, changes in the electrical properties of the flow stream itself, which are used in the electrical measurement, can introduce errors. For example, the capacitive type probe uses the flowing liquid as a dielectric medium. Numerous factors can cause the dielectric constant of the liquid to change, including temperature, presence of impurities, etc. A temperature change from 15° to 25° C will cause the dielectric constant of water to decrease approximately 5%. [5] Thus, a non-uniform dielectric medium can introduce a significant error into the level measurement system.

Manufacturer's claims of accuracy for electrical type level measuring devices are all in the range of $\pm 0.5 - 1.0\%$ of full scale level. These claims would appear to be warranted, provided the probe remains clean and the electrical property of the flow stream being measured does not vary with time.

Ultrasonic-This type of level measurement system utilizes the acoustic instrumentation principles developed for use in SONAR equipment during World War II. The liquid level is measured by determining the time required for an acoustic pulse generated by an ultrasonic transmitter to travel from the transmitter to the air-liquid interface (where it is reflected) and return to an ultrasonic receiver. The transit time of the pulse, then, is a measure of the liquid level. The transmitter and

receiver may be separate elements, or may be combined into a single transducer. As shown in Figure 4, the transmitter/receiver element may either be mounted above the flow stream, utilizing air path measurement, or mounted below the flow stream, utilizing liquid path measurement. [2]

A primary source of error in this type of level measurement system is with the instrumentation used to generate and receive the ultrasonic pulses, and to measure their transit time. There are difficult engineering problems involved with wave propagation, proper detection of the desired portion of the wave, signal-to-noise ratio problems, etc. The solutions to these problems are within the bounds of current electronic practice, but all must be carefully considered in instrument design. The accuracy of the system will be a function of the degree to which the designer has overcome these problems, and should be stated by the manufacturer. A second instrument problem results from variation in the velocity of sound. In air, the velocity of sound is mainly affected by variation in temperature; in liquids the velocity varies with temperature, pressure, and other factors. [6] Thus, an instrument measuring level using ultrasonic techniques must compensate for changes in the velocity of sound through the medium in which the ultrasonic pulses are being sent.

Other errors can result from the use of an ultrasonic measuring device in narrow channels, round pipes, or other applications with space restrictions. This could result in false echos, with a corresponding loss in accuracy. The surface of the flow stream itself can also cause problems. Foam on the surface will absorb the ultrasonic signal, and a choppy or turbulent surface could diffuse the ultrasonic pulse to the point where the return signal may not be properly detected. [7]

Manufacturer's claims of accuracy for ultrasonic type level measuring devices range from ± 0.001 ft. (for a 10 Ft. range) to $\pm 2.0\%$ of full scale level. Claims of $\pm 1.0\%$ of full scale are typical, and can probably be expected of a well designed and properly installed unit of this type.

Bubbler-In this type of level measuring device, a tube is anchored at a fixed depth in the primary device, and some type of gas is bubbled out of the tube at a constant rate, as shown in Figure 5. The pressure in the tube necessary to maintain the bubble rate corresponds to the hydraulic head of the liquid above the tube. Thus, the pressure in the tube is proportional to the liquid level in the primary device. This pressure can be measured either with a mechanical pressure sensor to provide a mechanical output or with an electronic pressure transducer to provide an electrical output, both types of outputs being proportional to the liquid level.

The primary source of error in a bubbler type level measuring system is usually connected with the device used to measure the backpressure in the bubble tube. Mechanical methods, usually consisting of a diaphragm or bellows type pressure element and a mechanical linkage, can suffer from hysteresis and non-linearity errors. Electronic methods, using various types of transducers, suffer from similar errors, with the added problems

of temperature related inaccuracies. All of these potential sources of error can be minimized or held to tolerable levels with competent pressure-measuring system design. However, there will always be a certain degree of inaccuracy present, and this should be clearly stated by the manufacturer.

Another potential problem is related to the density of the liquid in the flow stream. For any type of bubbler system, the bubble tube pressure is a function of the liquid density. Thus, if the density of the liquid changes, the indicated level will also change. An instrument system could be designed which would continuously measure the liquid density and make corrections for a changing density. However, this correction is rarely made, as the density of flow streams commonly encountered does not normally vary an appreciable amount. This potential error source should be recognized, though. [8]

If the exit end base of the bubble tube becomes appreciably reduced due to build-up of contaminants from the flow, erroneous readings will result even though the instrument may appear to be functioning normally. This problem can be overcome through periodic inspection and maintenance, and proper selection of bubble tube material.

A final possibility of error lies with the fact that the transmission of changes in the liquid level to be measured by the bubbler system may be delayed due to the effect of the charging time of the air volume in bubble tube under the liquid surface. This problem will occur if the liquid level increases at a faster rate than the gas supply can charge the bubble tube. Thus, the liquid will enter the tube through the outlet and the pressure sensing element will follow the level increase with a certain delay. [8] This error can be overcome by one of two strategies. First, by increasing the rate of gas flow and decreasing the bubble tube inside diameter the charge time can be decreased; however, this is wasteful of the gas supply. Alternatively, a level increasing faster than the charge rate can be detected electronically, and the gas flow rate momentarily increased until the bubble tube is fully charged. If one of these methods is not employed, the instrument will not respond as rapidly to rising levels as it will to falling levels, with a resultant tracking error.

Manufacturer's claims of accuracy for bubble type level measuring devices range from $\pm 1.0\%$ of full scale level to $\pm 1/4$ inch. Accuracies of $\pm 1.0 - 2.0\%$ of full scale can probably be typically expected from a well designed bubbler level detection system.

Dipping Probe-Of the five methods of level measurement discussed, the dipping probe type is probably the most recent development. In this technique, a probe mounted on the end of a cable is lowered, using a motor driven pulley, until it makes contact with the liquid surface, as shown in Figure 6. When the tip of the probe touches the surface, a microampere circuit through the liquid to a ground return is completed, and the probe is raised to a position just above the liquid surface. After a short period of time, the probe is again lowered and the cycle is repeated. In

a manner similar to a float operated device, the angular position of the cable pulley when the probe tip touches the liquid surface is a measure of the liquid level.

The dipping probe level measurement technique shares cable and pulley related error sources with float actuated systems. Changes in ambient temperature and/or humidity may cause the cable length to change, resulting in an inaccurate level indication. [7] Manufacturing inaccuracies (tolerance problems) in the diameter of the pulley around which the cable is wound will also lead to level tracking errors.

Collision with surface debris or the action of wind may cause an oscillation of the pendulum-like dipping probe, which would result in inaccurate measurement until the swinging motion subsides. It is also possible that the probe might become coated after extended periods of use, which would result in a level zero offset. [2]

Manufacturer's claims of accuracy for dipping probe type level measuring devices range from ± 0.005 ft. to $\pm 1.0\%$ of full scale level. It appears as though accuracies of $\pm 1.0\%$ of full scale can probably be expected from this type of device.

5. Level-To-Flow Rate Conversion Methodologies- Description And Error Analysis

The second of the two functions which a secondary measuring device must perform is that of converting the liquid level measured in the primary measuring device into a corresponding flow rate, according to the known liquid level-flow rate relationship of the primary device. Some of the more commonly used methods of converting level to flow rate are: mechanical cam, electronic analog function generator, electronic memory device, and opto-electronic function generator.

Mechanical Cam-The mechanical cam is probably the oldest method of accomplishing the level-to-flow rate conversion. In this method, a mechanical cam, whose profile follows the level-flow rate relationship of the primary measuring device in question, is rotated by the level measuring device to an angular position proportional to the liquid level in the primary device. The radial distance from the cam centerline to the cam follower centerline is then proportional to the flow rate, as shown in Figure 7.

The major error problem in a mechanical cam level-to-flow rate conversion system is the degree of accuracy with which the cam can be manufactured to match the level-flow rate relationship of the primary device. In any manufacturing process, there are limits to the precision with which any part can be economically made in quantity. These accuracy limits, of course, apply to the profile of a typical level-to-flow rate conversion cam, compounded by two additional factors. First, the usually non-linear, and often complex, level-flow rate relationship of most

primary measuring devices makes the manufacturing process difficult. And second, because of space limitations in the flow meter package, the cam must of necessity be relatively small, placing further limitations on its accuracy. The manufacturer should state the precision with which his cam matches the level-flow rate relationship of the primary device.

No published manufacturer's claims of accuracy for a mechanical cam level-to-flow rate conversion system could be found. However, normal accuracies of the level-to-flow rate conversion which can be expected from this type of device are probably in the $\pm 3-5\%$ range.

Electronic Analog Function Generator-In this type of level-to-flow rate conversion system, a solid state integrated circuit device is used to convert an electrical analog of the level into a flow rate analog, according to a presettable power formula. The heart of this type of system is an electronic algebraic module which essentially performs a transfer function defined by the following expression:

$$Q = KL^m$$

where: Q = flow rate

K = constant multiplier

L = liquid level

m = power

An electrical analog of the liquid level in the primary device, L , is provided by the level measuring system as an input to the algebraic module. The values of the multiplying constant K and the power m are established as reference analog signals by associated circuitry, and are usually selectable (within limits) by flow meter front panel controls. These values are selected so as to match the level-flow rate relationship of the primary device in question. The output of the module is then an analog signal proportional to the flow rate for the level input, according to the multiplier and power preset.

The major problem with electronic analog function generator type level-to-flow rate conversion systems is their inability to accurately reproduce the level-flow rate relationships of many of the commonly used types of primary measuring devices. The majority of primary devices have a level-flow rate relationship which can be expressed as a simple power function, similar to the above expression, and thus theoretically may be accurately accommodated by this type of conversion system. However, instruments using this system usually have only two or three discrete values of the power m available, for example 1.5 and 2.5. A number of primary devices have simple power formula type level-flow rate relationships, whose power is close to, but definitely different from 1.5 or 2.5. Thus, for these devices the instrument can only approximate the level-flow rate relationship of the device, with a resultant error in the conversion.

A fairly large minority of commonly used primary devices have level-flow rate relationships which do not fit a simple power function. Their level-flow rate relationships are expressed by more complex equations or by data only, and thus are not directly compatible with an analog function generator type conversion system. These types of primary devices can

be accommodated only by approximating their level-flow rate relationship with a simple power function. This, of course, necessarily leads to errors in the level-flow rate conversion.

Systems of this type also have difficult engineering problems regarding the application of the function generator module and the associated electronics. First, there is a certain amount of inherent inaccuracy in the accomplishment of the transfer function, an inaccuracy which may be compounded by improper electronic system design. [9] There are also problems associated with temperature sensitivity and long term stability of the module and of the analog references which establish the values of K and m . Proper design can minimize these errors, but they will always be present to a certain extent, and should be so stated by the manufacturer.

Again, no published manufacturer's claims of accuracy for an electronic analog function generator type level-to-flow rate conversion system could be found. However, for primary measuring devices having a simple power formula type level-flow rate relationship with a power exactly matching one found on the instrument, conversion accuracies of $\pm 1-2\%$ can probably be attained. For other primary devices whose level-flow rate relationships have to be approximated, conversion accuracies in the $\pm 3-6\%$ range would seem reasonable.

Electronic Memory Device-In this type of level-to-flow rate conversion system, a large scale integrated circuit memory device is programmed such that for a given level input, the output of the device is the flow rate corresponding to that level. The type of memory device most often used is a programmable read only memory (PROM). The PROM is programmed by the manufacturer with the level-flow rate relationship of the primary measuring device in question. The level measuring device supplies to the PROM a digital code representing the level in the primary device. The PROM is essentially a look-up table, in which each digital liquid level value has a corresponding flow rate value. Thus, for a given digital level input, the output of the PROM is a digital code for the flow rate corresponding to that level.

A PROM type level-to-flow rate conversion system does not have any actual "error" associated with the memory device; that is, for a correctly programmed PROM, a given level input will always result in the pre-programmed flow rate as an output. However, there are flow rate resolution problems. The inputs to the PROM are normally based on equal increments of liquid level, the outputs usually being the flow rate value corresponding to the level at the midpoint of the level increment. Because of the exponential nature of most primary measuring device level-flow rate relationships, equal level increments will result in nonequal flow rate increments, the flow rate increments for each level increment becoming increasingly larger at higher level values. Thus, the majority of the flow rate range will be contained within a minority of the level range, and vice versa. This results in a decreased resolution of the flow rate for higher level values.

The PROM's normally used in this type of instrumentation have 256 level-flow rate pairs (words), meaning that the level will be resolved

into 256 equal increments. Manufacturers commonly state for PROM's of this size that ". . .the level-flow rate function is accurate to better than 0.4%". What they actually mean is that the level resolution is better than 0.4% (1 part in 256). At low levels, the flow rate resolution is better than 0.4%; at high levels it is worse than 0.4%. Thus, the resolution of the flow rate (which is, after all, the desired quantity) varies over the level range and is much worse than the stated 0.4% at higher level ranges. In general, of course, the larger the PROM, the better the flow rate resolution.

Opto-Electronic Function Generator-In this final type of level-to-flow rate conversion system, a disk which has been optically coded with the level-flow rate relationship of the primary measuring device in question is used to accomplish the level-flow rate conversion. The coded disk (see Figure 8) is rotated to a level proportional angular position by the level measurement system. The disk is divided into a number of angular increments, the angles representing equal increments of flow rate (not equal increments of level). Each angular flow rate increment on the disk has its own numeric coded value corresponding to a flow rate value for that particular angular increment. An optical sensor electronically reads the coded flow rate value corresponding to the measured level, and transmits this value to further decoding and processing circuitry. Thus, liquid level is converted into a corresponding coded flow rate value by the interaction of the disk and the optical sensor.

The major problems of an opto-electronic function generator type level-to-flow rate conversion system are associated with the degree of accuracy with which the information can be encoded on the disk, and the degree of accuracy with which the instrument can read the information from the disk. The angular bands of flow rate information must be optically encoded on the disk by the manufacturer. There is a certain amount of inaccuracy inherent in the encoding process, which will be reflected by inaccuracies in the level-flow rate relationship recorded on the disk. There will also be errors resulting from the detection of the coded bands by the optical sensor. Both of these errors will affect the accuracy of the level-flow rate conversion.

The manufacturer of this type of device claims a level-to-flow rate conversion precision of $\pm 0.05\%$ of full scale flow rate for a 0.2% flow rate resolution device (1 part in 512). These claims would appear to be justified.

6. Flow Meter Accuracy Specifications

Various methods of accomplishing each of the two basic functions of an open channel flow meter have been discussed separately, along with the accuracies which might be expected from each. Any of the level measurement methods may be combined with any of the level-to-flow rate conversion methods to form a complete, functional flow meter. The temptation here is to combine level measurement accuracies with level-to-flow rate conversion accuracies, in an attempt to obtain a comprehensive flow meter

accuracy. Such a combined accuracy would not, however, be truly reflective of the situation, due to the non-linear relationship of liquid level and flow rate for most primary measuring devices. Errors in the liquid level are usually not reflected by equal errors in the flow rate, and a linear error in the level-to-flow conversion process often leads to non-linear (with respect to level) flow rate errors. Thus, it is usually better practice not to combine the two flow meter functions, but rather to specify the accuracy of each separately.

With this in mind, the following standard general format is proposed for open channel flow meter accuracy specifications. The format is proposed in the interest of promoting a uniformity of specifications to aid prospective users. This is, of course, only a general format, and certain categories may have to be added or deleted, dependent upon the design of the particular flow meter in question.

A. LEVEL MEASUREMENT

1. Accuracy: The accuracy of the level measurement system should be stated. May be combined total error or may be broken down to indicate linearity, hysteresis, repeatability, sensitivity, etc., errors separately. May be stated as an absolute level error, or error as a percentage of full scale level.
2. Temperature Error: Both the magnitude and applicable temperature range of any temperature related errors should be stated as error per unit of temperature.
3. Resolution: Any level resolution limitations inherent in the system should be stated, along with the resolution of the liquid level indication device (if applicable).

B. LEVEL-TO-FLOW RATE CONVERSION

1. Accuracy: The accuracy of the level-to-flow rate conversion system should be stated. Usually to be stated as a percentage of full scale flow rate.
2. Temperature Error: As Above.
3. Resolution: Any resolution limitations inherent in the system should be stated. Also to be stated is whether the limitation deals with input (level resolution) or output (flow rate resolution.)

A review of product literature revealed that many manufacturers currently state flow meter accuracies in a manner quite similar to the above proposed format. However, many manufacturers utilize a different format in quoting the accuracies of their respective instruments. In any case, typically a manufacturer's accuracy specifications are written in such a way as to emphasize the strong points of their instrument and de-emphasize any weak points. There is nothing untruthful or dishonest in this practice; it is simply an outgrowth of a competitive marketplace. However, a prospective purchaser and user of flow measuring instrumentation has the right to know the accuracy specifications of the instrument, in terms he can understand and which relate to his particular application. Most flow meter manufacturers are more than willing to discuss accuracy specifications, and a prospective customer should not be hesitant to ask the manufacturer exactly what his specifications mean in relation to

the prospective application. A flow meter is usually a fairly significant investment, and the user should know what he is paying for in terms of accuracy. While a user should not have to pay for more accuracy than the application demands, the flow meter should provide the accuracy required to supply meaningful results.

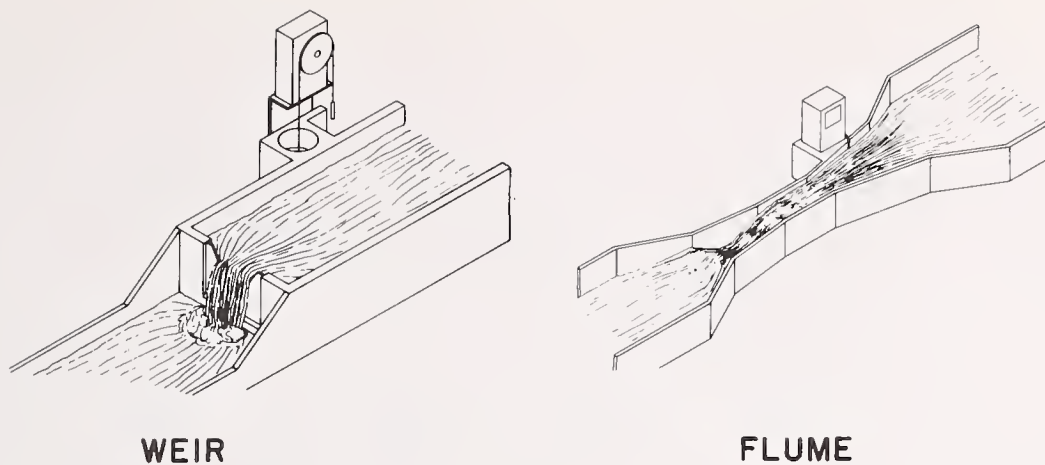
7. Conclusion

Instrumentation errors in open channel flow measurement systems have been discussed. While the errors associated with secondary (and primary) measuring devices are, of course, of vital concern in controlling the accuracy of an open channel flow measurement system, probably of equal concern should be the sizing of the system to minimize the effect of the errors associated with the measuring instrumentation. The accuracy tolerance of a flow meter is usually specified as a percentage of a full scale quantity, this being the position where the factors contributing to the error are most controllable. As the quantity being measured decreases, the possible error as a percentage of the actual reading increases. Consider, for example, a level measurement system which has a specified accuracy of $\pm 1\%$ of full scale for a 0 to 1.0 ft. level range. The potential maximum error at any position will then be ± 0.01 ft. At a 1 ft. level, the maximum error as a percentage of the reading will be 1 percent ($0.01 \text{ ft.}/1.0 \text{ ft.}$). However, if the level decreases to 0.2 ft., the maximum error as a percentage of the reading will increase to 5 percent ($0.01 \text{ ft.}/0.2 \text{ ft.}$). Thus, as is typical with many instrument systems, the user is advised to keep the magnitude of the quantity being measured as high up on the full scale range as possible.

This can be accomplished by proper selection and sizing of primary and secondary measuring devices. The primary device should be sized such that it generates as large a level as is practical for the flow rate expected. A nontraditional primary device, such as a combination of a V-notch and rectangular weir, may be employed to assure an acceptable level over a wide range of flow rates. The secondary device should be selected such that the anticipated levels in the primary device are well up in the liquid level range of the secondary device. In this manner, the effect of possible errors in the flow rate being measured can be minimized. This runs contrary to the popular practice of oversizing primary and secondary devices to allow for future expansion, a practice, however, which should be avoided if errors are to be minimized.

References

1. United States Department of Interior, Bureau of Reclamation, Water Measurement Manual, Second Edition, Superintendent of Documents, U.S. Government Printing Office, Washington, D.C. (1967).
2. Shelley, Philip E., and Kirkpatrick, George A., Sewer Flow Measurement-A State-of-the-Art Assessment, Environmental Protection Technology Series No. EPA-600/2-75-027, National Technical Information Service, Springfield, Va. (1975).
3. Kulin, Gershon, and Compton, Philip R., A Guide to Methods and Standards for the Measurement of Water Flow, National Technical Information Service, Springfield, Va. (1975).
4. Mougnot, G., 'Measuring Sewage Flow Using Weirs and Flumes', Water & Sewage Works, July 1974, pp 78-81.
5. Hodgman, Charles D., ed., Handbook of Chemistry and Physics, 43rd Edition, The Chemical Rubber Publishing Co., Cleveland, Ohio (1961).
6. Baumeister, Theodore, ed., Mark's Standard Handbook for Mechanical Engineers, 7th Edition, McGraw-Hill Book Company (1967).
7. Schontzler, Gordon J., 'Fact Sheet on the Use of Ultrasonic and Dipping Probe Flowmeter Application', Manning Environment Corp., Santa Cruz, Calif.
8. Buzay, K., 'Pneumatic Level and Open Channel Flow Measuring Systems', Water Resources Instrumentation, Vol. 1, Krizek, Raymond J., ed., Ann Arbor Science Publishers, Inc. Ann Arbor, Mich. (1974).
9. Sheingold, Daniel H., ed., Nonlinear Circuits Handbook, Analog Devices, Norwood, Mass. (1974).



WEIR

FLUME

Figure 1 - Primary Measuring Devices.

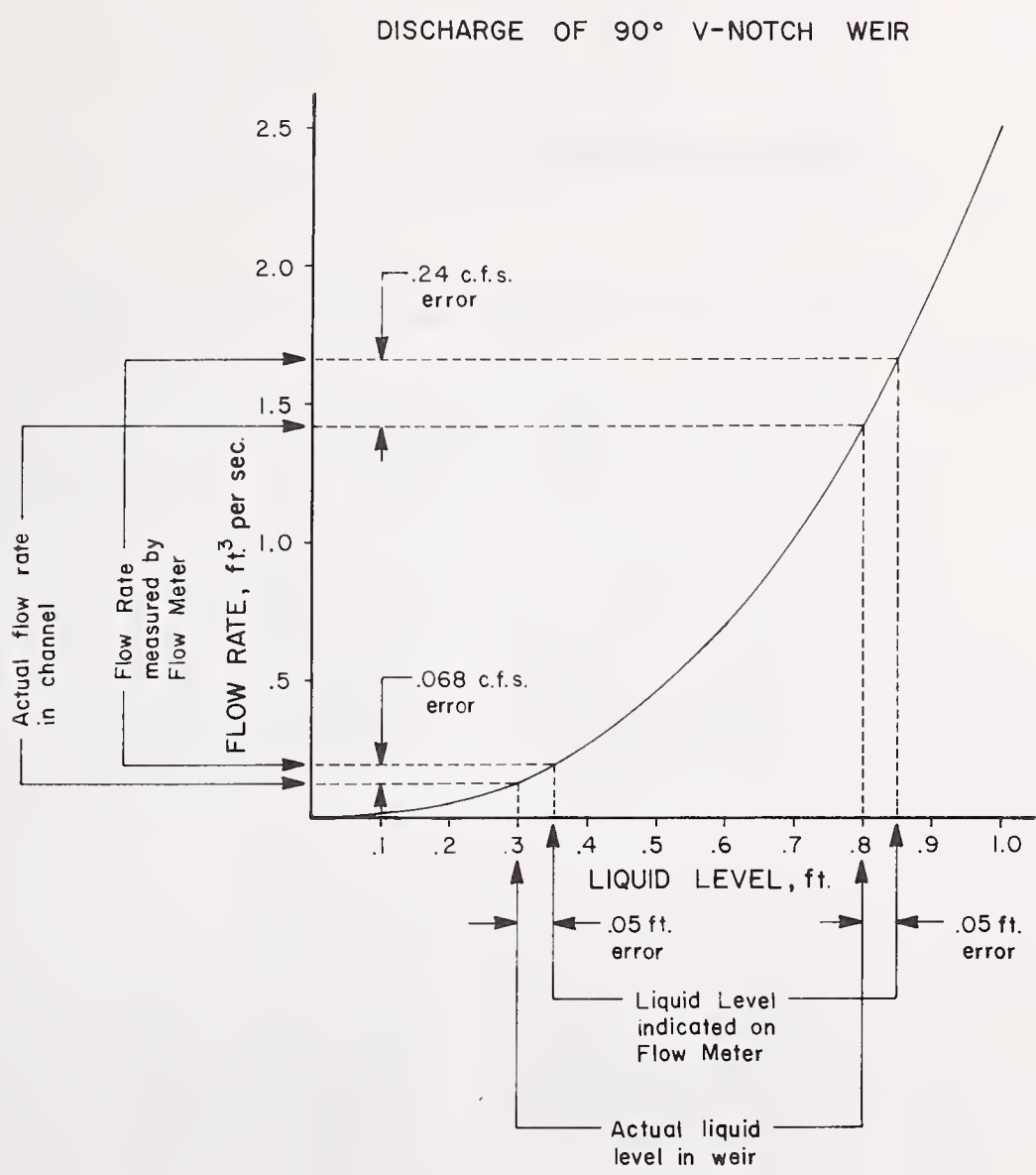


Figure 2 - Flow Meter "Zero" Errors.

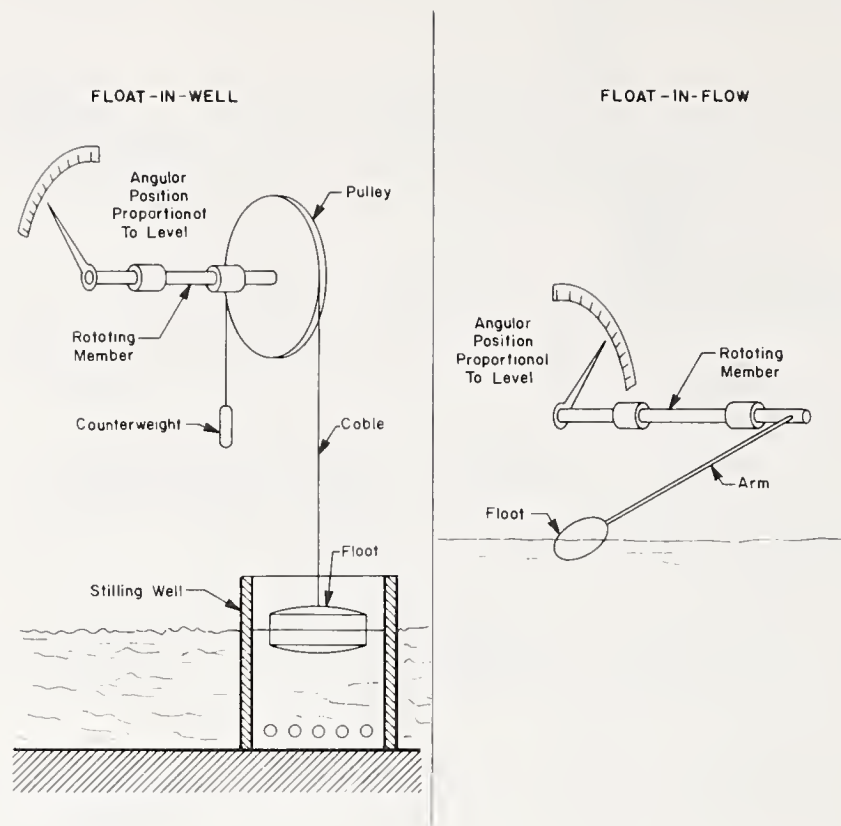


Figure 3 - Float Operated Level Measurement Device.

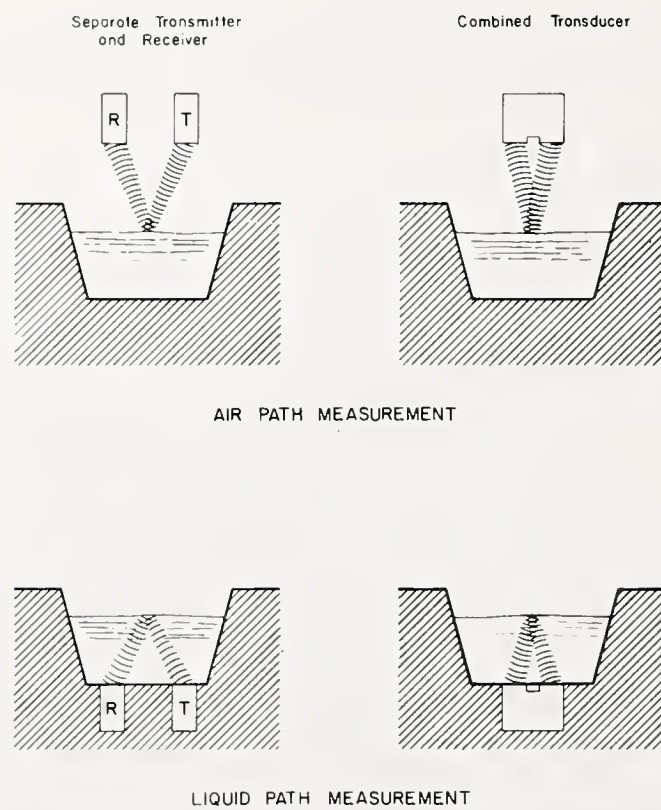


Figure 4 - Ultrasonic Level Measurement System.

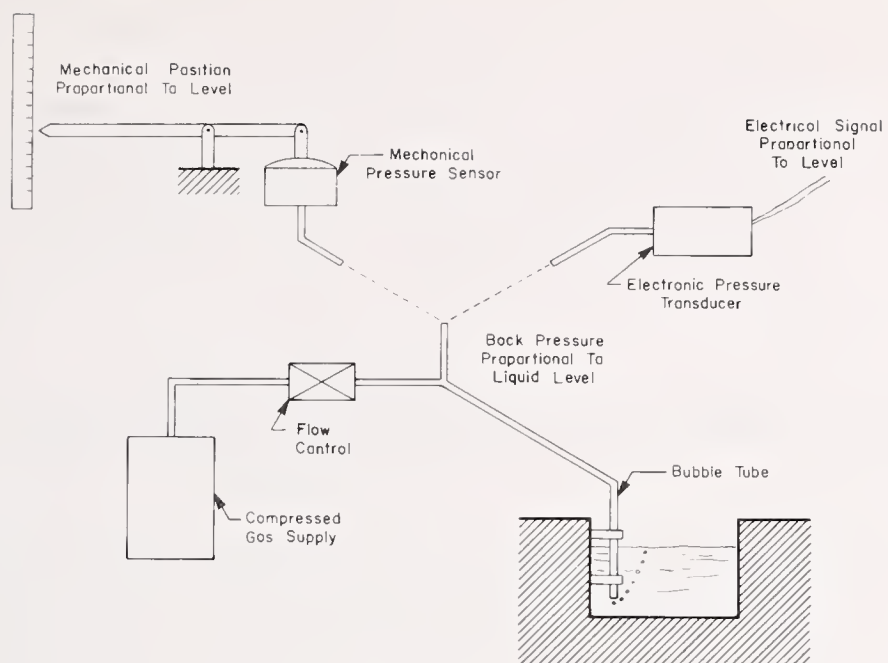


Figure 5 - Bubbler Level Measurement System.

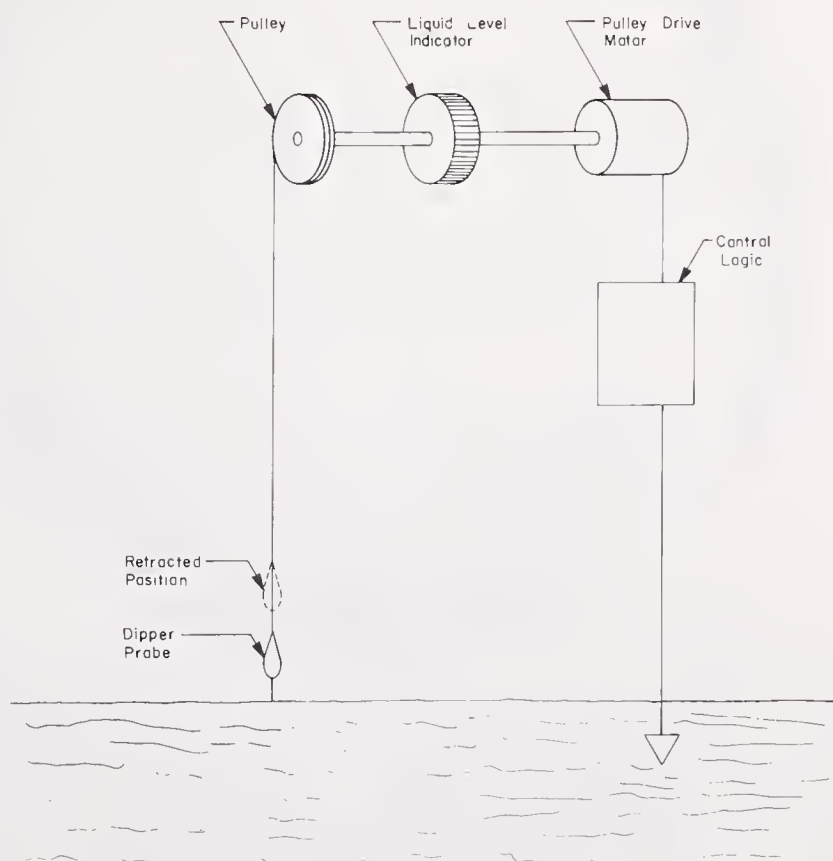


Figure 6 - Dipping Probe Level Measurement System.

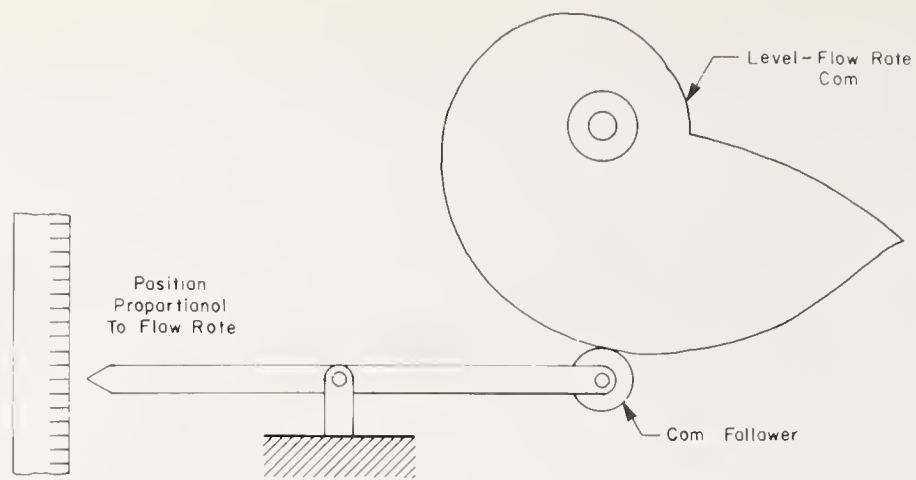


Figure 7 - Mechanical Cam Level-to-Flow Rate Conversion System.



Figure 8 - Opto-Electronic Function Generator Level-to-Flow Rate Conversion System.

MARINE DYNAMICS AND ITS EFFECTS ON CURRENT MEASURING TRANSDUCERS

Thomas Mero and Gerald Appell

Test and Evaluation Laboratory (T&EL)
National Oceanic and Atmospheric Administration

and

Raul S. McQuivey
Sutron Corporation
1925 North Lynn Street
Arlington, Va.

A growing interest in measuring current velocities in coastal zone and estuaries prompted the creation of a Dynamic Analysis Program at T&EL (formerly NOIC). The dynamics of near-shore current flows are more severe than that of the deep ocean. Therefore, it is important to qualify the performance of current measuring transducers in a dynamic environment. A study was contracted to determine what scales and intensities of turbulence exist in the near-shore environment. The major effort of the study is concerned with turbulence from 1 to 20 Hz and scales up to 30 cm.

Tests are being conducted to determine the response characteristics of several current measuring transducers including both rotor and electromagnetic instruments. These tests include grid-produced turbulence measurements as well as simulated mooring-line dynamics' tests. Measurements have revealed several transducers that have 10 to 20% sensitivity increases when turbulence intensities of 6 to 12% are present.

This paper contains a description of turbulence that exists in the marine environment along with dynamic response characteristics of several current measuring transducers.

INTRODUCTION

A growing concern about the preservation and management of our marine resources has precipitated the need for a more complete understanding of the physical, chemical, and biological processes in the marine environment. The estuarine and coastal zones are of particular interest because they are the receiving bodies for disposal of large

amounts of solid and liquid wastes, excess heat and many other chemical and radioactive materials. Understanding how pollutants are transported and how they affect the marine environment requires accurate, reliable instrumentation for measurement of mean and fluctuating flow characteristics.

The Test and Evaluation Laboratory (T&EL) formerly the National Oceanographic Instrumentation Center (NOIC) is involved in the calibration and testing of current measuring systems. Recognizing the lack of information available on the dynamic response characteristics of current measuring transducers and systems, T&EL established a laboratory testing program in 1975 to evaluate the effects of both large scale dynamics, i.e., wave generated and small scale (high frequency) turbulence. Preliminary results indicated some electromagnetic type flow sensors were biased by nearly 15 percent of actual flow velocity when certain scales and intensities of turbulence were present. Large scale dynamics created errors of over 50% of actual velocity on rotor-vane type instrumentation. T&EL expanded its dynamic analysis program in 1976 in an effort to better understand the range of dynamics present in the marine environment and to quantify their effect on current measuring transducers.

Sutron Corporation was awarded a contract to study marine environmental dynamics. A major objective of the study was to conduct a literature search to identify the mean and fluctuating flow measurements which have been made in describing the marine environment and to determine a realistic range of natural environmental dynamics. This information would then be utilized in establishing the relevancy of the dynamic test program and in the development of realistic laboratory simulation methods.

The following is a description of marine environmental dynamics as indicated from the study and laboratory simulation tests which have been conducted at T&EL to describe current measuring transducers performance in the dynamic environment.

THE MARINE ENVIRONMENT

The marine environment can be divided into three regions or zones: the estuarine zone, the coastal zone, and the deep ocean. It was attempted in the study to quantify a realistic range of environmental dynamics in each of these regions by summarizing the mean and fluctuating velocity measurements that have been reported in the literature. Each region experiences particular scales of dynamic behavior which are primarily dependent on environmental factors. A brief description follows of the flow structure in each region along with a range of environmental dynamics obtained from the literature review.

Estuarine

Estuarine flow structure is generated by many natural forces creating complex patterns of motion. In describing this flow structure,

the important characteristics to be considered are:

1. The cyclical rise and fall of the water surface which results from ocean tides and the periods of these tidal waves;
2. The geometry of tidal estuaries and the rise and fall of the tide at the mouth, which results in an exchange of water masses through the entrance with large amounts of sea water temporarily stored in the estuary during high tide;
3. The state of diffusion of fresh water to salt water;
4. The variation of salinity over the depth and the resulting internal density currents;
5. Surface waves and currents.

Estuarine flow dynamics are largely two-dimensional in nature with each estuary having distinct characteristics depending on location and geometry. Table 1 summarizes the range of environmental dynamics obtained from the literature review.

Coastal Zone

Coastal zone processes are important in designing coastal structures, understanding the stability of a coastline, and evaluating the effects of pollution on the coastal environment. The currents in the coastal zone are extremely complex, with wind-induced currents a primary source of energy.

An attempt at briefly describing the coastal circulation process follows. Coastal currents flow roughly parallel to the shore constituting a relatively uniform flow in the deeper water adjacent to the surf zone. A near-shore current system may be superimposed on the inner portion of the coastal current or, in the absence of a coastal current may exist independently. The near-shore system is associated with wave action in and near the breaker zone and consists of shoreward mass transportation of water caused by wave motion, movement of the water parallel to the coast as longshore currents, or seaward return flows (rip currents). In some cases local currents result in the near-shore area where water from rivers and nearly enclosed bays is discharged into the ocean with considerable momentum.

By comparison with the other zones, the coastal zone probably has more energy in the small-scale structure (turbulence) because of its three-dimensional dynamics and high intensities. Literature indicates that investigators are taking measurements of currents in the coastal zone with instrumentation that is not capable of responding to the three-dimensional dynamics. Many investigators are not aware of the problems associated with taking reliable/accurate measurements in the coastal zones. A summary of a range of dynamics obtained from a literature review is presented in Table 2.

Table 1. Estuarine Environmental Dynamics

<u>Characteristic</u>	<u>Fresh Water</u>	<u>Saline Water</u>
Currents (cm/sec)	0 to 500 cm/sec	0 to 500 cm/sec
Intensity of Turbulence (percent) $\frac{\sqrt{\overline{u^2}}}{\overline{U}}$	5 to greater than 50	5 to greater than 50
Scales: Tides (m)	10^3 to 10^5	10^3 to 10^5
Wind	1 to 10	1 to 30
Macro	1 to 10	1 to 10
Micro	0.01 to 0.1	0.01 to 0.1

Table 2. Coastal Environmental Dynamics

<u>Characteristic</u>	<u>Range</u>
Currents (cm/sec): Coastal	Up to 60
Longshore	Up to 50
Rip	Up to 75
Wave Induced	Up to 25
Intensity of Turbulence (percent) $\sqrt{\frac{\overline{u^2}}{\overline{U}}}$	5 to greater than 50
Scales (m): Tide	10^3 to 10^5
Wind	1 to 25
Macro	1 to 10
Micro	0.01 to 0.1

Deep ocean flow structure is generated by a variety of natural forces acting to keep the ocean in a continual, complex pattern of motion. Ocean currents can be categorized into several groups, one of which is currents related to the distribution of density in the sea. This class of currents include large-scale ocean current such as the Gulf Stream, the Kuroshio, and the equatorial currents. Wind stress on the sea surface directly causes currents, which in turn tend to alter the density distribution; tidal currents and those associated with internal waves are also present. In describing general oceanic flow structure, the ocean can be divided into: (a) the mixed surface layer, (b) the thermocline and interior layer, and (c) the bottom layer. The dynamics associated with the mixed layer is three-dimensional in nature while the thermocline and interior layer, and the bottom layer contain largely two dimensional dynamics. The range of environmental dynamics associated with these layers as indicated in the literature is summarized in Table 3. Considerable variation in these dynamics should be expected depending on location.

DYNAMIC PERFORMANCE TESTING OF CURRENT-MEASURING TRANSDUCERS

T&EL's Dynamic Analysis program was established to describe the dynamic performance of current-measuring transducers by first developing laboratory simulation methods. Dynamics in the marine environment has been categorized in the program into two groups: (a) turbulence being that from 1 to 10 Hz with length scales up to 10 cm, and (b) macroscale dynamics which describe motions from 0.05 Hz to 1 Hz with length scales greater than 10 cm.

Turbulence

T&EL's submerged jet facility at the Washington, D.C., Navy Yard is being used extensively in turbulence investigations. The mean flow turbulence intensity of the facility is less than 1 percent over its operating range of 0.5 to 200 cm/sec. Screens of various sizes are inserted at the outlet of the jet to produce turbulence with intensities up to 10 percent of mean flow. A Delft miniature propeller meter and a Disa hot-film system are being used as flow measurement standards.

Tests conducted on an Aanderaa rotor-type current measuring transducer found it to be largely unaffected by the turbulence generated in the facility. The rotor acted as a low-pass filter, averaging the small-scale velocity fluctuation. Mean flow measurement errors were generally less than 2 percent.

Several electromagnetic current meter (EMCM) sensors have been studied. A cylindrical EMCM sensor was tested having a 2.5 cm diameter with extended electrodes. Two spherical EMCM sensors having extended electrodes with a 1-cm diameter and a 3.8-cm diameter, respectively were evaluated.

Table 3. Deep Ocean Environmental Dynamics

<u>Characteristic</u>	<u>Mixed Surface Layer</u>	<u>Thermocline & Interior Layer</u>	<u>Bottom Layer</u>
Current Velocity (cm/sec)	Up to 250	Up to 250	Up to 25
Intensity of Turbulence (percent) $\frac{\sqrt{\overline{u^2}}}{\overline{U}}$	5 to greater than 5	1 to 5 (variable)	1 to 5
Scales: Tide (m)	10^3 to 10^5	10^3 to 10^5	
Wind	1 to 25	5 to 50	
Macro	1 to 10	1 to 25	
Micro	0.01 to 0.1	0.01 to 0.1	
Depth (m)	Up to 100	0 to 600	Below 100

A streamlined elliptical EMCM sensor of French design and an "open" design EMCM sensor developed by J. R. Olson of the Naval Undersea Center (NUC) were included in the testing. The "open" sensor utilized a Helmholtz coil design with its electrodes mounted in the center of the coil.

The operation of EMCMs is based on Faraday's law of electromagnetic induction. An electromagnetic field is generated, and as water (an electrical conductor) moves perpendicular to the magnetic flux lines an electromotive force (potential) is generated. Orthogonal electrode pairs sense two voltage components that define the magnitude and direction of the water velocity in a plane perpendicular to the magnetic field. The magnetic field strength diminishes as the square of the distance from the magnet; therefore, the largest electrical potential is produced closest to the surface of the transducer.

Mean flow measurement errors detected when turbulence scales of approximately 2 cm with intensities of 4 percent were introduced are shown in Figure 1. All the EMCM sensors tested but the small spherical and the "open" EMCM sensor indicated a positive averaging error of greater than 2%. These errors are believed the result of a disturbance in the boundary layer flow around the probes introduced by the presence of turbulence in the flow. The small spherical probe was relatively unaffected. It is conjectured that the probe size is small with respect to the scales of turbulence; therefore, the boundary layer flow was not significantly affected. The "open" design EMCM sensor was also unaffected because it measures free stream velocity and produces, by design, no boundary effect.

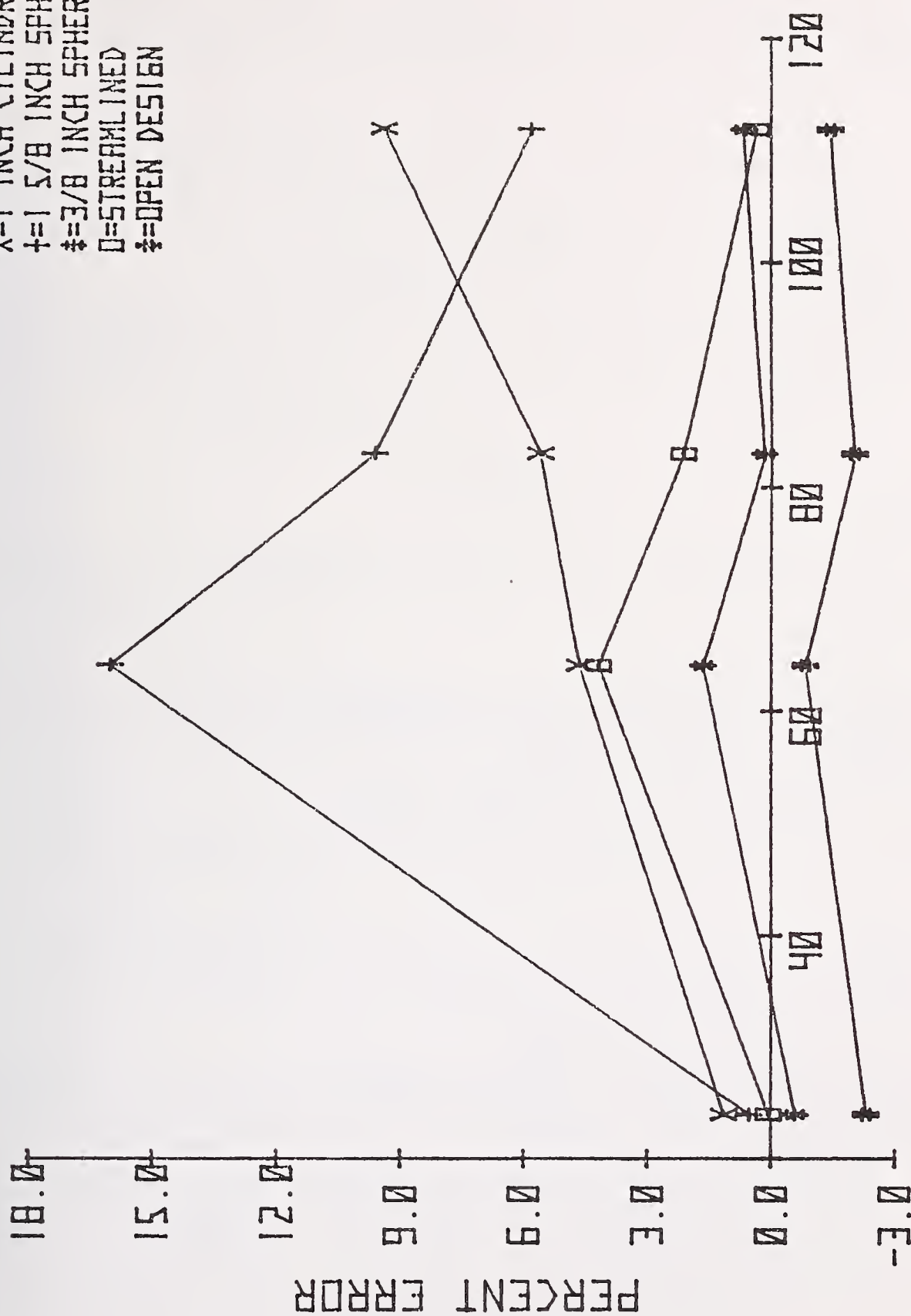
Investigations are continuing in an effort to more fully understand the dynamics of boundary layer flow and its resulting effects on EMCM sensors, and at improving laboratory simulation methods.

Macroscale Dynamics

Current measuring systems in the marine environment encounter macroscale dynamics from water partical motions and from system platform motions. In an effort to define the large-scale dynamic response of current-measuring systems in the laboratory, T&EL contracted the design and fabrication of a dynamic test apparatus to the Naval Ship Research and Development Center (NSRDC). The apparatus mounts on the No. 1 tow carriage at NSRDC and can produce nearly sinusoidal motions in the horizontal and vertical plane and circular motion in the vertical plane. These motions are generated while the tow carriage is underway, thereby simulating wave generated water partical motion or mooring line and platform-induced motions on current meter systems.

A 10-cm diameter spherical EMCM Marsh McBirney MMI-555, Aanderaa RCM-4 rotor type meter and a General Oceanics (G.O.) Model 2010 drag force type meter were selected as representative instruments for testing.

X=1 INCH CYLINDRICAL
 +=1 5/8 INCH SPHERICAL
 *=3/8 INCH SPHERICAL
 O=STREAMLINED
 ‡=OPEN DESIGN



MEAN FLOW SPEED (CM/SEC)

Figure 1. Turbulence effect on EMC; T&EL submerged jet facility. Turbulence scale \approx 2 cm, 4% intensity.

Test data from the Aanderaa and G.O. current meters were of limited value since only speed was sampled from these instruments precluding a vector analysis. However, test conditions in which the mean flow velocity exceeds the angular velocity of the sensor are valid measurements of vector magnitude and indicate significant over register from both meters. Analysis of motion picture films show unresponsiveness of the Aanderaa to high frequency and reversing type flows. The G.O. meter was more responsive to dynamics and yet, it became unstable under high-frequency oscillations.

The MMI-555 measures two components of the flow; therefore, a vector analysis was performed comparing the system input vector with the instrument output vector. Test results from averaging 100 data samples acquired at 2 per second are summarized in Table 4. Real-time vector analysis was also performed and sensor response to 32 cm/sec and 77 cm/sec orbital velocities are shown in Figures 2 and 3, respectively. A 1-second phase shift and attenuation at high orbital velocities results from the instrument's internal time constant. The MMI-555 was able to measure mean flow in the presence of the simulated large scale dynamics with errors generally below 4 cm/sec.

SUMMARY

The literature search conducted by Sutron Corporation confirmed that both micro and macroscale dynamics are present in the marine environment.

Laboratory tests conducted to define dynamic response characteristics of various current measuring transducers indicated that the electromagnetic sensors tested, accurately measured mean flow in the presence of macroscale dynamics with errors generally less than 4 cm/sec. However, microscale turbulence cause significant positive averaging errors in certain EMCM sensors. The rotor tested was relatively immune to microscale turbulence errors and yet, it over registered by over 18 cm/sec when subjected to macroscale dynamics.

Additional investigation is required in the form of improved laboratory simulation of marine dynamics as well as field measurements to verify the significance of laboratory test techniques.

Understanding both the dynamics of the environment and the response of various current sensors to those dynamics will enable investigators to select sensors and platforms which are best suited for each particular application.

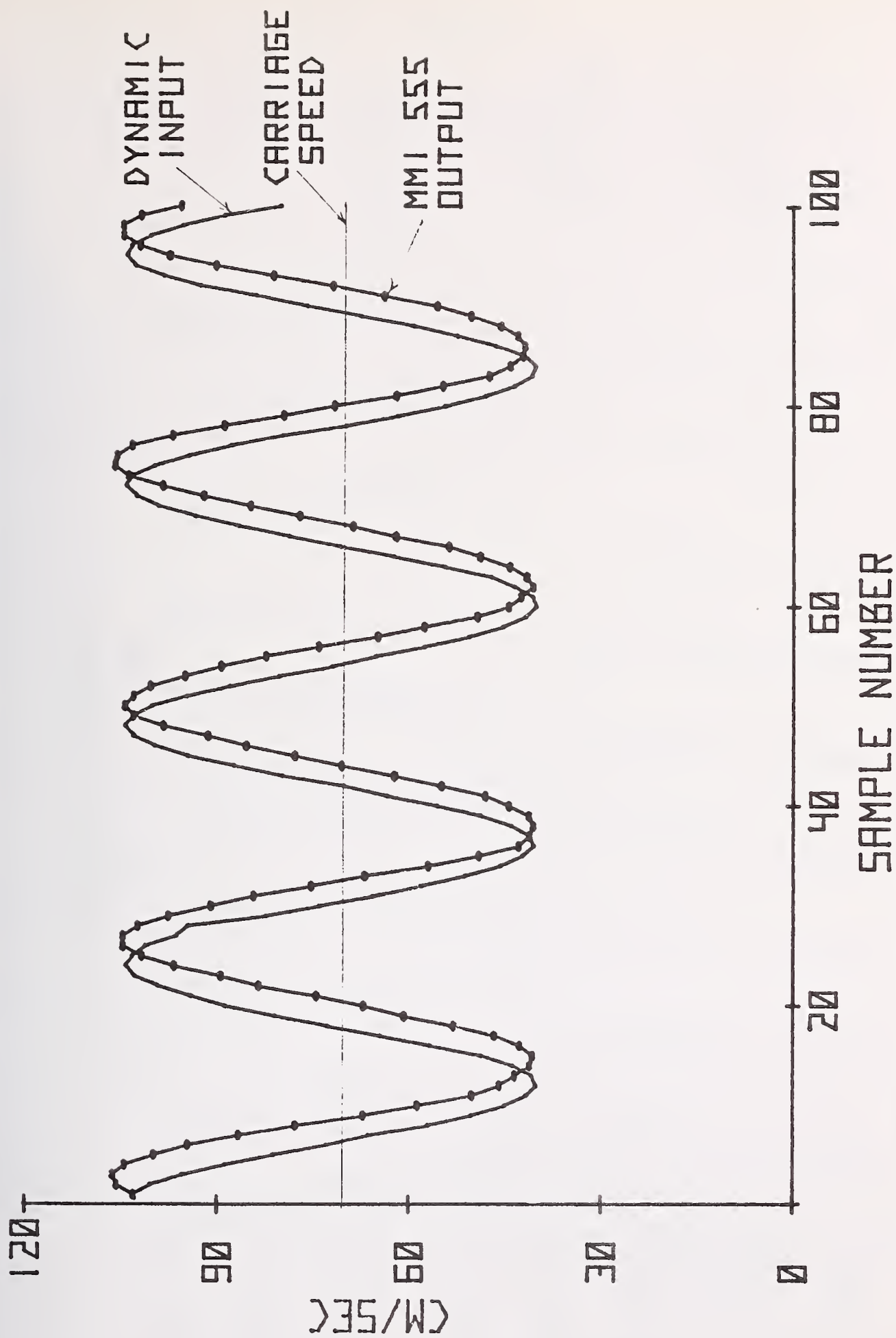


Figure 2. Dynamic test results utilizing the Dynamic Test Fixture. Displayed are the actual data samples taken during tests at 72 cm/sec carriage speed, 0° orbital velocity angle, and 32 cm/sec orbital velocity.

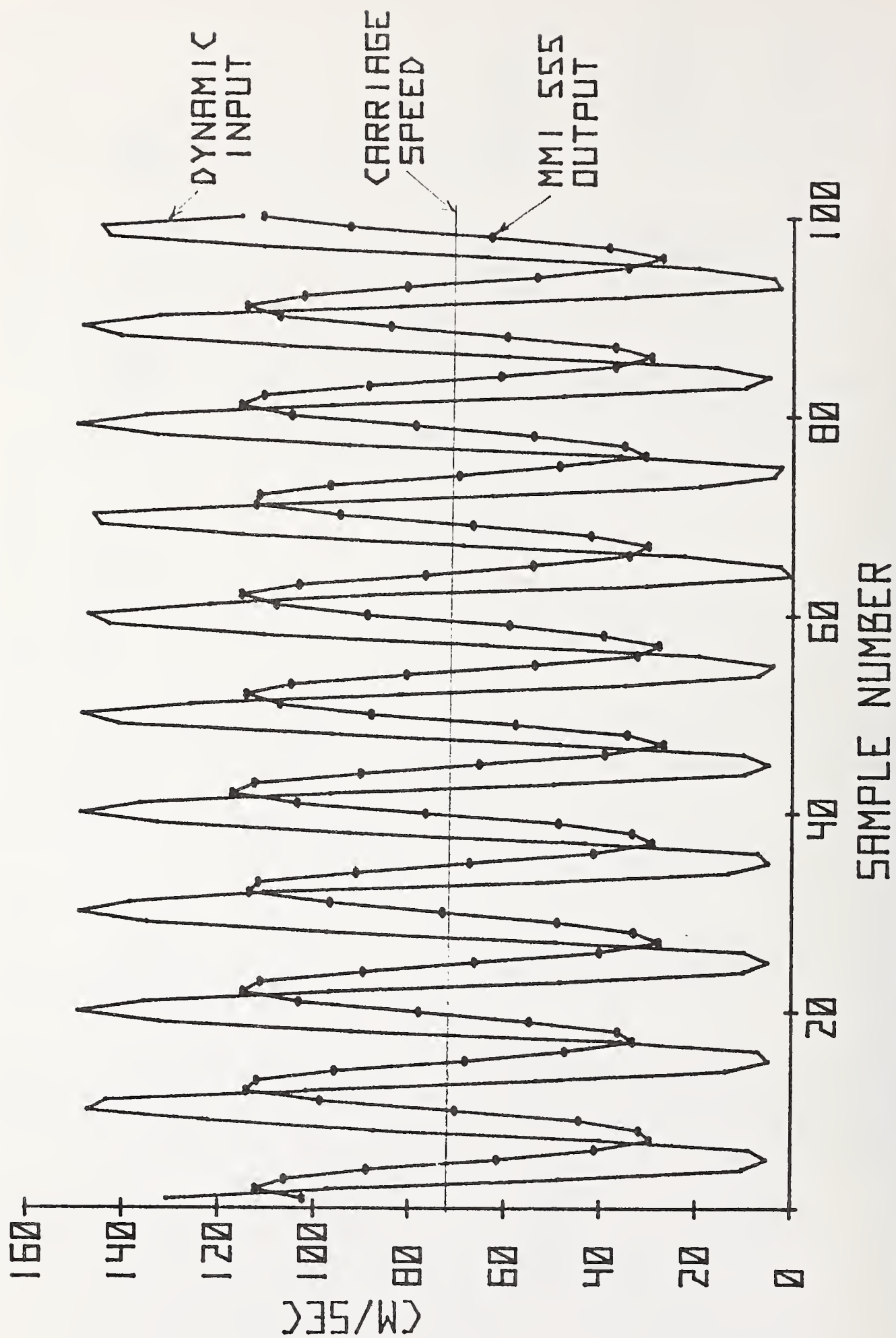


Figure 3. Dynamic test results utilizing the Dynamic Test Fixture. Displayed are the actual data samples taken during tests at 72 cm/sec carriage speed, 0° orbital velocity angle, and 77 cm/sec orbital velocity.

REFERENCES

1. Unpublished Report, "Mean and Fluctuating Measurements in the Marine Environment" by Raul S. McQuivey, Phd., Sutron Corporation, 1925 North Lynn Street, Arlington, Virginia.
2. Appell, Gerald F., "Evaluating the Performance of Flow Measuring Instrumentation", Plessey STD/Ocean Systems Conference, San Diego, California, January 19-21, 1977.
3. Bennett, George and Graham Wells, "Flow Improvement Modifications and Flow Quality Evaluation of the NOIC Current Meter Calibration Facility", Prepared by Engineering and Industrial Research Station, Mississippi State University, for National Oceanographic Instrumentation Center, NOAA, Department of Commerce, Report Number EIRS-ASE-75-2, April 1975.

Table 4
MMI MODEL 555
DATA SUMMARY OF THE DYNAMIC TEST RESULTS
STROKE AMPLITUDE = 122 CM NSRDC 7/21/76

FLOW CM/SEC	PERIOD SEC	ORBITAL VELOCITY CM/SEC	MMI 555 OUTPUT CM/SEC	SPEED ERROR CM/SEC	% SPEED ERROR CM/SEC
ORBITAL MOTION = INTO THE FLOW					
10.52	12	32.00	13.51	2.99	28.42
10.52	8	47.56	15.51	4.99	47.43
10.38	5	78.86	19.16	8.78	84.59
36.12	12	32.01	37.40	1.28	3.54
36.10	8	47.60	40.06	3.96	10.97
36.55	5	77.32	41.05	4.50	12.31
72.23	12	32.00	73.56	1.33	1.84
72.35	8	47.64	70.91	-1.44	-1.99
72.20	5	77.40	71.90	-0.30	-0.42
ORBITAL MOTION = 45 DEGREES TO THE FLOW					
10.67	12	32.04	11.86	1.19	11.15
10.62	8	47.65	13.19	2.57	24.20
10.39	5	76.98	14.85	4.46	42.93
36.60	12	32.07	35.75	-0.85	-2.32
36.26	8	47.76	39.06	2.80	7.72
36.16	5	77.26	38.40	2.24	6.19
72.23	12	32.08	72.90	0.67	0.93
72.23	8	47.85	69.91	-2.32	-3.21
72.25	5	77.08	70.90	-1.35	-1.87
ORBITAL MOTION = 90 DEGREES TO THE FLOW					
0.00	12	32.10	5.89	5.89	0.00
0.00	8	47.74	8.87	8.87	0.00
0.00	5	76.94	13.85	13.85	0.00
10.87	12	32.12	13.85	2.98	27.41
10.24	8	47.81	13.52	3.28	32.03
10.49	5	77.09	14.18	3.69	35.18
36.29	12	32.12	37.74	1.45	4.00
36.42	8	48.78	38.40	1.98	5.44
36.45	5	77.12	38.40	1.95	5.35
72.04	12	32.11	72.24	0.20	0.28
72.76	8	48.48	71.90	-0.86	-1.18
72.84	5	77.20	71.57	-1.27	-1.74

SOME ERROR SOURCES IN PRICE AND PYGMY
CURRENT METER TRAVERSES

Gershon Kulin

Mechanics Division
National Bureau of Standards

Some performance characteristics and effects of methods of calibration and use of Price and Pygmy water current meters are examined with emphasis on their application to velocity-area traverses for flowrate determination. The limits of applicability of group rating equations relative to individual ratings are discussed using available calibration data. The repeatability of meter performance at low velocities, $0.1 < V < 0.5$ ft/s ($3.0 < V < 15.2$ cm/s),¹ is investigated. The effect of cable-and-weight suspension relative to rod suspension of Price meters is examined experimentally and analytically for Columbus and Elliptic weights. Errors due to lateral velocity gradients and bottom and sidewall proximity effects on both types of meters are also investigated.

Key words: Current meter calibrations; current meters, water; flow measurement; Price meter suspensions; Pygmy meter performance; velocity-area method.

1. Introduction

Price and Pygmy water current meters, shown in figure 1, are vertical axis meters with rotating wheels composed of six conical buckets. The outside diameters of the Price and Pygmy bucket wheels are 5 inches (12.7 cm) and 2 inches (5.1 cm) respectively and the meter geometries are approximately similar. The Pygmy meter was developed specifically to replace the larger Price meter in very shallow flows [1],² but its actual use in the field is not restricted to such cases. These meters are among the most widely used devices in this country for open channel flowrate determination by the velocity-area method.

¹Non-metric units are given precedence in this paper because they are still customarily used in the field.

²Figures in brackets indicate the literature references at the end of this paper.

The accuracy of such flowrate determinations depends on some combination of current meter accuracy and the accuracy of the spatial and temporal sampling of the velocities. This note deals only with the first element, i.e., the current meter accuracy, and its purpose is to provide users with an estimate of the accuracy that can be expected from Price and Pygmy current meters calibrated and used in various ways. Accuracy requirements differ among various users, some needing perhaps only a few percent while others are anxious to shave every possible percentage point off of the uncertainty. It is reasonable to expect the latter category to increase as needs increase for accurate water and wastewater flow measurements.

In this work, more than routine attention has been given to low velocities, i.e., velocities less than one foot per second (30.5 cm/s). Although guidebooks generally caution users to make traverses in sections of moderate velocity, sometimes lower velocities are unavoidable, e.g., when traversing upstream to calibrate a weir or flume. Meters in good condition are assumed. Smoot and Carter [2] pointed out the sensitivity of Price meter performance to dented buckets, and because the low velocity performance of the meters can depend upon the internal friction, it is also assumed that the user continuously monitors the spin tests of the instruments.

The data included here were obtained from: low velocity, i.e., less than 0.5 ft/s (15 cm/s), experiments in a short towing tank; limited experiments in a 20-inch (50.8 cm) diameter gravity-flow water tunnel; and from the records of numerous NBS calibrations of submitted meters during the 1960's, when NBS was still operating a large towing-tank calibration station that was later transferred to the U.S. Geological Survey.

2. Calibrations in the Large Towing Tank

Price meters submitted to NBS were routinely calibrated at eight velocities between 0.25 ft/s (7.6 cm/s) and 8 ft/s (244 cm/s). Pygmy meters were calibrated at six velocities between 0.25 ft/s (7.6 cm/s) and 3 ft/s (91.4 cm/s). At each velocity two passes were made in opposite directions along the towing tank. The resulting 12 sets of velocity-rotation rate data for the Pygmy meters were fitted with a rating equation of the form

$$V = MN + A \quad (1)$$

where V is the velocity in feet per second, N is the rotation rate in revolutions per second, and M and A are constants. The 16 sets of velocity-rotation rate data for the Price meter were fitted with two straight line equations which matched at $N = 1$, so that

$$V_1 = M_1N + A_1, N < 1 \quad (2)$$

$$V_2 = M_2N + A_2, N > 1$$

$$V_1 = V_2, N = 1$$

where M_1 , M_2 , A_1 and A_2 are constants.

3. Repeatability of Rating Equations

Price meters. We consider first the dependability of the rating equations themselves. One rod-mounted Price meter was repetitively calibrated a total of 18 times. Five of these runs were made in 1968, shortly after the meter was purchased. Eight runs were made in 1972 and five more runs were made shortly thereafter with a new lower bearing and a sharper pivot pin replacing the older one which had been dulled. Between the 1968 and 1972 runs the towing carriage was completely rebuilt by the Geological Survey, so that effectively two different towing systems were involved.

The results are shown in terms of observed revolutions per foot of advance, N/V , in figure 2 for each of the three groups of calibrations. The lower curve of figure 3 shows the standard deviation of the rating equations from the average of the eighteen equations computed for selected velocities over the calibration range. (In these figures and in many of the following a logarithmic scale is used for the velocity abscissa for clarity in plotting the lower velocities.) The deviations are very small at moderate and high velocities and exceed 0.5 percent only at velocities below about 0.3 ft/s (9.1 cm/s). It is inferred from this result that a single carefully made calibration of a Price meter comes very close to describing the correct, i.e., average, V - N relation, at least for non-turbulent conditions.

Pygmy meters. The corresponding results for a Pygmy meter are shown in the lower curve of figure 4. In this case one meter was repetitively calibrated seven times over a period of a few days. Although the deviations at the higher velocities are slightly larger than for the Price meter, they are still small and one again can infer the utility of a single rating equation as a description of the "true" or average towing-tank rating for that meter in specified condition.

4. Calibrations of Groups of Meters

Price meters. Often, instead of having a meter individually calibrated, users employ a "standard" or representative equation developed by a manufacturer or by other means to describe the V - N relation for a group of meters. We examined the rating equations of Price meters, representing at least three different manufacturers, which were submitted in groups for calibration. It is assumed that the meters in each group were manufactured at the same time or under the same conditions. In figure 3 are shown the standard deviations of the individual rating equations from the average rating equation for each group. The dashed curve typifies the deviations, which are of course larger than the deviations for an individual calibration but are still quite small and could well be adequate for many applications. This result agrees with the conclusions of Smoot and Carter [2].

If this course is taken it is necessary to consider how closely a "standard" equation describes a group average. The U.S. Geological Survey handles this problem by supplying meter dies and forms, for which standard ratings have been developed, to the manufacturer which is awarded the meter

contract. However, these comments are intended mainly for individual purchasers of individual meters, and there is little information available on which to base a judgment. One manufacturer's standard rating that is known to us shows deviations from the average performance of its meters which exceed the meter-to-meter deviations shown in figure 3 and which exceed 2 percent for some batches of meters. Based on this limited evidence it is concluded that an individual calibration is necessary if a meter rating within 1 percent is desired.

Pygmy meters. Corresponding results for groups of Pygmy meters are shown in figure 4. The standard deviations are larger than those obtained for the Price meter groups, but might still be satisfactory for many applications.

Concerning standard or group ratings for Pygmy meters, many users apply the approximate rating equation

$$V = N \quad (3)$$

The results of this action are shown in figure 5. For velocities higher than about 1 ft/s (30.5 cm/s), standard deviations are within about 2 percent, again a value whose acceptability depends upon the application. As the velocity decreases, however, the deviations become unacceptably high for virtually all purposes. Actually the deviations at the low velocities are not entirely random; equation (3) always underestimates the velocity in that range. A simple albeit crude adjustment can be made by using the weighted average calibration equation for all of the meter groups of figure 4.

$$V = 0.969N + 0.043 \quad (4)$$

The standard deviation of the groups of calibration equations referenced to eq. (4) is typified by the dashed line in figure 5 and indicates a substantial improvement over the use of equation (3) at low velocities. Equation (3) is not presented here as a valid average equation for all Pygmy meters, except perhaps for those manufactured during the 1960's from which these data were derived. However, it is noted that when eq. (4) is compared with a more recent group average cited by Schneider and Smoot [3], agreement is within about 2 percent over the entire velocity range and within about 1 percent for velocities higher than 1 ft/s (30.5 cm/s).

5. Precision of Calibrations

The repetitive runs on the single Price and Pygmy meters were made differently than the routine calibration runs, in that between each velocity run a measured time interval was allowed which was longer than that used during the routine calibrations. Also, a stilling period of two hours was allowed after the highest velocity runs were completed before starting the 0.25 ft/s (7.6 cm/s) runs for the next calibration. The standard deviations of the measured values of N/V from the values computed at the same velocities using the calibration equations are shown in figure 6 for the Pygmy meters. The deviations are slightly smaller for the repetitive runs on the single

meters. However, this is not expected to affect the deviations of the calibration equations appreciably, and the conclusions drawn from figures 3 and 4 regarding the advantages of individual calibrations are still valid.

6. Deviation of Velocities from Rating Equations

The deviations shown in figure 6 can be due to: approximating the rating with straight-line equations, a factor which does not appear to be important for velocities greater than 0.25 ft/s (7.6 cm/s); factors inherent in the calibration method; and random differences in meter response. Usually it is not possible to separate the deviations due to meter response from those due to calibration method. By tacitly assigning all deviations to meter response we are being conservative. In any event, the deviations shown in figure 6 are small so long as the velocities are higher than 1 ft/s (30.5 cm/s). Also, if these deviations are random their probable contribution to the total velocity-area error can be estimated by dividing the deviation for each point velocity by the square root of the number of sampling points, making the resultant effect still smaller.

To further investigate meter responses at low velocities, where deviations are likely to be higher, a series of runs on two Price and two Pygmy meters was undertaken in a small towing tank 3 ft (91.4 cm) wide by 2 ft (61.0 cm) deep by 40 ft (12.2 m) long towing tank using velocities between about 0.1 ft/s (3.0 cm/s) and 0.5 ft/s (15.2 cm/s). This range overlaps the velocities from 0.25 ft/s (7.6 cm/s) to 0.5 ft/s (15.2 cm/s) covered in the usual calibrations in the large towing tank, thus serving in part as a check on the equipment. The limiting high velocity was governed by the short tank length. The limiting low velocity was essentially the lower limit of consistent meter behavior.

The deviations of N/V can be computed using each pass down the tank, as was done by Smoot and Carter [2] for deviations of V . Alternatively they can be computed using the "round trip" average N/V for each velocity, recalling that the rationale for using round trips in the calibrations is the cancellation of the effects of steady thermally induced currents in the tank [4]. Computing standard deviations based on each pass in effect charges the meter for such currents in the tank. On the other hand, using round trips could mask some deviations which should be blamed on the meter. Extreme examples are shown in Table 1, where run 6-11-74 exhibits obvious drift while run 6-12-74, made one day later, shows no such quasi-steady effect. For practical estimating purposes, a figure somewhere between the round trip and single-pass values is considered to be representative, a conclusion which is supported by data of figure 7 discussed later.

Results for two Price and two Pygmy meters repetitively run at constant velocities in the small towing tank are given in figure 7, which also includes available data from the full calibrations in the large towing tank. These results represent the deviations of measured N/V values from the average N/V at a given velocity. It should be noted also that the percentage standard deviation of N/V , which is equivalent to the percentage change in N for a fixed velocity, is not the same as the percentage deviation in V for the same N . But for velocities over 1 ft/s the two are the same for

practical purposes.

Pygmy meters. For meter no. 1 the spin test time was about one minute, a value which is below the desired time of approximately 1-1/2 minutes but above the practical minimum of 1/2 minute as recommended by the U.S. Geological Survey [1]. The reason for the larger internal friction was not apparent since the bearings appeared to be in good condition. Meter no. 2 had a spin test time longer than 2 minutes. The minimum speeds for reliable and consistent rotation were about 0.16 ft/s (4.9 cm/s) and 0.11 ft/s (3.4 cm/s) for meters no. 1 and no. 2 respectively.

Price meters. The spin tests on the two Price meters varied but in figure 7 only runs with similar spin tests are compared. The lowest velocity for consistent performance was about 0.1 ft/s (3.0 cm/s) for both meters. When the penta gear was removed from meter no. 2, the minimum velocity was reduced to about 0.07 ft/s (2.1 cm/s). However, at these velocities (not shown in figure 7) the deviations of N/V were high; for example, at $V = 0.075$ ft/s (2.3 cm/s), the standard deviation from the average N/V was 11 percent for each pass and 6 percent for a round trip computation.

Although the data of figure 7 were treated as though all deviations were random, deviations were noted in the day-to-day averages when runs were repeated over a period of several days. These are noted on the curves. It is possible that, as far as a day's field work is concerned, these have to be considered as systematic errors, so that at 0.25 ft/s (7.6 cm/s), for example, we should add about 1 percent uncertainty to the uncertainty in the calibration equations themselves.

The towing tank results of figure 7 are in reasonable agreement with the deviations obtained in a 20-inch (50.8 cm) diameter gravity flow water tunnel, where the Price and Pygmy no. 1 meters were subjected to velocities from 0.25 ft/s (7.6 cm/s) to 8 ft/s (2.44 cm/s) with runs repeated on several different days. In spite of the fact that only two meters of each type were used, the agreement between two such disparate testing methods suggests that figure 7 presents a usable and conservative picture of current meter reliability.

7. Calibration of Price Meters With Cable Suspension

The two most commonly used weight suspensions are shown in figure 8 using the 15-pound (6.8 kg) weight as an illustration, but heavier weights are available in both the Columbus and Elliptic weight series. Recommended spacing between meter and various sizes of Columbus weights can be found in references [5] and [6].

The deviations of the rating equations of groups of cable-rated Price meters from the group average are notably larger than the corresponding deviations for rod-mounted meters, as shown by the upper dashed curve in figure 3. The same figure also shows that the deviations for repetitive ratings of a single cable-suspended meter are larger than for the rod-mounted case. Probably part of the increased deviation is due to additional currents generated in the towing tank by the submerged weight.

8. Comparison of Rod and Cable Ratings

Columbus weights. One Price meter was repetitively calibrated, from 8 to 10 times, with rod suspension and with 15, 30 and 50-lb (6.8, 13.6 and 22.7 kg) Columbus weights. The rating equations are compared in figure 9. Also shown are results for a group of 11 Price meters which were calibrated both with rod and 15-pound (6.8 kg) Columbus weight suspensions. In general, the results support the contention of the U.S. Geological Survey that properly used Columbus weights cause no change from rod mounted ratings [5]. However, consistent deviations in the Columbus weight curves are noted, particularly at the lowest velocities.

Placing the results in terms of N/V in figure 10, it is seen that there are consistent trends toward slower rotation for cable suspensions at the lowest velocities and toward slightly faster rotation at the moderate velocities. Possible hydrodynamic explanations for this behavior will be noted later.

Elliptic weights. No single-meter repetitive runs were made with Elliptic weights, but the results of comparative rod-cable calibrations on two groups of meters are shown in figure 9. The meter-to-weight spacings are different for the two groups, 5.3 inches (13.5 cm) and 6.7 inches (17.0 cm). It is seen that both groups show a higher velocity for the cable rating throughout the range, with the difference increasing markedly at low velocities. The same effect in terms of N/V is shown in figure 11, where N/V is always smaller for cable mounting.

The slower rotation with decreasing velocity of cable-mounted relative to rod-mounted meters is common to both types of weights, and possible non-hydrodynamic causes were considered. First was considered the possibility that the rod-mounted results were too high at low velocities. There was a certain amount of "lurching" of the carriage which was apparent to the observer at low velocities. Conceivably this could have given a saw-tooth velocity vs. time curve of such shape that meter inertia rounded off the "teeth" and gave an erroneously high rotation rate. However, available rod-mounted meter data at low velocities for three different carriages do not account for differences of this magnitude. Second it was considered that the meters were not properly balanced on their pivots and therefore operated at a tilt when the velocities were too low for the fins to develop enough lift for balance. Such a tilt could increase the internal friction and make the meters rotate more slowly. To check this, a meter was repetitively run at low velocities with a deliberate tilt of 1.5 degrees but no consistent effect was found.

9. Hydrodynamic Effects of Weights

The most obvious hydrodynamic effect of the weight is the distortion of the velocity field around it. Figure 12 shows the velocity distribution for potential flow around a shape closely approximating that of the 15-pound (6.8 kg) Elliptic weight as developed by Lofquist [7]. A typical position for the bucket wheel is shown by the dashed rectangle, and the center of the wheel is seen to be in a zone of little or no velocity distortion. The rear of the wheel is subject to an increased ambient velocity of more than one percent. Because most of this part of the periphery exerts a retarding

torque, this could be translated into a fractional percentage reduction in N , but not enough to account for the differences in figure 11.

Figure 13 shows the potential flow velocity distribution around a 15-pound (6.8 kg) Columbus weight [7]. Here the meter is situated in a zone of at least + 1 percent in velocity. This can account for part of the effect seen at moderate velocities in figure 10, but cannot account for the observed change in the apparent suspension effect with decreasing velocity. We note in passing that this change cannot be accounted for by a larger boundary layer thickness at the low Reynolds numbers because such an increase, even if significant, would provide an effect in the opposite direction.

A remaining potential source of the increased cable-weight effect at the low velocities is the interaction between the rotary motion induced by the bucket wheel and the supporting strap and fin. The strap is about 2 inches (5.1 cm) closer to the wheel than the rod (see figure 8), and the fin also is a little closer than when the rod is used. Figure 12 suggests that data available for a 6.7-inch (17.0 cm) spacing between meter and Elliptic weight would be essentially free of velocity-distortion effects. These data for a group of 12 meters, plotted in the manner of figure 11, suggest a strap interference effect of about 1 percent at 8 ft/s (244 cm/s) gradually increasing to about 4 percent at 0.25 ft/s (7.6 cm/s). These values are supported by limited data available for a 50-pound (22.7 kg) weight at 9.8-inch (24.9 cm) spacing. Also, in configurations where the meter is particularly close to the top of the weight, there can be an additional meter-weight interference as is suggested by the 30-pound (13.6 kg) Columbus results of figure 10. However, there is insufficient data to evaluate this effect for all situations. Because the various interference effects are at least as large as the theoretically obtainable velocity-distortion effect, it remains necessary to experimentally determine any needed adjustments to rod-mounted calibrations, and the curves of figure 9 can be used for that purpose.

10. Measurements With Wading Rod

Recommended practices for wader position relative to the current meter are cited in the literature, e.g., [5], but the data base or analytical reasons for these recommendations are not given. As a result, users have no guidelines as to the errors involved in failure to adhere to recommended practice.

If the wader can be considered as a vertical circular cylinder immersed in a low Froude number potential flow, the solution is well known and is shown in figure 14 in terms of local-to-undisturbed velocity ratio [7]. Recommended practice places the bucket wheel somewhere within the dashed rectangle in the figure, depending upon the particular geometry and upon whether a Price or Pygmy meter is used. In that area the increases in velocity average about 3 percent. Slenderizing the water to an elliptical cylinder of 3:4 breadth-length ratio reduces the velocity increase to about 2 percent. Experimental verification is needed here with shapes more closely simulating a body. Existing field data on wading-cable suspension comparison are very limited. Schoof and Crow [8] actually found differences in the opposite direction but some of their field work was done under adverse

conditions. In the meantime this idealized analysis has been presented to show that a potential for systematic error exists in wading measurements.

11. Effect of Lateral Velocity Gradient

Figure 15 shows the elements of a theoretical model of bucket wheel current meters developed by Lofquist [7]. The torque is an integral around the periphery of the product of a drag coefficient, the square of the tangential component of the relative velocities felt by the buckets, and obvious geometric factors. It is assumed that the drag coefficient has only two discrete values depending upon whether the open or closed side of the bucket faces the relative tangential velocity. One result of this analysis is that the change in rotation rate, ω , in rad/s, can be expressed as

$$\Delta\omega/\omega = (2+k^2)(\bar{a}\Omega/V)/3k \quad (5)$$

where k is the value of $(\bar{a}\omega/V)$ at large V , and \bar{a} and Ω are the wheel radius and velocity gradient as defined in figure 15. For example, if the velocity increases (in the direction shown in figure 15) by 10 percent over a lateral distance of 1 foot (30.5 cm), and if we use experimentally determined values of k of 0.34 and 0.30 for the Price and Pygmy meters respectively, the rotation rate is increased by 2.9 percent for the Price meter and 1.2 percent for the Pygmy. These numerical results have not been confirmed experimentally. But if they are even approximately correct their magnitude is sufficient to produce errors in traversing a badly skewed profile if the sum of the gradients at the sampling points is not zero. The possibility of lateral gradient effects should also be considered when using figure 16 to position meters for wading measurements.

12. Wall and Bottom Proximity Effects

Wall effect. We assume that the total "wall effect" in flowing water is due to the velocity gradient created by the wall, superposed upon another effect due only to wall proximity. The velocity gradient effect has already been considered and the proximity effect can be treated separately by making near-wall experiments in a towing tank. This was done by repetitive towing of meters in the small NBS tank at various positions near the wall and along the centerline, with the runs for each position repeated over a period of several days. Because of the short length of the towing tank, experiments were restricted to velocities of 0.5 ft/s (15.2 cm/s). The results obtained are expected to be conservative for velocities higher than 0.5 ft/s (15.2 cm/s), since the cable-suspension data analysis indicated that interference effects decrease as velocities increase. Unfortunately, this low velocity introduces considerable scatter into the results.

A dimensional analysis shows that the relative change in rotation rate, $\Delta\omega/\omega$, where ω is the rotation rate unaffected by boundary proximity, is a function of a Reynolds number and of s/a' , where s is the distance from the meter vertical axis to the wall and a' is the outside radius of the bucket wheel. Assuming a negligible effect of Reynolds number [7], $\Delta\omega/\omega$ becomes a function only of s/a' for each meter. The experimental data

for this relationship are shown in figure 16 for both meters. Each point of Pygmy meter data represents the average of one day's runs, which typically consisted of about 6 near-wall and 6 centerline runs. For the Price meter only the overall averages are plotted.

The response of the current meters to wall proximity clearly depends upon the meter orientation, i.e., whether the "upstream-facing" or "downstream facing" cups are next to the wall. The results in figure 16 suggest that wall proximity effect does not exceed about 0.5 percent if the meter is kept a dimensionless distance of $s/a' = 2$ from the wall, corresponding to bucket tip clearances of 1 inch (2.5 cm) and 1-1/2 inches (3.8 cm) for the Pygmy and Price meters respectively.

Bottom effect. Neglecting any possible Reynolds number dependence, $\Delta\omega/\omega$ due to bottom proximity is a function of h/a , where h is the distance from the horizontal axis of the meter to the bottom and " a " is the radius of the bucket face. Experimental results are shown in figure 17, with the individual points again representing daily averages. The interpretation of these data is somewhat more uncertain than for the wall effects, but it appears that bottom proximity effects can be kept under 1 percent if h/a is larger than about 8 for the Pygmy meter and about 6 for the Price, corresponding to axis distances of about 3 inches (7.6 cm) and 6 inches (15.2 cm) respectively. These figures are in reasonable agreement with existing U.S. Geological Survey recommendations [6]. Surface proximity errors were not investigated because free-surface effects cannot be covered with such a limited velocity range.

13. Summary

Some performance characteristics and effects of methods of calibration and use of Price and Pygmy water current meters have been examined with a view toward their application to velocity-area traverses for flowrate determination. The improved accuracy obtained by calibrating meters individually as opposed to the use of group or type calibrations is shown, based on NBS calibration experience. The repeatability of meter performance at low velocity, $0.1 < V < 0.5$ ft/s ($3.0 < V < 15.2$ cm/s), was investigated with the results shown in figure 7. Differences between rating equations for rod-mounted and cable-suspended Price meters were determined experimentally and explained analytically where possible for Columbus and Elliptic weights. These differences were found to be generally small for Columbus weights, except at low velocities. For both types of weights no single constant correction factor could adjust for the cable-rod differences over the entire 0.25 to 8.0 ft/s (7.6 to 244 cm/s) velocity range. The potential for systematic errors of 2 to 3 percent in wading measurements and a consequent need for further research was pointed out. A theoretical model for vertical-axis bucket-wheel current meters was outlined which permitted an estimate of a substantial effect of lateral velocity gradients. The effects of wall proximity in the absence of velocity gradient and of bottom proximity were investigated experimentally at a velocity of 0.5 ft/s (15.2 cm/s) with the results shown in figures 18 and 19. The potential hydrodynamic effect of turbulence in the flowing stream on Price and Pygmy meters has not been considered here and will be the subject of future NBS research.

14. Acknowledgment

The repetitive runs for comparison of rod-mounted and Columbus-weight suspended Price meter ratings described in figure 11 were made by T. Robusto of NBS using the U.S. Geological Survey towing tank. We gratefully acknowledge this U.S.G.S. cooperation.

15. References

- [1] Smoot, G. F. and Novak, C. E., Calibration and Maintenance of Vertical-Axis Type Current Meters, *Techniques of Water-Resources Investigations of the United States Geological Survey*, Book 8, Ch. B2, 1968.
- [2] Smoot, G. F. and Carter, R. W., Are Individual Current Meter Ratings Necessary?, *Proc. Amer. Soc. Civ. Eng.*, 94, HY2, March 1968, pp. 391-397.
- [3] Schneider, V. R. and Smoot, G. F., Development of a Standard Rating for the Price Pygmy Current Meter, *Jour. Research, U.S. Geol. Survey*, 4, 3, May-June, 1976, pp. 293-297.
- [4] Dickman, R. H., The Rating of Water Current Meters, *Water Power*, Sept. 1951, p. 330.
- [5] Buchanan, T. J. and Somers, W. P., Discharge Measurements at Gaging Stations, *Techniques of Water Resources Investigations of the United States Geological Survey*, Book 3, Ch. A8, 1969.
- [6] Bureau of Reclamation, Water Measurement Manual, *U.S. Dept. Interior, Second Ed., Revised Reprint*, 1974.
- [7] Lofquist, K. E. B., Notes on Current Meter Thoery, unpublished manuscript, Fluid Mechanics Section, National Bureau of Standards, 1975.
- [8] Schoof, R. R. and Crow, F. R., Discussion of Reference (3), *Proc. Amer. Soc. Civ. Eng.*, 94, HY6, Nov. 1968, pp. 1596-1601.

Table 1

Evidence of Effect of Drift Currentat $V = 0.24$ ft/s, Pygmy Meter

<u>Round Trip</u>	<u>Run of 6-11-74</u>		<u>Run of 6-12-74</u>	
	<u>N/V</u>		<u>N/V</u>	
	<u>Northbound</u>	<u>Southbound</u>	<u>Northbound</u>	<u>Southbound</u>
1	0.837	0.896	0.862	0.862
2	0.826	0.913	0.857	0.840
3	0.861	0.880	0.876	0.845
4	0.843	0.900	0.876	0.890
5	0.841	0.885	0.874	0.882
6	0.847	0.894	0.871	0.884
7	0.835	0.905	0.885	0.878
8	0.849	0.900	0.880	0.870
9	0.846	0.895	0.877	0.878
10	0.842	0.915	0.880	0.883
11	0.846	0.902	0.874	0.871
12	0.855	0.904	0.870	0.878
13	0.837	0.920		

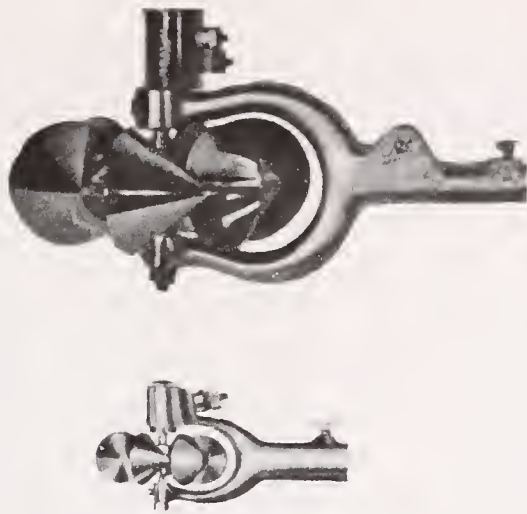


FIGURE 1. PRICE AND PYGMY WATER CURRENT METERS.

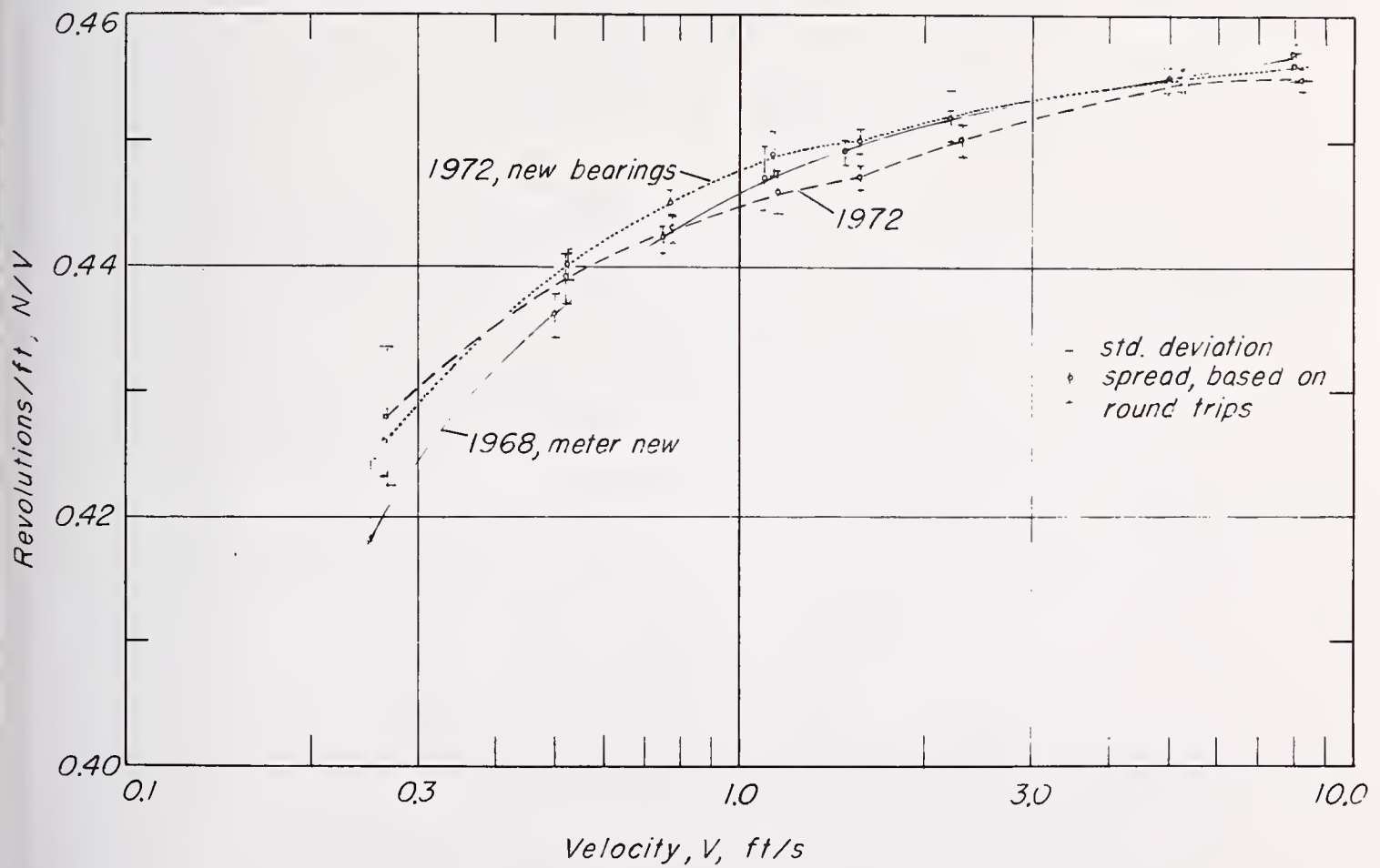


FIGURE 2. N/V FOR THREE SETS OF REPETITIVE CALIBRATIONS OF A SINGLE ROD-MOUNTED PRICE METER.

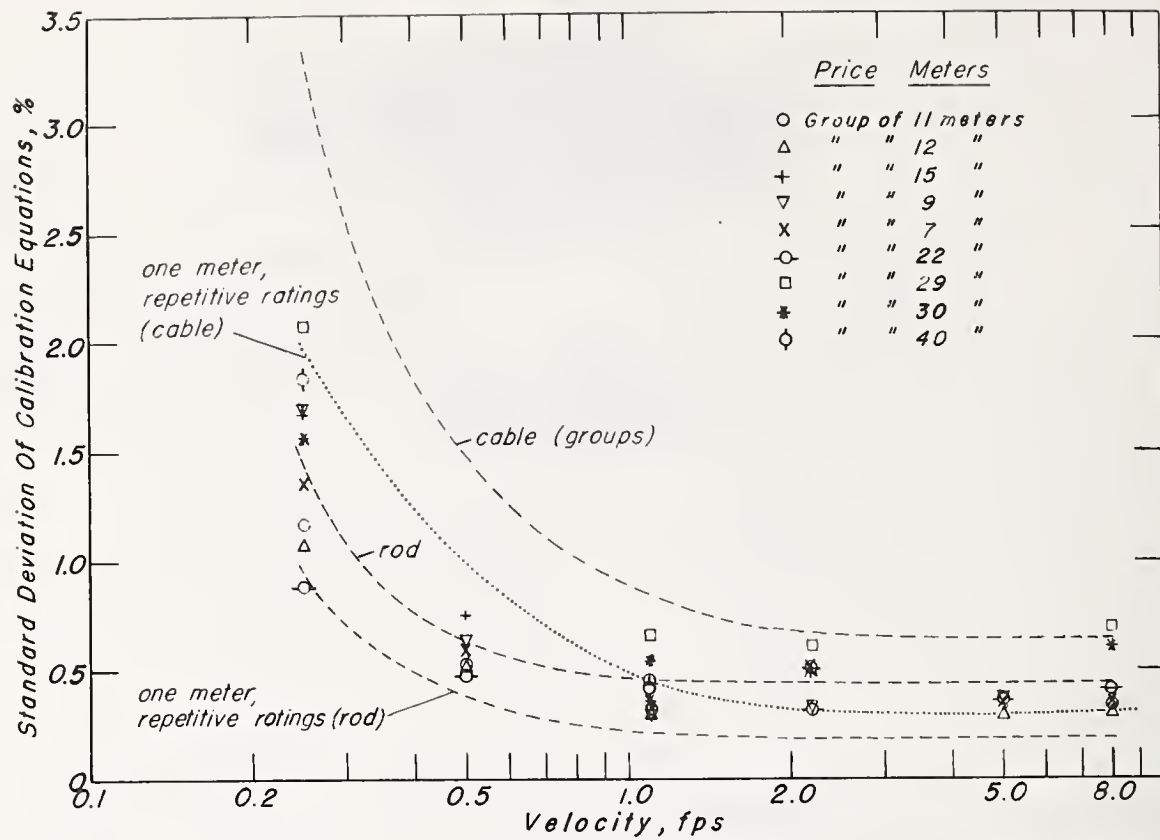


FIGURE 3. STANDARD DEVIATIONS OF CALIBRATION EQUATIONS FOR PRICE METERS.

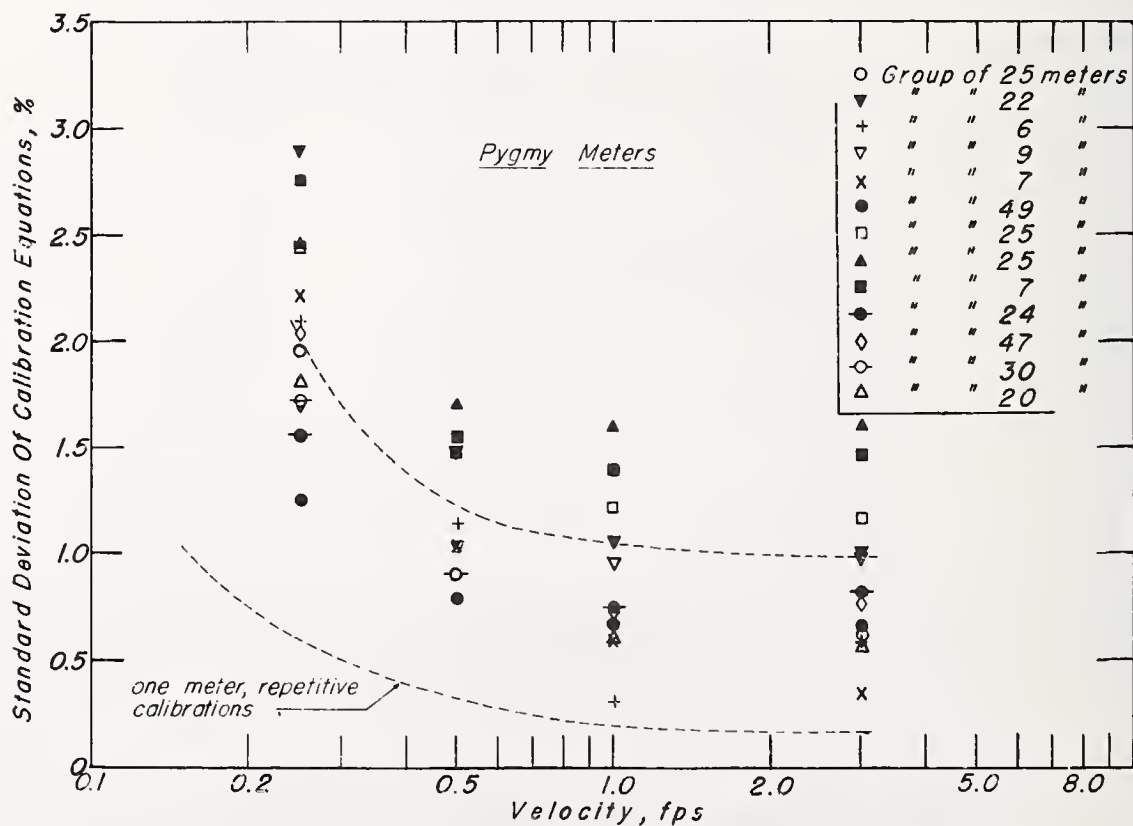


FIGURE 4. STANDARD DEVIATIONS OF CALIBRATION EQUATIONS FOR PYGMY METERS.

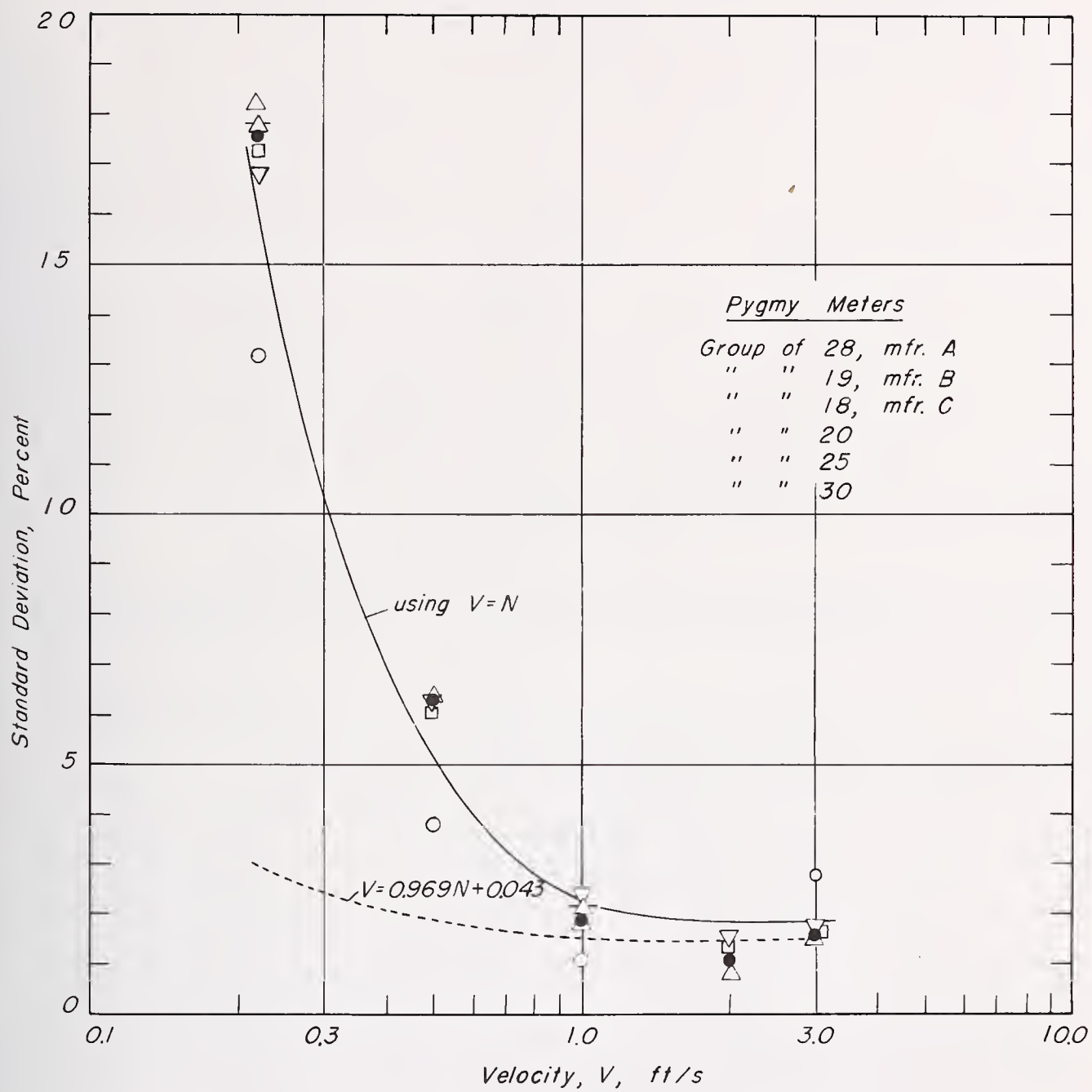


FIGURE 5. STANDARD DEVIATIONS OF PYGMY METER RATING EQUATIONS FROM GROUP EQUATIONS.

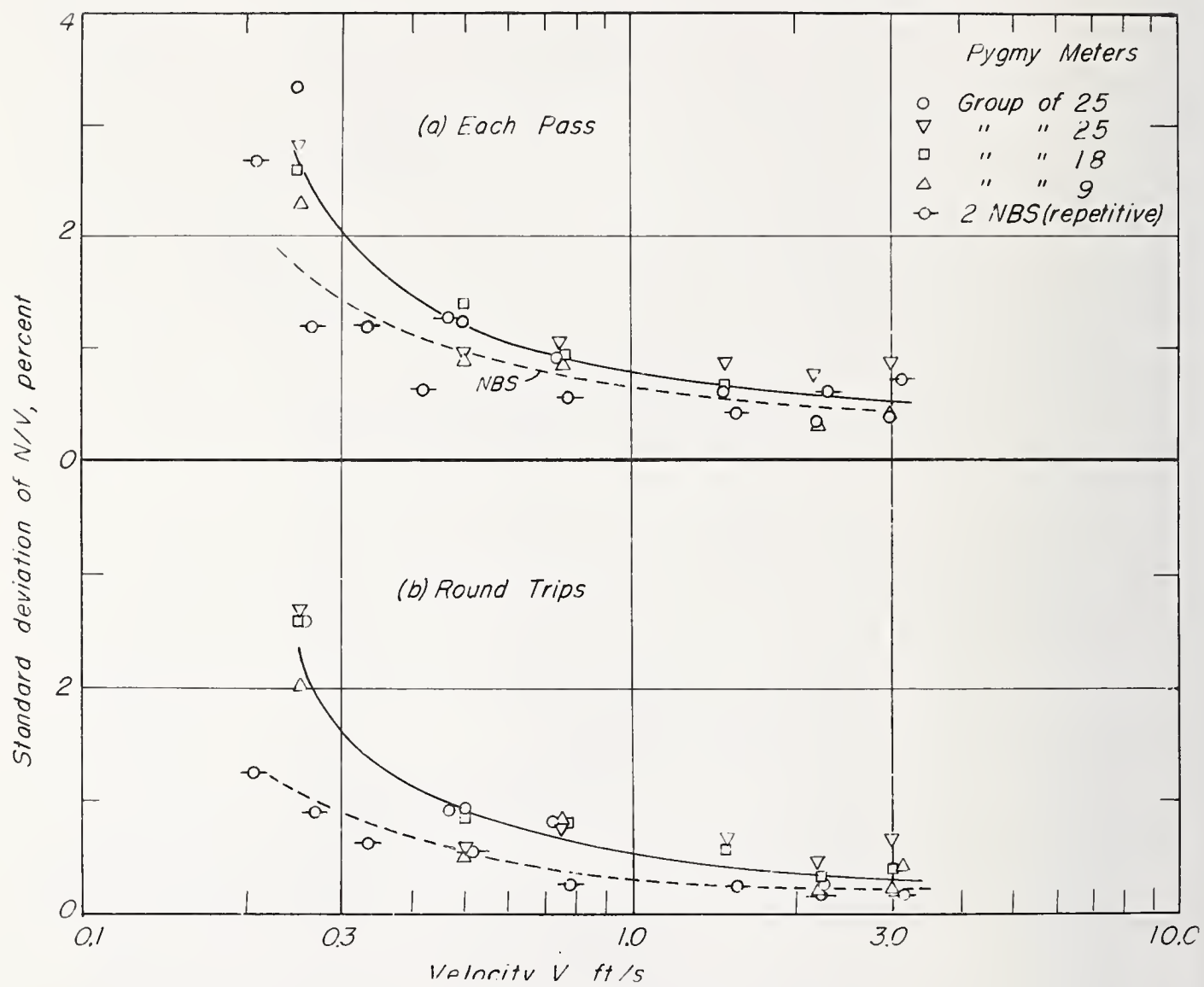


FIGURE 6. DEVIATIONS OF MEASURED VELOCITIES FROM INDIVIDUAL CALIBRATION EQUATIONS.

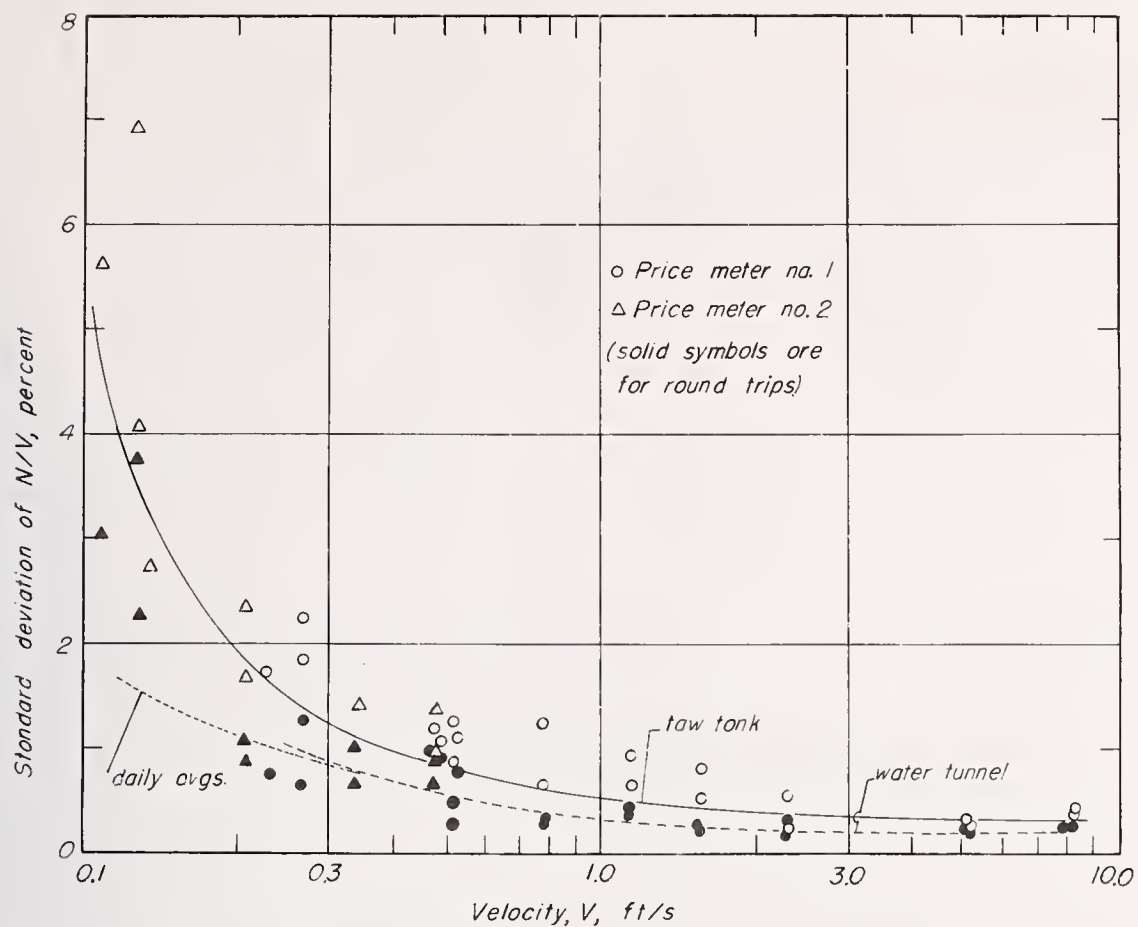


FIGURE 7(a). DEVIATIONS OF N/V FOR TWO PRICE METERS.

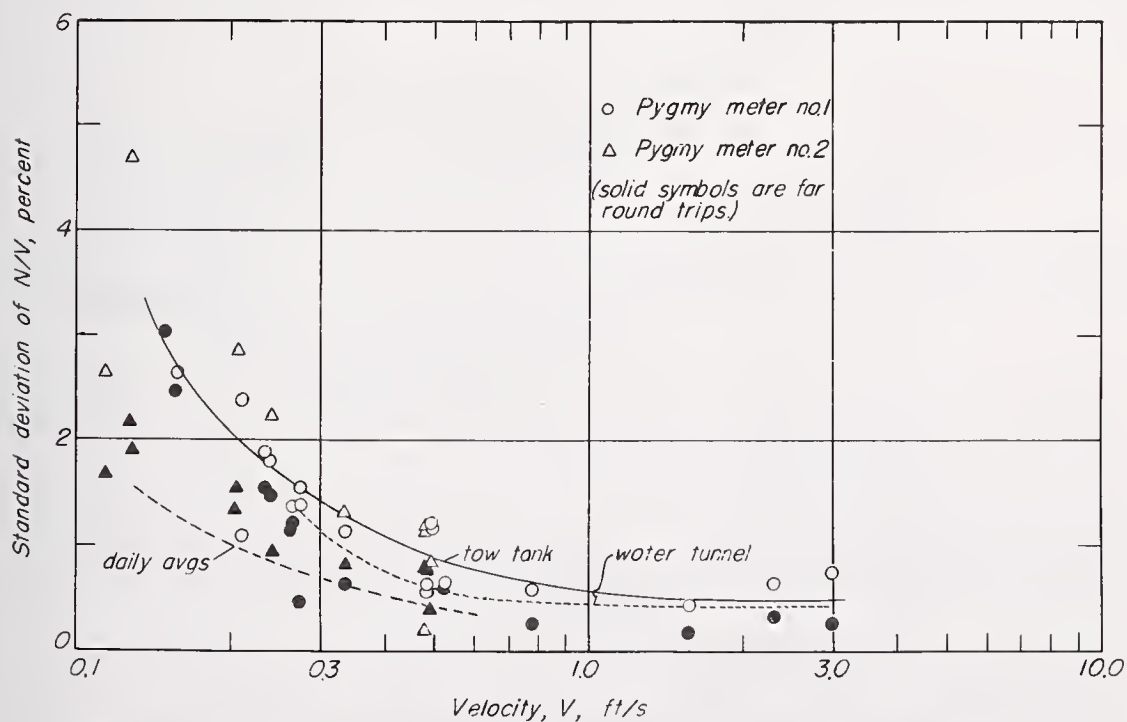
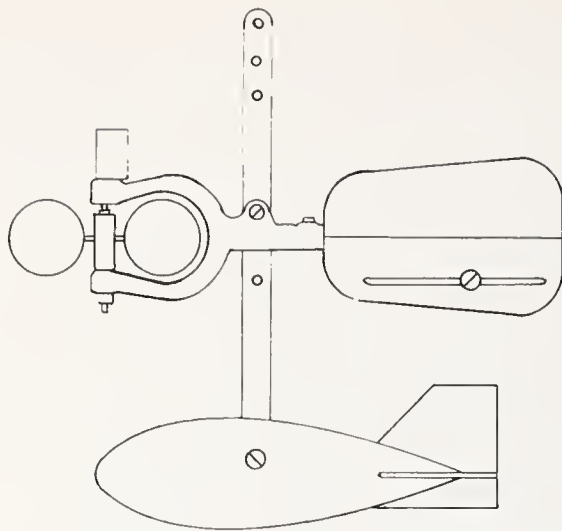
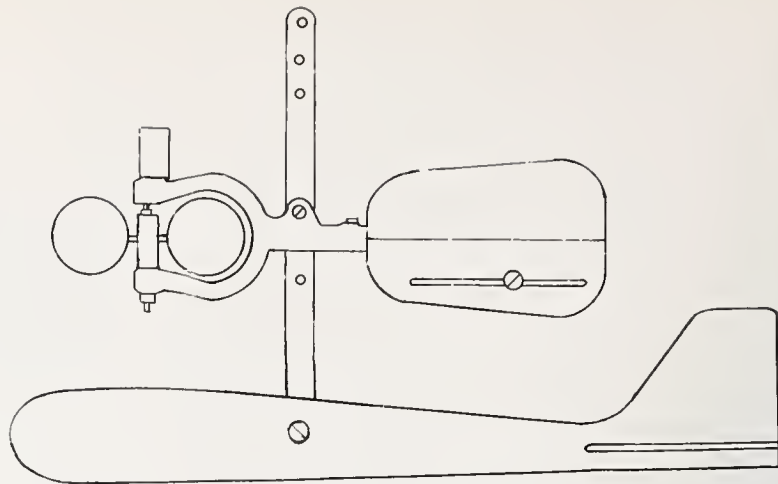


FIGURE 7(b). DEVIATIONS OF N/V FOR TWO PYGMY METERS.



15-pound Elliptic weight



15-pound Columbus weight

FIGURE 8. PRICE METERS SUSPENDED WITH ELLIPTIC AND COLUMBUS WEIGHTS.

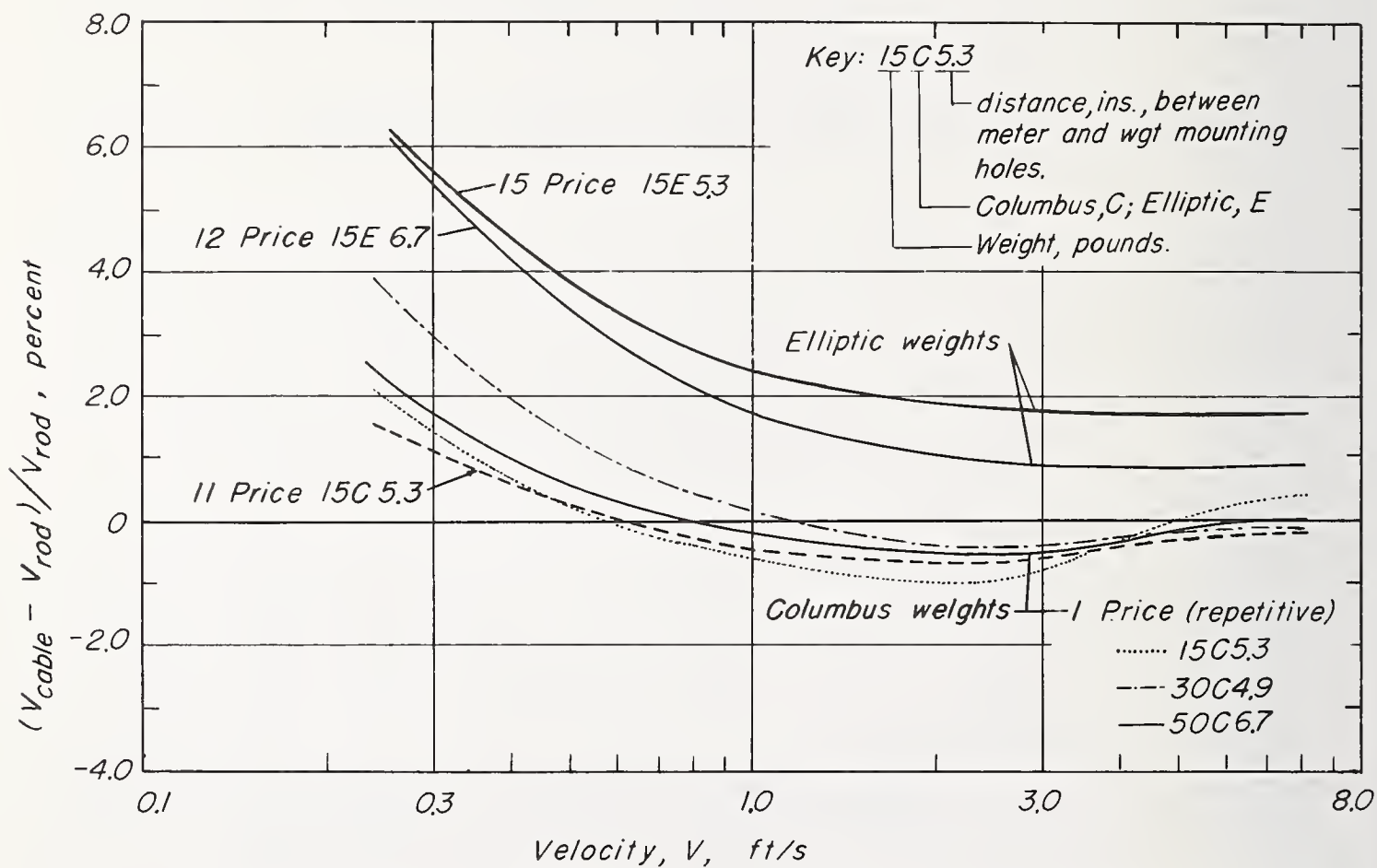


FIGURE 9. COMPARISON OF RATING EQUATIONS FOR CABLE AND ROD SUSPENSIONS.

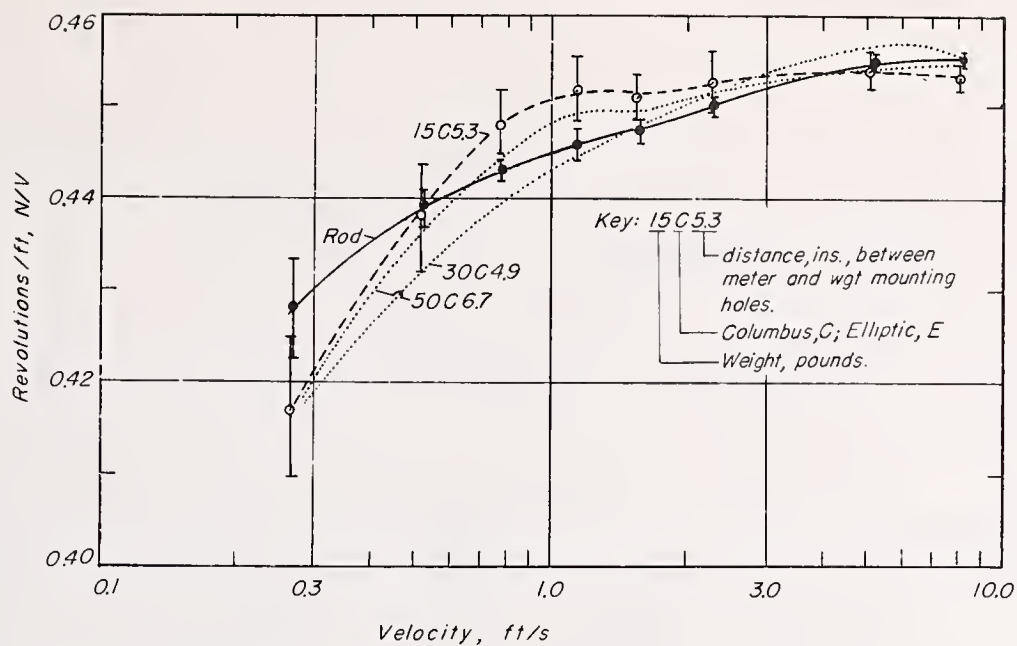


FIGURE 10. REPETITIVE CALIBRATION OF A PRICE METER WITH ROD AND COLUMBUS WEIGHT SUSPENSIONS.

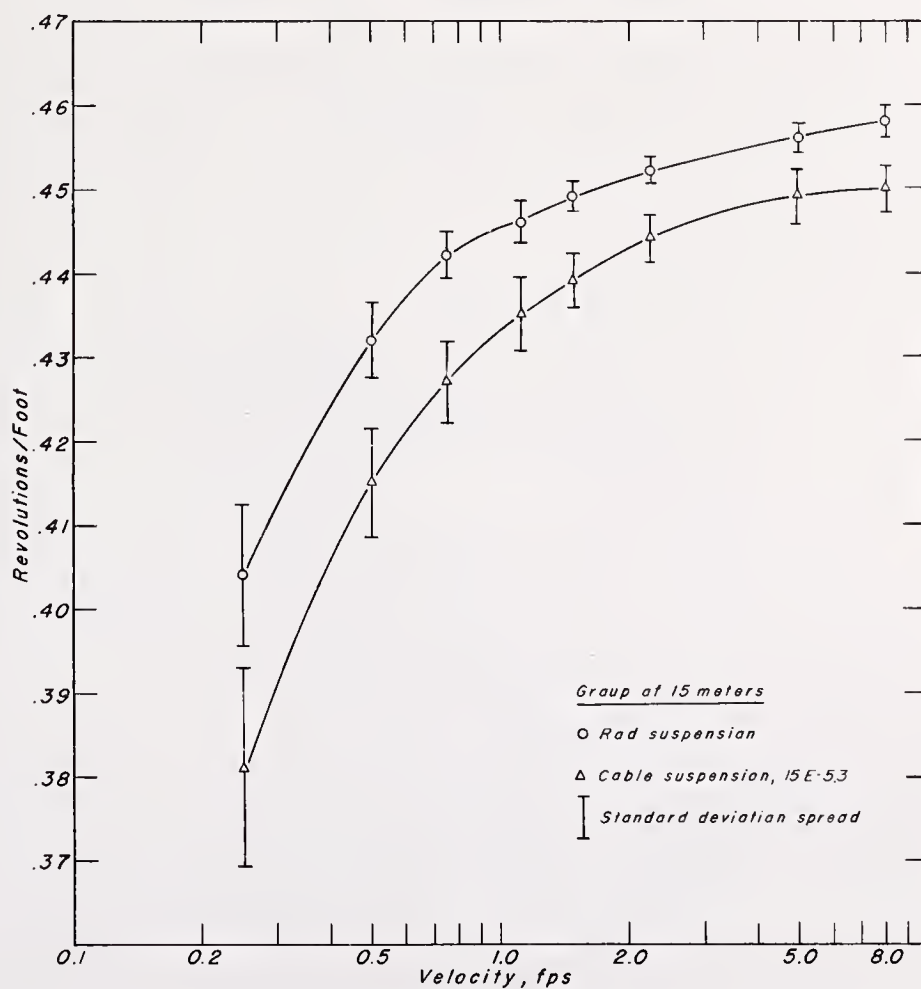


FIGURE 11. COMPARISON OF N/V FOR ROD AND ELLIPTIC WEIGHT CALIBRATIONS.

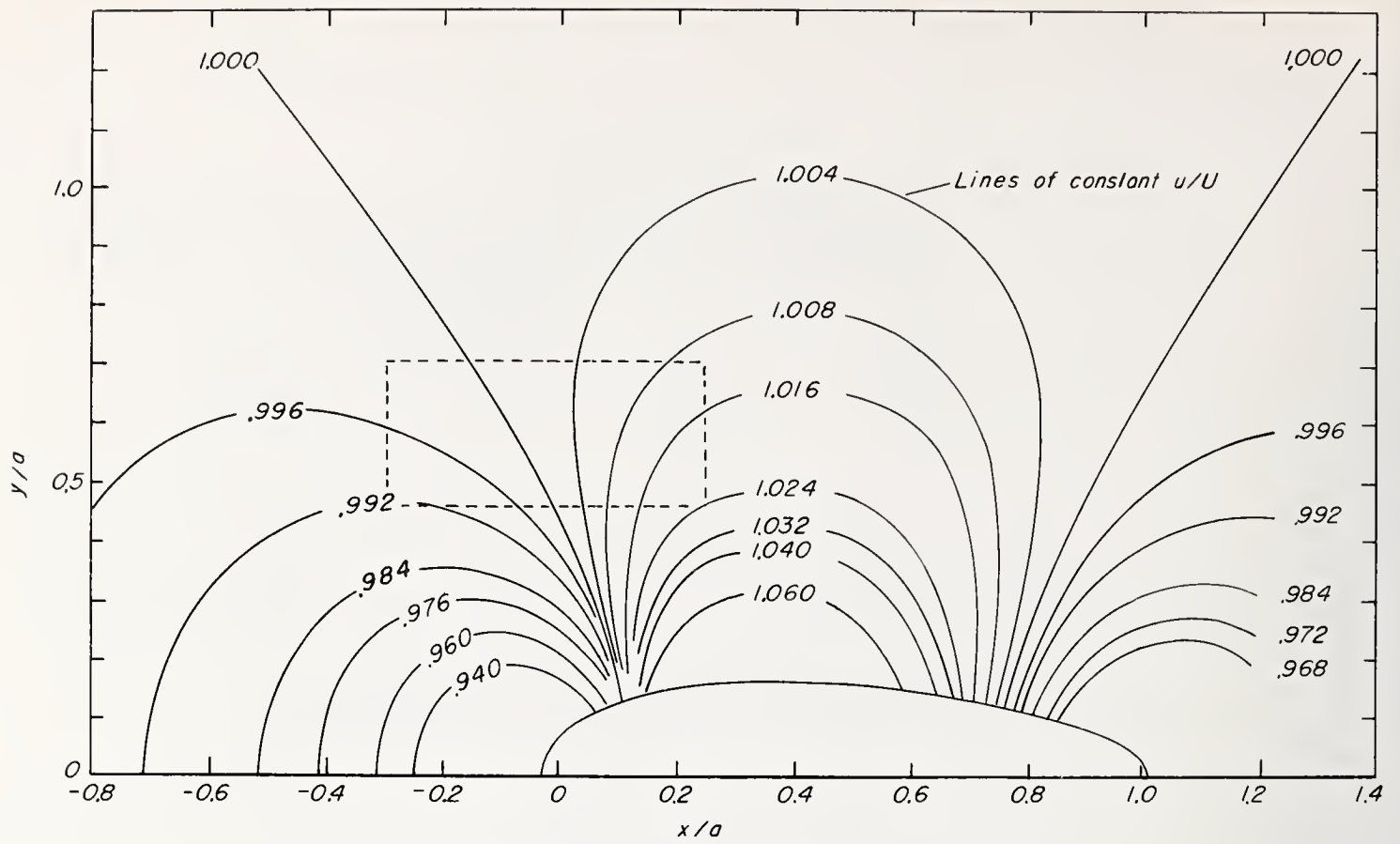


FIGURE 12. VELOCITIES AROUND AN ELLIPTIC WEIGHT.

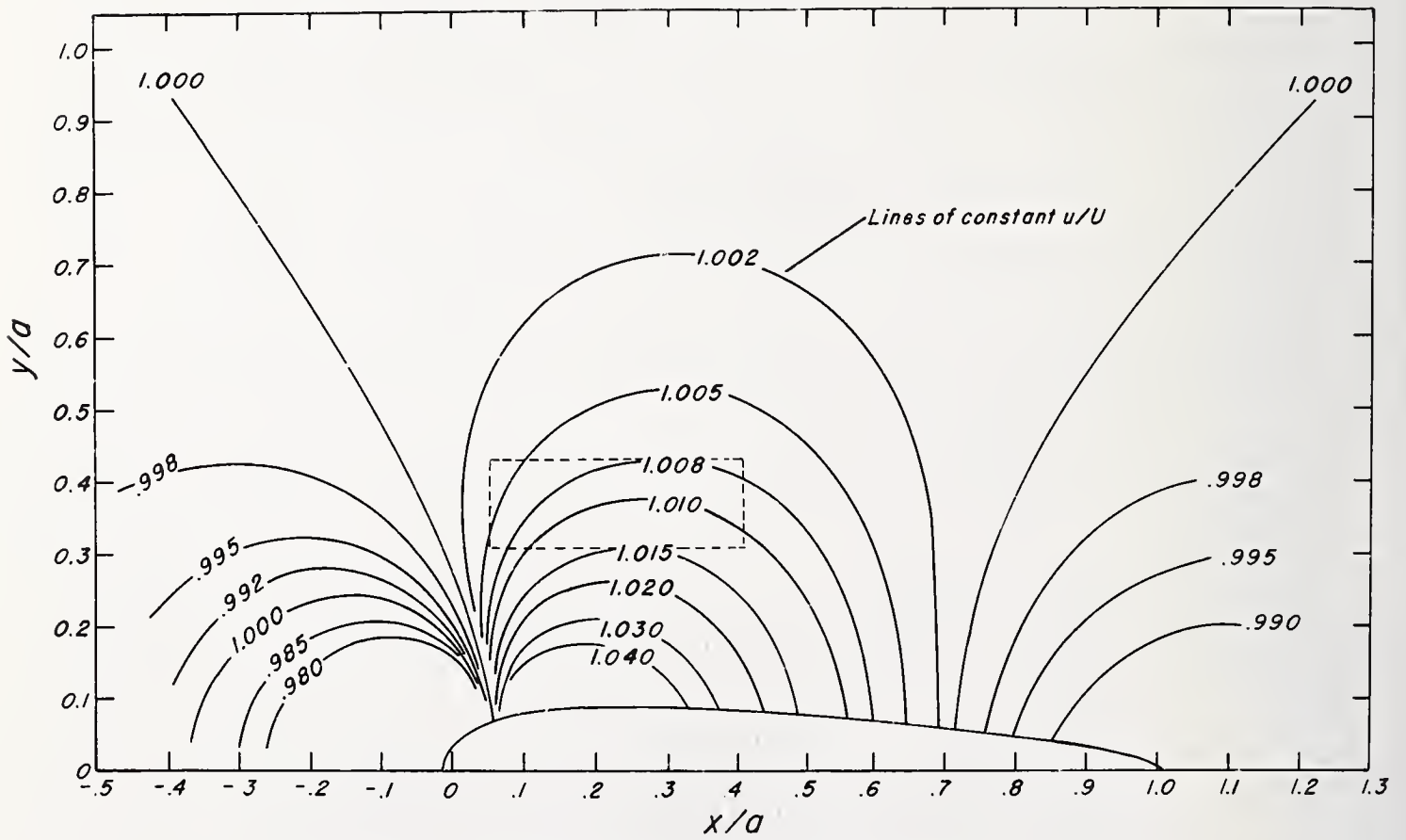


FIGURE 13. VELOCITIES AROUND A COLUMBUS WEIGHT.

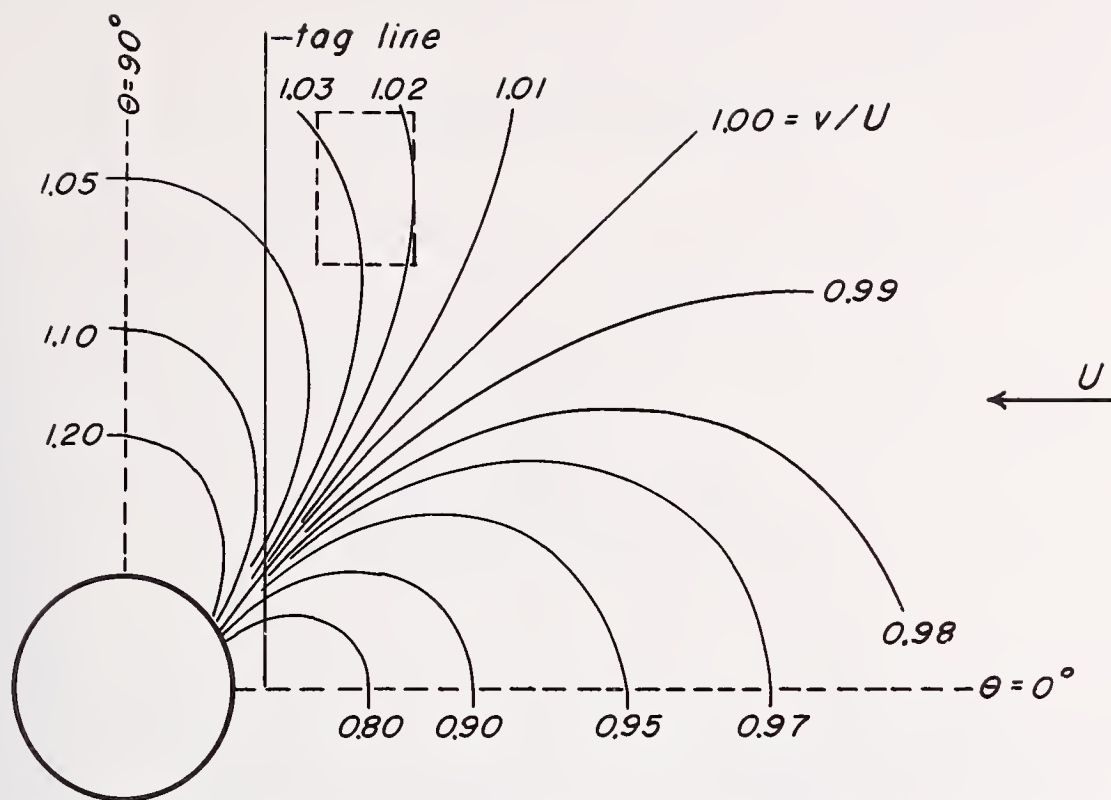
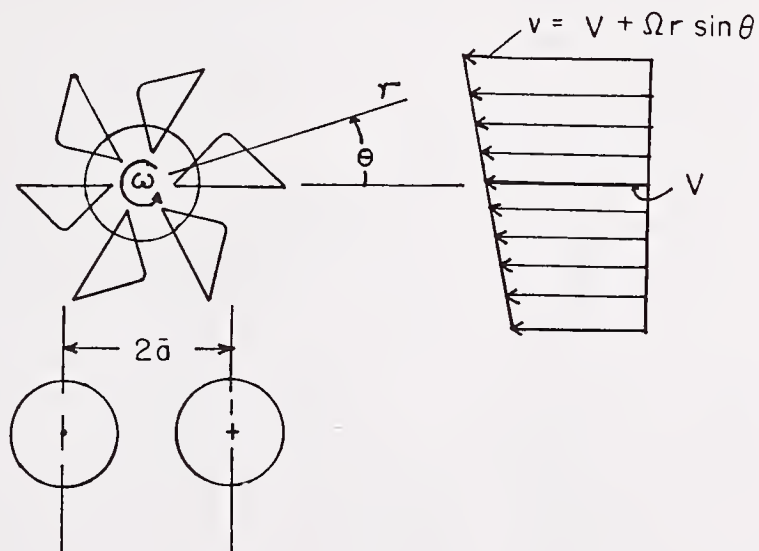


FIGURE 14. EFFECT OF "CYLINDRICAL WADER" ON VELOCITIES.



$$T = \rho a^3 \int_0^{2\pi} C_\theta (v_\theta - \omega a)^2 d\theta$$

$$C_\theta = C + \Delta C, \text{ for } (v_\theta - \omega a) > 0$$

$$C_\theta = -(C - \Delta C), \text{ for } (v_\theta - \omega a) < 0$$

$$v_\theta = v \cos \theta$$

FIGURE 15. ELEMENTS OF ANALYTICAL MODEL.

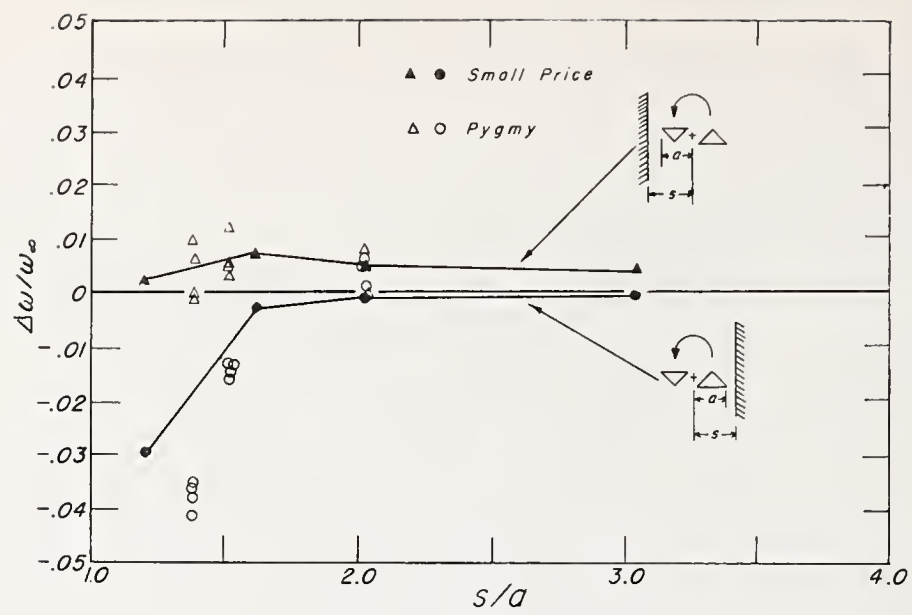


FIGURE 16. WALL EFFECT

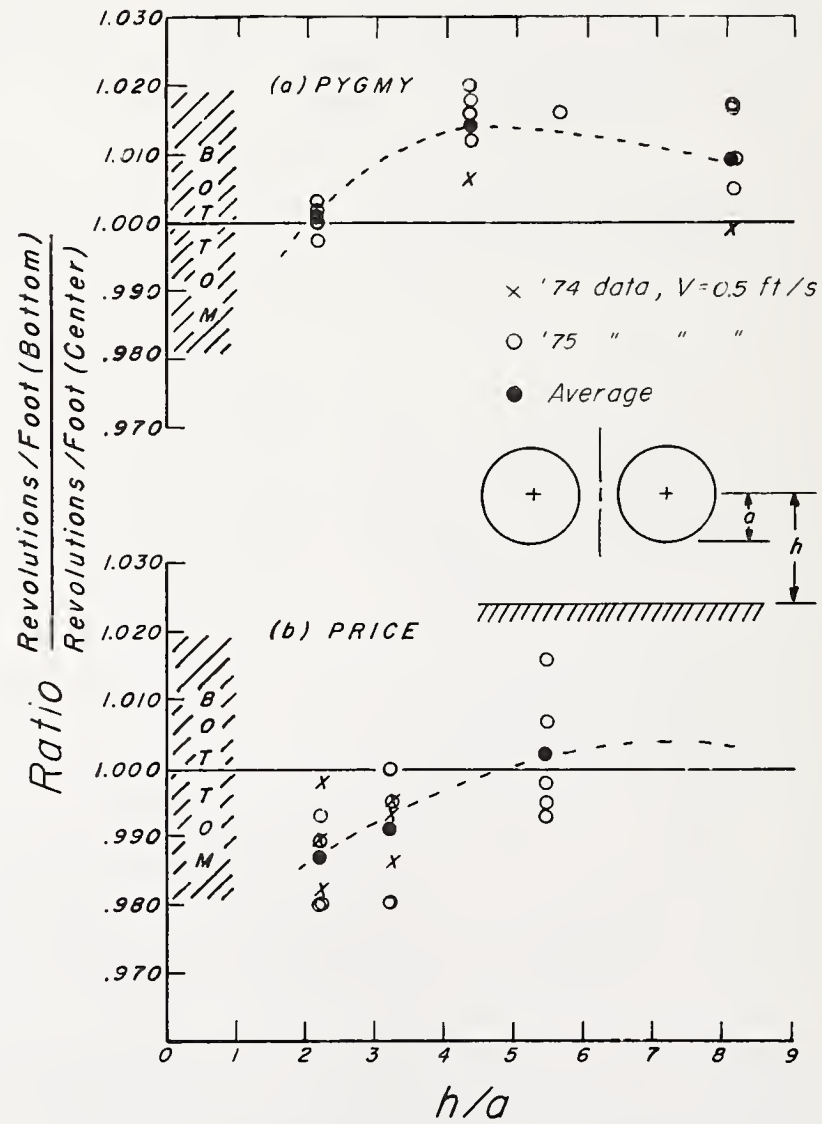


FIGURE 17. BOTTOM EFFECT

FLOW MEASUREMENTS IN THE CANALS OF POWER PLANT
CLOSED LOOP COOLING SYSTEMS

Joseph F. O'Brien, James Skridulis, John Annett, and G. Wayne Singley

NUS Corporation
Rockville, Maryland 20850

Harold L. Koenig
Commonwealth Edison Company
Chicago, Illinois 60690

Measurements were made of the flows in the intake and discharge canals of three large power plants as part of a comprehensive study on the thermal performance of various closed loop cooling systems. The types of cooling systems studied were spray canal, cooling lake, and spray canal/cooling lake combination. The flows were measured using velocity-area and dye dilution techniques. Velocity-area flow measurements were made at two of the plants under constant plant operational conditions. Analysis showed that the experimental error in these measurements was generally less than the estimated total standard error. This result was expected because of the relatively uniform nature of the canal cross-sections. At one of the plants, dye dilution and velocity-area flow measurements were used to develop a stage-discharge equation for a wing-tipped weir. Subsequent validation measurements indicated that the variation of the measured flow rates from the flow rates predicted by the weir equation was less than the probable experimental error. Discharges calculated by the velocity distribution method were compared to those found by the one-point and two-point methods for various numbers of verticals per transect. It was found that the calculated discharge was not particularly sensitive to the number of points per vertical, but was affected by the number of verticals per transect.

Key Words: closed-loop cooling system; cooling lake; dye dilution method; error analysis; flow rate measurement; open channel flow measurement; power plant; spray canal; stage-discharge equation; velocity-area method; weir equation.

1. Introduction

Flow measurements were made in the intake and discharge canals of three large power plants with different types of closed loop cooling systems: spray canal, cooling lake, and spray canal/cooling lake combination. These measurements were part of a comprehensive study on the thermal performance of the cooling systems carried out for Commonwealth Edison Company. Data on canal flows were required to obtain mass balances for the plant steam electric system. In addition, plant discharge flows were used in conjunction with condenser heat rejection models to determine variable heat loading on the cooling system. The flows were measured by the velocity-area and dye dilution methods.

Approximately 50 transects of the various canals were made using an Ott propeller current meter. The data generated in these transects were used to compute canal flow rates by velocity-area techniques. For two of the transects, sufficient vertical resolution was maintained so as to allow a comparison of flow rates calculated by the velocity-distribution method with those found by the one-point or two-point methods. Another area of investigation involved transects made while plant operational conditions were constant. The flow rates calculated for these transects permitted an assessment of potential errors in measurement procedures. At one of the plants, data from dye dilution and velocity-area flow measurements were used to derive a stage-discharge equation for a wing-tipped weir. Subsequent velocity-area measurements were made to validate the derived weir equation.

2. Description of Plants

Powerton Station (Figure 1) consists of two 840 MWe(net) coal-fired fossil units. The station is designed for closed-cycle operation using a cooling lake. Circulating water is discharged from the condensers into a discharge canal which flows to a 1,426 acre cooling lake. Water withdrawn from the lake passes through an intake canal and is returned to the condensers by six circulating water pumps (each rated at 256.6 cfs).

Dresden Nuclear Station (Figure 2) consists of three boiling water reactors: one 200 MWe unit and two 809 MWe(net) units. The smaller unit is designed for once-through operation. The larger units are designed for closed-cycle operation using a spray canal/cooling lake combination. Circulating water is discharged from the condensers of the larger units into a discharge/spray canal where the water passes through an array of spray modules. Six lift pumps (each rated at 372.4 cfs) raise the water approximately 22 feet to a 1,275 acre cooling lake. Water from the lake flows over a gated-spillway structure to the intake canal and is delivered to the condensers by six circulating water pumps (each rated at 350.1 cfs).

Quad Cities Nuclear Station (Figure 3) consists of two 809 MWe(net) boiling water reactors. The station is designed for closed-cycle operation using a spray canal. Circulating water is discharged from the condensers to the discharge canal where six lift pumps (each rated at 372.4 cfs) raise the water approximately 17 feet to the spray canal. The water passes through an array of spray modules and over a wing-tipped weir to an intake bay where six circulating water pumps (each rated at 350.1 cfs) deliver the water back to the condensers.

3. Velocity-Area Method

Measurement of flow rate by the velocity-area method [1,2,3,4,5,6]¹ is explained by reference to Figure 4. The depth of each sub-area is measured at prescribed width stations. The velocity is measured with a current meter at one or more points in the vertical. The measured widths, depths, and velocities are used to calculate the flows for each sub-area. These flows are then summed to give the total flow.

An Ott current meter² with a type 1 propeller was used for the velocity measurements (Figure 5). The current meter propeller is designed to be accurate when set to within $\pm 5^\circ$ of the flow direction. The meter is mounted on a relocating device that slips over a 20 mm diameter support rod. The support rod is marked at 0.1 foot intervals. Propeller revolutions are counted over a pre-set time by an Ott counter. The meter was calibrated by the manufacturer.

¹ Figures in brackets indicate the literature references at the end of this paper.

² Model C31 Ott universal current meter and Model Z100 counter. Epic, Inc., 150 Nassau St., New York, N.Y.

Steel cables stretched across the width of each canal were marked at 5 foot intervals. Depth and velocity measurements were made at these 5 foot intervals from a flat-bottomed boat attached to the cable. Measurement procedure involved lowering the support rod, with current meter attached, until it touched the canal bottom. After careful positioning to insure that the rod was vertical, the canal depth was measured to the nearest 0.1 foot. Then, after checking that the propeller was directed into the flow, the velocity at each desired point in the vertical was measured by counting propeller revolutions for 60 seconds.

The average velocity for each width station was determined by the two-point and/or the velocity-distribution method. For the two-point method, the velocity was measured at 0.2 and 0.8 of the water depth. For the velocity-distribution method, the velocity was measured at 0.2, 0.4, 0.6 and 0.8 of the water depth for depths between 2 and 5 feet, and at every tenth of the water depth for depths greater than 5 feet. For both methods, the velocity was measured at 0.6 of the water depth for depths less than 2 feet. The average velocity at each station was the arithmetic mean of the measurements.

The total flow rate for the cross-section was calculated by the mid-section method as follows.

$$Q = d_1 V_1 \left[\frac{b_1}{2} + \frac{b_2}{2} \right] + d_2 V_2 \left[\frac{b_2}{2} + \frac{b_3}{2} \right] + \dots \quad (1)$$

where (referring to Figure 4)

- Q = flow rate (cfs)
- d_1, d_2 = water depths at Station 1 and 2, respectively (ft)
- V_1, V_2 = velocities at Stations 1 and 2, respectively (fps)
- b_1, b_2, b_3 = distances along water surface from shore to Station 1, Station 1 to Station 2, and Station 2 to Station 3, respectively (ft)

4. Dye Dilution Method

Measurement of flow rate by the dye dilution method [3,7,8,9,10] involves injecting a known amount of dye into the flow and determining the dye concentration downstream. Two methods are commonly used for dye injection: slug injection and continuous injection. The latter method, which was the one used in this study, involves the injection of a dye solution of known concentration at a known, constant rate. The point of injection should be sufficiently upstream to insure uniform dye concentration throughout the downstream measurement cross-section. As shown in Figure 6, a plateau, or level of concentration, develops at the measurement cross-section. Under these conditions, and, assuming that the injection rate is much less than the stream flow, the rate of flow is given by

$$Q = q \frac{c}{C} \quad (2)$$

where

Q = flow rate (cfs)

q = dye injection rate (cfs)

c = dye concentration in injection
solution

C = dye concentration at measurement
cross-section

The dye concentrations can be determined by measuring fluorescence. However, since the ratio c/C is the dilution factor, absolute values of the concentrations are not required. A set of standards is usually prepared by serial dilution of the injection solution. Thus, if F_1 is the fluorescence of the injection solution diluted by a factor K , and F_2 is the fluorescence of flow sample, then the flow rate is given by

$$Q = q K \frac{F_1}{F_2} \quad (3)$$

Rhodamine WT dye³ was diluted with water to give an approximate injection solution concentration of 10%. A serial dilution process was

³Rhodamine WT (20% aqueous solution), E.I. Du Pont, P.O. Box 96240, Chicago, Ill. 60693

used to prepare a set of dilution standards. The dilutions were made using 5 ml volumetric pipets and Class A volumetric flasks. The tolerance for the pipets was ± 0.01 ml, while the tolerances for the volumetric flasks were ± 0.2 ml, ± 0.3 ml, and ± 0.5 ml for 500 ml, 1000 ml, and 2000 ml flasks, respectively.

The dye solution was injected by a positive displacement pump.⁴ The pump was driven by an A.C. frequency locked motor to assure constant pumping rates. The stroke length was variable to allow pumping over a range of from near 0 to 108 ml/min. The pumping rate was measured before and after injection by pumping into a 500 ml graduated cylinder for a time interval measured with a stopwatch.

Samples at the measurement cross-section were collected in polyethylene bottles at five minute intervals. Samples were checked for fluorescence⁵ as collected to determine the arrival of the dye cloud. With the arrival of the dye cloud, three samples across the width of the cross-section were taken in each time interval. Sampling continued at this schedule until the dye concentration decreased to the pre-injection level.

Fluorescence of Rhodamine WT is affected by changes in temperature as follows

$$F_r = F_s \exp \{ 0.026 (T_s - T_r) \} \quad (4)$$

where

F_r = calculated fluorescence at reference temperature T_r

F_s = measured fluorescence at sample temperature T_s

T_s = sample temperature ($^{\circ}\text{C}$)

T_r = reference temperature ($^{\circ}\text{C}$)

⁴ Model RP-1-G-400 positive displacement pump, Fluid Metering, Inc., 48 Summit St., Oyster Bay, N.Y. 11771

⁵ All fluorescence measurements were made using a Turner Model 111 fluorometer. (G.K. Turner Associates, 2524 Pulgas Ave., Palo Alto, Calif. 94303)

A 1°C rise in sample temperature will result in a decrease in the fluorescence of about 2.6%. Thus it is essential that the fluorescence of samples and dilution standards be measured at the same temperature. The samples and the dilution standards were allowed to reach room temperature before fluorescence levels were determined. The arithmetic mean of all the fluorescence values in the plateau was used in calculating the flow rate.

5. Powerton Station Measurements

Flow rate measurements at the Powerton Station were made using the two-point velocity-area method. The locations of the measurement cross-sections are shown in Figure 1. The cross-sections are located in straight reaches of the canals and are remote from bends and artificial obstructions. Both the intake and discharge canals are trapezoidal in shape with a bottom and a top width of about 35 feet and 95 feet, respectively, and a depth of about 10 feet (Figure 7). The bottoms of both canals are fine dirt with an occasional 12 inch stone. The sides are covered with 1-2 foot stone rip-rap.

Seven measurements were made with one unit (3 circulating water pumps) operating. Plant operational conditions were essentially constant for these measurements. The results are shown in Tables 1 and 2 for the intake and discharge canals, respectively. The mean flow in the intake canal was 786.5 cfs, with a maximum deviation from the mean of 15.2 cfs (1.9%) and a standard deviation of 8.8 cfs. The mean flow in the discharge canal was 853.8 cfs, with a maximum deviation from the mean of 38.5 cfs (4.5%) and a standard deviation of 20.9 cfs.

6. Dresden Nuclear Station Measurements

Flow rate measurements at the Dresden Nuclear Station were made using the two-point velocity-area method. The locations of the measurement cross-sections are shown in Figure 2. The cross-sections are located in straight reaches of the canals and are remote from bends and artificial obstructions. Both the intake and discharge canals are trapezoidal in shape (Figure 8). The intake canal has a bottom and top width of about 25 feet and 85 feet, respectively, and a depth of about 9 feet. The discharge canal has a bottom and top width of about 45 feet and 95 feet, respectively, and a depth of about 15 feet. The bottoms of both canals are fine dirt with an occasional 12 inch stone. The sides are covered with 1-2 foot stone rip-rap.

Five measurements were made with one unit (3 circulating water and 3 lift pumps) operating. Plant operational conditions were essentially constant for these measurements. The results are shown in Tables 3 and 4 for the intake and discharge canals, respectively. It should be pointed out that the relatively large variations in canal top width and flow cross-sectional area noted in the discharge canal data (Table 4) are due to imbalances between lift and circulating water pumps. These variations should not materially effect the magnitudes of the flows being measured. The mean flow in the intake canal was 1110.4 cfs, with a maximum deviation from the mean of 24.2 cfs (2.2%) and a standard deviation of 16.8 cfs. The mean flow in the discharge canal was 1079.8 cfs, with a maximum deviation from the mean of 14.1 cfs (1.3%) and a standard deviation of 8.7 cfs.

7. Quad Cities Nuclear Station Measurements

Flow rate measurements at the Quad Cities Nuclear Station were made using the velocity distribution and two-point velocity-area methods and the continuous injection dye dilution method.

The location of the measurement cross-section for the velocity-area measurements is shown in Figure 3. The cross-section is about 50 feet upstream from a wing-tipped weir and about 50 feet downstream from an array of spray modules. The spray canal is trapezoidal in shape with a bottom and top width of about 120 feet and 190 feet, respectively, and a depth of about 10 feet (Figure 9). The canal bottom is sand over a PVC liner. The sides are covered by 3-6 inch stone rip-rap.

The locations of the injection and measurement cross-sections for the dye measurements are shown in Figure 3. The measurement cross-section is about 1,000 feet downstream from the weir. Before reaching the cross-section the flow traverses a concrete-lined flume and an energy dissipater. Dye concentrations at the measurement cross-section were not well mixed when the dye was injected at the weir or from a bridge about 1,100 feet upstream from the weir. Injection from a bridge about 11,000 feet upstream from the weir did give good mixing for 2 and 3 lift pump operation, but not for 5 lift pump operation. For the 5 lift pump case, injection at the lift pumps, about 16,000 feet upstream from the weir, resulted in good mixing. The time histories of dye concentrations at the measurement cross-section for 2, 3, and 5 lift pumps are shown in Figure 10.

An initial set of dye and velocity-area measurements was made at Quad Cities to determine a stage-discharge equation for the wing-tipped weir in the spray canal. The form of the equation was

$$Q = C_e L_e H^{3/2} \quad (5)$$

where

Q = flow rate (cfs)

C_e = effective discharge coefficient

L_e = effective crest length (ft)

H = depth of water above weir crest
upstream from the weir (ft)

The data from these measurements are presented in Table 5. A subsequent set of flow measurements was made to confirm the validity of the derived relationship. These data are given in Table 6.

8. Analysis and Discussion

Analyses were carried out in three areas with regard to the flow measurement data collected for the present study. These included: (1) the estimation of the total standard error expected for the velocity-area method measurements; (2) an assessment of the calibration and validation of the stage-discharge equation developed for the weir in the Quad Cities spray canal; and (3) a comparison of the discharges calculated by the one-point, two-point, and velocity distribution methods. Each area of investigation is discussed below.

Velocity-Area Measurements: Error Analysis

The overall error associated with a physical measurement consists of a random component and a systematic component. A simplified estimate of the random standard error for flow meter measurements of the type performed for this study is given by [5] as

$$X'_Q = \pm \left\{ X_m^2 + \frac{1}{m} \left(X_d^2 + X_v^2 \right) \right\}^{1/2} \quad (6)$$

where X'_Q is the percentage random standard error in the discharge Q . The other quantities in equation (6) are defined as follows.

X_m = error associated with the number of verticals per cross-section. Typical values of X_m are $\pm 5, 3$ and 1% for 8, 15, and 50 verticals/cross-section, respectively [5].

X_d = error associated with depth measurement. A value for X_d of $\pm 0.7\%$ has been estimated for alluvial channels of the depths encountered in this program [5].

X_v = error associated with the determination of the mean velocity for each vertical.

m = number of verticals per cross-section.

The error associated with the determination of the mean velocity for each vertical can be expressed by combining the local point velocity error with that for the number of points at which velocity measurements are made [5]. That is,

$$X_v = \pm \left\{ \frac{X_f^2}{p} + X_o^2 \right\}^{1/2} \quad (7)$$

where

X_f = error associated with the local point velocity measurement

X_o = error associated with the number of points per vertical

p = number of points per vertical

A value for X_f of $\pm 6\%$ has been suggested where the period of each measurement is 40 seconds or approximately 100 propeller revolutions [5]. These conditions are similar to those in the present study. Guides as to the value of X_o have been given as $\pm 3.5, 3.0$, and 0.5% for the one-point, two-point, and velocity-distribution methods, respectively [5].

The major source of systematic error for velocity area measurements will arise from errors in current meter calibration. This error is on the order of ± 0.5 to $\pm 1\%$ for an individually rated meter [5]. A second potential systematic error may be caused by differences in water temperatures at calibration and under field conditions. The manufacturer of the Ott current meter used in this program states that special oil used in the hub of the propeller allows measurements to be made at various temperatures without any decrease in accuracy [11]. However, an Ott propeller current meter of a different type exhibited a change in velocity of about 1% for a change in temperature of from 70° to 40°F [6]. Since water temperatures in the canals were frequently more than 90°F , the 1% value for this constituent of the systematic error was adopted. As a consequence, by using an equation similar to (6), and by assuming the calibration error to be $\pm 1\%$, the systematic standard error (X''_Q) can be estimated as being $\pm 1.4\%$.

The overall estimate of the standard error in the discharge is given by [5]

$$X_Q = \pm \left\{ X'_Q{}^2 + X''_Q{}^2 \right\}^{1/2} \quad (8)$$

X_Q was calculated for various numbers of verticals per cross-section for the one-point, two-point, and velocity distribution methods. The estimated values for the individual error components presented in the foregoing were used in the calculations. The calculation results are presented in Table 7.

The total percentage standard error for the two-point velocity-area measurements (15-20 verticals) at Dresden and Powerton were 1.5 and 0.8% for the Dresden intake and discharge canals, respectively, and 1.1 and 4.5% for the Powerton intake and discharge canals, respectively. From Table 7 it can be seen that these experimental errors are generally less than the estimated total standard errors. This result would be anticipated because of the relative longitudinal and cross-sectional uniformity of the canals and the generally well-behaved nature of the measured flows. The reason for the higher than expected experimental errors in the Powerton discharge canal is not known at this time.

Weir Equation Calibration and Validation

As discussed in Section 7, an initial set of dye and flow meter measurements were made at the Quad Cities Nuclear Station to determine a stage-discharge equation for the wing-tipped weir in the spray canal.

These data are shown in Table 5. The form of the proposed weir equation was

$$Q = C_e L_e H^{3/2} \quad (9)$$

where the quantities in equation (9) are the same as those defined for equation (5). The terms C_e and L_e in equation (9) are functions of weir head (H), velocity of approach (v), and weir geometry. It was assumed that the dependency of C_e and L_e on these parameters could be expressed through a representation similar to the Francis formula. That is,

$$C_e L_e = M \left\{ \left(1 + \frac{v^2/2g}{H} \right)^{3/2} - \left(\frac{v^2/2g}{H} \right)^{3/2} \right\} \quad (10)$$

To complete the discharge equation development, the velocity of approach was correlated to weir head by making use of the Ott meter data, and the constant M was determined from a statistical analysis of both the Ott meter and dye dilution data. The resulting weir equation is given below.

$$Q = 772 \left\{ (H + h)^{3/2} - h^{3/2} \right\} \quad (11)$$

where

$$h = (0.78H - 0.31)^2 / 2g$$

$$g = \text{gravitational acceleration (ft}^2/\text{sec)}$$

A plot of the weir equation, along with the initial set of data is presented in the upper graph of Figure 11.

A subsequent set of flow measurements were made to validate the weir equation. These data are shown in Table 6 and the lower graph of Figure 11. From Table 6 it can be seen that the validation flow measurements agreed with the weir equation predictions to within 2%. From Table 7 it can be seen that this variation is less than the probable experimental error for the measurement procedures used.

Velocity-Area Measurements: Comparison of Methods

The velocity-distribution method was used for a mid-canal transect made in conjunction with the weir equation validation tests at Quad Cities. The data from this transect were used to compute discharges by the

one-point and two-point methods as well as by the velocity-distribution method. These calculations were carried out for mid-section intervals of 5, 10, and 20 feet. The mid-section intervals correspond to about 40, 20, and 10 verticals per transect, respectively, or about 2.5, 5, and 10% of canal width per interval, respectively. The results of the calculations are given in Table 8.

These results show that the calculated discharge was not particularly sensitive to the number of velocity measurements per vertical. For example, for the 5 foot mid-section interval, the discharges calculated by the three methods differed from the mean of the three discharges by less than 0.5%. This finding, which is consistent with the standard error estimates given in Table 7, was an important one for the present study. This was because of a more than four-fold decrease in measurement time for the two-point method as compared to the velocity distribution procedure. Another finding, also consistent with the standard error estimates, is that experimental error increases relatively quickly with decreasing number of transects per cross-section. For example, the means of the flows computed for the 10 and 20 foot intervals differed from the 5 foot interval mean by 0.4% and 6.9%, respectively. This error, however, appears to be more systematic than random in that the increased flows calculated for the larger intervals were primarily due to over estimates of mean velocity in near shore areas.

9. Conclusions

The following conclusions are reached regarding the flow measurements and analyses reported herein.

(1) The experimental error in the flow rates measured at Powerton Station and Dresden Nuclear Station were, as expected, generally less than the estimated total standard error.

(2) For measurements of flow rate by dye-dilution methods, preliminary experiments should be carried out to insure complete mixing at the measurement cross-section under all expected flow conditions.

(3) The stage-discharge equation for the weir in the Quad Cities Nuclear Station spray canal predicts flow rates to within the probable experimental error of validation measurements.

(4) Flow rate calculations for these canals are not particularly sensitive to the number of points per vertical, but are affected by the number of verticals per transect.

10. References

- [1] Buchanan, T.J. and Somers, W.P., "Discharge Measurements at Gaging Stations," Book 3, Chapter A8 of Techniques of Water-Resources Investigations of the U.S. Geological Survey, Geological Survey, U.S. Department of the Interior, 1969.
- [2] "Current Meters," Chapter 5 of Water Measurement Manual, Bureau of Reclamation, U.S. Department of the Interior, Second Edition, Revised Reprint, 1974.
- [3] "Instruments and Methods of Observation," Chapter 2 of Guide to Hydrometeorological Practices, WMO-No. 168. TP. 82, World Meteorological Organization, 1970.
- [4] Kulin, G. and Compton, P.R., "A Guide to Methods for the Measurement of Water Flow," NBS Special Publication 421, National Bureau of Standards, U.S. Department of Commerce, May 1975.
- [5] "Liquid Flow Measurement in Open Channels - - Velocity-Area Method," International Standard I.S.O. 748, 1973. (Obtainable from American National Standards Institute, 1430 Broadway, New York, N.Y. 10018).
- [6] Johnson, R.L., "Laboratory Determination of Current Meter Performance," Technical Report No. 843-1, Division Hydraulic Laboratory, North Pacific Division, U.S. Army Corps of Engineers, November 1966.
- [7] Wilson, J.F., "Fluorometric Procedures for Dye Tracing," Book 3, Chapter A12 of Techniques of Water-Resources Investigations of the U.S. Geological Survey, Geological Survey, U.S. Department of the Interior, 1968.
- [8] Replogle, J.A., Myers, L.E., Brust, K.J., "Flow Measurements with Fluorescent Tracers," Journal of the Hydraulics Division, ASCE, Vol. 92, HY5, pp. 1-15, September 1966.
- [9] Kirkpatrick, F.A., Sayre, W.W. and Richardson, E.V., "Flow Measurements with Fluorescent Tracers" Journal of the Hydraulics Division, ASCE, Vol. 93, HY4, pp. 298-308, July 1967.

[10] Kirkpatrick, F.A., "Flow Calibration by Dye-Dilution Measurement," Civil Engineering, February 1968, pp. 74-76.

[11] "Instruction Manual," Ott Universal Current Meter C31 (10.002).

Table 1. Flow Rate Measurements for the Powerton Station Intake Canal

Date	Top Width	Cross-Section Area	Flow Rate	Average Velocity
	(ft)	(ft ²)	(cfs)	(fps)
21 Aug 75	95.3	658.3	801.7	1.22
30 Aug 75	92.8	641.2	778.0	1.21
30 Aug 75	92.7	647.9	790.2	1.22
31 Aug 75	94.0	646.8	786.1	1.22
31 Aug 75	94.1	647.9	787.7	1.22
1 Sept 75	94.0	653.8	774.4	1.18
1 Sept 75	94.2	654.5	787.3	1.20

Table 2. Flow Rate Measurements for the Powerton Station Discharge Canal

Date	Top Width	Cross-Section Area	Flow Rate	Average Velocity
	(ft)	(ft ²)	(cfs)	(fps)
21 Aug 75	91.2	714.4	866.1	1.21
29 Aug 75	90.5	705.5	857.1	1.21
30 Aug 75	90.0	705.0	883.2	1.25
31 Aug 75	91.2	699.1	857.5	1.23
31 Aug 75	91.5	696.7	852.8	1.22
1 Sept 75	91.5	702.7	815.3	1.16
1 Sept 75	91.5	701.8	844.5	1.20

Table 3. Flow Rate Measurements for the Dresden
Nuclear Station Intake Canal

Date	Top Width	Cross-Section Area	Flow Rate	Average Velocity
	(ft)	(ft ²)	(cfs)	(fps)
7 Aug 75	85.0	483.3	1111.0	2.30
7 Aug 75	85.0	479.3	1126.1	2.35
8 Aug 75	85.3	480.4	1125.9	2.34
9 Aug 75	85.0	475.4	1086.2	2.28
10 Aug 75	84.7	472.2	1102.6	2.34

Table 4. Flow Rate Measurements for the Dresden Nuclear
Station Discharge Canal

Date	Top Width	Cross-Section Area	Flow Rate	Average Velocity
	(ft)	(ft ²)	(cfs)	(fps)
7 Aug 75	91.5	916.3	1081.5	1.18
7 Aug 75	93.0	930.4	1077.9	1.16
8 Aug 75	86.5	832.2	1093.9	1.31
9 Aug 75	93.8	928.6	1072.9	1.16
10 Aug 75	94.8	948.0	1073.0	1.13

Table 5. Quad Cities Nuclear Station Flow
Measurements (Weir Calibration)

Date	Number of Lift Pumps	Weir Head	Flow Rate (dye dilution)	Flow Rate (Ott meter)
		(ft)	(cfs)	(cfs)
10 July 75	2	1.07	833	804
8 July 75	3	1.33	1252	1216
22 May 75	3	1.38	1269	—
19 July 75	5	1.90	—	2043
3 Aug 75	5	1.92	2072	—

Table 6. Quad Cities Nuclear Station Flow Measurements
(Weir Validation)

Date	Number of Lift Pumps	Weir Head (ft)	Flow Rate (A) (Ott meter) (cfs)	Flow Rate (B) (weir equation) (cfs)	Percent Difference (A-B/B) (%)
28 July 76	3	1.34	1221	1208	1.1
13 Aug 76	3	1.36	1241	1236	0.4
14 Aug 76	3	1.35	1202	1222	-1.6

Table 7. Estimated Total Standard Error
in the Discharge (%)

<u>Method</u>	<u>Number of Verticals</u>			
	10	15	20	40
One-Point	5.1	3.8	3.4	2.4
Two-Point	4.9	3.6	3.3	2.3
Velocity Distribution	4.7	3.4	3.1	2.1

Table 8. Comparison of Calculation Procedures

Mid-Section Interval	Q (one-point method)	Q (two-point method)	Q (velocity- distribution method)	Mean
(ft)	(cfs)	(cfs)	(cfs)	(cfs)
5	1295	1289	1296	1293
10	1302	1289	1304	1298
20	1382	1377	1389	1383



FIGURE 1. POWERTON STATION

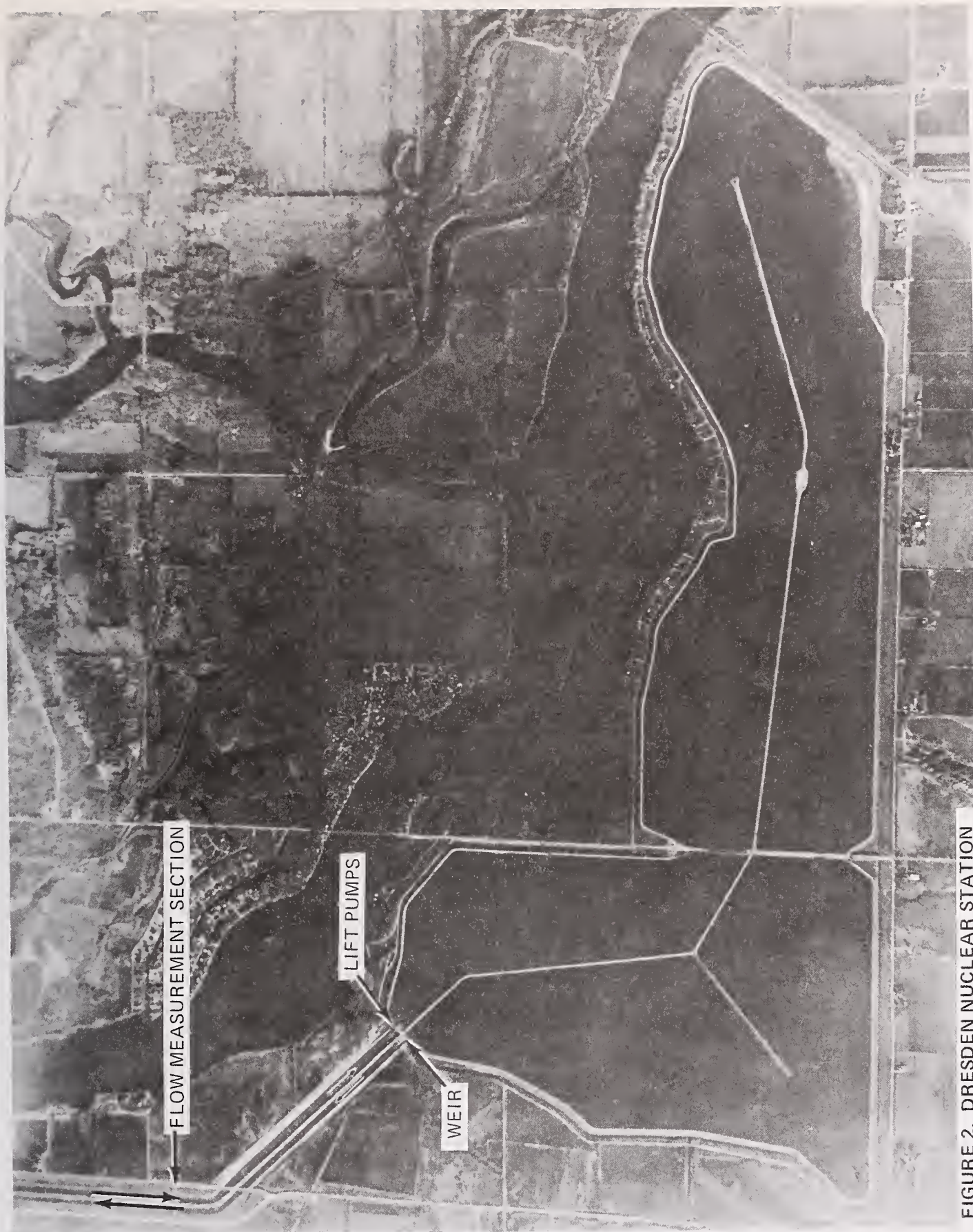


FIGURE 2. DRESDEN NUCLEAR STATION

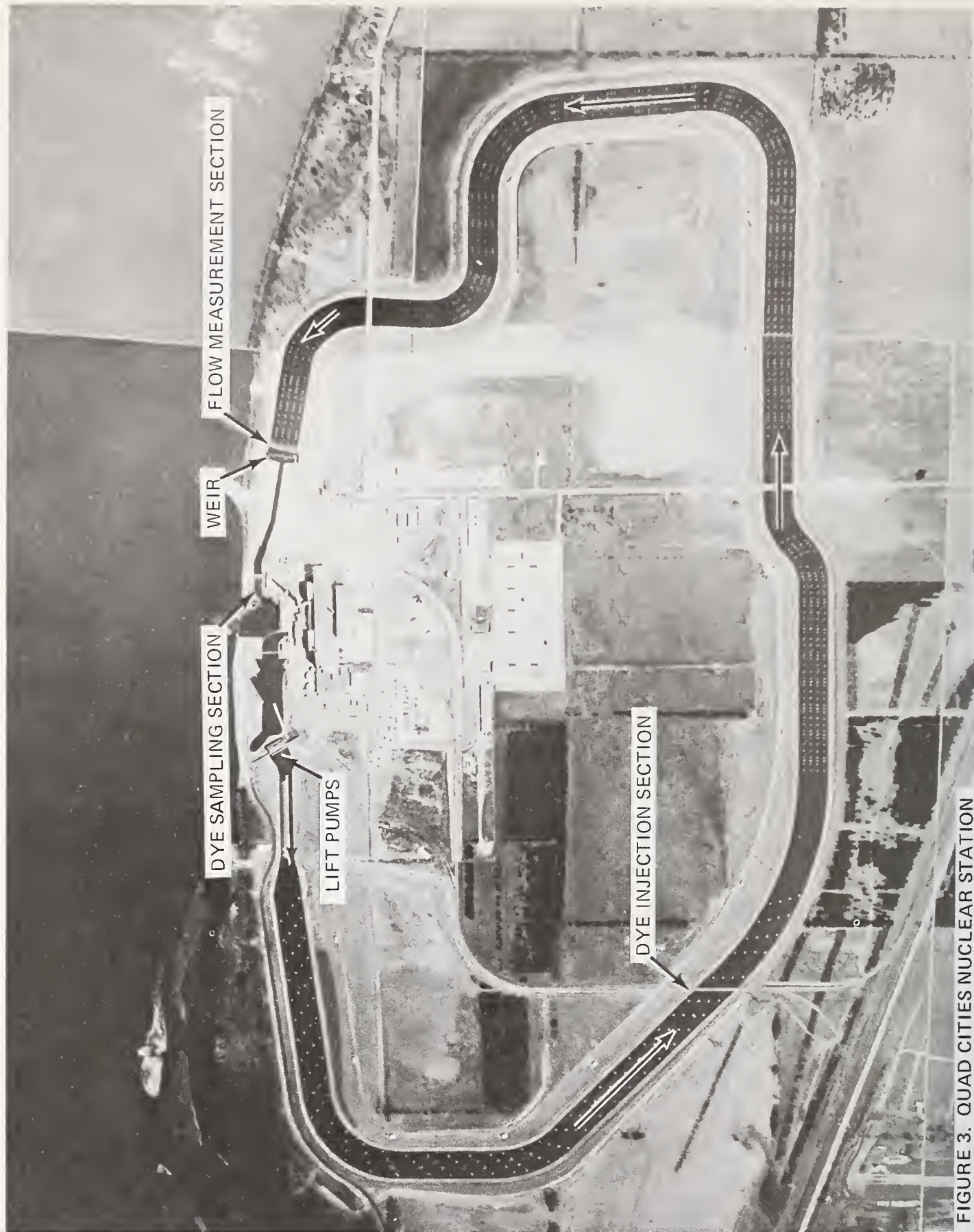


FIGURE 3. QUAD CITIES NUCLEAR STATION

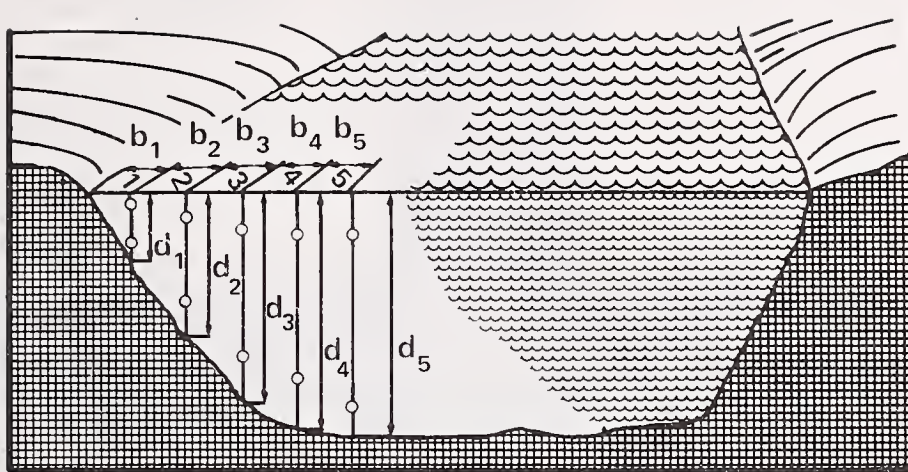


FIGURE 4

CROSS-SECTION SHOWING
LOCATION OF POINTS OF
VELOCITY MEASUREMENTS

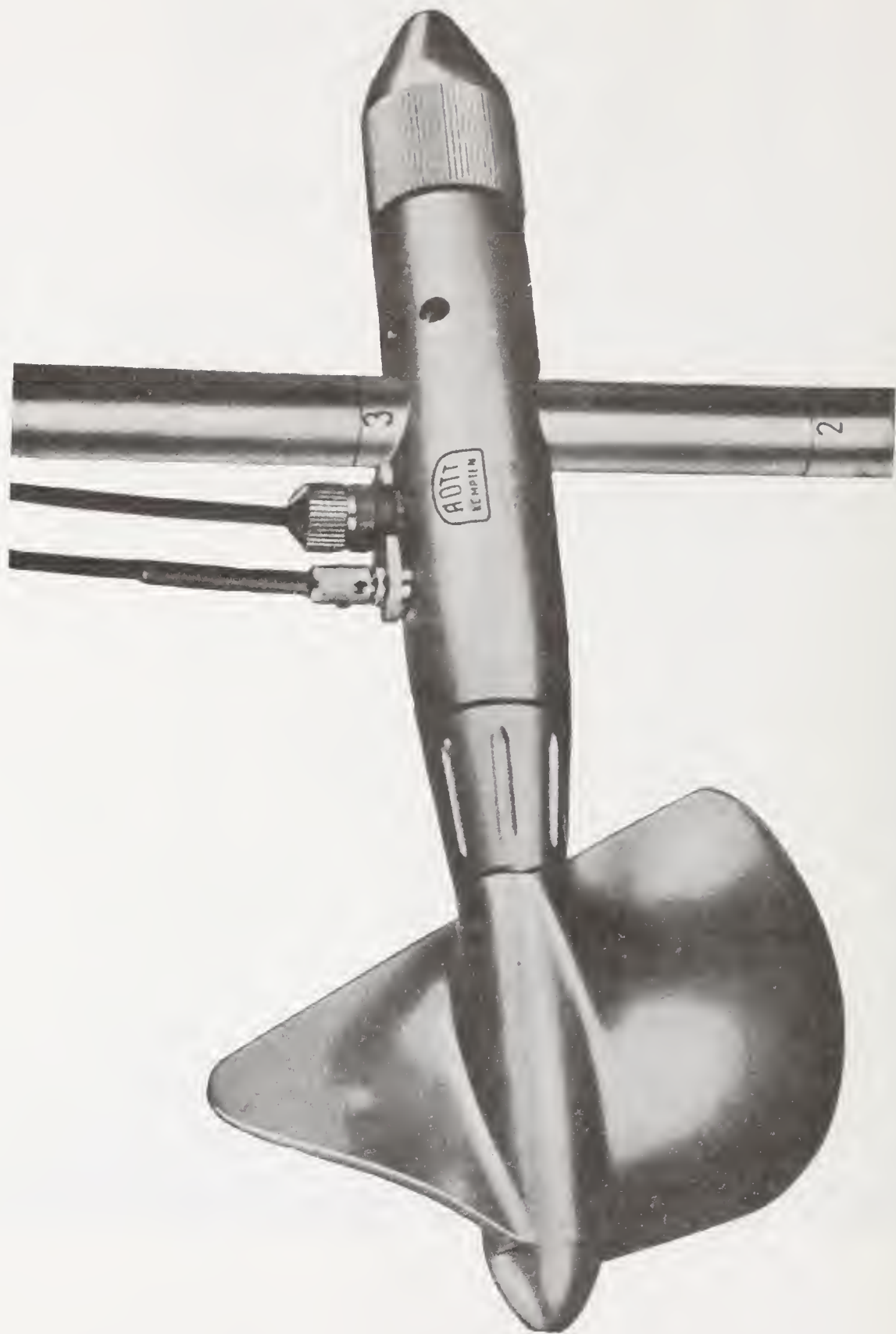
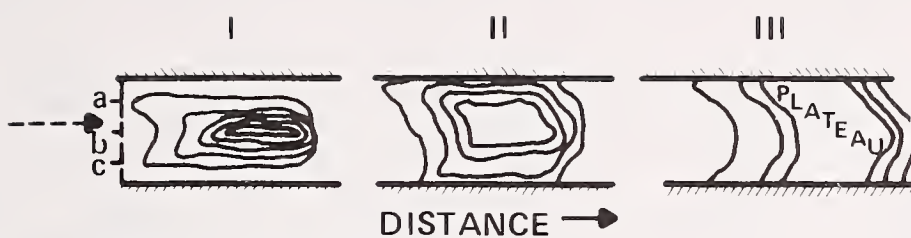
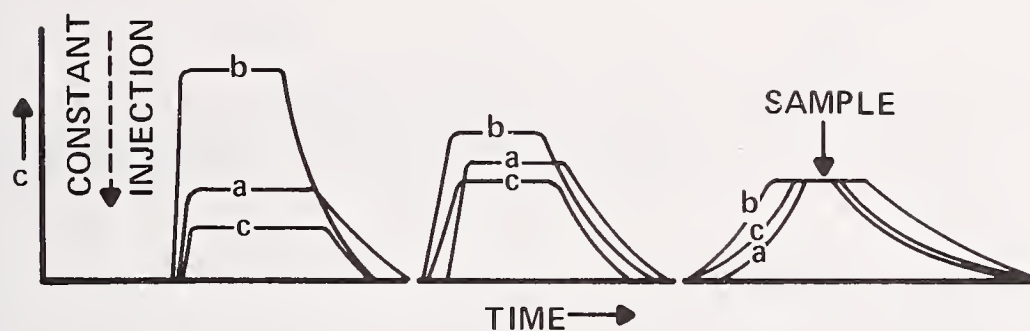


FIGURE 5. OTT PROPELLER CURRENT METER



(a) SPATIAL DISTRIBUTION



(b) TIME - CONCENTRATION CURVES

FIGURE 6

DYE CLOUD AS IT DISPERSES DUE
TO SINGLE POINT, CONSTANT RATE
OF DYE INJECTION UPSTREAM, AFTER
KIRKPATRICK, ET AL., [9]

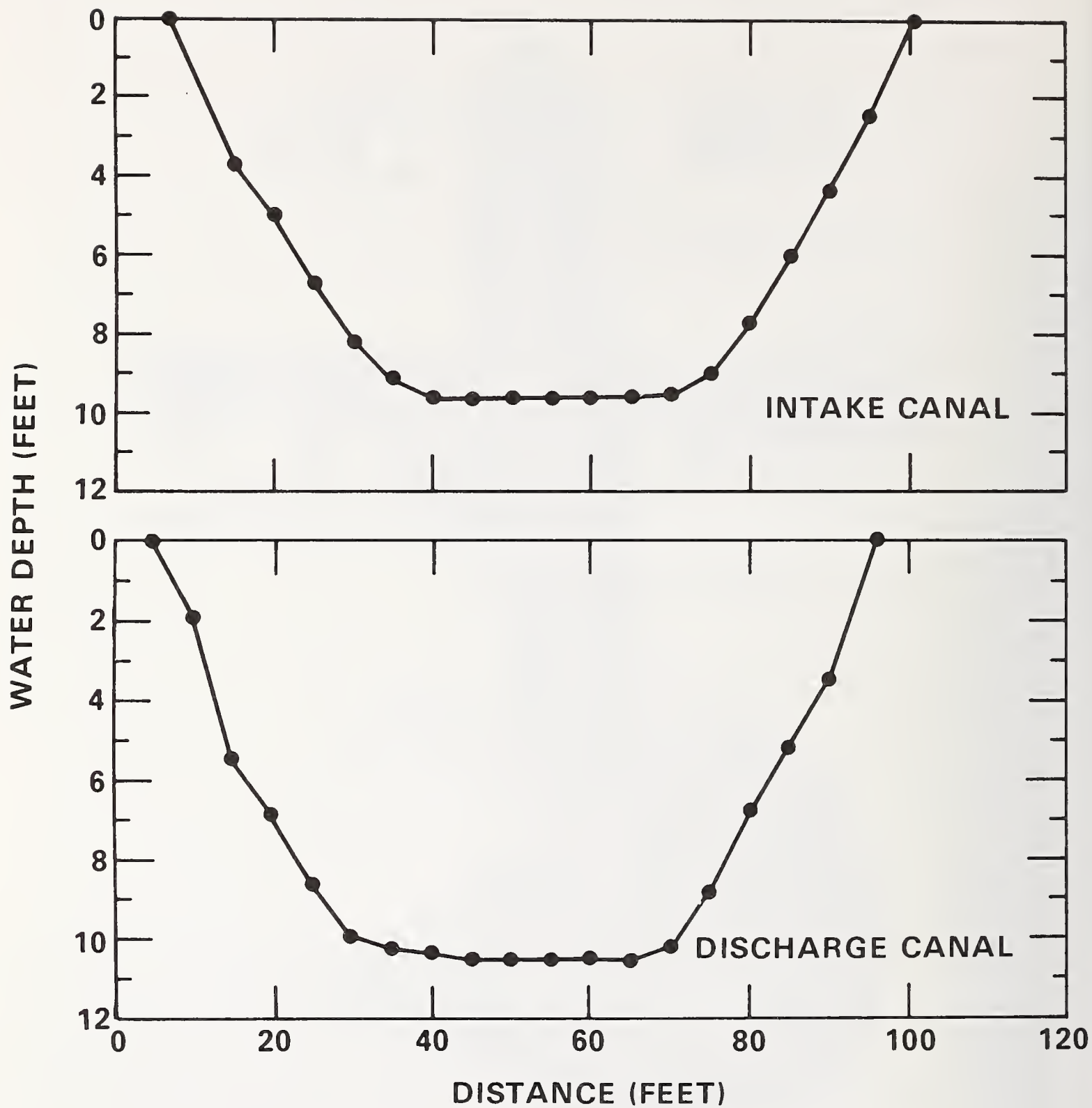


FIGURE 7
CROSS-SECTIONS OF POWERTON STATION CANALS
ON 1 SEPTEMBER 1975

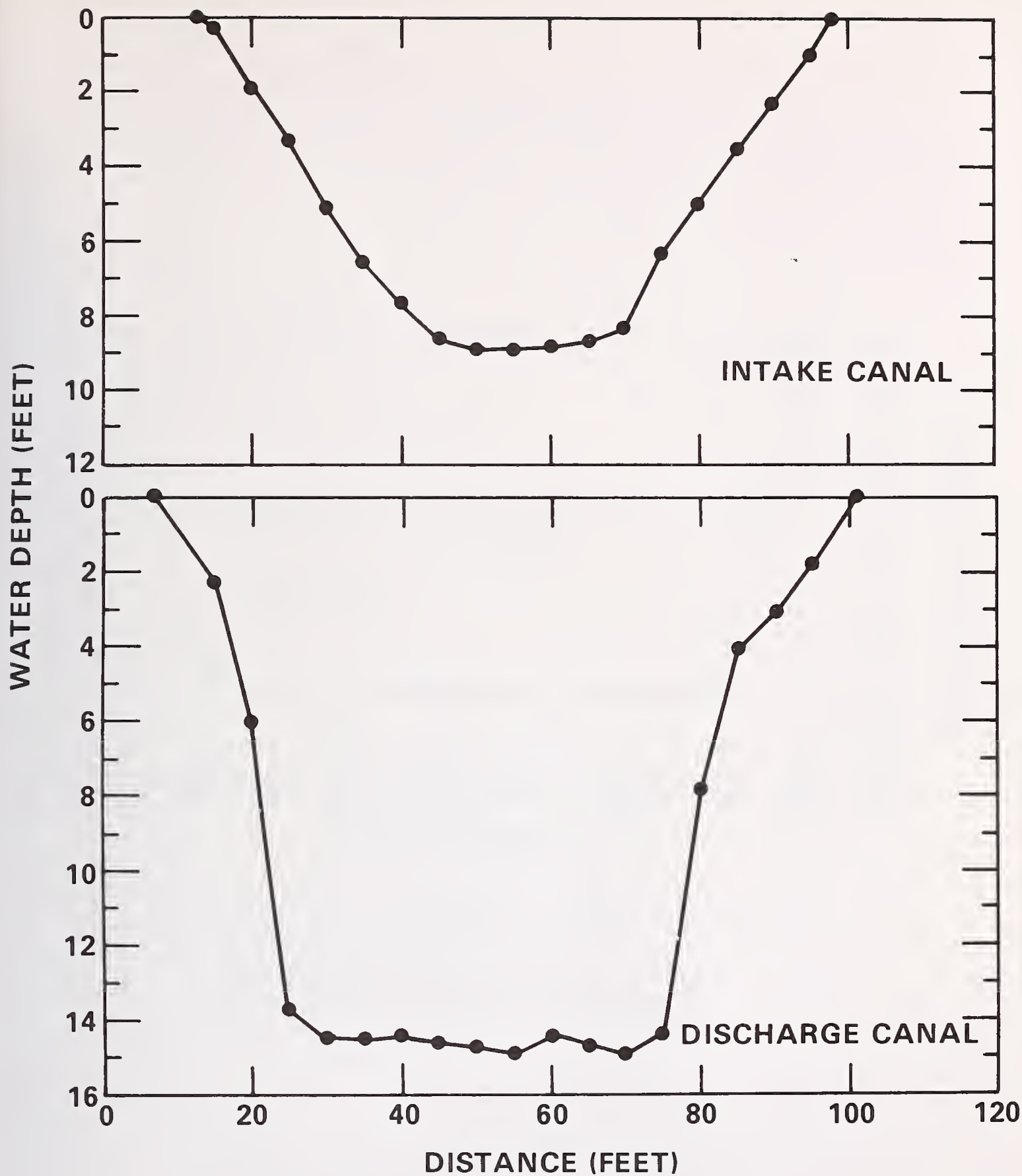


FIGURE 8

CROSS-SECTIONS OF DRESDEN NUCLEAR STATION
CANALS ON 9 AUGUST 1975

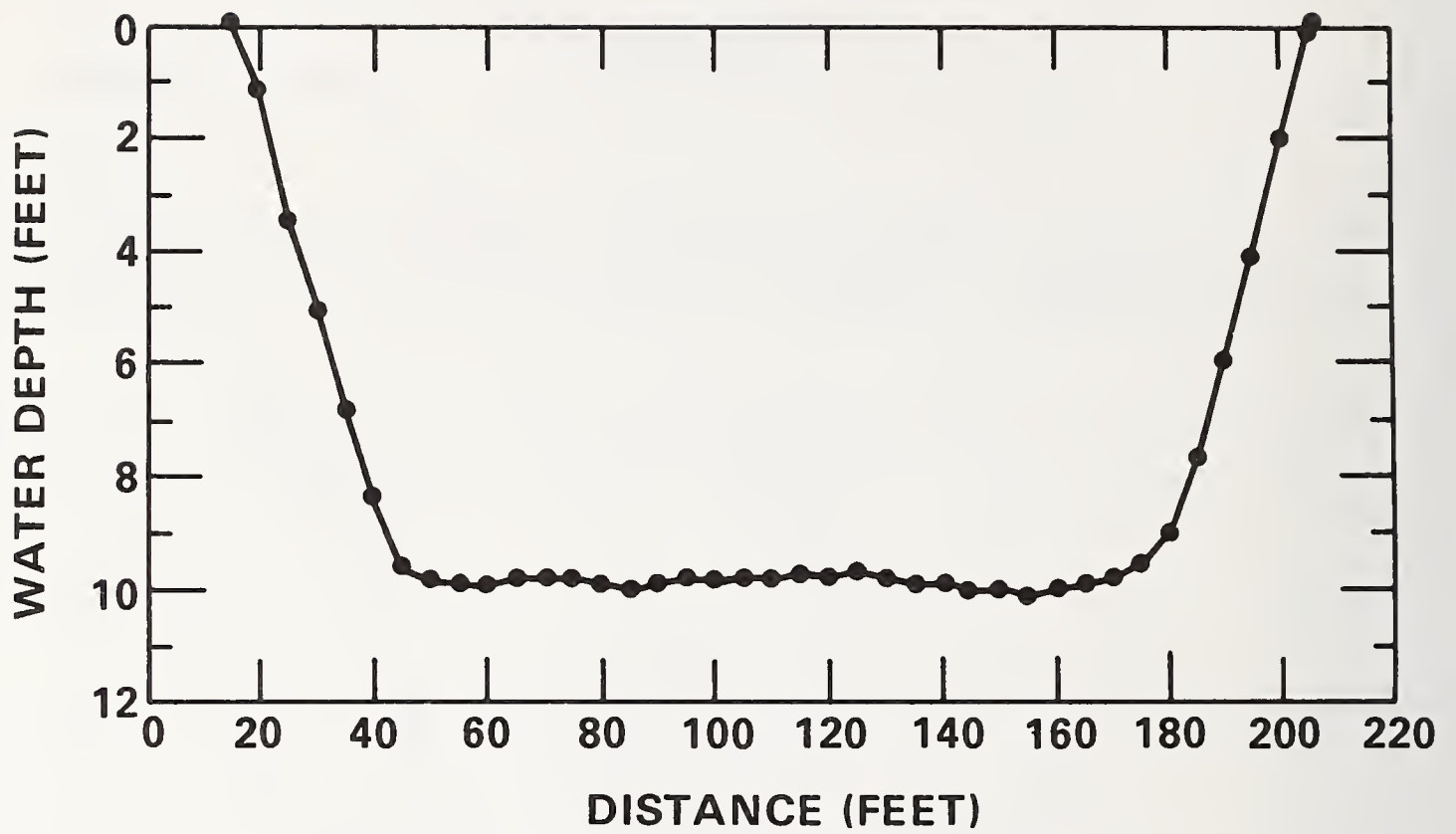


FIGURE 9

CROSS-SECTION OF QUAD CITIES NUCLEAR
STATION SPRAY CANAL ON 13 AUGUST 1976

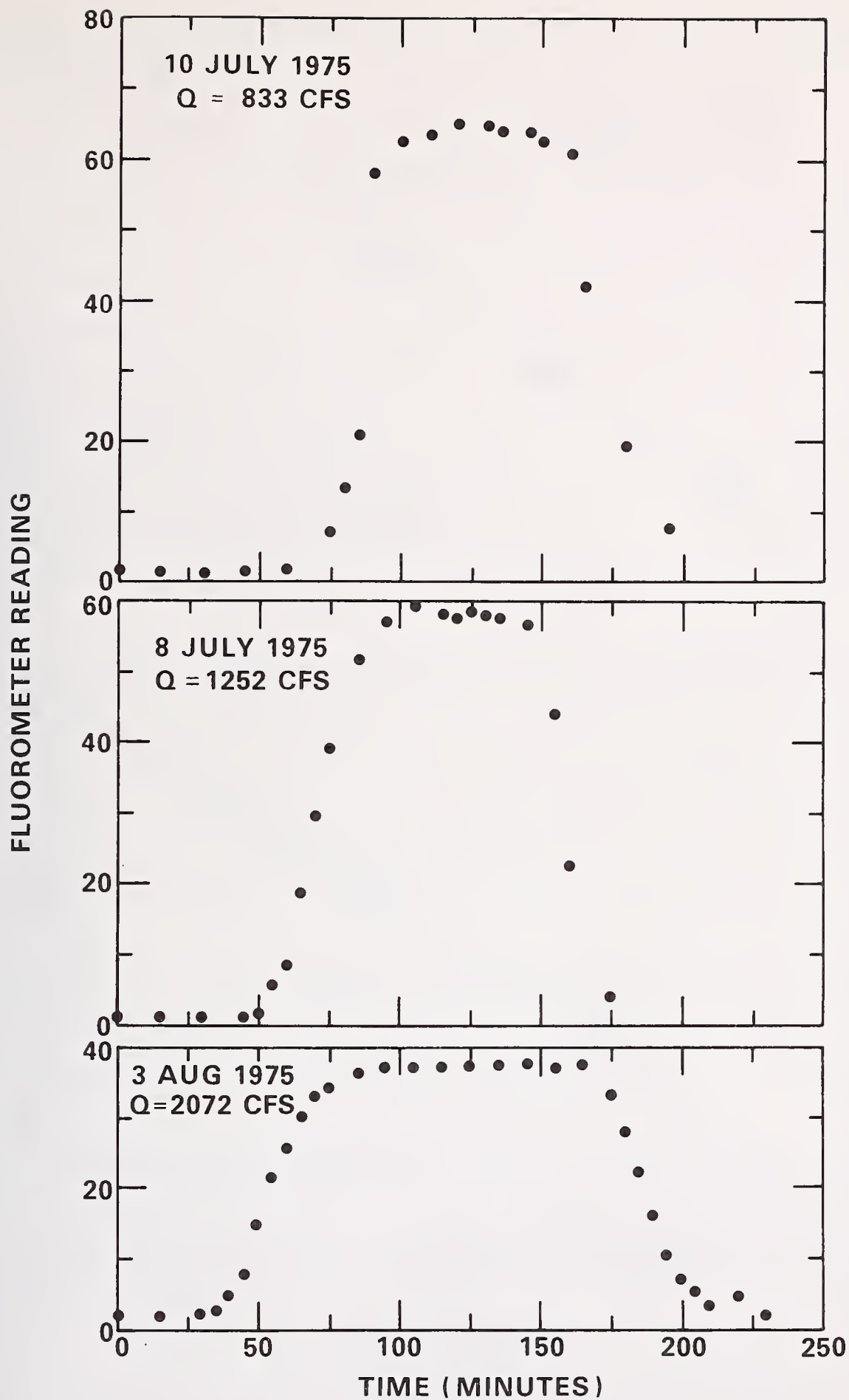


FIGURE 10

SAMPLE FLUORESCENCE AT MEASUREMENT
CROSS-SECTION

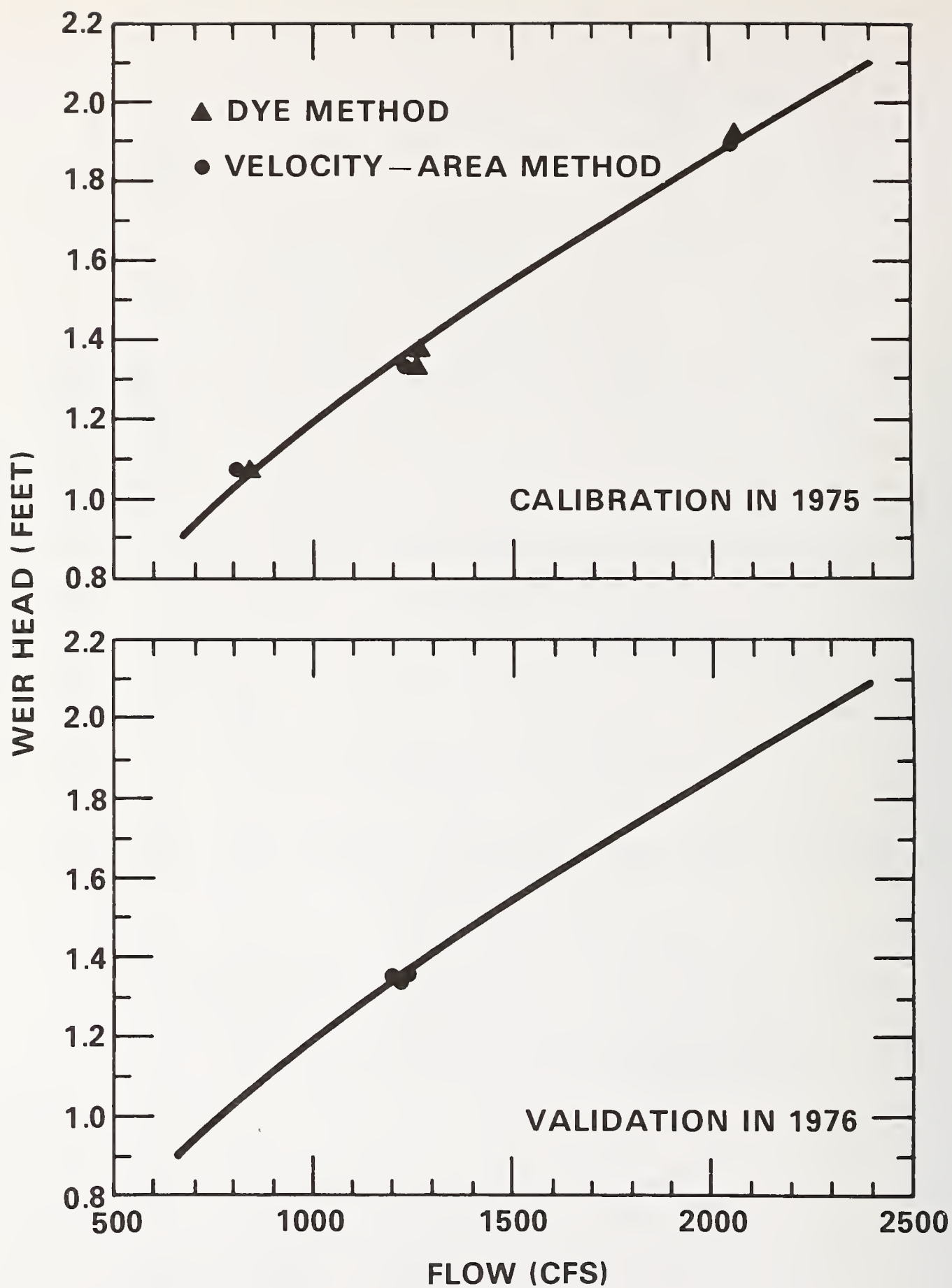


FIGURE 11

WEIR FLOW CALIBRATION AND VALIDATION
IN THE QUAD CITIES NUCLEAR
STATION SPRAY CANAL

ERRORS IN FLOW MEASUREMENT AND THEIR IMPORTANCE IN
INFILTRATION/INFLOW ANALYSIS

D. L. Guthrie
Environmental Quality Systems, Inc.
Rockville, Maryland

D. R. Washington and C. Vincenty
Donald R. Washington and Associates
Residencial Tintillo, Bayamon, Puerto Rico

For infiltration/inflow analysis, flow measurement problems encountered in warm weather and humid climates include rapid build-up of floc particles and solids caused by high bacterial growth rates. Environmental in situ factors not only have a tendency to shorten equipment life but also to reduce the accuracy of flow determinations and to lengthen the time required for field study of infiltration/inflow problems.

Several common flow-measurement devices including the weir, Parshall flume, and scow were used in field studies of infiltration/inflow in Puerto Rico. Mathematical determinations of infiltration/inflow were made by calculating the hydraulic gradient, the height of water in the sewer, and the velocity head loss. Both of these instrumental and physical-mathematical methods for flow determination are reviewed, stressing the advantages and disadvantages of each, their sources of error, and methods used to resolve that error, wherever possible.

Results of infiltration/inflow studies are presented, emphasizing flow determination errors and their effect upon the inherent errors in infiltration/inflow assessment. Sewer system evaluations are not discussed because they are concerned with the evaluation of the physical problems of the existing sewer system which would increase infiltration/inflow.

Errors resulting from operational problems with physical flow-measurement devices are presented, along with a strategy to reduce these errors. The impact of operational problems in flow determination on infiltration/inflow assessment are also presented, along with field-tested resolutions for those problems.

1. Introduction

Flow determination is one of the most important and critical steps in infiltration/inflow analysis. There are many ways to measure flow, depending upon the application of the chosen flow-measurement device.

The infiltration/inflow (I/I) studies providing the data base for this paper were conducted in Puerto Rico. Isabela [1]¹ and Bayamon [2], Puerto Rico, including ten other urbanizations were studied by the authors under contract to the Puerto Rico Aqueduct and Sewer Authority (PRASA).

Errors in flow measurement can result from many sources in the field. The errors, of course, are different for different flow measurement devices. The most commonly used devices for measuring flow in semi-closed conduits or sewers are:

- (1) Water level recorder
- (2) Manning "dipper"
- (3) Parshall flume
- (4) Pitot tube
- (5) Weir
- (6) Scow

These devices are either universal in concept and design or are manufactured commercially.

Sewer flows can also be measured physically. There are two methods:

- (1) Hydraulic grade line measurements
- (2) Hand measurement of depth of flow

Both instrumental and physical methods will now be reviewed in respect to their (1) installation, where applicable; and (2) sources of error. Some field-tested approaches to minimize the error in flow results will be detailed.

Water Level Recorder

Several water level recorders are commercially available. The recorders used by the authors were manufactured by the Stevens Company.² Other variations of this instrument have been modified for use as tide gauges and test well recorders for depth-to-water table measurements. The authors used the Stevens recorders to measure the head (1) above weirs, (2) in Parshall flumes, and attached to a scow.

The recorder is mounted on either wooden, metal, or plastic platform, attached to the wall of the manhole (or flume, etc.) by brackets and nail studs. Care must be taken to align the float carefully over the exact center of the usually semi-circular channel in the middle of the manhole. A stilling basin must then be constructed using PVC pipe, for example, so that the float will maintain a relatively stable position and will not be subjected to the force of the current. Only through experience and judgment on a case-by-case basis can the installer select the correct length of PVC pipe so periodic high flows will not cause wastewater to spill over on top of the float, perhaps dislodging it from the stilling basin.

¹Figures in brackets indicate the literature references at the end of this paper.

²Leupold and Stevens Company, Beaverton, Oregon.

Debris accumulation is a problem in using the water level recorder method. A scum layer of 1/2 to 3 inches invariably forms. It must be frequently removed (every one to two days) to insure accurate measurements and to minimize errors.

Another source of error is the dislodging of the stilling basin. The stilling basin was usually positioned by the authors by wire to nail studs shot into the walls of the manhole in a triangular fashion radiating from the stilling basin. During periods of surcharging, not only are the chances of the stilling basin to be dislodged great, but the recorder itself may be inundated. Either of these events would cause a loss of data for a significant period of time.

Calibration of the chart may also cause problems. The water level must be measured from the bottom of the invert. With an inexperienced field crew, more training must be initiated by the field engineer to ensure that this is done properly. The water level must be measured at the same place in the manhole every time. Slight construction irregularities in the sewer can introduce a significant source of error to an infiltration/inflow study. The pen ink must be regularly changed to minimize ink dry-ups and ink blotting the chart.

Manning "Dipper"

A very common device used in infiltration/inflow studies is the "dipper," developed by the Manning Corporation.³ The instrument consists of a cylindrical housing and a probe. Dippers are available in several lengths, the most common of which are 15 and 18 feet. Upon contact with the water surface completing the circuit by grounding, the probe retracts slightly to descend again. Electronic circuitry transforms the change in the water or wastewater elevation to a circular chart recorder. The unit is powered externally by a battery.

This device was found to be reliable for only short periods of time. Over extended time periods, the chance for problems to occur is increased. The units had to be regularly serviced every one to two weeks. Field problems are as follows:

- (1) Dead batteries (batteries should be charged every 2 days at a minimum)
- (2) Acid spills
- (3) Failure to establish a proper ground
- (4) Cable corrosion
- (5) High temperature and humidity causing arcing and short-circuiting
- (6) Fouling of the probe with scum, trash and debris
- (7) Inking problems on the chart

Each of these seven field problems, if not rectified promptly and efficiently, could result in significant data losses. During an I/I study in Bayamon, Puerto Rico, an 80 percent data loss was sometimes realized at certain

³Manning Environmental Corporation, Santa Cruz, California.

stations. Again, the dipper (and probe) must be centralized in the middle of the channel so that the water level can be measured as accurately as possible.

Parshall Flume

As a temporary field measurement technique, the use of the Parshall flume is ludicrous from the standpoint of capital expenditure, construction practicality, and cost-effectiveness. Therefore, their use is largely confined to permanent facilities, such as sewage treatment plants.

Parshall flumes were found to work well under normal conditions. The deposition of solids and debris is not extensive, reducing errors in flow measurement caused by that deposition. The largest problems encountered by the authors, especially at the Levittown and Sierra Bayamon sewage treatment plants, were that the flow meters operated by the Puerto Rico Aqueduct and Sewer Authority were inoperative a large percentage of the time. They had to be replaced by Stevens meters. Unfortunately, the flow in Parshall flumes was never calibrated with another flow measurement device such as a weir so that the discrepancy in flow resulting from using the two methods was never calculated.

Pitot Tube

A usually reliable and accurate flow measuring device, the pitot tube, has been used for measurement of closed conduit liquid flow for many years. However, due to the accumulation of solids and debris in open channel sewers, a pitot tube would become clogged within several minutes. This tendency for solids build-up increases in small diameter sewers because, in warmer climates, higher evaporation rates cause the percent solids in the wastewater to be substantially higher than larger diameter sewers, where dilution tends to reduce the solids concentration. Thus, the pitot tube is completely impracticable for wastewater flow measurement.

Weir

Because Manning "dippers" are impracticable for flow measurement in shallow, small diameter sewers (their probes do not retract far enough), Parshall flumes are impracticable as temporary flow measurement devices, and pitot tubes have too many fouling difficulties, the weir becomes a reasonable alternative for wastewater flow measurement. It is used in conjunction with a Stevens or other equivalent water level recorder.

Many problems result in searching for a complete weir formula due to the inconsistency of the nomenclature and the specificity of the formulas presented. The foremost of these is the problem of a submerged weir. The authors have found that V-notch weirs tend to be the most reliable. The formulae most commonly given for the low flows caused by infiltration are very limited in their accuracy as their flow approaches the average sewage flow. For normal and peak flow, a suppressed rectangular weir is preferred. In an effort to obtain the benefits afforded by both types of weirs, a combination weir was developed which, in the authors' experience, is a preferable method of metering sewage flow to either component part. The derivation of a weir formula will be discussed subsequently.

Although the weir is a relatively good and maintenance-free flow measurement device, its installation is rather difficult. First, a manhole in good structural condition, having no sediments on the apron, and preferably 4-7 feet in depth should be selected. After selection, the manhole surfaces should be cleaned by scrubbing or water spraying.

Measurements for weir construction appear in Figure 1. These measurements are optimal, but they can be easily modified depending upon field conditions. The weir is pre-cut to reduce labor and ensure standardization. Then, the sluice gate must be cut. Obtaining a proper fit of the sluice gate is very important to reduce leakage and therefore increase weir accuracy. Several refittings are necessary to obtain a tight fit, done while the wastewater is flowing. Finally, a rubber gasket is placed around the edge of the sluice gate to maintain a waterproof seal.

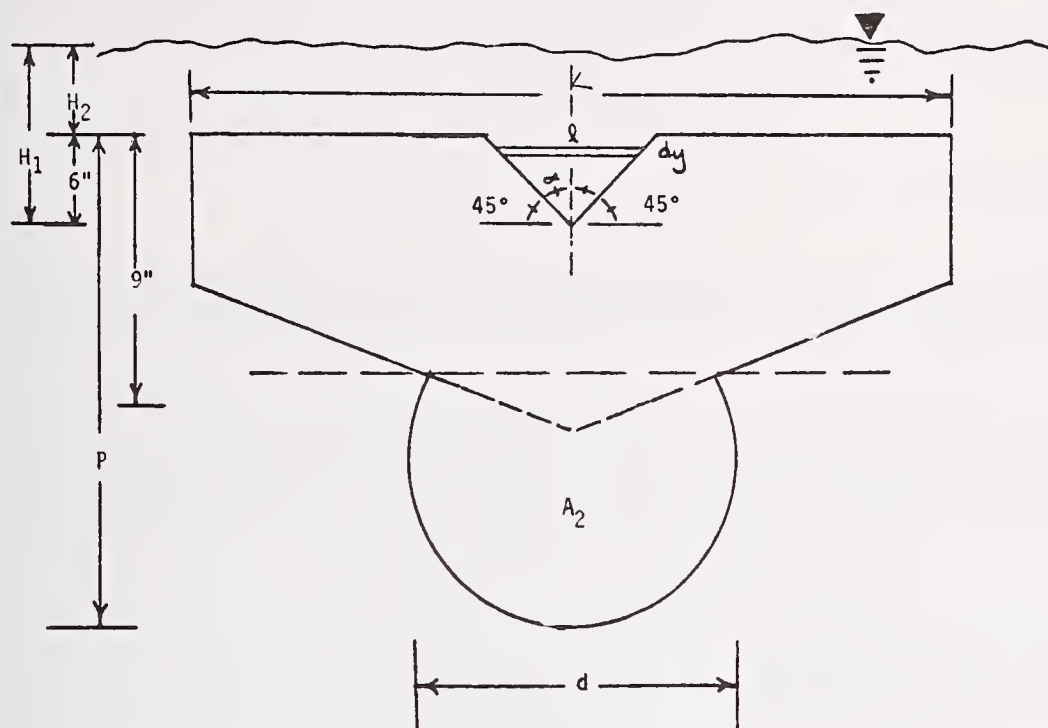


FIGURE 1. WEIR PLAN VIEW

Before actual weir installation, the sluice gate is fitted to the pre-cut weir, marking screw hole locations. Four screws or bolts are usually sufficient. The weir is then installed, placing the aluminum strip on the upstream side. Two wood braces attached to the weir hold it in position against the manhole wall using nails shot into the concrete.

Packing material must then be placed around the weir sides. It should be somewhat flexible, allowing for the seal to hold when the wood bends due to water pressure. The following materials are recommended:

- (1) hydraulic cement
- (2) tar
- (3) plastic.

After the weir is installed, the sluice gate must be positioned. In order to do this, the flow must be stopped with buckets, sandbags, inflatable stoppers, or whatever else is available.

The sluice gate is lowered and forced into its final position. This is a real "boots and gloves" job. Once installed, more insulation is placed around the weir and attached sluice gate, if needed. Finally, the water level recorder platform and stilling basin are installed on the upstream side of the weir, and the water level recorder (Stevens or equivalent) is placed in operation.

Two major problems are created by weir installation which can result in significant flow measurement problems. These are:

- (1) Solids accumulation behind the weir can become rather extensive. At a weir installed in the Sierra Bayamon system, a scum mat six inches thick accumulated [1].
- (2) Leaks often create critical flow measurement problems. There is no actual method for determining the percent volume of wastewater leaking from the weir, but either regular maintenance to add packing should be done or a percent volume leak could be estimated.

A derivation of a combination flow equation for the combination weir was presented in a recent Water and Sewage Works Journal article [3]. The final expression is a result from a combination of Bernoulli's equation and the standard weir formula for a 90° V-notch weir, and integrating to yield the formula for the combination weir. Taking into account the expression for C as revealed by King [4], the final equation for the combination weir including velocity of approach is:

$$Q_T = 2.52 \left(H_1^{2.47} - H_2^{2.47} \right) + 3.34 L H_2^{1.47} \left[1 + 0.56 \left(\frac{L H_2}{A} \right)^2 \right] \quad (a)$$

This equation says that A is the area of (L) (P + H), or more correctly, in a weir with the dimensions shown in Figure 1, A =

$$\frac{3}{2} L + 6L + \frac{10}{12} \pi + H_2 L \quad (b)$$

Tables for the solution of the second term in equation (a) are given in reference 4 starting on page 4-54. A graphical solution for a 90 degree V-notch weir with $L = 44$ in. shows that there is little difference for ten-inch and 16-inch diameter sewers. These appear in the aforementioned Journal article by the authors.

Despite the small differences between sewers in the 10 to 16-inch range, it is very easy to have errors. The authors noted that it is most difficult to measure flow closer than $1/4$ inch in the field to set the zero points on graphs. For example, in an eight-inch sewer at Bajura, Isabel, Puerto Rico, this amounts to a range of $12,000 \pm 5,000$ gal/day [1] - a 143 percent maximum error! For low flow over the weir, using equation (a), the flow at $H_1 = 1/4$ in. is 115 gal/day. At $H_1 = \pm 1/4$ in., the average relative error, or the average of the maximum and minimum errors divided by the accepted value, is 176 percent.

If weirs are to be used for making infiltration/inflow analyses, these corrections should be noted. Despite their occasional difficulties of installation, they have proven to be one of the most reliable and efficient methods for determination flow in small diameter sewers.

Scow

A scow is a flutable block attached to the side of a manhole by a vertically-pivoting rod. A wire from the top center of the scow is connected to a water level recorder located at the top of the manhole.

The scow is particularly useful in estimating flows in extremely deep manholes or in manholes subject to wide flow fluctuations. The total change in head allowed for by a scow using a 5 foot radius is approximately 8-9 feet. This type of scow was installed in the Calle Marina section of Bayamon, where manhole depths approximated 15-20 feet.⁴

Errors can occur when frequent and violent surcharging are evident. In the Calle Marina system, the manhole covers would blow off during periods of high-intensity, short-duration rainfall, which were frequent. Obviously, this does not tend to prolong equipment life!

Other problems were created during surcharging conditions. The most notable of these were:

- (1) The balled cable sometimes fell off the cylinder pulley. A man had to be sent down to retrieve the cable.
- (2) During one particularly violent surcharging (exact rainfall data could not be easily obtained because of convective precipitation. A standard USGS rain gauge several kilometers away was not representative of areawide precipitation), the scow was completely ripped off the wall of the manhole. It was never recovered.

⁴ It should be noted that in the installation of the scow, the field workers must wear gas masks when working in such a hazardous environment.

- (3) When the water level drastically and quickly changed, the drum recorder charts were almost impossible to read. Sometimes the ink smeared, blending several lines into one very thick one.

Hydraulic Grade Line Measurements

Flows were occasionally calculated by measuring the height of water and in order to compute the hydraulic grade line. The technique is useful for measuring flows in sewers located directly upstream from pumping stations. This method's reliability, however, is jeopardized by only periodically measuring the flow. A constant flow record is impracticable to obtain by this method.

Hand Measurement of Depth of Flow

When rapid measurements of wastewater flow are needed to cross-check previous measurements and/or calculations, the water level in the sewer can be measured by an extremely heavy plumb-bob and wire. The Manning equation [4] could be used to calculate the flow, if the slope is known. However, this is only a rough estimate for one point in time and should not be relied upon to contribute toward the study data base.

Measuring Flow in the Field

Field problems are sometimes created by circumstances independent of the measuring device used. These problems usually require an innovative approach in their solution and have the potential of causing a great loss of data.

Major considerations in attempting to measure sewer flow in the field are:

- (1) Traffic diversion problems
- (2) Sewer gas buildup and the risk of explosion
- (3) Theft of equipment
- (4) Deep manholes
- (5) Vibrations caused by heavy traffic flow.

These will be further explored at this point. Traffic diversion problems are minor, but they create a nuisance. Standard orange colors must be worn by all field workers, and flashing yellow lights may be necessary. An additional worker may have to be given the job of flagman. This creates the need for more fieldworkers, reduces the speed with which the survey is conducted and thereby reduces the number of stations which can be monitored daily, and lengthens the duration of the sampling program.

Sewer gas buildup and the risk of explosion tends to increase during periods of warm or hot weather. In the installation of weirs, the monitoring of flow patterns, and the other miscellaneous tasks necessary to conduct an I/I study, the manhole must be removed and several minutes be allowed to pass before entry. Even so, gas masks protecting the eyes, nose, and throat must be worn upon entry. Common sense prevails here.

Not necessarily a cause of error but a cause of data loss, is the theft of equipment. In an I/I study for Levittown, Puerto Rico [2], a theft rate of approximately 30 percent was noticed. In other words, something was stolen one out of every three days. Heavy chains and padlocks were insufficient. The study had to be extended an extra two months in this area.

Deep manholes present problems previously mentioned. Again, these are:

- (1) Difficulty in measuring water elevation
- (2) Difficulty in assessing groundwater elevation
- (3) Difficulty in centralizing "dipper" probe in the channel

At first thought, a discussion of vibrations from heavy traffic may appear to be irrelevant to this paper. Several years ago, the authors thought that also. However, not so. In a manhole in Sierra Bayamon, a Manning dipper was securely installed. Several days later when it was checked, the dipper, battery, cables and rack were gone. It showed up on the bar rack of the Puerto Nuevo sewage treatment plant approximately two months later! Needless to say, a week's data was lost, and the company would not repair the dipper!

Examples of Flow Measurement

Three examples of flow measurement are given, from the best-case to the worst-case. These flow measurements were made during August-November 1974 [2]. The sampling locations are shown in Figures 2 and 3.

The first case is shown in Figure 4 and represents wastewater flow and rainfall vs. time for the Bayamon Gardens Sewage Treatment Plant effluent. A continuous wastewater flow measurement was obtained, which correlated very nicely with precipitation in the same area.

Figure 5 shows a worsening field condition, where only a partial flow measurement was able to be obtained. The sampling station was located in the Calle Zinia area in Bayamon. The "S" indicates a surcharging condition. However, for more than 50 percent of the time period, rainfall could be correlated to wastewater flow and/or surcharging conditions.

The worst case of infiltration/inflow causing a loss of data appears in Figure 6 and represents data from the Calle Columbia Station in Bayamon. Rainfall could not be correlated to wastewater flow, as the rainfall gauge was more than two miles away from the sampling station. Additionally, the sewer surcharged more than 80 percent of the time. The peak flow was more than 300 percent greater than the highest measurable wastewater flow by conventional methods.



FIGURE 2

CENTRAL BAYAMON AREA

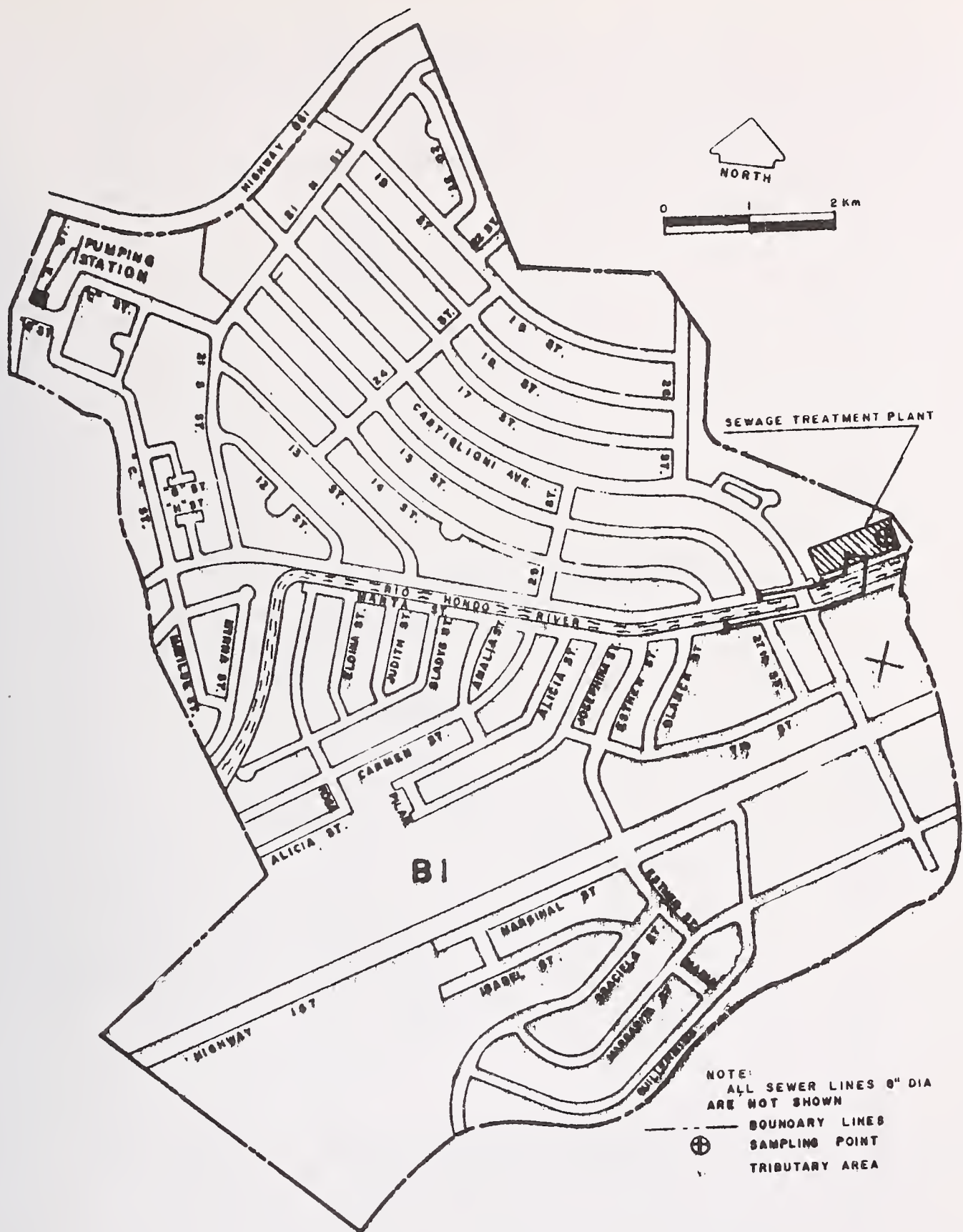
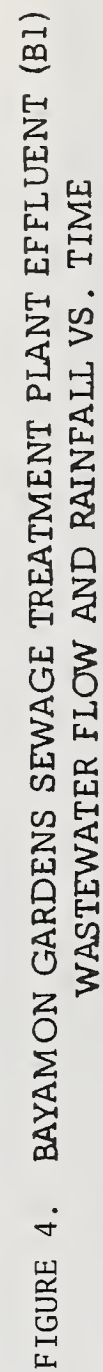


FIGURE 3. SAMPLING LOCATIONS



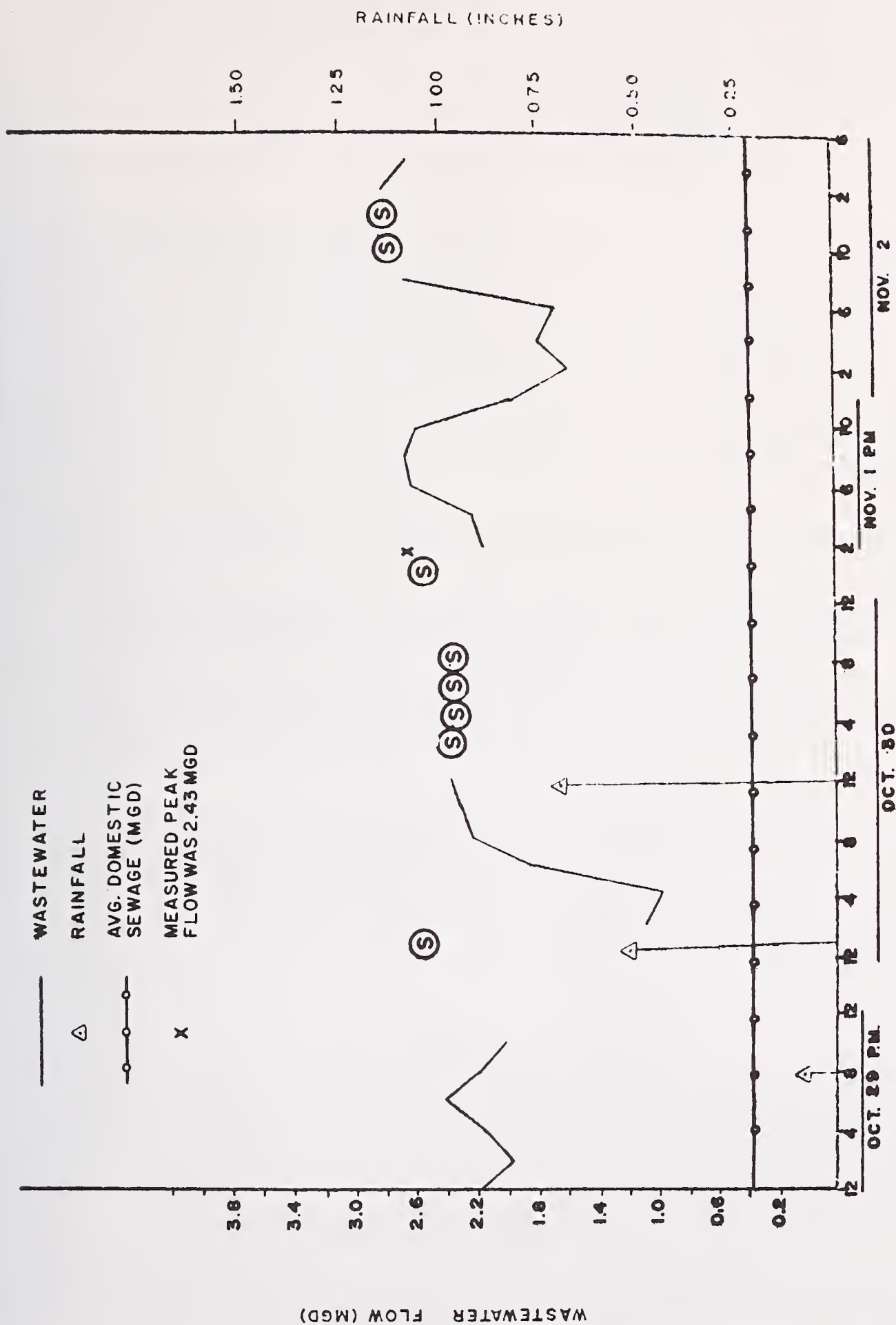


FIGURE 5. BAYAMON, CALLE ZINIA (A1b) WASTEWATER FLOW AND RAINFALL VS. TIME

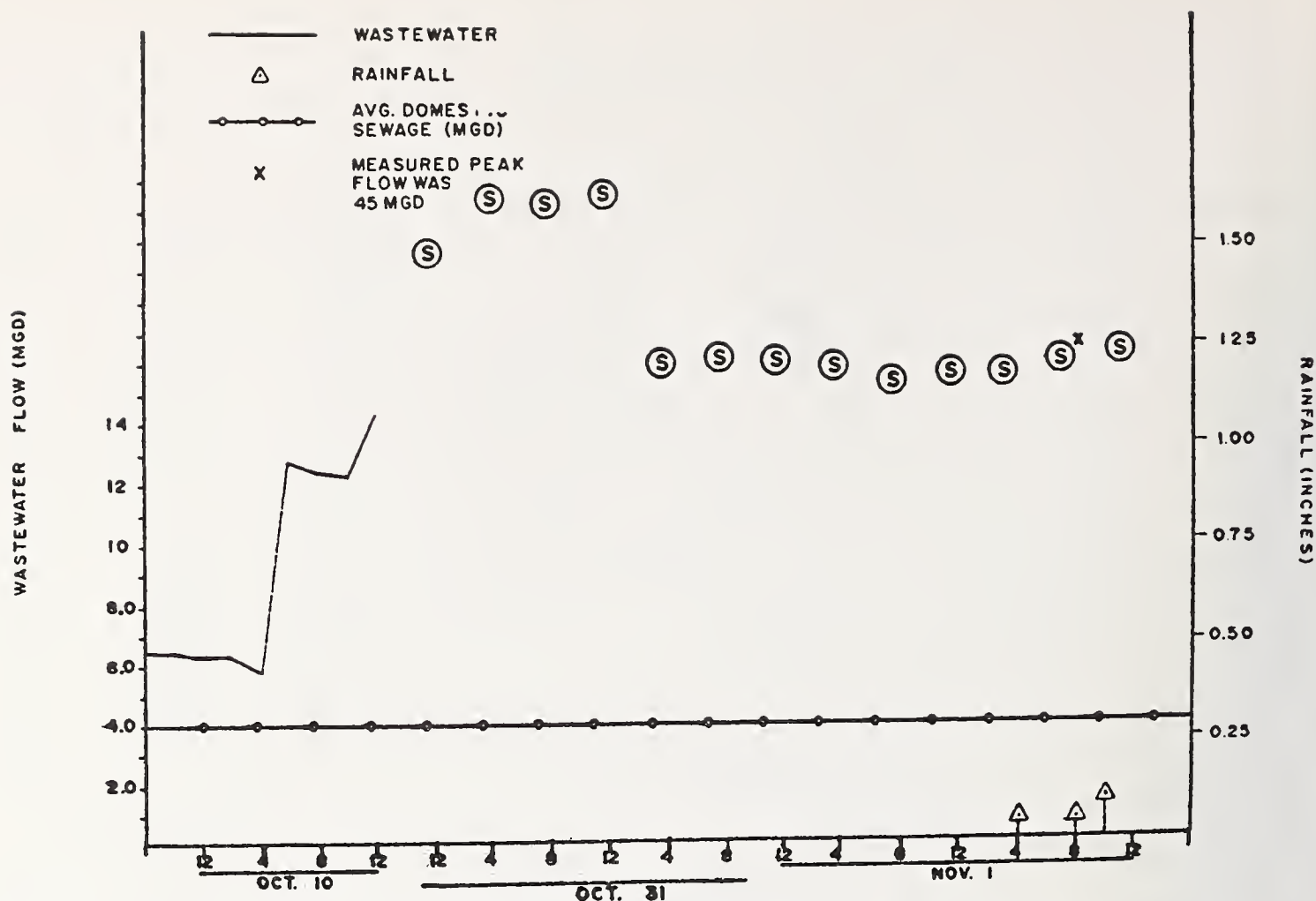


FIGURE 6. BAYAMON, CALLE COLOMBIA (A5a) WASTEWATER FLOW AND RAINFALL VS. TIME

These problems cover the range of those expected in the field. Not every I/I study will encounter such difficult environmental conditions. However, the techniques presented herein can serve as a guide to those attempting to minimize errors while conducting I/I studies, especially in tropical or semi-tropical environments.

References

1. Donald R. Washington, Inc. and Ing. P. Tejada, Inc. Infiltration/Inflow Study, Isabela, Puerto Rico for PRASA (in print). 1975.
2. Basora and Rodriguez, A. Heres Gonzalez and Donald R. Washington, Inc. Facilities Planning for the Bayamon Wastewater Region. Vol. IV: Infiltration/Inflow Analysis for PRASA. April, 1976.
3. Guthrie, D. L. and Washington, D. R. "Using the Weir in Infiltration/Inflow Analysis." Journal of Water and Sewage Works. 123, 10, 26 (1976).
4. King, H. W. and Brater, E. F. Handbook of Hydraulics. 4th ed., New York: McGraw-Hill. 1954.

RATING BROAD-CRESTED V-NOTCH WEIRS
WITH NARROW, SLOPING APPROACH CHANNELS AND SEDIMENT DEPOSITS¹

James F. Ruff, Assistant Professor
Civil Engineering, Colorado State University
Keith Saxton, USDA-ARS, Washington State University
Clement Dang, Engineer, Grinnel Fire Protection Systems Inc.

An accurate and reliable precalibrated streamflow measuring device is required to determine the discharge from small watersheds because rapidly rising and falling streamflow stages prevent accurate field determination of flow rates by conventional stream gaging techniques. Broad-crested, V-notch weirs were developed and calibrated by the U. S. Soil Conservation Service about 1940 to meet these requirements and they have been used extensively. Because field calibration of these weirs is difficult and inaccurate, the calibration curves often have not been verified. Recent evidence has shown that different approach channels cause significant deviations from the original calibrations.

Model studies were conducted to investigate the effects of the different approach channels slopes, cross-sections, and sediment deposits on the weir calibrations. The fixed-boundary channels were tested at slopes of 0.0, 0.5, 1.0, and 1.5 percent. Rectangular, trapezoidal, and circular cross-sections were tested with sediment deposits of 0.0, 0.5, and 1.0 feet depth. The calibration curves developed from the broad-crested V-notch weirs, will provide more accurate discharge measurements for small watersheds with narrow sloping channels.

Key Words: Broad-crested V-notch Weirs; small watersheds; streamflow measurements; calibration; approach channels; stream gages; weirs.

1. Introduction

Streamflow measurements are an important requirement of many research and design activities. These measurements have greater significance with the increased emphasis on environmental water quantity and quality. The economic, social, and scientific interpretations based on these streamflow measurements require that the measurements be accurate and reliable. Numerous measurement techniques and instruments have been developed for a wide range of flow conditions and criteria, and each system has unique characteristics. Watersheds with areas of less than 1 mi² (2.59 km²) often have streamflow with stages that rise and fall rapidly. Measurement of streamflow from small watersheds where maximum peak rates are expected to be 300 to 1,000 cfs (8.49 to 28.3 cms) presents gaging requirements that

¹This study supported in part by USDA-ARS Specific Agreement No. 12-14-3001-556.

are best met by precalibrated flumes or weirs because these watersheds often have rapidly varying, short-duration streamflow, where field calibration is difficult or impossible. Additional measurement problems exist because good accuracy is required throughout a wide range of flow rates, and the flow often contains significant amounts of trash and sediment which may interfere with the gaging device.

A broad-crested, V-notch weir was developed and tested by researchers of the U. S. Soil Conservation Service (SCS) for use as a precalibrated streamflow measuring device for small watersheds [3, 4, 5, 6].² The calibrations were developed using laboratory models with fixed-bed approach channels with geometric cross sections. These weirs have been used extensively, often with no further laboratory or field calibration verification. However, the weir calibrations are dependent on the approach channel conditions; thus, only when the laboratory condition is closely duplicated can the laboratory rating be reliably applied to field installations.

Although most hydraulic handbooks for flow measurements describe the required approach channel conditions for the weir ratings listed, few suggest the consequences if these conditions are not met. In many situations, appropriate approach channels cannot be constructed and, often, properly constructed approach channels are later significantly modified by sediment deposition. In this article, we review the effect of approach channels on weir ratings, and present preliminary research results that indicate the potential effect of approach channels on the calibration of broad-crested, V-notch weirs.

2. Determining Weir Calibrations

The theoretical discharge of a sharp-crested, triangular weir is

$$Q = \frac{8}{15} (2g)^{1/2} \tan\left(\frac{\theta}{2}\right) H^{5/2} \quad (1)$$

where Q is the discharge, $L^3 T^{-1}$, g is the gravity constant, $L T^{-2}$, θ is the internal weir angle and H is the head above notch, L .

The assumptions are: (1) no approach velocity, (2) parallel flow, (3) no energy loss within the approach reach, and (4) an energy coefficient of unity. Since these ideal conditions do not exist, Equation (1) is modified to account for the approach velocity by the addition to the static head, H , of the velocity head, $\alpha \frac{V^2}{2g}$; where α is the kinetic energy correction factor and V is the average approach velocity at the gaging section. Also, a coefficient is incorporated with the constants of Equation (1) to form a discharge coefficient, C_D , so that the discharge is expressed by

$$Q = C_D \tan\left(\frac{\theta}{2}\right) \left(H + \alpha_1 \frac{V_1^2}{2g}\right)^{5/2} \quad (2a)$$

$$\text{or} \quad Q = C_D \tan\left(\frac{\theta}{2}\right) H_T^{5/2} \quad (2b)$$

²Figures in brackets indicate the literature references at the end of this paper.

where C_D is the discharge coefficient, $L^{1/2} T^{-1}$, α_1 is the kinetic energy correction factor, V_1 is the average approach velocity, $L T^{-1}$, and H_T is $H + \alpha_1 \frac{V_1^2}{2g}$ is total head L . The discharge coefficient is assumed to

account for losses, the gravitational constant, and for other changes without having to alter the other variables, i.e. H , V , and θ .

To precalibrate V-notch weirs, then, requires that the discharge coefficient, C_D , be determined for the entire flow range by laboratory models or other means. This coefficient is primarily dependent on the weir angle, weir cross section, and approach channel geometry. Usually, the coefficient is not constant through the full range of flow. The weir ratings are commonly expressed as graphs of C_D versus Q or as Q versus H .

Field installations must closely simulate the laboratory setting to allow application of the laboratory-developed discharge coefficients, or some method must be used to modify these coefficients. For rectangular, thin-plate weirs with rectangular, level approach channels, Kindsvater and Carter [7] developed modification criteria to estimate discharge coefficients for a variety of weir heights and approach channel widths. The calibrations for the SCS broad-crested V-notch weir, were made dependent on the upstream cross section (which can be expressed as weir coefficients); but, again, only level channel slopes were considered [2].

3. The Broad-Crested, V-Notch Weir

The broad-crested, V-notch weir developed by SCS researchers at Cornell University, the National Bureau of Standards, and the University of Minnesota was economical to construct, durable, and accurate throughout the flow range for small channel slopes. The weir thickness was 16 in. (40.6 cm). The crest cross section had 6-in. (15.2 cm) wide sections sloping 3 horizontal to 1 vertical on the upstream and downstream side and a 4-in. (10.2 cm) wide horizontal section at the center. Weir section details are presented by Holtan [2], page 35.

Weirs with side slopes of 2, 3, 5, and 10 horizontal to 1 vertical were calibrated using the head 10 ft. (3.0 m) upstream of the weir. The approach channels for the weir calibrations had several sizes of rectangular or trapezoidal cross sections, a 0.0-percent grade, and bottom elevations 6 in. (15.2 cm) or more below that of the weir notch. These calibrations were first reported by Huff [3, 4, 5, 6]; again by Harrold and Krimgold [1]; and later by Holtan [2].

Early field installations soon disclosed that sediment transported by the streamflow often deposited in the approach channel, which resulted in a channel gradient and an effective channel bottom at or above the weir notch elevation. Further testing was done on several modified approach channels for alleviating the deposition problem and head-discharge relationships were determined [6]. Many of these tests showed significant deviations from the published ratings, irregular rating curves due to standing waves,

and approach velocities near critical--but the summary reports were not widely disseminated.

The broad-crested, V-notch weir remains a useful stream-measuring device for numerous applications, both in the U. S. and in other nations. Usually, the field sites closely approximate those represented by the laboratory conditions; thus, the laboratory ratings are applicable. For cases of obvious approach channel deviations from the calibrated weir geometry or weir modifications, field calibration is necessary and accomplished; in other situations, field calibration is necessary, but is impossible or impractical. The only recourses here are either to accept the inaccuracy (usually of unknown magnitude) or to use a different measurement device, but suitable devices are often neither available nor practical. Thus, the broad-crested, V-notch weir continues to be used despite the difficulties of accurate ratings.

Weirs cause hydraulic characteristics conducive to upstream sediment deposition. Streams carrying even moderate suspended sediment loads or those with mobile beds naturally assume some channel gradient and equilibrium cross section. If this results in a weir approach channel different from that represented in the laboratory, there may be significant rating shifts and inaccurate streamflow measurements. Streams carrying heavy bedloads, such as sandbed streams, or those with suspended loads greater than 50,000 to 100,000 ppm are particularly susceptible.

The sediment deposition in the approach channel may be dynamic during a flow event. These deposition changes may cause a variable rating shift that is difficult to document and assess. The deposit may become apparent only as the flow recedes, and only then if observers are tending the measurement station. Even with reasonable estimates for deposition depths, cross sections, and slopes during an event, no reliable method is available to adjust the weir rating.

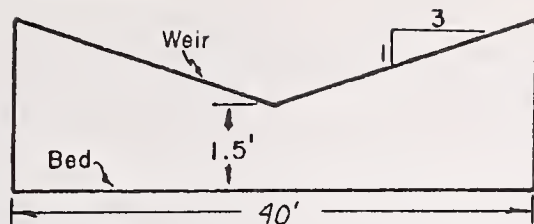
4. Recent Weir Tests

Model tests were conducted to further define approach channel effects on the calibrations of broad-crested, V-notch weirs [9]. Fixed-bed models with a model-to-prototype ratio of 1 to 5 were installed in a 4 x 8 x 200 ft. (1.2 x 2.4 x 60.8 m) tilting flume. The weirs tested had side slopes of 2 and 3 horizontal to 1 vertical (127° and 143° internal weir angle, respectively). Head measurements were made 10 ft. (3.0 m)(prototype) upstream of the weir center line.

The approach channel cross sections tested are shown in Figure 1. Cross sections 1 and 6 were the entire rectangular flume width. Cross sections 2 and 9 were similar to the original weir calibration tests [3, 4, 5, 6] and were used to verify similarity of results between the two test series. Cross sections 3, 4, 5, 7, and 8 represent alluvial channels being gaged on research watersheds in western Iowa, near Treynor [8, 10].

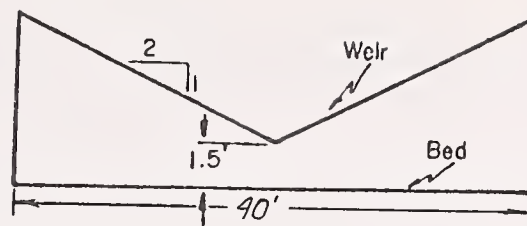
Channel slopes of 0.0, 0.5, 1.0 and 1.5 percent were tested for all cross sections by tilting the test flume. The rating curves in Figure 2 indicate the effects caused by channel slope. All curves are for the number

3:1 Weir

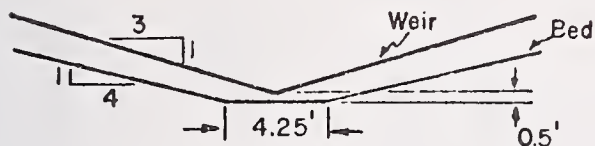


(1) Rectangular Channel

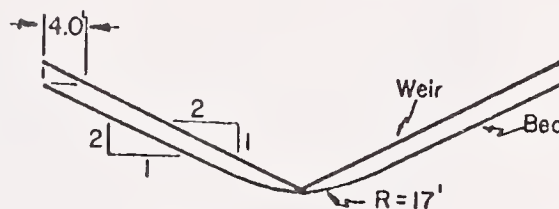
2:1 Weir



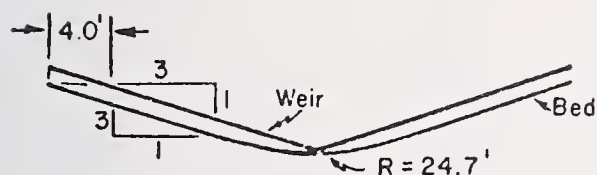
(6) Rectangular Channel



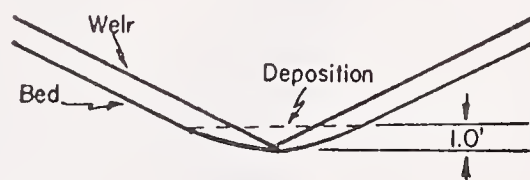
(2) 4:1 Trapezoidal Bed Channel



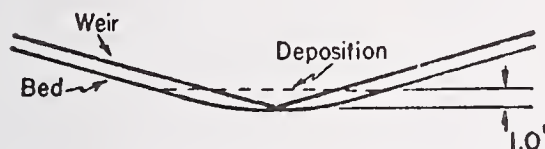
(7) 2:1 Circular Bed Channel



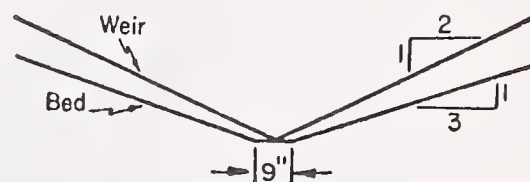
(3) 3:1 Circular Bed Channel



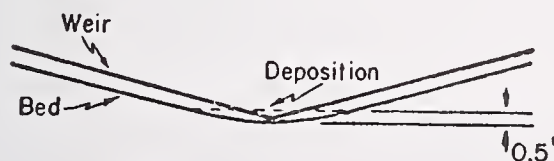
(8) 2:1 Circular Bed Channel with Severe Deposition



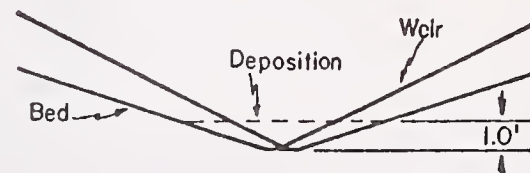
(4) 3:1 Circular Bed Channel with Severe Deposition



(9) 3:1 Trapezoidal Bed Channel

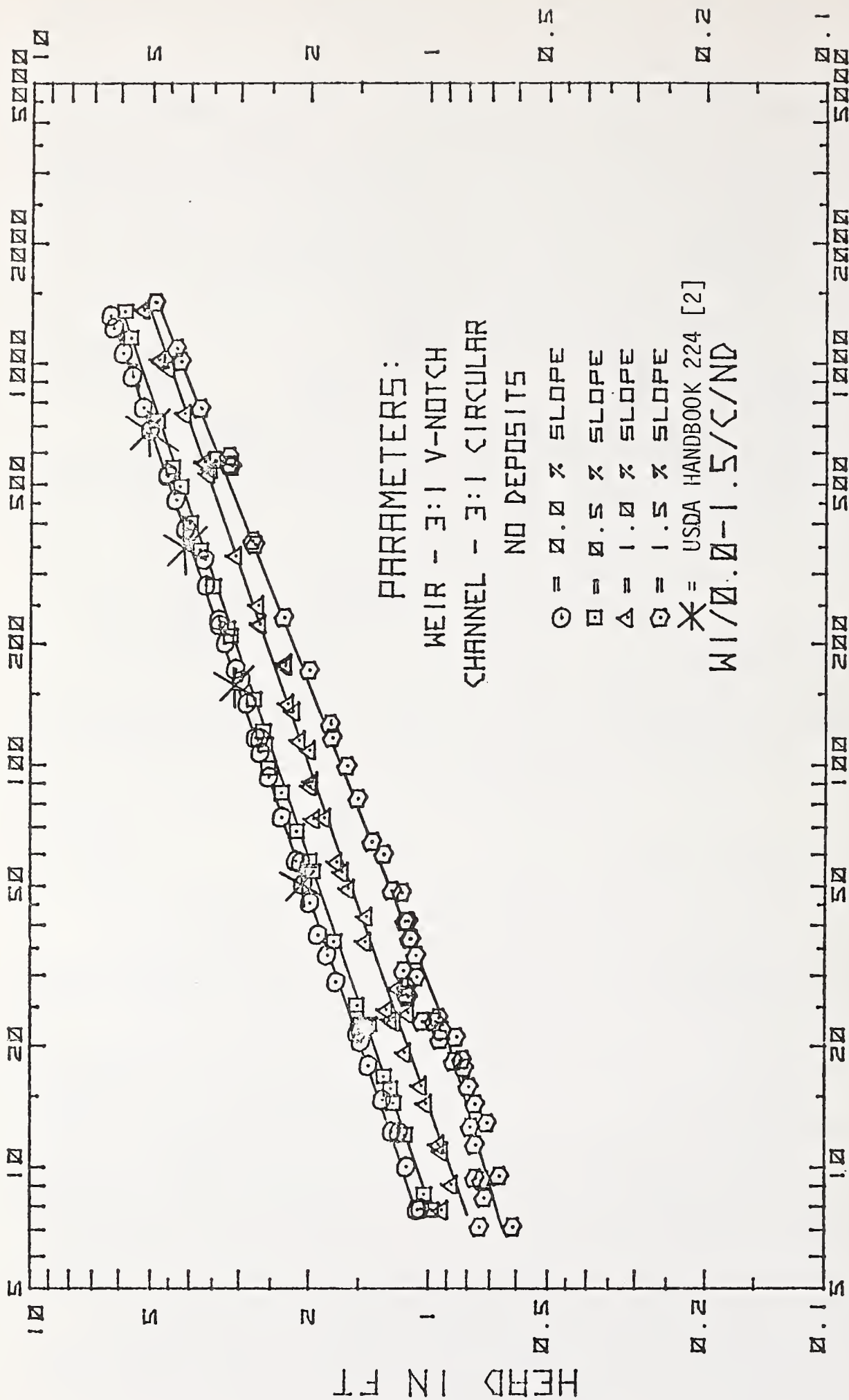


(5) 3:1 Circular Bed Channel with Moderate Deposition



(10) 3:1 Trapezoidal Bed Channel with Severe Deposition

Figure 1 - Approach channel cross sections used in tests.
All dimensions in prototype units (1 ft = 0.30 m)



DISCHARGE IN CFS

Figure 2 - Rating Curves of Static Head versus Discharge
(1 ft = 0.30 m; 1 cfs = 01028 cms)

3 channel cross section (Figure 1). As expected, the channels with steeper slopes cause higher flow rates for a given head as a result of increased approach velocity. Some small irregularities in the rating curves for 1.0- and 1.5-percent slopes caused by standing waves at the measuring section were smoothed. The slope effects were not as large nor as irregular for the 4:1 trapezoid channel cross section (No. 2, Figure 1).

The rating curve for 0.0-percent channel slope developed from the 1938 to 1941 tests and reported by Holtan [2] is also presented on Figure 2. The rating curves for the other slopes based upon Holtan's rating table do not vary significantly from that for the 0.0-percent slope. The discrepancies between the rating curves developed in the recent tests and those based on the rating table in Agricultural Handbook No. 224 [2] are evident in Figure 2. The rating table accounts for slope and channel geometry only indirectly by a change in area. This indirect approach is not satisfactory and the ratings may be in error by as much as 100-percent when comparing the Handbook No. 224 results with those at 1-percent slope. For example, representative discharge values are given in Table 1 for discharges read from the rating curves at different channel slopes and for discharges based upon the Handbook rating table.

Table 1

Representative discharge values for effects of channel slope, 3:1 Weir; Circular Bed Channel; No Deposition (1 ft = 0.03 m, 1 cfs = 0.028 cms)

Head ft	Discharge, cfs					
	From Figure 2			From Ag. Handbook 224		
	Slope, %			Slope, %		
	0.0	0.5	1.0	0.0	0.5	1.0
2	52.0	58.0	100.0	51.4	51.7	52.5
3	170.0	175.0	300	155.5	156.5	156.5
4	375	420	700	344	360	370
5	710	810	1360	667	695	~775 ^{1/}

^{1/} Value extrapolated beyond table.

The effect of approach velocity is demonstrated in Figure 3. The curves of Figure 3 are derived from the same data as those shown in Figure 2. The velocity head is added to the static head to obtain the total head. A value of $\alpha = 1.116$ was used for the calculations and is the average value determined from velocity profiles for all channel slopes and cross sections tested. By using the total head, the rating curves tend to converge toward a single curve. Determination of the discharge is easier since the differences are smaller for a given total head.

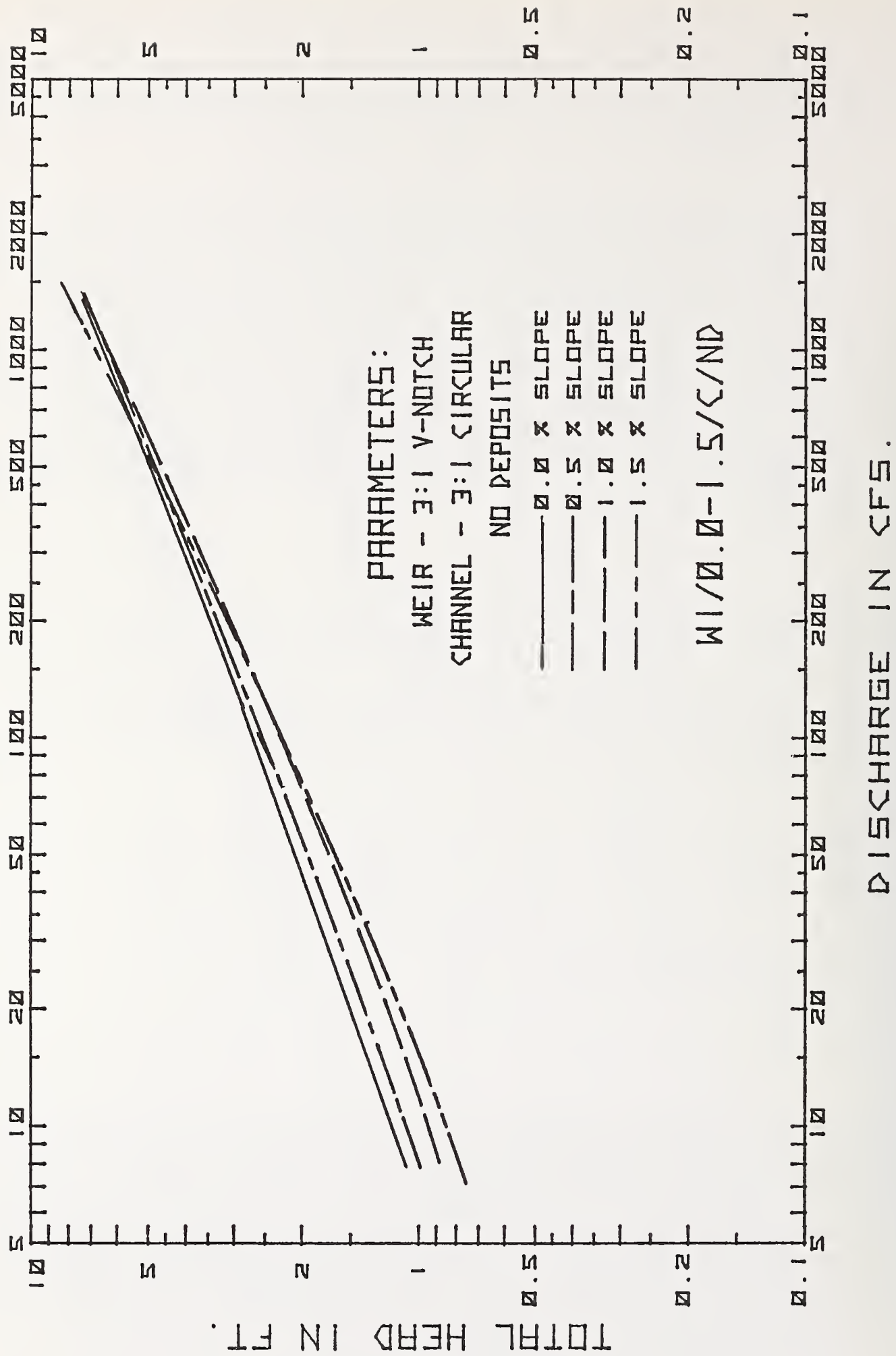


Figure 3 - 3:1 V-notch Weir Rating Curves of Total Head versus Discharge
 (1 ft = 0.30 m; 1 cfs = 0.028 cms).

The effect of sediment deposition was tested by filling the channel bottom as shown by the dashed lines on cross sections 4, 5, 8, and 10 of Figure 1. Two deposit depths were tested to represent 0.5 and 1.0 ft. (15.2 and 30.5 cm) depths (prototype) at the channel section 10 ft. (3.0 m) (prototype) upstream from the weir. The deposit depths were linearly reduced to zero at the weir notch and 25 ft. (7.6 m)(prototype) upstream.

The effect of deposition in the approach channel at 0.5% channel slope is demonstrated in Figure 4 for the 0.5 and 1.0 ft. (15.2 and 30.5 cm) (prototype) deposits in the number 4 and 5 cross sections. For the 0.5-percent channel slope, the discharge for specified heads was significantly reduced below about 50 cfs by the 1.0 ft deposit. This general trend was observed at all channel slopes with more deviation from the no deposit case evident at greater slopes. The use of total head gave more consistant results and less deviation in the rating curves. However, most rating curves used in the field still relate to static head. Therefore, representative discharge values relative to static head are given in Table 2 to aid in assessing the effects of channel deposition on such rating curves. If the discharge rating for the 1.0-percent channel slope is representative of field site situations, discharge measurements based on ratings of 0.0-percent slope may be more than 100-percent in error throughout the flow range. However, the laboratory model is probably smoother than most field sites; thus the expected error would be somewhat less, but further comparisons with field data are needed for verification.

Table 2

Representative discharge values for the effects of channel deposition, 3:1 Weir; Circular Bed Channel (1 ft = 0.30 m, 1 cfs = 0.028 cms).

Head ft	Discharge, cfs ^{1/}								
	0.0% Slope			0.5% Slope			1.0% Slope		
	Deposition, ft			Deposition, ft			Deposition, ft		
	0.0	0.5	1.0	0.0	0.5	1.0	0.0	0.5	1.0
2	46.5	45.0	52.5	58.0	49.5	60.8	109.0	78.3	73.2
3	165.4	160.3	166.5	184.6	180.0	176.4	316.9	270.6	303.8
4	374.2	360.0	365.8	407.4	412.9	403.3	700.0	648.9	597.4
5	670.1	661.0	676.3	806.3	789.1	758.6	1169.6	1044.0	1017.6

^{1/} Values taken from head versus discharge data used to develop Figure 4.

Observations in the flume showed that the deeper deposit caused high velocities between the weir and 10 ft. (3.0 m)(prototype) upstream. An alluvial stream bed would probably not maintain this situation for any length of time.

The effects of approach channel cross section at 0.5-percent channel slope are demonstrated in Figure 5. As expected the smaller channel cross sections caused increased flow rates due to increased approach velocities. Similar results were observed for all other slopes and for the 2:1 weir

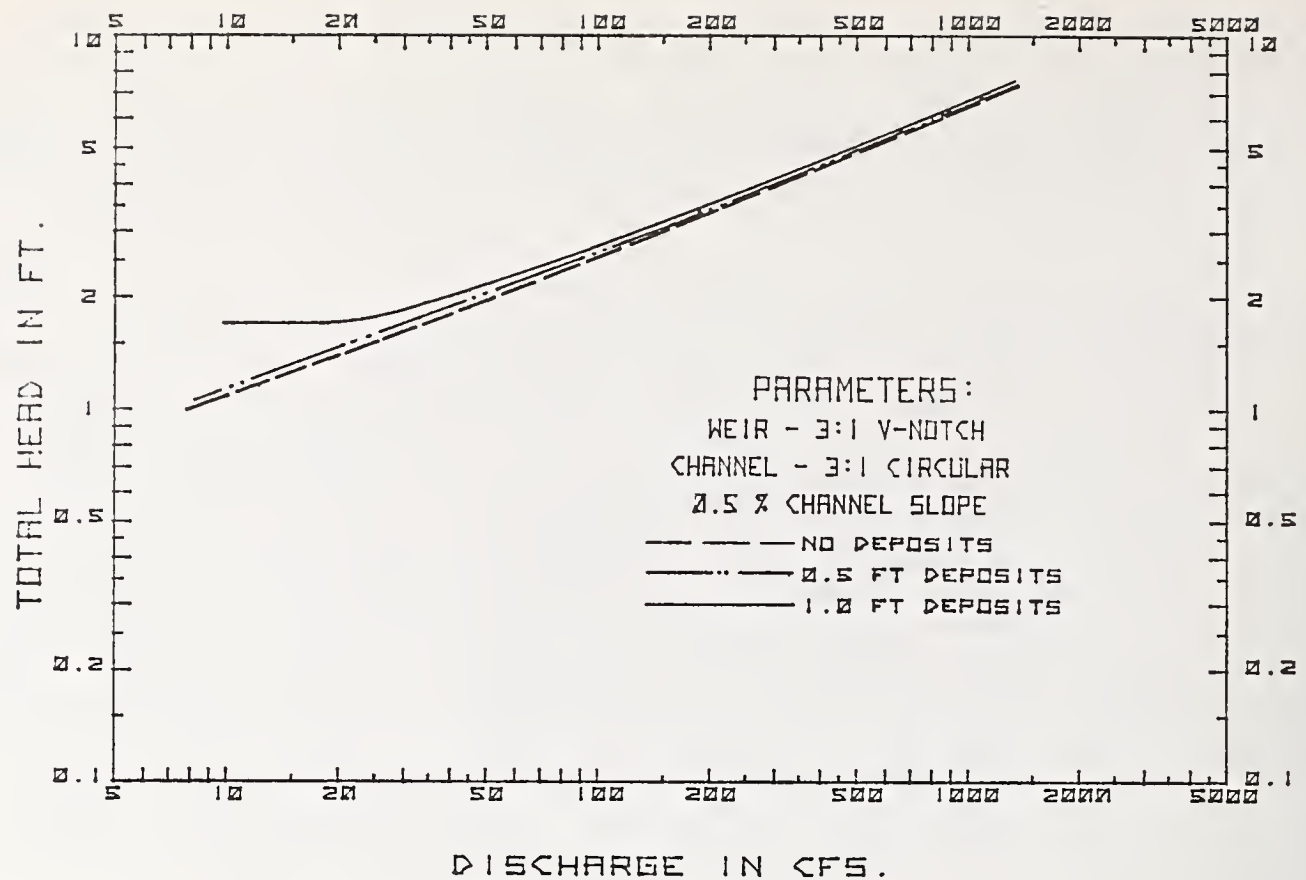


Figure 4 - The Effect of Deposition in the Approach Channels on the 3:1 V-notch Weir Rating (1 ft = 0.30 m; 1 cfs = 0.028 cms).

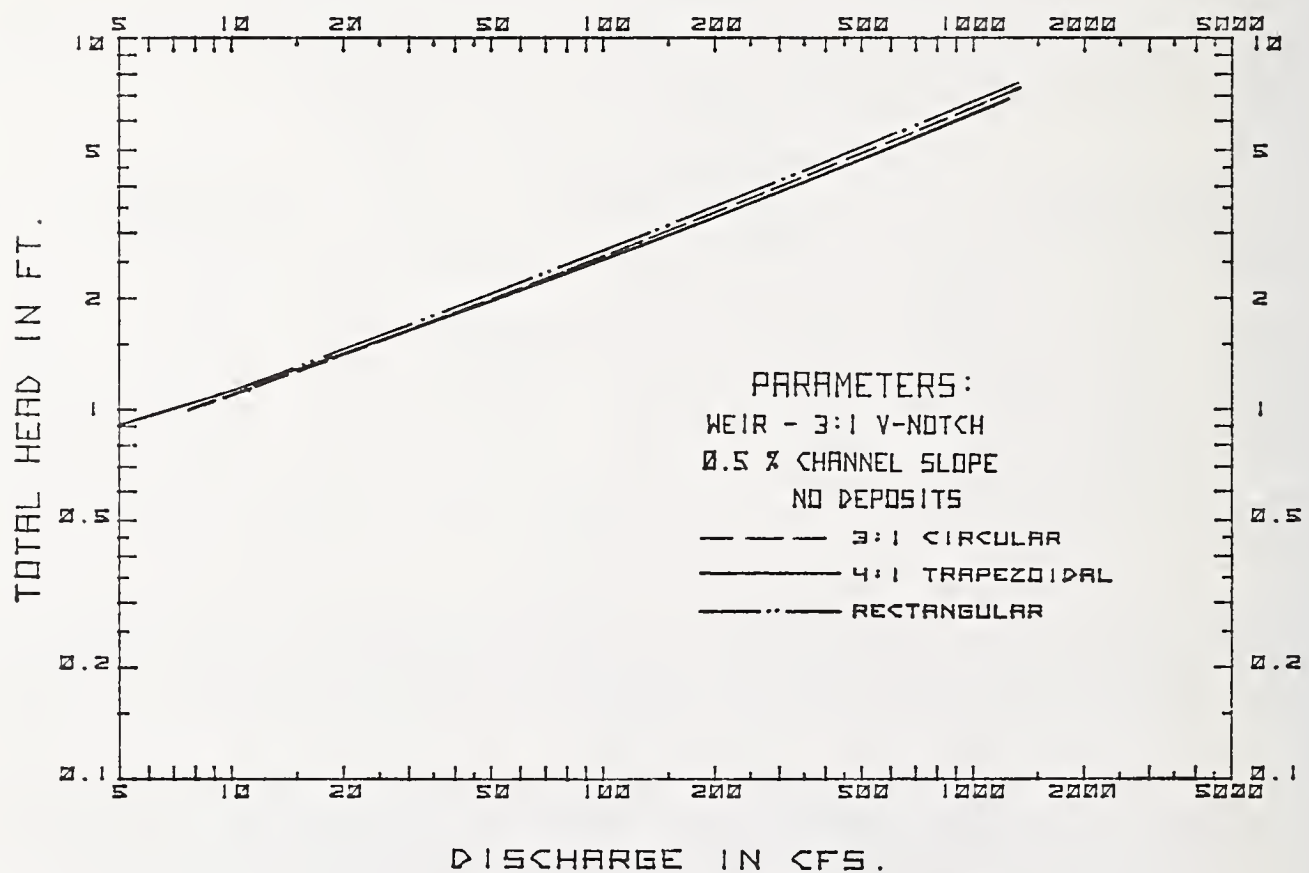


Figure 5 - The Effect of Approach Channel Cross Section on the 3:1 V-notch Weir Rating (1 ft. = 0.30 m; 1 cfs = 0.028 cms).

with a few exceptions below total heads of 1.5 ft. For those cases below 1.5 ft, the trapezoid or circular channel would indicate less discharge for a specified head. This occurred at the lower discharges tested, generally less than 20 cfs (0.56 cms), and the differences when compared to the rectangular channel were on the order of 20-percent or less.

The results obtained for the 2:1 weir and different approach channels were similar to those described for the 3:1 weir. For example, the effect of channel slope on the 2:1 weir rating curves for the number 7 channel cross section (Figure 1) is demonstrated in Figure 6. The 0.0 and 0.5-percent slopes are essentially coincident over the full range of discharges. The 1.0 and 1.5-percent rating curves deviate at the lower discharges, but tend to converge toward the 0.0-percent curve at the higher discharges. Errors on the order of 100-percent can also be obtained if the 0.0-percent channel slope rating curve is used for a channel with a slope of 1.0-percent.

The discharge coefficient, C_D , was defined in Equation 2b. The relationship of C_D with the total head provides another means of determining the rating curve for a weir-channel system.

The discharge coefficient curves obtained for the data used to develop Figure 6 are shown in Figure 7. The curves for 1.0 and 1.5-percent slopes also tend to deviate from the curves for 0.0 and 0.5-percent slopes as was evident in Figure 6. In some cases, it may be necessary to develop a discharge rating curve. The discharge rating curve can be developed for the total head versus discharge coefficient relationship in a more satisfactory manner than using the rating curves. This is because the values of C_D , although subject to some scatter, tend to group much closer together, and interpolation is easier since the graphs are plotted on rectilinear scales rather than logarithmic scales.

5. Summary and Conclusions

Broad-crested, V-notch weirs have many characteristics that make them desirable for streamflow measurements where expected peak flow rates range from 300 to 1,000 cfs (8.4 to 28.0 cms). A weir developed by the U. S. Soil Conservation Service is often used. This weir was originally calibrated with varying approach channel cross sections but with the channel bottom level and at least 0.5 ft. (15.2 cm) below the weir notch. For alluvial streams carrying sediment, the approach channels establish a slope, and the channel bottom at the weir is usually near the notch elevation. Because the weir head-discharge relationships are dependent on approach channel conditions, any deviation from the original calibration conditions causes a rating change.

Recent model tests have been conducted to determine the effect of approach channel slope and cross section and of deposition on the ratings of these broad-crested, V-notch weirs. These laboratory results provide improved predictions for the head-discharge relationships of these weirs for many common field sites. Further, improvements between the model and field installations can be obtained if one or two field data points are available to adjust for differences in roughness between model and prototype.

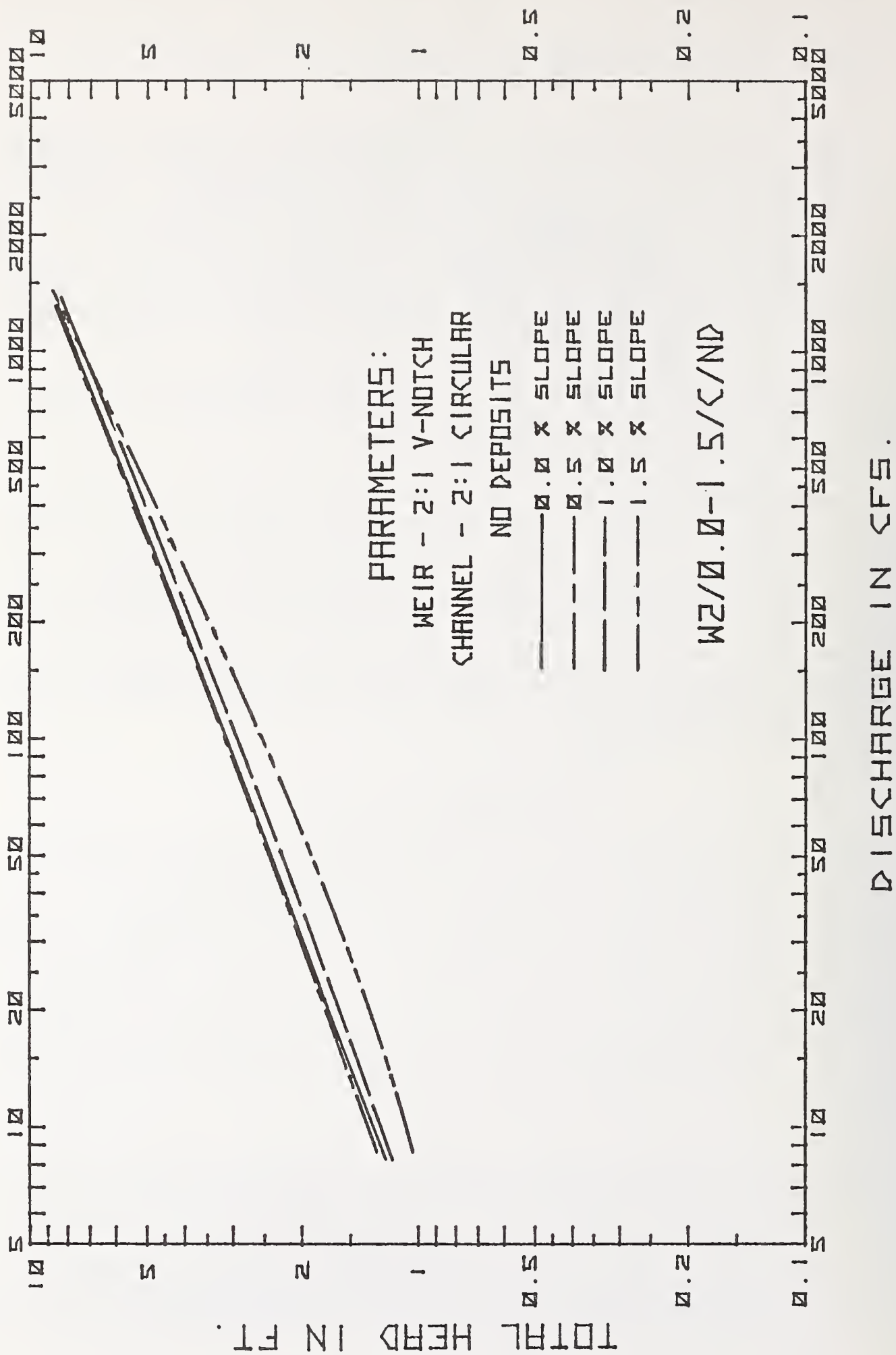


Figure 6 - 2:1 V-notch Weir Rating Curves of Total Head versus Discharge
(1 ft. = 0.30 m; 1 cfs = 0.028 cms).

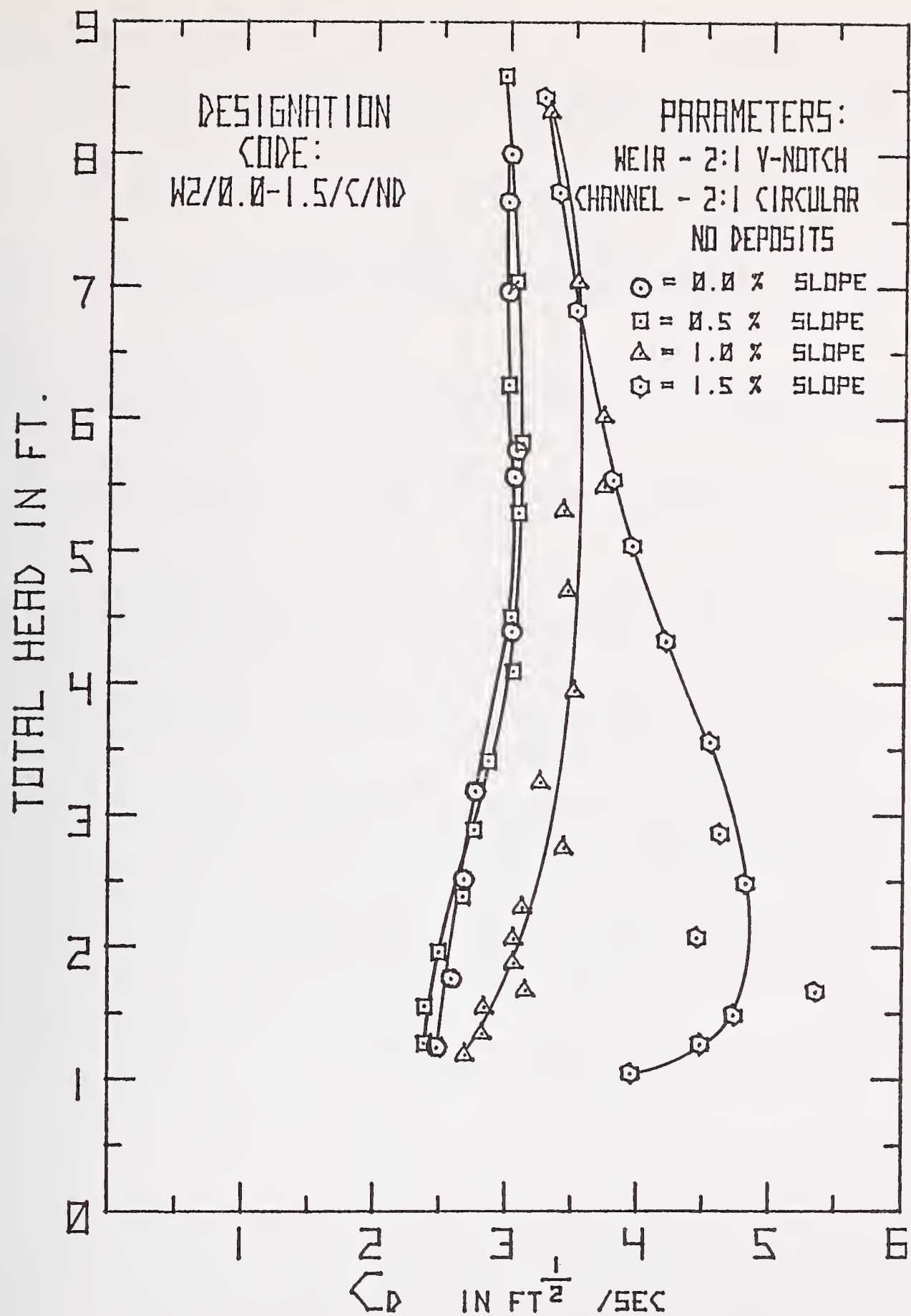


Figure 7 - Discharge Coefficient Curves

6. References

- [1] Harrold, L. L., and Krimgold, D. B., 1943, Devices for Measuring Rates and Amounts of Runoff, USDA, Soil Conservation Service, SCS-TP-51.
- [2] Holtan, H. N., Minshall, N. E., and Harrold, L. L., 1962, Field Manual for Research in Agricultural Hydrology, Agriculture Handbook 224, USDA, Agricultural Research Service.
- [3] Huff, A. N., 1938, Tests of 16-inch Weir and Comparison with 30-inch Weir, Report No. 1, Cornell University, Section of Watershed and Hydrology Studies.
- [4] Huff, A. N., 1941a, Calibration of 2:1 V-notch Measuring Weirs, St. Anthony Falls Hydraulic Laboratory, Minneapolis, Minnesota, Report No. MN-R-3-6.
- [5] Huff, A. N., 1941b, Calibration of 3:1 V-notch Measuring Weirs, St. Anthony Falls Hydraulic Laboratory, Minneapolis, Minnesota, Report No. MN-R-3-8.
- [6] Huff, A. N., 1942, Calibration of 3:1 and 5:1 V-notch Measuring Weirs, Supplement to Calibration of 2:1 V-notch Measuring Weirs, St. Anthony Falls Hydraulic Laboratory, Minneapolis, Minnesota, Report No. MN-R-3-7.
- [7] Kindsvater, C. E., and Carter, R. W., 1959, Discharge Characteristics of Rectangular Thin-plate Weirs, Transactions of the American Society of Civil Engineers, 124, 772-822.
- [8] Minshall, N. E., and Spomer, R. G., 1965, New Type Weir Construction for Small Watersheds, Proceedings of the American Society of Civil Engineers, 91 (IR1), 11-15.
- [9] Ruff, J. F., and Dang, C., 1977, Rating Broad-Crested V-notch Weir, Interim Report prepared for USDA, Agricultural Research Service. Colorado State University, Engineering Research Center, CER77JFR-CD42.
- [10] Saxton, K. E., Spomer, R. G., and Kramer, L. A., 1971, Hydrology and Erosion of Loessial Watersheds, Proceedings of the American Society of Civil Engineers, 97 (HY11), 1835-1851.

COMPENSATING FOR CONSTRUCTION ERRORS IN
CRITICAL-FLOW FLUMES AND BROAD-CRESTED WEIRS ¹

John A. Replogle
Research Hydraulic Engineer
U. S. Water Conservation Laboratory
Agricultural Research Service, USDA
4331 East Broadway, Phoenix, Arizona 85040

Critical-flow flumes and broad-crested weirs can now be routinely and accurately calibrated ($\pm 2\%$) by computer techniques over a wide range of flow rates and flume cross sections, including trapezoidal and complex shapes. This ability permits detailed compensation for errors introduced by construction anomalies. Procedures were developed and used on a series of primary devices in irrigation canals, including trapezoidal flumes and broad-crested weirs, which identified construction errors and accurately related a readout mechanism to the primary device, as constructed, so that the original intended accuracy could be restored. Templates were used to accurately define field dimensions of the flume throat section, its most sensitive portion. Errors in defining the throat cross-sectional area can be shown to be nearly equal to the error in discharge. Errors in the approach and converging sections are about one-tenth as important. The accurate field measurements of flume dimensions were then used to compute a tailored calibration table for the particular construction. The template can also be used to accurately relate the readout device to the flume. Direct reading discharge gages that were prestamped could be mounted, using a modification of the technique, to reserve the highest accuracy for any selected flow rate on the gage. Discharge errors, if any, could thus be relegated to the least used flow range.

Key Words: Broad-crested weirs; errors; flow measurement; flumes; open-channel flow.

1. Introduction

Calibrations of flumes and broad-crested weirs have traditionally been based on laboratory ratings which, if done carefully, can produce a discharge calibration for a particular structure that is repeatable and accurate to within $\pm 1\%$ of reading over a 20:1 range in flow rate. This same

¹ Contribution from the Agricultural Research Service, U. S. Department of Agriculture.

device when translated to field construction and read by field installed instruments, too frequently produces errors of more than $\pm 5\%$. Part of the problem may be that no general understanding of the error sources or guidelines for correcting construction anomalies and registration errors are available at the field level. The main objective of this paper is to discuss calibration, construction, and registration errors, and to suggest techniques for accurately compensating for their presence or reducing their influence. A realistic goal would be to reduce errors in the primary device to less than half the total system error, including the readout method, i.e., for a 5% desired total accuracy, a flume, itself, should be within $\pm 2.5\%$.

2. Errors -- Types and Sources

Errors associated with flow measurements using flumes or broad-crested weirs can usually be traced to primary calibration errors, construction anomalies, zero registration problems, and readout-device shortcomings. These errors can be classified as systematic, random or spurious -- the latter linked to mistakes and malfunctions. Many errors are random when applied to a population of flumes but are systematic when applied to a single flume. For example, several flumes constructed by the same method would be expected to have random errors associated with the dimensional tolerances of the variables listed in Table 1, Appendix 1. These dimensional errors would cause a random spread of indicated discharge from flume to flume, but each flume would show a systematic, not random, deviation from calibration. Since it is possible and practical to measure the flume dimensions "as constructed" these will, therefore, be treated as systematic errors. Likewise, registration errors (zero determination) will be treated as systematic errors. Both construction and registration errors, with proper technique, can be reduced to less than $\pm 1\%$, at least for the most frequently used flow range on a particular irrigation canal.

Other error sources are associated with the secondary or readout device. The methods available to detect flow depth are many and varied, ranging from direct-indicating staff gages, point gages, and float operated indicators, to pressure transducers, purge-bubbler systems, sonic-level indicators and capacitance-level detectors. They may be used with or without separate stilling wells. The types of errors associated with these secondary devices have been adequately described in measurement handbooks, and the effects of errors in detecting flow depth of weirs and flumes has been well documented (reference [5]).²

Yet another source of error results from the method for obtaining the discharge rating for a particular flume. As mentioned earlier, a laboratory rating on an individual device may be within $\pm 1\%$, especially if a

² Numbers in brackets refer to appended references.

good primary standard like a weighing-tank system, is used. Inferring the calibration from scale models and from similar devices of a type is often and successfully used, but at some sacrifice of accuracy in exchange for more flexibility to mass produce similar structures. More recently, computer modeling has been applied to produce individual ratings for mass-produced structures.

3. Computer Model for Flumes

Critical-flow flumes and broad-crested weirs can now be routinely calibrated by computer modeling, accurate to about $\pm 2\%$ for a wide range of flume cross-sectional shapes, including trapezoidal and complex shapes [6, 8]. Typically, laboratory data fit to a third-degree polynomial, coincides with the computer-predicted calibration curve, within $\pm 2\%$ in the upper two-thirds of the maximum design flow depth, and be within $\pm 5\%$ at one-tenth of the maximum flow stage. Figure 1 illustrates a typical comparison of computed discharge coefficient and laboratory-measured discharge coefficient for a trapezoidal flume.

Flumes must have nearly parallel flow in the contracted throat section (Section 3, Figure 2) and in the approach channel (Section 1, Figure 2, for the stage discharge relation to be computer predictable. Also, the converging section (Section 2, Figure 3) should not produce flow separation. This requires converging the flow into the flume throat with rounded entrances, or with flat-surface construction, at less than 1 unit laterally to 3 units longitudinally. Also, the throat section and the approach sections should each be at least twice as long as the depth of flow to insure nearly parallel flow. However, when the throat is twenty times larger than the flow depth, frictional effects, whose prediction at deeper flows could be rather casual, now dominate and can cause rating errors over 5%. Thus, the practical measuring limits for a critical-depth flume, or a broad-crested weir with rounded upstream edge is:

$$\frac{L3}{20} < Y1 < \frac{L3}{2} \quad (1)$$

where $Y1$ is the water depth in Section 1 referenced to the elevation of the floor in Section 3, and $L3$ is the length of Section 3.

Long-throated flumes with proper diverging sections can withstand up to 0.95 submergence, while causing no more than a 1% change in discharge. This is the definition of "modular limit" (2). Shorter throated devices have modular limits that are 0.65 or less, which causes submerged flow operation to be frequently encountered or else forces the design of extra overfall height into a canal system.

Other advantages of these computer-rateable flumes include the ability to tailor the flume for a particular canal measuring problem, most often eliminating the requirement for measuring with submerged flume flow, which is inconvenient and inaccurate, as is discussed in more detail in reference [8].

Computer Model Programs: A simple version of a Basic computer program that will compute the depth-discharge relation for trapezoidal flumes is given in Appendix 1. This version will not print out Froude Number information or channel velocity information. More complex programs have been presented elsewhere [6, 7].

4. Model Verification

Laboratory Verification: Many shapes of measuring flumes -- trapezoidal, rectangular, triangular, and complex -- have been successfully calibrated with the computer model and verified by laboratory tests [6, 8]. These shapes have included structures with bottom sill only (broad-crested weirs), side contractions only, contractions from one side only, and even side contractions with a depressed floor (negative sill). Discharge ratings for all can be predicted, if the basic length criteria for parallel flow, (mentioned above) are observed. Historical data, as published, usually fit the model. When it did not fit, recalibration, when possible, has confirmed the computer prediction. Usually, the differences were on the order of 5 to 7% and were reduced by recalibration to about $\pm 2\%$, indicating that the original calibration had a systematic or registration error.

Computational Verification: Computational verification of the computer model can be established by comparison to hydraulic modeling. Suppose that a scale model were made of a flume. If the model is made of plexiglass and the prototype made of concrete, an appropriate length ratio would be 1:7. Now, if we use the computer technique to directly compute the rating curves for both the model and the prototype, then appropriately expand the rating for the model by Froude Modeling Techniques, the Froude Model expansion and the direct prototype rating by computer will differ by only a fraction of a percent. This small difference probably represents the slight calibration change caused by Reynolds Number effects, which Froude modeling assumes is negligible.

Field Verification: Field checks by others have also confirmed the model. Four separate examples include the following:

I. A complex-flume [6] having discharges ranging from 30 to 220 cfs, was field-checked with a series of 64 current meter traversings over a 2-year period. The current-meter ratings substantiated the computer predicted ratings to within $\pm 5\%$.

II. Flume Number 2, ASAE Standard S359.1, was originally calibrated using an outdoor flow facility. At flow depths below about half the maximum flow depth, the published flume calibration deviates from computer prediction by 5 to 7%. Recent recalibration³ against a suppressed rectangular

³ Recalibration made by Allan Humpherys and James Bondurant, Snake River Conservation Research Center, Agricultural Research Service, USDA, Kimberly, Idaho, fall of 1976.

weir confirmed the computer prediction within a standard deviation of $\pm 1\%$. The original calibration, although systematically overpredicting discharge by only 5 to 7% in a seldom-used flow range for this size flume, will be updated in future standards and publications, since better information is now available.

III. A trapezoidal flume, designed for use in concrete canals, was field-checked against a constant-head orifice that was carefully adjusted to 20 cfs. The flume, installed downstream and fitted with a staff gage attached to the canal wall, confirmed this discharge.

IV. A sill placed in a trapezoidal canal was fitted with a sloping approach. Thus, it was a trapezoidal broad-crested weir with the equivalent of a rounded upstream edge. A staff gage was fastened to the sloping canal wall. Irrigation District personnel, using a propeller meter in the delivery pipe to the canal lateral, reported the meter read slightly over 15-1/2 cfs when the meter was in place. About 1000 ft downstream, 15.7 cfs was read, indicating excellent agreement.

The nearly universal capability to rate flumes permits detailed examination of the magnitude of discharge errors introduced by construction anomalies, registration problems, and aging effects of erosion or deposition on the flume surface.

5. Error Evaluation and Compensation

Deriving an error equation for the flumes that involves so many variables is impractical. The most straightforward approach is to examine the influence of introducing an incremental change of $\pm 1\%$ in each variable, in turn, and noting the corresponding change in indicated discharge rate. A problem arises when applying this percentage formula to a quantity like sideslope, Z1 and Z3. These quantities, for example, are zero for a rectangular flume, so a percentage change is meaningless. However, for both of these examples, the sideslope is 1, and changing these values by 1% is consistent with changing the flow areas by 1%, if a corresponding 1% change is simultaneously made in bottom widths. A specified rotation applied to the sideslopes is a viable alternative.

The effects of construction and registration error on discharge prediction were examined using the model for two specific types of field installations, a broad-crested weir and a trapezoidal flume. The specific variables examined were those listed in Table 1, Appendix 1.

Broad-crested Weir Example: A broad-crested weir was designed to measure irrigation canal discharges primarily at 15 cfs with an expected range of 12 to 16 cfs, and an occasional need to measure as low as 2 cfs. A one-time measurement, using a portable, adjustable, trapezoidal flume [7] indicated that 16.1 cfs was flowing in the canal at a depth of 1.8 ft. This left a freeboard of 0.7 ft, more than adequate for installing a critical-flow device to obtain the desired measurements. The weir was designed to

cause 0.25 ft of water-depth increase upstream at 15 cfs to avoid submergence. This was a liberal allowance since this configuration is expected to operate with a head difference of only about 0.15 ft at 15 cfs. (Equal to 85% submergence (modular limit) with water depths referenced to the floor or weir crest elevation, not the channel floor). Since the tailwater control in this case was primarily due to channel friction, this liberal allowance was needed to handle seasonal changes in channel roughness due to algae growth and Bermudagrass infringements over the canal edges. For construction economy, diverging Section 4 was omitted. This could be added later if submerged flow were threatening to increase the modular limit to nearly 95%. The sill could also be easily raised by pouring a concrete cap over the original sill and recomputing the calibration, but at sacrifice of some upstream freeboard.

Construction Procedure: The broad-crested weir was poured directly into an existing trapezoidal concrete canal with nominal 2-ft bottom, 1:1 sideslopes, and 2.5-ft depth. Calculations with the computer model indicated the need for a 1.1-ft sill height to achieve the proper submergence limits discussed previously. Plywood end forms (1.1 ft high) for the sill were pre-cut to fit the channel shape. These were held upright in the canal with 2-ft-long timber spacers and wire ties. The top edges of the forms were carefully leveled across the channel and with respect to each other before pouring the concrete. The form tops served as finishing guides for the top surface of the sill. After the initial set of the concrete in the sill, the upstream form was removed and a concrete ramp was formed. This was essentially hand plastered into place with little requirement for accuracy, except that there be no sharp discontinuities between this section and the previously poured sill. The sill was 2 ft long and the ramp approximately 3 ft long.

A carefully measured sheet-metal template, pre-cut to match the intended finished cross-sectional shape, and with a height corresponding to the design flow depth at 15 cfs, was inserted to check the finished dimensions. The fit was not very close because the nominal existing canal had a sideslope which, measured with the template, was 0.931 horizontal to 1-unit vertical instead of 1:1. When the two end forms were finally level, the top sill surface ended up about 0.05 ft higher than planned, making $Y_8 = 1.15$ instead of 1.1. The width of the sill was 4.25 ft instead of the intended 4.2 ft. The only measurements remaining unchanged were the cross leveling and longitudinal leveling of the sill surface, as read with a 4-ft carpenter's level. No special effort was exerted to correct or maintain the dimensions, except for leveling, since the other dimensions could be readily handled in the final calibration.

The template was used for two purposes -- to determine the true constructed dimensions of the contracted throat section (Section 3), and to minimize errors due to mounting a gage on a rough canal wall that may not be exactly on a 1:1 slope. After recalibrating by computer modeling, a side-wall gage scale was calculated and marked directly in cubic feet per second. This pre-marked gage was mounted about 1 ft upstream from the end of the sloping transition section (Section 2) using the 15-cfs mark for registration at the appropriate elevation above the throat section floor. The actual

registration was transferred with a surveying level from the top of the template, placed near the center of Section 3, to the appropriate mark on the gage in Section 1. Thus, small depressions or high spots on the sill that a surveying rod might encounter became quickly apparent and were somewhat averaged when the template was appropriately placed. Ponded water over the sill can sometimes be used in place of the surveying technique, but the template is needed, using either method. By registering on the most frequently expected flow, errors in gage mounting slope or even in gage marking are relegated to seldom-used ends of the gage.

Detailed discussions on location of depth sensing and construction precautions are found in References [1], [2], [3], [5].

Error Detection and Compensation: The systematic errors that field measurements revealed were evaluated with the computer model. Recapitulating, the noted differences in dimensions and slopes, Δ , from intended were:

$$\Delta B3 = 0.05 \text{ ft} = + 1.19\%$$

$$\Delta Z3 = 0.069 \text{ ft} = - 6.90\%$$

$$\Delta Y8 = 0.05 \text{ ft} = + 4.55\%$$

From calibration tables computed for the uncorrected weir, 15 cfs occurs at a Y1 reading of 0.95 ft. Figure 3 shows the computed change in discharge corresponding to a 1% change in the respective variable. At 0.954-ft flow depth or a Y1/L3 ratio of 0.477, these three variables caused the following indicated changes in discharge:

$$B3: \quad \Delta Q = + 1.19\% \times 1.05 = + 1.25\%$$

$$Z3: \quad \Delta Q = - 6.90\% \times 0.17 = - 1.17\%$$

$$Y8: \quad \Delta Q = + 4.55\% \times 0.38 = + 1.73\%$$

The absolute value of the combined detected error is 4.15%. In this case, the errors cancel somewhat to yield a net systematic error in ΔQ of only +1.81% from the intended original calibration for a flow of 15 cfs.

Recalibration using the actual dimensions placed the 15 cfs mark at 0.954 ft above the throat bottom elevation. The gage scale which had been premarked based on the expected dimensions was still useable by registering on the most used flow range. Applying the calculated corrections and the registration-with-template procedure restored the flume to intended accuracy.

Sensitivity: The relation between discharge, Q , and changes in upstream depth, $Y1$, can be readily studied with the model. A familiar approach is to obtain a power function for the weir by plotting the computed head and discharge values on log-log paper. The calibration equation for this particular weir can be approximated to within $\pm 1\%$ by

$$Q = 16.1(Y1)^{1.65}$$

for between 2 and 16 cfs. Thus, a 1% error in Y_1 will cause 1.65% error in Q . A more complete representation of variation, dQ , with Y_1 is shown in Figure 3 (plotted as $Y_1 \div 10$ to accommodate the figure). To hold the error contribution from the readout device to less than 2.5%, the weir gage must be capable of less than $(2.5/1.65) = \pm 1.52\%$ random error of detection. At 15 cfs, this translates into detecting $\pm .0144$ ft vertically or ± 0.02 ft on the sloping wall gage. In the field, even with gusting winds of 20 to 30 MPH, the canal water surface was stable enough to be easily read to within half of 0.02 ft on the gage. Thus, sensitivity in the most used flow range was no problem. For 2 cfs, however, similar reasoning requires detecting $\pm .006$ ft on the sloping gage, a much more difficult task but certainly not unusable.

This particular broad-crested weir was not field rated with any planned field test program. However, an opportunity presented itself to check at least one flow rate using a propeller meter in the 30-in supply line from the main canal. The check is that mentioned earlier as the example IV of field verification of flumes and weirs.

All other dimensional errors associated with the remainder of the variables caused 0.2% or less change in discharge for each percent change in that variable, except for the variable A_3 , which is really a combination of errors in B_3 and Z_3 (Figure 3). Discharge errors are almost directly proportional to errors in the determined area of flow, A_3 , related to a particular flow depth. The template, when fitted to the throat of a flume or broad-crested weir, visually shows whether area determinations will be suitable, assuming that proper zero registration is made. Even some cross-slope error, if properly accounted for by the registration-with-template procedure, is not critical because the correct flow area will be closely approximated.

Trapezoidal Flume Example: A trapezoidal flume (Figure 2) was designed with a constant throat (Section 3) cross-sectional shape, but could be constructed using variable sill heights, Y_8 , to adjust for submergence situations. This type flume was built using an inside mold or form for Section 3 that was reused for many flumes of the same style. It was not subject to inaccuracies due to canal shape and could be used in unlined canals with proper channel protection. This has advantages for contractors because standard tables can be established for a range of sill heights, and individual calibration by computer modeling is not required. Also, they have greater sensitivity than the broad-crested weir, and will drain down after use better than the weir without having to use special drain pipes.

Provided the original form is accurate, and the flume throat is level in the direction of flow, registration becomes the major source of error. Using prestamped gages, the template method should be applied to align the most used flow range to the correct registration, and relegate any error of gage or canal slope to the little-used ranges.

For this style of flume, plotting the rating curve on log-log paper produces:

$$Q = 5.34(Y_1)^{2.11}$$

for the region of 10 to 20 cfs. Thus, a 1% error in Y_1 causes 2.11% error in discharge. As was computed for the broad-crested weir, this requires that the readout device be readable to no more than $\pm 1.17\%$ random error to retain less than 2.5% error in discharge. At 15 cfs, this means detecting ± 0.019 ft vertically or ± 0.028 ft on the sloping gage. Thus, accuracy of readout should be no problem. At 2 cfs, the equation changes to $Q = 5.31(Y_1)^{1.86}$ and the gage must be readable to ± 0.011 ft which is still detectable. At 1 cfs, this flume would require detecting ± 0.008 ft, which is getting near the limit of accurately reading a wall-mounted staff gage. However, if 5% random error in Q is acceptable, the gage may still be useable.

Since this flume has a throat length of 4 ft it will be somewhat more sensitive to roughness changes than the broad-crested weir, so it may be instructive to examine the expected calibration shifts due to deposits, etc.

Irrigation waters are sometimes used to apply anhydrous ammonia fertilizer to the crops. In hard waters this leaves a wall deposit on the canal and flume that may be 1/8 in. thick, or more, but will dissolve during a clear-water flow period. Other temporary changes are caused by sediment deposits in the approach section (Section 1). The changes in discharge due to a 1/4-in. throat deposit, a roughness change from glass smooth to broomed concrete, and sedimentation (Section 1) equal to the sill height, are shown in Figures 4 and 5. These coating effects are almost the same as a registration error of the same magnitude. Very subtle differences result from the coatings in the approach channel and the way that the uniform coating would geometrically change the flow areas.

Figures 3 and 4 show how changes in B_3 and Z_3 influence the discharge difference, but the combined influences plotted as changes in A_3 for both structures are similar.

More than 50 of these trapezoidal flumes, designed for the Soil Conservation Service (SCS), have been installed by contractors, and checked by the SCS for conformance to specifications. Upstream from one flume an existing constant-head orifice structure was used to obtain a flow of 20 cfs. This is one of the field checks discussed previously as example III of field verification of flumes and weirs. The example output of the computer model in Appendix I is for this style flume with a 0.2-ft sill height. The flume calibration curve of Y_1 vs Q can be plotted directly from this table.

6. Summary and Conclusions

Critical-flow flumes and broad-crested weirs can now be routinely calibrated by computer techniques accurate to about $\pm 2\%$ over a wide range of flow rates and flume cross-sections, including trapezoidal and complex shapes. This ability permits detailed compensation for errors introduced by construction anomalies. Procedures were developed and used on a series of primary devices in irrigation canals, including trapezoidal flumes and broad-crested weirs that identified construction errors and accurately

related a readout mechanism to the primary device, as constructed, so that the original intended accuracy could be restored. Templates can accurately define field dimensions of the flume throat section, which is the most sensitive portion of a flume. Errors in defining the cross-sectional area of the throat can be shown to be nearly equal to the error in discharge. Errors in the approach section and converging section are about one-tenth as important.

The accurate field measurements of flume dimensions were then used to compute a tailored calibration table for the particular construction. A registration-by-template procedure accurately relates the readout device to the flume.

Direct reading discharge gages that were prestamped could be mounted, with the registration technique, to reserve the highest accuracy for any selected flow rate on the gage. Discharge errors, if any, are thus relegated to the least-used flow range.

References

- [1] American Society of Agricultural Engineers, ASAE Standard: ASAE 359.1, Trapezoidal flumes for irrigation flow measurement, pp 565-7 (1976).
- [2] Bos, M. G. (Ed.), Discharge measurement structures, Publication No. 161, Delft Hydraulics Laboratory, Delft, Netherlands (1976).
- [3] British Standards Institution, Standard No. 3680-4B, Methods of measurement of liquid flow in open channels, 4B: Long-base weirs, Available from American National Standards Institute, 1430 Broadway, New York, NY (1969).
- [4] King, Horace Williams, Handbook of hydraulics, Fourth Edition, McGraw-Hill, New York, NY (1954).
- [5] Kulin, Gershon, and Philip R. Compton, A guide to methods and standards for the measurement of water flow, NBS Special Publication 421, U. S. Department of Commerce, National Bureau of Standards, 89 pp (1975).
- [6] Replogle, John A., Critical-flow flumes with complex cross section, Proc. of ASCE Irrigation and Drainage Division Specialty Conference held at Logan, Utah, August 13-15 (1975).
- [7] Replogle, John A., Portable, adjustable flow-measuring flume for small canals, Paper No. 75-2558, presented at the 1975 Winter Meeting, American Society of Agricultural Engineers, December 15-18, Chicago, Illinois (1975).
- [8] Replogle, John A., Tailoring critical-depth measuring flumes, In Flow: Its measurement and control in science and industry, Rodger B. Dowdell, Editor, Vol. 1, Instrument Society of America, pp 123-32 (1974).

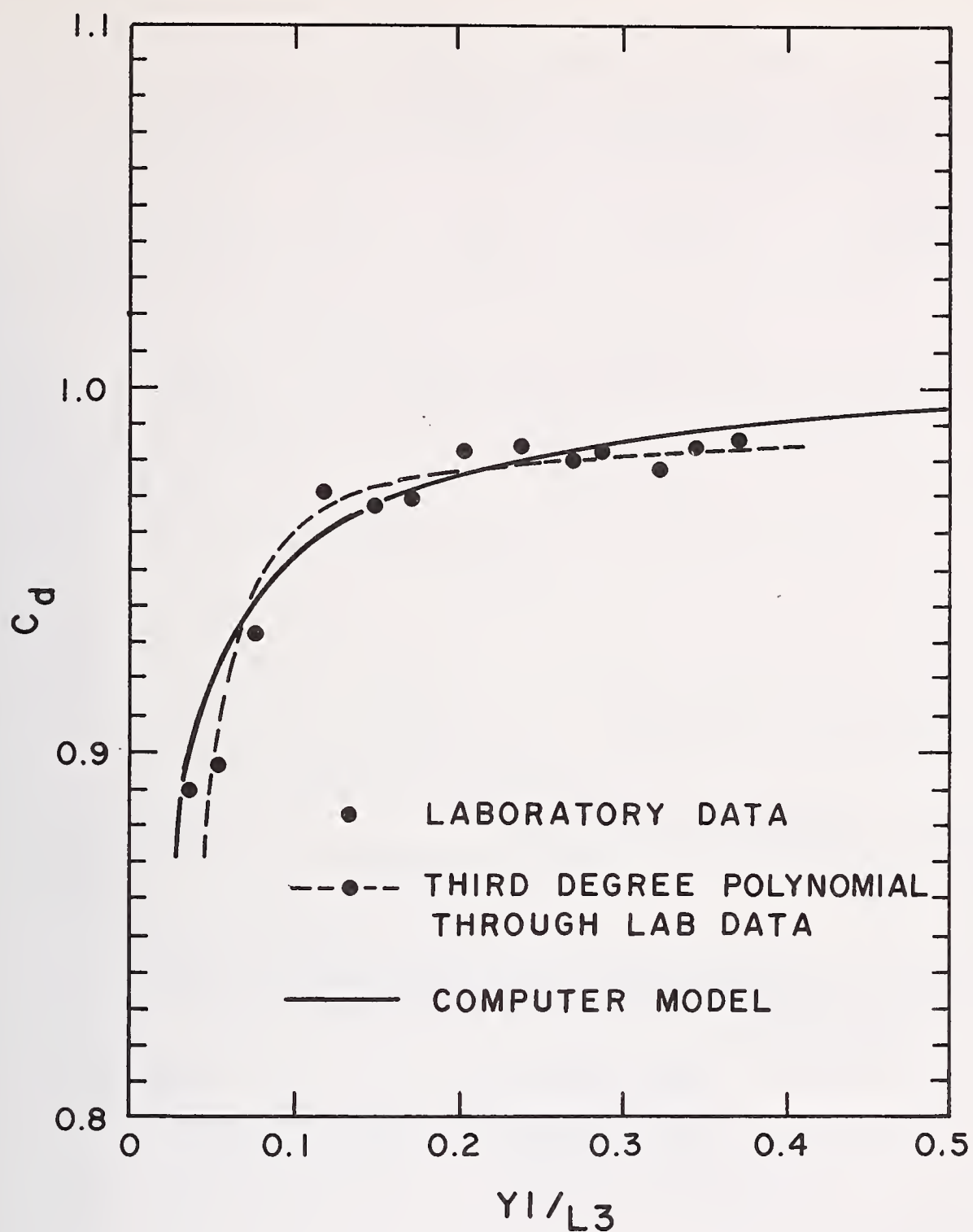


Figure 1: Typical laboratory results fitted with a third-degree polynomial and computer model prediction of discharge coefficient, C_d , for a trapezoidal flume.

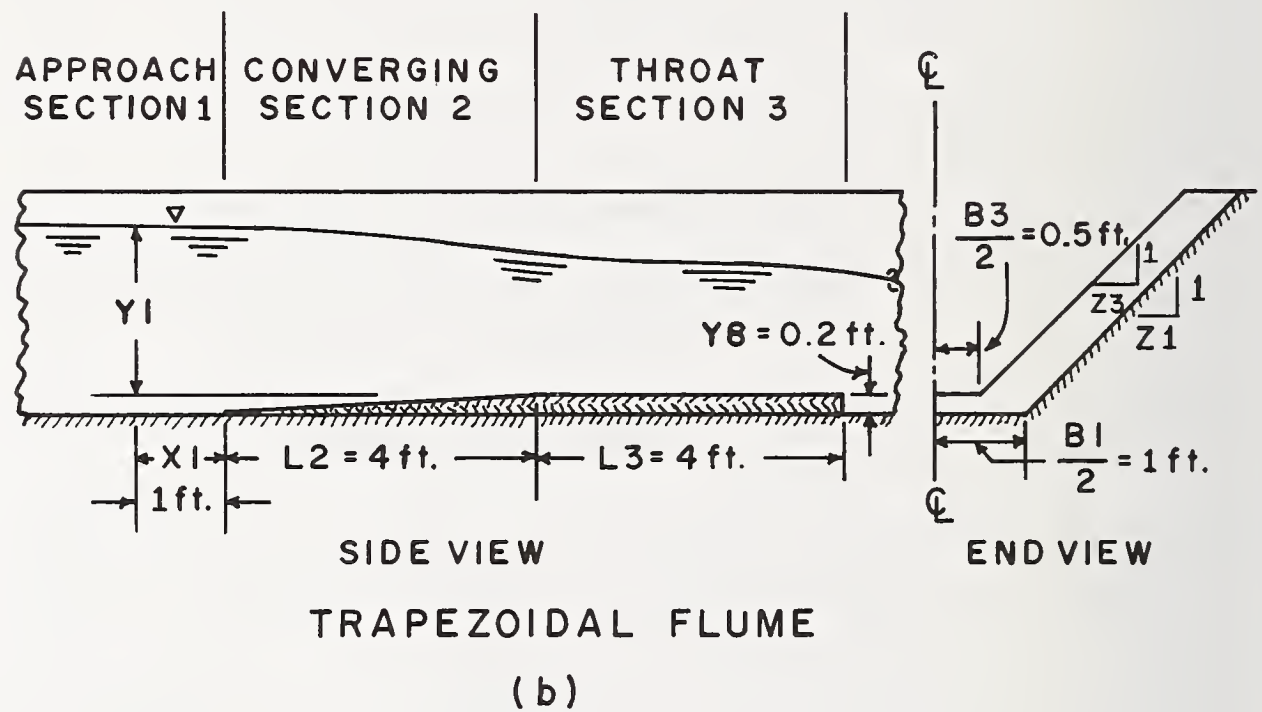
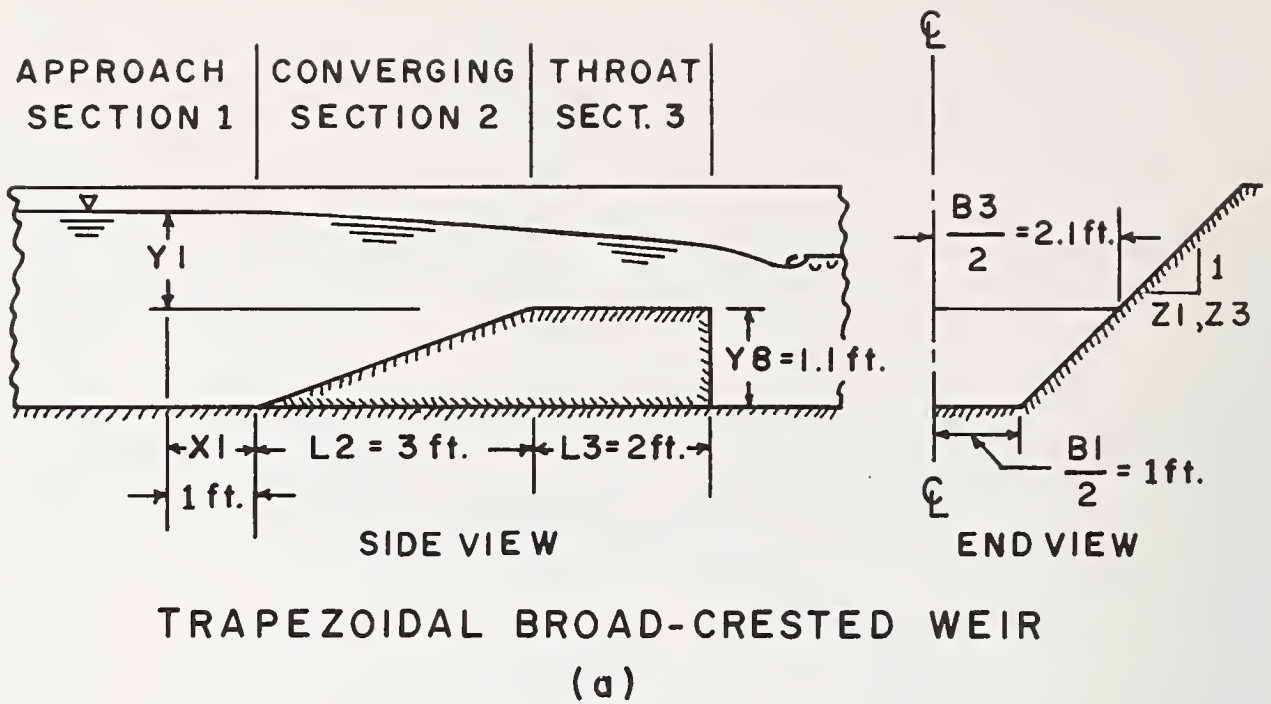


Figure 2: (a) Broad-crested weir in concrete canal.
(b) Trapezoidal flume in concrete canal.

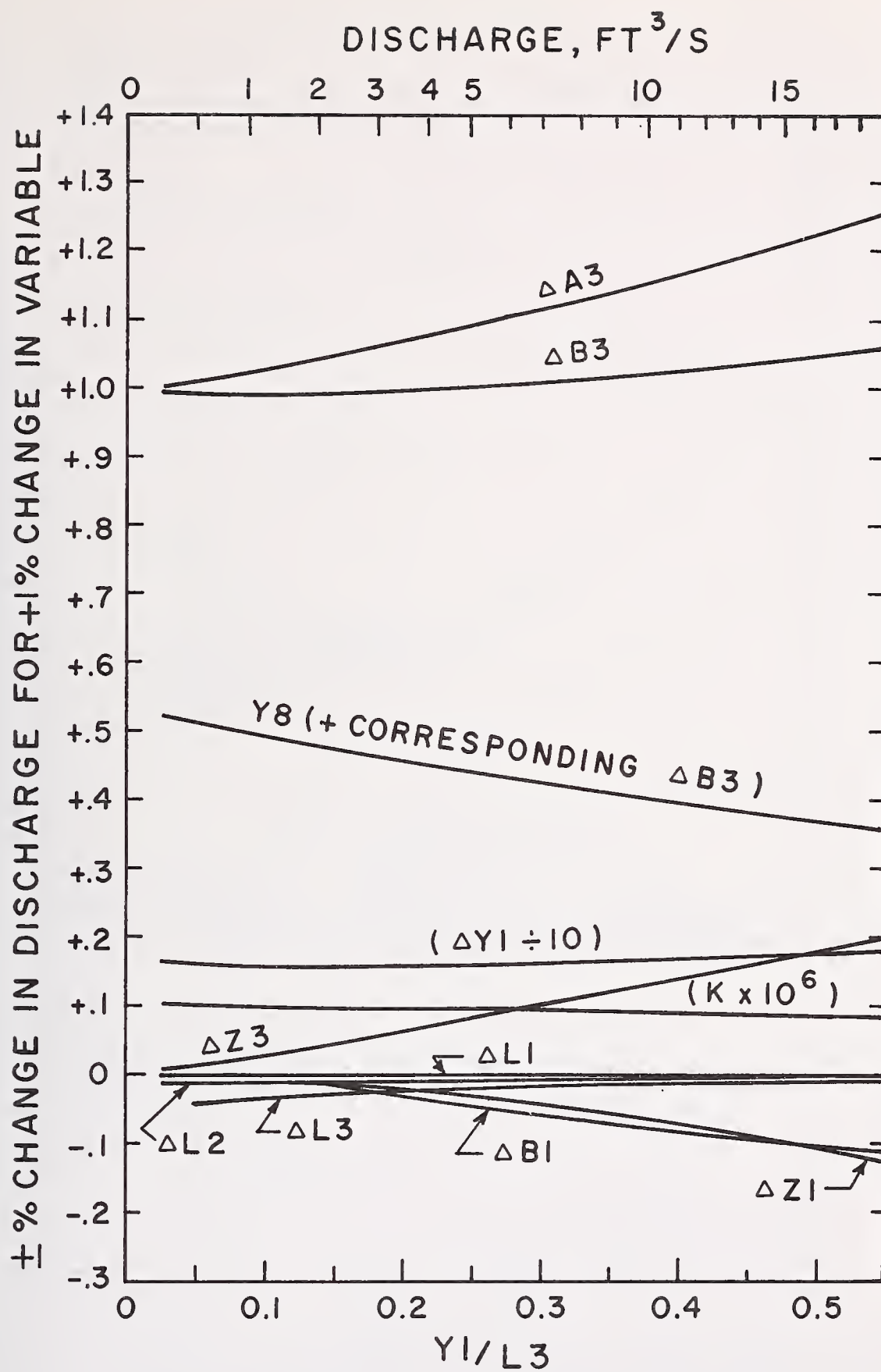


Figure 3: Effects on discharge through a broad-crested weir caused by changes in weir dimensions.

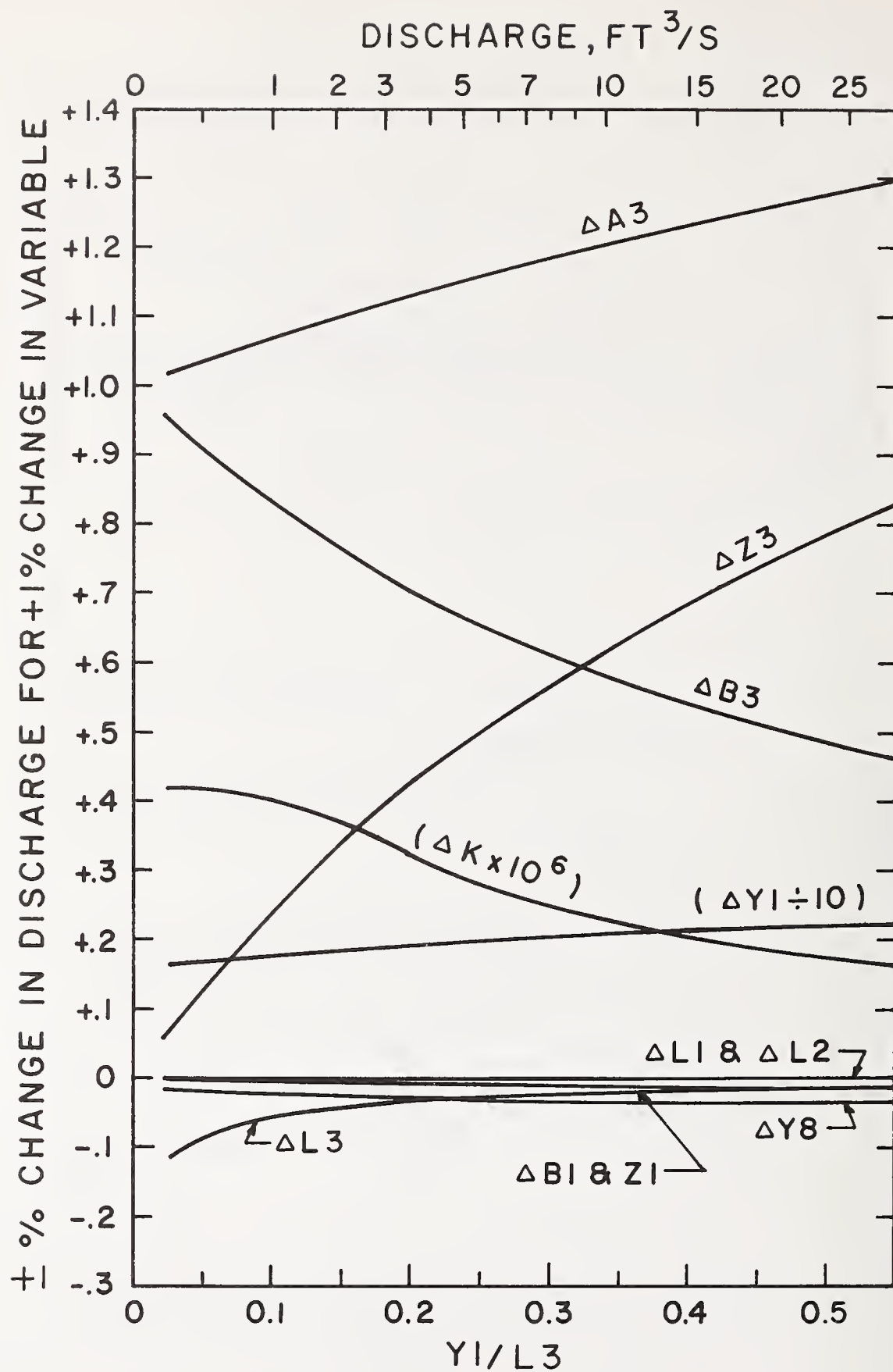


Figure 4: Effects on discharge through trapezoidal flume caused by changes in flume dimensions.

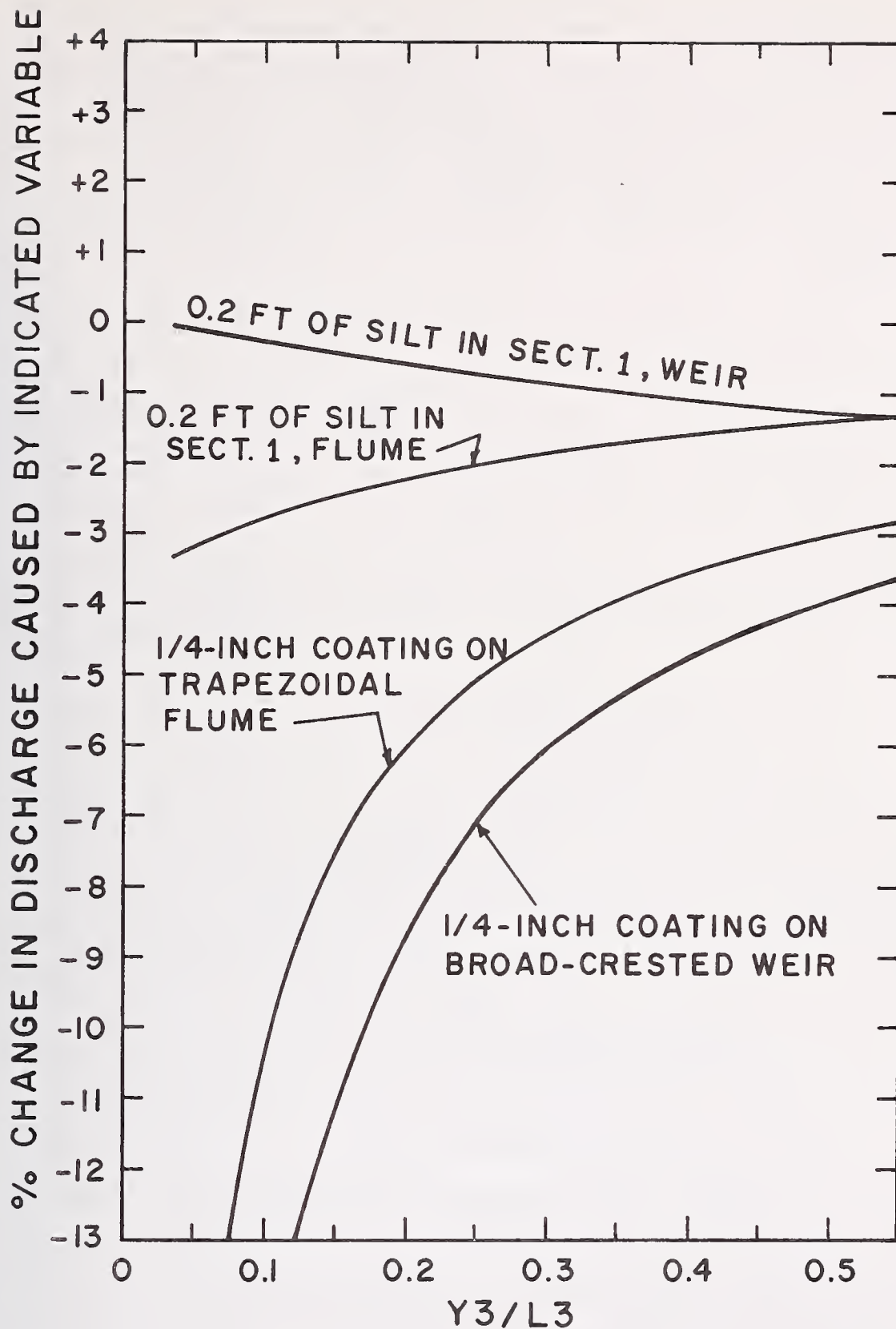


Figure 5: Effects on discharge through trapezoidal flume and broad-crested weir caused by fertilizer coatings and canal siltation.

The attached BASIC computer program prints out the depth, Y_1 , in feet or meters, and discharge, Q , in ft^3/s or m^2/s , depending on the units of the input data. More extended versions provide critical depth, Froude Number, velocities in Sections 1 and 3, discharge coefficient, and the estimated value for the velocity distribution coefficient (listed as A_3 in the program, not to be confused with area, A_3 , of the text and Table 1, which the program uses in the form of $\text{FNC}(X)$). Program versions of this type can be found in references [6] and [7]. The differences are only in the information format printed out, not in the values computed.

The remarks statements refer to an equation number. These are the equations as described and used in reference [6].

This version is suitable for trapezoidal flumes, and the limiting cases, triangular and rectangular. The approach channel and the throat need not be similar. A rectangular channel approach section may have a trapezoidal throat section, but the converging section will have to be warped or multiplaned.

For parabolic, circular, and non-symmetrical channels, the five functions at the beginning of the program need to be modified to give area, top width and wetted perimeter, for each shape required. For more complex shapes, refer to reference [6].

Table 1

DATA INPUTS TO PROGRAM:		Comments
B_1, B_3	Bottom widths Sections 1 and 3.	(Feet or meters).
Z_1, Z_3	Sideslopes, Z (horizontal): 1 (vertical), Sect. 1 and 3.	
$S, 1, L_0$	Starting depth, increment and limiting depth for Y_1 .	(Feet or meters)
K	Absolute roughness height.	(Feet or meters).
L_3	Length of Section 3.	(Feet or meters).
Y_8	Sill height.	(Feet or meters).
L_1	$L_1 = X_1$; distance, depth-sensing location from downstream end of Section 1.	(Feet or meters).
G	Gravitational constant	$(32.16 \text{ ft/s}^2 \text{ or } 9.803 \text{ m/s}^2)$.
T	Water temperature	$(^{\circ}\text{C})$.
Y_1	Flow depth in Section 1 referenced to elevation of flume floor in Section 3.	
A_1	Flow area of Section 1 (not input directly but computed from B_1, Z_1 as $\text{FNE}(X)$)	
A_3	Flow area of Section 3 (not input directly but computed from B_3, Z_3 as $\text{FNC}(X)$).	

```

0001 REM          COMPUTER MODEL FOR TRAPEZOIDAL FLUMES
0005 REM  FUNCTIONS FOR A1,T3,A3,P1,P3 RESPECTIVELY
0016 DEF FNE(X)=(B1+Z1*X)*X
0028 DEF FNN(X)=B3+2*Z3*X
0038 DEF FNC(X)=(B3+Z3*X)*X
0048 DEF FNP(X)=B1+2*X*(1+Z1*Z1)†.5
0058 DEF FNO(X)=B3+2*X*(1+Z3*Z3)†.5
0109 READ B1,B3,Z1,Z3,S,I,L0,K,L3,Y8,L1,L2
0110 DATA 2,1,1,1
0120 DATA .1,.2,2.5
0140 DATA .0005,4,.2,1,4
0189 READ G,V1
0190 DATA 32.16,1.228E-5
0200 PRINT "Y1","Q"
0210 FOR Y1=S TO L0 STEP I
0220   LET Y=Y8+Y1
0236   LET M=0
0237   LET Q5=0
0238   LET H6=0
0239   LET Q=0
0240   LET A1=1
0250   LET A3=1
0260   LET Y3=.7*Y1
0261   LET Q3=Q
0279   REM          COMPUTE Q   (EQ. 1)
0280   LET Q=(G*FNC(Y3)†3/(A3*FNN(Y3)))†.5
0290   IF ABS(Q-Q3)<.0001*Q THEN GOTO 0360
0300   LET Y4=Y3
0309   REM          COMPUTE Y3 (EQ. 4)
0310   LET Y0=Q*Q/(2*G*FNE(Y)†2)
0312   LET Y0=Y0*A1+Y1-H6
0314   LET Y3=Y0-FNC(Y3)/(2*FNN(Y3))
0330   IF ABS(Y3-Y4)<.0001*Y4 THEN GOTO 0261
0350   GOTO 0300
0360   IF M>0 THEN GOTO 0390
0380   LET M=1
0390   IF ABS(Q5-Q)<.001*Q THEN GOTO 0510
0400   LET Q5=Q
0410   GOSUB 0570
0429   REM          COMPUTE A3 (EQ. 17-21)
0430   LET E=1.77*C6†.5
0440   LET A2=1.5*FNO(Y3)/FNN(Y3)-.5
0450   IF A2<2 THEN GOTO 0460
0455   LET A2=2
0460   LET A4=.025*L3/(FNC(Y3)/FNO(Y3))- .05
0465   IF A4>0 THEN GOTO 0470
0468   LET A4=0
0470   IF A4<1 THEN GOTO 0480
0475   LET A4=1
0480   LET A3=1+(3*E*E-2*E†3)*A2*A4
0489   REM          ASSIGN A1 A VALUE FOR OPEN CHANNELS
0490   LET A1=1.04
0500   GOTO 0310
0510   PRINT Y1,Q
0540 NEXT Y1
0550 END

```

```

0560 REM                      SUBROUTINE FOR FRICTION LOSS
0569 REM                      COMPUTE A LENGTH REYNOLDS NO. BASED ON L3
0570 LET R=Q/FNC(Y3)*L3/V1
0579 REM                      COMPUTE A CRITICAL LENGTH REYNOLDS NUMBER (EQ. 8)
0580 LET R5=350000+L3/K
0589 REM                      COMPUTE A LAMINAR DRAG COEF., C1 (EQ. 10)
0590 LET C1=1.328/R+.5
0609 REM                      COMPUTE THE TOTAL DRAG COEF. (CORRECTED),C7 (EQ. 7)
0610 LET X1=R
0620 LET X2=L3
0630 GOSUB 0780
0640 LET C6=C0
0645 IF R<R5 THEN GOTO 0710
0650 LET X1=R5
0660 LET X2=R5*V1/(Q/FNC(Y3))
0670 GOSUB 0780
0680 LET C8=C0
0690 LET C7=C6-(R5/R)*(C8-C1)
0700 GOTO 0720
0710 LET C7=C1
0719 REM                      COMPUTE FRICTION IN THROAT, H3 (EQ. 13)
0720 LET H3=C7*FNO(Y3)*L3*Q*Q/(2*G*FNC(Y3)+3)
0729 REM                      ESTIMATE Y2 (EQ. 15)
0730 LET Y2=Y3+(5/8)*(Y1-Y3)
0739 REM                      COMPUTE FRICTION, SECT. 2, H2 (EQ. 16)
0740 LET H2=FN(Y)*L2*Q*Q/FNE(Y)+3
0742 LET H2=H2+FN(Y2)*L2*Q*Q/FNC(Y2)+3
0744 LET H2=H2*.00235/(4*G)
0749 REM                      COMPUTE FRICTION, SECT. 1, H1 (EQ. 14)
0750 LET H1=.00235*FN(Y)*L1*Q*Q/(2*G*FNE(Y)+3)
0759 REM                      COMPUTE TOTAL FRICTION, H6 (EQ. 5)
0760 LET H6=H1+H2+H3
0770 RETURN
0779 REM                      COMPUTE C0 (EQ. 9)
0780 LET C0=.005
0790 LET C9=C0
0800 LET J=(.544*C0+.5)
0805 LET C0=J/(5.61*C0+.5-.638-LOG(1/(X1*C0)+1/(4.84*X2/K*C0+.5)))
0810 IF ABS(C0-C9)>.00001 THEN GOTO 0790
0820 RETURN

```

Y1	Q
.1	9.26352E-2
.3	.585946
.5	1.4546
.7	2.7227
.9	4.42691
1.1	6.60579
1.3	9.29756
1.5	12.5397
1.7	16.3688
1.9	20.8202
2.1	25.9286
2.3	31.7275
2.5	38.2499

NUMERICAL MODELING OF TWO-DIMENSIONAL FLUMES

Ronald W. Davis

Mechanics Division
National Bureau of Standards

Flumes are commonly used devices for the measurement of open-channel flow rates. Their range of operation has been limited, however, because, outside of experimentally calibrating each configuration used, one has had to resort to one-dimensional theory for flow rate determination. This theory is restricted to fairly low values of upstream-head to crest-length ratio, as well as to almost level flumes with a reasonably uniform incoming velocity profile and non-converging sidewalls. The present study is concerned with extending the operational range of a particular type of flume (the two-dimensional version of the Palmer-Bowlus flume) into areas where one-dimensional theory loses its validity. The determination of the head-discharge relationship for this flume is done numerically by use of the SOLA finite difference routine for two-dimensional free-surface flows. Effects of changes in flume geometry, channel slope, and upstream velocity profile are investigated. The numerical results are verified experimentally.

Key Words: Flumes; hydraulic models; hydraulics; numerical models; open-channel flow; weirs.

1. Introduction

Flumes are commonly used devices for the measurement of open-channel flow rates. The fluid depth at a particular location in a flume is measured, this depth then being related to the discharge by means of a head-discharge calibration curve. This paper will present a new means of determining this calibration curve. Previously it has been determined either experimentally or by means of one-dimensional flow theory. It will be shown here that, under certain conditions, the use of a two-dimensional numerical flow field simulation has significant advantages over these other two methods in determining the calibration curve. As will be seen, it is clearly far cheaper and less time-consuming to calibrate by computer program than to experimentally rate each type of flume prior to field installation. Also effects of errors in field installation of the flume can often be more readily assessed on the computer than in the laboratory. The use of one-dimensional flow theory [1]¹ can lead to errors in discharge determination for flumes with such features as converging sidewalls, short crests, steeply sloping channel beds, and severely

¹ Figures in brackets indicate the literature references at the end of this paper.

distorted incoming flow profiles. It is in situations such as these that the numerical simulation to be discussed here will be shown advantageous.

As noted previously, the present investigation is concerned with the application of two-dimensional theory to flow through measuring flumes. The particular flume chosen for study is the two-dimensional version of the Palmer-Bowlus flume (i.e., a broadcrested weir), which is often used in sewers [2]. This flume serves as a convenient test case for the present study and provides the first data on this device not derived from either experiment or one-dimensional theory [2,3,4]. The computation of flow through this flume is performed numerically by use of the SOLA finite difference routine recently developed at the Los Alamos Scientific Laboratory [5]. This code solves the complete two-dimensional, time-dependent Navier-Stokes and continuity equations for incompressible flows with free surfaces. It is one of a line of Marker-and-Cell codes for the computation of free-surface flows which have appeared during the past decade [6, p. 196]. SOLA is used here to determine the head-discharge relationship of the given flume for situations in which one-dimensional theory is generally inadequate. These include large upstream-head to crest-length ratios, sloping channel beds, and highly nonuniform incoming velocity profiles. In addition, effects of changes in flume geometry are investigated. In order to verify the numerical results, an experimental investigation of the baseline flume is made. The experimental apparatus consists of a flume set at the exit from a constant-width plexiglass channel. The head-discharge relationship and the effects of channel slope on this relationship are obtained experimentally and compared with the numerical results. Free-surface profiles traced off the plexiglass sidewall are compared with those generated numerically. Results of all these comparisons are seen to be satisfactory.

2. Numerical Scheme

The SOLA finite difference routine is a simplified version of the Marker-and-Cell (MAC) method first proposed by Harlow and Welch [7] for incompressible free-surface flow problems. Since a complete description of SOLA can be found in ref. [5], only a brief review of the numerical scheme will be presented here.

The Navier-Stokes and continuity equations for incompressible flow are written in primitive variables as

$$\frac{\partial \vec{q}}{\partial t} + (\vec{q} \cdot \nabla) \vec{q} = - \nabla p + \vec{\Phi} + \nu \nabla^2 \vec{q} \quad (1)$$

$$\nabla \cdot \vec{q} = 0 \quad (2)$$

in which $\vec{q} = (u,v)$, where u and v are the velocity components in a two-dimensional cartesian reference frame (x,y) ; p is the ratio of pressure to constant density; $\vec{\Phi}$ is the body acceleration (gravitational here); ν is kinematic viscosity (zero for the present study); and t is time. The two components of eq. (1) are put in conservation form [8, p. 28] and finite differenced using an explicit marching scheme in time. The convective terms $(\vec{q} \cdot \nabla) \vec{q}$ are differenced using a mixture of central and upwind differencing [6, p. 19 and 73]. The precise mix can be varied by means of a parameter. Thus, the velocity field computed from eq. (1) at time step $(N + 1)$ is solely a function of the velocity and pressure fields at time step (N) . However, this velocity

field at time step $(N + 1)$ is determined only from eq. (1) and will probably not satisfy the continuity equation, eq. (2). Incompressibility is imposed by adjusting the pressure in each computational cell until the velocity divergence for that cell approaches to within a certain tolerance, ϵ , of zero, where ϵ is usually of order 10^{-3} or less. Thus, if there is a net inflow into a cell, p is increased to eliminate this; for a net outflow, p is decreased. Since the pressure adjustment to a given cell affects the velocity divergence of neighboring cells, this process must be done iteratively. The velocity changes in each cell which occur as a result of these pressure changes are computed from a finite difference form of

$$\frac{\partial \vec{q}}{\partial t} = - \nabla p \quad (3)$$

which is the appropriate form of eq. (1) for impulsively applied pressure gradients [8, p. 471]. Once the divergence condition for each cell is satisfied, the iteration stops. Since eq. (3) has not changed the vorticity field determined from eq. (1), both vorticity and divergence are correct at time step $(N + 1)$. Thus, the correct velocity and pressure fields at time step $(N + 1)$ are now known, and the calculation can proceed to time step $(N + 2)$ once the free-surface location has been updated.

In the original MAC code, massless marker particles moved with the fluid and determined the location of the free surface. These particles have been eliminated from SOLA. Instead, the location of the free surface is determined from the kinematic equation

$$\frac{\partial h_s}{\partial t} + \vec{q} \cdot \nabla h_s = v \quad (4)$$

in which h_s is free-surface height. The pressure along the free surface is maintained^s constant (zero) by appropriately adjusting the pressures in the computational cells through which the free surface passes. In addition to computing free surfaces, SOLA can also handle rigid curved boundaries by appropriate modifications to the pressure iteration along these boundaries.

As with most explicit numerical schemes [6], there are time step restrictions required to maintain numerical stability. For the present investigation

$$\Delta t = \frac{1}{3} \min \left\{ \frac{\Delta x}{|\vec{u}|}, \frac{\Delta y}{|\vec{v}|} \right\} \quad (5)$$

in which Δt is the time step; and Δx and Δy are the cell dimensions. After each time step, the mesh was swept to find the value of the right hand side of eq. (5). Thus Δt changed as the computation proceeded. Also for numerical stability reasons, the differencing of the convective terms in eq. (1) was split equally between central and upwind differencing.

3. Numerical Modeling of Flume

The model of the Palmer-Bowlus flume that is used in this study is shown in figure 1. The values of θ for both bottom slopes are the same. The flow enters parallel to the channel bed on the left and leaves almost parallel to the bottom slope on the right. The exit condition on the right was chosen so as to simulate free flow over the brink and also to avoid the computing dif-

iculties associated with any hydraulic jump that might occur downstream. The length of the bottom slope downstream of the brink was adjusted until further increases had negligible effect on the flow upstream of the brink. Typical distances in the x-direction traversed by this slope are between L and 2L, depending on flume geometry. The components of gravitational acceleration, g , are denoted by g_x and g_y . The value of g_y is always negative, while g_x is non-zero only if the entire flume is sloped. A positive g_x denotes positive flume slope, i.e., flume tilted downward to the right.

The problem being considered here is time-dependent, as the location of the free surface, $\lim_{t \rightarrow \infty} h(x,t) = h_s(x,\infty)$, is not known a priori. Thus, $h(x,0)$ must be guessed; the better the guess, the less computer time required. The incoming velocity profile, $U(y,t)$, is arbitrarily specified at each time step at a distance approximately $L/2$ upstream of the base of the crest. The draw-down of the free surface begins downstream of this point. The outgoing velocity on the right is closely approximated from Bernoulli's equation for flow parallel to the bottom slope [9, p. 40]. It is specified at each time step, but only prior to the pressure iteration required to satisfy the continuity equation, eq. (2). Thus, the outgoing velocity at a given time step changes as pressure changes, as do all other velocities except $U(y,t)$. This makes for minimum interference with the upstream flow [5], which is insensitive to disturbances at this location anyway since the flow downstream of the brink is supercritical [1, p. 192]. The upstream depth, h , is allowed to vary with time. Because of this, the discharge through the flume can also vary with time. The computation proceeds until the greatest change in $[h_s(x,t) + P + y_o]$ from one time step to the next is less than 0.01 percent. The final value of h is then $h_s(0,\infty)$, which is the primary quantity sought from the calculation. This allows the head-discharge relationship to be determined for the specified geometry, channel slope, and inlet velocity profile.

As the fluid being modeled is nearly inviscid, the kinematic viscosity in eq. (1) was set equal to zero. Thus, viscous boundary-layer effects in the flume were ignored. This is justified by the relatively large upstream-head to crest-length ratios being considered here. Also, boundary layer effects upstream of the flume can be accounted for by an appropriately specified upstream velocity profile. A typical mesh consisted of 29 cells horizontally and 9 fluid-filled cells vertically at the inlet location. All computations were done in double precision on the NBS UNIVAC 1108. Computation times ranged from one to five minutes.

4. Numerical Results

A summary of the cases to be presented is given in table 1. Flume 1 is the baseline configuration. Effects of changes in slope and inlet velocity profile on the head-discharge relationship are evaluated using this flume. Flumes 2 and 3 show the effect on this relationship of geometry changes from the baseline configuration.

The definitions of discharge, Q , and head, H , to be used here are as follows:

$$Q = \int_{y_o}^{y_o + P + h} U(y) dy \quad (6)$$

$$H = h + \frac{1}{2g} \left(\frac{Q}{P + h} \right)^2 \quad (7)$$

in which y_0 and P are defined in figure 1; $g = \sqrt{g_x^2 + g_y^2}$; $h = h_s(0, \infty)$; and $U(y) = U(y, \infty)$, as time is now irrelevant. All quantities can be nondimensionalized according to the following:

$$d' = \frac{d}{L}, \quad \vec{q}' = \frac{\vec{q}}{\sqrt{gL}}, \quad Q' = \frac{Q}{L\sqrt{gL}}, \quad \frac{H}{L} \quad (8)$$

in which d is an arbitrary length. Primes will now be dropped; all quantities referred to hereafter are nondimensionalized according to eq. (8) and are steady-state values.

The main purpose of this study is to extend determination of the head-discharge relationship into areas where one-dimensional theory is inadequate. For values of H less than about 0.33, one-dimensional theory should generally provide satisfactory results, at least for level flumes with reasonably uniform incoming flow profiles [1, p. 212]. Thus, this investigation is concerned solely with values of H between the approximate limits of 0.33 and 1.30. The upper limit of about 1.30 is rather arbitrary. It was chosen partially on the basis of computer costs and partially because h is approximately 1.0 near the upper limit of H . It will be seen that the results presented here do in fact approach the one-dimensional results as H tends to its lower limit.

Figure 2 shows discharge versus head for flume 1 with zero slope and constant inlet velocity profile, $U(y) = U$. The head-discharge relationship, $Q = .581 H^{1.550}$, is obtained by least-squares curve-fit. The RMS error of the fit is about 0.6 percent. This is based on percentage error in Q for a given H . Figure 3 shows the same least-squares curve-fit along with those for flumes 2 and 3. Also shown is the one-dimensional relationship [1, p. 211]. The RMS errors of the fits for flumes 2 and 3 are about 1.0 percent and 0.6 percent, respectively. All three curve-fits are based on from 21 to 28 data points, which are equally weighted. It can be seen that the effect of the change in θ (flume 2) is much greater than the effect of the change in P (flume 3). In fact, the increase in P has almost no effect. Figure 4 presents the difference between the two-dimensional and the one-dimensional values for Q taken from the curves in figure 3. As expected, these differences decrease as H decreases.

Figure 5 illustrates the effect on the head-discharge relationship of sloping flume 1. The effect is, of course, greatest at low values of H where gravitational considerations are most important. In fact, the inlet Froude number, $U/\sqrt{h + P}$, is about 2/3 near the top of the curve and 1/3 near the bottom.

Figure 6 is a comparison between the linear inlet velocity profile and the uniform inlet profile for flume 1 with no slope. For the linear profile, the surface velocity is 2.33 times greater than the bottom velocity. This profile is chosen so as to give typical values of energy and momentum coefficients, α and β , of 1.16 and 1.05, respectively [9, p. 28]. The effect of inlet velocity profile on the velocities at two points along the crest of the flume is depicted for two values of H . The two locations chosen to depict the profiles are at distances of 0.56 and 0.19 upstream from the brink. At the first of these locations, the Froude number, $u/\sqrt{h_s}$, is equal to one

(critical) for the solid line with $H = 0.37$. If there were a free overfall at the brink, the critical depth would be about 1.40 times the brink depth [1, p. 195]. For the present case, the corresponding value is 1.39. Figure 7 shows the negligible effect that the distorted inlet profile has on the head-discharge relationship. The maximum change in Q for a given H is about 2 percent.

5. Experimental Flume

In order to try and assess the accuracy of the numerical results, it was decided to set up an experimental model of flume 1. Figure 8 shows the experimental apparatus. It consisted of an 8-foot (2.44 meter)-long clear plexiglass channel with a constant width of 6 in. (15.2 cm). The flume was set at the exit from the channel and terminated in a free overfall. The crest length, L , was 6 in. (15.2 cm). Flow entered the channel through a 1-in. (2.5 cm)-wide slot in the vertical 2-in. (5.1 cm)-diameter pipe at the upstream end. An orifice meter in the pipe upstream of the slot was used to measure flow rate. In order to smooth out the high level of turbulence produced by the flow into the settling basin just downstream of the pipe, two screens and a series of spaced honeycomb sections were employed as shown in figure 8. To assess the effectiveness of these elements in smoothing the flow, pitot tube and propeller meter traverses were made at the depth measuring station 3 in. (7.6 cm) ($L/2$) upstream of the base of the flume. The traverses came to within 0.37 in. (0.9 cm) of the side-wall and 1.30 in. (3.3 cm) of the bottom. Water depth varied from 3 in. (7.6 cm) to 7 in. (17.8 cm). As observed from the numerical results (figure 7), vertical variations in velocity were not deemed as important as transverse variations. Two-dimensionality of the flow required a reasonably uniform velocity profile across the channel. The traverses showed that the greatest change in velocity in any given transverse or vertical plane within the region covered was about 15 percent. This was felt to be about as good as could be expected in a channel of this size, and the experiment proceeded.

The experimental procedure consisted of reading the pressure drop across the orifice meter with a mercury manometer and obtaining the upstream height at the depth measuring station using a point gage. Free-surface profiles were traced off the channel sidewall at the flume location with the aid of a floodlight. Flume slopes of 1 percent, 2 percent, and -1 percent were obtained by simply sloping the entire channel. At the conclusion of the experiment, the orifice meter was calibrated in place using a weighing tank.

6. Experimental - Numerical Comparison

Figure 9 shows the least-squares fit to the experimental head-discharge data at zero slope. The fit is based on 20 data points and has an RMS error of approximately 0.7 percent. Head, H , and discharge, Q , are defined here as previously. Discharge, Q , is obtained by dividing the total flow rate measured with the orifice meter by the channel width. Figure 10 is a comparison between the experimental and the numerical head-discharge relationships. Also shown for comparison is the one-dimensional relationship. For $H = 0.33$ ($\log H = -0.48$), the difference between the numerical and experimental values of Q is about 3.3 percent. For $H = 1.30$ ($\log H = 0.11$), the difference is about 1.6 percent. The experimental curve does not approach the one-dimensional curve with decreasing H as it should for an ideal fluid, such a fluid being assumed in the numerical computations. In fact, it is suspected that viscous boundary-layer effects along the channel sidewalls, which grow in importance

as H decreases, are largely responsible for the difference between the experimental and numerical results. In the present study, the thickness of these boundary-layers was not measured. Further, the exact nature of the boundary layers in the channel is difficult to estimate because of the honeycomb and turbulence upstream. However, if one can assume that a turbulent boundary layer begins to grow just downstream of the final honeycomb, then the following formula for boundary-layer displacement thickness on a flat plate is appropriate [10, p. 599]:

$$\delta_1 = .04625 D (\text{Re}_D)^{-1/5}, \quad \text{Re}_D = \frac{(\frac{Q}{P+h})D}{\nu} \quad (9)$$

in which δ_1 is the nondimensional (with L , as usual) displacement thickness; D is the nondimensional distance from the final honeycomb to the depth measuring station (about 4); ν is the nondimensional kinematic viscosity; and Re_D is the Reynolds number based on D . The boundary layers along the channel sidewalls will reduce the effective channel width and thus effect the experimentally calculated values of Q and H . Note that the boundary layer along the channel bottom does not effect the experimental calculation of Q and has only a negligible effect on the experimental calculation of H . Also, the numerical results indicate that the effect of vertical variations in velocity is negligible. If the experimental data is corrected for the assumed sidewall boundary layers, then the curve-fit indicated by the dashed line in figure 10 results. The RMS error for this fit is about 0.6 percent. The values of Re_D that occur in the fitted region are roughly between 2.0×10^5 and 5.0×10^5 . This is in the laminar-turbulent transition region for flow over a flat plate [10, p. 600], but because of the high levels of turbulence in the channel, it is sufficient for this approximation to assume that the boundary layer is always turbulent. For $H = 0.33$, the difference between the numerical and boundary-layer-corrected experimental values of Q is about 1.0 percent, while for $H = 1.30$, it is about 0.2 percent. Table 2, which summarizes the curve-fits obtained in this study, clearly shows that the boundary-layer-corrected curve-fit more closely approximates the numerical curve-fit than does the uncorrected experimental fit. Also, it is seen from figure 10 that the boundary-layer-corrected experimental curve now approaches the one-dimensional curve for small H . Thus, the suspicion that sidewall boundary-layer effects in the channel are important appears to be justified, at least based on this approximate analysis. It is unfortunate that the experiment could not have been performed in a wider channel, thus reducing boundary-layer blockage as percentage of width.

Figure 11 compares numerical and experimental free-surface profiles over the unsloped flume for two values of H . The energy $(h_s + |\vec{q}|^2/2)$ along the computer-calculated profiles is constant to within five percent within the region shown. It is noted that one-dimensional theory gives no free-surface profile for the case $H = 0.96$, while the one-dimensional flow for the case $H = 0.37$ is subcritical everywhere. Figure 12 shows the difference between the zero-slope curve-fit value of Q , denoted by Q_0 , and the value of Q at the same H for a sloped flume. This difference is plotted as a function of head for the experimental, the boundary-layer corrected experimental, and the numerical cases. The computed slope effect is seen to agree quite well with the experimental effect for each of the three slopes studied.

7. Conclusions

It has been shown that a relatively simple, easily obtained numerical

routine, SOLA, can provide significant advantages over current methods of calibrating two-dimensional flumes. The routine can easily accommodate upstream velocity profile and channel slope effects, as well as changes in flume geometry. The accuracy of the method has been demonstrated by experimental means. The head-discharge relationships presented in table 2 show both the high quality (small RMS error) of the curve-fits and the very good agreement between computer and experiment. It is recalled that this agreement was obtained under the simplifying assumption of inviscid flow for the numerical computations. Thus, the convenience and low cost of using this code make the excellent numerical-experimental comparison quite impressive.

The main conclusion of this investigation is that the computer in general and SOLA in particular have an important part to play in the study of two-dimensional measuring flumes. Such things as the effect of sediment build-up (i.e., geometry change) on the flume calibration curve can now be readily determined. Errors produced by incorrect flume installation are easily assessed. The limits of validity of one-dimensional theory can now be defined for a given flume and use of this theory suitably restricted. Outside of these limits of validity, the errors associated with the currently common practice of using one-dimensional theory are now amenable to calculation.

It is hoped that other open-channel flow researchers will make use of SOLA. In particular, it can readily be adapted to compute fully three-dimensional flows [5]. Thus, the study of three-dimensional flumes with converging sidewalls should be possible with this code. The main limitation in this regard would seem to be computer time.

8. Acknowledgments

The author gratefully acknowledges the helpful advice of Drs. Gershon Kulin and George Mattingly. He is also grateful for the assistance of Mr. Louis Lembeck in performing the experiment.

9. References

- [1] Henderson, F. M., *Open Channel Flow*, (The Macmillan Company, New York, 1966).
- [2] Kulin, G. and Compton, P. R., A guide to methods and standards for the measurement of water flow, *National Bureau of Standards Special Publication 421*, (U. S. Government Printing Office, Washington, D. C., 1975).
- [3] Ludwig, R. G. and Parkhurst, J. D., Simplified application of Palmer-Bowlus flow meters, *J. Water Pollution Control Federation* 46, 2764 (1974).
- [4] Wells, E. A. and Gotaas, H. B., Design of venturi flumes in circular conduits, *Proc. Amer. Soc. Civ. Engr.* 82, Proc. Paper 928 (1956).
- [5] Hirt, C. W., Nichols, B. D., and Romero, N. C., SOLA - A numerical solution algorithm for transient fluid flows, *Los Alamos Scientific Laboratory Report LA-5852*, (U. S. Government Printing Office, Washington, D. C., 1975).
- [6] Roache, P. J., *Computational Fluid Dynamics*, (Hermosa Publishers, Albuquerque, New Mexico, 1972).
- [7] Harlow, F. H. and Welch, J. E., Numerical calculation of time-dependent viscous incompressible flow, *Physics of Fluids* 8, 2182 (1965).
- [8] Batchelor, G. K., *An Introduction to Fluid Dynamics*, (Cambridge University Press, London, 1967).
- [9] Chow, V. T., *Open-Channel Hydraulics*, (McGraw-Hill Book Company, New York, 1959).
- [10] Schlichting, H., *Boundary-Layer Theory*, (McGraw-Hill Book Company, New York, 1968).

10. Notation

The following symbols are used in this paper:

D = distance from final honeycomb to depth measuring station in experimental channel;

d = arbitrary length;

g = gravitational acceleration;

g_x = component of gravitational acceleration parallel to channel bed;

g_y = component of gravitational acceleration normal to channel bed;

H = upstream head;

h = height above crest of upstream flow;

h_s = height above crest of free surface;

L = crest length;

N = N^{th} time step;

P = crest height;

p = ratio of pressure to constant fluid density;

Q = discharge through flume;

Q_0 = baseline flume discharge from zero-slope curve-fit;

\vec{q} = velocity vector;

Re_D = Reynolds number based on $D = \frac{(\frac{Q}{P+h})D}{v}$;

t = time;

U = inlet velocity profile;

u = component of velocity parallel to channel bed;

v = component of velocity normal to channel bed;

x = coordinate parallel to channel bed;

y = coordinate normal to channel

y_0 = height of channel bed in xy -coordinate system;

α = energy coefficient =
$$\frac{\int_{y_0}^{y_0+P+h} [U(y)]^3 dy}{Q^3/(P+h)^2};$$

β = momentum coefficient =
$$\frac{\int_{y_0}^{y_0+P+h} [U(y)]^2 dy}{Q^2/P+h};$$

Δt = computational time step;

$\Delta x, \Delta y$ = computational cell dimensions;

δ_1 = boundary-layer displacement thickness;
 ϵ = maximum bound on velocity divergence for a computational cell;
 θ = flume bottom slope angle;
 ν = kinematic viscosity;
 Φ = body acceleration; and
 ∇ = gradient operator.

TABLE 1

NUMERICALLY MODELED FLUMES

Flume No.	P/L	Tan θ	Flume Slope, %	Inlet Velocity Profile, U(y)
1	0.19	0.25	0, 1, 2, -1	constant
			0	linear
2	0.19	0.33	0	constant
3	0.33	0.25	0	constant

TABLE 2

LEAST-SQUARES CURVE-FITS OF HEAD-DISCHARGE RELATIONSHIP
FOR UNSLOPED FLUMES

FLUME	HEAD-DISCHARGE RELATIONSHIP (RMS Error, %)		
	NUMERICAL	EXPERIMENTAL	EXPERIMENTAL (Boundary-Layer Corrected)
1	$Q = .581 H^{1.550}$ (0.6)	$Q = .570 H^{1.563}$ (0.7)	$Q = .579 H^{1.556}$ (0.6)
2	$Q = .596 H^{1.572}$ (1.0)	-	-
3	$Q = .584 H^{1.555}$ (0.6)	-	-

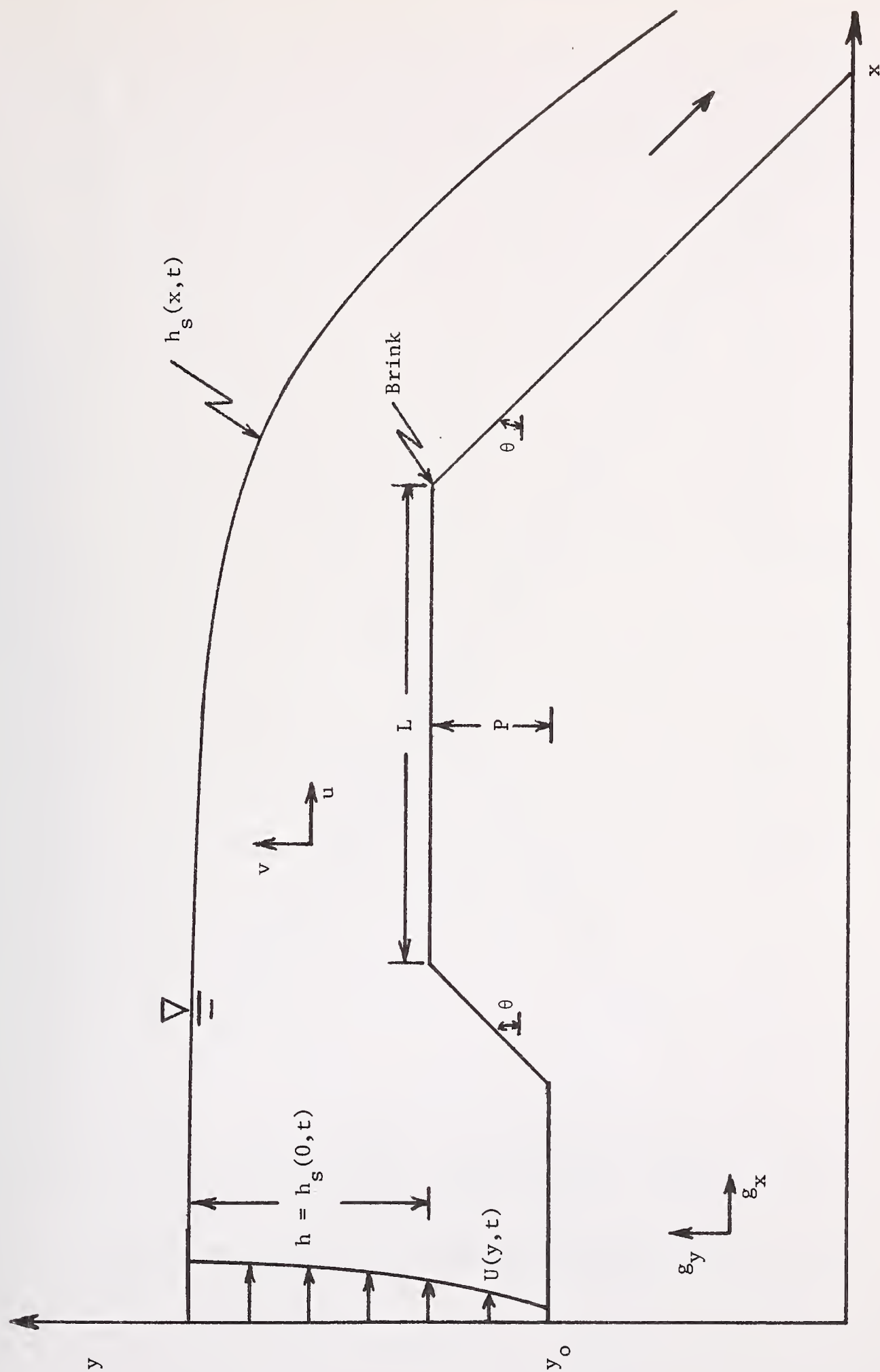


FIGURE 1. MODEL OF PALMER-BOWLUS FLUME

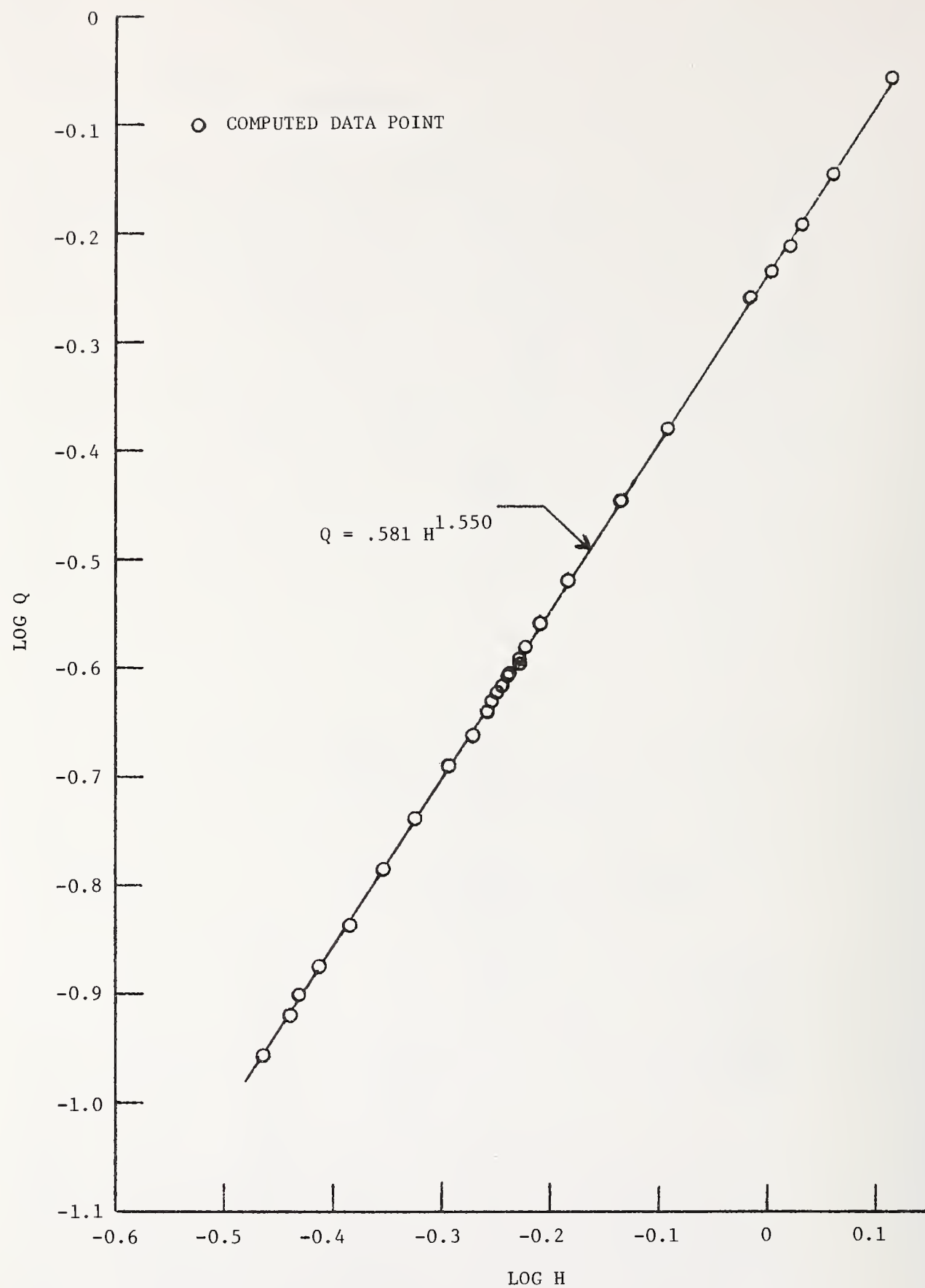


FIGURE 2. COMPUTER-CALCULATED HEAD-DISCHARGE RELATIONSHIP FOR FLUME 1

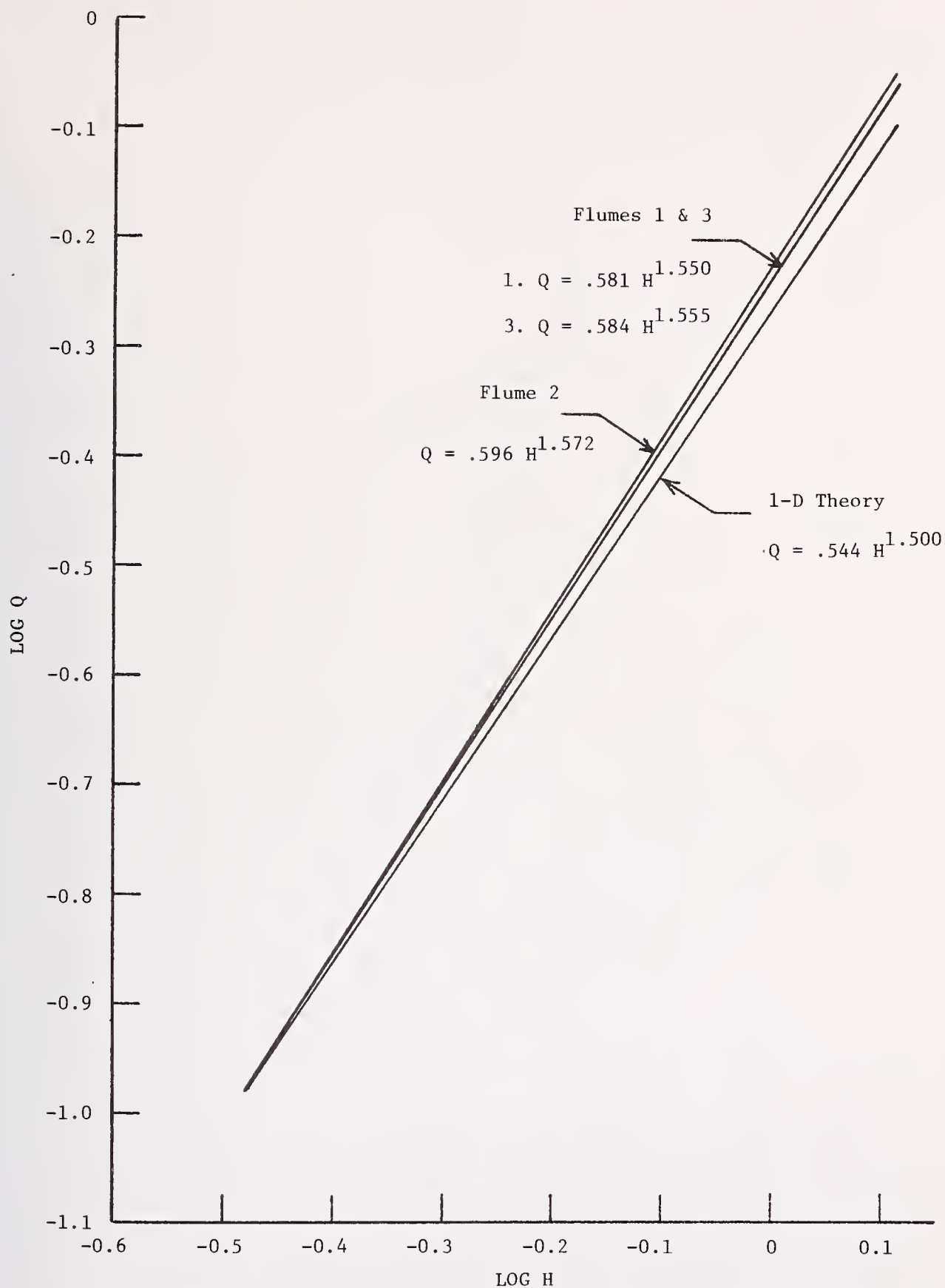


FIGURE 3. LEAST-SQUARES CURVE-FITS FOR NUMERICALLY MODELED FLUMES

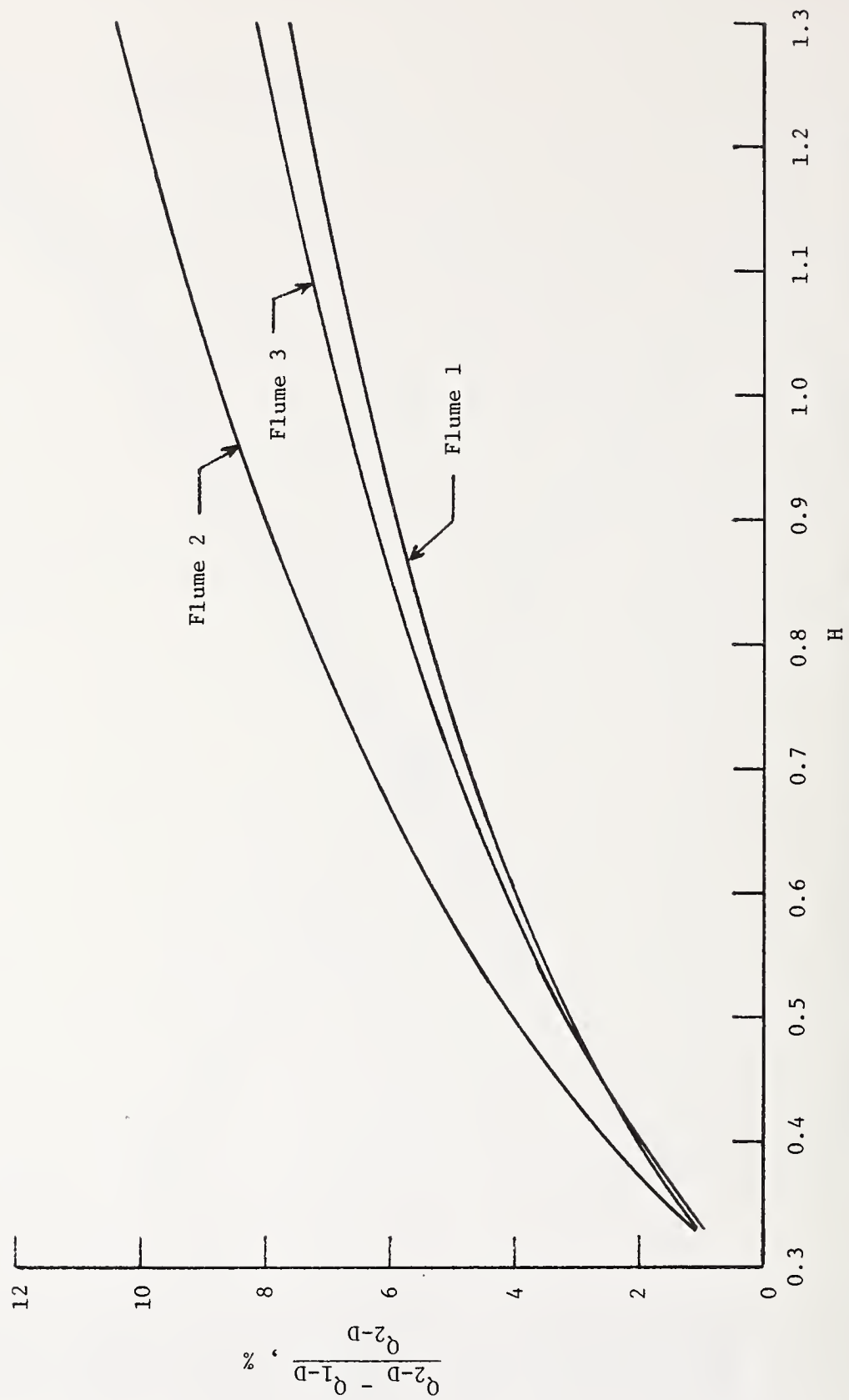


FIGURE 4. DIFFERENCE BETWEEN 2-D AND 1-D DISCHARGE DETERMINATION

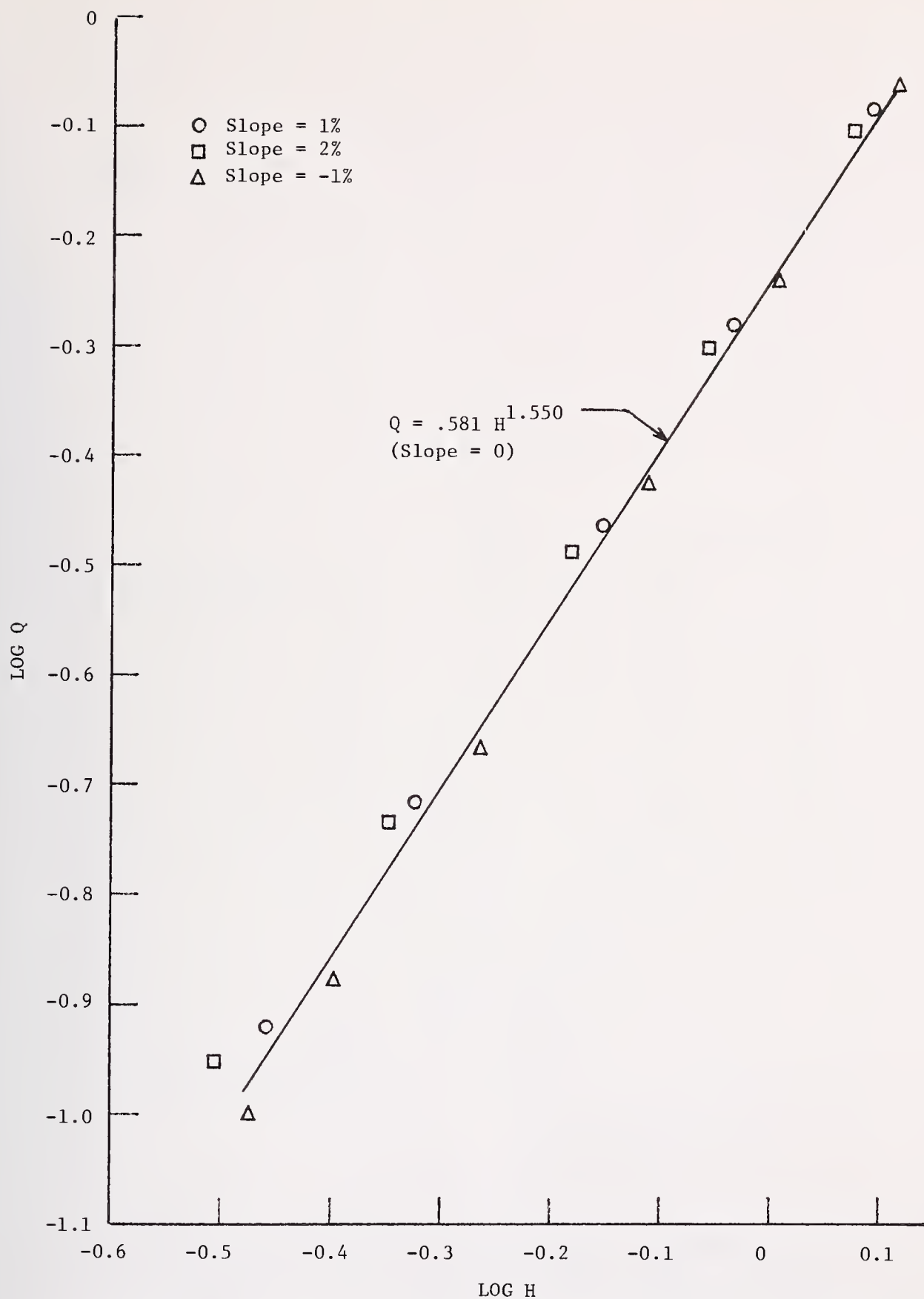


FIGURE 5. EFFECT OF SLOPE ON HEAD-DISCHARGE RELATIONSHIP

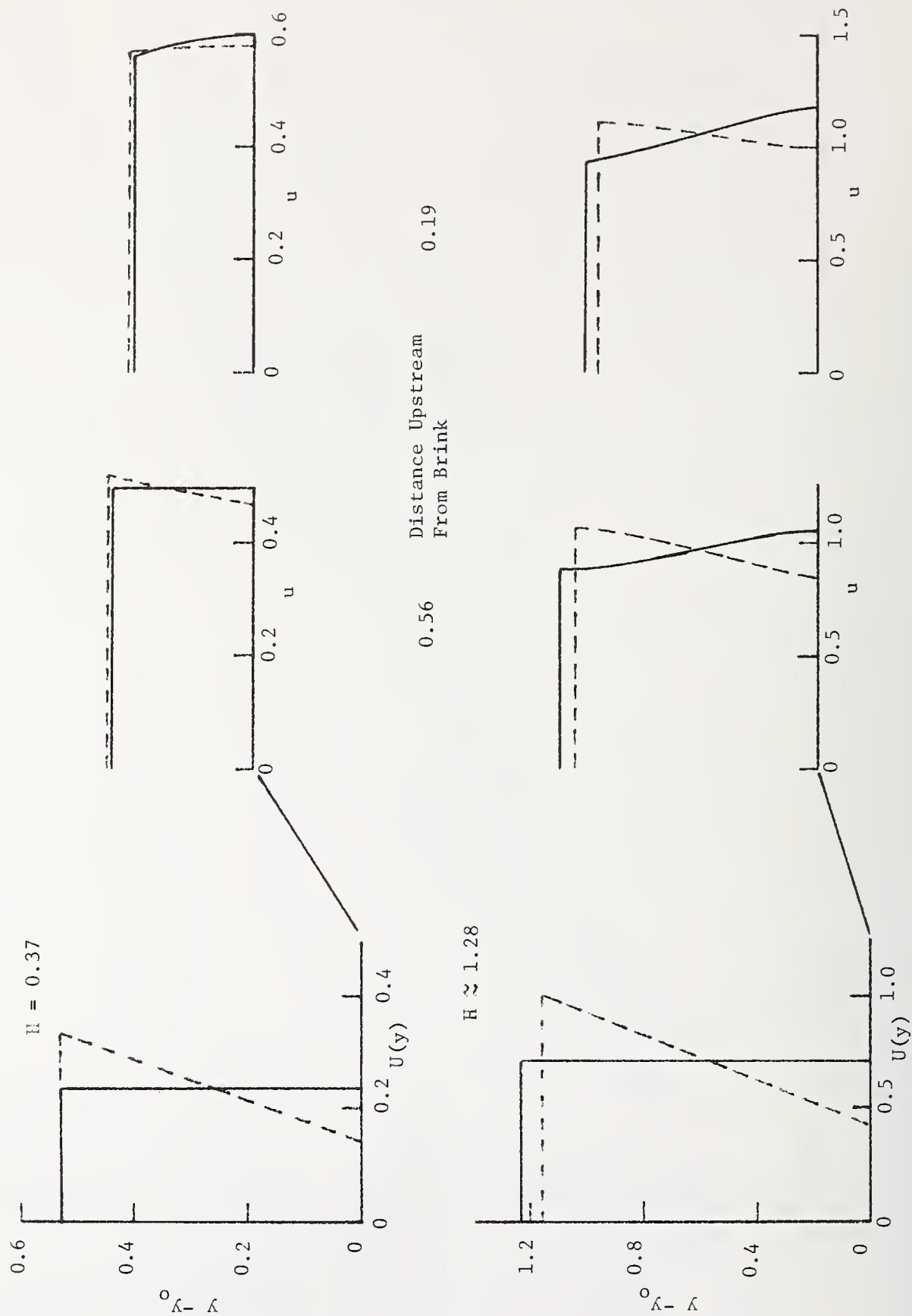


FIGURE 6. VELOCITY PROFILES IN FLUME 1

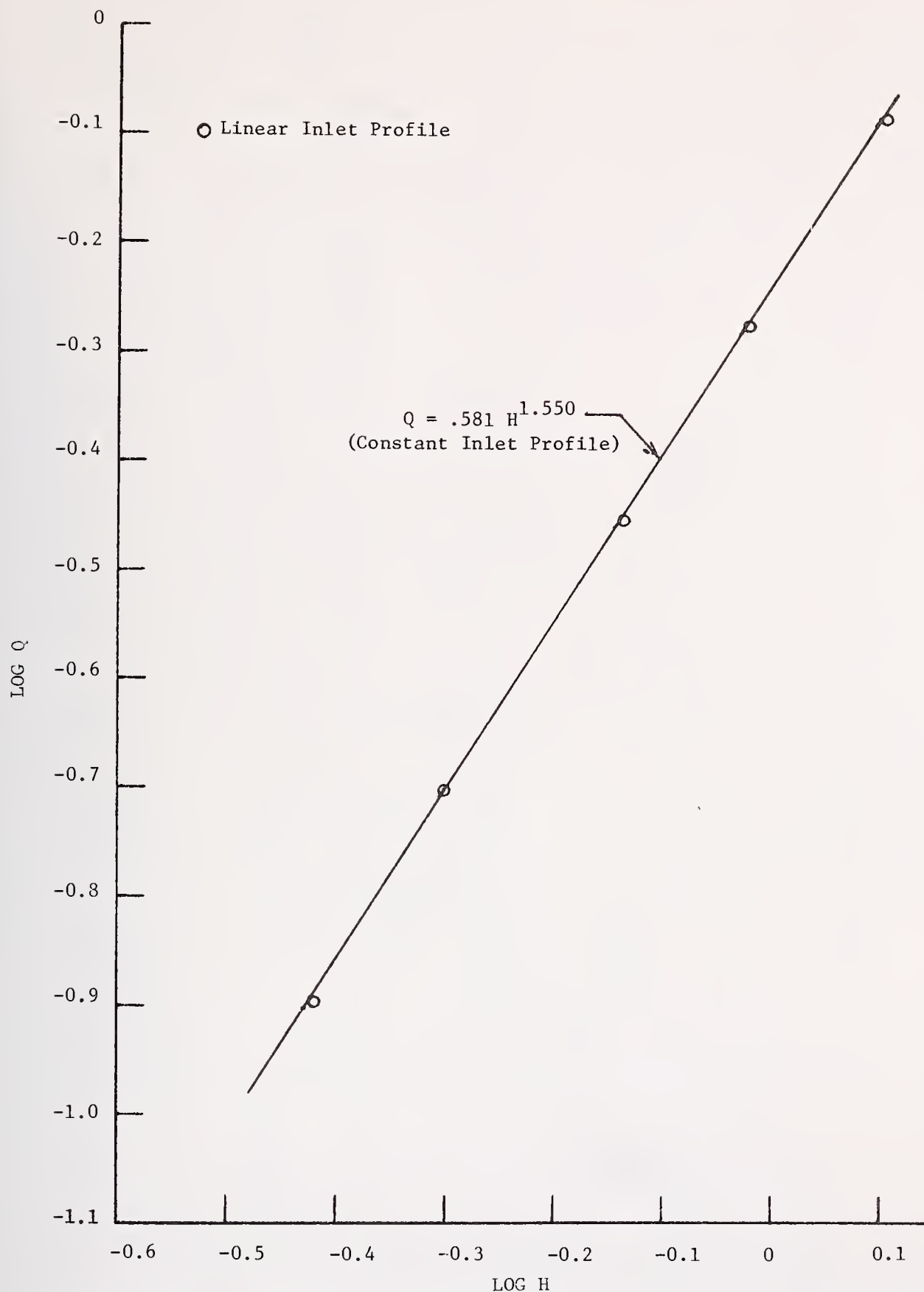


FIGURE 7. EFFECT OF INLET VELOCITY PROFILE ON HEAD-DISCHARGE RELATIONSHIP

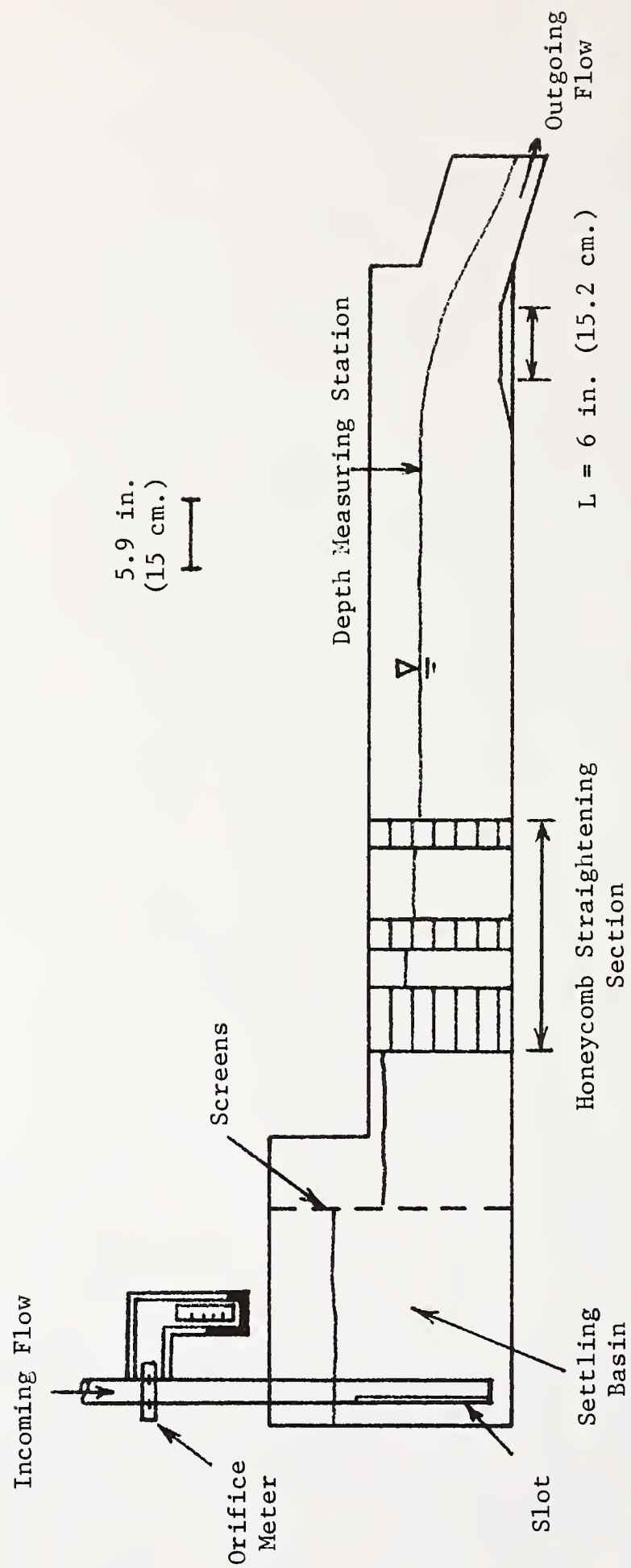


FIGURE 8. EXPERIMENTAL APPARATUS

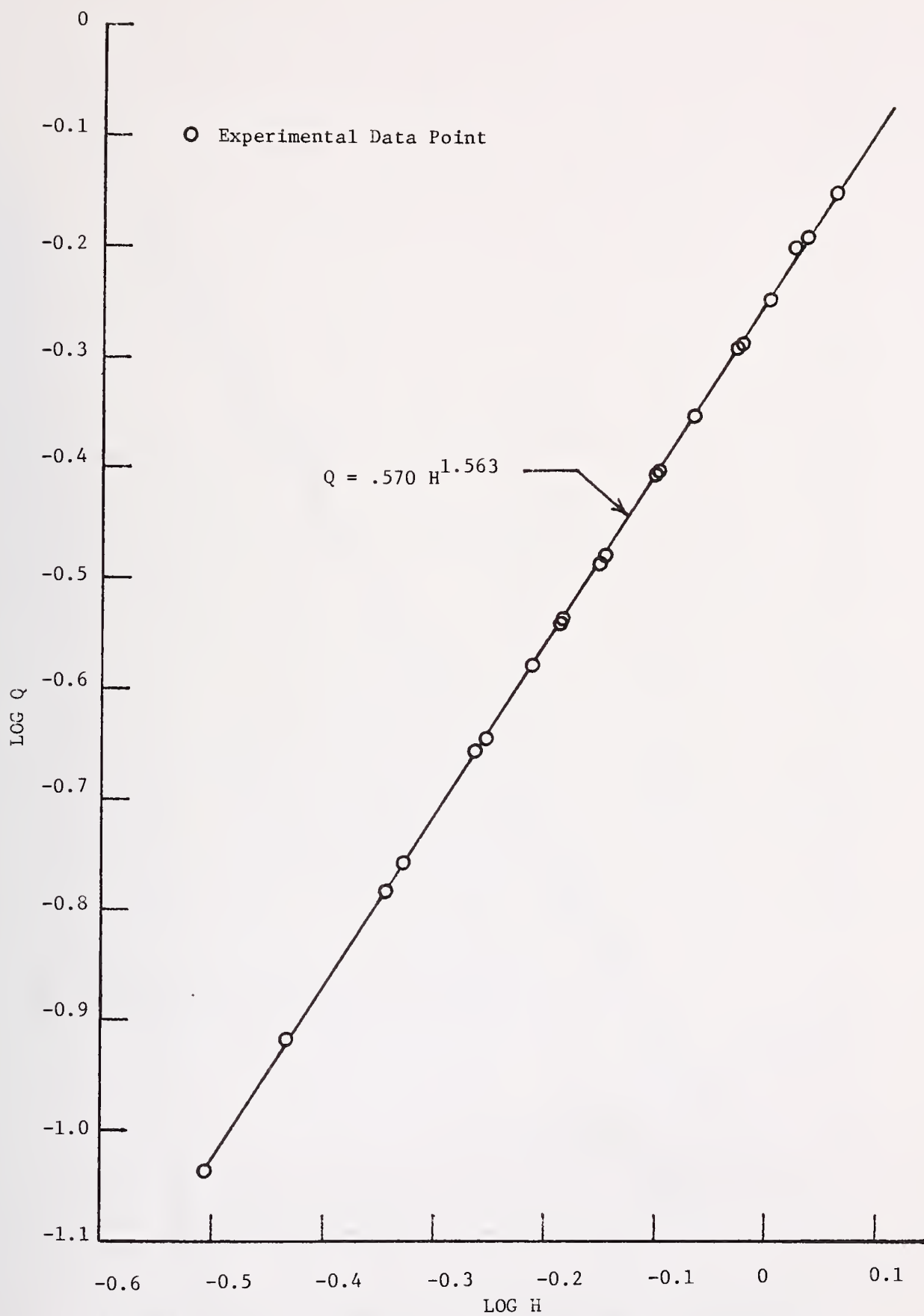


FIGURE 9. EXPERIMENTAL HEAD-DISCHARGE RELATIONSHIP FOR FLUME 1

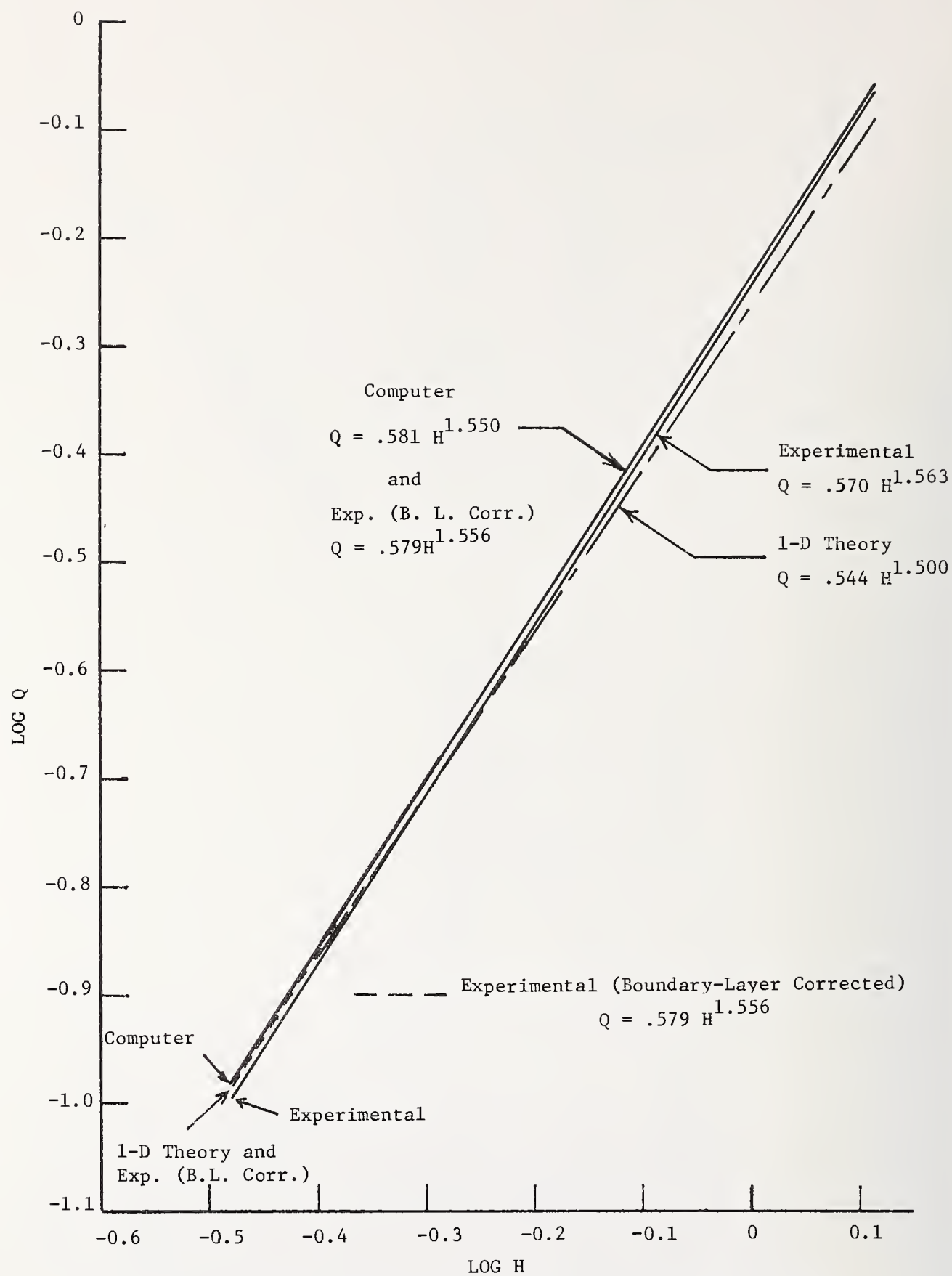


FIGURE 10. EXPERIMENTAL AND NUMERICAL HEAD-DISCHARGE RELATIONSHIPS

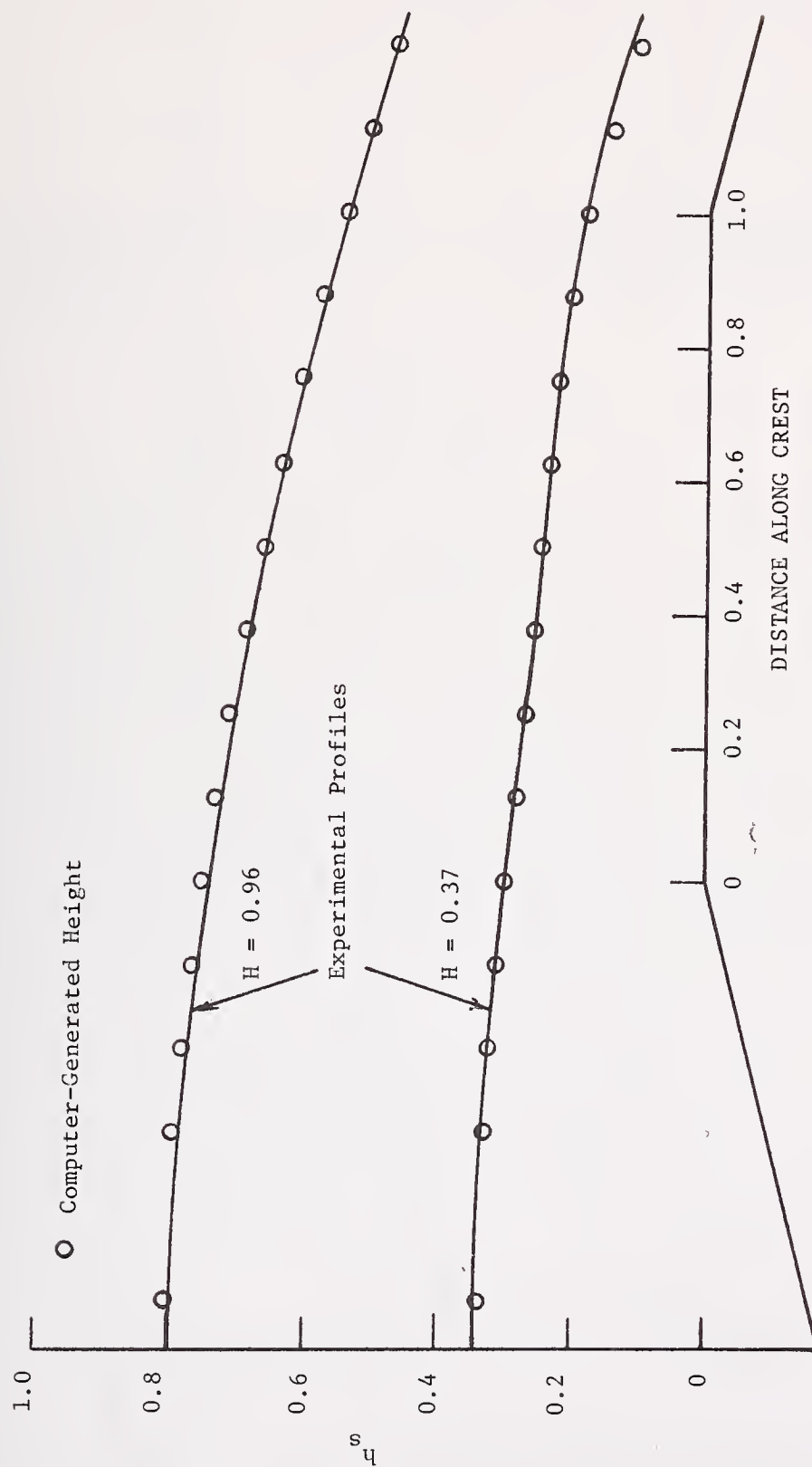


FIGURE 11. EXPERIMENTAL AND NUMERICAL FREE-SURFACE PROFILES

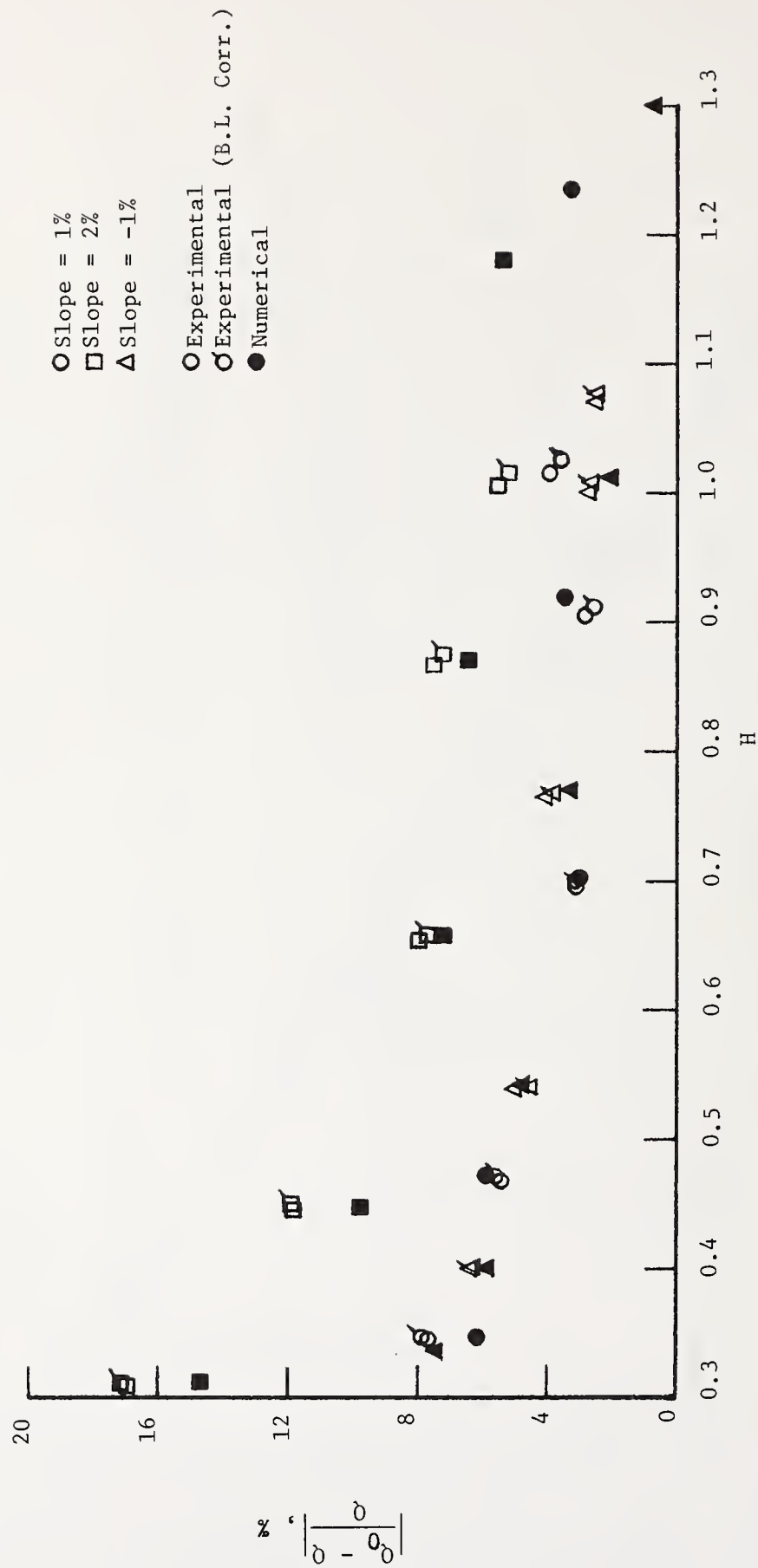


FIGURE 12. EXPERIMENTAL AND NUMERICAL SLOPE EFFECT COMPARISON

THE DESIGN OF OPEN CHANNEL ACOUSTIC FLOWMETERS FOR
SPECIFIED ACCURACY: SOURCES OF ERROR AND CALIBRATION
TEST RESULTS

Francis C. Lowell, Jr.

Ocean Research Equipment, Inc.
Accusonic Division
Falmouth, Massachusetts 02541

The design of open channel acoustic flowmeters is more difficult than the design of pipeline flowmeters because of errors introduced by the free surface, as well as because the open channel environment is usually more susceptible to attenuation and multipath conditions which can inject large errors unless special signal recognition and filtering techniques are employed. The sources of error in open channel acoustic flowmeters are tabulated and discussed. These include 1) Line velocity errors 2) Level measurement errors 3) Integration errors. Assuming that the required sophisticated techniques are used to prevent the large errors (20-50%) which can occur due to signal attenuation and multipath, the total flow rate error contribution of Items 1 and 2 above can be kept below 1% for liquid velocities greater than .5 FPS. Any error in excess of 1% of flow is contributed by Item 3, Integration error. For an accurately known cross section, this error is a function of the number and spacing of acoustic paths and the integration method used, and can be predicted in advance. Therefore, the desired overall system accuracy should be taken into account during the design phase in order to establish the minimum number of paths required. Two design examples are given for 2% specified accuracy with maximum flow rates of 1000 and 6000 CFS. In both cases the meters were calibrated using standard stream gauging techniques and demonstrated accuracies of better than 2%.

Key Words: Acoustic velocity, acoustic flow rate, flow rate, liquid flow rate, liquid velocity, open channel flow rate, open channel velocity.

1. Introduction

Acoustic methods have been used for velocity and flow rate measurement for several years {1}¹{2}.

Their chief advantages and limitations are summarized in Figure 1, and typical applications are listed in Figure 2. In general, they are economically practical for use where one or more of the following apply: (1) high accuracy is required, (2) channel widths are large, (3) head loss must be avoided, (4) calibration or rating costs are prohibitively high.

This report discusses the use of acoustic flowmeters to determine volume flow rate in open channels with particular emphasis on sources of error and the design approach required to produce a meter of specified accuracy for a given application.

The design problem is more difficult for open channels than for pipelines because of errors introduced by the free surface, as well as because the open channel environment is usually more susceptible to attenuation and multipath conditions which can inject large errors unless special signal recognition and filtering techniques are employed. Nevertheless, relatively high accuracies have been achieved in a wide variety of applications.

2. Theory of Operation

Acoustic flowmeters operate on the established principle that the propagation velocity of acoustic signals in liquids is changed when a component of the liquid velocity is parallel to the direction of acoustic propagation.

The average liquid velocity on each path is determined by measurement of the acoustic traveltime in each direction. These paths have one acoustic transducer at each end, and are located at various elevations in the flowing cross section. The liquid velocity measured at each path is integrated across the flowing area to determine the total volume flow rate. Figure 3 summarizes a mathematical derivation for the acoustic line velocity.

¹Figures in brackets indicate literature references at the end of this paper.

An acoustic flowmeter (see Figures 4, 5, and 6) consists of an electronics/processing unit and several pairs of acoustic transducers and associated cabling. In addition, it must include one of several possible means to measure water level (stage). Normally, the measurement section is part of the channel, and a separately fabricated "meter section" is not required.

When several acoustic paths are to be located in a given cross section, there are limits to the proximity of the acoustic path to the surface and bottom. This limitation results from acoustic multipath reflections at the boundary which interfere with the direct signal arrival from the opposite transducer (see Figure 7). The time required to detect the presence of a signal (say one carrier frequency period), establishes the interval required before the first interfering signals can arrive. Thus the acoustic path must be located a certain minimum distance (clearance height) from the surface or bottom, a distance which depends on operating frequency and path length.

The operating frequency chosen depends on the application, but the following general rules apply.

1. - Higher operating frequencies increase system accuracy by providing higher timing accuracies and hence smaller line velocity errors. Higher frequencies also allow path locations closer to reflecting surfaces; e.g. surface and bottom, hence velocity estimation errors can be reduced.
2. - Lower operating frequencies yield reduced signal attenuation, particularly where silt or entrained air may be a problem. This increases system reliability.
3. - For a given liquid velocity and acoustic path angle, ΔT becomes smaller as the channel becomes narrower, thus requiring a higher operating frequency to maintain system accuracy. Thus, "small" systems tend to be high frequency systems. Typical values of frequency and path length are shown in Figure 8.

3. System Design

Acoustic flowmeter design is, like many other things, an iterative process.

Usual specifications include range of volume flow rate, type of channel, type of access available for transducer installation, maintainability requirements, accuracy, type of outputs, and others.

Additional information required includes a knowledge of the general hydraulic conditions around the meter, and its location relative to sources of entrained air such as pumps, turbines, and spillways upstream. Furthermore, in river systems the expected silt or sediment load should be considered, as well as shipping traffic.

There are several possible system trade-off's. The most usual one is to trade-off the cost of increasing system accuracy by incorporating additional acoustic paths, vs the cost to obtain the same increase in accuracy by performing more extensive post installation tests and calibrations.

A related problem with open channel flowmeter installations is that the velocity distribution in the channel is not well known, either because it changes with different flow/stage conditions or the channel is new and of a sufficiently unusual design that the velocity profile cannot be predicted accurately. In either of the above cases, additional acoustic paths can reduce system errors.

The economics of open channel flowmeters strongly favor the addition of acoustic paths because the marginal cost of additional paths is low given that the site work, electronics, stage measuring system, cable runs/conduits and transducer mounting means have already been paid for. Therefore increased system accuracy can often be achieved more economically with an increased number of acoustic paths than by field calibration after installation. Furthermore, as the channel wall and bottom roughness change between maintenance and cleaning cycles the velocity distribution will change, and even if a calibration is performed after installation, the meter coefficient may change with time, unless a sufficient number of acoustic paths are installed.

A second trade-off is the relation of system cost to site location and site development work required. An example of this is whether the system should be installed in a location requiring extensive site work for a favorable measurement section vs. the possible cost savings of reduced site work on the channel and more complex acoustic path placement to compensate for unknown cross flow components and velocity distributions.

Needless to say, the best system designs occur when the flowmeter is considered in the planning process so that an optimum meter location can be picked at minimum cost.

4. Sources of Error

There are several important sources of error which must be considered when acoustic flowmeters are being designed. These are summarized below:

A) Line Velocity Errors

(1) Installation or Survey Errors

a) Referring to Figure 3, it can be seen that the measured line velocity is proportional to L/T^2 , and since T is proportional to L , then V is proportional to $1/L$. Therefore any error in L will introduce the same error in V . In general, this is not a problem because L can be measured to a high degree of accuracy.

b) Path angle error. Since $v \sim 1/\cos\theta$, any error in θ will produce an error in V . For example, at a 45° path angle, a 1 degree error in θ will produce a 1.7% error in the line velocity.

c) Non-liquid and/or stationary liquid delays: Any delays in the system which add to T without changing ΔT will introduce errors in the meter and must be compensated for. These errors include:

- i) Cable/logic/detector delays
- ii) Acoustic delays associated with transducer windows
- iii) Liquid delays which occur when transducers are separated from the moving fluid, for example, recessed in the walls of an aqueduct.

(2) Errors introduced by transducer installation

These can be caused by transducer projection, if any, into the streamflow, and any unsampled flowing area behind the transducers. Correction for these errors requires analysis of the exact installation configuration. In general the errors produced by the projection effect are less than the ratio of transducer diameter to channel width, which is generally less than 0.1 to 0.5 percent, and can be compensated for.

(3) Errors due to variable acoustic signal strength, receiver circuits, and timing accuracy.

The signals traveling along any acoustic path are subject to variable attenuation in addition to normal spreading loss. This attenuation can be caused by silt, entrained air, marine life, shipping or fouling to name a few. Furthermore, acoustic signals can be distorted by multipath reflections from shipping or debris.

The most serious manifestation of this problem in its effect on flowmeter accuracy occurs when the acoustic signals are sufficiently weakened or distorted so that the receiver detector misses the desired detection point on the waveform by one acoustic wavelength (one period) the effect on accuracy can be very severe. Typical errors resulting from this problem are shown in Figure 8.

If the meter is to be installed in areas where weak or distorted signals are a possibility, then it is essential that signal recognition circuits be incorporated into the system receiver in order to prevent this type of error.

(4) Crossflow Errors

One of the most frequent problems in acoustic flow-meter design efforts is the prediction of streamline direction components which are not parallel to the measurement section axis. The errors produced by this effect are exactly analogous to angular errors in the assumed path position (survey errors) covered in Section 4A(1)b except that the crossflow component is, in general, a function of flow rate and stage.

These errors can occur, for example, when the measurement section is too close to an upstream bend, transition or obstruction which causes the flow to become detached from one or both walls, thus producing asymmetrical and/or diverging streamlines in the meter section. The problem may be aggravated in bi-directional flow installations because any correction factor used for one direction may not be correct when the flow is in the other direction.

A third case occurs in unlined channels where the sidewalls are so irregular that it is impossible to determine the "axis" of the channel.

In any of the above cases, errors can be reduced by the addition of one or more acoustic paths, at the same elevations as the original ones but installed at the opposite angle (see Figure 9). Exact cancellation of errors can be accomplished on the crossed paths, and an estimate of the cross flow component can be used to adjust the readings on the non-crossed paths.

(5) Other Sources of Error

a) Errors due to time base accuracy are generally negligible because crystal oscillators are used which have very high stability and accuracy ($\pm 0.005\%$).

b) Differential detector traveltime measurement errors are eliminated by using the same detector for time measurement in both directions, or by careful balancing of two detectors if simultaneous measurements are made in both directions. The use of one detector, while eliminating one source of error, adds one, at least theoretically in that the two traveltimes must be measured sequentially rather

than simultaneously. However, in practice, this does not introduce significant error because the time required to make a complete pair of measurements is short compared to the rate of change of velocity in the measurement section, even under very turbulent conditions, and the possibility of long term differential delays developing between two separate receivers is eliminated.

c) Errors associated with the discrete traveltime counting periods or quanta, are reduced by using a relatively high counting frequency (10-40 mHz, depending on channel width) and the averaging of many individual line velocity readings. This is possible because while an error of ± 1 count is, in general, made with every traveltime measurement, this is a true random error and can be reduced by averaging over a suitable period (usually 10 sec-10 min, depending on the rate of change of flow rate).

B) Level Measurement Error

The effect of a given uncertainty can be easily calculated given a specific application, as it has a direct effect on the flowing area between the highest acoustic path and the surface.

C) Integration Error

Integration error is defined as the difference between the flow rate calculated by an exact integration of the velocity profile and the flow rate calculated using exact line velocities measured on the several acoustic paths in the system.

The error associated with flow rate integration is conveniently divided into three parts. They are: (1) Highest layer error: the volume flow rate between the highest acoustic path and the surface is uncertain to the extent that the velocity distribution is uncertain. The highest acoustic path cannot be placed arbitrarily close to the surface because of multipath effects. Therefore an estimate of the velocity distribution must be made, usually on the basis of the velocity gradient between the two highest paths extrapolated to the surface. (2) Lowest layer error: the region bounded by the lowest acoustic path and the channel bottom has a flow rate uncertainty resulting from the unknown velocity distribution near

the bottom. The error contribution here is generally less, however, because the velocities are lower, and the boundary condition that the velocity is zero at the bottom is known. (3) Layers bounded by acoustic paths: the errors associated with layer flows which are bounded by acoustic paths are completely under control of the designer.

5. Designing For Specified Accuracy: Worst Case Analysis For Acoustic Path Placement

With proper system design, it is possible to keep the total error contributions due to line velocity error and uncertainty in stage to within +1% of flow for average velocities in excess of .5 FPS (.15 m/sec), (see Figure 16).

Any error in excess of 1.0% of flow results from integration error. For an accurately known cross section, this error is a function of the number and spacing of acoustic paths and the integration method used, and can be predicted in advance. Therefore, the desired overall system accuracy should be taken into account during the design phase in order to establish the number of paths required.

It is not possible to produce a standard "cookbook" design for open channel flowmeter acoustic path placement because variable stage, and high Reynolds numbers and thermal gradients can produce velocity distributions which bear no resemblance to theoretical curves which are derived assuming fully developed turbulent flow. Thus numerical integration techniques which require a specific distribution of acoustic paths are of limited usefulness, and every system should be designed with its particular characteristics in mind.

In this and the following section, two designs are discussed. In each case the design required an accuracy of 2% of flow rate. In both cases, the aqueduct was mortar lined and its cross section was accurately known. The location, angle and elevations of the acoustic paths were accurately determined by standard surveying techniques, and the water level was determined by a stilling well and float connected to a digitizer yielding an overall resolution of $\pm .005$ ft ($\pm .0015$ m) of stage.

A) In the first example, the channel was rectangular in cross section, with a 30' width and 10' depth (9.14 m by 2.74 m deep). The water level varied from 2 feet to 10 feet (.61 m to 2.74 m). An overall accuracy of +2% was specified.

The design sequence involved first, the determination of the number of acoustic paths required to meet an integration accuracy of approximately 0.5% using a theoretical logarithmic velocity distribution (4 paths).

A "worst case" velocity distribution or gradient was then constructed which produced additional integration error. The "worst case" profile, which consisted of a linear velocity gradient between the highest acoustic path and water surface, was chosen to represent the uncertainty in flow rate which could possibly occur, but which could not be corrected for, since the gradient occurred above the highest acoustic path and therefore could not be detected. The magnitude of this gradient was chosen to be +5% of the average surface layer velocity. This average velocity was determined by a weighted average of the velocity measured on the highest acoustic path and the surface velocity estimated by linear extrapolation from the two highest acoustic paths.

Using this "worst case" velocity gradient, the integration error was calculated as the stage was increased. At the stage where the integration error approached 1%, a 5th acoustic path was added at the minimum distance below the water surface (.5 ft in this case, or .15m). This procedure was repeated, adding acoustic paths as required up to maximum stage.

Finally, the positions of the acoustic paths were adjusted to equalize the estimated error peaks, since the highest acoustic path, in general, did not fall at the maximum distance from the highest water elevation. The final path elevations are shown in Figure 10.

B) This system was built and installed at the inlet canal to Lake Skinner, near Hemet, California, and was subsequently calibrated by Metropolitan Water District of Southern California and U. S. Geological Survey personnel,

using standard stream gaging techniques {3}. On the first calibration, agreement was better than $\pm 2\%$ on all readings except for two at low stage, where flow separation and excessive turbulence made accurate conventional stream gaging impossible. A subsequent low stage calibration with the stream gaging equipment installed upstream of the turbulence produced readings within the 2% tolerance. (see Figure 12).

The turbulence observed at low stage was caused by an S bend and transition from trapezoidal to rectangular cross section upstream of the meter section (see Figure 5). This caused separation of flow, turbulence and non-axial flow streamlines through the meter section. The effect of this can be seen on the calibration curve, since the meter error varies from $-1.5-2\%$ at stages over 7 ft (2 m) to $+1.5-2\%$ at a stage of approximately 3.5 ft (1 m). From Figure 9, the average cross flow component at this stage is therefore about 2° , and is a function of stage. The statements above are supported by streamflow direction data taken by Metropolitan Water District personnel {3}.

This calibration illustrates a problem common to high accuracy open channel meters of any type: the available standards to which the meters can be compared are of comparable accuracy to the meter being calibrated. Therefore, it is difficult to determine an error or accuracy for the acoustic meter on this basis.

C) Recently, computer simulations have been run on this flowmeter design at O.R.E. The purpose of the simulation was to obtain a more accurate estimate of integration errors produced by different vertical velocity profiles. Two types of tests were performed. The first consisted of several runs using undistorted or "typical" velocity profiles produced by several possible logarithmic curves simulating different degrees of channel surface roughness. Velocity profiles used during these runs are shown on Figure 10, and the resulting errors are shown on Figure 11a. The important thing to notice here is that the integration errors are small, and that the several assumed flow profiles do not effect the error significantly.

In the second set of runs, see Figure 10, one of the assumed logarithmic distributions was distorted with two

different profiles. These profiles were scaled so that the maximum distortion velocity occurred at maximum stage, with a linear decrease with lower stages so as to maintain a constant maximum near surface velocity gradient. These velocity profiles were chosen to represent the possible results of a strong upstream or downstream wind or other effects such as ice or debris which could cause unpredictable velocity gradients near the surface.

The two velocity distortion profiles used differ in that one is mostly confined to areas relatively near the surface, and hence cannot be "seen" by the two upper acoustic paths at all stages. The other, while more gradual, has a larger total flow rate effect but it can be "seen" by the upper paths. The flow rate change caused by the distorted profile can thus be partially corrected for.

The plots in Figure 11b show the effect of these assumed profiles. In order to make the worst case integration error approximately 1%, the velocity distortion was increased to +20% of the undistorted surface velocity at maximum stage. (The 20% distortion figure was regarded as unrealistically high and hence conservative). The maximum integration errors occur at water depths .5 ft (.15 m) above each transducer elevation, which corresponds to a maximum velocity extrapolation distance.

Since, in our opinion, a 20% surface velocity distortion is unrealistically large, our conclusion is that we were conservative in our acoustic path spacings and we could have made the meter meet specification with one or two fewer acoustic paths. Also, given that all nine paths were to be used, we could have distributed them more favorably, so as to reduce the peak error slightly.

However, in the real world of fixed price contracts, penalty clauses and performance bonds, one or two extra acoustic paths is a small price to pay for a conservative design, customer confidence, and a shorter acceptance period.

D) Two additional flowmeters were designed and built for the State of California Department of Water Resources, and install in the California Aqueduct near check structures 12 and 21. Both meters operate in trapezoidal cross

sections of very similar dimensions, and have overall design accuracies of $\pm 2\%$ of flow. The pertinent dimensions and acoustic path locations for Check 12 are shown in Figure 13.

The main difference between these trapezoidal meters and the previous example, other than size and shape, is the relatively small variation in stage (27 to 31 ft or 8 to 9 m at Check 12).

This design problem differed from the preceeding example because the potential surface layer flow rate estimation error was relatively small due to the small variation in stage. However, because of the anticipated daily variation in flow rate (pumping of aqueduct water is normally done during off-peak hours) and the strong density gradients which could be produced by near zero flow during the daylight hours, irregular velocity profiles could develop which would not resemble the classical logarithmic velocity profiles.

This problem was illustrated by several profiles, taken by The Department of Water Resources at the flowmeter locations, which were examined during the design stage {4}. Some of these have subsequently been published {5}. An error analysis was performed using "worst case" criteria for this application, based on the measured velocity profiles. The resulting design is shown on Figure 13. The analysis showed that the total flow rate error contribution of upper and lower paths was constant with equal path spacing because the upper layers had larger areas and lower velocity gradients while the opposite was true of the lower layers.

E) Computer simulations have been run on this design, in this case using several actual velocity profiles. The curves selected for computer analysis did not represent a random sample of expected velocity profiles, but were selected to include the "worst" ones from the point of view of possible integration error, together with one considered more nearly typical (Check 21 Run 144). These curves are shown on Figure 15, together with the integration errors.

Four of the six velocity profiles show integration errors of less than 1%, and demonstrate the ability of the flowmeter to provide accurate results even when the velocity profile does not resemble theoretical curves. Even the two worst profiles demonstrated errors of less than 2% and the velocity distribution producing this error could only be expected to persist for a small fraction of the time since they were probably produced by system flow transients.

After installation, the flowmeter was calibrated by Department of Water Resources personnel {6}. The results of the calibrations are shown in Figure 14A, together with the velocity distributions which were obtained (Figure 14B). The calibration results demonstrate the high accuracy which is achieved when near-typical velocity profiles occur in the meter section.

F) A summary of error sources for a typical open channel application is shown in Figure 16. From this illustration it is clear that for high accuracy flow rate measurement, the potentially large errors associated with incorrect determination of traveltime (Item 5b) must be positively eliminated by suitable design.

Summary and Conclusions

Acoustic flowmeters can be used to measure volume flow rate in a wide variety of applications.

Using the design approach discussed above, system flow rate accuracies of two percent or better are achievable over a broad range of flow rates for mortar lined channels. Similar design techniques are applicable to any open channel acoustic flowmeter requirement.

In all cases, total installed system cost can be minimized during the design stage by a suitable trade-off between equipment, site work and calibration costs on the one hand, and desired accuracy on the other.

Acknowledgements

The author wishes to thank the Metropolitan Water District of Southern California and the State of California Department of Water Resources for making calibration and flow profile data available for this paper.

In addition, valuable ideas, particularly concerning acoustic design and error analysis have been provided from discussions with personnel of the Hydro-Instrumentation Department of Rijkswaterstaat, the Netherlands.

Within our own organization I would like to thank Mr. Tom Campbell for his help and suggestions used in the computer analysis portion of the work.

References

- {1} Smith, W., Experience in the United States of America with acoustic flowmeters, Symposium on river gauging by ultrasonic and electromagnetic methods, University of Reading, England, Dec 1974.
- {2} Schuster, J.C., Measuring water velocity by Ultrasonic Flowmeter, Proc ASCE. 5 of Hydraulics Div., 101:HY12, Dec 1975
- {3} Whitsett, A.M., Ramsay, W.B., Angularity flow tests at acoustic flowmeter installation, Lake Skinner, Unpublished Report, Metropolitan Water District of Southern California, 29 Jan 1975.
- {4} Ohriti, R., L.E. Flowmeter flow profiles near Check 12 and 21, Unpublished Data, State of California Department of Water Resources, 20 April 1970 thru 10 Feb 1971.
- {5} Lanning, C., Ehrhart, R.W., Application of Acoustic Velocity Flowmeters, J.Am.Water Works, 69 Feb 1977.
- {6} Innes, G., Trefethen, G., Gage, D., Current meter measurement, California Aqueduct bridge at Acoustical flow meter site near Check 12, Unpublished Data, State of California Department of Water Resources, Dec 10, 11, 1975; Jan 4, 1976.

ADVANTAGES

- HIGH ACCURACY. CAN BE MADE INDEPENDENT OF FLOW RATE, VELOCITY PROFILE, AND TEMPERATURE.
- SUITABLE FOR ANY LIQUID WHICH PROPAGATES HIGH FREQUENCY SOUND.
- BI-DIRECTIONAL FLOW MEASUREMENT.
- NO OBSTRUCTION IN THE CHANNEL CROSS SECTION. NO HEAD LOSS.
- NO MOVING PARTS.
- NO PRACTICAL UPPER LIMIT ON LIQUID VELOCITY.
- PERIODIC CALIBRATIONS NOT REQUIRED.
- AUTOMATIC SIGNAL AND DATA TESTING CAN INSURE THAT ONLY ACCURATE READINGS ARE ACCEPTED FOR OUTPUT.
- ELECTRONICS CAN ACCOMMODATE MANY METERED SECTIONS.
- EXCELLENT SERVICABILITY.
- COST RELATIVELY INDEPENDENT OF SIZE.
- CAN ALSO PROVIDE AVERAGE TEMPERATURE.

LIMITATIONS

- CONTINUOUS QUANTITIES OF ENTRAINED GASES AND/OR SUSPENDED SOLIDS AFFECT ACOUSTIC PERFORMANCE.
- RELATIVELY HIGH COST IN SMALL SINGLE INSTALLATIONS.
- NOT SUITABLE FOR WIDE, VERY SHALLOW CHANNELS.
- MAY NOT BE SUITABLE FOR AREAS WITH HIGH RATES OF MARINE GROWTH.

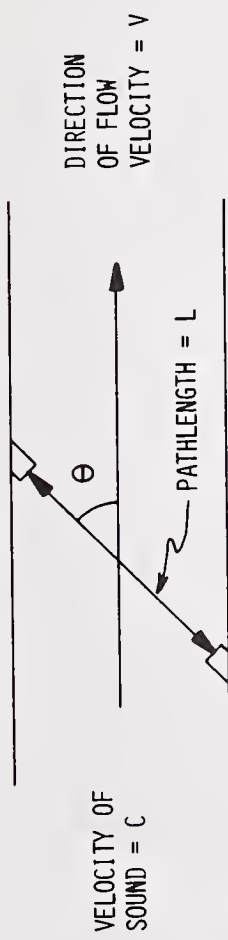
FIGURE 1 - ADVANTAGES AND LIMITATIONS OF
ACOUSTIC FLOW MEASUREMENT

APPLICATIONS

- CUSTODY TRANSFER OR REVENUE METER.
- POTABLE AND WASTE WATER TREATMENT PLANTS; CAN BE USED AS CONTROL SYSTEM INPUT.
- HYDROELECTRIC POWER PLANT MANAGEMENT.
- NUCLEAR/FOSSIL POWER PLANT COOLING WATER FLOW MEASUREMENT.
- ACCEPTANCE TESTING AND PERIODIC RETESTING OF LARGE HYDRAULIC MACHINERY SUCH AS PUMPS, TURBINES, AND COOLING TOWERS.
- WATER RESOURCE MANAGEMENT.

FIGURE 2 - APPLICATIONS OF ACOUSTIC FLOW MEASUREMENT

THE UPSTREAM AND DOWNSTREAM ACOUSTIC TRAVELTIMES ARE MEASURED ALONG THE DIAGONAL ACOUSTIC PATH. SOUND WAVES TRAVELING DOWN-STREAM PROPAGATE AT HIGHER VELOCITIES THAN THOSE TRAVELING UP-STREAM.



$$\begin{aligned}
 \text{TRAVELTIME UPSTREAM} &= T_{UP} = \frac{L}{c - v \cos \theta} \quad (1) \\
 \text{TRAVELTIME DOWNSTREAM} &= T_{DN} = \frac{L}{c + v \cos \theta} \quad (2) \\
 \text{TRAVELTIME DIFFERENCE} &= \Delta T = T_{UP} - T_{DN} \quad (3) \\
 \text{SUBSTITUTING AND SIMPLIFYING} &= \Delta T = \frac{2vL \cos \theta}{c^2 - v^2 \cos^2 \theta} \quad (4) \\
 \text{SINCE } \cos \theta \leq 1 \text{ AND } v^2 \ll c^2, & \quad \Delta T \approx \frac{2vL \cos \theta}{c^2} \quad (5) \\
 \text{BUT } c \approx \frac{1}{T} \text{ WHERE} & \quad \bar{T} = \frac{T_{UP} + T_{DN}}{2} \quad (6) \\
 \text{SOLVING FOR } v, & \quad v \approx \frac{\Delta T}{\bar{T}^2} \cdot \frac{L}{2 \cos \theta} \quad (7)
 \end{aligned}$$

FIG.3 DERIVATION OF ACOUSTIC LINE VELOCITY EQUATION

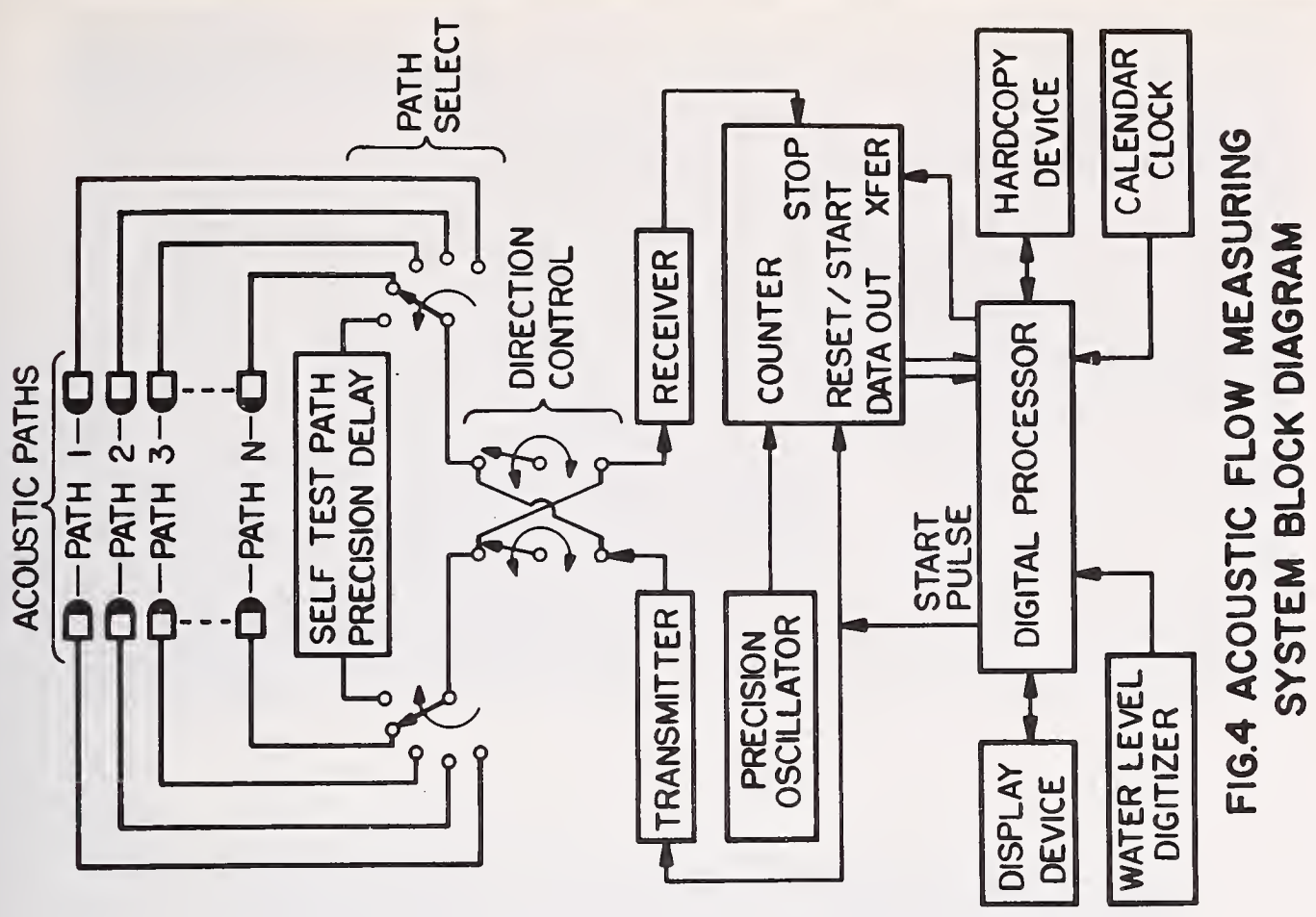


FIG.4 ACOUSTIC FLOW MEASURING SYSTEM BLOCK DIAGRAM

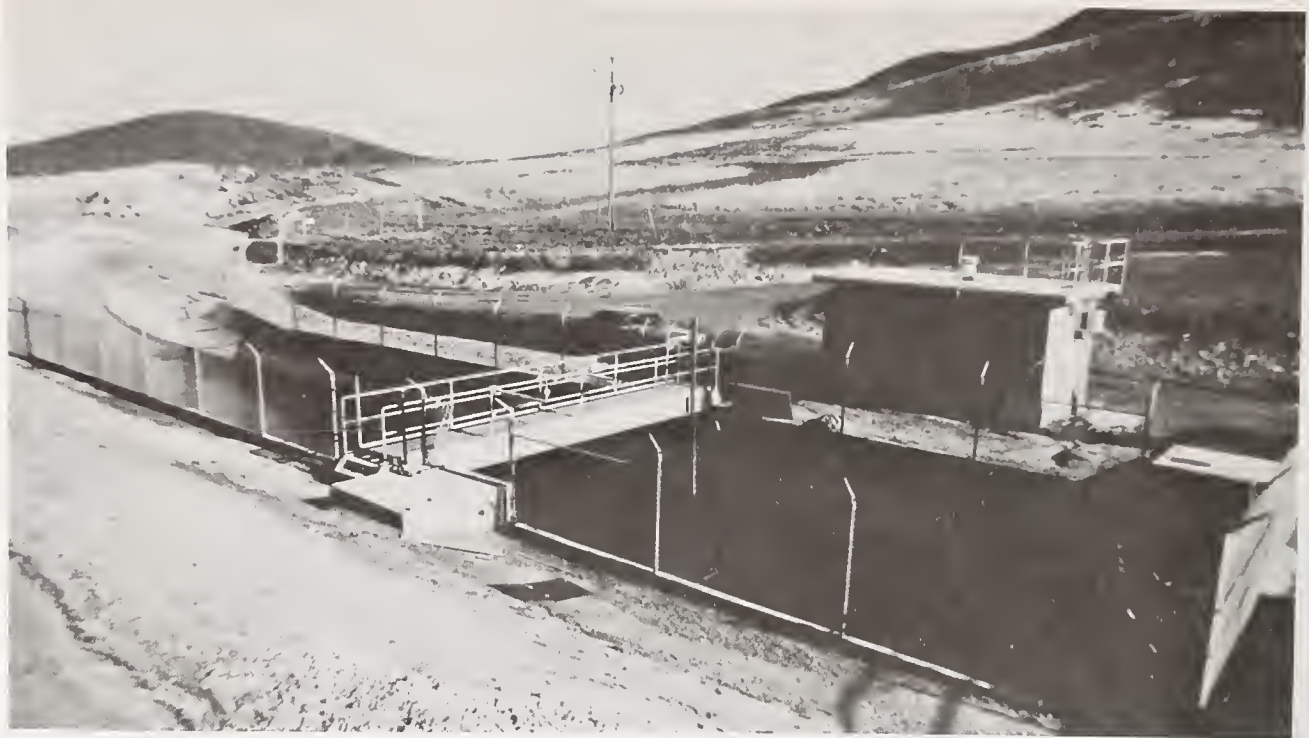


FIG.5 TYPICAL FLOWMETER INSTALLATION

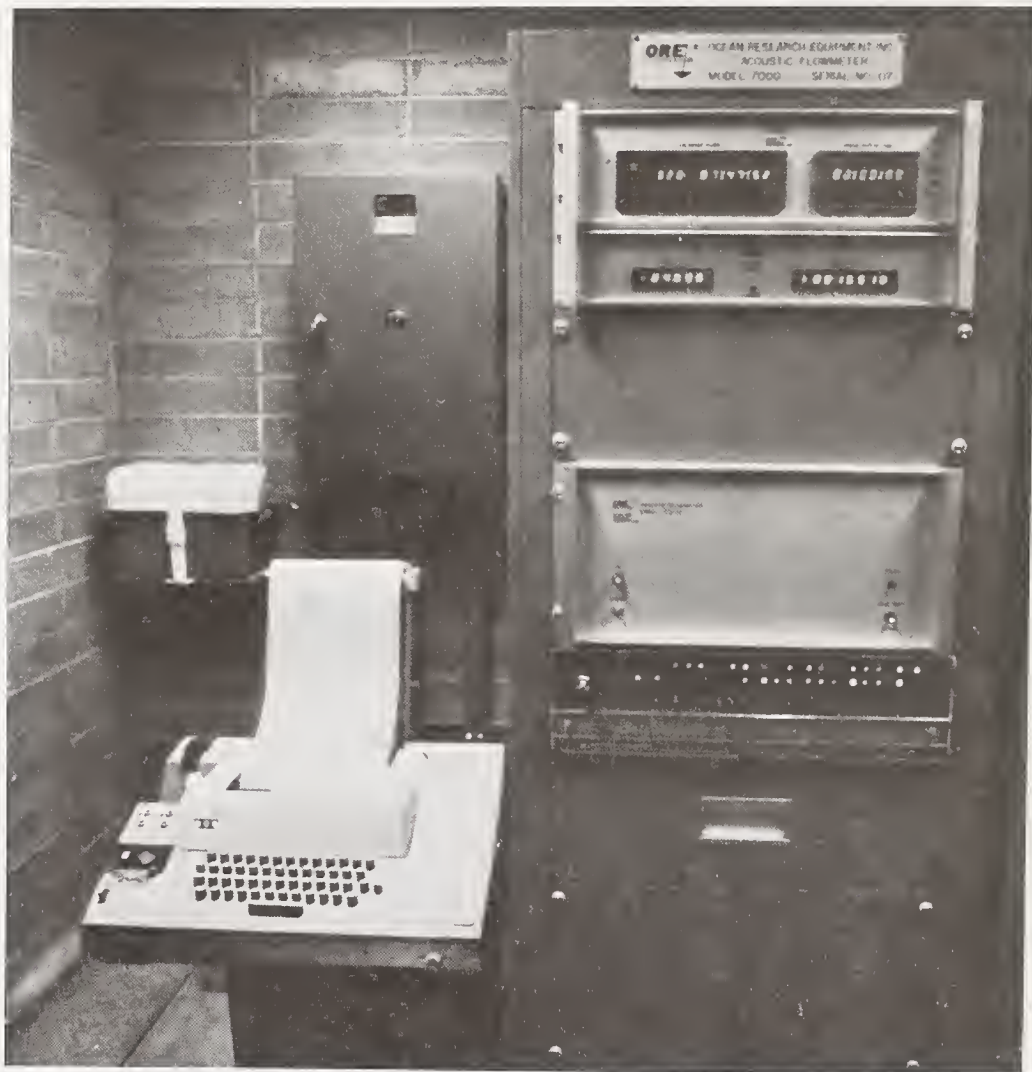
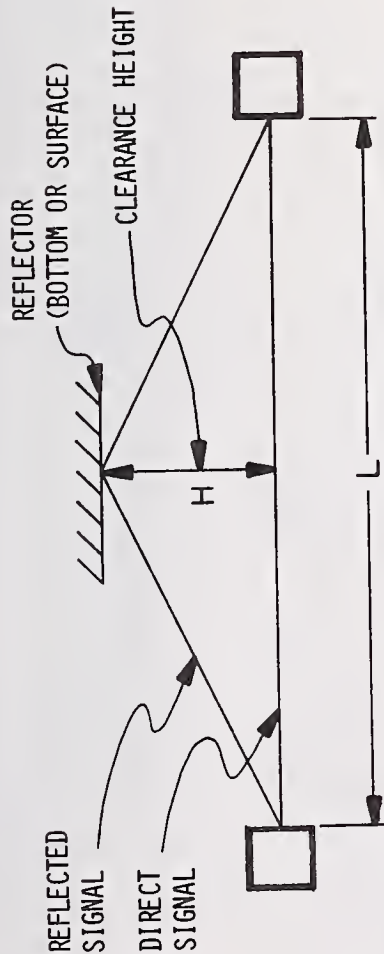


FIG.6 TYPICAL FLOWMETER ELECTRONICS CONSOLE



REFLECTED SIGNAL
DIRECT SIGNAL
REFLECTOR (BOTTOM OR SURFACE)
CLEARANCE HEIGHT
H
L
REQUIREMENT: SIGNALS ARRIVING VIA ANY REFLECTED SIGNAL PATH MUST ARRIVE AT LEAST ONE WAVELENGTH LATER THAN DIRECT ARRIVAL.

LET λ = WAVELENGTH
 F = FREQUENCY
 C = VELOCITY OF SOUND
 H = CLEARANCE HEIGHT

THEN $\lambda = C/F$ (1)

THEREFORE, BY PYTHAGOREAN THEOREM,

$$L + \lambda = 2 \left[\left(\frac{L}{2} \right)^2 + H^2 \right]^{\frac{1}{2}} \quad (2)$$

SQUARING BOTH SIDES AND SOLVING FOR H,

$$H = \sqrt{\frac{2L\lambda + \lambda^2}{4}} \quad (3)$$

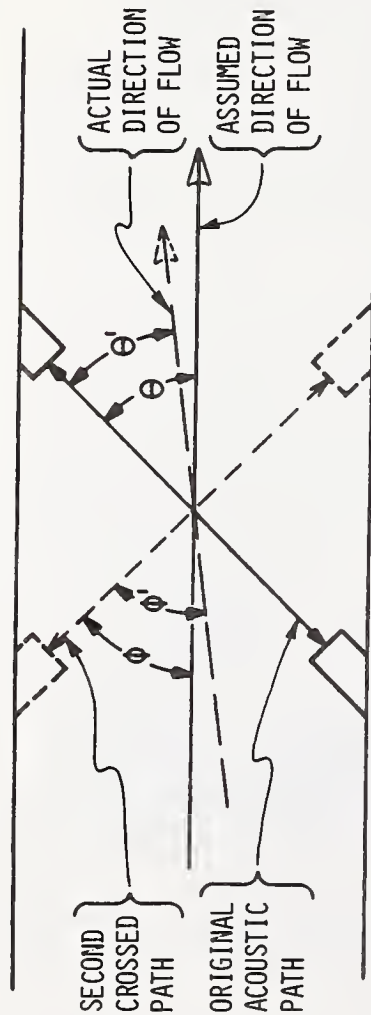
SINCE $\lambda \ll L, \lambda^2 \approx 0,$ (4)

THEREFORE, SUBSTITUTING FROM (1) WE HAVE, $H \approx \sqrt{\frac{L\lambda}{2}}$ (5)
 $H \approx \sqrt{\frac{LC}{2F}}$

FIG. 7 ACOUSTIC LINE VELOCITY MULTIPLE REFLECTION (MULTIPATH) PROBLEM

PATH LENGTH L, FT	OPERATING FREQUENCY F, KHZ	CLEARANCE HEIGHT H, FT	VELOCITY ERROR FOR 1 CARRIER CYCLE TIMING ERROR, FT/SEC
500-1500 FT	100 KHZ	3.5-6.1 FT	.035 - .012 FT/SEC
200-500 FT.	200 KHZ	1.5-2.5 FT	.446 - .178 FT/SEC
75-200 FT.	300 KHZ	.8-1.3 FT	.785 - .295 FT/SEC
20-75 FT.	500 KHZ	.32-.62 FT	1.78 - .476 FT/SEC
2-20 FT.	1000 KHZ	.07-.22 FT	8.75 - .875 FT/SEC

FIGURE 8 - TYPICAL PATH LENGTH VS OPERATING FREQUENCY, CLEARANCE HEIGHT AND EFFECTS OF ONE CARRIER CYCLE TIMING ERROR



ASSUME: BOTH PATH LENGTHS = L
 ORIGINAL PATH ANGLE = $\theta = \phi = 45^\circ$
 ACTUAL DIRECTION OF FLOW = $\theta' = 43^\circ$, $\phi' = 47^\circ$
 ACTUAL VELOCITY = V

MEASURED
$$\Delta T = \frac{2VL \cos \theta'}{C^2} = K \cos \theta' \quad (1)$$

WHERE K = CONSTANT = $2LV / C^2$ (2)

CORRECT
$$\Delta T = K \cos \theta \quad (3)$$

∴ ERROR =
$$E1 = \frac{K \cos \theta}{K \cos \theta'} = \frac{\cos 45^\circ}{\cos 47^\circ} = 1.034 \quad (4)$$

IF THE SECOND PATH WERE INSTALLED,
 SECOND MEASURED $\Delta T = \Delta T' = K \cos \phi'$

∴ ERROR =
$$E2 = \frac{K \cos \phi}{K \cos \phi'} = \frac{\cos 45^\circ}{\cos 43^\circ} = .967 \quad (5)$$

CORRECTED ERROR
$$E = \sqrt{(E1^2 + E2^2)/2} = 1.000 \quad (6)$$

FIG.9 CROSSFLOW ERROR

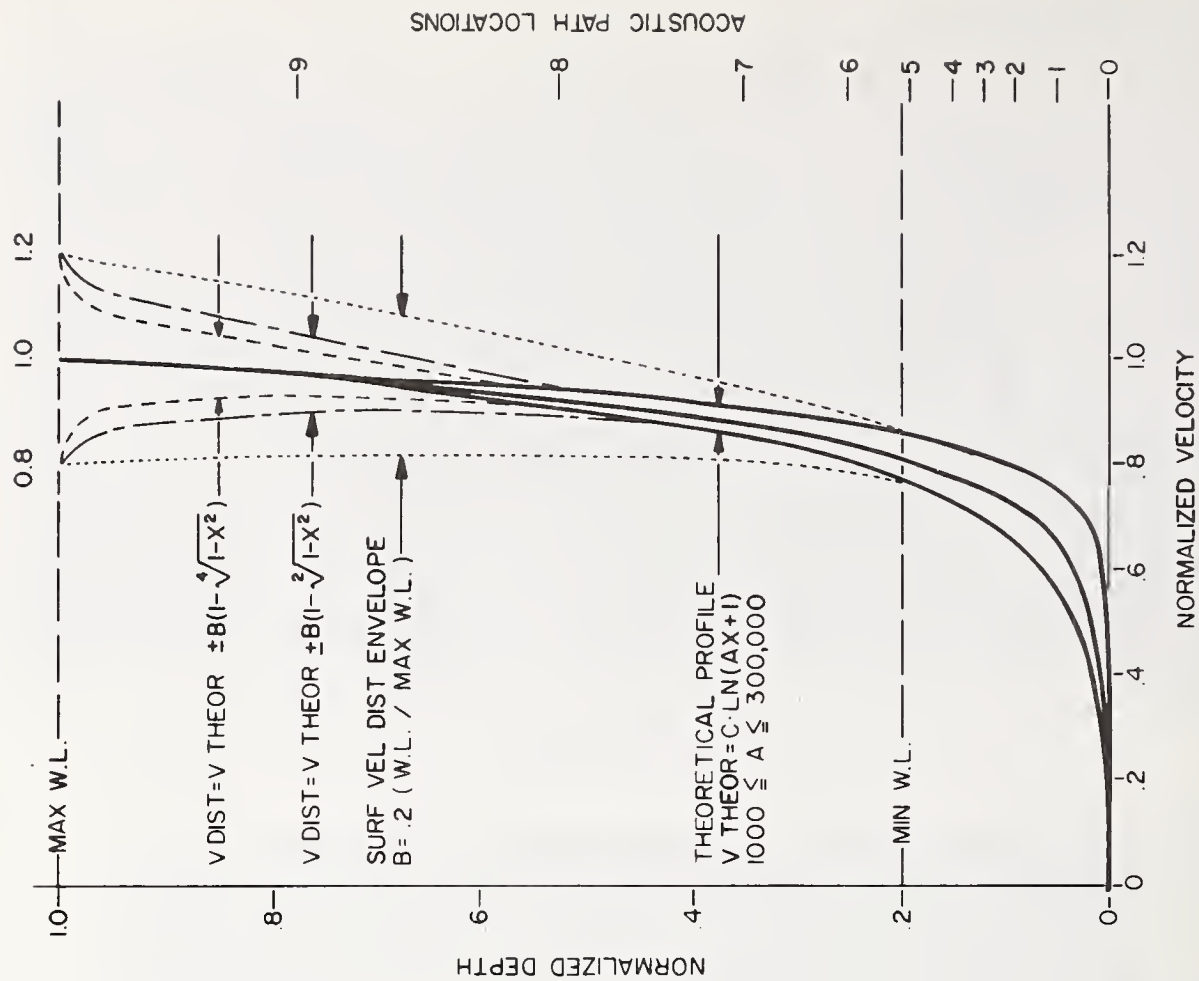
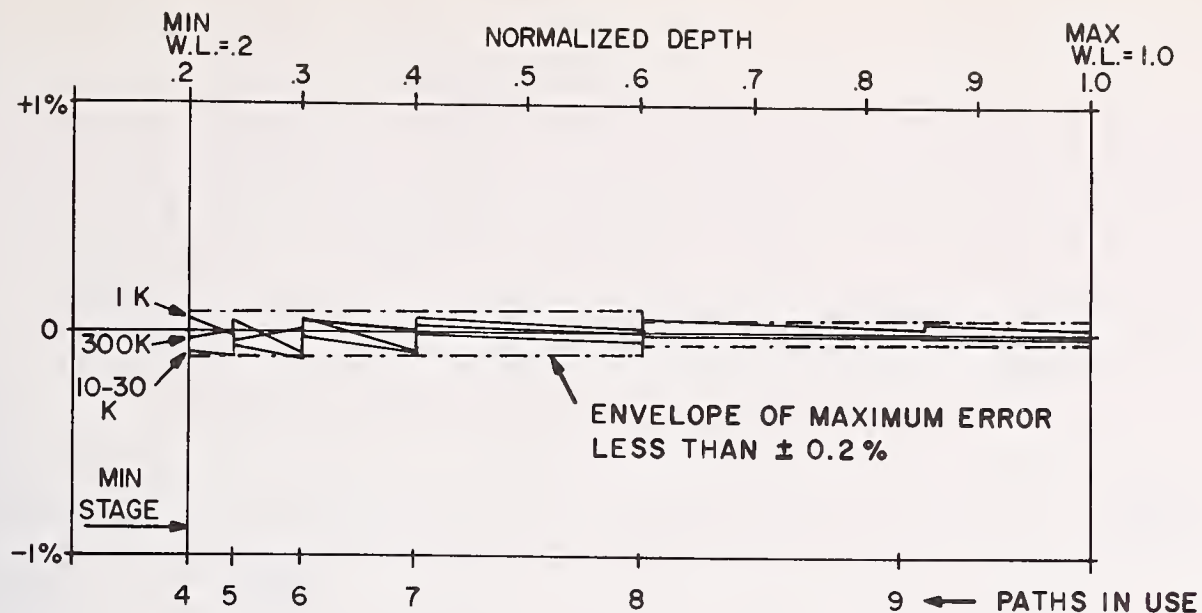
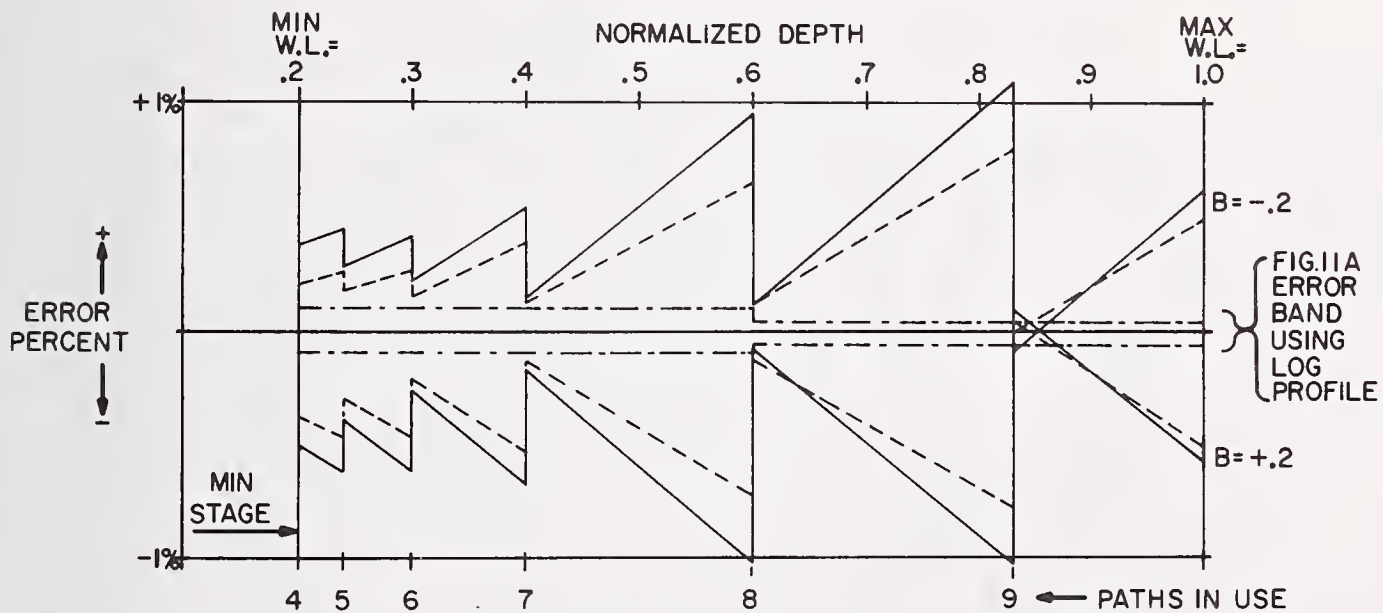


FIG.10 THEORETICAL & DISTORTED VELOCITY PROFILES
 USED IN COMPUTER ACCURACY SIMULATION
 INLET CANAL TO LAKE SKINNER



ALL CURVES: $V = C \cdot \ln(A X + 1)$
 WHERE C = NORMALIZING CONSTANT
 $A = 1,000 ; 3,000 ; 10,000 ; 30,000 ; 300,000$
 $X = \text{NORMALIZED DEPTH}$

FIG.IIA INTEGRATION ERROR VS STAGE FOR DIFFERENT THEORETICAL PROFILES OF FIG.10



SOLID CURVES: $V = C \cdot \ln(30,000 X + 1) \pm B \cdot Z \left[1 - \sqrt{1 - (X/Z)^2} \right]$

DOTTED CURVES: $V = C \cdot \ln(30,000 X + 1) \pm B \cdot Z \left[1 - \sqrt[4]{1 - (X/Z)^2} \right]$

WHERE C = NORMALIZING CONSTANT, Z = STAGE, X = NORMALIZED DEPTH, B = 0.2

FIG.IIB INTEGRATION ERROR VS STAGE FOR DISTORTED PROFILES OF FIG.10

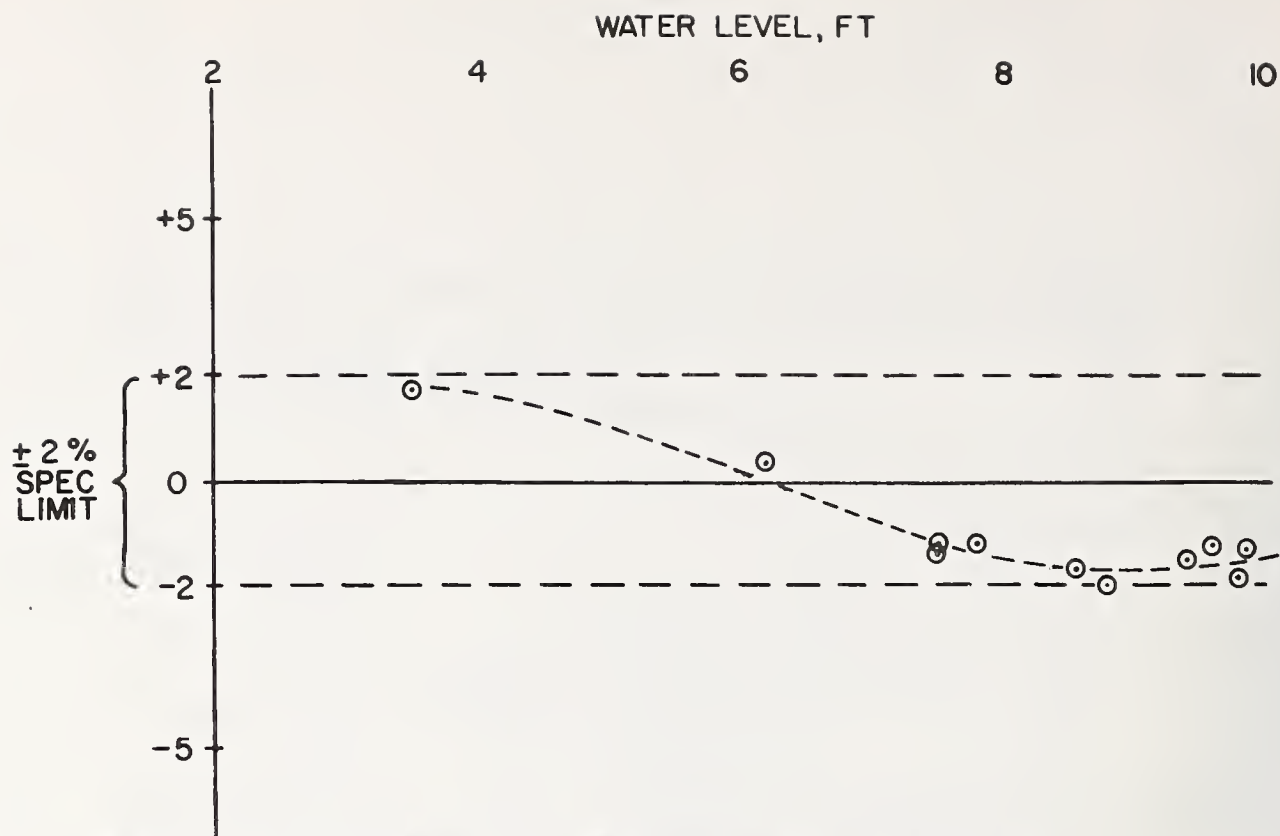


FIG.12 FLOWMETER CALIBRATION RESULTS
INLET CANAL TO LAKE SKINNER (REF 3)

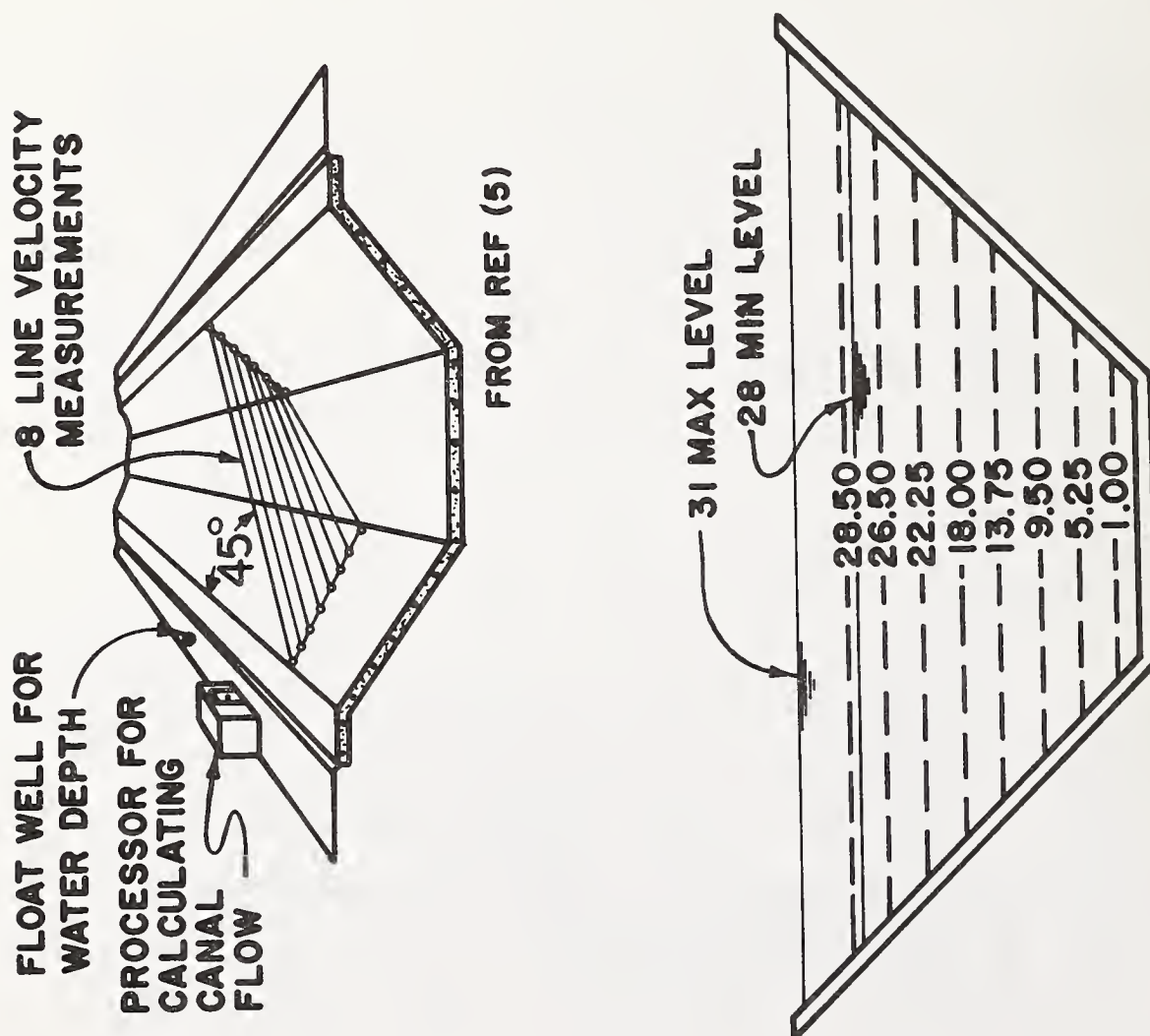


FIG.13 CHECK 12 / 21 CROSS SECTION
AND ACOUSTIC PATH PLACEMENT

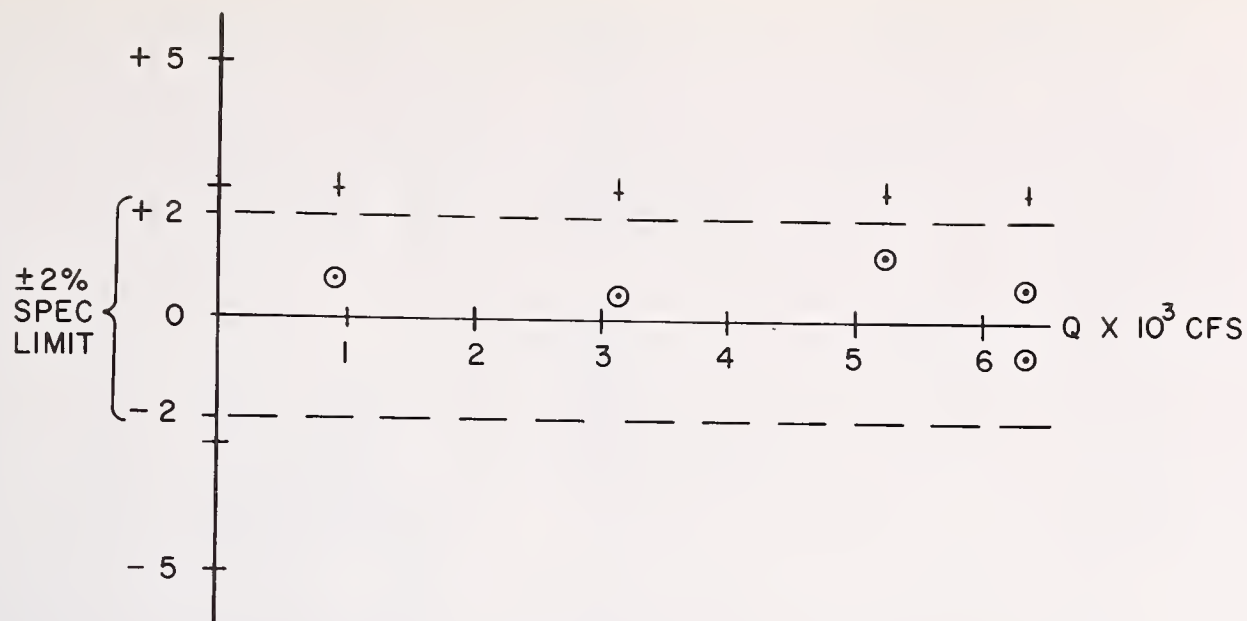


FIG.14A FLOWMETER CALIBRATION RESULTS
AT CHECK 12 (REF 4)

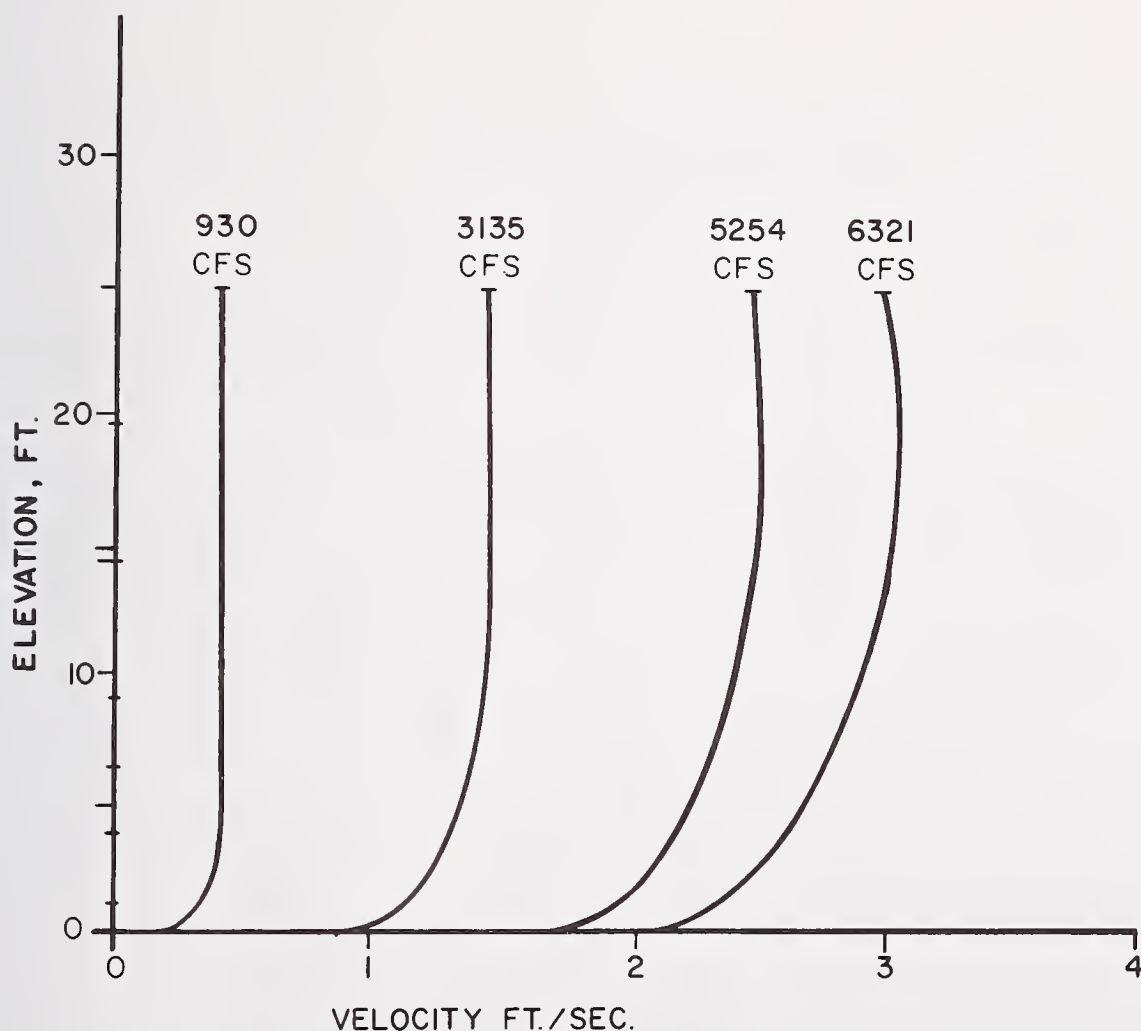
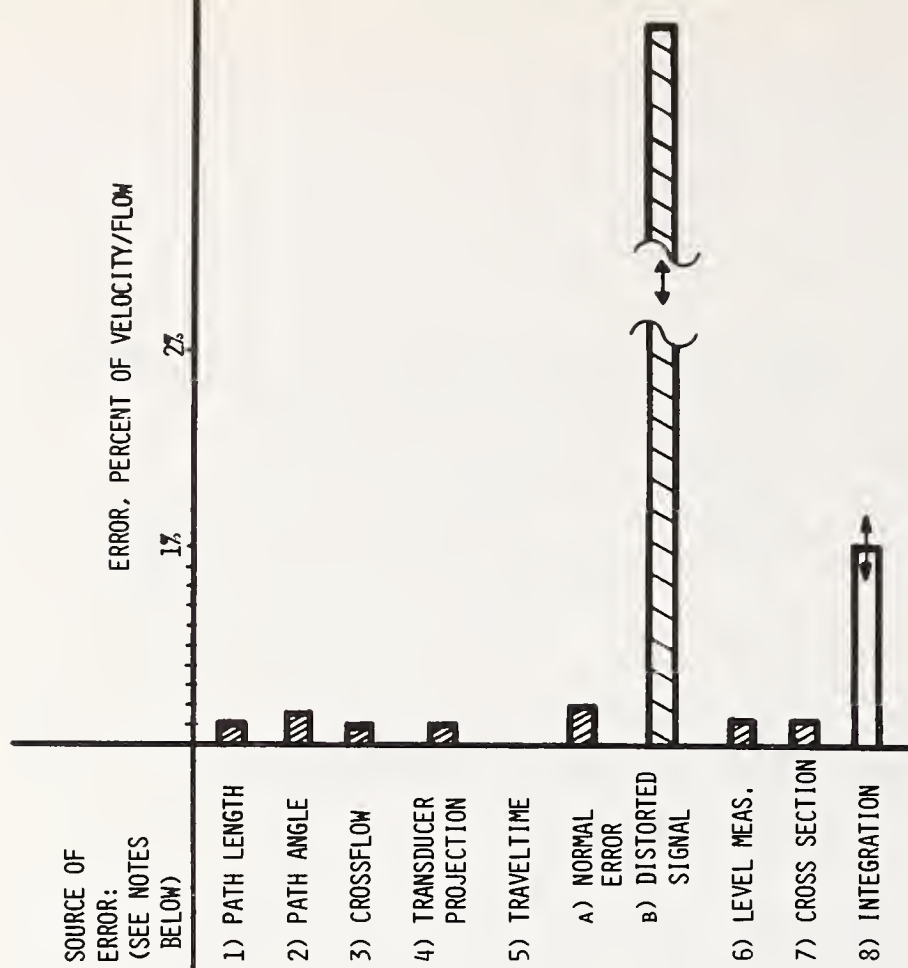


FIG.14B VELOCITY PROFILES MEASURED
DURING CALIBRATION AT CHECK 12



NOTES

- 1) ASSUMES DIRECT FACE TO FACE MEASUREMENT.
- 2) ASSUMES $\pm 0.1^\circ$ SURVEY ACCURACY.
- 3) ASSUMES CROSSED PATHS IF REQUIRED.
- 4) THIS ERROR DEPENDS ON RATION OF TRANSDUCER DIA TO PATH LENGTH.
- 5A) RANDOM VELOCITY ERROR, REDUCED BY MULTIPLE MEASUREMENT AVERAGING, PERCENT DEPENDS ON VELOCITY.
- 5B) THIS ERROR CAN BE BETWEEN 1 AND MORE THAN 100% DEPENDING ON VELOCITY OF FLOW, PATH LENGTH AND OPERATING FREQUENCY. SEE SECTION 4A(3).
- 6) ERROR DEPENDS ON DEPTH AND METHOD USED.
- 7) ASSUMES MORTAR LINED CHANNEL.
- 8) TYPICALLY 1-3%, DEPENDING ON SYSTEM REQUIREMENTS.

**FIG.16 OPEN CHANNEL ACOUSTIC FLOWMETER
ERROR SUMMARY**

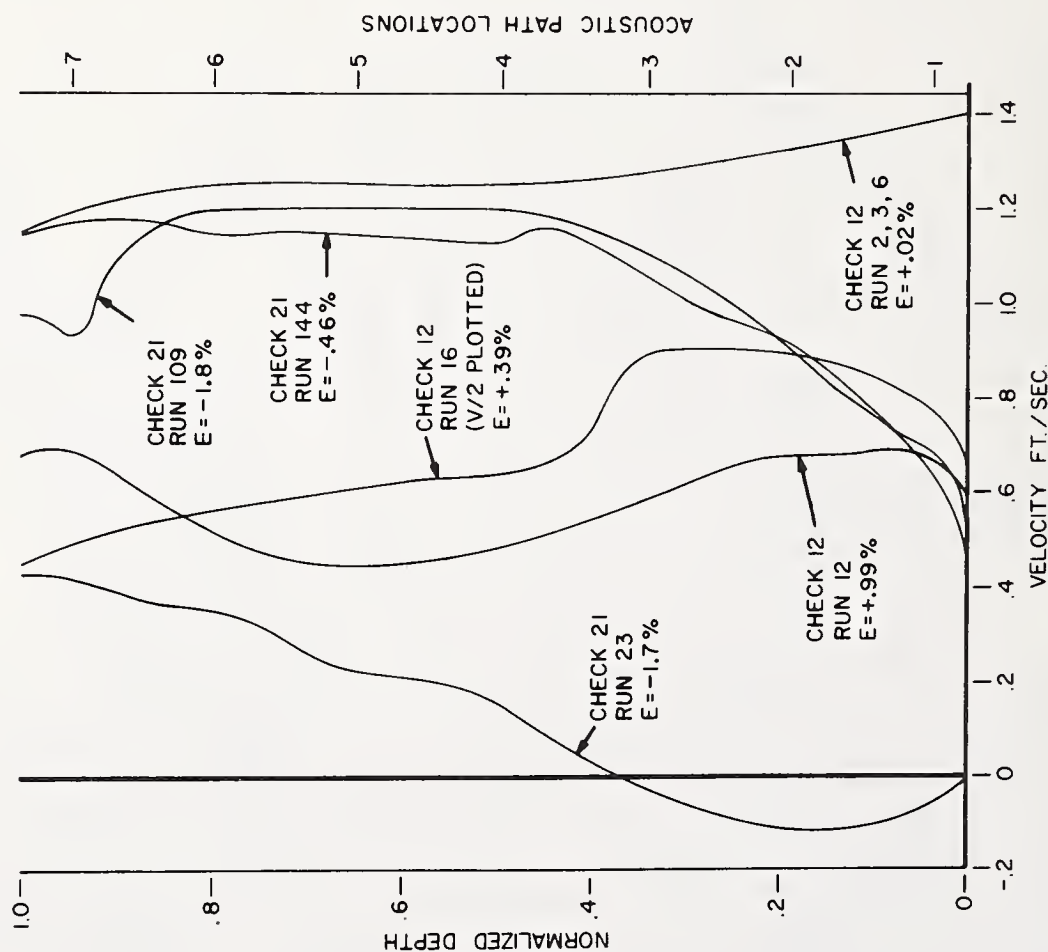


**FIG.15 VELOCITY PROFILES MEASURED
AT CHECK 12/21 (REF. 4) USED
FOR "WORST CASE" SIMULATION**

APPLICATION CONSIDERATIONS & PERFORMANCE CAPABILITY
OF THE TIME DIFFERENTIAL
CLAMP-ON ULTRASONIC FLOWMETER

J. Baumel
Controlotron Corporation
111 Bell Street
West Babylon, New York 11704

ABSTRACT

Substantial information has been developed on the application history and performance capability of the time differential clamp-on ultrasonic flowmeter during approximately four years of in-service experience. These application considerations and performance capabilities are reviewed together with a review of the principles of operation and listings of the types of uses to which this instrument has been applied.

1. INTRODUCTION

The impact of a practical clamp-on flowmetering device would be significant enough for many users who are faced with the need to measure flow rate of liquids whose physical or chemical properties make conventional flowmeters difficult or impossible to apply. But the availability of a clamp-on flowmeter whose basic performance characteristics challenge and, in many cases, exceed the performance capabilities of conventional flowmeters, permits application of the time differential clamp-on ultrasonic flowmeter to ordinary applications with significant economic and performance benefits not previously available.

Such a device is the time differential clamp-on ultrasonic flowmeter. This device works on the principle of transmitting an ultrasonic beam between two transducers merely clamped to opposite sides of an existing defined pipe in such a way as to transmit the beam at a definable angle relative to flow. A flow display computer obtaining data from these transducers is charged with the task of extracting the relatively minute effect of flow rate on the upstream versus downstream transmission time of the sonic beam through the liquid. (See Fig.1) This flow display computer converts the data which it has obtained to those forms which are standard in industry, i.e., a digital display in engineering units of choice, a scalable analog display with settable high and low flow alarms, plus analog outputs 0-10V and 4-20ma, a pulse rate output proportional to flow (100 Hz per foot per second), and a totalizer register in units of liquid volume.

The time differential clamp-on ultrasonic flowmeter (hereinafter referred to as the ΔT clamp-on ultrasonic flowmeter) should not be confused with the Doppler ultrasonic flowmeter which uses only a single transducer mounted

on one side of the pipe which obtains data from the change in apparent reception frequency of a continuous ultrasonic beam being reflected from bubbles or solid particles which may be suspended in the liquid. Nor should it be confused with insertion time differential ultrasonic flowmeters which employ a spool section having sonic transducers embedded within fixed holders welded into the side of the spool section. The former device has the convenience of the ΔT clamp-on flowmeter, but is highly dependent on the presence of free solids or gases in the stream for operation, and has a calibration factor dependent upon the sonic velocity of the liquid - a factor very frequently unknown or variable.

The spool insert time differential ultrasonic flowmeter has the accuracy capability of the clamp-on ΔT flowmeter, but of course does not have its convenience of installation or maintenance.

2. DESCRIPTION OF ΔT CLAMP-ON ULTRASONIC FLOWMETER

The clamp-on ΔT ultrasonic flowmeter consists of a set of ultrasonic transducers mounted on opposite sides of the pipe at a preferred displacement ordinarily fixed by a spacing bar interconnecting the two elements. Installation on a pipe whose diameter, wall thickness and Material has been previously designated is accomplished by merely applying a sonic coupling compound between each transducer element and pipe exterior, and tightening a self-contained clamp mechanism. This simple mounting procedure makes practical the use of this device as a portable flowmeter.

The flow display computer operates the transducers and measures the time differential between transmission and reception of sonic energy. It then converts this time differential, which is proportional to flow, to conventional data format. Models are available which provide digital display in preferred flow units, analog display, analog outputs (0-10V & 4-20ma), totalizer display, and pulse rate proportional to flow. Thus the ΔT clamp-on ultrasonic flowmeter provides any of the functions ordinarily provided by any conventional flowmeter of any type, and in many applications can be used interchangeably.

In general, it is necessary to specify only the pipe size, schedule and material as the flow display computer will automatically correct for the effects of changes in sonic velocity of the liquid regardless of the cause of such change (i.e., temperature changes or changes in liquid chemistry).

This flowmeter has been used in applications on pipes as small as $\frac{1}{2}$ " and is available for pipes larger than 60". In principle, there is no upper limit so long as the liquid is sonically conductive - a property of most homogeneous liquids free of excessive undissolved gases or solids.

3. APPLICATION CONSIDERATIONS

The prime requirement for operation of the clamp-on flowmeter is that the sonic beam which is injected into the exterior wall of the pipe be

successfully transmitted through that wall, through the liquid, and then through the far wall of the pipe so as to be received with sufficient amplitude at the receive transducer to permit signal detection. For this to be achieved only two conditions are required --

1. The pipe wall must be sonically conductive (including the effects of any internal coatings or linings).
2. The liquid must be sufficiently sonically conductive.

These two conditions are almost always achieved in real applications. All metallic pipe has been found to be an excellent conductor of sonic energy. Many lined pipes have also been found to be sufficiently sonically conductive, provided that the lining is well bonded to the interior of the pipe wall. Most linings themselves such as plastics are excellent sonic conductors. However, some linings such as cement may be absorptive of the sound beam if during the mixing of the cement air bubbles have been retained during the curing of the cement.

Most plastic pipes are excellent sonic conductors. Included in this class are PVC and filament wound FRP pipe. However, FRP pipe made of woven mat generally includes sufficient entrapped air within the mat to seriously interfere with the sonic conductivity of the pipe wall.

Nature has been very kind to us in that all homogeneous, non-aerated liquids have been found to be excellent sonic conductors. The only property of the liquid other than its sonic conductivity which is of any material importance is the sonic velocity of the liquid itself, which for most liquids lies in the range of 1000-2000 meters per second. The ΔT clamp-on flow display computer computes the sonic velocity from the data which is received from the ultrasonic beam and uses this data to correct the scaling of the system so that the system calibration is essentially independent of the sonic velocity.

However, there are conditions under which a liquid will lose part or even all of its sonic conductivity. A primary cause of this condition is what is commonly called aeration. Aeration is a condition in which free bubbles of either air or of the vaporized liquid pass through the sonic beam. These bubbles tend to disperse and diffuse the sound beam if present. However, this is a condition which can generally be avoided since its causes are rather well defined. For example, aeration can be caused by adding liquid to a holding tank with the inlet above the liquid level, causing air to be mixed as the stream passes through the surface of the liquid. A low inlet (below the surface) has always avoided this condition. Other causes of aeration are leaky fittings at the suction end of a pump, or cavitation caused by a defective pump or an upstream throttling valve. Since these causes are generally destructive in themselves, their effect on the flowmeter which is announced by the flowmeter's "fault monitoring system", enables the user to be aware of the condition and take the necessary corrective action.

Undissolved solids in the liquid can also serve to reduce the liquid's sonic conductivity. In general, this condition is considerably more tolerable than aeration. Examples of systems providing excellent operation with free solids content of up to 50% have been found on many occasions. While no hard and fast rule has been established, it has been found that solids whose acoustic impedance is reasonably similar to the liquid itself (such as paper pulp), are more tolerable than solids whose acoustic impedance is considerably higher (sand particles).

Since the principle of operation of the ΔT flowmeter does not in itself depend upon the physical properties of the liquid, operation is generally not affected adversely by reasonable variations of liquid temperature. The only effect of viscosity will be on the flow profile - an effect which is among those for which means of correction are available within the computer. Means also exist for taking into account non fully developed flow profile or flow profile skew, which may exist if the pipe section on which the clamp-on transducers are placed is immediately after an elbow. Correction is effected by placing the transducer in a plane which is coincident with the plane of the elbow itself, so that the sonic beam passes through the peak of the flow profile itself.

Transducers have been supplied for applications ranging from cryogenic temperatures up to 500°F. Since introduction of the sonic beam from the transducer to the pipe wall requires use of a coupling compound to fill any gaps which may otherwise exist between the pipe surface and the transducer surface, it is necessary to use a coupling medium which is suitable for the temperature at which the process will operate. A variety of liquids such as oil, greases, and settable rubbers and epoxies have been found which cover all of these conditions very satisfactorily.

4. PERFORMANCE CAPABILITY

The performance parameters of interest to the user of the ΔT clamp-on ultrasonic flowmeter are the same as those parameters which are currently used to rate conventional flowmeters. These parameters include:

1. Linearity
2. Stability (freedom from drift)
3. Range of operation
4. Resolution
5. Calibration accuracy
6. Response time

Linearity

The independent linearity of the clamp-on ultrasonic flowmeter approximates 0.25-0.5% for liquids and pipes of normal sonic conductivity. Evidence of this capability is presented in Fig.2 representing data obtained at Alden Research Laboratories on a typical production unit manufactured for Atomic Energy of Canada Ltd.

Stability

Zero drift stability of the ΔT clamp-on flowmeter has been found not to exceed variations of .05 ft/sec independent of pipe size. In many cases where flow can be shut down at will, any long term zero drift can be eliminated even though .05 ft/sec represents an exceedingly small maximum drift.

Span drift has not been found to exceed 0.5% of reading over long periods of time approximating one year. This high stability is due to the digital nature of the computation not ordinarily subject to variation. Portable calibration equipment is available to permit testing span calibration without removing the flow display computers from their installations.

Range of Operation

The operating range of the ΔT clamp-on flowmeter is guaranteed from -30 ft/sec to +30 ft/sec including zero flow. This is evidenced by incorporation of a $3\frac{1}{2}$ digit display which has the capacity to display flow in any pipe size for velocities of up to at least 30 ft/sec. An automatic flow direction indicator is also provided.

Resolution

The resolution is defined as the smallest change in flow which can be detected and displayed by the flow display computer. The resolution of the ΔT clamp-on ultrasonic flowmeter is of the order of magnitude of 1/1000 ft. per second independent of pipe size. The reason for this extremely high resolution is because friction is not a factor in the measurement technique. A particular benefit of this high resolution is that very low flow velocities can be displayed with very high resolution. For example, a flow velocity of 1 ft/sec in a $2\frac{1}{2}$ " pipe can be displayed with a resolution of 1/100 of a gallon per minute. Thus, even at this nominally low velocity, 1% resolution can be obtained.

Calibration Accuracy

Calibration accuracy refers to the degree to which the data displayed by the ΔT flowmeter truly represents actual flow. Since the linearity specification defined above applies primarily to the degree to which a change in flow causes a correspondingly proportional change in indication, the calibration accuracy can be viewed as a statement as to how closely the proportionality constant corresponds to unity.

In general, the clamp-on flowmeter can be calibrated either intrinsically, which is basically an electronic calibration method, or by setting its calibration controls while the flowmeter is operating on a flow calibration stand. As would be expected, calibration performed under actual flow conditions will be more accurate in general than that performed intrinsically. This does not mean to imply that an intrinsic calibration cannot be perfectly accurate, but rather that the confidence factor associated with an actual flow calibration is greater. It has been found by many tests performed

at recognized flow laboratories that the calibration of the clamp-on flowmeter can achieve accuracies of 0.5% or better. Intrinsic calibrations have generally fallen within the range of 1-4% when performed electronically and then checked on an actual flow calibration stand. Continued experience in intrinsic calibration, which is of course less expensive than actual flow calibration, has shown a general improvement as experience has been gained. There is the expectation that intrinsic calibrations should lie in the 0.5%-2% region in the relatively near future.

It should be noted that the clamp-on flowmeter is somewhat responsive to the flow profile of the liquid which it is measuring. This, of course, is similar to the flow profile sensitivity of many conventional flowmeter techniques.

The clamp-on flowmeter has the ability to compensate for the difference between the flow profile shape in actual service as compared to the flow profile shape achieved during calibration which is ordinarily performed with a liquid such as water. This correction is performed by the flow display computer by means of an internal program into which the user of the machine merely provides an instruction as to the Reynolds number of the process being monitored. The flow display computer then automatically corrects for this new flow profile shape on the presumption that it is fully developed. Non-fully developed flow requires a special program which in general can be provided.

Response Time

Since the clamp-on flowmeter operates on the basis of a sonic beam sent through the liquid, there is no inertia involved in extracting flow data from the flowing stream. For that reason, the response time of the clamp-on flowmeter can be extremely fast. Raw data is available with each transmission passing through the pipe. In general, for liquids similar to water, that transmission travels through the pipe in a time equal to approximately sixteen millionths of a second per inch of pipe diameter. For most practical models of the clamp-on flowmeter, the data processing uses approximately 1/100 of a second so that actual output data is available at a frequency bandwidth of approximately 100 Hz. This is considerably faster than most flowmeters and, in fact, is considerably faster than that required for most applications. For that reason, the flow display computer is generally equipped with a user selected control of response time which can be made as fast as .01 second or as slow as 10 seconds for applications in which a smoothing of a normally fluctuating flow is desired.

5. APPLICATION LIST

Successful applications of the ΔT clamp-on ultrasonic instrument are found in essentially every industry. A representative list of such applications follows:

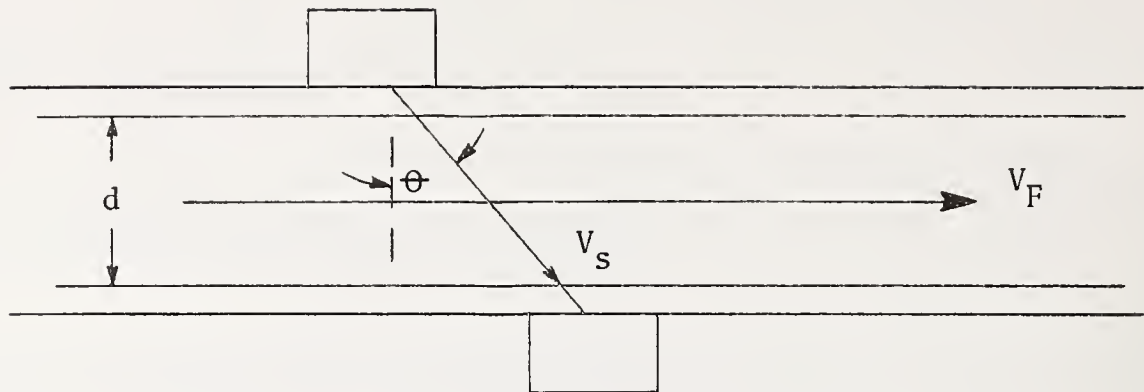
<u>INDUSTRY</u>	<u>APPLICATION</u>
Paper	Black liquor reactor two 10 channel multiplex operation for 3/4" carbon steel schedule 80 lines
Nuclear power	Reactor cooling balance, pipe sizes sizes from 2-4" and multipipe surveys to 36'
Petrochemical	Crude oil and other petrochemical flow measurements and control functions. 1 through 24" pipes
Pharmaceutical	Measurement and control of products for the preparation of antibiotics
Chemical processing	Numerous and diverse chemicals in pipes from 1" to 12"
Government	Measurement of cryogenic liquids, liquid TNT, phosphorous and other liquids
Municipal	Waste water and sewage with pipes up to 42" in diameter
Aerospace	Jet engine fuel flow (aircraft tubing)
Food	Quality and batch control in food processing. 1" to 4" pipes
Marine	Submarine ballast measurement and control (3" copper nickel pipe)

6. CONCLUSION

The clamp-on ultrasonic flowmeter is a new tool available to industry, enabling it to accomplish flow measurements with a convenience, economy and performance capability not previously available in one instrument. Substantial field experience and calibration test results have established its capability in a wide diversity of practical applications. The availability of performance data, limits of acceptable application, and the body of knowledge governing successful installation and use, has been established and is available to industrial users as a base for the increase in the utilization of this instrument.

1.

SKETCH



2.

$$T_s = \frac{d}{V_s \cos \theta}$$

3.

$$\Delta T_s = \frac{V_F \sin \theta}{V_s} T_s$$

Let $d=1''$, $V_s= 5000 \text{ ft./sec.}$, $V_F = .001 \text{ ft./sec}$ $\theta=30^\circ$

$$T_s = \frac{1}{(60 \times 10^3) (.866)} = 19.25 \mu\text{sec}$$

$$\Delta T_s = \frac{.001 (0.5) (19.25 \times 10^{-6})}{5000}$$

$$\Delta T_s = 1.925 \times 10^{-12} \text{ seconds}$$

Figure 1. ΔT clamp-on flowmeter differential time computation.

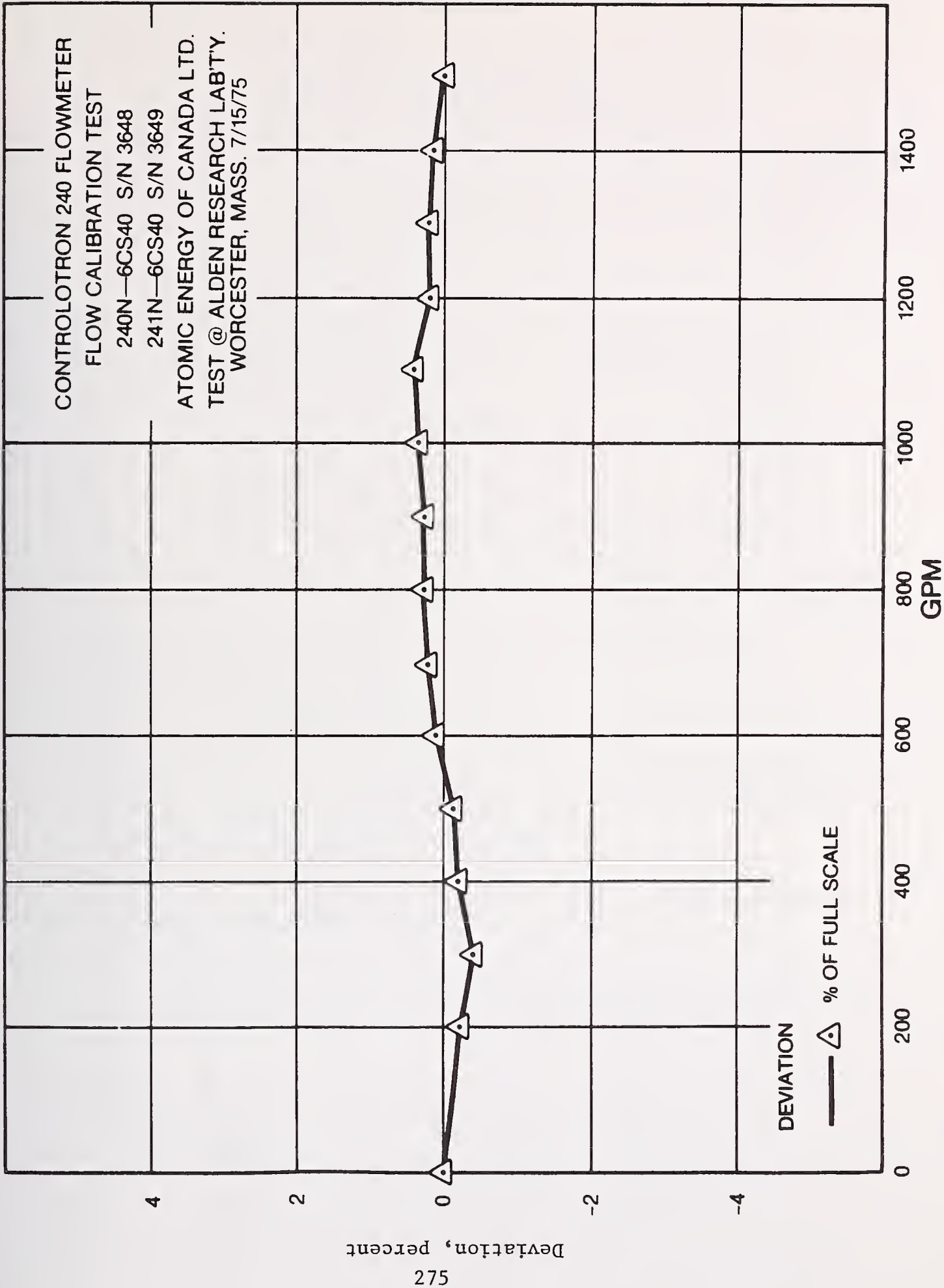


Figure 2. Controlotron 240 flowmeter calibration curve.

PERFORMANCE

Zero Stability	.05 1/sec
Linearity	1% of reading above 1 fps.
Accuracy	
Intrinsic Calibration	1-4% of range (typical)
Actual flow Calibration	0.5-1.5% of range (typical)
Repeatability	<u>+3</u> digits of s.d.
Flow Range	0 to 30 ft/sec (minimum)
Digital Display Resolution	20,000 digits (two ranges)
Digital Display Update Interval	4 seconds
Analog Update Interval	0.1 sec (nom) Faster update on special order
Totalizer Update Rate	Continuous (Real Time)
Liquid Characteristics Standard:	Homogeneous No Undissolved solids or gases, V_L from 900 to 2100 m/sec.
Approval Required:	Non-homogeneous liquids or undissolved solids in liquid

Note: For nominal pipe size, wall thickness, in specified pipe material and for homogeneous non-aerated liquids.

Figure 3. 241 flow display computer specification.

THEORETICAL AND EXPERIMENTAL
ASSESSMENT OF UNCERTAINTIES IN
NON-INTRUSIVE, ULTRASONIC FLOW MEASUREMENT¹

Ronald F. Bruner
Naval Ship Engineering Center
Philadelphia Division
Philadelphia, PA 19112

In recent years the development of commercially available², externally mounted, ultrasonic flow measuring systems has made it possible to measure liquid flow rate without disturbing the flow or modifying the ducting. Such systems rely on the highly accurate measurement of both the time for sound pulses to travel from an upstream transducer to an oppositely mounted downstream transducer, and the time for sound pulses to travel from downstream to the upstream transducer. (This technique does not employ the Doppler shift, and scattered sound is undesirable.) This paper treats only the steady flow of homogeneous liquid in full ducts, although the theory is easily extended to open channel and gas flow.

In making such measurements the duct itself becomes part of the measuring system, as the path and intensity of the transmitted sound depend on the material composition, wall thickness, and surface condition of the duct. Furthermore, the outside dimension of the duct (i.e. diameter), velocity of sound in the liquid, and flow velocity field also figure in the theoretical determination of the flow rate. Add to the uncertainties in the above parameters the positional (i.e. mounting) uncertainties plus uncertainties in the electronic equipment, and the feasibility of accurate flow measurement outside the laboratory becomes questionable.

A theoretical analysis is developed which aims to quantify the uncertainties associated with these parameters, and to determine their effects on overall system accuracy and repeatability. Experimental data have been obtained for estimating the uncertainties which might normally be encountered. These are presented for comparison with the theory. The result is a clearer picture of what we can realistically expect for the overall accuracy of non-intrusive, ultrasonic flow measurement both in the field, and under controlled conditions.

Key Words: Ultrasonic flowmeter; acoustic rays; flow measurement.

¹The opinions expressed herein are those of the author and not necessarily those of the Department of Defense nor the Navy Department.

²The flow measuring system referred to for the experimental data in this paper was manufactured by Controlotron Corp., 111 Bell Street, West Babylon, NY 11704.

1. Introduction

The development of commercially available, externally mounted, ultrasonic flow measuring systems may well be the most significant advance in flow measurement technology in recent years. In principle, this type of system leaves little to be desired for the measurement of homogeneous liquid flow. It is portable, and does not require any disturbance of the flow or the piping, other than removal of lagging and/or scale from the pipe surface. The essential idea behind this type of flow measurement is that it takes longer for ultrasound to traverse the flow when directed against the flow (upstream) than when it is directed with the flow (downstream) (see Figure 1). The greater the flow, the greater is the difference between these two traverse times.

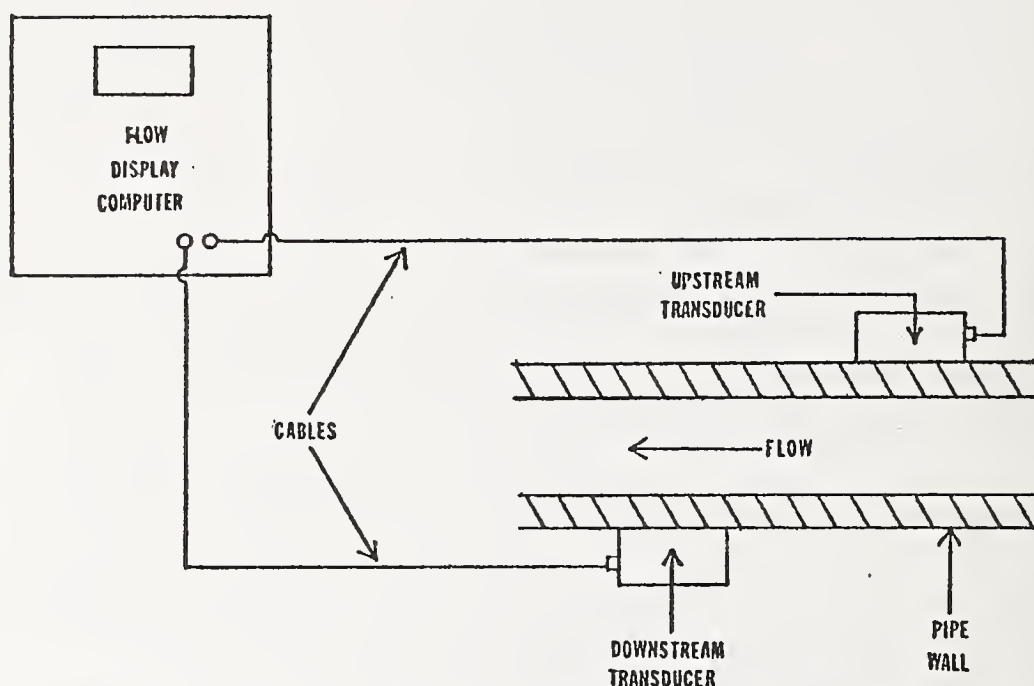


FIGURE 1 SKETCH OF FLOW MEASURING SYSTEM

The major elements of the system are seen in Figure 1. The flow computer is the originator and receiver of electrical pulses. For example, a pulse is sent to the downstream transducer. Natural frequency vibrations are thus induced in the transducer crystal (usually in the 100kHz-5MHz range) and an ultrasonic pulse travels across the pipe, exciting the upstream transducer crystal. This results in an electrical signal which is received and analyzed by the flow computer to give a measure of the upstream traverse time. The direction of the signal is reversed (i.e. sent to upstream transducer and received by downstream transducer) to obtain a measure of the downstream traverse time. These two measurements must be the bases for the subsequent calculation of flow. Approximately 13,000 measurements per second were made by the unit tested, so that averaged readings, displayed about every four seconds, were relatively sta-

ble, with most fluctuations less than 1/2% of reading from the average (except near zero flow).

2. Laboratory Experience

The simplest setup for testing the flow measuring system is a long straight pipe with a "standard" flowmeter of proven accuracy and reliability installed in series, downstream. This was done for the specific case of water flow in an 8 foot (2.4m) section of 4 inch (10cm) (IPS), schedule 40, carbon steel pipe. A 4 inch (10cm) turbine flowmeter was used as the standard. Periodic in situ calibration of the turbine meter, using gravimetric (weight-time) methods, verified its accuracy within $\pm 1/2\%$ of reading throughout. The transducers were mounted with approximately 20 diameters of straight piping upstream and a silicone base sonic couplant applied between them and the pipe surface to enhance acoustic transmission.

The flow display computer offered two readouts, one indicating flow in gallons per minute (gpm), the other indicating total gallons of flow since the last scale resetting (1 gallon = 3.785 liters). At least 25 displayed readings were averaged for each flow measurement. Each of these averages was accomplished in less than 30 minutes, a sufficiently short time to consider the data randomly distributed about a constant mean {1}.³ The totalizer was calibrated versus the standard six times over a period of twelve days, and the flow display was calibrated five times over the last seven of those days. After the initial zero setting and calibration scale setting were made, nothing was changed in the setup during the twelve day period except to disconnect and secure the flow computer each night. To estimate the magnitude of random changes in calibration over several days in this permanent type installation, the average meter correction factor (true flow divided by measured flow) and its standard deviation were calculated at each flow rate for the number, n, of reliable calibration points obtained. The results are given in Tables 1 and 2.

Table 1 Summary of Permanent Installation Data from Flow Display

<u>Nominal Flow Rate (gpm)</u>	<u>Average Correction Factor</u>	<u>Standard Deviation</u>	<u>n</u>
580	1.0100	.0032	4
480	1.0169	.0032	5
380	1.0193	.0086	5
280	1.0359	.0019	4
180	1.0342	.0075	5
80	1.0452	.0233	5

³Figures in brackets indicate the literature references at the end of this paper.

Table 2 Summary of Permanent Installation Data from Totalizer

<u>Nominal Flow Rate (gpm)</u>	<u>Average Correction Factor</u>	<u>Standard Deviation</u>	<u>n</u>
580	.9991	.0048	6
480	1.0003	.0062	6
380	1.0022	.0085	6
280	1.0095	.0121	6
180	1.0111	.0223	6
80	1.0063	.0502	6

It is apparent from these data that the standard deviation tends to increase with decreasing flow rate. It is surmised that this is due to drifts in the zero setting. To check the consistency of this assertion with the data, all readings were corrected for zero drift by taking the average of true zero (no flow) readings before and after each calibration and subtracting this from the flow readings. The resulting, zero-corrected data are presented as Tables 3 and 4. The decrease in standard deviation is quite apparent at the lower flow rates, supporting the contention that zero drift is an additive correction to the flow readouts.

Table 3 Summary of Zero-Corrected Permanent Installation
Data from Flow Display

<u>Nominal Flow Rate (gpm)</u>	<u>Average Correction Factor</u>	<u>Standard Deviation</u>	<u>n</u>
580	1.0002	.0048	4
480	1.0072	.0051	5
380	1.0048	.0067	5
280	1.0163	.0042	4
180	1.0018	.0030	5
80	0.9717	.0077	5

Standard Deviation of Average Correction Factors 0.0135

Table 4 Summary of Zero-Corrected Permanent Installation
Data from Totalizer

<u>Nominal Flow Rate (gpm)</u>	<u>Average Correction Factor</u>	<u>Standard Deviation</u>	<u>n</u>
580	.9924	.0034	6
480	.9920	.0031	6
380	.9918	.0030	6
280	.9974	.0051	6
180	.9885	.0066	6
80	.9554	.0134	6

Standard Deviation of Average Correction Factors 0.0174

There are two other prominent tendencies in the data in Tables 3 and 4. First, the meter correction factor is different (lower) for the totalizer than for the flow display by about 1.4% on average, with a slight trend towards larger discrepancies at lower flow rates. Furthermore, the correction factor is dependent on flow rate. This is borne out by the fact that the standard deviation of the average correction factors (center column) is greater than the standard deviations computed at each flow rate (right column). Also, there is an obvious decrease in correction factor with decreasing flow for the three lowest flow rates.

To summarize further the data obtained in the permanent installation, it is assumed that the variations in meter correction factor can be divided into two independent components: one originating from a simple, additive zero drift (which may be minimized by setting true zero before reading), the other originating in electronic and mechanical drifts in calibration factor and expressible as a percentage of flow rate. This latter source of variation is estimated from the root-mean-square (rms) of the standard deviations listed in Tables 3 and 4. For the flow display the rms deviation is 0.00552, and for the totalizer, 0.00683. If the uncertainty in a flow reading, R , is taken to be 2.576 standard deviations (which would include 99% of normally distributed data), then we have $\pm 0.0142R$ uncertainty in the flow display, and $\pm 0.0176R$ uncertainty in the totalizer. In addition, the zero drift standard deviation was estimated at 1.30 gpm for the display calibrations and 2.47 gpm for the totalizer calibrations. However, the flow display zero drift decreased monotonically over the twelve days, starting at true zero, and decreasing to -7.1 gpm. Based on this observation it seems reasonable to assign an uncertainty of at least ± 7 gpm to the zero setting if true zero is not set for several days. It should be recalled that the overall uncertainty in this circumstance is the square root of the sum of the individual squared uncertainties. Also, all of the above data refer to a system which is accurately calibrated in place, and therefore does not include uncertainties due to piping differences, installation procedures, or any other observed parameters.

Next the removal and reinstallation of the transducers (on the same pipe) was isolated as a source of uncertainty. This variable is present in the common case whereby the ultrasonic flowmeter is calibrated at one location for use at another location with similar piping. The zero-corrected data for this temporary type installation is summarized in Tables 5 and 6.

Table 5 Summary of Zero-Corrected Temporary
Installation Data from Flow Display

<u>Nominal Flow Rate (gpm)</u>	<u>Average Correction Factor</u>	<u>Standard Deviation</u>	<u>n</u>
580	.9289	.0146	10
480	.9617	.0264	10
380	.9741	.0155	10
280	.9670	.0234	10
180	.9677	.0248	8
80	.8758	.0566	8

Table 6 Summary of Zero-Corrected Temporary
Installation Data from Totalizer

<u>Nominal Flow Rate (gpm)</u>	<u>Average Correction Factor</u>	<u>Standard Deviation</u>	<u>n</u>
580	.9580	.0141	10
480	.9601	.0141	10
380	.9620	.0146	10
280	.9617	.0179	10
180	.9545	.0186	10
80	.9481	.0268	8

The rms standard deviation from Table 5 (excluding data at 80 gpm where unavoidable zero drift during the calibration may make a significant contribution) is 0.0214, and, from Table 6, 0.0160. With the same interpretation as for the permanent installation data, this implies an estimated uncertainty of $\pm 0.0551R$ in flow display readings, temporary installation, and an estimated uncertainty of $\pm 0.0412R$ in totalizer readings, temporary installation. The increase over the corresponding permanent installation uncertainties ($\pm 0.0142R$ and $\pm 0.0176R$ respectively) must be due to uncertainties originating from removal and reinstallation, without recalibration, as this was the only additional variable.

To summarize Tables 1 through 6, lumping flow display and totalizer data together, a repeatability of $\pm 1.6\%$ of reading is estimated for permanently installed, undisturbed, transducers if true zero setting is maintained. If in situ calibration is performed, this is also equal to the estimated uncertainty. If transducers are calibrated in one place and used in another, the estimated uncertainty is $\pm 4.9\%$ of reading, assuming true zero setting, and not counting the uncertainties due to piping differences.

Finally, in discussing experimental data, it should be recalled that the above data are from only one flow measuring system which is not a large enough sample to infer reliably the parameters which characterize the performance of this type of flowmeter. However, calibration and shipboard data have been obtained with several different flow measuring systems of this type {1, 2, 3} and they indicate comparable linearity, data scatter, and repeatability to the estimates reported herein.

3. Theoretical Analysis

The evaluation of uncertainties associated with additional variables, such as pipe diameter and wall thickness, acoustic velocity in the pipe wall, and flow profile and acoustic velocity in the liquid, would require a fairly long and costly program if done experimentally. A theoretical analysis was undertaken instead, which permits direct calculation of the uncertainties in flow measurement due to each of these variables except flow profile. Furthermore, this analysis provides considerable insight into the acoustic principles underlying the operation of externally mounted ultrasonic flowmeters in general.

The idealized model used to simplify the analysis incorporates the following: (1) The sound is emitted and received at a geometric point in each transducer. (2) The sound wavelength is sufficiently short that geometric acoustics pertains. (3) The sound path lies entirely in a plane containing the point transducers and the pipe axis. (4) The pipe is exactly symmetric about its axis. (5) The flow velocity is constant everywhere inside the pipe, and in time. Figure 2 depicts this model.

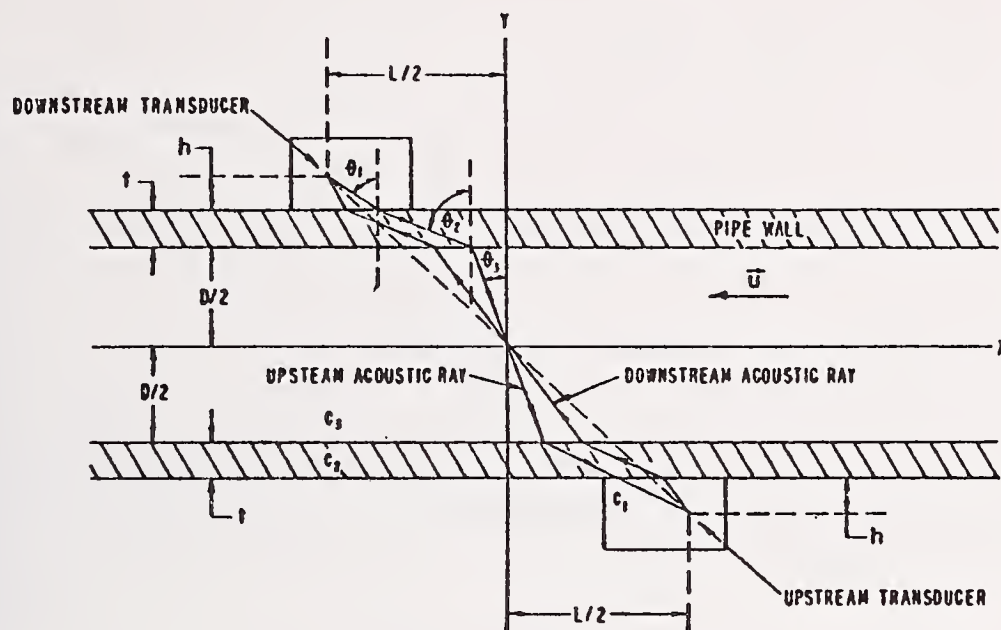


FIGURE 2 DIAGRAM FOR ANALYSIS OF ACOUSTIC RAY TRANSMISSION BETWEEN ULTRASONIC TRANSDUCERS

A simple argument based on symmetry and the identity of the transducers leads to the conclusion that any sound ray traveling between the two transducers must pass through the midpoint of the line joining them. To see this consider the symmetry operation of time reversal. Inasmuch as the transducers are identical, this operation must result in no real physical change to the system. However, if it is conjectured that the sound ray path does not go through the midpoint of the line joining the transducers, then time reversal (which amounts to a reversal in the directions of sound propagation and flow) would not leave the path unchanged (i.e. A path which crossed the x-axis upstream of the midpoint initially, would cross the x-axis downstream of the midpoint if time were reversed). Since time reversal is a fundamental symmetry of classical physics, it follows that the upstream and downstream ray paths must intersect each other, and the pipe center line, at a point midway between the transducers.

The space and time dependence of a sound wave in a uniformly moving liquid has the form {4} :

$$\exp\{i(\vec{k} \cdot \vec{x} - (kc + \vec{k} \cdot \vec{u})t)\} \quad (1)$$

This result shows that the sound will travel along a straight line in the idealized flow considered. The central problem now is to determine the angle of refraction of the sound as it enters the liquid. To do this, we notice that the boundary conditions on the solution to the wave equation lie only in the plane normal to the y-axis. The correct solution must therefore be invariant under translation along the x direction {4}. This requires that the x component of the wave vector be continuous across the solid-liquid interface:

$$k_{2x} = k_{3x} \quad (2)$$

where the notation of Figure 2 applies, and k is the magnitude of the wave vector. Geometric analysis gives the expression for k_{3x} (see Appendix):

$$k_{3x} = \frac{\omega/c_3 \left[\sin\theta_3 \left(1 - \frac{u^2}{c_3^2} \cos^2\theta_3 \right)^{1/2} + \frac{u}{c_3} \sin^2\theta_3 - \frac{u}{c_3} \right]}{1 - \frac{u^2}{c_3^2} \cos^2\theta_3 + \frac{u}{c_3} \sin\theta_3 \left(1 - \frac{u^2}{c_3^2} \cos^2\theta_3 \right)^{1/2}} \quad (3)$$

Since k_2 is simply ω/c_2 , and since the angular frequency, ω , is the same in both media, equations (2) and (3) combine to give the desired generalization of Snell's law relating the refraction angles at the interface of the pipe wall and the moving liquid:

$$\frac{\sin\theta_2}{c_2} = \frac{\sin\theta_3 \left[1 - \frac{u/c_3 \csc\theta_3}{\left(1 - \frac{u^2}{c_3^2} \cos^2\theta_3 \right)^{1/2} + \frac{u}{c_3} \sin\theta_3} \right]}{c_3 \left(1 - \frac{u^2}{c_3^2} \cos^2\theta_3 \right)^{1/2}} \quad (4)$$

while, at the interface of the transducers with the pipe wall we have the usual form of Snell's law:

$$\frac{\sin\theta_1}{c_1} = \frac{\sin\theta_2}{c_2} \quad (5)$$

Equations (4) and (5) together with the equation constraining the sound ray path to begin and end at the transducer locations, namely,

$$L/2 = h \tan \theta_1 + t \tan \theta_2 + D/2 \tan \theta_3 \quad (6)$$

uniquely determine the ray path. The resulting equation is developed in the Appendix, and it determines θ_3 only implicitly. A program was developed to calculate $\sin\theta_3$ iteratively on a hand-held programmable calculator. The calculated value of $\sin\theta_3$ was used then to calculate the time of traversal of a sound pulse. (The equations, as listed herein and in the Appendix are for downstream traversal, and the same relations pertain for upstream traversal except the sign of u is changed.) Since the ultrasonic flow measuring system under discussion must determine flow based on measurements of upstream and downstream traverse times, the ability to calculate these as a function of the various parameters permits a theoretical determination of the effects which changes in these parameters will have on actual flow measurements.

Before listing the results of the numerical investigation, it is interesting to note that the upstream and downstream paths are not coincident (This is somewhat exaggerated in Figure 2). However, the fact that both paths intersect the midpoint of the line joining the transducers requires that each path be symmetric about that point. This means that the analysis may be restricted to the portion of each path which is between a transducer and the midpoint since the remainder of the path is just a reflection of this. As may be expected, the upstream pulse takes a more direct path across the liquid in an "effort" to avoid the retarding effects of the flow, while the downstream ray is lengthened in the liquid to "take advantage" of the free boost in velocity. This is in accord with Fermat's principle, which states that sound takes the path of least time.

The calculations were made using an idealized version of the system actually used to obtain the experimental data of section 2. The nominal parameters were: pipe inside diameter, $D = 4.026$ in. (10.23cm); pipe wall thickness, $t = 0.237$ in. (0.602cm); acoustic velocity in carbon steel pipe, $c_2 = 5940$ m/s; axial separation of transducers, $L = 5.57$ in. (14.1cm); distance between transducer crystal and pipe surface, $h = 1.0$ in. (2.54cm); acoustic velocity in liquid (fresh water), $c_3 = 1496.7$ m/s; and, acoustic velocity in transducer housing, $c_1 = 2620$ m/s. With these nominal parameters, it was calculated that $\sin\theta_3 = 0.2497474683$ for $u=0$, and the traverse time, for a sound pulse was $\tau = 107.4664$ μ s. With $u = 5$ m/s, for example, the difference between upstream and downstream traverse times was $\Delta\tau = 117.740$ ns.

It was found that the difference between upstream and downstream traverse times, $\Delta\tau$, is linearly proportional to the flow velocity, u , to an accuracy of better than $1.4 \times 10^{-3}\%$ for velocities up to 50 m/s. The difference in the reciprocal times, $\Delta(1/\tau)$, is similarly a linear function of u over all commonly experienced flow velocities. More importantly, though, $\Delta(1/\tau)$ was calculated, with $u = 10$ m/s, for six values of liquid acoustic velocity ranging from $c_3 = 800$ m/s to 2000 m/s and found to be independent of the liquid acoustic velocity to better than $1.8 \times 10^{-4}\%$! This means that the flometer calibration may indeed be considered independent of the metered liquid provided an acceptable signal/noise ratio can be maintained. Furthermore, the product of the liquid acoustic veloc-

ity with the average of the upstream and downstream traverse times is essentially constant (to better than $6.2 \times 10^{-5}\%$) over the same range of acoustic velocities, so that the flow computer may actually "know" what liquid it is metering (i.e. the acoustic velocity of the liquid). This is important in the case where the transducers must be repositioned to improve the signal to noise ratio, since a correction factor for the change in position can be calculated only if the liquid acoustic velocity is known.

The uncertainties associated with certain parameters were calculated using the nominal values listed previously, and are given in Table 7. The uncertainties assigned to pipe wall thickness and pipe inside diameter correspond to tolerances given in military specifications for carbon steel pipe. The uncertainties in pipe acoustic velocity, liquid acoustic velocity, and transducer axial separation were chosen arbitrarily to illustrate their effects on $\Delta\tau$ and $\Delta(1/\tau)$.

Table 7 Uncertainties Arising in
Measured Quantities Due to Uncertainties
in Certain Parameters

<u>Parameter</u>	<u>Uncertainty in</u> <u>Parameter (%)</u>	<u>Resulting</u> <u>Uncertainty in</u> <u>$\Delta\tau$ (%)</u>	<u>Resulting</u> <u>Uncertainty in</u> <u>$\Delta(1/\tau)$ (%)</u>
Pipe wall thickness	± 12.5	-0.24, +0.22	-0.31, +0.28
Pipe inside diameter	± 0.65	± 0.62	± 0.15
Pipe acoustic velocity	± 1.0	-1.0, +1.1	-0.76, +0.78
Transducer axial separation	± 2.24	+0.06, -0.07	± 0.92
Liquid acoustic velocity	± 50	-56, +400	$< 2 \times 10^{-4}$

It is apparent that the values in Table 7 are considerably smaller than the uncertainties determined experimentally in Section 2. Apparently, the electronic stability and signal processing techniques are the principle sources of uncertainty. For example, implicit in the idea of averaging out the noise in the signal by taking a large number of measurements is the assumption that noise is entirely random. In fact, signals from the transmitting transducer might reach the receiving transducer via certain other "favored" paths in addition to the idealized path used for the analysis. This could skew the distribution of the received noise, resulting in a biased flow reading. (It has been pointed out by the inventor that a higher signal/noise ratio generally leads to improved readings).

In closing this section, it should be emphasized that all calculations were made assuming a constant velocity profile. Although the constancy in time is not expected to alter the results significantly (based on calculations done by the author describing the interaction of sound with turbulence {5}, and on laboratory observations which showed no significant increase in readout fluctuations as the flow was increased from laminar

to turbulent), the assumed constancy of velocity throughout the pipe overlooks the essentially non-linear changes in the real velocity profile as the Reynolds number and pipe roughness change. In reality, therefore, $\Delta\tau$ and $\Delta(1/\tau)$ are not linearly related to the flow rate, a fact borne out by the data of Tables 1 through 6. Also, it is hoped that this analysis will help permit the eventual use of a single flow measuring system for use in various piping situations, for, so long as an acceptable signal can be transmitted across the pipe, it is possible, in principle, to correct for the various parameter changes and infer the flow from the measured upstream and downstream traverse times.

4. Conclusions

The development of non-intrusive, ultrasonic flow measurement systems represents a significant advance in our technology. They enable flow measurement, by means of portable instruments, of homogeneous liquid flow in systems which may not be opened, a capability previously unavailable. Experimental and theoretical results indicate that, while commercially available models may be adequate for many industrial and military applications, there remains significant room for improvement in overall accuracy and repeatability.

There is a need for additional work in this area of flow measurement to provide improved statistics on a representative sample of instruments, and to extend and deepen our understanding. For example, scant information is available on the effects of upstream piping, a problem commonly encountered in flow measurement applications. Also, an accurate analysis of sound propagation in real, viscous and turbulent, shear flows could help to improve linearity. These and other problems are under investigation presently by the author.

APPENDIX

The derivation of the equations determining the sound ray paths and traverse times is most easily visualized using Figure 2 of the text. The central problem is to find a means of calculating the upstream and downstream traverse times for sound pulses given D , t , h , c_1 , c_2 , c_3 , L and u . As discussed in the text, the analysis may be confined to half of the ray path, due to symmetry, and the traverse time calculated will be half the complete traverse time.

The most difficult of the necessary relationships to establish is the one which relates the refraction angle, θ_3 , in the moving liquid to the angle θ_2 in the pipe wall. If there were no flow, Snell's law would be adequate, as it is in the case of refraction at the transducer-pipe wall interface:

$$\frac{\sin\theta_1}{c_1} = \frac{\sin\theta_2}{c_2} \quad (1A)$$

To determine the necessary generalization of Snell's law when one medium is moving we consider the boundary condition that the x component of the wave vector be continuous across the interface:

$$k_{2x} = k_{3x} \quad (2A)$$

In the pipe wall, the magnitude of \vec{k}_2 is simply ω/c_2 , and the direction of \vec{k}_2 is along the direction of the ray path. In the moving medium, however, neither the magnitude nor direction of \vec{k}_3 is so simple. As seen from the expression in the text giving the time dependence of the wave, the angular frequency is {4}:

$$\omega = c_3 k_3 + \vec{u} \cdot \vec{k}_3 \quad (3A)$$

By a general theorem of physics, the velocity of this wave is {4}:

$$c_3' = \frac{\partial \omega}{\partial k_3} = c_3 \frac{\vec{k}_3}{k_3} + \vec{u} \quad (4A)$$

Transposing \vec{u} , squaring both sides, and solving for c_3' gives:

$$c_3' = c_3 \left[\left(1 - \frac{u^2}{c_3^2} \cos^2 \theta_3\right)^{1/2} + \frac{u}{c_3} \sin \theta_3 \right] \quad (5A)$$

Now, solving for \vec{k}_3 in (4A) and substituting the result in (3A), we obtain the relationship between ω and k_3 :

$$\omega = k_3 c_3 \left[1 + \frac{c_3' u}{c_3^2} \sin \theta_3 - \frac{u^2}{c_3^2} \right] \quad (6A)$$

Substituting for c_3' , from (5A) and solving for k_3 yields:

$$k_3 = \frac{\omega/c_3}{1 + \frac{u}{c_3} \sin \theta_3 \left[\left(1 - \frac{u^2}{c_3^2} \cos^2 \theta_3\right)^{1/2} + \frac{u}{c_3} \sin \theta_3 \right] - \frac{u^2}{c_3^2}} \quad (7A)$$

In order to determine k_{3x} , we take the scalar product of k_3 with u which, by definition is $k_{3x}u$. Using (4A) as well as (7A), we obtain:

$$k_{3x} u = \frac{u k_3}{c_3} (c_3' \sin \theta_3 - u) \quad (8A)$$

Substituting the previously determined expressions for c_3' and k_3 from (5A) and (7A) respectively gives:

$$k_{3x} = \frac{\omega/c_3 \left[\sin\theta_3 \left(1 - \frac{u^2}{c_3^2} \cos^2\theta_3 \right)^{1/2} + \frac{u}{c_3} \sin^2\theta_3 - \frac{u}{c_3} \right]}{1 - \frac{u^2}{c_3^2} \cos^2\theta_3 + \frac{u}{c_3} \sin\theta_3 \left(1 - \frac{u^2}{c_3^2} \cos^2\theta_3 \right)^{1/2}} \quad (9A)$$

Factoring $\sin\theta_3$ from the numerator and $\left(1 - \frac{u^2}{c_3^2} \cos^2\theta_3 \right)^{1/2}$ from the denominator, and equating with k_{2x} gives the explicit expression of (2A):

$$\frac{\sin\theta_2}{c_2} = \frac{\sin\theta_3 \left[1 - \frac{u/c_3 \csc\theta_3}{\left(1 - \frac{u^2}{c_3^2} \cos^2\theta_3 \right)^{1/2} + \frac{u}{c_3} \sin\theta_3} \right]}{c_3 \left(1 - \frac{u^2}{c_3^2} \cos^2\theta_3 \right)^{1/2}} \quad (10A)$$

Equation (10A) is the generalization of Snell's law to the case where medium 3 is moving with velocity u relative to medium 2. In order to determine the ray path completely, we must also require that it begin at one transducer and end at the other. This condition is expressed mathematically from a direct analysis of the geometry in Figure 2:

$$L/2 = h \tan \theta_1 + t \tan \theta_2 + D/2 \tan \theta_3 \quad (11A)$$

Equations (1A), (10A), and (11A) uniquely determine the three unknowns, θ_1 , θ_2 and θ_3 . Unfortunately, these three equations cannot be solved explicitly for the angles. If we can determine θ_3 , however, θ_2 and θ_1 may be calculated from (10A) and (1A) directly.

Before developing an exact expression for the implicit determination of θ_3 , we shorten the notation in (10A) by letting:

$$x = \sin\theta_3 \quad (12A)$$

$$\epsilon = u/c_3 \quad (13A)$$

$$y = \cos\theta_3 \quad (14A)$$

$$F = \frac{\epsilon}{(1 - \epsilon^2 y^2)^{\frac{1}{2}} \left[(1 - \epsilon^2 y^2)^{\frac{1}{2}} + \epsilon x \right]} \quad (15A)$$

$$G = \frac{x}{(1 - \epsilon^2 y^2)^{\frac{1}{2}}} - F \quad (16A)$$

$$n_{13} = c_1/c_3 \quad (17A)$$

$$\text{and} \quad n_{23} = c_2/c_3 \quad (18A)$$

Now, (10A) becomes:

$$\sin \theta_2 = n_{23} G \quad (19A)$$

and (1A) becomes:

$$\sin \theta_1 = n_{13} G \quad (20A)$$

Substitution of (19A) and (20A) into (11A) leads to an implicit expression which determines x:

$$L/2 = \frac{h n_{13} G}{(1 - n_{13}^2 G^2)^{\frac{1}{2}}} + \frac{t n_{23} G}{(1 - n_{23}^2 G^2)^{\frac{1}{2}}} + \frac{Dx}{2(1 - x^2)^{\frac{1}{2}}} \quad (21A)$$

Although the actual numerical solution of (21A) for x is a fairly lengthy and tedious undertaking, it can be done iteratively on a programmable calculator of 224 step capacity. Once the value for x is determined for given conditions, the next problem is to calculate the traverse time for the path corresponding to x. This is accomplished by dividing the length of the ray path in each medium by the acoustic velocity in that medium and summing (see Figure 2). The traverse time, in terms of the new variables, is:

$$\tau = \frac{2h}{c_1 (1 - n_{13}^2 G^2)^{\frac{1}{2}}} + \frac{2t}{c_2 (1 - n_{23}^2 G^2)^{\frac{1}{2}}} + \frac{D}{c_3 y ((1 - \epsilon^2 y^2)^{\frac{1}{2}} + \epsilon x)} \quad (22A)$$

This expression applies to a pulse traveling from the upstream to the downstream transducer when ϵ is positive, and vice versa when ϵ is negative.

References

- {1} "Evaluation of Controlotron Corporation Ultrasonic Clampitron Flowmeter", by Fania Wanenchak, Naval Ship Engineering Center, Philadelphia Division report of Project A-1811 (August 6, 1976).
- {2} "Report on Performance Testing of Main Propulsion and Auxiliary Machinery Using Presently Installed and Portable Instrumentation", by Paul Drnjevic, Code 1861, PERA (CV), Puget Sound Naval Shipyard, Bremerton, Washington 98314 (August 1976).
- {3} "Test Equipment Application Project Report: Controlotron Model 240 (Clampitron) Ultrasonic Flowmeter (3" and 4" Pipe Size)", by John Flude, SMMSO, Naval Ship Engineering Center, Washington, DC, (June 1975).
- {4} L.P. Landau and E.M. Lifshitz, Fluid Mechanics, Pergamon Press, New York (1959), pp. 254-259.
- {5} Unpublished paper, "Sound Propagation in a Turbulent Medium", by Ronald F. Bruner, Naval Ship Engineering Center, Philadelphia Division.
- {6} A.R. Wenzel, "Propagation Speed and Attenuation Coefficient for Plane Coherent Acoustic Waves in a Turbulent Medium", J. Acoust. Soc. Am., v51, 1683-1687 (1972).
- {7} S.F. Clifford and E.H. Brown, "Acoustic Scattering from a Moving Turbulent Medium", J. Acoust. Soc. Am., v55, 929-933 (1974).
- {8} Lynnworth, L.C., "Clamp-on Ultrasonic Flowmeters: Limitations and Remedies", Instrumentation Technology, v22, n9, Sep 1975 pp. 37-44.
- {9} Segall, J., "Application Considerations For Controlotron Ultrasonic Clampitron Flowmeter", ISA Industry-Oriented Conference and Exhibit, paper 822, Milwaukee, WI, Oct. 6-9, 1975.

A NEW ULTRASONIC FLOWMETER FOR THE NATURAL GAS INDUSTRY

N. E. Pedersen, J. E. Bradshaw,
L. C. Lynnworth and P. R. Morel

Panametrics, Inc.
221 Crescent St.
Waltham, MA 02154

An ultrasonic flow metering system is being developed for the measurement of the flow of natural gas in pipelines having diameters from less than 1 ft to 3 ft or more. The system is designed to measure flow over a line pressure range from less than 100 psig to 1500 psig. Problems relating to high frequency dispersion and attenuation by the gas are avoided by the use of a patented ultrasonic flow metering technique which utilizes the accurate measurement of the absolute phases as well as the phase difference of various discrete low frequency (25 Hz and 5 kHz) components in the identical but sequential upstream and downstream transmitted waveforms. The measurement system utilizes a dedicated microcomputer which has been programmed to provide outputs of flow rate (ft/sec), supercompressibility, flow rate (std cu ft/hr), totalized flow (std cu ft), Reynolds number, energy flow rate (btu/hr) and totalized energy flow (btu), as well as a real time statistical analysis of intermediate data. A prototype system has been tested on an in-service gas line of 2 ft diameter. Good tracking was observed between the ultrasonic meter and a downstream orifice station on a point-by-point basis at 30 second intervals, although the flow rate varied rather substantially over such intervals. Representative preliminary data are presented.

1. Introduction

The standard of measurement of the flow of natural gas in pipelines has traditionally been the multiple tube orifice station. Such systems represent a substantial capital investment, and require a significant amount of space for their location. By contrast, the utilization of ultrasonic techniques makes possible the measurement of natural gas flow at a relatively low cost and with essentially zero pressure drop. The space requirements are minimal. Although it is not the primary objective of the present development to replace orifice metering stations as custody transfer devices, it is believed that a substantial number of measurement requirements exist in which an ultrasonic system of proven reliability and reasonable accuracy is of benefit to the natural gas industry. An example of such an application is the metering of flow from new gas sources.

In a previous ultrasonic gas flowmeter development,^{1,2} a mechanical device produced sonic shock waves which were alternately propagated upstream and downstream along a diagonal path within the pipeline. Measurement of the individual transit times permitted calculation of the gas flow velocity within the pipeline. The device was capable of providing one gas flow measurement in a period of several minutes, and utilized a rather expensive and complex electromechanical shock generator.

The present system is being developed for gas flow measurement in pipelines having diameters ranging from less than one foot to three feet or more, and over a gas pressure range of from less than 100 psig to 1500 psig. Although the macroscopic parameters (pipe diameter, flow velocity, sound speed, etc.) affecting the system point to the use of ultrasonic pulses having frequency components on the order of 1 MHz or higher, the dispersion and attenuation by the gas at such frequencies are very high. The resulting need for very high energy transmission is avoided by the use of a patented ultrasonic flow metering technique which accurately measures the absolute phases as well as the phase differences of various discrete low frequency (25 Hz and 5 kHz) components in identical but sequential upstream and downstream transmitted waveforms. These waveforms are efficiently transmitted by means of modulating a carrier wave, whose frequency is high enough (100 kHz) to provide good directionality, but low enough to be below the high attenuation region of the predominantly methane gas mixture. The rate of data acquisition of the present system is approximately 4500 times higher than that of the aforementioned ultrasonic system. Upon reception and after demodulation of the carrier wave, the above mentioned 25 Hz and 5 kHz signal components are passed through high Q bandpass filters. These filters serve the dual purpose of providing a high signal-to-noise ratio,

and of isolating the particular frequency components, of the received waveform, whose phases are to be measured. The utilization of these narrow-band and highly directional techniques permits the use of piezo-electric transducers of relatively conventional design, operated at very modest voltage and power levels.

The measurement system utilizes a dedicated microcomputer to provide the various outputs such as flow rate (ft/sec), supercompressibility, volumetric flow rate (std cu ft/hr), totalized volumetric flow (std cu ft), Reynolds number, flow profile correction factor, flow velocity statistics, profile corrected flow rates, energy flow rate (btu/hr) and totalized energy flow (btu). The computations relating to energy flow rate are dependent upon a priori knowledge of the mole fractions of the various gas constituents. The supercompressibility computation also utilizes the above data on gas constituents, as well as continuously measured values of flowing gas temperature and pressure. The various site parameters, such as pipe diameter, gas constituents, etc., are entered via front panel thumbwheel switches. The microcomputer also provides a real time statistical analysis of intermediate data. Individual flow measurements and computations are made at the rate of 25 per second. Upon accumulation of a statistically meaningful (e. g. 100) number of preliminary flow computations, the mean and the standard deviation among the measurements are computed. Then a statistical criterion is invoked to test the individual intermediate results. Those values which do not satisfy the criterion are rejected, and a new mean flow is computed.

To date, a prototype system, developed under contract to Columbia Gas System Service Corporation, has been tested over a period of several months on an in-service gas line of 2 ft diameter. The measurement site included a large orifice metering station, thereby permitting direct comparison of the outputs of the two measuring systems over periods as short as 30 seconds and as long as several days. The standard deviation among the individual ultrasonic flow measurements, made at 1/25 second intervals, was used to evaluate the very short term fluctuation in the diameter averaged flow, while the 30 second and longer intervals were compared with the orifice measurements averaged over the corresponding time periods.

2. The Required Measurement

The geometry of the measurement is sketched in Fig. 1, which shows an ultrasonic propagation path at an angle of 45° to the pipe axis, and intersecting the axis. Ultrasonic energy is consecutively transmitted upstream and then downstream. The flow velocity is determined by means of accurate measurement of the upstream and downstream transit times, as well as the time difference between upstream and downstream transits.

ULTRASONIC FLOW MEASUREMENT GEOMETRY

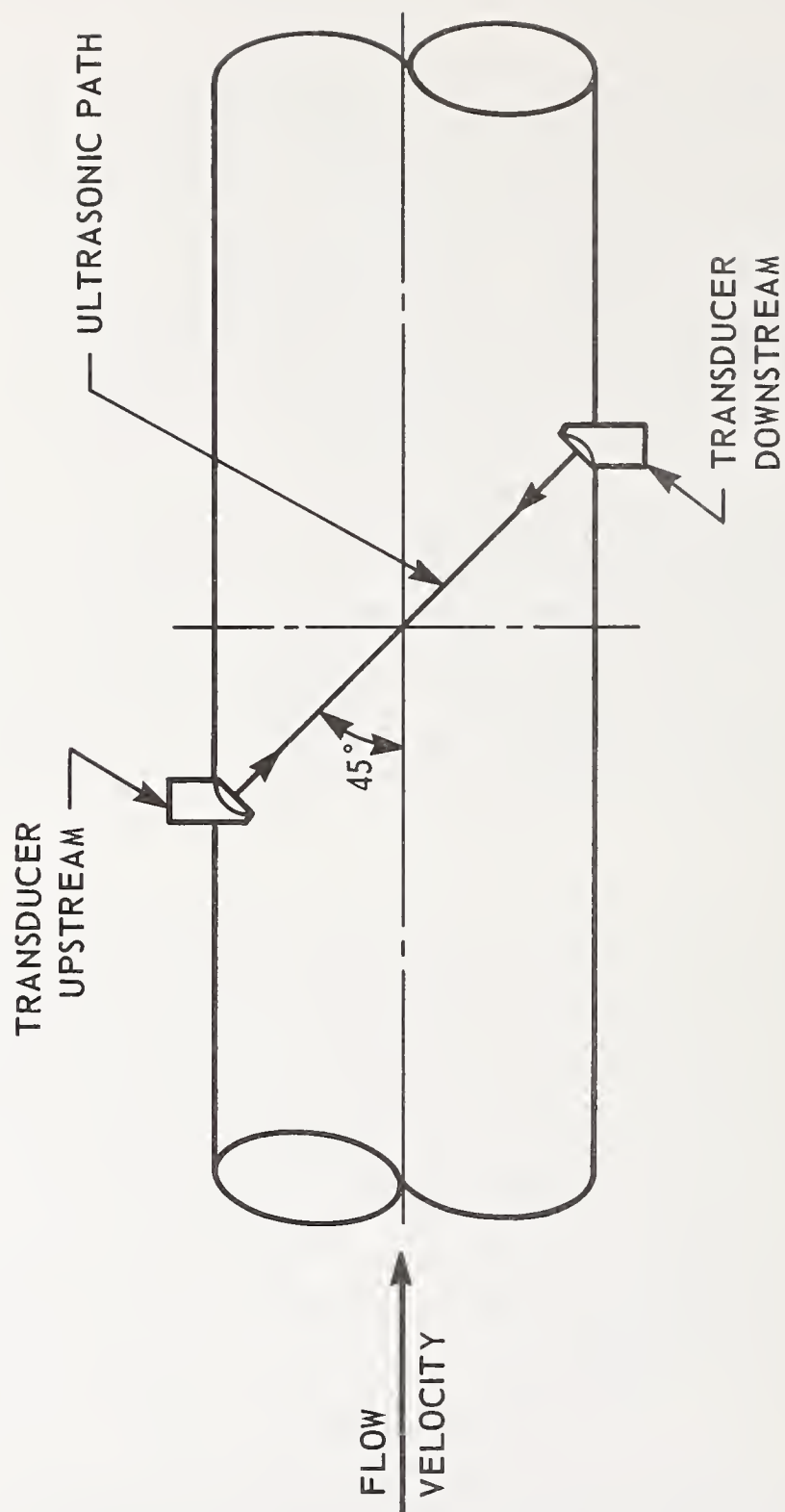


FIGURE 1

The basic equation which is solved by the flowmetering system is given below.

$$\dot{Q} = (\bar{v})(PCF) \left(\frac{P_f}{P_s} \frac{T_s}{T_f} \right) (F_{PV})^2 \quad (1)$$

In the above equation, \dot{Q} is the area averaged gas flow rate in units of standard cubic feet per second and \bar{v} = diameter averaged flow as measured by the ultrasonic flowmeter. PCF represents the flow profile correction factor, and takes into account the fact that the area averaged flow is not generally the same as the diameter averaged flow. P_f , T_f , P_s and T_s are the flowing and "standard" pressure and temperature, respectively. The quantity F_{PV} is the supercompressibility of the gas and arises from its non-ideal properties insofar as the gas law is concerned. This quantity depends upon P_f , T_f , and the mole fractions of the various constituents of the gas mixture.

3. Theory of Operation

Electronics:

The basic mode of operation of the flowmetering system is such that most of the desirable features of narrow band coherent cw operation are obtained, while many of the shortcomings of such operation are avoided. As mentioned earlier, the system measures flow by means of measuring the absolute phases of and phase differences between various frequency components of a composite waveform which is consecutively transmitted upstream and downstream along a 45° path which intersects the pipe axis.³ In considering the operation of the system, it is convenient to represent the transmitted signal as a cw wave of frequency ω_o , modulated by a rectangular wave whose repetition frequency is ω_m . Since the modulation waveform can be represented as a Fourier series, we can express the transmitted waveform as follows:

$$E_T \sim \sin \omega_o t \sum_{n=0}^{\infty} [A_n \sin n\omega_m t + B_n \cos n\omega_m t]. \quad (2)$$

Since the modulation waveform has zero amplitude during the "off" period and finite amplitude during the "on" period, its mean value is non-zero and therefore the B_0 Fourier coefficient is non-zero. Therefore, rewriting (1), we have

$$E_T \sim \sin \omega_o t \left\{ B_0 + \sum_{n=1}^{\infty} [A_n \sin n\omega_m t + B_n \cos n\omega_m t] \right\} \quad (3)$$

From the above equation, it can be seen that contained within the transmitted waveform is a spectral component of frequency ω_o . Side band components at frequencies given by $(\omega_o \pm n\omega_m)$ also occur. The received

waveform is passed through a bandpass filter having a sufficiently high Q so that these sideband frequency components are rejected, and only the ω_0 component is passed. Thus, a replica of the original (unmodulated) cw wave is retrieved. Of course, the phase shift due to the transit through the pipe will be present in the retrieved ω_0 component of the signal. A switching arrangement is provided, which passes the "downstream" waveforms to one ω_0 filter, and the "upstream" waveforms to a second ω_0 filter. If the phases of these waves are

$$\left. \begin{aligned} \phi_1 = \omega_0 t_1 &= \frac{\omega_0 D}{\sin \theta} \frac{1}{c - v \cos \theta} \\ \phi_2 = \omega_0 t_2 &= \frac{\omega_0 D}{\sin \theta} \frac{1}{c + v \cos \theta} \end{aligned} \right\}, \quad (4)$$

where t_1 and t_2 are the upstream and downstream transit times respectively, D = pipe diameter, and v = average flow velocity over the ultrasonic path, and c = sound speed in the gas.

The phase difference is

$$\phi_1 - \phi_2 = \frac{\omega_0 D}{\sin \theta} \frac{v \cos \theta}{c^2 - v^2 \cos^2 \theta} \quad (5)$$

It can be seen from the above equation that, although the phase difference $(\phi_1 - \phi_2)$ is proportional to the flow velocity, it is also proportional to the reciprocal of the sound speed. This dependence is eliminated by another narrow band technique which is described below.

The modulation waveform (the Fourier series of equation (2)) has a large Fourier component (ω_m) at its fundamental frequency. This waveform is obtained by means of an amplitude detector, and is passed through a bandpass filter of sufficiently high Q to reject all of the harmonics $n\omega_m$. Thus, in a manner analogous to the above ω_0 case, a cw wave of frequency ω_m emerges from the bandpass filter. In the flow-metering system, the detected modulation waveforms of the received downstream and upstream transmissions are (by means of a sequential switching system) passed to two ω_m bandpass filters. The phases of these two waves are, respectively,

$$\left. \begin{aligned} \psi_1 = \omega_m t_1 &= \frac{\omega_m D}{\sin \theta} \frac{1}{c - v \cos \theta} \\ \psi_2 = \omega_m t_2 &= \frac{\omega_m D}{\sin \theta} \frac{1}{c + v \cos \theta} \end{aligned} \right\} \quad (6)$$

We next combine equations (5) and (6) to obtain

$$\frac{\phi_1 - \phi_2}{\psi_1 \psi_2} = v \left(\frac{\omega_o \sin 2\theta}{\omega_m^2 D} \right), \quad (7)$$

which is independent of sound speed.

The phases ψ_1 and ψ_2 are measured by means of separately comparing the filtered ω_m signals with an internally generated reference wave at frequency ω_m , whereas the $(\phi_1 - \phi_2)$ phase difference is determined by direct comparison of the filtered upstream and downstream ω_o signals. Thus, three independent measurements are made. Each of these measurements is conducted on a cycle-by-cycle basis on the continuous waves emerging from the four ω_o and ω_m filters.

From the above, it is clear that all measurements leading to the computation of flowing gas velocity are made under substantially coherent, narrow band conditions. This type of operation is most advantageous in the case of ultrasonic measurements in a gas because the accompanying improvement in signal-to-noise ratio goes far to offset the decrease in received power due to the large impedance mismatch at the gas/transducer interfaces.

It turns out that the optimum (ω_o) frequency for the phase difference $(\phi_1 - \phi_2)$ measurement is about 5 kHz for a 2 foot diameter pipeline, and a maximum natural gas flow rate of ~ 30 ft/sec. Physical and practical constraints limit the transducer active diameter to less than 1.5". Since the sound speed in the gas is on the order of 1300 ft/sec ($\sim 1.6 \times 10^4$ in/sec), the wavelength λ of a 5 kHz ultrasonic signal is 3.1 in. Since the (disc) radiator is only $1/2\lambda$ to $1/3\lambda$ in dimension, it would exhibit a very wide radiation pattern. This excessive beam width would result in a disastrously low power level at the receiver. This problem was solved by means of utilizing a carrier wave (100 kHz) which has the desired beam width of about 10° for a ~ 1 " diameter transducer. The "information" waveform (i.e. the modulated 5 kHz wave) amplitude modulates the 100 kHz carrier. The received composite waveform is prefiltered through a 100 kHz filter (see Fig. 2) which is just wide enough to pass the ± 5 kHz modulation components of the information waveform. Following demodulation of the prefiltered 100 kHz signal, those frequency components of importance are retrieved. In this way, the ultrasonic energy is efficiently transmitted through the gas and the pertinent information is recovered at the receiver.

The implementation of the approach described above is shown in block diagram form in Fig. 2. A 10 MHz crystal controlled clock is the source from which all waveforms, switch timing, and reference signals

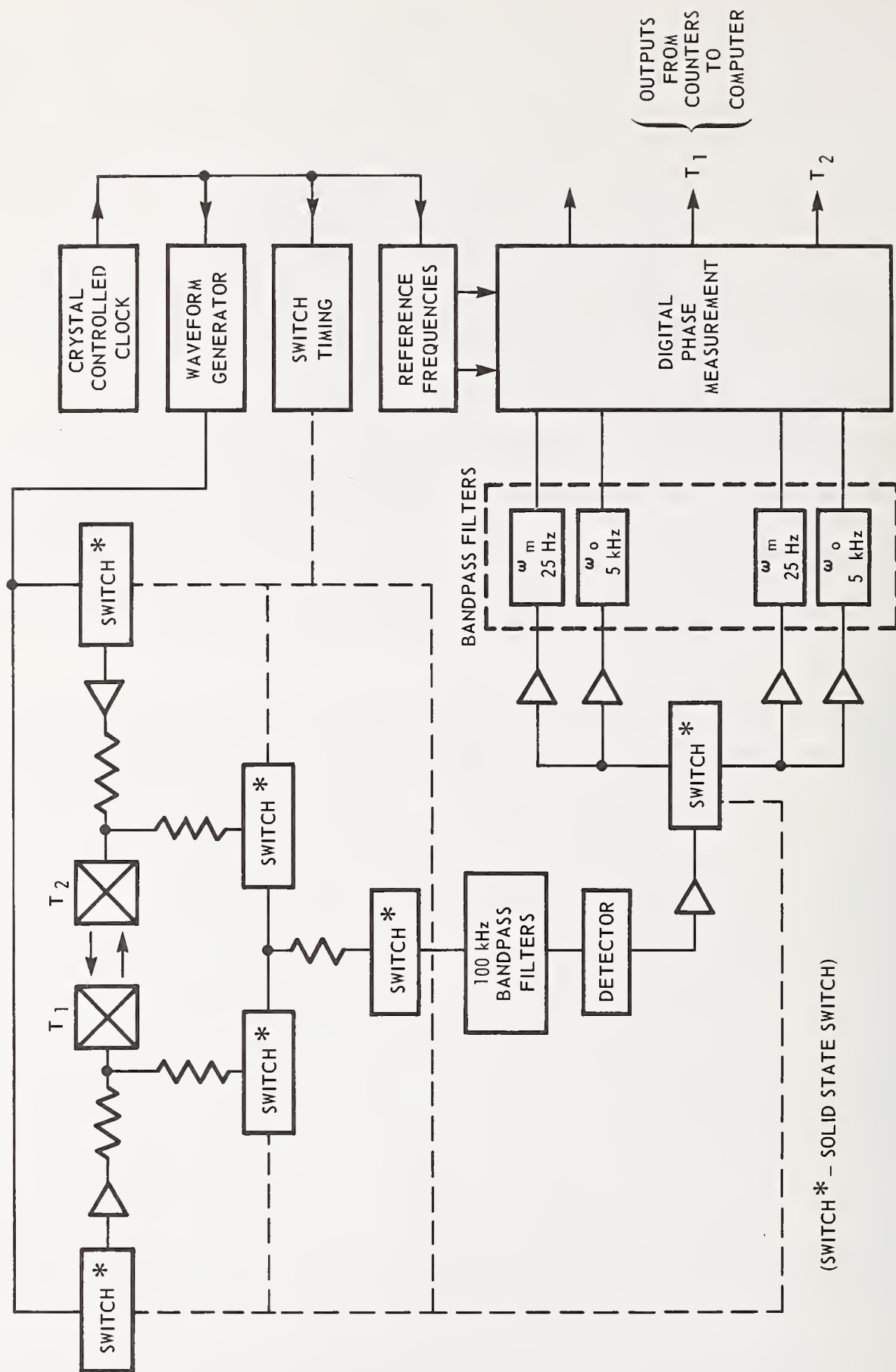


FIGURE 2 SIMPLIFIED BLOCK DIAGRAM OF ULTRASONIC FLOWMETER

are derived. The (solid state) switching is arranged so that, when transducer T_1 is transmitting (coupled to the waveform generator), transducer T_2 is receiving (coupled to the 100 kHz bandpass filter, and vice versa. After detection of the 100 kHz carrier, the information waveform, with T_2 receiving, is coupled (via a solid state switch) to the lower set of 5 kHz and 25 Hz bandpass filters. When T_1 is receiving, the information waveform is coupled to the upper set of 5 kHz and 25 Hz filters. As discussed earlier, these filters are sufficiently narrow that only the pure frequencies ω_0 and ω_m sinusoidal waveforms are passed.

The digital phase measurements are accomplished by means of passing the above sine waves to zero-cross detectors. In the case of the $\phi_1 - \phi_2$ measurement, the 5 kHz phase difference is digitally measured by means of counting the number of 5 MHz pulses which fit in the time slot equal to the overlap time of the two 5 kHz square waves. In the case of ψ_1 and ψ_2 , these phases are individually measured by counting the number of 5 MHz pulses which fit in the time slot equal to the overlap between each ω_m square wave and a 25 Hz reference square wave. The outputs of the phase measuring system are therefore three counter outputs. Let ΔT , T_1 , and T_2 be the number of counts associated with the $\Delta\phi$, ψ_1 , and ψ_2 measurements, respectively. The counter outputs, scaled down by 2π , are related to the phases as follows:

$$\left. \begin{aligned} \Delta T &= 2.5 \times 10^6 \left(\frac{\Delta\phi}{\omega_0} \right) \left(\frac{\omega_0}{\omega_m} \right) \\ T_1 &= 2.5 \times 10^6 \left(\frac{\psi_1}{\omega_m} \right) \\ T_2 &= 2.5 \times 10^6 \left(\frac{\psi_2}{\omega_m} \right) \end{aligned} \right\}, \quad (8)$$

where the factor of (ω_0/ω_m) has been included in the first of the above equations to take into account the fact that the ΔT count occurs more frequently than the T_1 , T_2 counts by this ratio.

Combining equations (8) and (7), we obtain the equation for diameter averaged flow velocity:

$$v = 1.25 \times 10^4 \left(\frac{D}{\sin 2\theta} \right) \left(\frac{\Delta T}{T_1 T_2} \right) \quad (9)$$

The ΔT , T_1 , and T_2 counts are transferred to the computer at a rate of 25 times per second, and separate "v" computations are made at this rate. After a predetermined statistically large (e.g. 100) number of individual flow (v) computations are made, the statistical mean and the standard deviation among the v's are computed. Chauvenet's criterion^{4,5} gives an optimum deviation from the mean, beyond which a data

point should be considered to be invalid. This criterion depends upon the number of data points as well as the standard deviation. For 100 points, it turns out that (assuming a normal distribution) all points deviating from the mean by the statistical limit of error (3σ) should be disregarded. This criterion is applied to the one hundred accumulated v 's, and a new mean value, \bar{v} , is computed.

After this computation, the sequencing of the switching (Fig. 2) is automatically modified so that the inputs to the 5 kHz filters are reversed. This "configuration change" has the effect of providing a measurement of $|\phi_2 - \phi_1|$, rather than $|\phi_1 - \phi_2|$. If the phase shifts of each of the 5 kHz filters is identical, then of course the two phase measurements will be the same. But, if a difference in phase shift exists between the two filter circuits (including associated zero-cross detectors), an error in velocity measurement will occur. The following operation

$$\overline{\Delta\phi} = 1/2 \{ |\phi_1 - \phi_2|_A + |\phi_1 - \phi_2|_B \} \quad (10)$$

removes the effect of differences in phase shift between these two filters, as long as the (assumed small) phase disparity, $|\delta\phi_2 - \delta\phi_1|$ is less than the magnitudes $|\phi_1 - \phi_2|_A$ and $|\phi_1 - \phi_2|_B$. The product $T_1 T_2$ is unaltered by the configuration change, and the overall cycle time, including all computations, is slightly less than 30 seconds. Therefore, the simple averaging of the measured velocities suffices to null any filter drift. Thus, if "A" and "B" represent the two configurations, the computation of the averaged velocity,

$$\bar{v} = 1/2 (\bar{v}_A + \bar{v}_B), \quad (11)$$

provides the desired result. \bar{v}_A and \bar{v}_B are each independently the result of the statistical analysis already discussed.

Microcomputer:

The computing and data handling functions of the flowmetering system are accomplished with an 8 bit microcomputer which utilizes the well known 8080 CPU chip, along with 7000 words of ROM and 8000 words of RAM.

The software utilizes a priority interrupt routine with data inputs, teletype I/O and power failure all being interrupt driven. The supercompressibility calculation is the normal background program, being replaced by the data processing routines when a complete set of input data has been accepted. A teletype readout routine is provided, and serves the dual function of providing information useful for troubleshooting, as well as detailed short term data analysis. Any of several

output formats is selected by typing a single key. For example, continuously updated arrays of all ΔT , T_1 , and T_2 data and intermediate velocity computations for up to 100 sets in "A" and "B" configurations may be printed. Three LED readouts are provided, each of which can present final and intermediate computations of any one of 38 (thumbwheel) selectable) parameters.

4. Prototype System Fabrication

Figure 3 is a photograph showing the complete electronics package. The portion of the system schematically described in Figure 2 is contained in the four circuit boards in the upper left of the cabinet. All other boards constitute the microcomputer. The power supply is housed at the bottom of the cabinet.

The front panel layout is shown in Figure 4. A resettable electro-mechanical counter can be seen at the upper left. Its function is to integrate the flow velocity, and its unit of output is millions of standard cubic feet. Three LED displays are provided. The thumbwheel switches to the right of these allow any one of 38 different quantities to be displayed, including error codes in case of equipment malfunction or maladjustment of some thumbwheel inputs. The center of the panel contains thumbwheel switches which input the mole percentages of the various gas constituents, while the lower left column of switches input site parameters such as pipe diameter, base temperature and pressure, and gas specific gravity (in case its constituents are not known). The right column of thumbwheel switches inputs the various statistical quantities to be utilized in the automatic data analysis.

Note that the front panel is provided with a lockable door having a transparent window. This provides an element of safety from tinkering by unauthorized personnel.

The electronics package is designed to be housed up to 250 feet from the pipeline.

5. Supercompressibility

Since the important unit of measurement of natural gas flow is standard cubic feet, and since the gas under measurement is at elevated pressure, it is necessary to compute the supercompressibility of the gas in order to provide instrumental readouts in units of standard cubic feet. The computation utilizes the base equation adopted by the American Gas Association.⁶

The computer inputs needed to perform the computation are flowing gas pressure and flowing gas temperature. These are both measured at

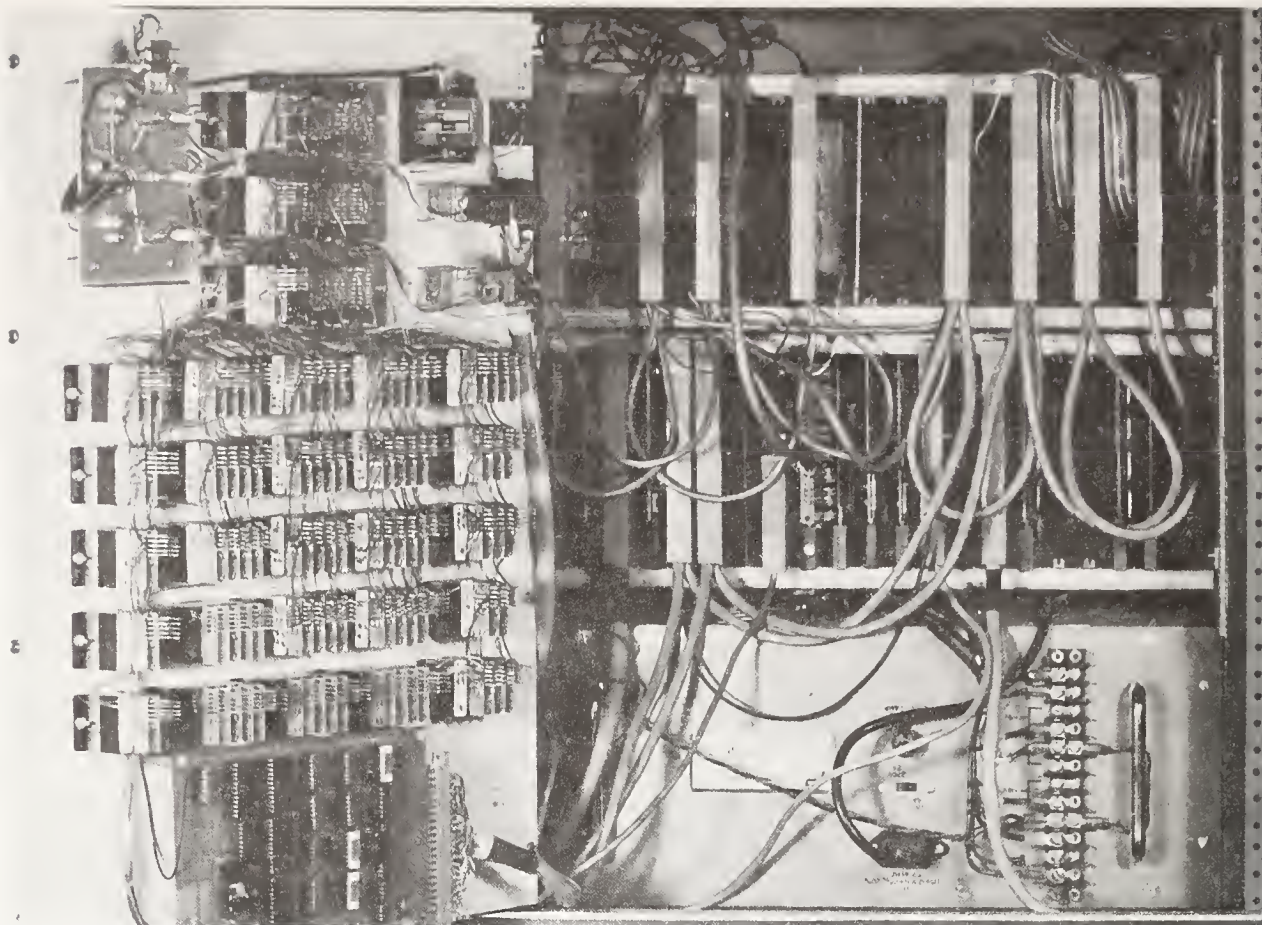


FIGURE 3 ULTRASONIC GAS FLOWMETER ELECTRONICS.

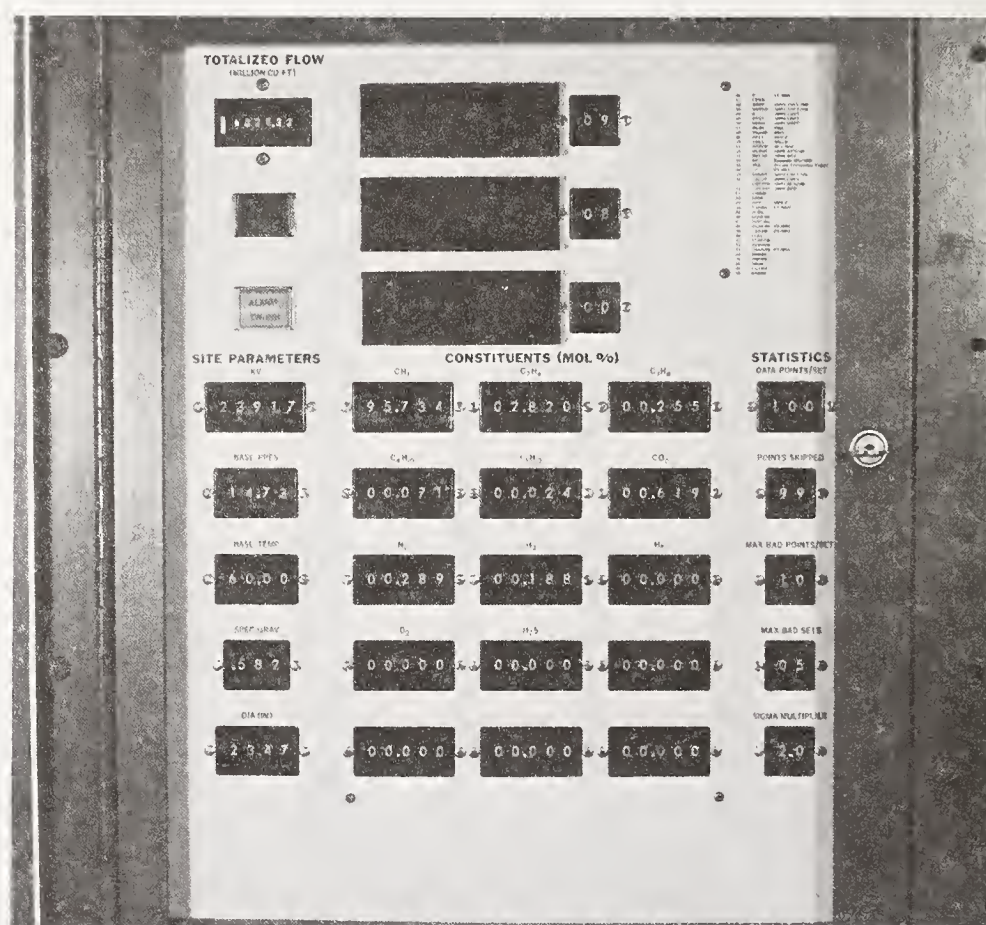


FIGURE 4 ULTRASONIC GAS FLOWMETER FRONT PANEL.

the pipeline just downstream of the ultrasonic transducer locations and appear as DC analog inputs to the microcomputer. Also used in the calculation are the mole percentages of the following gas constituents:

CH_4 , C_2H_6 , C_3H_8 , C_4H_{10} , C_5H_{12} , H_2 , O_2 , N_2 , He, and H_2S .

6. Energy Computation

Since the system depends upon a priori knowledge of the proportions of the above gas constituents, it is a relatively simple task to combine this information with the known energy content (BTU/Std cu.ft.) of each of the constituents, and to thereby provide outputs of energy flow rate and integrated energy flow down the pipeline. If and when reliable on-line gas constituent measurement means become available, the present system could be easily adapted to accept such inputs and thus provide measured energy flow and its time integral.

7. Profile Correction

The correction of the measured diameter averaged flow for velocity profile variations with Reynolds number has not constituted a main objective of the work to date. Instead, the primary objective thus far has been to first provide a flowmetering system having the required stability and reproducibility. The field tests to be described were conducted at fairly constant flowing gas pressure and temperature, the flow rate varied over less than one order of magnitude, and its composition was constant. Therefore, a total variation in Reynolds number of less than one order of magnitude was encountered. Since this represents a very modest perturbation in flow profile at a nominal Reynolds number of 10^6 , a relatively simple correction was utilized. This assumes that the flow can be expressed as

$$v(r) = v(o) \left[1 - \left(\frac{r}{R} \right)^{\frac{1}{n}} \right]^{\frac{1}{n}}, \quad (12)$$

and is the well known Power Law approximation for flow profile. In the above equation, n is determined by the Reynolds number, and varies by about 10% over the measured flow range. Although the merits and deficiencies of the Power Law assumption have been discussed at length, we believe that its use is appropriate under the stated flowing gas conditions.

A calibration program, planned for the near future, will involve comparative measurements between the present system and an orifice station over the entire range of about three orders of magnitude in Reynolds number. Since Reynolds number is directly computed by the flowmeter, it is believed that a comprehensive calibration effort will

provide the profile correction data required for operation under essentially straight pipeline conditions. Effects which must be considered are pipe wall roughness as well as possible perturbations due to the small discontinuities at the pipe wall caused by the ultrasonic transducers.

Should the results of the above measurements demonstrate the need in certain applications of ultrasonic flow measurement over more than one path, this can be mechanically and electronically implemented within the framework of the present design.

8. Insertion Mechanism

The ultrasonic transducer insertion mechanism used in this program is shown in Fig. 5. It consists mainly of stainless steel or nickel plated standard hardware and fittings, and an adapter to the ball valve. It accommodates the required seal-offs and explosion-proof equipment, yet allows for probe rotation and translation adjustments which are useful in the set-up procedure to maximize signals.

9. Ultrasonic Transducer

Requirements include: center frequency, 100 kHz; 3 dB bandwidth, $\pm 5^\circ$; beam orientation, 45° to axis of insertion mechanism or pipe axis; holder O.D. less than ~ 50 mm; center frequency and bandwidth to be retained from -20 to $+150^\circ\text{F}$ and 30 to 1500 psig; means to be included for damping of vibrations potentially induced by shed vortices.

A variety of transducer shapes was fabricated and tested, such as truncated cones, chamfered discs and elliptical discs, in attempts to control and broaden bandwidth by geometrical, non-attenuating means. Since these geometrical approaches did not provide an adequate solution in the available time, a more conventional combination of a radial-mode resonator epoxied to a circuit board disc was used. This combination was silicone-grease-coupled to an epoxy-impregnated graphite impedance-matching disc.

The reason for selecting the radial mode follows. Low-frequency piezoelectric transducers, if operated in the thickness mode, are too large for the present application. However, theory and experience with acoustic emission transducers in the 100 kHz range have shown that cross coupling between radial and axial modes in piezoelectric materials such as PZT enables one to make thick disc transducers in approximately the same diameter as common contact transducers in the megahertz range. The thick disc resonant frequency equation derived by Lucey⁷ is

$$f = N_p / D \left[1 - 1/3 (N_p / N_{33}) (L/D)^2 \right]^{1/2}, \quad (12)$$

where L = length, D = diameter, N_p = planar frequency constant and N_{33} = axial frequency constant. This equation is valid for $0 \leq L/D \leq 0.7$. For a typical PZT element, if $D = 19$ mm and $L = 7.6$ mm, equation (12) predicts $f = 100$ kHz.

10. Field Test Setup

The field tests were conducted at the Alexandria, KY orifice metering station operated by Columbia Gas Transmission Corporation. The facility is a custody transfer station for the Cincinnati, Ohio area and contains ten individual tubes. A photograph of a portion of the facility is shown in Fig. 6.

The ultrasonic flowmeter was housed in a small trailer on the site. The location of the ultrasonic, pressure, and temperature transducers was about 400 ft upstream of the orifice meters. All pertinent pressure and temperature data from the orifice station, as well as profile corrected flow data from the ultrasonic system, are fed to a data logger. This device reads all inputs at approximately 30 second intervals and stores the (digital) records on magnetic tape. In this manner, about three days accumulation of data can be collected before a new tape reel is inserted. The taped data were processed and analyzed with an IBM 370 computer by Columbia Gas System Service Corp. personnel at Columbus, Ohio.

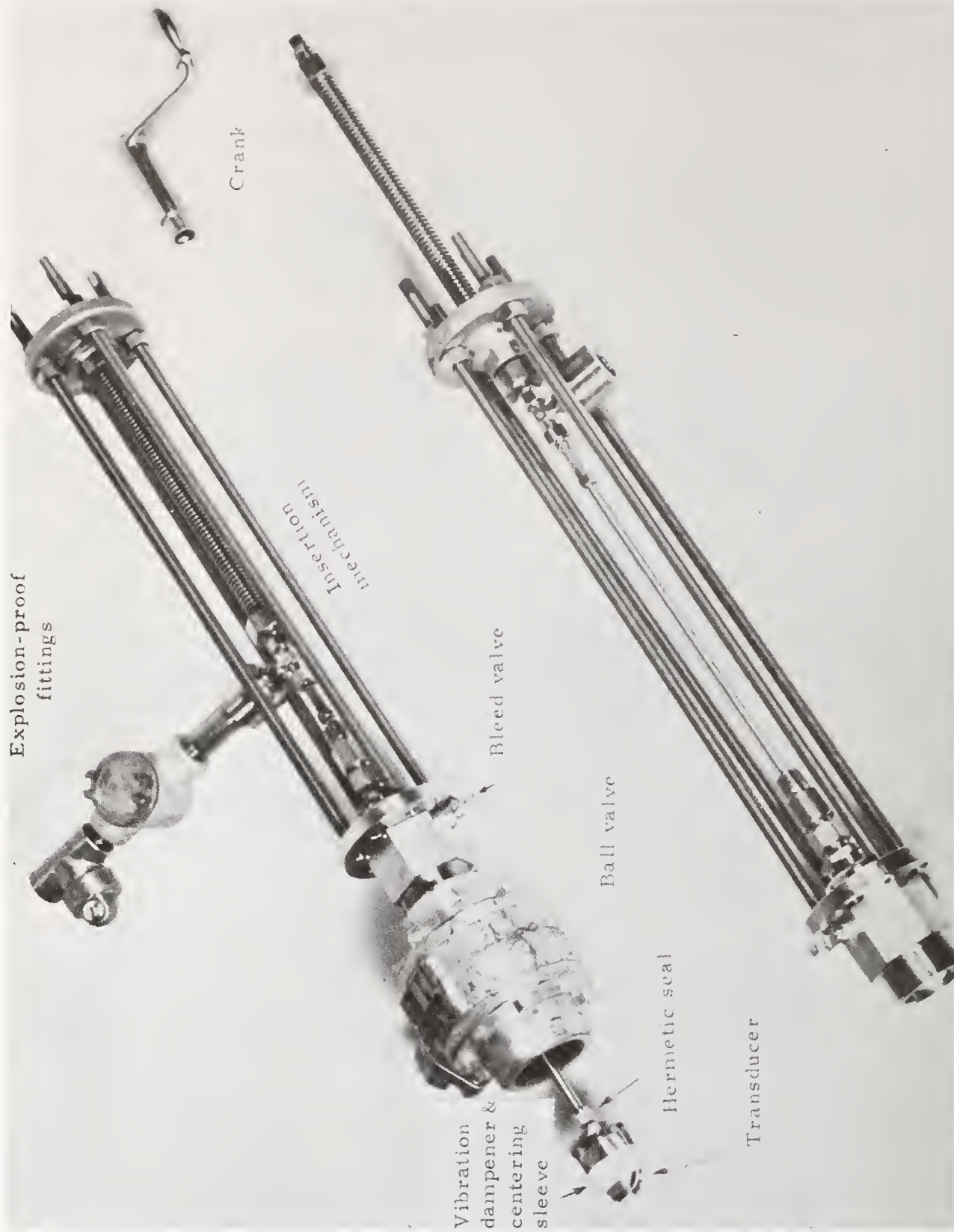
Coaxial cables were used to couple the ultrasonic transducers to the electronics. These were approximately 200 ft in length and introduced an overall attenuation of about 10 dB.

11. Experimental Results

The ultrasonic flowmetering system, as delivered to the test site, was uncalibrated. The purpose of the tests at Alexandria was to determine the short term and long term tracking between the ultrasonic meter and the orifice meter. However, since the outputs of both meters were simultaneously recorded on magnetic tape and computer processed, it was a relatively simple matter to use a small portion of the comparative data for the purpose of calibration of the ultrasonic meter, and to treat the remainder as experimental data. This was done for two consecutive periods. Each period was approximately 65 hours in duration and included more than 8000 individual measurements of flow velocity.

The ultrasonic system calibration was done under the assumption that the meter has linear response, but that there may be a zero offset and a slope error. These potential errors are taken into account by means of experimentally determining the values of K_1 and K_2 in the

INSERTION MECHANISM



Ultrasonic transducer, insertion mechanism for use on hot-tapped 24" pipe, and explosion-proof hardware. Designed and fabricated by Panametrics in 1976 to measure flow of natural gas at pressures ranging up to 1500 psig. Tested in 1976 at ~ 500 psig, $\sim 55^{\circ}\text{F}$, $\lesssim 10$ to $\gtrsim 20$ ft/s natural gas flow velocity.



FIGURE 6 **ORIFICE MEASUREMENT STATION, ALEXANDRIA, KY.**

following equation

$$V'_p = V_p(1 + K_1) + K_2, \quad (13)$$

where V_p and V'_p are the uncorrected and corrected flow velocity readings, respectively. The values of K_1 and K_2 for the two above mentioned ~65 hour periods are given below:

First Period

$$\begin{aligned} K_1 &= 0.1603 & \bar{\epsilon} &= -0.16\% \\ K_2 &= 0.1343 \text{ ft/sec} & N &= 8100 \end{aligned}$$

Second Period

$$\begin{aligned} K_1 &= 0.1792 & \bar{\epsilon} &= 0.061\% \\ K_2 &= 0.0059 \text{ ft/sec} & N &= 8178 \end{aligned}$$

In the above, $\bar{\epsilon}$ is the percentage of full scale difference between the orifice data and the corrected ultrasonic data over the interval of N data points. Thus,

$$\bar{\epsilon} = \frac{\sum_{n=1}^N V_o - \sum_{n=1}^N V'_p}{30} \times 100 \quad (14)$$

where V_o = flow velocity measured by the orifice meter.

The factor of $100/30$ is introduced because the full scale output is 30 ft/sec and $\bar{\epsilon}$ is expressed as percent of full scale.

It should be noted that $\bar{\epsilon}$ represents the agreement between the two integrated flowmeter readings over each 65 hour period, following on-site calibrations. We consider the first value $\bar{\epsilon} = -0.16\%$ to be reasonable, considering the long integration period. However, the second value $\bar{\epsilon} = 0.061\%$ is probably not representative of the instrumental stability, reproducibility, or linearity. Rather, this small a variation must be considered the result of a lucky choice of calibration point sets.

To get an estimate of the shorter term statistical deviations between the two flowmeters, the two above data sets were each divided into sets of 1000, 100, 10, and single points, and the standard deviation of the average of each of these point sets was computed. The standard deviations were relative to the orifice station. The results are

plotted in Fig. 7. The data for the Second Period are more representative of the instrumental stability, since we have already shown that $\bar{\epsilon}$ for that period is vanishingly small. Therefore, the standard deviations for the second period do not include any significant calibration error. (The σ 's of the First Period include a calibration error which results in an offset of 0.16%, and the σ 's would therefore be expected to be somewhat higher than those of the Second Period.)

A direct comparison between (5 minute averaged) computed flow velocity readouts of the ultrasonic and orifice meters is shown in Fig. 8. This particular segment was chosen because of the abrupt 2:1 change in flow velocity. Also plotted in the figure are the differences (% of full scale) between the two meter readouts.* The abruptness of the above change in flow is further exemplified in Fig. 9, which is a direct comparison between the 30 second averaged flow velocity readouts of the two meters.** Note that the statistical fluctuations in the data are somewhat greater than those of Fig. 8. This is because the data of Fig. 8 have been averaged over 5 minutes, while the data of Fig. 9 are taken at 30 second intervals. We are virtually certain that the observed short term (30 second) fluctuations are the result of the very short term (~ 40 millisecond) fluctuations due to turbulence. The short term fluctuations of the electronics system, as measured in the laboratory, was of the order of 0.02% of full scale. Although such a discontinuous change in flow velocity is rare in occurrence, these data segments were chosen for presentation for the purpose of demonstrating the tracking between the two flowmeters.

Finally, we present the (100 point averaged) data representing the two entire ~ 65 hour periods. These are shown in Figs. 10 and 11. The large ($\sim 4:1$) excursions in flow velocity are due to the periodic daily energy demand variations of the city of Cincinnati.

12. Discussion

It is important to stress the fact that the calibration of the ultrasonic flowmeter was done at the test site and utilized data from the orifice meter. Therefore, the agreement between the two measurements cannot be interpreted in terms of absolute accuracy. It should also be pointed out that the time duration between "calibration" and "test" data was in no case more than about 65 hours.

*Note that $\pm 1\%$ of full scale corresponds to ± 0.3 ft/sec in flow velocity.

**It should be noted that, although nearly perfect tracking is evident in the data shown, two other similar abrupt flow changes (< 30 seconds) did not demonstrate such good tracking.

STANDARD DEVIATION OF DATA SETS VS. INTEGRATION PERIOD

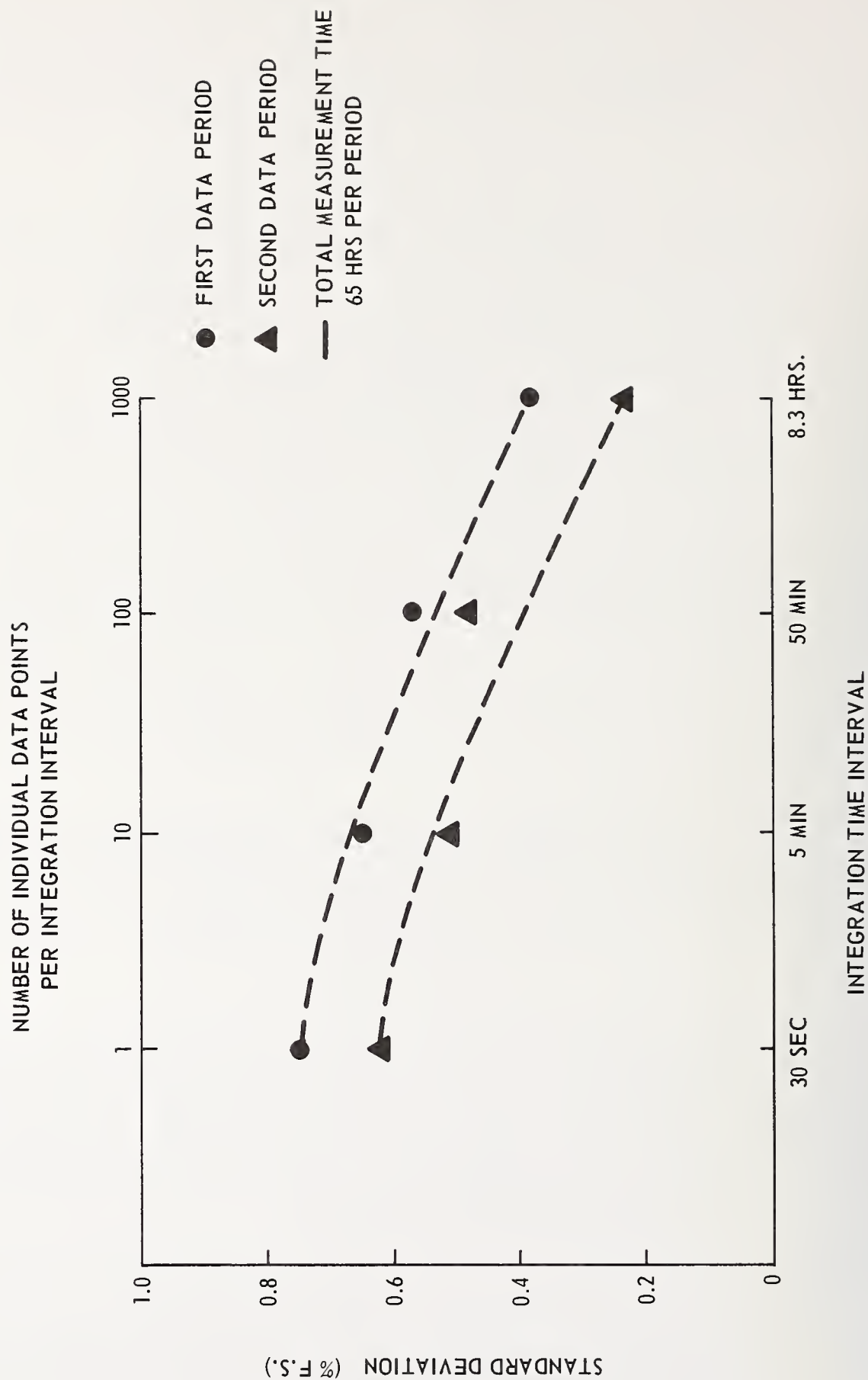


FIGURE 7

COMPARISON OF ULTRASONIC AND ORIFICE METER READINGS 10 POINTS AVERAGED DATA (5 minute)

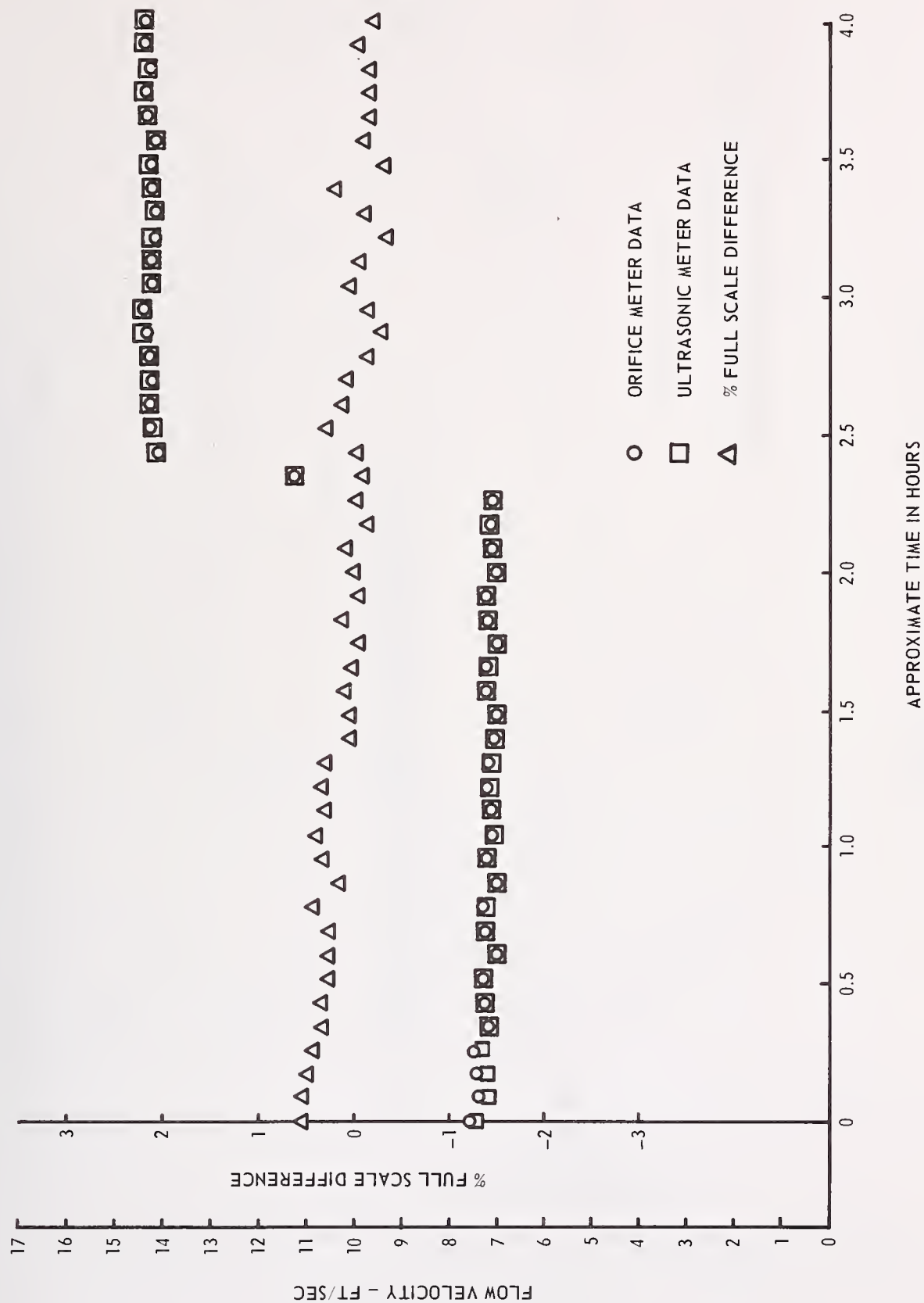


FIGURE 8

COMPARISON OF ULTRASONIC AND ORIFICE METER READINGS SINGLE POINT DATA (30 second)

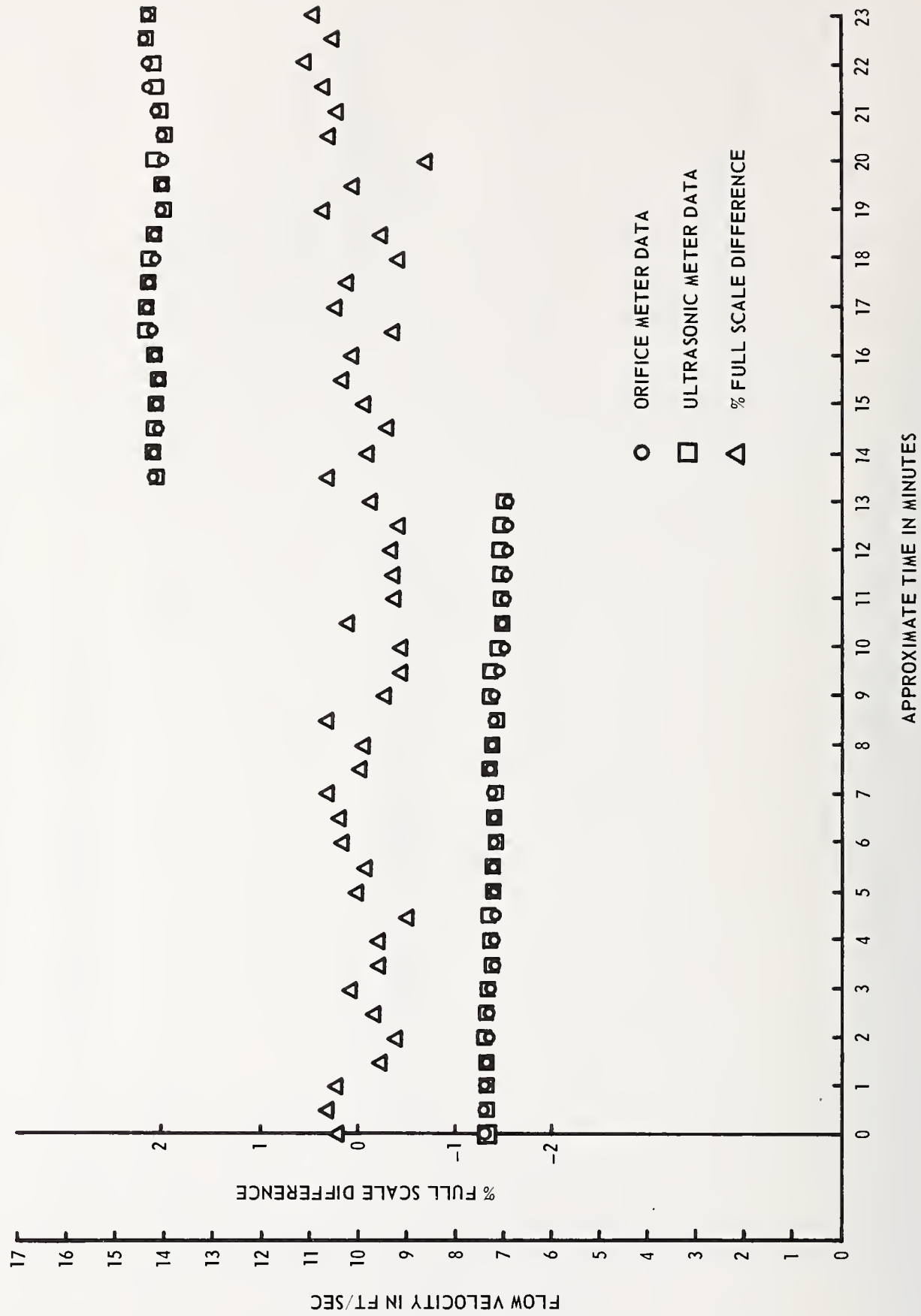


FIGURE 9

COMPARISON OF ULTRASONIC AND ORIFICE METER VELOCITIES TEST PERIOD NO. 1 100 POINT AVERAGED DATA (50 min)

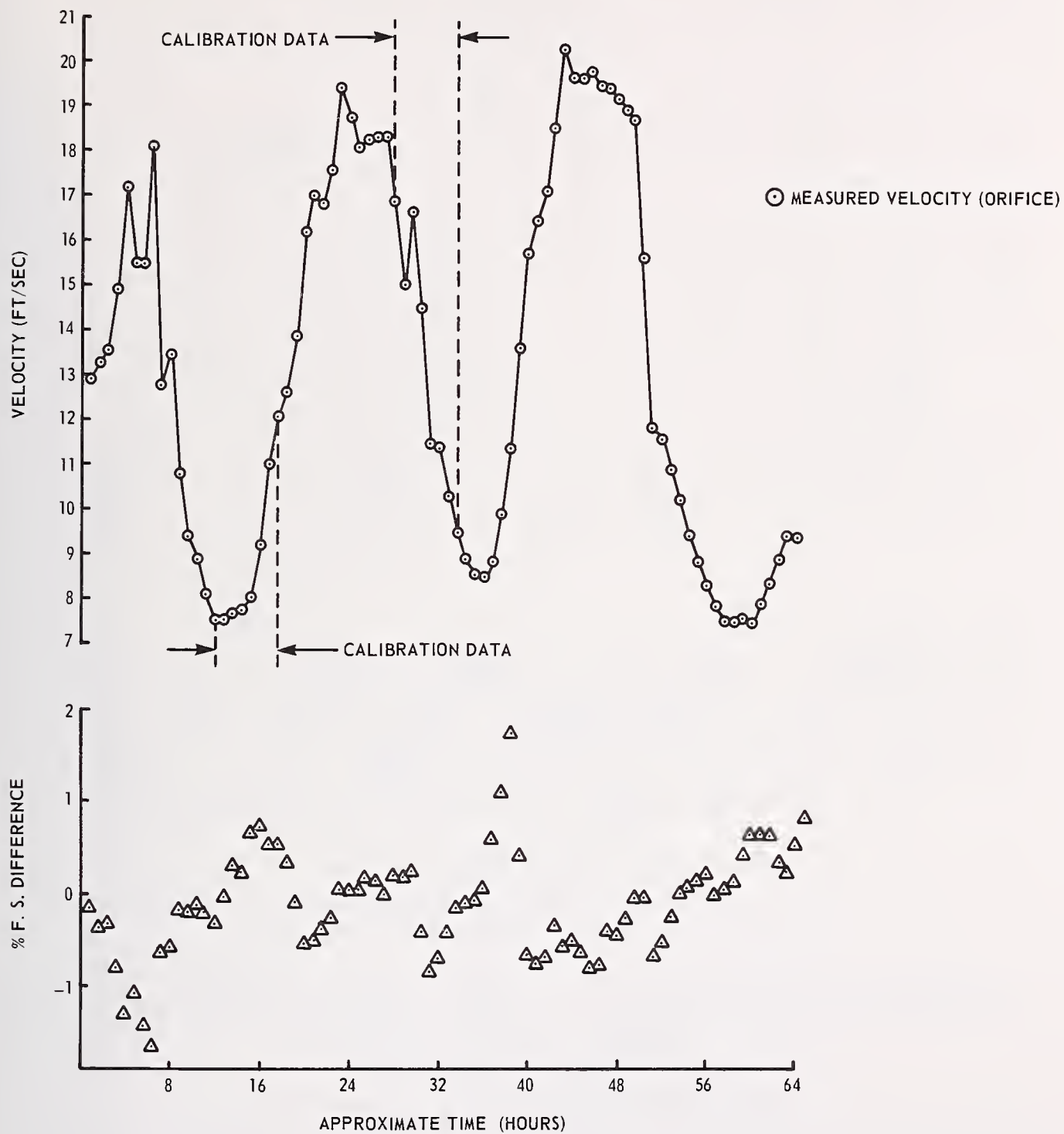


FIGURE 10

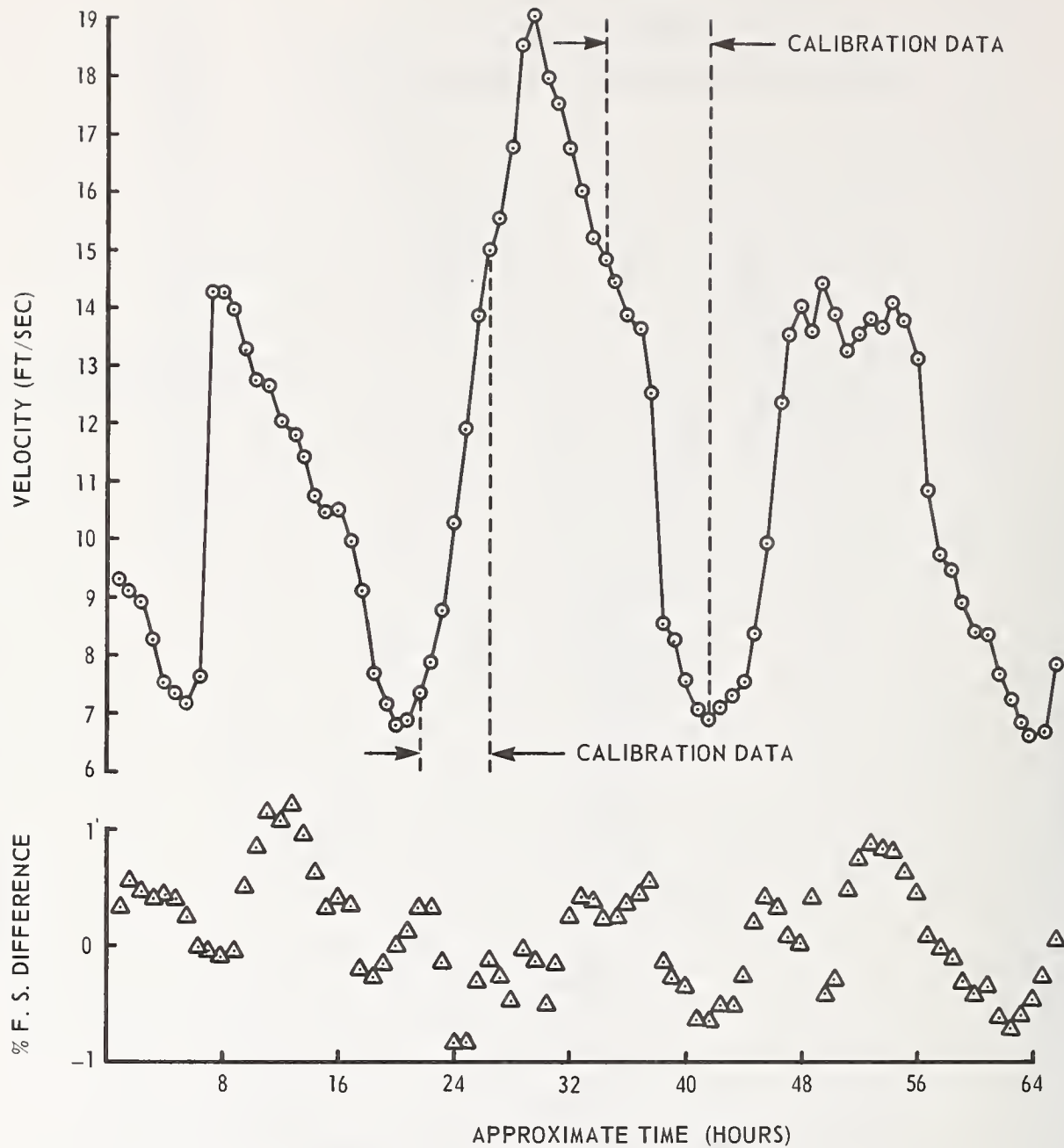


FIGURE 11

**COMPARISON OF ULTRASONIC AND ORIFICE METER VELOCITIES
TEST PERIOD NO. 2
100 POINT AVERAGED DATA (50 min)**

The conclusions which one can draw from the above results are the following:

1. With on-site calibration, the ultrasonic gas flowmetering system has demonstrated a potential overall accuracy of about $\pm 0.4\%$ of full scale (standard deviation) over an integration period of one hour, and of about $\pm 0.25\%$ of full scale over an integration period of between 8 hours and 65 hours.
2. Long term stability over periods of weeks and months has not yet been demonstrated. A calibration program planned for the near future will provide numerical results in this regard.
3. The tracking agreement between the ultrasonic and orifice flowmeters was demonstrated to be very good over integration periods of 30 seconds and five minutes. It appears as though local turbulence was the limiting factor in this agreement, and gave rise to relative measurement fluctuations of the order of $\pm 0.6\%$ of full scale (± 0.18 ft/sec) for a 30 second integration period, and about 0.5% (± 0.15 ft/sec) for a 5 minute integration period. Since these (assumed random) local fluctuations appear at both meter locations, we could attribute the effects due to local turbulence of about ± 0.13 ft/sec and ± 0.10 ft/sec for the two time periods, respectively.
4. Velocity dependent changes in flow profile were compensated adequately by assuming the well known Power Law flow profile, and making the appropriate Reynolds number dependent correction in the single path integrated flow velocity measurement. The necessity and/or desirability of using multiple cords will be another subject of study in the calibration work.
5. Modifications to the present ultrasonic flowmeter are underway to improve its temperature stability, as well as the phase measurement accuracy. A second system is presently being fabricated and will include these improvements. An improved ultrasonic transducer is also under development and is expected to result in a low pressure limit of less than 50 psig.

13. Acknowledgments

A large portion of this work was supported by Columbia Gas System Service Corporation. In addition, significant technical contributions were made to the program by Mr. James Hager,* Mr. William Munk, and Mr. Richard Colburn, all of Columbia Gas System Service Corporation. The contributions of Mr. Ken Fowler and Mr. Dana Patch in the transducer development are also acknowledged.

* Mr. Hager is presently with McFadden Sales, Inc., Columbus, Ohio.

14. References

1. E. Moffatt and K. Fetterhoff, "Large Volume Flow Measurement by Sonic Techniques", Proc. A.I.P. Symposium on Flow, Pittsburgh, PA, May, 1974.
2. F. B. Cook and E. M. Moffatt, "Flow Meter for High Pressure Gas Using Sonic Pulses", Proc. I.S.A. Conference, New York, NY, October 1974.
3. N. E. Pedersen, L. C. Lynnworth, J. E. Bradshaw, "Improved Ultrasonic Fuel Mass Flowmeter for Army Aircraft Engine Diagnostics", USAAMRDL TR-75-8, June 1975.
4. Y. Beers, "Theory of Errors", Chap. 7, Addison-Wesley Publishing Company, Reading, MA, 1953.
5. W. Price, "Nuclear Radiation Detection", Chap. 3, McGraw-Hill Book Company, New York, NY, 1958.
6. A.G.A. Gas Measurement Committee Report No. 3, "Orifice Metering of Natural Gas", 1955, 1956.
7. G. K. Lucey, Jr., Resonant and Antiresonant Frequencies of Thick Discs and Thick Rods, J. Acoust. Soc. Amer. 43(6), 1324-1328 (May 1968).

A NEW NON-INTRUSIVE FLOWMETER

R. S. Flemons

Canadian General Electric Co. Ltd.
Peterborough, Ontario
Canada K9J 7B5

A new type of flowmeter is described which can be clamped to the outside of existing pipes and can measure liquid velocity without calibration. Two diametral ultrasonic beams are used to interact with the liquid and to detect passage of inherent tracers such as turbulent eddies. Cross-correlation analysis is used to determine the transit time of the eddy pattern and thus the liquid velocity. The operating principles of the signal processing electronics and the digital cross-correlator are outlined. Comparisons with accurate gravimetric flow measurements and field applications are briefly described.

Instruments to measure fluid flow have a long history of development and application. In spite of this they possess limitations which can seriously limit their suitability for use in many situations. This situation was encountered in 1971 with conventional instruments installed on a Heavy Water separation plant, where the process fluid is an extremely corrosive and toxic solution of Hydrogen Sulphide. The high cost of shutting down the plant to check and replace the flowmeters forced an assessment of alternative measuring systems. All systems known to us at that time required penetration of the piping, which introduced potential leak sites and exposed the instruments to deterioration from the corrosive fluid. In addition, routine inspection and calibration of the primary elements entailed shutting down the plant to gain access to the exposed parts. This resulted in a serious loss of production and an increased possibility of leakage of the toxic fluid.

The work of Dr. M.S. Beck and his colleagues at the University of Bradford, England [1] suggested that using a combination of ultrasonics to interact with the liquid through the pipe walls and a cross-correlation analyser to determine the liquid transit time, a new type of flowmeter might be developed with none of these limitations. The development of a practical instrument of this type was carried out by Canadian General Electric with technical support from Dr. Beck and later with financial assistance from Atomic Energy of Canada Limited.

The transducers* of the ultrasonic cross-correlation flowmeter (USCCFM) may be clamped to the outside of existing pipes ranging from 4 to 30 inches O.D. Pipe wall thickness and material impose no problems because the ultrasonic energy propagates across a pipe diameter and is not refracted at the pipe wall. Since one set of transducers may be used on all sizes of pipe, the instrument is particularly attractive for use on large pipes where the installed cost of conventional instruments is often very high. The range of flows which may be measured is indicated in the following table.

Pipe Size	4"	8"	16"	30"
Flow Range (USGPM)	25 - 500	200 - 4,000	800 - 13,000	8,000 - 80,000

With some minor modification these ranges can be somewhat extended.

Installation is rapid and inexpensive. Pipe preparation is confined to removing loose paint or scale from the outer surface. Since the pipe wall is not penetrated there is no leakage hazard and the process fluid cannot corrode or erode the sensors. Calibration is never required since the instrument simply measures fluid transit time over a known distance. For the same reason the instrument accuracy is unaffected by changes in fluid properties such as temperature, density and viscosity. Fluid conditions such as turbulence and traces of gas or particulate matter, which often cause errors in other instruments, form the signals which are utilized by the USCCFM. Long straight pipes upstream are not required, in fact the preferred location is within 5 pipe diameters of an elbow.

Relationship to the Ultrasonic Travel Time Difference Meter

At the time this development started (1971) we were not aware that a form of the ultrasonic travel time difference meter [2] had been developed in which the transducers are placed on the outside of a pipe wall [3]. Since this meter may appear to be similar to the USCCFM, it is important to contrast the principles of operation. The travel time difference meters send ultrasonic energy through the flowing fluid in two directions. The effective propagation velocity of energy travelling in the direction of fluid flow is the sum of the sonic velocity and the fluid velocity, whereas for energy travelling against the fluid flow the effective propagation velocity is the sonic velocity minus the fluid velocity. By comparing the ultrasonic transit time in the two directions, the average fluid velocity may be determined. Since the sonic velocity is far greater than normal flow velocities the fractional changes are small and sophisticated electronic circuits are required to achieve precise fluid velocity measurements.

* In this paper, "transducer" means simply an element which transforms electrical to acoustic energy, or vice versa. This transducer is not a calibrated component which affects the accuracy of the instrument.

The form of the travel time difference meter in which the transducers are mounted on the outside of the pipe has another feature which distinguishes it from the USCCFM. As is apparent from the operating principle outlined above, it is ultrasonic energy propagating in the direction of the pipe axis which is affected by the fluid velocity. To provide a component of energy flow in this direction, the ultrasonic beams are sent diagonally across the pipe. This causes the beams to be refracted at the interfaces between the transducers and the pipe wall and between the pipe wall and the liquid. The angle of refraction is a function of the liquid properties and of the pipe wall material and thickness. For this reason the transducer system has to be carefully designed to match pipe and liquid parameters.

Interaction of the Ultrasonic Beams with the Flowing Liquid

The operating principle of the USCCFM is illustrated in Figure 1. Two continuous-wave ultrasonic beams are directed diametrically across the pipe at locations spaced a known distance apart, typically between $\frac{1}{2}$ and 2 pipe diameters. As in the case of the travel time difference meter the sonic propagation is affected by velocity although in this case it is the transverse velocity components of turbulent eddies that are of interest. The eddy represented in Figure 1 will first accelerate and then decelerate the upstream beam. It will be swept downstream by the fluid flow and will then produce a similar effect on the second beam. In each beam the eddy pattern interacts with the ultrasonic wave causing its phase to be disturbed or "modulated".

Arrangement of Ultrasonic Transducers

The ultrasonic energy is generated by a simple thickness-mode piezo-crystal which is supported in a cylindrical mount and pressed against a silicone rubber coupling block. The coupling block is in turn pressed against the pipe wall. A drop of heavy silicone oil is used on both surfaces of the block to exclude air from the interface. Identical crystals and mounts are used to receive the ultrasonic energy on the opposite side of the pipe.

Figure 2 shows the mounting arrangement. The cylindrical mounts containing the crystals are supported normal to the pipe surface and confined by the white nylon caps shown surrounding the coaxial connectors. Rotating the caps advances the cylindrical mounts and presses the coupling block against the pipe surface. The only critical dimension is the spacing in the direction of the pipe axis between the upstream and downstream pairs of transducers. This is established by four spacers which link the pairs of mounts. Longer spacers are used when the mounts are used on larger pipes.

Figure 3 shows a block diagram of the signal circuits. The upstream and downstream channels are identical up to the point where their signals are fed to the correlator. Each has a low power sinusoidal oscillator operating between 0.7 and 1.5 MHz at 1 watt level. Coaxial cables, which can be at least 100 feet long, couple the oscillator to the transmitting transducer. Similar cables couple the receiving transducers to a broad-band R.F. amplifier which presents amplitude-limited square waves to a synchronous demodulator. The received R.F. signals are normally about 0.1 volt, although the amplifier will provide full limiting for signals of 1 mV.

The phase demodulator consists of two balanced mixers which are synchronized by direct and quadrature signals from the associated transmitting oscillator. Four output signals are generated which are direct and inverted sine and cosine functions of the instantaneous phase difference between the transmitted and received signals. A selector circuit chooses the signal having a suitable polarity of change-of-voltage with respect to the change-of-phase-delay. Voltages so selected are fed via a high pass filter to the correlation analyser from each of the upstream and downstream channels. The selector circuit overcomes the ambiguity caused by the large and somewhat unstable phase delay (typically 50,000 degrees) which exists in each ultrasonic transmission path. Note that a complete set of electronics from oscillator to selector is provided for each channel. To avoid interference the two oscillators operate on slightly different frequencies.

The signals fed to the correlator from the demodulators are low frequency random voltages which are replicas of the phase modulation imposed on the ultrasonic beams by the passage of turbulence patterns through them. There is a significant probability that a pattern which intercepts the upstream beam will also intercept the downstream beam. Therefore the output signals from both demodulators will contain similar voltage variations but the voltage pattern from the downstream channel will tend to lag in time by an amount corresponding to the transit time of the turbulence patterns between the beams. It has been found that this closely corresponds to the liquid transit time.

Although turbulence patterns have been found to be the source of most of the phase modulation, similar modulation is produced by minute variation of temperature and density which also travel at the liquid velocity.

The Basic Cross-Correlation Analyser

In the initial development stages of the USCCFM, the demodulated signals were fed to a Hewlett Packard 3721A Correlation Analyser [4] which displayed the signal delay time as a peak position on an oscilloscope. Although this instrument was invaluable for circuit

development, its size, cost and the lack of an electrical output representing peak position made it impractical as a component of an industrial flowmeter.

It has proved possible to build a correlator on four 4" x 6" circuit cards which provides a continuous readout of flow velocity and other features suitable for use in a flowmeter. The operating principle is indicated in Figure 4. The demodulated analogue signals from the upstream and downstream channels are applied to zero-crossing detectors which generate binary pulse trains, indicating the instantaneous polarities of the signals. The serial pulse train derived from the upstream signal is applied to a serial-in parallel-out shift register where it is shifted under control of a sampling clock. At each output a serial pulse train appears which duplicates the input pulse train delayed in time by a known amount. Each of these outputs is applied to a separate binary multiplier where it is compared with the non-delayed pulses derived from the downstream signal.

If both inputs to a multiplier are truly random, its output will be in the 0 state as often as in the 1 state. If both inputs are always coincident, the multiplier output will always remain in the 1 state. For lesser degrees of coincidence, the 1 state will predominate to a degree which indicates the degree of coincidence (or correlation) between the multiplier inputs. Each multiplier feeds a separate multi-bit binary counter which fills to capacity (i.e. overflows) at a rate dependent upon the proportion of 1's at its input. Since all counters are reset to zero whenever one overflows, the ordinal position of the counter which overflows indicates the channel where the greatest correlation exists. The upstream signal applied to this channel has been delayed by a time which is determined by the number of shift register stages multiplied by the time delay per stage, i.e. the product of the ordinal position of the channel, multiplied by the period of the sampling clock. Since this delay produced the maximum correlation with the downstream signal, it corresponds to the travel time of the fluid between the ultrasonic beams.

This basic principle has been used in a number of cross-correlation analysers [4,5]. To enable such an analyser to be constructed economically, a LSI chip was developed at the University of Edinburgh which contains a 12 stage shift register with corresponding multipliers, counters and auxiliary circuits which determine the overflow position. The correlator which forms part of the USCCFM uses 5 such chips, which largely accounts for its compact form.

Features of the Correlator used in the USCCFM

The conventional cross-correlation analyser described above is not very suitable for use in a flowmeter. One problem is due to the discrete steps of delay time represented by the successive output of the shift register. Particularly for short delay times, adjacent steps

can differ by a large fractional amount. Another undesirable feature is that the output is in terms of delay time which is the reciprocal of the desired output, flow velocity. To overcome these problems, the frequency of the sampling clock has been made variable and is servo-controlled to hold the average overflow position constant, in a chosen channel. If the overflow actually occurs in a lower numbered channel (indicating a time delay which is too short) the clock frequency is increased so that each stage of the shift register represents a shorter delay and more stages are required to match the transit delay. If the overflow occurs in a higher numbered channel the opposite control action occurs and the clock frequency is lowered until the overflow occurs in the chosen channel. If the flow velocity changes, the instrument adjusts the clock frequency to follow the changing transit delay. The control loop is an analogue circuit with integral feedback, providing a continuously variable clock frequency with infinite resolution and avoiding the discrete steps of the overflow channels. Since the clock frequency is inversely proportional to the delay in the shift register, the readout can be easily made directly proportional to flow velocity. The time delays provided by the overflowing counters and by the integral servo feedback provide smoothing of the statistical nature of the delay measurement.

Of course many auxiliary circuits are necessary in such an analyser which will not be explained in detail. One such circuit gives the correlator the ability to recognize and lock-on to correlatable signals. Another circuit determines the degree of correlation between the inputs (or the cross-covariance) and indicates to the operator the quality of the signals. Three types of output are provided; a pulse train related to the sampling clock frequency which is directly proportional to the flow velocity, a digital readout of the sampling clock frequency measured against a crystal controlled standard and a scaleable, isolated analogue current output suitable for interconnection with conventional plant instrumentation.

Sources of Measurement Error

An important feature of the USCCFM is that it measures flow velocity in terms of two fundamental quantities, T , the time required for the fluid to travel d , the distance between the two beams. The velocity $v = d/T$. Thus the instrument does not depend upon or require calibration. If volumetric flow Q is required, the pipe area A must be determined and $Q = \frac{dA}{T}$. Mass flow, of course, entails multiplying by the fluid density.

The beam separation d is set by the mechanical construction which introduces a negligible uncertainty, and by the acoustic symmetry of the transducers which is estimated to be ± 2 mm. At the minimum value of d (0.1 m) used on small pipes this could introduce a $\pm 2\%$ error. It becomes proportionally less on larger pipes.

The pipe area A may be calculated as

$$\pi/4 \{(\text{circumference}/\pi) - 2 \times \text{wall thickness}\}^2$$

(If the pipe is out-of-round, the circumference measurement effectively averages the O.D.). Permissible thickness variations from handbook values for standard pipes can cause a 3% error in the calculated area. It is preferable to measure the wall with an ultrasonic thickness gauge which will probably reduce the error in area to 1% or less.

The error in determining the transit delay T has several components. The time delay in the shift register is obtained by measuring the frequency of the sampling clock which can easily be done with negligible error. The factors which relate this time delay to T are more difficult to assess. It can be shown mathematically, and we have demonstrated in practice that, on the average, the time delay which produces the maximum number of coincidences in the multipliers corresponds to the time delay inherent in the signals from the two receiving transducers, providing that the bandwidth and phase response of the two electronic channels are identical for the correlatable components of the signals. The use of a simple polarity-correlator does not affect this relationship (5,6).

Because of statistical scatter due to both the axial velocity of the turbulence patterns and presence of uncorrelated noise in the signals, there is a variance in the measured flow rate. This can be reduced by increasing the averaging time at the expense of response time. The averaging time is adjustable and an acceptably steady output can usually be obtained with an averaging time in the order of 10 seconds.

The other factor which affects the relationship between the measured time delay and the average liquid velocity is the flow profile. The meter measures the average velocity across a diameter of the pipe whereas the volumetric flow is proportional to the average velocity integrated over the pipe area. The error due to this cause has been calculated by Birger [7] for the ultrasonic travel time difference meter in fully developed turbulent flow. His analysis also applies to the USCCFM. It is presented in Figure 5 as a flow coefficient k, which is a weak function of Reynold's number. True flow is k times the indicated flow.

In practice, the USCCFM has been found to operate better in a more turbulent flow than the "fully developed" condition. A suitable location is about 5 diameters below an elbow. This additional turbulence flattens the velocity profile somewhat and the effective value of k differs slightly from Birger's calculations. The effective value as determined by our laboratory calculations is indicated by a broken line in Figure 5. Since the flow near an elbow has a somewhat uncertain velocity profile a further error source is introduced probably amounting to +2%.

The error sources are independent so it is reasonable to combine them as a root-sum-square. Taking as an example an 8 inch pipe with measured wall thickness

Maximum error in d +1%

Maximum error in A +1%

Maximum error in k +2%

Net maximum error $(2^2 + 1 + 1)^{\frac{1}{2}} = 2.4\%$

No allowance has been made for statistical scatter since it is assumed the averaging time is long enough to make this negligible.

Laboratory Tests of System Performance

To investigate the instrument performance a series of careful comparisons has been made between flow as measured by prototype USCCFMs and as determined by precise mass/time measurements. The first such tests were conducted at the hydraulic laboratories of the National Research Council in Ottawa, Canada, before the correlation analyser section of the instrument was designed. The transit times were measured with a Hewlett Packard 3721A Correlator. These tests demonstrated the ability of the ultrasonic, signal electronics and demodulation systems to produce correlatable data without introducing erroneous time delays. A scatter in the value of k of up to +0.04 from Birger's value was observed in tests covering a wide range of flow conditions. This included the human error in reading the delay time from the oscilloscopic display, which is not a problem with the present instrument.

A more recent series of tests at the Chalk River Nuclear Laboratories of AECL, using the final form of the instrument with its own correlation analyser and digital readout of flow velocity, has shown that accuracies of +0.02 (2%) of the measured value (at 1 σ limits) can be maintained over a 10 to 1 range of flow without adjustment. A full report of these tests is in preparation [8]. This performance is particularly encouraging when it is realized that there are no calibrated transducers or other sources of progressive deterioration in the system. The linear response and the fact that accuracies do not have to be expressed in terms of the full scale value are also advantages.

Field Experience

The instrument has been used on numerous occasions at Heavy Water production plants at Port Hawkesbury, Nova Scotia and Tiverton, Ontario. Since these plants are built out-of-doors to avoid possible concentration of toxic Hydrogen Sulphide in confined areas, the conditions of application are often very difficult, entailing rain, snow and difficulties of access. It has been demonstrated that the meter can be installed in a new location and measure flow within an hour or two even in adverse conditions. In these locations, comparisons were made with plant instrumentation. In all cases the measurements agreed within the likely uncertainties of the existing instruments.

On another occasion the instrument was used to investigate the partitioning of flow in a part of the moderator system during commissioning of the Bruce Nuclear Generating Station. The only accessible measuring locations were short pipes between valves and other sources of flow disturbance. Nevertheless, useful measurements were obtained which enabled modification of the hydraulic design.

Summary

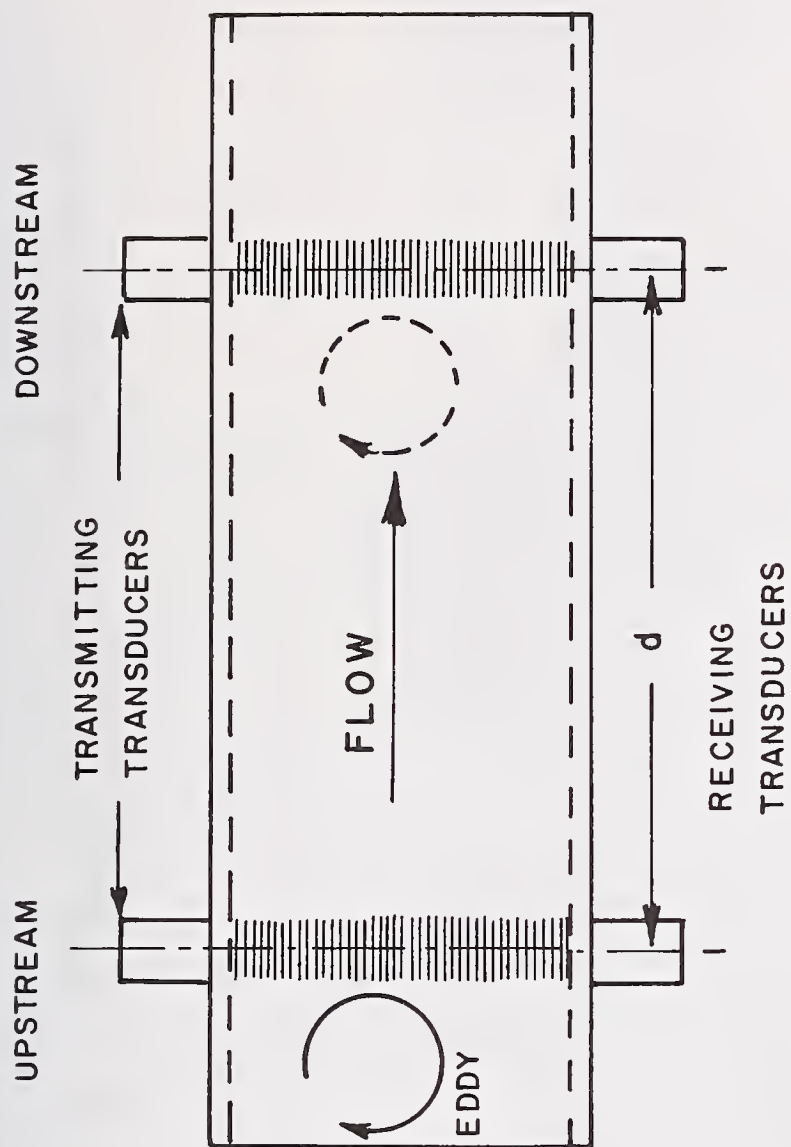
The USCCFM utilizes an old principle of flow measurement, that of timing the passage of a tracer a known distance along a flow path, but it does this in a new way. The tracer used is the inherent turbulence pattern present in fast flowing liquid. The tracer is monitored from the outside of existing piping without penetration. A compact correlation analyser is used to continuously determine the transit time of the tracer pattern and provide a real-time readout of flow in velocity, volumetric or mass units. Because of the use of the tracer principle, calibration is not required and a small correction for velocity profile provides sustained accuracies of $\pm 2\%$ of the reading over a 10 to 1 range of flow in a given location. The existing hardware can be applied to pipes ranging from 4 to 30 inches, which accommodate a flow range from 25 to 80,000 USGPM.

Acknowledgements

The author wishes to acknowledge the contributions to this development made by Dr. M.S. Beck and Dr. C.N. Wormald of the University of Bradford, Dr. K.J. Serdula of AECL Chalk River, Ontario, the staffs of the Port Hawkesbury and Bruce Heavy Water Plants and of his colleague Mr. D.L. Freeman.

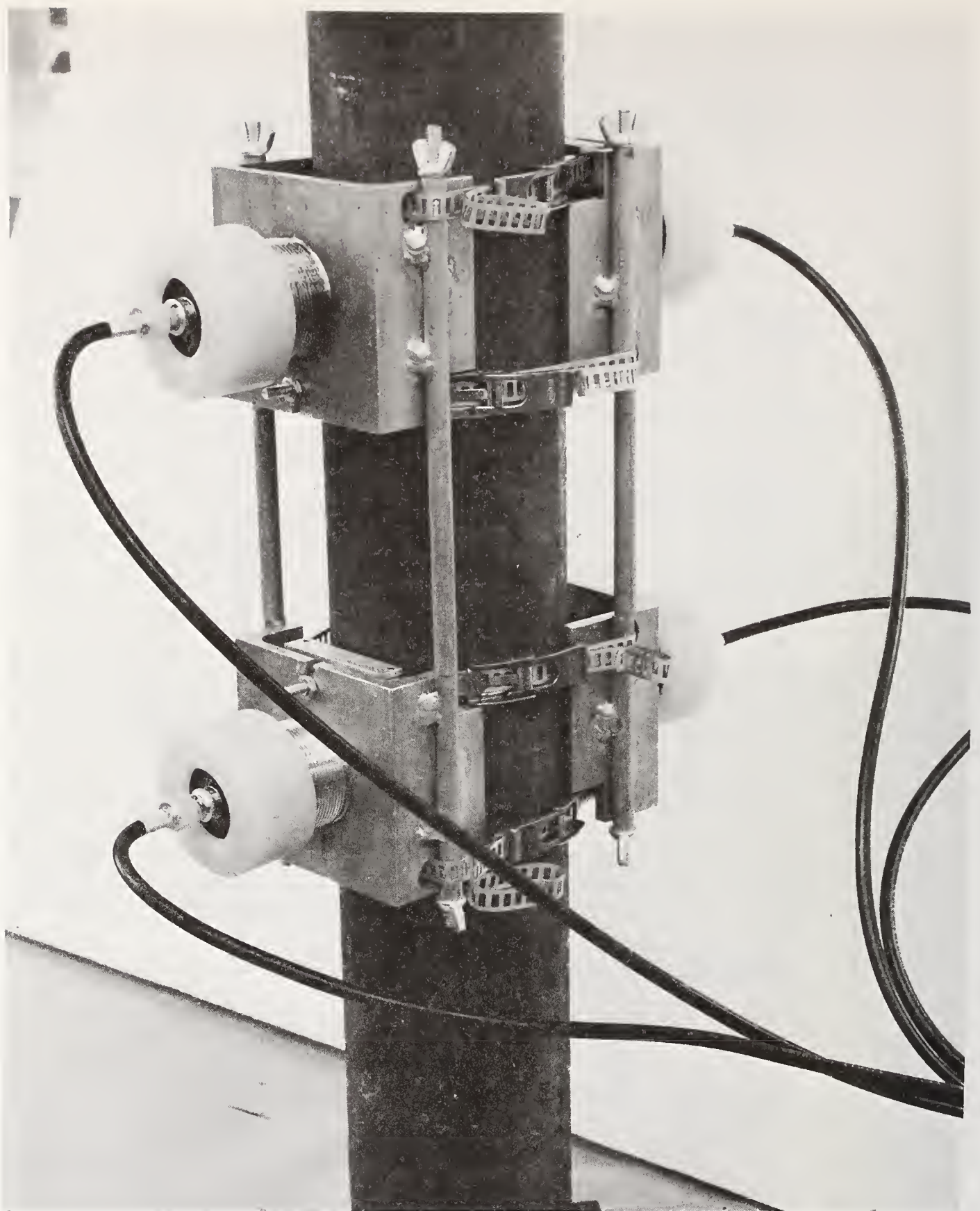
References

- [1] Beck, M.S., Calvert, G., Hobson, J.H., Lee, K.T., Mendies, P.J., "Total Volume and Component Flow Measurement in Industrial Slurries and Suspensions using Correlation Techniques", *Measurement and Control*, Vol. 4, No. 8, pp T133 - T138, August 1971.
- [2] McShane, J.L., "Ultrasonic Flowmeter Basics", *Instrumentation Technology*, pp 44 - 48, July 1971.
- [3] Torrance, J.W., "Confusion and Delusion in Sonic Flow Metering", Paper presented at 28th Annual Instrumentation-Automation Conference and Exhibit, I.S.A., Houston, Texas, October 15 - 18, 1973.
- [4] Anderson, G.C., and Perry, M.A., "A Calibrated Real-Time Correlator/Averager/Probability Analyser", *Hewlett-Packard Journal*, Vol. 21, No. 3, pp 9 - 15, November 1969.
- [5] Jordan, J.R., "A Correlation Function and Time Delay Measuring System Designed for Large Scale Circuit Integration", Paper presented at International Symposium on Measurement and Process Identification by Correlation and Spectral Techniques, Institute of Measurement and Control, University of Bradford, England, 2 - 5 January, 1973.
- [6] Boonstoppel, F., Veltman, B., and Vergouwen, F., "The Measurement of Flow by Cross-Correlation Techniques", Paper presented at IEE Conference on Industrial Measurement Techniques for On-Line Computers, June 1968.
- [7] Birger, G.L., "Certain Problems in Calibrating Ultrasonic Flowmeters", *Izmeritel'naya Tekhnika*, No. 10, pp 53 - 55, October 1962.
- [8] Bazerghi, H., and Serdula, K.J., "Evaluation of the Performance of the CGE Ultrasonic Cross-Correlation Flowmeter", Paper to be presented at Canadian Nuclear Association Conference, Montreal, Canada, June 1977.



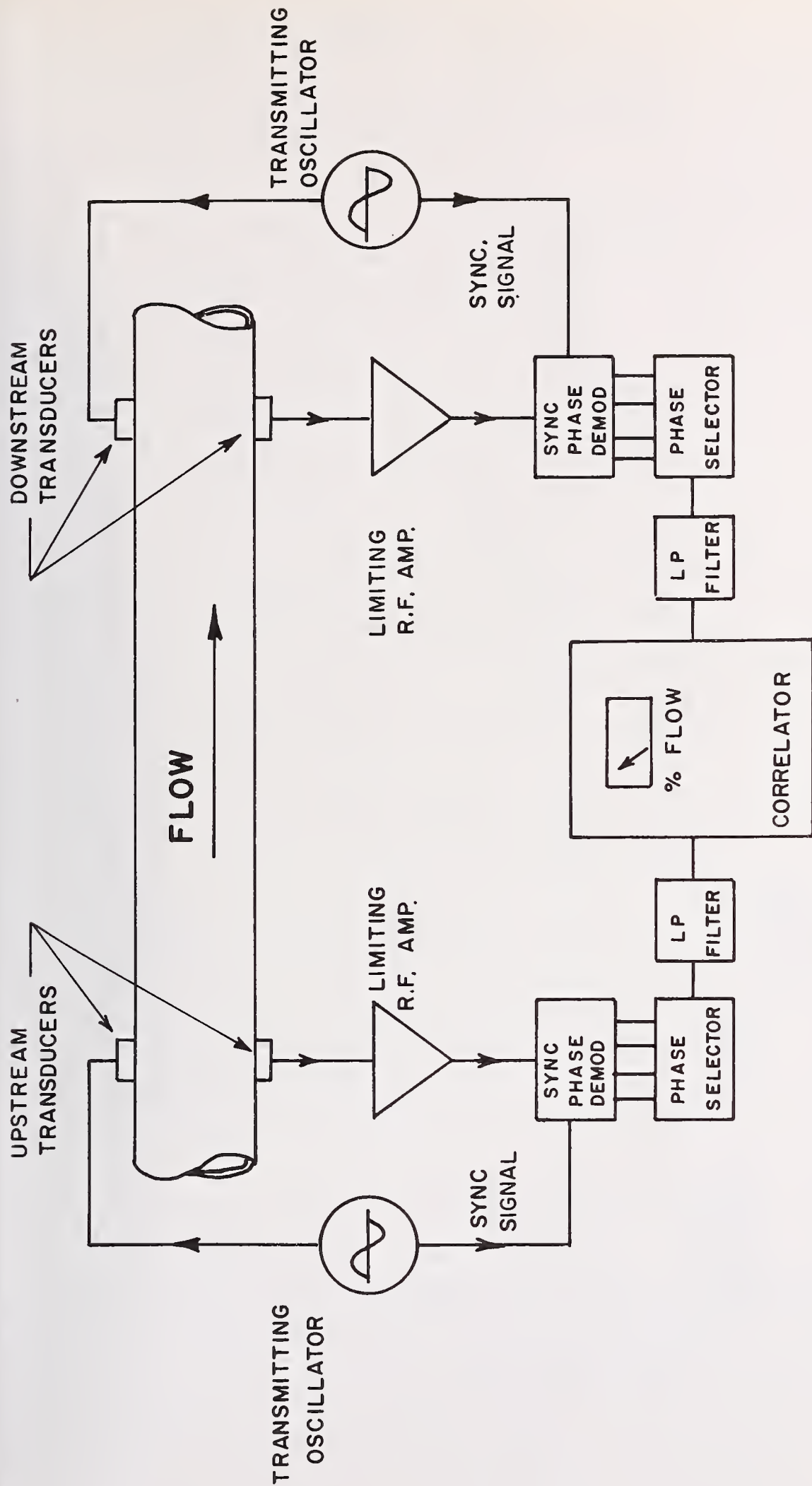
OPERATING PRINCIPLE OF ULTRASONIC FLOW MEASUREMENT

FIGURE 1



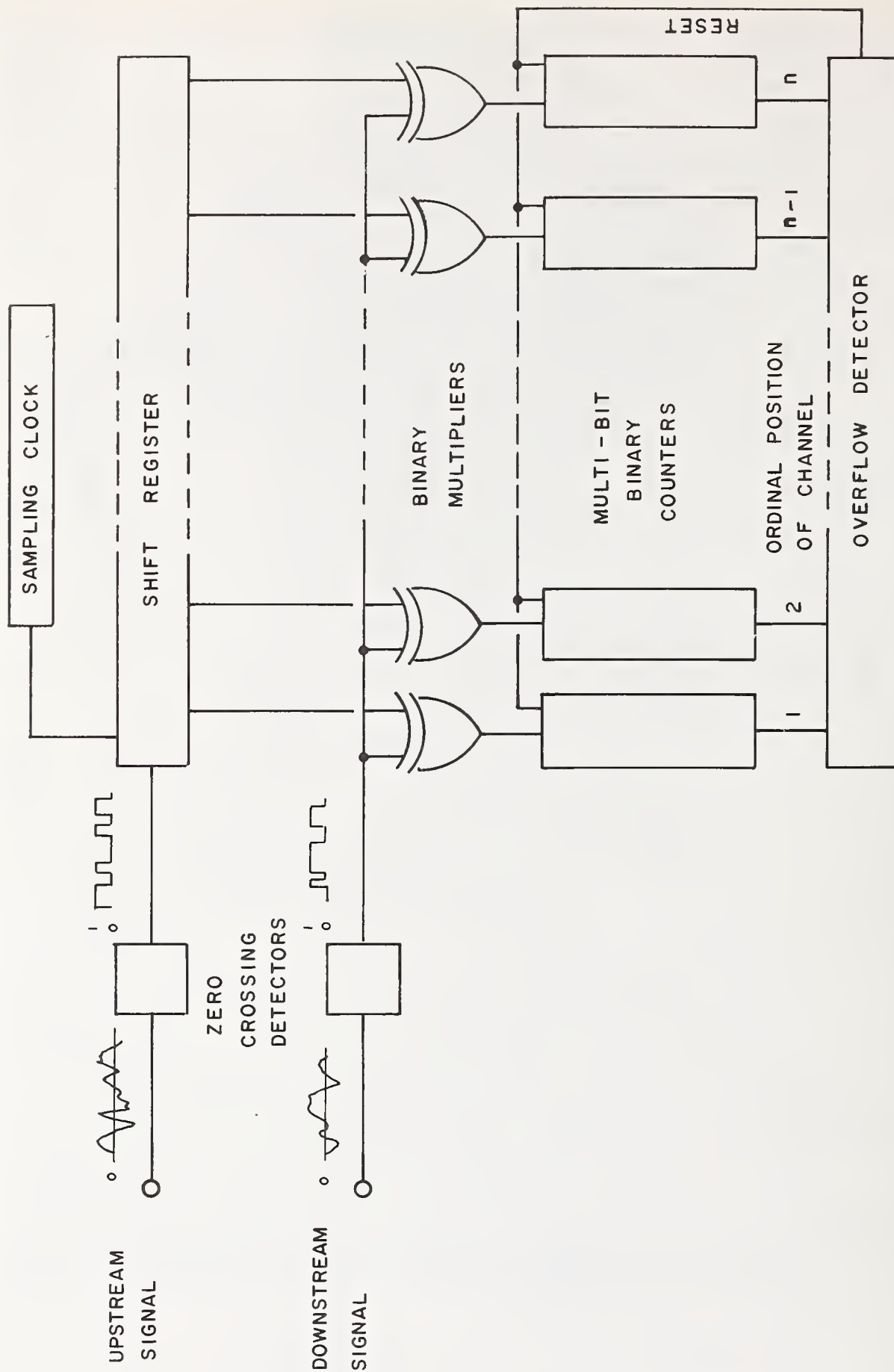
TRANSDUCER MOUNTING ARRANGEMENT

FIGURE 2



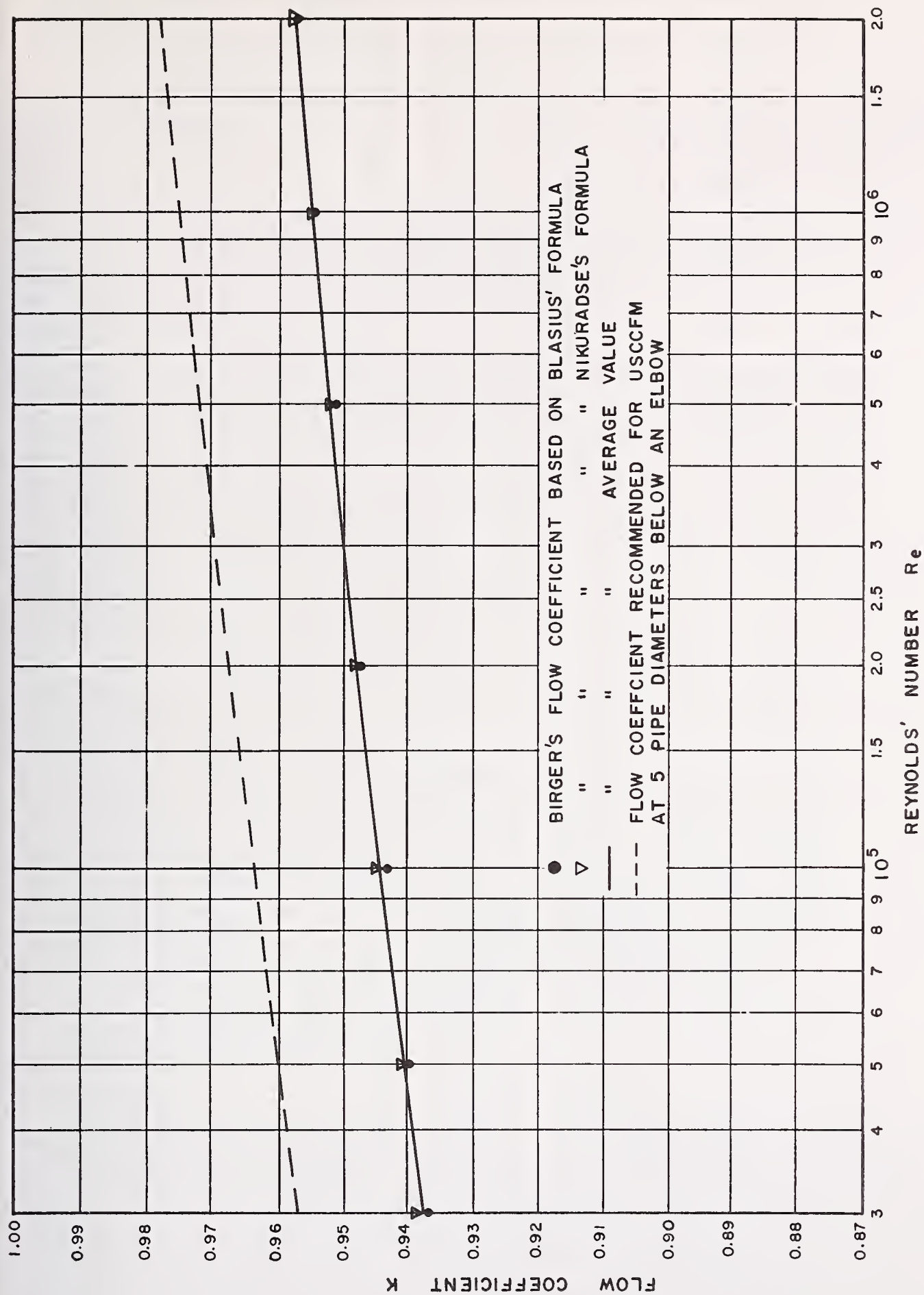
BLOCK DIAGRAM OF SIGNAL CIRCUITS

FIGURE 3



OPERATING PRINCIPLE OF THE BASIC CORRELATOR

FIGURE 4



FLOW COEFFICIENT FIGURE 5

RECONSTRUCTING THREE-DIMENSIONAL FLUID VELOCITY VECTOR
AND TEMPERATURE FIELDS FROM ACOUSTIC TRANSMISSION MEASUREMENTS

S. A. Johnson, J. F. Greenleaf, M. Tanaka and G. Flandro*

Biodynamics Research Unit
Department of Physiology and Biophysics
Mayo Foundation
Rochester, Minnesota 55901

A theory with supporting experimental evidence is presented for reconstructing the three-dimensional fluid velocity vector field and temperature field in a moving medium from a set of measurements of the acoustic propagation time between a multiplicity of transmitter and receiver locations on a stationary boundary surface. The inversion of the integrals relating the acoustic propagation path to the propagation time measurements is affected by linearization and discrete approximation of the integrals and application of an algebraic reconstruction technique (ART). The inversion of these integrals provides reconstructions of both acoustic refractive index and vector fluid velocity. Temperature reconstructions are obtained from the temperature dependence of acoustic refractive index. The problem of the presence of certain invisible fluid functions is treated. Since this technique does not require the presence of scattering centers or the optical transparency of the medium, it may be applied in many cases (i.e., turbid, opaque, or chemically pure media) where Doppler or optical (e.g., laser holography) methods fail.

1. Introduction

Methods for the measurement and description of the flow of fluids (both liquids and gases) may be divided into two main classes: invasive techniques and non-invasive techniques. Invasive methods make use of devices such as probes, the introduction of markers, the measurement of pressure changes across restrictions, etc. The non-invasive methods make use of the external measurement of some flow-dependent property such as

* Mechanical Engineering Department, University of Utah, Salt Lake City, Utah.

those relating to changes in optical properties, acoustic properties, electro-magnetic properties, etc. At the present time, several optical methods exist for gaining information about fluid flows. Laser Doppler, Schlieren optics, interferometric, holographic, etc., methods are known to the art. These methods require that the fluid be nearly transparent to the incident light. In addition to near perfect fluid transparency, Doppler methods require the presence of scattering centers or particles. Natural or artificial dust particles or fluctuations in density can serve this purpose. Low scattering center concentration provides longer ranges but sensitivity suffers. Higher scattering center concentration provides higher sensitivity but limits the range (depth) of measurement. The use of higher transmit power levels increases range and provides a stronger scattered signal but power is usually restricted by practical upper limits. Schlieren, interferometric, and holographic methods work well in general only for gas flows where density variations may be larger than for liquids.

Acoustic methods have also been proposed and applied which make use of either the Doppler scattered sound or transmitted sound along a single beam. The use of pulsed Doppler methods allows measurement of the component of fluid velocity (not the true fluid velocity) along the acoustic beam. The same trade off between sensitivity, which governs laser Doppler measurements, also exist for acoustic doppler techniques.

The average fluid velocity component along a transmitted beam can be determined from the measured time of propagation along the beam. Flow meters designed around this principle are well known.

All of these methods suffer from several common weaknesses: first, only the component of flow parallel to the beam is determined; second, only that region of the flow traversed by the beam is sampled. Thus, none of the previously mentioned methods in their simplest form measure true three-dimensional flow.

This paper will demonstrate that three-dimensional fluid flow can be determined by a new transmission method which overcomes the range and sensitivity problems of doppler methods and which overcomes the averaging problem (determining only the average parallel component) of the single beam transmission delay method.

It has been suggested that fluid flow within a measurement region may be determined by transmitting and receiving acoustic energy through the measurement region along a plurality of rays such that each volume element is traversed by a set of rays having components in each direction for which flow

components are to be reconstructed [1]¹. The propagation time of the acoustic energy along the plurality of rays constitutes the only measurements required by the method [1].

Each ray propagation time measurement is an integral of a function of acoustic speed and fluid velocity along the ray and the set of such measurements constitute a simultaneous set of integral equations which may be inverted (solved) to obtain the unknown fluid velocity vector field [1]. The equation which relates the propagation time along each ray from a source a to a receiver b is given by (see Figure 1 and 2)

$$t_{ab} = \int_a^b ds / || \vec{\tau}_m C(\vec{r}) + \vec{V}(\vec{r}) || \quad (1)$$

where $\vec{\tau}_m$ is the unit tangent vector along the acoustic ray as seen from the moving medium, $C(\vec{r})$ is the local acoustic speed as seen in the moving media, and $\vec{V}(\vec{r})$ is the fluid velocity vector as measured in the laboratory.

In general the actual ray path taken by acoustic energy from the source a to the receiver b is not known a priori even though the time of propagation may be measured quite accurately. It will be shown that the actual paths may be found either by appropriate simplifying assumptions or from proper mathematical consideration of the complete set of propagation times between many sources and receivers on a boundary surface surrounding (but not necessarily enclosing) the flow. This paper will proceed with the simplest case of fluid velocities much less (10% or less) than the speed of sound and then generalize to higher fluid velocities.

When the velocity of the fluid is everywhere much less than the speed of sound, the denominator in Equation 1 can be approximated by the expression $(C + \vec{\tau}_m \cdot \vec{V})$ where it is assumed that the ray tangent vector $\vec{\tau}_m$ as seen from a coordinate system embedded in the fluid is almost identical to the ray tangent vector $\vec{\tau}$ as seen in the laboratory coordinate system. In most fluids, when $|\vec{V}| \ll C$, the variations in $C(\vec{r})$ are also correspondingly small. With these assumption, Equation 1 can be written as:

$$t_{ab} = \int_a^b (1/C) (1 - \vec{\tau} \cdot \vec{V}/C) ds \quad (2)$$

The assumption that $\vec{\tau}_m$ is nearly equal to $\vec{\tau}$ allows the further assumption that the acoustic rays are nearly straight lines. Thus, the ray paths may be found in terms of the known source point a and receiver point b. The use of straight line rays

¹ Figures in brackets indicate the literature references at the end of this paper.

provide a further benefit, namely, a simple method for separating the dependence of the time t_{ab} on both $C(\vec{r})$ and $V(\vec{r})$. This separation is obtained by forming the linear combinations $(t_{ab} + t_{ba})$ and $(t_{ab} - t_{ba})$ where now t_{ba} refers to the propagation time between b and a when b serves as the source and a as the receiver.

$$t_{ab} + t_{ba} = 2 \int_a^b (1/C(\vec{r})) ds \quad (3)$$

$$t_{ab} - t_{ba} = -2 \int_a^b (\vec{r} \cdot \vec{V}/C^2) ds \quad (4)$$

Thus, even if $C(\vec{r})$ is a function of position \vec{r} it may be found by the inversion of the multiple set of equations (3) corresponding to a well chosen set of ray paths. This solution may be used to define C^2 in Equation 4 so that V may be found from the same or a similar set of ray measurements used to solve Equation 3.

It is important to choose a set of ray paths which provide a unique solution to Equations 3 and 4. One such good arrangement of transducers which provide paths with linear independent integrals is shown in Figure 1. Flow is assumed in a cylinder formed by translating a closed plane curve, nowhere convex inward, in a straight line (square and circular pipes are members of this set) as shown in Figure 1. The source and receiver transducers are placed on the intersection of this cylinder and two parallel planes. These planes are shown arranged such that the axis of the cylinder is normal to both plane a and plane b. Ray paths are used from any transducer a_i in plane a to any other transducer a_j in plane a or to any transducer b_j in plane b. As shown in Figure 1, both intraplane rays and interplane rays are utilized in this arrangement.

Geometric Arrangement of Transducers

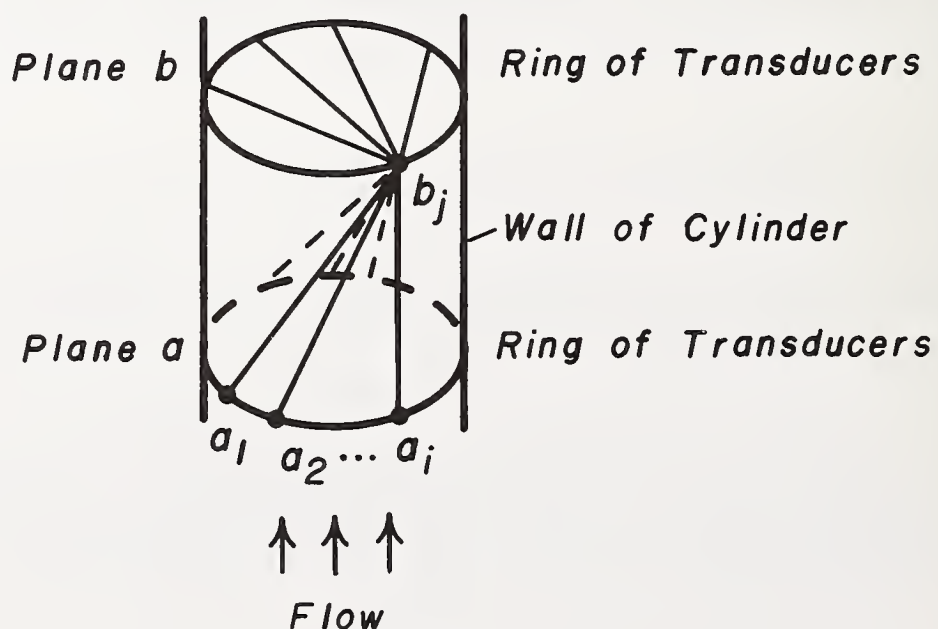


Figure 1 Illustrates a geometry in which three-dimensional fluid flow can be reconstructed with a few simplifying assumptions. Two of many planes a, b, c, \dots containing transducers $a_1, a_2, \dots, a_2, b_1, b_2, \dots, b_2$, etc. are shown.

The mathematical form of $\vec{r} \cdot \vec{V}$ can be derived by reference to Figure 2 which shows a coordinate system in the fluid flow field with the z axis in the direction of the axis of cylindrical symmetry. \vec{r} is the unit tangent vector to an acoustic ray at an arbitrary point, i.e., $\vec{r} = d\vec{r}/ds$, while $\hat{i}, \hat{j}, \hat{k}$ are unit vectors along the x, y, z axes which are fixed in direction. Let $\vec{r} = \vec{R} + z\hat{k}$, then $\vec{R}_0 = d\vec{R}/ds$ and then \vec{R}_0 and dR are the projections of \vec{r} and ds respectively onto the xy plane. The magnitude of $d\vec{r}$ is ds , the magnitude of $d\vec{R}$ is dR . Here α, β, γ are the direction angles and (R_0, θ) are the polar coordinates of \vec{R}_0 .

Coordinate System in Flow Field (C-Axis in Direction of Cylindrical Channel)

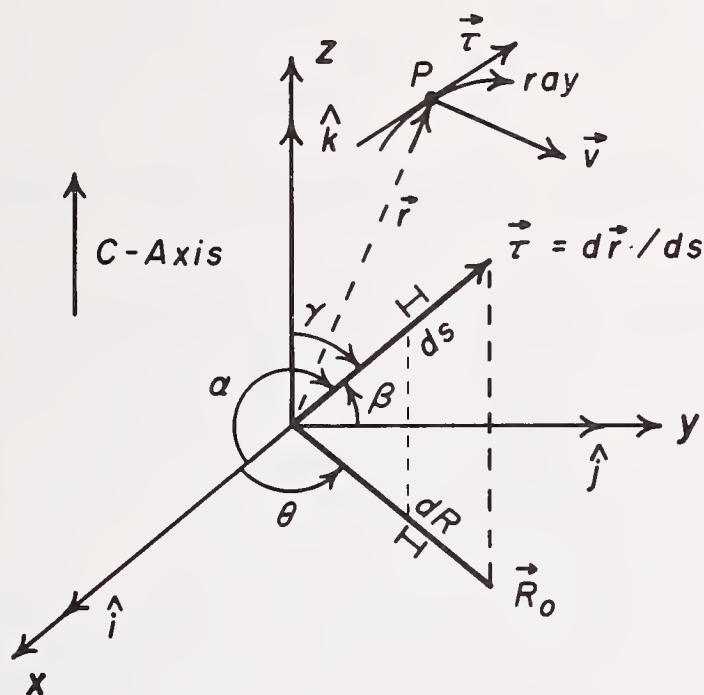


Figure 2 Coordinate system in flow field with z -axis in direction of cylindrical channel axis (C-axis). $\vec{r} = d\vec{r}/ds$ is unit tangent vector to acoustic ray at an arbitrary point P , but $\hat{i}, \hat{j}, \hat{k}$ unit vectors along x, y, z axes are fixed in direction. Note $|d\vec{r}| = ds$ and the projection of ds is dR , i.e., $|d\vec{R}| = dR$. Note also the fluid flow vector $\vec{V}(\vec{r})$ at point P .

With this notation, an expression for $\vec{V} \cdot \vec{r}$ may be written in terms of components V_x, V_y, V_z of \vec{V} and the cylindrical coordinates of \vec{r} . Noted^x that $dR = (\sin \gamma)ds$ where $\vec{r} = R_0 + \hat{k} \cos \gamma$. With this substitution for $\vec{r} \cdot \vec{V}$ Equation 4 becomes (note, in this paper the symbol \equiv will indicate a definition)

$$I_0(a_i b_j) \equiv t_{a_i b_j} - t_{b_j a_i} = -2 \int_a^b (1/C^2) [(V_x \cos \theta + V_y \sin \theta) \sin \gamma + V_z \cos \gamma] ds \quad (5)$$

which may be written

$$I_2 \equiv [I_0(a_i b_j) - I_1(a_i b_j)] = -2 \cos \gamma \int_{a_i}^{b_j} (1/C^2) V_z dR \quad (6)$$

where

$$I_1(a_i b_j) \equiv -2 \int_{a_i}^{b_j} (1/C^2) (V_x \cos \theta + V_y \sin \theta) dR \quad (7)$$

The advantage of writing Equations 6 and 7 in place of Equation 5 is made more clear by noting that I_1 from Equation 7 is independent of γ . Thus, V_x and V_y may be found by taking a sufficiently large set of rays in either plane a or plane b (not from plane a to plane b) and solving the corresponding set of Equations 7 for V_x and V_y . In other words, $I_0(a_i a_j) = I_1(a_i a_j)$ when $\gamma = \pi/2$ and where a_j is the projection of b_j onto the a-plane.

The function V_z may be found without solving Equation 7 for V_x and V_y if the value of I_2 can be found for each a_i and b_j . If a_i and b_j are in different planes and if a_i and a_j are their projections along the cylindrical axis onto one plane, then $I_1(a_i b_j)$ is identical in value to $I_1(a_i a_j)$. With I_2 determined for each ray in a sufficiently large set of rays from I_0 and I_1 , it is then possible for Equation 6 to be inverted. Thus, Equation 6 may be replaced by the following practical equation, relating V_z to actual time measurements.

$$I_2 = [(t_{a_i b_j} - t_{b_j a_i}) - (t_{a_i a_j} - t_{a_j a_i})] = -2 \cos \gamma \int_{a_i}^{a_j} (V_z / C^2) dR \quad (8)$$

Thus, V_z is found from data consisting of measurements between transducer pairs both in the same plane and between distinct planes. The integral in Equation 7 or Equation 8 may be written in terms of an approximate discrete sum by subdividing planes a or b into finite elements or pixels. Then dR corresponds to the length of the ray in each pixel. Using this notation, Equation 7 and 8 become

$$I_1(a, i, j)_s = -2 \sum_k (1/C^2) [V_x(k) \cos \theta_s + V_y(k) \sin \theta_s] L_{sk} \quad (9)$$

$$I_2(a,b,i,j)_s = -2\cos \gamma_s \sum_k (1/C^2) V_z(k) L_{sk} \quad (10)$$

where L_{sk} is the length of ray s in pixel k . Methods for solving Equations 9 and 10 are well-known [2].

The case of nonconstant speed of sound C is also described by Equations 3, 6, and 7 or their extensions, such as Equation 9. Thus, both \vec{V} and C can be reconstructed even in those cases where C is not a constant. The case where flow changes rapidly with coordinate z can be treated by the use of more than two measuring planes, i.e., more planes than a and b , and by spacing those planes closer together.

The ART method is usually applied to reconstruct scalar quantities from their projections. In the operation of this technique, the reconstruction of vector quantities is required. This is accomplished by writing $(\vec{r} \cdot \vec{V})$ as $(V_x \cos \alpha + V_y \cos \beta + V_z \cos \gamma)$. At each point along the ray $\cos \alpha$, $\cos \beta$, and $\cos \gamma$ are known. The quantities V_x , V_y , and V_z are each sought in the N^2 pixels (picture elements) in a square array with N pixels on a side. One way to accomplish this task is to modify the ART algorithm to reconstruct a scalar U in a rectangular array of $3N^2$ pixels where the value of U is V_x in the first square sub array of N by N , where U is V_y in the middle square sub array of N by N , and where U is V_z in the last square sub array of N by N . In the case of cylindrical symmetry such as used in Equation 9 and 10, only two such square sub arrays are used to solve Equation 9 and only one such square sub array is required to solve Equation 10.

2. Fast Flows

The problem of reconstructing fluid flows where the velocity of the flow is not significantly small compared to the speed of sound requires a more accurate treatment of the ray paths than the straight line approximations of Equation 9 and 10 [1]. Thus, the ray paths may bend significantly due to both the transformation from moving to laboratory coordinate systems and from acoustic speed variations due to density variations (the latter being more common in gases than liquids). If a complete set of acoustic ray paths could be determined, then Equation 1 could be inverted notwithstanding its nonlinear nature. Techniques are known for finding the ray paths when $\vec{V}(\vec{r})$ and $C(\vec{r})$ are known. One such technique is called ray tracing and has been previously described [1,3]. Thus, it seems that either the ray paths or \vec{V} and C can be found independently even in fast flows.

While many methods could be suggested for finding both the ray paths and \vec{V} and C , for purposes of illustration only, an iterative technique will be described. First, linear ray

paths are assumed on a sufficiently coarse grid (i.e., large pixels). Second, the speed C and velocity \vec{V} are reconstructed. Third, more accurate ray paths are found by ray tracing. It may be necessary to smooth the reconstructions obtained from the previous step before ray tracing. Fourth, Equation 1 is solved again for new values of C and \vec{V} using the ray path from step three. Steps three and four may be repeated many times as the grid size is made smaller.

The case for supersonic flow requires special treatment because there may be transducer pairs for which it is impossible to find linking rays (sound cannot travel upstream in supersonic flows). Although it seems probable that a suitable set of invertible equations may be obtained in many cases of this type when proper consideration is given to transducer placement, a proof of this conjecture is not presently known to the authors.

3. Invisible Fluid Flow

Under some circumstances, Equations 3 and 4 cannot be inverted. A simple example is the case of radial flow in a plane from a point source in that plane. If this flow has angular symmetry, then $t_{ab} - t_{ba} = 0$. Any such flow in a plane which contains $\vec{\tau}$ (i.e., $\vec{\tau}$ has no components perpendicular to this plane) is invisible. However, the flow may be detected if $\vec{\tau}$ has components perpendicular to the plane. See Figure 3 for the geometry of this example.

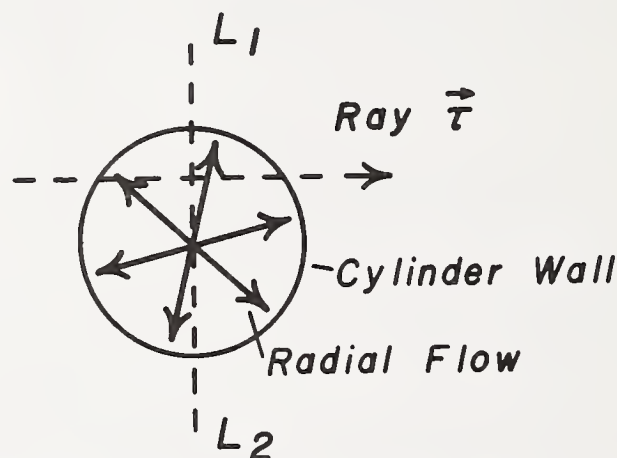


Figure 3 Invisible radial flow. See text for explanation.

From Figure 3, it is seen that a decrease in speed on the left of symmetry axis $L_1 L_2$ is equal to the increase in speed on the right of axis $L_1 L_2$. It should be noted that radial flows are not invisible to the second order terms in the expansion of Equation 2 since $(\vec{\tau} \cdot \vec{V}/C)^2$ does not change sign upon

reflection about L_1 , L_2 , although the contribution from the second order term is usually negligible for $|\vec{V}| < C/5$.

Under some circumstances the integral in Equation 8 may not vanish, as it does in the case of angularly symmetric radial flow, yet the system of Equations 7 and 8 are still not invertable because each integral in a set corresponding to different rays is not linearly independent. A simple example of this situation is the case of two-dimensional flow in a channel with rays taken between points on opposing walls of the channel. The geometry of this case is given in Figure 4 below.

ULTRASONIC QUANTITATION OF AVERAGE TWO-DIMENSIONAL FLOW IN A CYLINDER

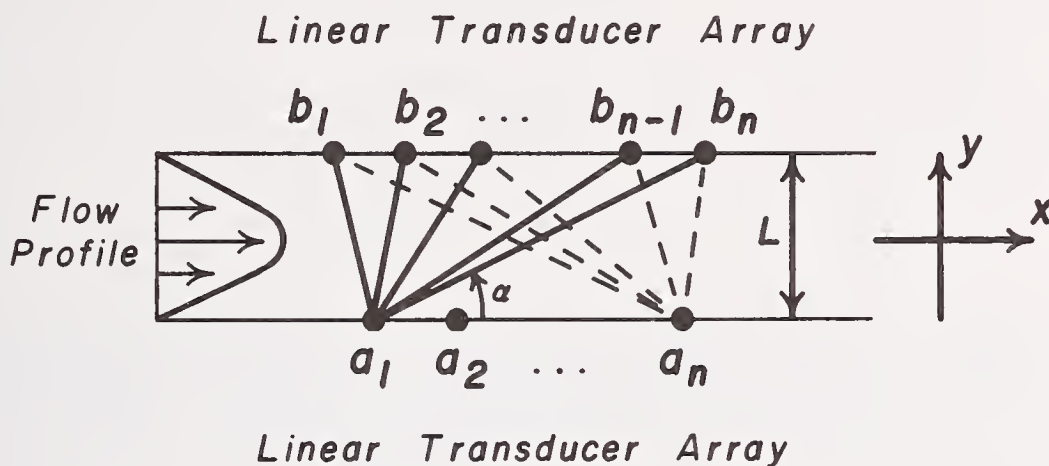


Figure 4 Two-dimensional flow in a channel cannot be reconstructed by linear approximation with the geometry shown. However, the average flow is determined by forward and backward measurements along each ray. See text for explanation.

In Figure 4 transducers a_1, \dots, a_n are located on the lower wall and transducers b_1, \dots, b_n are located on the upper wall. Let $\alpha(a_i, b_j) = \alpha_{i,j}$ be the angle which the ray between a_i and b_j makes with the x -axis. The x -axis is parallel to the parallel channel walls. Let the shortest distance between the channel walls be L . The integrals (Equation 4) can be evaluated by changing the parameter of integration by the formula $ds = (\sin \alpha_{i,j})^{-1} dy$ and noting that $\vec{V} \cdot \vec{\tau} = V_x \cos \alpha_{i,j}$. Here we assume $V_y \equiv 0$ for steady state flow.

Thus Equation 4 becomes

$$t_{a_i b_j} - t_{b_j a_i} = -2 \cot \alpha_{i,j} \int_{a_i}^{b_j} \frac{V_x}{C^2} dy \quad (11)$$

If the fluid is incompressible then C^2 is constant. The continuity equation and the assumption $V_y = 0$ implies that $\frac{\partial}{\partial x} V_x = 0$. Thus the integral in Equation 11 is a constant independent of the path $a_i b_j$ and all such equations are linearly dependent. Note $t_{a_i b_j} - t_{b_j a_i} = -2 \langle V_x \rangle X_{a_i b_j} / C^2$ where $\langle V_x \rangle$ is the average flow and $X_{a_i b_j}$ is the x-axis distance between a_i and b_j .

The problem of possible invisible fluid flows may be minimized by two approaches: first, the second order terms in the expansion of Equation (1) or (2) may be used, second, three-dimensional (3-D) rather than two-dimensional (2-D) geometries may be used. This latter approach could make use of the notion that many invisible flows in 2-D are detectable in 3-D. An additional help may be found in requiring the 3-D reconstruction to be consistent with fluid dynamic equations such as the continuity and momentums equations.

4. Reconstruction of Temperature Fields

The theory developed in the preceding sections may be applied under certain conditions to the determination of the three-dimensional distribution of temperature. If, for example, it is known that the material to be probed by the measuring acoustic fields is homogeneous then the reconstruction of the velocity field may be related to the temperature of the material by a simple function which maps velocity of sound to temperature. A similar method has been proposed by [4] Sweeney using optical rather than acoustic properties of matter.

If the substance is pure degassed water, then the velocity of sound in the neighborhood of 19°C is given by the formula

$$c[\text{m/sec}] = 1461 [\text{m/sec}] + 3.44 (T-19^\circ\text{C}) + .0185 (T-19^\circ\text{C})^2 + \dots \quad (12)$$

where T is measured in °C. Thus, the inverse function giving T as a function of c is the required mapping function. A difference of 20°C for water produces about the same percent change in velocity of sound as the difference between striated muscle and water. Reconstruction accuracy may be increased if the difference in temperature is required. Thus, circulation and metabolic heat generation may possibly be reconstructed. A map of mixing of two identical fluids of different temperatures may be also be reconstructed. Thus, a reconstruction of c can be transformed to a reconstruction of T . The reconstruction of c is obtained by solving the system of Equations 3.

5. Use of a Priori Information

The fluid dynamic equations may be written in finite difference form to provide additional equations of constraint to the previous equations. This makes possible more accurate reconstructions or reconstructions from fewer projections. For example, the equation of continuity (here d = density, \vec{V} = velocity)

$$\nabla \cdot (d\vec{V}) + \frac{\partial d}{\partial t} = 0 \quad (13)$$

produces the following set of finite difference equations in two dimensions

$$\begin{aligned} d_{i+1,j,t} V_{x,i+1,j} - d_{i,j,t} V_{x,i,j} + \\ d_{i,j+1,t} V_{y,i,j+1} - d_{i,j,t} V_{y,i,j} + \\ d_{i,j,t+1} - d_{i,j,t} = 0 \end{aligned} \quad (14)$$

where here $\Delta x = \Delta y = 1$ by a choice of coordinates. Note $k = (i,j)$ when comparing V_x , V_y , and d in the two notations (e.g., $V_{x,k} = V_{x,i,j}$, etc.)

In a similar manner the momentum and energy equations could be written in finite difference form and used with equation. The use of Laplace's equation as a priori information in reconstruction has been reported by Radulovic [5].

6. Computer Simulation Studies

Digital computer simulation studies were conducted in FORTRAN language on a CDC 3500 computer to test the previously described theory. Computer simulation permits the testing of a wide range of flow configurations and acoustic path geometries. In our case, both two-dimensional parallel ray projection and fan beam projections were simulated. Such projection data were made either by integrating Equation 2 by analytic or numerical means for a specific velocity function $\vec{V}(\vec{r})$. The set of acoustic propagation times $\{t_{ab}\}$ thus obtained was then used as measurement data to reconstruct the velocity function $\vec{V}_R(\vec{r})$. The similarity of $\vec{V}_R(\vec{r})$ and $\vec{V}(\vec{r})$ is a measure of the accuracy of the reconstruction method. A modified algebraic reconstruction technique (ART) with an underrelaxation parameter of 0.75 was used [6].

The angular velocity of several vortex models with angular symmetry were reconstructed from simulated parallel projection data. The velocity of a natural fluid vortex measured in a plane perpendicular to the vortex axis may be modeled by

$$\vec{V}_{Pl}(\vec{R}) = \frac{wA^2}{R} (1 - e^{-R^2/A^2}) \hat{e} \quad (15)$$

where $\hat{\theta}$ is a unit vector defined to be perpendicular to \vec{R} and to \hat{k} . This function behaves like wR for very small R and like wA^2/R for very large R . The maximum value occurs near $R = A$.

In order to simplify the simulation and reconstruction algorithms it is desirable to study a function which vanishes outside a finite radius B and yet corresponds closely to the behavior of $\vec{V}_{p1}(\vec{R})$ defined in Equation 15. The function $\vec{V}_{p2}(\vec{R})$ defined by Equation 16 was chosen to meet these requirements

$$\vec{V}_{p2}(\vec{R}) = \begin{cases} (w - \frac{wA}{B})R\hat{\theta}, & R \leq A \\ (\frac{wA^2}{R} - \frac{wA^2}{B})\hat{\theta}, & A < R \leq B \\ 0, & B < R \end{cases} \quad (16)$$

The three-dimensional velocity $\vec{V}(\vec{R})$ for a point in a plane is given by $\vec{V}(\vec{R}) = \vec{V}_p(\vec{R}) + V_z(\vec{R})\hat{k}$. In these simulations, the function $V_z(\vec{R})$ was defined to have a parabolic shape representing a downward flow given by

$$V_z(\vec{R}) = \begin{cases} -K[(R/B)^2 - 1], & R < B \\ 0, & R \geq B \end{cases} \quad (17)$$

The constants of geometry and flow were given values of $A = 4.24$ cm, $B = 9.55$ cm, $w = 50$ radians/sec, $K = 91$ cm/sec and simulated projection data were computed. A graph of $|\vec{V}_{p2}(R)|$ vs. R along a diameter and the corresponding generated fan beam projection data ($t_{ab} - t_{ba}$) are shown in Figure 5. Also shown in the same figure is the function $V_R(\vec{R})$ which is a reconstruction of $|\vec{V}_{p2}(\vec{R})|$ from the set projection data $t_{ab} - t_{ba}$. The geometry of the flow and transducer locations (the geometry corresponds to that given in Figure 1) is also described in Figure 5.

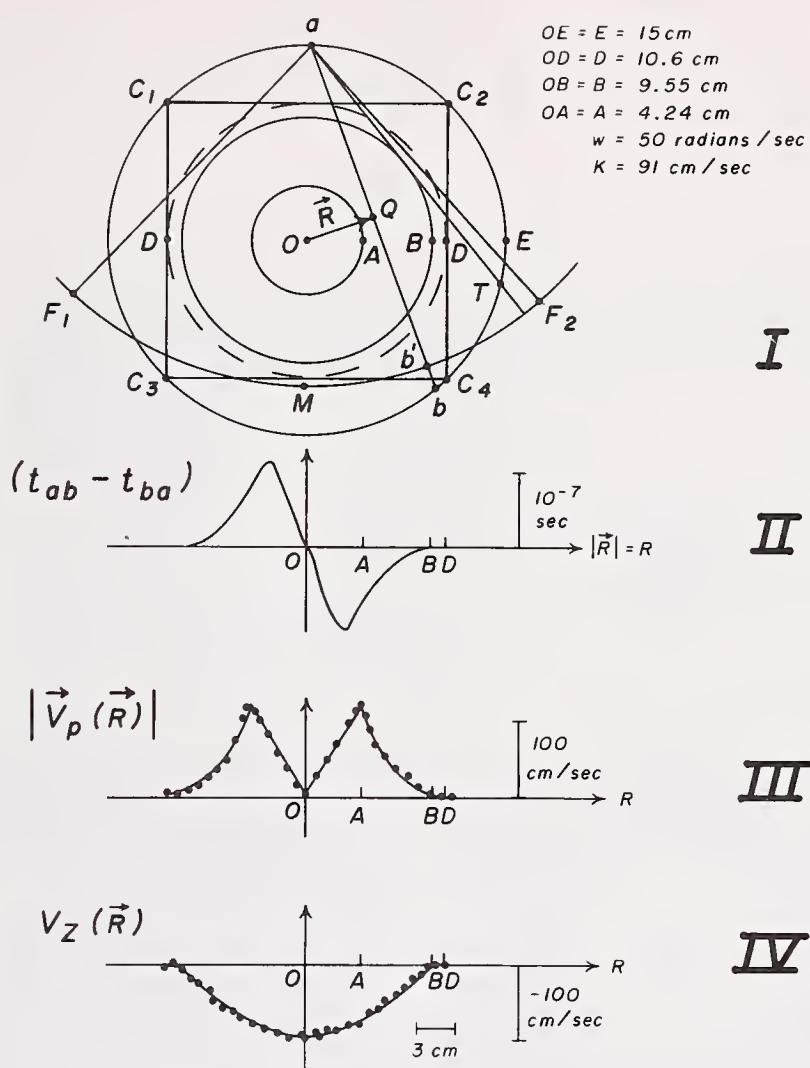


Figure 5 Experimental geometry for vortex reconstruction. **Line I:** shows the source and detector geometry transducers at a and b on circle of radius OE. Square $C_1C_2C_3C_4$ is area reconstructed. Radius OB is 0.9 of OD. OA is 0.4 of OD. For simulation, transducers on radius $Oa = Ob$. For experimental data collection source at a and receiver at b and receiver moves on arc of circle F_2 b MF, with a at center. **Line II:** shows the simulated time difference $(t_{ab} - t_{ba})$ ordinate calibration shown for values of A,B,w,k given in this figure. The abscissa R is the perpendicular distance from 0 to ray ab. **Line III:** shows assumed planar fluid speed function (solid line) and reconstructed values sampled along line ODE (solid dots). **Line IV:** shows assumed perpendicular (V_z) fluid component (solid line) and reconstructed values sampled along line ODE (solid dots).

Gray scale pictures of the three components V_x , V_y , V_z of the reconstructed function $\vec{V}_R(\vec{R})$ and of the planar magnitude $(V_x^2 + V_y^2)^{1/2}$ are shown in Figure 6. The picture of $(V_x^2 + V_y^2)^{1/2}$ shows the circular nature of the concentric flow lines. In these studies, 153 views each with 153 rays were used.

RECONSTRUCTION OF SIMULATED FLOW

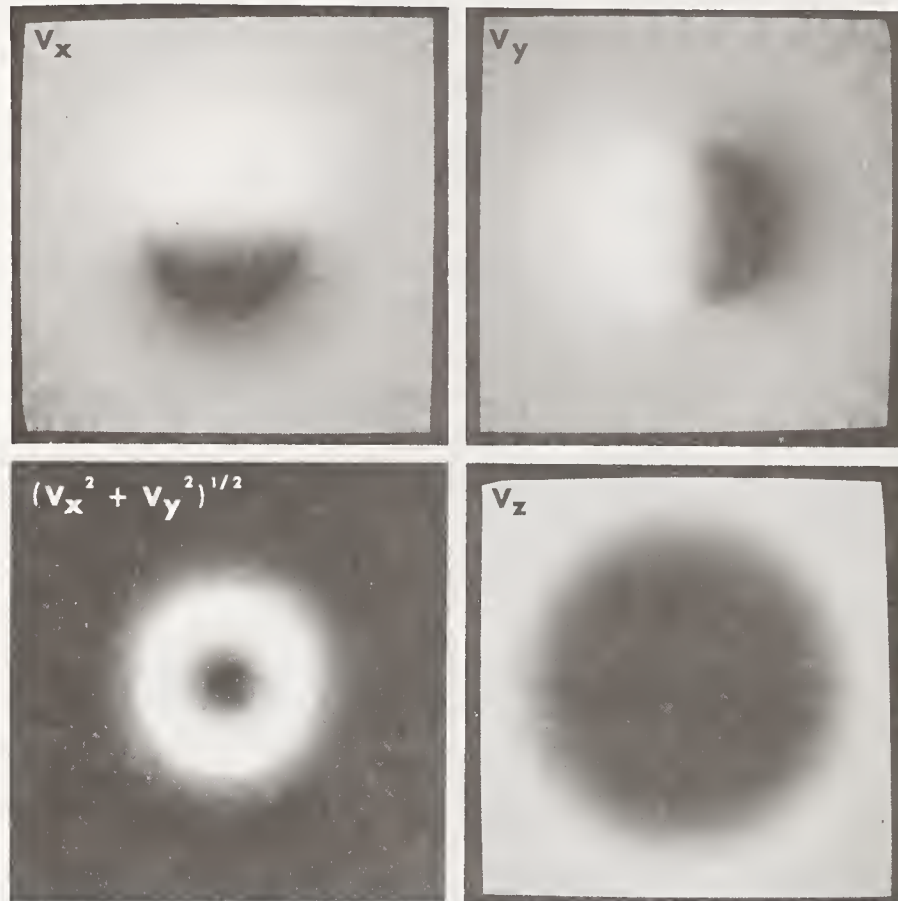


Figure 6 Reconstruction of vector components of simulated fluid vortex. Top left shows x component V_x . Top right shows y component V_y . Bottom right shows z component V_z . In these fluid velocity component reconstructions black is negative, gray is zero and white is positive in values. Bottom left is the magnitude of the xy planar component $(V_x^2 + V_y^2)^{1/2}$. Note circular equal speed contours. Images are 64×64 pixels per side.

7. Experimental Flow Studies

The success of the computer simulation studies prompted an experimental verification of these results in the laboratory. Accordingly, an experiment was conducted with a flow and transducer geometry which matched the simulation studies as closely as possible. Although a circular transducer array like that shown in Figure 1 was not available, a fan beam

geometry corresponding to the fan F_1 a F_2 MF, shown in Figure 5 was possible by using an ultrasound scanner designed for breast cancer detection studies [7]. The source moved on a circle of radius 21 cm while the detector moved around the source on a circular arc of radius 26 cm on the opposite side of the center. All source intervals are equal.

The difference $(t_{ab} - t_{ba})$ was digitized, separate measurements of t_{ab} and t_{ba} provided by a time of flight detector. The values of $(t_{ab} - t_{ba})$ were determined for 60 views with 150 rays per view and processing by the same algorithm used in the simulation studies. All ray intervals are equal.

The raw data for all rays in all views is shown in Figure 7. Also shown are the gray scale pictures for the components V_x and V_y and the magnitude (speed) $(V_x^2 + V_y^2)^{1/2}$. No measurements of the component V_z were made.

RECONSTRUCTION OF EXPERIMENTAL FLOW

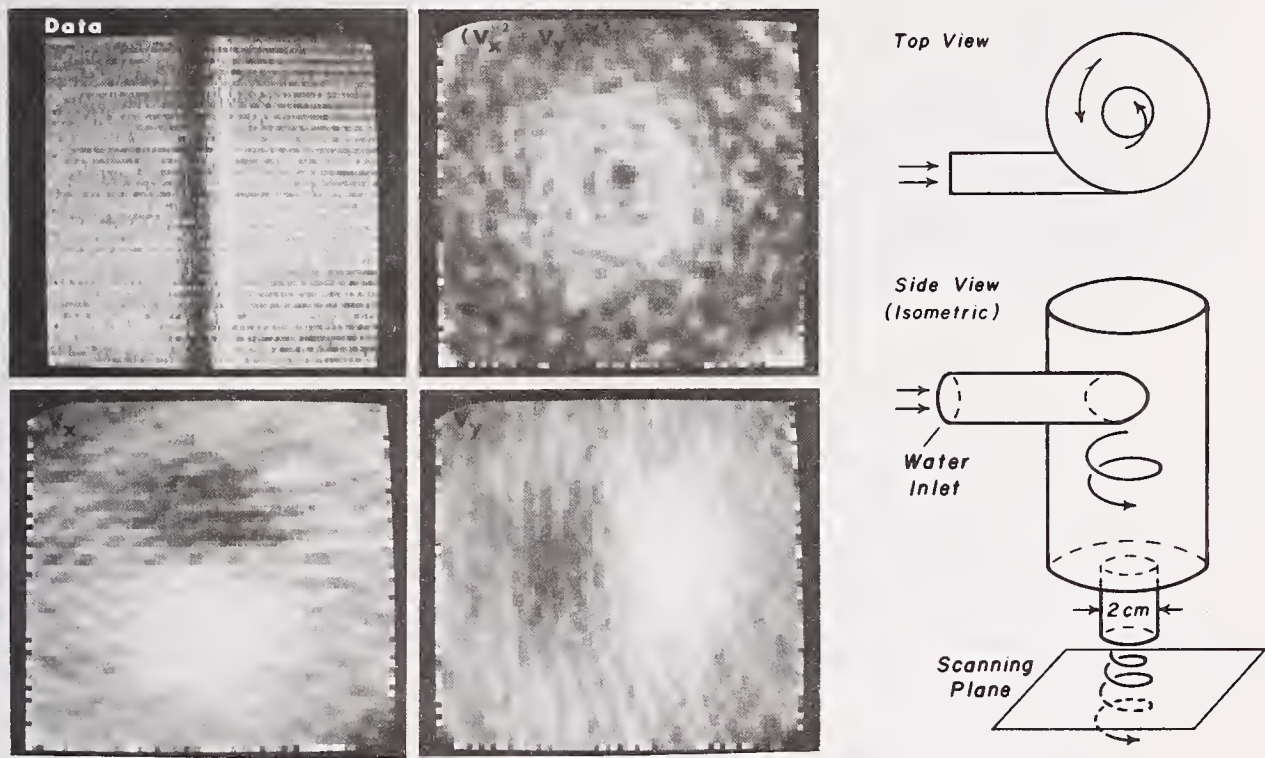


Figure 7 Experimental data and reconstruction of vector components of fluid vortex. Top left shows experimental data and is an image of the difference between the time of flight with flow and without flow (fast arrival = white, no change = gray, slow = black) vs. scan position (left to right) vs. angle of view (top to bottom). Top right shows reconstructed planar fluid speed $(V_x^2 + V_y^2)^{1/2}$, black is zero, white is positive. Bottom left shows x component of velocity V_x . Bottom right shows y component of velocity V_y . In V_x , black is negative, gray is zero, and white is positive.

Reconstructed flow is maximum (73 cm/sec) at a radius of 0.62 cm. Reconstructions are 64 pixels per side. Geometry of vortex, scanning plane, and vortex generator are shown in top and side views in right margin.

8. Experimental Temperature Tomography

The theory presented allows the reconstruction of temperature fields in moving or static fluids. This process might be termed temperature tomography or thermotomography. A reconstruction of a temperature static fluid was made before attempting the reconstruction of temperature in a flow field. A static temperature field was produced by circulating water from a constant temperature bath through three long sausage shaped balloons. The three balloons were arranged to form an equilateral triangle with sides of about three inches in a second constant temperature bath containing the ultrasound scanning transducers (5 MHz, wide band). A fourth balloon with no water circulation, filled with dilute sodium chloride located near the center of the triangle provided a constant nontemperature dependent refractive index area. The horizontal scanning plane passed through the center of the four balloons mounted at equal heights with their axis parallel and vertical. Sixty projection views of about 150 samples each were collected for each configuration of a preset constant temperature difference between the scanning bath and the balloons. The bath temperature was kept at 22°C for each configuration. The salt solution filled balloon provided a large refractive index constant temperature object to test the hypothesis that a reconstruction of only temperature changes in a nonhomogeneous object is possible. Figure 8 shows the result of the reconstruction of refractive index for four different balloon temperatures. The high contrast central salt solution filled balloon dominates the four temperature variable balloons. In the temperature difference tomograms in Figure 9, the evidence of the presence of the salt solution filled balloon is nearly removed by subtracting a reconstruction of all four balloons at 22°C from each reconstruction of different configuration. This single, initial experiment indicates this technique holds promise for reconstructing temperature differences in inhomogeneous materials.

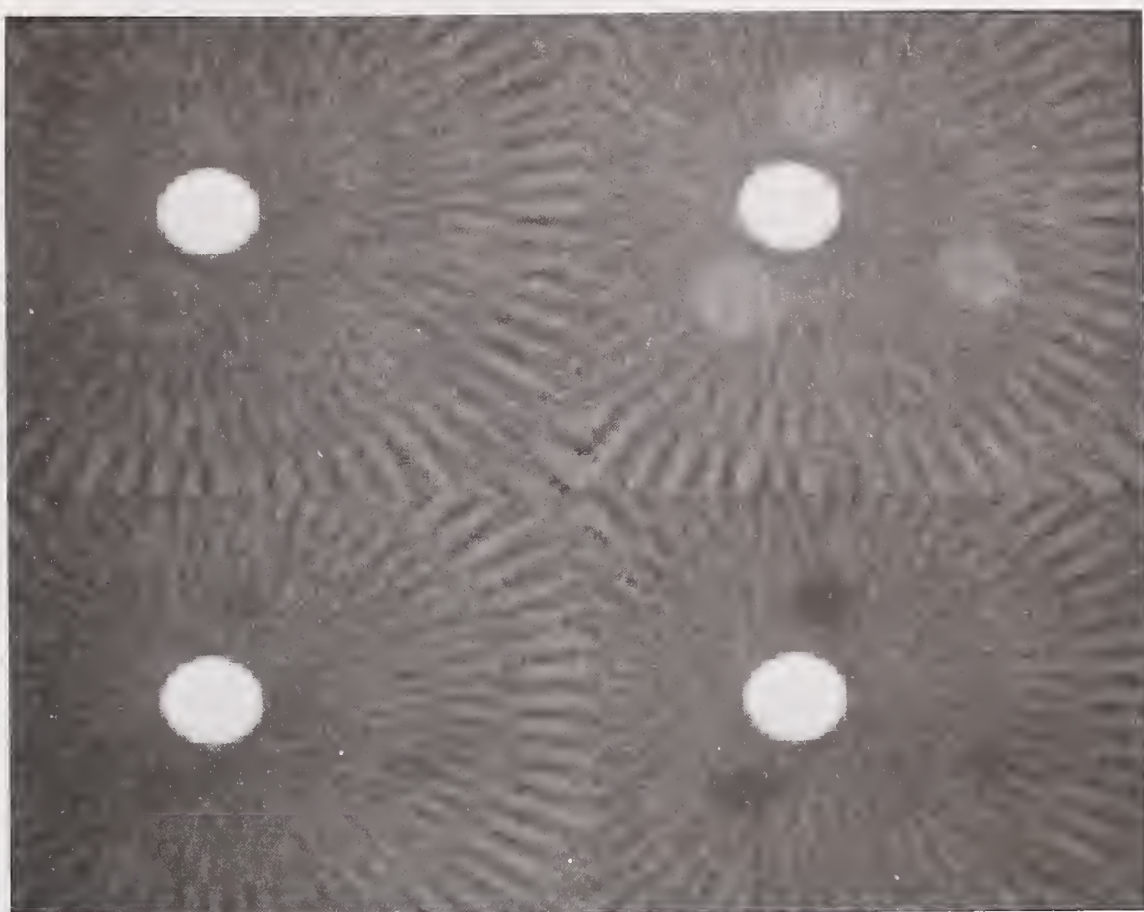


Figure 8 Initial temperature reconstruction experiments with water and saline filled balloons. Three water filled balloons and one saline balloon at 22°C are shown in top left. Water balloons at 23°C in top right. Water balloons at 21.5°C in bottom left and at 20.5°C at bottom right. Images were made with a convolution reconstruction algorithm from 60 views. The scan time was five minutes. In all images the saline filled balloon is in the center.

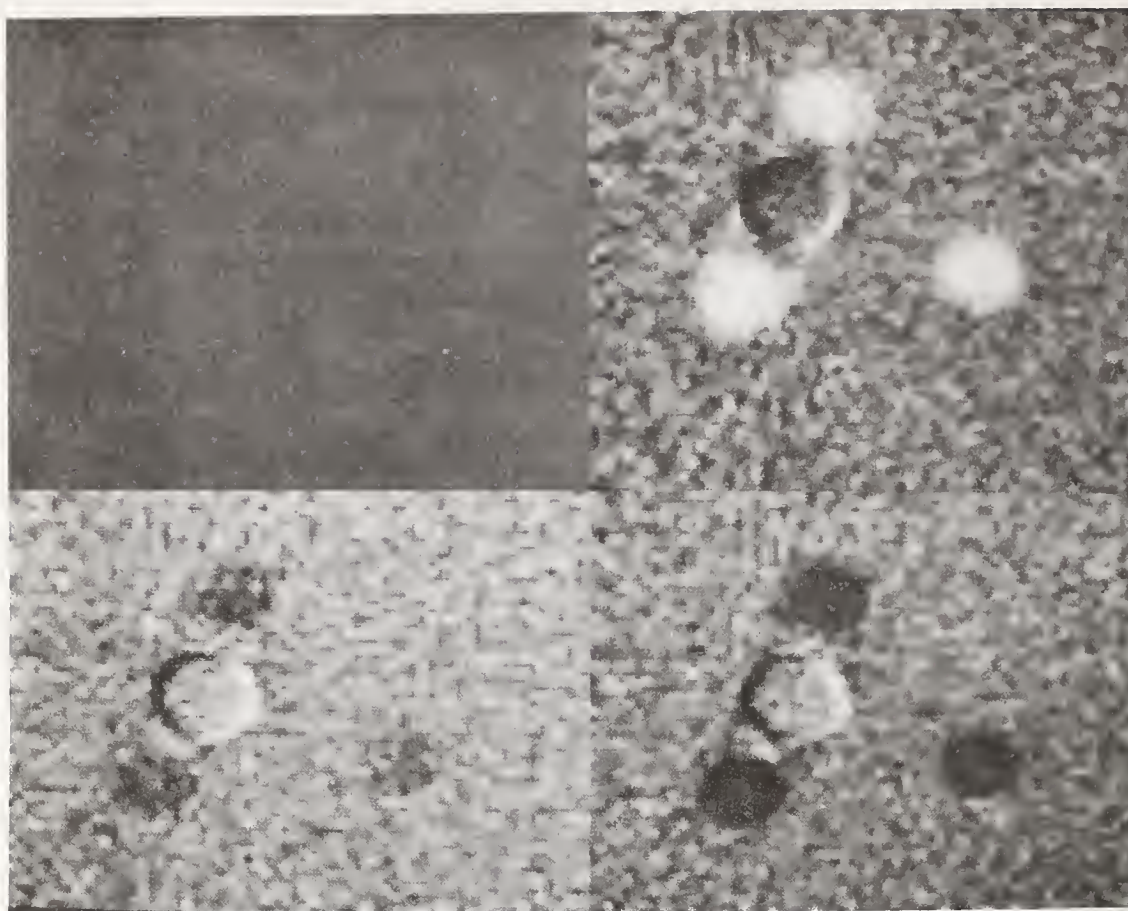


Figure 9 Reconstruction of temperature differences. This figure uses the data of Figure 8 to subtract out constant temperature background from the changing temperature objects. In each case, the 22°C constant temperature reconstruction shown in top left of Figure 8 is subtracted from:

- top left - top left of Figure 8 (not complete cancellation)
- top right - top right of Figure 8
- bottom left - bottom left of Figure 8
- bottom right - bottom right of Figure 8

Note the almost complete suppression of the saline balloon compared to Figure 8; thus, only temperature differences are reconstructed. (The particular subtraction routine used here actually gives the absolute value of the differences.)

9. Experimental Reconstruction of Mixing and Fluctuation

The previously described theory provides a means for obtaining a tomographic image of the mixing of two fluids or the fluctuation in fluid velocity of one fluid. If the data collection period is shorter than fluctuation time of regions larger than or equal to the spatial resolution of the instrumentation, then a "snap shot" or time resolved fluctuation reconstruction is possible. Repetition of this process as short time intervals would result in a time and spatial reconstruction of flow and fluctuation in flow. Such high speed instrumentation would require parallel data collection techniques.

Statistical characterization of mixing and fluctuation of flows with stationary statistical properties is possible with nonsimultaneous sampling techniques. The mixing of a tracer element in a flow has been characterized by some writers [8] by a stream segregation function I_s defined by dividing the variance of the percent concentration of a tracer at a point in the flow by the square of the mean of the percent concentration at that same point. The parameter I_s thus defined is a unit-less measure of mixing or fluctuation.

The reconstruction of the statistical properties in a plane must be obtained from the statistical properties in the projections. It can be shown that the mean value at a point in a reconstruction is the reconstruction of the mean values of the projection data (this follows because reconstruction and the mean are linear operators). It can also be shown under certain conditions that in a series of experiments the variance in refractive index at each point in a cross-section in the fluid can be reconstructed by applying the reconstruction algorithm to the variance of the projection data (this follows if the fluctuations from pixel to pixel along a ray are independent).

An experiment to collect data for such a statistical analysis of mixing and fluctuation at each point in a reconstructed tomographic plane has been performed. A spinning vortex plume of warm (24°C) water was directed downward into a tank of cold (15°C) water. Fluctuations are enhanced by the angular velocity and the more bouyant nature of the warm plume. Data for the reconstruction of refractive index cross-sections at the same spatial position was collected.

The reconstruction of the mean of these cross-sections of refractive index (i.e. temperature) is shown in Figure 10. The reconstruction of the variance of this set shown in Figure 11.

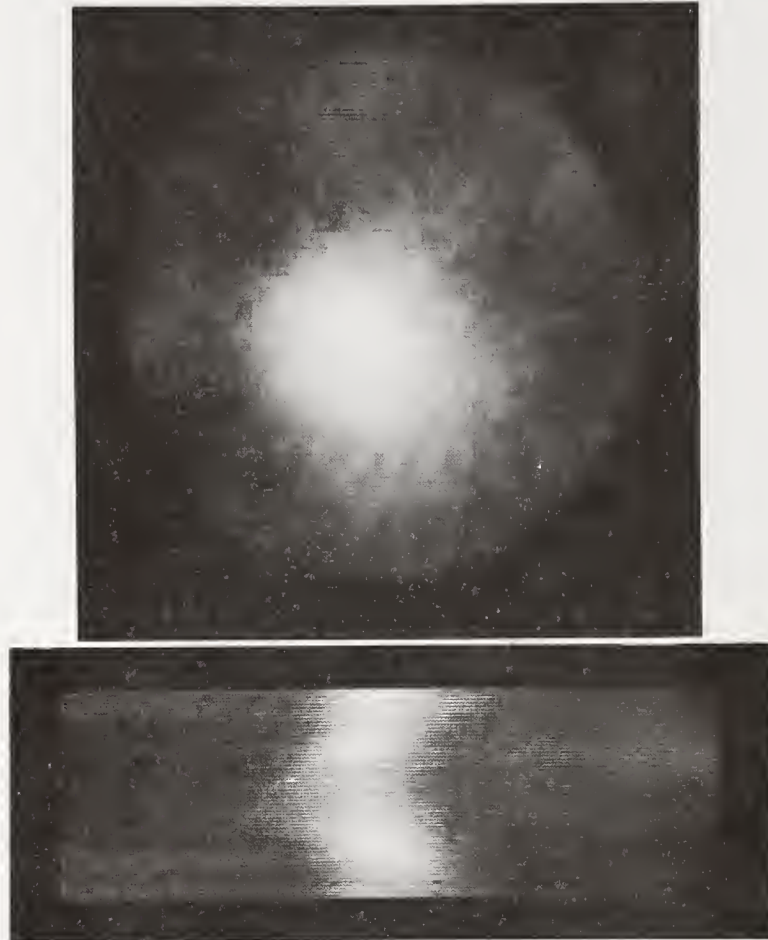


Figure 10 The top image shows a two-dimensional reconstruction of the mean temperature (the acoustic refractive index is temperature dependent) in a spinning warm vortex of water in a tank of cold water from eleven experiments. The image on the bottom is the data used to make the above reconstruction following the same format used to describe the data displayed in Figure 7.



Figure 11 The top image shows a two-dimensional reconstruction of the variance in refractive index (temperature dependent) from eleven experiments. The image on the bottom is the profile data used to make the reconstruction at the top. The profile data shown represents the variance of eleven profiles, each corresponding to one of eleven experiments. See Figure 7 for data format.

10. Potential Applications

One application of this method is the design and construction of improved flow meters for liquids and gases. The ability to reconstruct the local speed of sound allows inference of local density and temperature changes. The combination of velocity and density reconstructions permits the reconstruction of local and net mass flow rates. The inclusion of percent mass per volume of trace materials or pollutants permits the calculation of total mass flow of such materials in pipes, flues, or smoke stacks. Also, the total energy flow may be calculated in regions around wind power extraction machines such as windmills, wind turbines, or vortex towers or vortex power devices. In some circumstances, the temperature of a gas flow may be reconstructed. That this is possible may be seen by observing that the speed of sound in a monoatomic gas is given by

$$C = ((C_p/C_v)kT)^{1/2} \quad (15)$$

where C is the speed of sound C_p and C_v are the heat capacities at constant pressure and constant volume respectively, k is a constant proportional to the molecular weight of the gas, and T is the temperature of the gas in degrees Kelvin. Thus, a reconstruction of C when squared and rescaled provides a reconstruction of the temperature T (or the molecular weight, if T is known).

If the gas has no sources or sinks, then the continuity equation

$$\nabla \cdot (\rho \vec{V}) = 0 \quad (16)$$

where ρ is density and \vec{V} is velocity, may be integrated throughout the region where C and \vec{V} were previously reconstructed. This integration will require some assumptions on the value on some suitable boundary. The integral of Equation 16 is a reconstruction of the density function ρ . The pressure distribution may be obtained by using the gas law, $P = \rho RT/M$ (here, M is the gas molecular weight, R is the gas constant, P is the pressure, ρ = density, T = absolute temperature) and the reconstructions of ρ and T . Thus, a reconstruction of pressure is possible. The technique of measuring temperature might be extended to mixtures of gases using average molecular weights.

As has been seen, the data collected by the apparatus may be processed by algorithms of various levels of sophistication (e.g., straight lines or curved line reconstructions). One further level of improvement would involve the use of certain fluid dynamic equations such as the continuity equation, the momentum equation, and/or the energy equation (or their equivalents) as constraints in the solution of Equation 1. This may lead to greater accuracy in reconstruction or allow reconstruction with less data [1].

One further potential application is the reconstruction of the statistical moments of flow at each voxel (cubic volume element) in space.

Biomedical applications such as measuring flows of blood, respiratory gases, and other fluids both in and out of the body are possible when suitable measuring boundary conditions exist. For example, fluid carrying prosthetic devices could be tested by this noninvasive technique. However, where a suitable measurement collecting boundary does not exist (e.g., flows in the heart can only be viewed from a narrow view angle due to shielding of the lungs), Doppler methods will remain unchallenged.

11. Image Display Methods

The capability to reconstruct the value of a scalar or vector physical parameter in two or three dimensions calls for the use of compatible display methods. Gray scale pictures are useful for 2-D scalar display. The display of vectors sampled

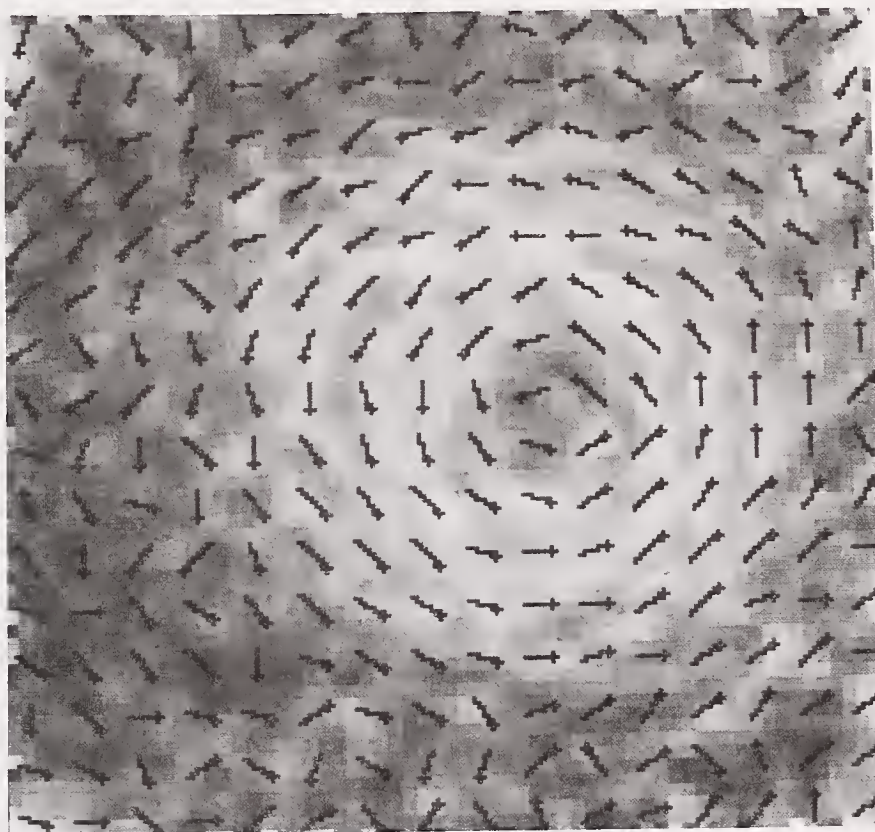


Figure 12 Gray scale (magnitude) and vector array (direction) computer generated image of a reconstructed vortex in a water tank. The array of vectors simulates a square array of yarn tufts, each tuft attached at one end to a stationary button. Thus, the tufts are inclined downstream in the clock-wise flow shown above.

on a 2-D plane may use a separate gray scale images for each component. This techniques was used in Figure 6. Another possible display method could color code the vector field with a color here governed by direction and with brightness or saturation governed by magnitude. Another method, which works well for fluid flow, is to display the stream lines or to display a 2-D array of arrows aligned with the stream lines. A display of the reconstruction of a fluid vortex using a field of arrows superposed upon a gray scale image of flow magnitude is shown in Figure 12. The display of functions in 3-D may be done by use of set of parallel cross-sections or by the use of special three-dimensional display hardware.

SUMMARY

A mathematical theory and computational algorithms are presented for an acoustic method for reconstructing fluid velocity vector fields. Computational FORTRAN programs were written and tested with simulated and real data for the case where the fluid speed is much less than the speed of sound. These tests indicate the method has the capacity for reconstructing three-dimensional fluid flows and net flows. It seems likely the method can be extended to reconstruct mass flow fields (variable density) and temperature fields. The method is capable of reconstructing flows with or without the presence of scattering centers [9].

ACKNOWLEDGEMENTS

The authors wish to thank Miss Pat Snider and associates for the secretarial and graphic assistance in preparing the manuscript. The photographic help of Mr. Leo Johnson is appreciated. The use of Mr. Willis VanNorman's gray scale and color computer graphic programs is appreciated. The support from Dr. Earl H. Wood, Chairman, Biophysical Sciences Unit, Mayo Clinic, and Dr. Erik Ritman, also at Mayo Clinic, is appreciated. Discussion with David T. Pratt, Ph.D. of the University of Utah, M. E. Department, on fluid mixing is appreciated. This research was supported by Grants HL-00170, HL-00060, RR-00007, HL-04664, N01-HT-4-2904 from the National Institutes of Health, United States Public Health Service; N01-CB-64041 from the National Cancer Institute.

REFERENCES

- [1] Johnson, S. A., Greenleaf, J. F., Samayoa, W. F., Duck, F. A., and Sjostrand, J.: Reconstruction of three-dimensional velocity fields and other parameters by acoustic ray tracing. 1975 Ultrasonics Symposium Proceedings, IEEE Cat. #75 CHO 994-4SU.
- [2] Johnson, S. A., Greenleaf, J. F., Chu, A., Sjostrand, J., Gilbert, B. K., and Wood, E. H.: Reconstruction of material characteristics from highly refraction distorted projections by ray tracing. Image Processing for 2-D and 3-D Reconstruction from projections: Theory and practice in Medicine and the physical Sciences. A Digest of Technical Papers, August 4-7, 1975, Stanford, California, pp TUB 2-1 - TUB 2-4.
- [3] White, R. W.: Acoustic ray tracing in moving inhomogeneous fluids. Journal, Acoustical Society of America, Vol. 53, No. 6 (1973).
- [4] Sweeney, D. W., Attwood, D. T., and Coleman, L. W.: Interferometric reconstruction of electron-number densities in laser-induced plasmas, Proc. Image Processing for 2-D and 3-D Reconstructions from Projections, Technical Digest, Optical Soc. Amer., Stanford University, August 4-7 (1975).
- [5] Radulovic, P. T.: Use of a priori information in holographic interferometry of asymmetric refractive index fields. Proc. International Symposium on 3-D Reconstruction, Brookhaven, New York, July (1974).
- [6] Herman, G. T., Lakshminarayanan, A. V., and Rowland, S. W.: The reconstruction of objects from shadowgraphs with high contrasts. Pattern Recognition, Vol. 7, pp 157-165 (1975).
- [7] Greenleaf, J. F., Johnson, S. A., Samayoa, W. F., and Hansen, C. R.: Refractive index by reconstruction: use to improve compound B-scan resolution. Proceedings, Seventh International Symposium on Acoustical Imaging and Holography, August 30-31, 1976, Chicago, Ill.
- [8] Pratt, D. T.: Mixing and chemical reaction in continuous combustion. Prog. Energy Combust. Sci. Vol. 1, 1976, pp 73-86, Pergamon Press, Great Britian.
- [9] Johnson, S. A.: Patent pending.

VALIDATION OF USE OF DYE-DILUTION METHOD FOR FLOW
MEASUREMENT IN LARGE OPEN AND CLOSED CHANNEL FLOWS

W. H. Morgan
Peerless Pump
An Indian Head Company
Montebello, CA 90640

D. Kempf
CEL Laboratories
FMC Corporation
Santa Clara, CA

R. E. Phillips
Turner Designs
Mountain View, CA

The use of water soluble tracers for determining flow rates of rivers and streams has been practiced for several decades, both in the United States and abroad. During the last 15 years the economical availability of water soluble dyes, coupled with the considerable technical improvement in fluorometry equipment, has made feasible the use of dye-dilution methods for in situ calibration of flumes and other flow measurement devices.

In July 1976 a validation of the precision of flow measurement by dye-dilution techniques was undertaken at the St. Anthony Falls Hydraulic Laboratory, University of Minnesota, by comparing volumetrically measured flows over the range of 50,000 to 80,000 GPM. Subsequently, the method was applied in a field acceptance test of a large variable speed vertical turbine pump handling effluent from a wastewater treatment plant.

In both the validation and acceptance tests a dye of the Rhodamine family was continuously injected at a low precisely controlled rate into the flow stream. Several precise dilutions of the injected dye concentrate were prepared so as to bracket the anticipated dilution expected of the measured flow. A fluorometer was used to detect levels of dye concentration in the fully mixed flow at downstream sampling point as well as that of the prepared volumetric diluents.

The most serious of the measuring problems encountered, at the field test site, was the variation in turbidity which was overcome by a change in the type of Rhodamine dye used and through carefully controlled volumetric dilution of samples.

This paper describes the apparatus and procedures used during the validation test as well as those of similar activities pursued during the conduct of verification tests of hydraulic performance for the two installed variable speed pumps. Results of the validation tests are demonstrated to be within 3% of volumetrically determined flows and the field application of the dye-dilution method for determining hydraulic performance are shown to be within 1.5% of the predicted head-capacity pump curve.

1. Introduction

In late 1972 a Mid-West headquartered pump company was awarded a contract to furnish four large single stage mixed flow vertical turbine pumps for installation in a new addition to an existing wastewater treatment plant serving metropolitan Louisville, Kentucky. These pumps handle secondary treatment effluent. The design point of each is 101 MGD (70,000 GPM) at 93 ft. TDH when operating at 600 rpm. Two pumps are each driven by vertically mounted direct connected 2000 HP synchronous motors. The remaining two pumps are each driven through a right angle gear and horizontal Eddy-current coupling connected to a horizontal 2000 HP synchronous motor. Each of the above furnished two types of mounted units are illustrated in Figures 1 and 2. Though the pump manufacturer has facilities to test full size and complete pumping equipment, an agreement was reached with the Consulting Engineers to provide hydraulic performance data for the prototype units based upon the results of model testing.

A brief description of certain aspects of pump location within the Station's pump house will provide background to better appreciate subsequent discussion. A combination of one constant and one variable speed unit is installed in one of two interconnected sump bays. Each unit is served by a 54" diameter steel discharge line in which neither flow measuring devices nor pressure regulating mechanism is installed. Beginning at the pump house the inverts of discharge piping are buried some eight feet below grade. The total length of discharge piping for each variable speed unit is approximately 665 feet (B₁) and 717 feet (B₂) as measured between pump house and outfall located in the levee adjacent to the Ohio River. At the top of the levee each 54" line contains a siphon breaker made from 20" diameter pipe and extending approximately 10 feet above grade. The elevation difference between centerlines of the 54" diameter pipe at pump discharge and at levee is 59.95 feet. After primary treatment the effluent passes through chlorine contact basins and then through a Parshall Flume located just ahead of the sump bays. Though provisions were included for chlorination treatment of the effluent, this process has not as yet been activated. Station layout, Parshall Flume, and discharge line profile are illustrated in Figures 3 - 5.

During September 1975 Station personnel conducted quasi hydraulic performance acceptance tests on each of the installed pumps. These tests were run to verify performance at design point conditions and to establish as well the maximum capacity obtainable under field head conditions without cavitation. The Parshall Flume, with ball-float integrating flow totalizer, was used to measure the effluent in-flow to individual pump bays. Because the Station at that time was not in full operation, only limited quantities of effluent were available which precluded sustained high volume flow rates. This condition caused significant variations of water level both in the flume and sump bays during testing periods. Results of these tests indicated that the pumps were delivering considerably less flow than the specified capacity. Subsequent analysis of forwarded test data

strongly suggested numerous areas of uncertainty in the flow data. In large measure these discrepancies centered around the effect on capacity measurement from undesirable entrance conditions to the flume, inadequate flow and head measuring equipment, and suspect accounting of flow-volume diverted into latent cisterns. Even though the foregoing test data was obscure in certain vital areas, it was left to the pump manufacturer to demonstrate that the installed pumping equipment did, in fact, meet the specified hydraulic conditions.

Throughout a period extending into early 1976 an extensive search was carried on to determine and evaluate the suitability of commercially available flow measuring devices other than the already existing flume. Initially, search was restricted further to flow devices sanctioned by the Standards of the Hydraulic Institute. In addition to instrument accuracy, the cost of the total package required to perform verification testing was of paramount importance to the pump manufacturer.

A variety of flow metering equipment was investigated. These included velocity sampling devices such as the pitot tube, insert turbine meter and insert vortex shedding meter. Single and multi-plane response ultrasonic meters, magnetic and magnetic resonance meters were considered. Devices such as the foregoing were either too costly or were dependent upon assuming a profile for fully developed flow. In this latter connection, recent investigations had demonstrated that even for straight pipe of adequate upstream length random and significant variations from fully developed profiles occurred under steady flow conditions (1). From among differential producing meters the venturi type, flow tube, and orifice plate (end-cap or otherwise) were entertained. Here again initial cost and/or expense of calibration, excavation or installation tended also to rule out these devices as suitable substitutes for the flow measuring flume.

During the foregoing quest, a number of references were encountered citing the use of tracer dyes for flow measurement of streams, rivers, and estuaries (2, 3, 4); calibration of ultrasonic and large venturi meters (5, 6); establishing of flow patterns in forebays of large generating plants as well as the determination of hydraulic performance (7, 8). It became rapidly apparent that only one group of tracers, fluorescent dyes, deserved serious consideration. Such characteristics as low dye cost, being environmentally acceptable, and with portable equipment easier to make quantitative measurements of flow rate in any shape and size of conduit. This method was suited ideally for our purpose with one exception, i.e., the method was not sanctioned by the Hydraulic Institute.

After a number of discussions between representatives having job site vested interests, agreement was reached for the use of the dye-dilution technique at the job site for measuring pump flow. Acceptance of this proposed method was qualified, however, by the proviso that a measuring accuracy to within 3% of true flow be demonstrated through validation testing.

Figures in parentheses indicate the literature references at the end of this paper.

To meet the requirements for a validation test proved to be a formidable challenge. Foremost of these was in assessing the degree of accuracy obtainable for controllable flows bracketing the 70,000 GPM design point of the pump. A further prerequisite was for a large reservoir capacity of unrecirculated water that would provide an approximate constant head during capacity draw off. An additional desirable condition would be to have a water composition that contained a minimum amount of suspended solids. Obviously, for reasons of economy, the location should be within the continental United States. Fortunately, these requirements were realized at the University of Minnesota's St. Anthony Falls Hydraulic Laboratory under the direction of Professor John F. Ripken. Figures 6 and 7 show certain of the facilities of this Laboratory used for validation testing.

This paper deals not only with the activities and results connected with the validation test, but also includes the procedures used and results from the use of dye-dilution techniques during subsequent hydraulic performance verification tests of installed equipment.

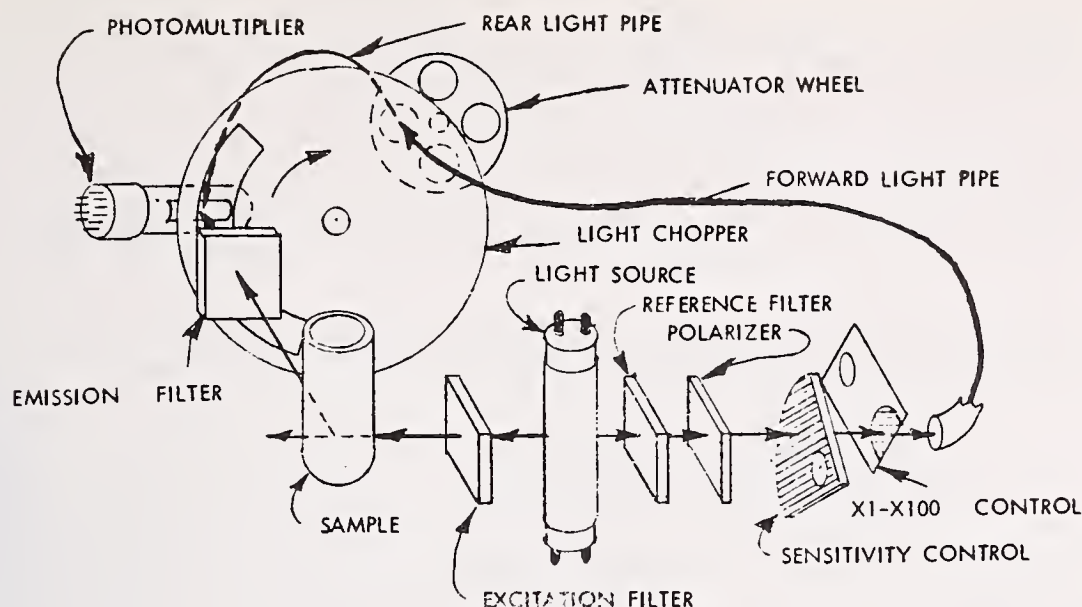
2. Validation Tests

A special physical phenomenon called fluorescence characterizes certain tracers and it is this distinctive property upon which the dye-dilution technique depends. A fluorescent substance is one which absorbs light of one wavelength (color) and emits light of a different wavelength.

- a. Dye: From a number of fluorescent tracers available, two from the organic Rhodamine family were chosen as being suitable for use at either test location. They are Rhodamine B and/or WT. At the validation test site only Rhodamine B was used. Each of these dyes has a detection limit of 10 ppt or less. Rhodamine B, in powder or liquid form, is more available commercially than the liquid Rhodamine WT. In liquid form Rhodamine B comes in an acetic acid solution of 40% (by wt.), while Rhodamine WT is supplied in a 20% aqueous solution. These tracers are highly persistent and great care must be exercised during their handling and in the preparation of dilutions. It is essential that once a flask or pipette is used for a particular dilution that those pieces of glassware be thereafter dedicated for that same dilution. Both of the Rhodamines absorb readily to some plastic containers. Therefore it is recommended that flasks, pipettes, and sampling bottles be of borosilicate glass (Pyrex), polyethylene, or polypropylene materials (9).

- b. Equipment

- 1) Fluorometer: The fluorometer measures the strength of the fluorescence in a diluent. A schematic diagram of the Turner Designs Model 10 Series portable fluorometer used for both the validation and verification tests is shown on the following page:



OPTICAL SYSTEM

With this instrument set in automatic mode, should a reading fall below 20% of full scale, a more sensitive range is automatically selected. Adjustment for background fluorescence is made only on one range and, if during operation other ranges are selected, the proper correction will be made automatically. Zero light also gives zero reading. Its sensitivity permits detectability to less than 10 parts/trillion and provides response linearity to within $\pm 1\%$. The instrument is portable and can be operated on conventional AC or powered by battery. Because the instrument is water-proofed, it can be used in a high moisture-laden environment without affecting its operation or accuracy of response. The instrument contains telemetry outputs for driving recorder equipment.

- 2) **Injection Pump:** The constant-rate injection pump contains a 1/4" diameter polished and ground piston operating within an accurately honed cylinder block. The pump is driven by a 1/8 HP synchronous motor. This type driver assures that the established flow of injected dye will be maintained at a constant rate of delivery over extended periods of continuous operation. The desired flow rate is obtained by micrometer adjustment of stroke. During validation tests, the injection rate was set at 78.7×10^{-6} cfs. The injection pump recirculated dye stock for a minimum of 1/2 hour to insure that pump parts reach a stable operating temperature. After warm-up the rate of injection flow is determined by the time required to fill a two-liter volumetric flask.
- 3) **Digital Voltmeter:** A digital voltmeter, Model 5900 with BCD output is plugged into telemetry outputs of the fluorometer. This displayed visual response to relative change in fluorescence of the diluent.

- 4) Digital Printer: A Model 5505A printer was used to make a permanent record of the change in millivolts - a function of a change in fluorescence.
- 5) Assorted Glassware:
 - a) Volumetric Flasks - Class A; six two-liter and two one-liter.
 - b) Volumetric Pipette - Class A; three each of 5, 10, 20, 50, and 100 millileters.
 - c) Sample Bottles - Polyethylene Plastic with screw-on Polypropylene caps.
- 6) Mixing Vessel for "Stock"; 30 gallon plastic container.

Definition of terms used in connection with the dye-dilution technique described in this paper.

- 1) STOCK A concentration of dye contained in the mixing vessel that is not only injected into the flow path, but is used also to make the STANDARDS dilutions.
- 2) BASE SOLUTIONS Intermediate dilutions of the STOCK from which STANDARDS dilutions are prepared.
- 3) STANDARD A "standard" is a known concentration or dilution of the injected dye. The dilution is made using precisely measured volumes of the flow media and dye being injected. Dilutions, known here as alpha, beta, and gamma standards are of such a concentration as to bracket the anticipated concentration level of the SAMPLE.
- 4) BLANK The amount of fluorescent materials occurring naturally in the system expressed as a concentration of the fluorescent material being measured. The fluctuation of blank during a measurement period is the important factor and not the absolute magnitude.
- 5) SAMPLE An amount drawn from the flowing media, downstream from the point of dye-injection, that contains a concentration of dispersed dye.
- 6) DILUTION RATIO This is the entire basis of the technique. The ratio is formed by the relative concentrations of injected dye and that of the SAMPLE collected.
- 7) CUVETTE A glass sample holder of specific dimensions inserted into the fluorometer for subsequent analysis of the fluorescence level of contained media. The cuvette was used to hold quantities of BLANK, STANDARD, and SAMPLE from each test run.

PREPARATION OF DILUTIONS: One of the most critical preparatory phases in the use of the dye-dilution method is the preparation of the STANDARDS. It is essential that all flasks and pipettes be thoroughly rinsed with undiluted media and that each flask or pipette once used for the preparation of a specific dilution be dedicated thereafter to the particular dilution for which the glass hardware was first used. This precaution cannot be overly emphasized since Rhodamine dye is extremely persistent.

1. In succession and proper sequence, approximately fill each 2-liter flask to graduated line with undiluted flow media obtained from the Station at which SAMPLES will be drawn.
2. Dilute the STOCK concentration by preparing at least two BASE dilutions. Using dedicated flasks and pipettes draw a 20 ml volume of the STOCK and slowly drip into 2-liter flask of first BASE. Using a dedicated pipette top off to graduated line with undiluted flow media. The second BASE is prepared similarly using again a dedicated 20 ml pipette and 2-liter flask. However, the second BASE is prepared by withdrawing 20 ml of the resultant first BASE dilution.
3. Again in a similar manner the three STANDARDS, alpha (α), beta (β), and gamma (γ) are prepared, except that specific volumes used in their preparation are each drawn from the second BASE.
4. A diagram for preparing these separate dilutions is shown in Fig. 8.
5. It will be noted that each of the STANDARDS bear to each other a concentration ratio of 1, 2, and 4.

DETERMINATION OF DISCHARGE FLOW - CONSTANT RATE INJECTION: When using the dye-dilution method it is not necessary to know the exact concentration of either the dye injected or that of the sample collected downstream. It is necessary only to know the dilution factor. In both validation and verification tests the constant-rate injection method was used. The flow rate to be determined (Q) is related to the dilution factor and the rate of dye injection as follows:

$$Q = q \left[\frac{C}{c} \right] \text{ where} \quad (1)$$

Q = Flow rate in test channel (or discharge flow)

q = Flow rate of the constant-rate injection pump

C = Concentration of the dye being injected

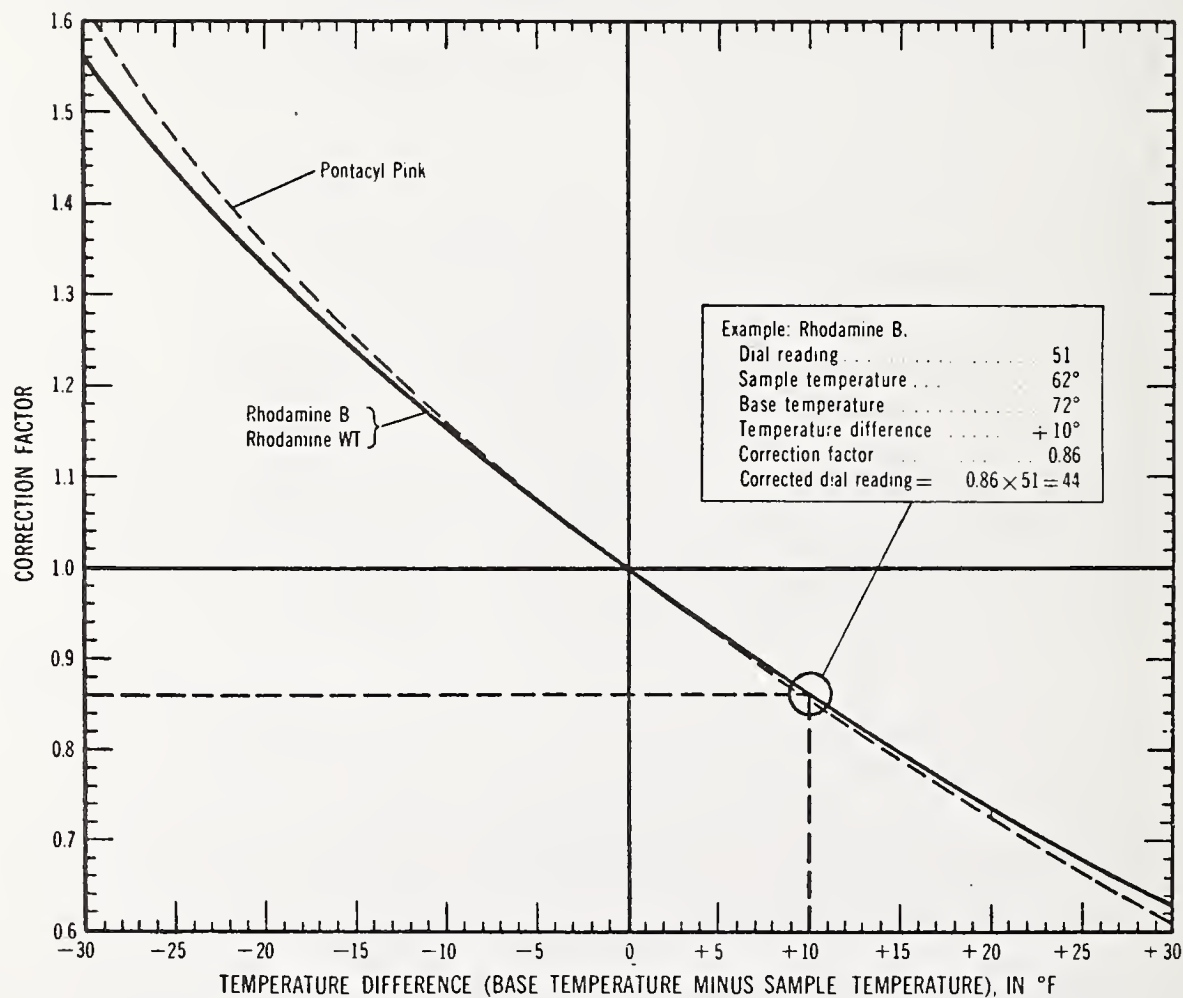
c = Concentration level of dye dispersed throughout the flow media and collected as SAMPLE downstream

The point at which samples are drawn must be located sufficiently downstream of the point of dye injection to assure complete mixing across the plane of flow.

To account for background fluorescence a BLANK of undiluted media is drawn at the sampling point before and after each test run. A numerical value of the BLANK'S fluorescence is determined by the fluorometer. In our case, this value is transmitted through the instrument's telemetry output terminals and converted into signal levels to drive the printer. The numerical value of the BLANK (B) is subtracted from each term in the DILUTION RATIO before determining discharge flow rate. To account for the fluorescence of the BLANK the foregoing relationship is modified to read as follows:

$$Q = q \left[\frac{C - B}{c - B} \right] \quad (2)$$

Should a temperature difference exist between quantities in the dilution rates, each should be temperature compensated before the determination of discharge flow. A temperature correction curve is shown below (10):



TESTS AND RESULTS: A sketch of the test setup is shown in Fig. 9. Two sampling Stations were used in the validation test. Station No. 1 was located approximately 190 feet downstream from the point of constant-rate injection. A second Station was subsequently set up out on the walkway between the two volumetric tanks. An approximate flow rate was established by adjusting the variable orifice plate at upper river pool. The final flow rate was determined by flow measurements in the Hydraulic Laboratory's two calibrated volumetric basins. A continuous and constant rate of flow was assured by virtue of the large upper pool reservoir being a flow branch of the Mississippi River. By means of a unique system of diverter valves located upstream and just preceding the volumetric basins the established flow rate in the test channel can be switched rapidly (in less than 2 seconds) from one volumetric basin to another and without flow interruption.

After flow is established in the test channel, BLANKS are drawn before the dye is injected. After dye injection a period of 10 minutes was allowed for complete dispersion of dye in the flow stream and before the start of filling volumetric basins as well as simultaneous taking of SAMPLES.

The first few days of testing were unproductive. The dye technique was consistently yielding calculated flows approximately 8% lower than the volumetric calibration. A common technique was being used in which the sample water from the flume was continuously pumped through a flow cell in the fluorometer. The fluorometer was calibrated by pouring standard dilutions of the stock solution dye through the flow cell. The water for the standards was collected from the river upper pool just prior to entry into the flume. The intention was to provide an automatic correction for any masking effect of suspended solids by preparing the standards in the same water whose flow rate was being measured. It was some time before it was recognized that the water at the sampling point was grossly different from the entry water. The extreme turbulence in the flume introduced massive amounts of air bubbles, some of which were microscopic, and rose very slowly. These air bubbles scattered the exciting light in the fluorometer and this scattered light was causing the instrument to effectively add a constant 0.08 ppb of dye to the measurement. Had the dye concentration been 50 ppb, instead of 1.0 ppb, the error introduced would have been only 0.16%. Lack of dye prevented increasing the concentration, so the effect was largely overcome by collecting dilution water at the sample point, and measuring some thirty discrete samples. Standards and samples were allowed to stand for as closely as possible the same length of time in the hope that the scattering effect would be the same. At this point, time and available storage vials did not permit letting the samples stand long enough to permit the bubbles to completely dissipate. Had it been possible to use higher dye concentration, or permit overnight standing, it is believed correlation with the volumetric calibration would have been even better than reported. From a practical standpoint accuracies of better than 1.% are difficult to obtain with this method in other than laboratory conditions.

By adopting the above control techniques the resultant determination of discharge flow by the dye-dilution method correlated well with that determined by volumetric basin measurements. The accompanying Percent Deviation Curve, Fig. 10 displays the results of test runs 9 through 15, shown in Table 1.

TABLE 1. DATA AND RESULTS FROM SIX TEST RUNS

DATE		7/30	7/31	7/31	7/31	7/31	7/31
TEST RUN		9	10	11	12	13	14
INJECTION FLOW cfs x 10 ⁻⁶		78.7	78.8	78.8	78.8	78.8	78.8
FLUOROMETER OUTPUT - mv	BLANK	7.5	15.0	17.0	125.5	106.33	125.0
	STANDARDS						
	Alpha	*	2653	2679	8624.16	**	**
	Beta	1123	1314	1348.25	4332.92	4530	4370
	Gamma	*	665	683	2197.5	**	**
	SAMPLES	2433.4	3869	1945.17	3678.84	4162.2	4477.35
DISCHARGE FLOW; DYE-DILUTION, cfs		72.377	53.11	198.81	186.61	171.89	153.71
DISCHARGE FLOW; VOLUMETRIC BASINS, cfs		74.031	54.463	106.012	198.352	175.096	155.793
PERCENT ERROR		-2.23	-2.48	+2.64	-5.92	-1.83	-1.34

*These STANDARDS compromised

**These STANDARDS not read due to curtailed test schedule

The scatter pattern of results, with the exception of run #12, fell within a tolerance zone of $\pm 3\%$. The regression line for all points, including test run #12, lies almost wholly within the -3% error zone which, together with its correlation coefficient of $+0.998$, supports the contention that, under prevailing conditions at the validation test site, the dye-dilution method for determining discharge flow will produce results at least within the objective of a $\pm 3\%$ error.

A sample calculation for determining the discharge flow by the dilution method follows.

SAMPLE CALCULATION

From Run #10

Injection Flow Rate (q):

1. Time to fill 2-liter flask = 14.95 minutes

2. $q = \frac{2.000 \text{ l} \times 0.2642 \text{ gal/l}}{14.95} = 35.34 \times 10^{-3} \text{ GPM}$

$q = 78.8 \times 10^{-6} \text{ cfs}$

Flow Rate in Channel by Dye-Dilution Q:

1. $Q = q \left[\frac{C - B}{c - B} \right]$

where C = B Standard; C = 1314 mv at ratio 2×10^6

B = Blank B = 15 mv

c = Sample c = 3869 mv

2. $Q = (78.8 \times 10^{-6}) \left[\frac{1314 - 15}{3869 - 15} \right] (2 \times 10^6)$

$= 78.8 \left[\frac{1299}{3854} \right] 2$

$Q = 53.11 \text{ cfs}$

CONCLUSIONS: The following observations pertain to the procedures used and results obtained during validation testing:

1. At the outset, turbidity of the Mississippi River was believed to be the prime factor affecting correlation between volumetrically determined discharge flows and those obtained by dye-dilution. Due to the change in preparatory procedures prior to fluorometric analysis, the subsequent correlation between each method of flow determination was greatly improved. Therefore, it was felt that turbidity had negligible effect on the correlation results.
2. Highly turbulent flow created by the waterfall effect at the bottom of the dye-injection shaft created microscopic bubbles that caused a positive measurement error. This effect was the most significant factor in not being able to correlate better between flow rates obtained by the two measuring methods. The detrimental effect on the data from this condition was largely overcome by procedures adopted during the last day's activities.
3. Taking undyed water for the preparation of STANDARDS, as well as taking of BLANKS and SAMPLES, all from the same test Station, improved data correlation.
4. Placing STANDARDS, BLANKS, and SAMPLES in a constant temperature bath for at least 30 minutes greatly contributed toward improvement in the results. This time period also allowed a share of the entrained bubbles to rise from solution and partially overcame their undesirable effect on data.
5. The overall conclusions, based on data and activities associated with validation testing, confirmed the contention that discharge flows could be determined within the permissible error of $\pm 3\%$ provided that extreme care was used in the preparation and handling of dilutions; adopting proper procedures for collecting, storing, and handling of the various dilutions prior to fluorometric analysis; having on hand an adequate amount of dye concentrate to, if necessary, adjust downstream concentrations for extended periods of time to levels in excess of 50 ppb; and the availability at a test site of the services of a chemist or chemical engineer.

3. Verification Tests

Job-site verification tests began the week of September 26. However, on the evening of September 27, the day prior to the start of the testing, the area was drenched by torrential rainfall which did not abate till mid-day October 2. Postponement to a more favorable period was ruled out due to customer scheduling and prior commitments of personnel involved in the tests. Climatic conditions created a number of untoward problems previously unencountered. The greatest of these was the direct passage through the treatment plant of raw sewage and

heavy silt loads from overflowing catch basins. As a result, some procedures established during the Minnesota validation test were modified, of necessity, to procedures that require more time-consuming dye-dilution techniques before obtaining final fluorescence values of specific dilutions.

The Pump Station contained four pumping units that were designated by the Station as B1 and B2 for variable-speed pumping units, Fig. 2 and by B3 and B4 for the constant-speed units, Fig. 1. As mentioned previously in the Introduction, there were no provisions for controlling pump discharge pressure so that only by speed regulation could flow rates and discharge pressure be varied. Therefore, field performance tests were performed only on the variable speed units. Capacity was determined by the dye-dilution method while discharge head was observed by pressure indication on a calibrated pressure gage whose sensing line was connected to a pressure manifold tapped into the pump column.

a. Dye: Both Rhodamine B and Rhodamine WT tracer dyes were used. After the first test, only Rhodamine WT was used due to its lower absorption characteristic.

b. Equipment:

- 1) The same Fluorometer, Injection Pump, Digital Voltmeter, and Digital Printer were used during job-site tests as were used at the validation test site. Volumetric flask glassware, of similar make and size, and STOCK mixing vessel were duplicated.
- 2) Submersible Pump: 3 gpm capacity.
- 3) Calibrated pressure gage: Range 0-200 feet H₂O; graduated in 2/10 foot increments capable of interpolation to 1/10 foot; 8: dial.
- 4) Digital Counter: Model 521A; interfaced with an electromagnetic tack-generator pick-up having 60 tooth gear head.
- 5) Cuvettes: #9820 rimless Pyrex culture tubes, 13 mm x 100 mm.

PREPARATION OF DILUTIONS: Precautions similar to those practiced during validation were applied in the preparation of dilutions used in the verification test. Concentrations of these dilutions were prepared by procedures described earlier.

1. STOCK

- a) For run #0 only a STOCK solution was prepared by diluting 40 percent active Rhodamine B to approximately 1.6 percent.
- b) For runs #1, 2, 3 and 4 a STOCK solution was prepared by diluting 20 percent active Rhodamine WT to approximately 4.0 percent.

2. STANDARDS

- a) The Alpha, Beta, and Gamma STANDARDS were prepared from the second BASE by diluting 30 ml, 20 ml, and 10 ml respectively to 2000 ml.
- b) For all tests the relative concentrations of Alpha, Beta and Gamma were in the order of 3, 2, and 1 respectively.

All dilutions were prepared using undyed effluent drawn from the downstream sampling test station.

DETERMINATION OF DISCHARGE FLOW: Constant-rate injection was used. Therefore, as described previously, the DILUTION RATIO, BLANK, and dye-injection rate were related in the same manner to obtain discharge flow.

TEST AND TEST PROCEDURE: Fig. 11 and Fig. 5 illustrate the test setup and test station locations.

The siphon breaker, in the discharge line of test pump, was unbolted at grade flange and pivoted out of the way. The sump pump fastened to its 3-inch diameter support pipe was inserted through the exposed opening down to approximately the centerline depth of the 54-inch discharge pipe. The support was then anchored to siphon breaker flange. Through use of the sump pump a continuous stream of the discharging effluent was brought to grade. One pint polyethylene bottles were rinsed several times with the effluent, then filled. Thus, from the sampling station, undyed effluent was drawn for use not only in preparing the STANDARDS but also in detecting background fluorescence of the flow stream (BLANKS). All of the SAMPLES of the effluent containing injected dye were collected in similar manner and from the same sampling station. Preceding each test run, and at the sampling station, a number of BLANKS were drawn as well as a quantity of undyed effluent for the making of STANDARDS.

For test runs #0 and #1 stop gates in the Station's flow-through channel were regulated so that a portion of effluent passed through the flume and into the test pumps' sump bay. A stabilized flow rate was obtained by a combination of stop gate regulation and pump speed. Sump levels were read on a tide board that was installed by transit in each sump. Stabilization was achieved when the sump level remained essentially constant. The 10 foot mark on the tide board was used as the reference datum and corresponded to Pump Station's elevation 400.0.

When flow into pump sump had stabilized and with pump speed steady dye was injected through the delivery tube and into pump suction. After a minimum of 5-minutes had elapsed, to allow for pipe surface coating and diffusion of dye in the flow path, a number of SAMPLES were drawn from the downstream sampling point. Thirty SAMPLES were obtained for each test run except #4 in which only nine SAMPLES were collected.

For each test run, and covering the same time period during which SAMPLES were being obtained, pressure gage levels, pump speed and sump elevation were being monitored and recorded. Table 2 includes a sample of such data.

After SAMPLES were collected, an interval lasting approximately 20 minutes, dye-injection was stopped. It is to be noted that the injection pump is not stopped. The dye is diverted to the mixing vessel and then recirculated. A ten minute period was considered sufficient to allow the system to be purged of residual dye after which final BLANKS and undyed effluent for the making of new STANDARDS were drawn. All SAMPLES and BLANKS were transported to the Treatment Plant's chemical laboratory and there placed in a temperature stabilizing bath. STANDARDS were placed also in the same bath.

On October 3 the Wastewater Treatment Plant's capacity could keep up with incoming flow without having to "pass-through" untreated effluent. Thus, for test runs #2, #3, and #4 secondary treatment effluent entered sump bays.

In order to complete the tests as scheduled, which had been complicated and delayed by weather conditions, BLANKS were not drawn nor STANDARDS prepared between runs #2 and #3 and between runs #3 and #4.

LABORATORY PROCEDURES: The effect of the high and variable turbidity on the accuracy of discharge flow was directly dependent upon the amount of dye that might be absorbed by substances in the effluent.

Filtration and absorption recovery tests were made of the Rhodamine B dye from the effluent. Dilutions were prepared with a 5 ml solution of Rhodamine B dye using distilled water. By comparing fluorometric readings of these filtered and unfiltered dilutions it was noted that Rhodamine B dye was partially lost by sorption on the filter medium. Further recovery studies on equal dilutions in the effluent and in distilled water indicated an apparent loss of 27% in the effluent. An automatic correction factor applied to the data could take this into account were it not for the distinct possibility that a variable solids load existed. One can appreciate the error introduced if, for example, a 10% change in solids (undiluted) would yield a 2.7% error. Filtration of the test dilutions was unacceptable since the resulting fluorometer readings would be lower, indicating higher than actual flow rates.

An additional recovery study was made consisting of further specific dilutions to test specimens of dye-effluent solutions. Ten milliliters of the specimens were diluted to 100 milliliters with distilled water. The result of this study showed that the effect from variable turbidity on the determined flow rate would introduce an error less than 0.3%. It was also proved by this study that the tracer was masked by the solids and not absorbed on the solids. Therefore, for each test run all BLANKS, STANDARDS, and SAMPLES were diluted tenfold with distilled water before analysis.

A portion of each BLANK, STANDARD, and SAMPLE was poured into individual cuvettes that had been previously washed. These cuvettes

were then placed in a room temperature water bath whose level was at approximately 1/4 inch above the fluid level in the cuvette. After a 15 minute period to allow the fluid to temperature stabilize, each cuvette was placed in the warmed-up fluorometer and analyzed. For each cuvette sample 10 readings were recorded at approximately 0.8 second intervals initiated after a 10 second stabilizing period. An average of the printout readings of SAMPLES and the before and after BLANKS and STANDARDS were used in the dye-dilution relation as described previously.

RESULTS: This section is divided into two parts. First, the determination of discharge flow rate (capacity - gpm) and second, the determination of the pump's total field head (TDH - feet) as measured across the plane of pump discharge.

1. Capacity: Hand calculations done in the field were refined later by statistical methods. Steps in the statistical analysis included the following operations:

- a) A mean and standard deviation of ten readings for each SAMPLE, BLANK, and STANDARD were calculated.
- b) A calibration curve was generated for each set of SAMPLES by plotting the calibration standard means as a function of relative dye concentration. A least squares linear regression analysis was performed. Utilizing the calibration curve, each SAMPLE mean was converted to a relative dye concentration, and a flow value was calculated.
- c) A statistical analysis was performed of the flow values obtained for each test run. This includes calculations of mean flow values, standard deviations and 95 percent confidence limits. See Appendix for a sample calculation.
- d) The capacity determined by the foregoing analyses is tabulated below:

<u>Run No.</u>	<u>Date</u>	<u>Pump No.</u>	<u>Mean Flow + 95% Confidence Limit (GPM)</u>
0	9-30	B ₁	51.2 (+3) \pm 1.4 (+3)
1	10-1	B ₁	54.2 (+3) \pm 0.3 (+3)
2	10-3	B ₂	63.0 (+3) \pm 0.5 (+3)
3	10-3	B ₂	59.8 (+3) \pm 0.5 (+3)
4	10-3	B ₂	67.1 (+3) \pm 1.6 (+3)

2. TDH(Field): In the test set-up drawing, Fig. 11, a distance is given from the floor to centerline of gage for unit B₁ and B₂. Converted to Station elevations these are 419.52 and 420.79

respectively. The average of water surface elevations for a given test run was subtracted from the respective gage elevation to obtain the vertical distance Z in the equation:

$$H_{\text{gage}} + \frac{V^2}{2g} + Z = \text{Pressure at manifold location, feet} \quad (3)$$

The value for $V^2/2g$ is calculated using an inside diameter of 54 inches for both column and discharge piping. The value used for acceleration of gravity, g , is 32.17 ft./sec.².

To obtain total field discharge head, at outlet face of discharge elbow, the head loss for the column (above pressure manifold) and that of the discharge elbow are each subtracted from the results obtained in (3) above, i.e.

$$\text{TDH (Field) = } H_{\text{gage}} + \frac{V^2}{2g} + Z - (H_{\text{Col}} + H_{\text{Disch elbow}}), \quad (4)$$

feet

Table 3 gives the result of combining these head values for each pump flow rate as was determined by the dye-dilution method.

The values shown in Table 4 result from applying corrections to Table I values for RPM, GPM, and TDH so as to obtain the pump's head-capacity characteristic at the constant design speed of 600 rpm. The corrections applied to the data are based on the use of certain of the Affinity Laws which relationships are used throughout the pump industry and which are also in accordance with the Standards of the Hydraulic Institute (11).

3. Figure 12 provides a plot of pump field performance based on the separate results of the above two steps.
4. Because of an electrical power failure to the B1 variable speed unit (requiring more time to repair than was available within the time allocated for testing) only runs #0 and #1 were made with this unit. The remaining test runs #2, #3, #4 and #5 were made using the B2 variable speed unit.

During the dye-dilution tests, Station personnel took comparative flow readings using the Parshall Flume's instrumentation. Based on the results from this parallel activity Station operators determined that their integrating flow totalizer equipment was out-of-calibration. As a consequence their previously obtained flow measurements were erroneous, producing flow readings that were low by as much as 15 percent. It was determined also that this error was not constant throughout the flow range.

The capacity shown for test run #5 was obtained after the dye-dilution tests were completed. The purpose of this test was to determine the maximum flow rate available to the Station under one pump operation should such a contingency arise.

TABLE 3

TOTAL DYNAMIC HEAD-FIELD

TEST RUN NO.	RPM	GPM	GAGE PRESS. FEET	* ☒ OF GAGE TO WATER SURFACE "Z" FEET	VELOCITY HEAD $V^2/2g$ FEET	** ELBOW PLUS COLUMN LOSSES FEET	TDH FIELD FEET	MGD
0	492	51,200	45.8	22.5	0.795	0.312	68.8	73.7
1	495	54,200	46.1	22.5	0.898	0.350	69.2	78.0
3	506	59,800	46.3	20.2	1.093	0.428	67.2	86.1
2	517	63,000	46.3	20.8	1.213	0.474	67.8	90.7
4	532	67,100	46.6	20.3	1.376	0.538	67.8	96.6
5	602	84,000	46.2	21.8	2.156	0.840	69.3	120.9

*To Water Surface: Elevation of Gage ☒ Minus Elevation of Water Surface in Wet Well

**Calculated: Based on Procedures Contained in References (12) and (13)

TABLE 4

TABLE 3 DATA CONVERTED TO 600 RPM

TEST RUN NO.	RPM	GPM	TDH FIELD FEET	RPM	GPM	TDH FIELD FEET	MGD
0	492	51,200	68.8	600	62,439	102.3	89.9
1	495	54,200	69.2	600	65,697	101.7	94.6
3	506	59,800	67.2	600	70,909	94.5	102.1
2	517	63,000	67.8	600	73,114	91.3	105.3
4	532	67,100	67.8	600	75,677	86.2	109.0
5	602	84,000	69.3	600	83,720	68.8	120.5

To perform this test both of the chlorine contact tanks were filled to almost overflowing as well as each of the interconnected sump bays. The pump speed was adjusted to approximately design speed and the decrease in surface level of the channels recorded. This test was based on volumetric changes in the artificially created reservoir. These latter readings, plus the Parshall Flume's readout values were used to approximate the capacity. The previously determined error in the Parshall Flume's instrumentation was taken into account in arriving at this approximate value for capacity.

CONCLUSIONS: The following observations pertain to the procedures used and results obtained during pump verification testing.

1. Extreme turbidity of the effluent and its variable solids content required the use of dye-dilution techniques different from those practiced at the validation test. Dye recovery studies demonstrated that Rhodamine B was absorbed on the glass filter medium during attempts at filtration. It was demonstrated that by using distilled water to make tenfold dilutions of the various samples that 99.5% of full recovery was assured.
2. It is advisable to use high concentrations of injected dye, consistent with EPA regulations, so as to ensure that the dye concentration of the SAMPLE is sufficiently high to nullify background fluorescence and the effects from minor turbidity on fluorometric analysis. The change to Rhodamine WT, obtained locally, permitted a 2-1/2-fold increase in the concentration of the injected dye over that used with Rhodamine B, which had been brought to the job site in limited quantity.
3. Before fluorometric analysis, place all STANDARDS, BLANKS, and SAMPLES in a room temperature water bath for as long a temperature stabilizing period, as is consistent with the test schedule, but for not less than 1/2 hour.
4. It is recommended that a chemist be retained as consultant during the first three or four times the dye-dilution method is applied for the determination of flow rate.
5. The dye-dilution technique based on the procedure and results outlined in this paper is an economical method for field use where metering and valving are not included in a buried or otherwise inaccessible discharge line. By using this technique, the field performance of the tested units met specified hydraulic design conditions and was within 1-1/2% of predicted H-Q curve.

ACKNOWLEDGMENT is given to Messrs. G. W. Allen, S. G. Sharp, and Ms. L. A. Enriquez, R&D, PG&E, Ca.; and also to Messrs. G. W. Crabtree, and F. Martin (illustrations), Peerless Pump, for their expertise and valuable assistance during the course of one or both of the tests.

4. REFERENCES

- (1) Alden Research Laboratories, Worcester Polytechnic Institute, Evaluation of the Westinghouse Leading Edge Flow Measurement System, Report ARL M71-83.
- (2) Pritchard, D. W., and Carpenter, J. H., Measurements of Turbulent Diffusion in Estuarine and Inshore Waters, in International Assoc. Sci. Hydrology Bulletin 20, 37-50 (1960).
- (3) Nickerson, D. H., Gloucester-Forced Circulation of Babson Reservoir, in Sanitalk, Quarterly Review, Mass., Division of Sanitary Engineering, 1-10 (1961).
- (4) Kilpatrick, A. M., Flow Calibration by Dye-Dilution Measurement, in Civil Engineering, 74-76 (1968).
- (5) BATTELLE, Pacific Northwest Laboratories, Performance Evaluation of --- 96 Inch, 900 cfs Venturi Flowmeter, Report (1973)
- (6) Allen, G. W. and Sharp, S. G., Moss Landing Dye-Dilution Pump Test, Report (1976).
- (7) Hutton, S. P. and Murdock, Comparative Flow-Measurement Tests at Finlarig Power Station, 395-404 (1962).
- (8) U. S. Dept. of Interior, Bureau of Reclamation, Pump Acceptance Test - Dos Amigos Pumping Plant, Report HM-17 (1973).
- (9) Turner Designs Brochures; Fluorometric Facts-Flow Measurements; and Flow Measurements in Sanitary Sewers by Dye-Dilution.
- (10) U. S. Dept. of Interior, Techniques of Water-Resources Investigations of the United States Geological Survey, Fluorometric Procedures for Dye Tracing, Book 3, Chapter 12A, 28 (1968).
- (11) Hydraulic Institute Standards, 13th Edition, Test Code, 62 (1975).
- (12) Hydraulic Institute Standards, Pipe Friction Manual, 24 (1961).
- (13) Miller, D. S., Internal Flow - A Guide to Losses in Pipe and Duct Systems, Part I, Design Data, 19 (1971).

SAMPLE CALCULATION, RUN 3b1. CAPACITY:

SAMPLE #22

- a. Results of ten telemetry readings, (mv) from fluorometer analysis
 3644, 3739, 3599, 3554, 3585
 3592, 3395, 3569, 3519, 3505

b. Mean Response (R) of above data = 3579 mv

c. Standard Deviation (S) = 44.9

d. Linear Regression Equation - based on Run 3b calibration curve

$$R = 143.1413C + 158.99$$

$$\text{Intercept} = 158.99$$

$$\text{Slope} = 143.1413$$

Where C = relative dye concentration, ppb, of the SAMPLE
 to STOCK concentration

$$e. C = \frac{(R - 158.99)}{143.1413} = \frac{(3579 - 158.99)}{143.1413} = 23.89 \times 10^{-9}$$

f. C_1 = Concentration of injected Rhodamine WT (0.04)

g. q = Mean flow rate of injection pump (based on time to fill a
 2-liter volumetric flask)

$$q = \frac{2.000 \text{ L} \times 0.2642 \text{ gal/L}}{14.82 \text{ min}} = 35.65 \times 10^{-3} \text{ gpm}$$

h. Discharge Capacity:

$$Q = \frac{(0.04)(35.65 \times 10^{-3})}{23.89 \times 10^{-9}} = 59,690 \text{ GPM}$$

Note: If the mathematical mean of all 29 SAMPLES was used, the tabulated discharge capacity of 59,800 GPM would be obtained.

2. TOTAL DYNAMIC HEAD-FIELD:

- a. By proper substitution of applicable values from Run 3, Table 3, into the head equation (4), the total field head at outlet face of discharge elbow for 506 rpm pump speed will be obtained.
- b. The right hand portion of Table 4 gives the CAPACITY and TOTAL DYNAMIC HEAD-FIELD for the pump's design speed of 600 RPM. These values are obtained by using the following Affinity Law relations:

$$\text{GPM}_2 = \text{GPM}_1 \frac{\text{RPM}_2}{\text{RPM}_1} \quad \text{and} \quad H_2 = H_1 \frac{\text{RPM}_2}{\text{RPM}_1}$$

Where the subscript 1 relates to the capacity and head obtained at test speed while subscript 2 relates to the change in those parameters when the test speed is changed to design speed.

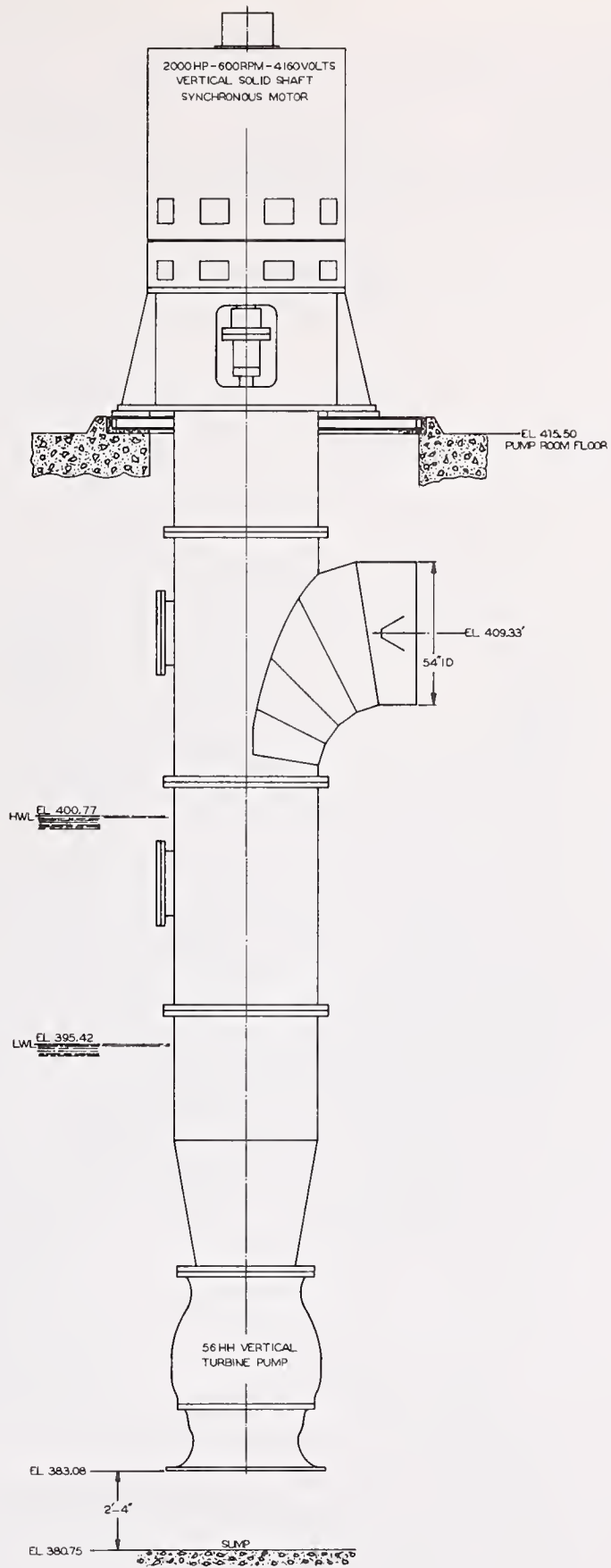


FIG. I

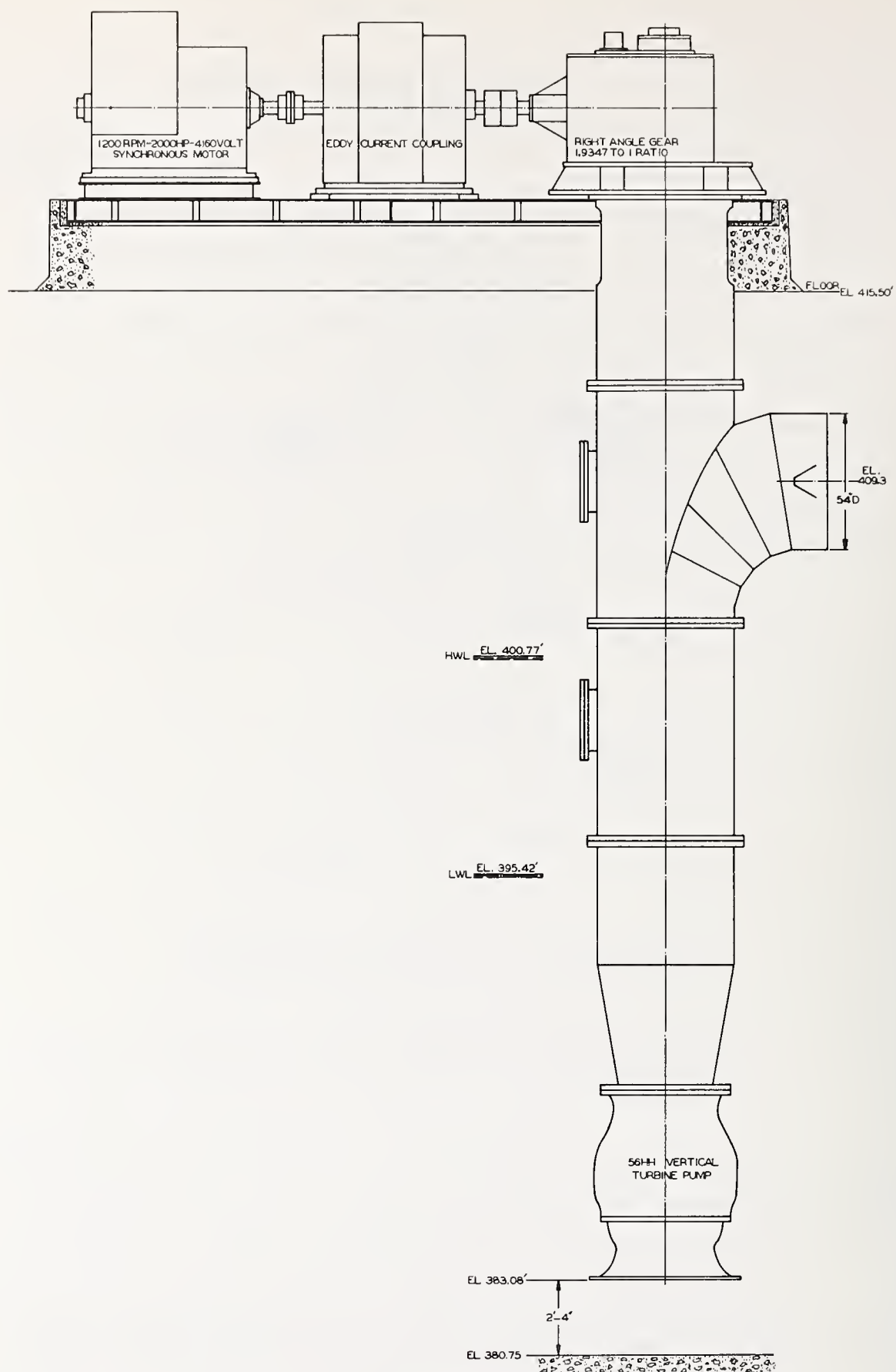


FIG. 2

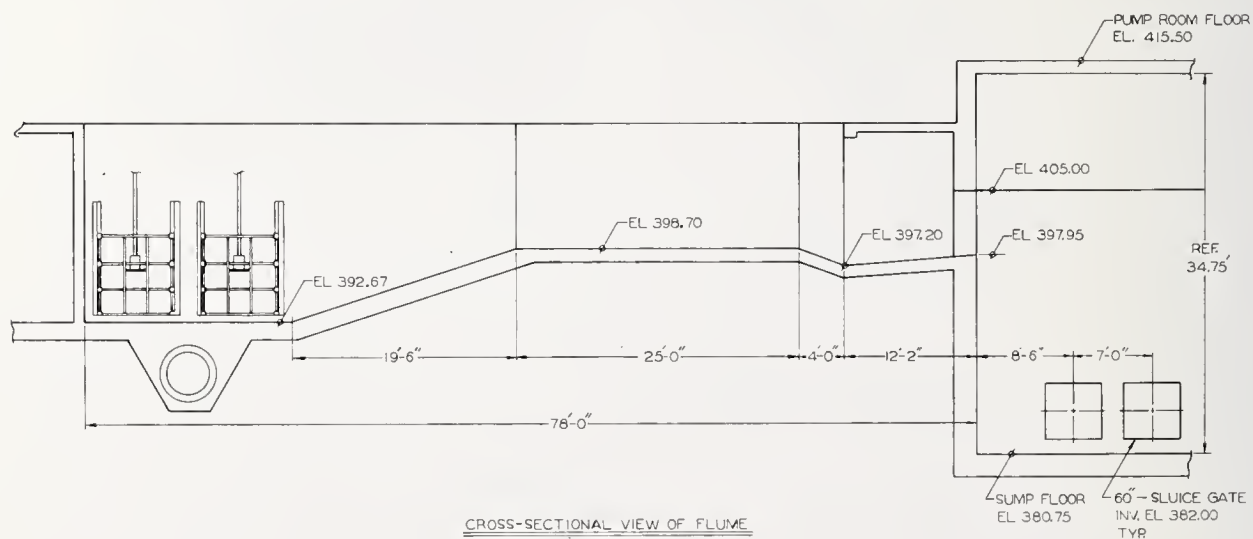
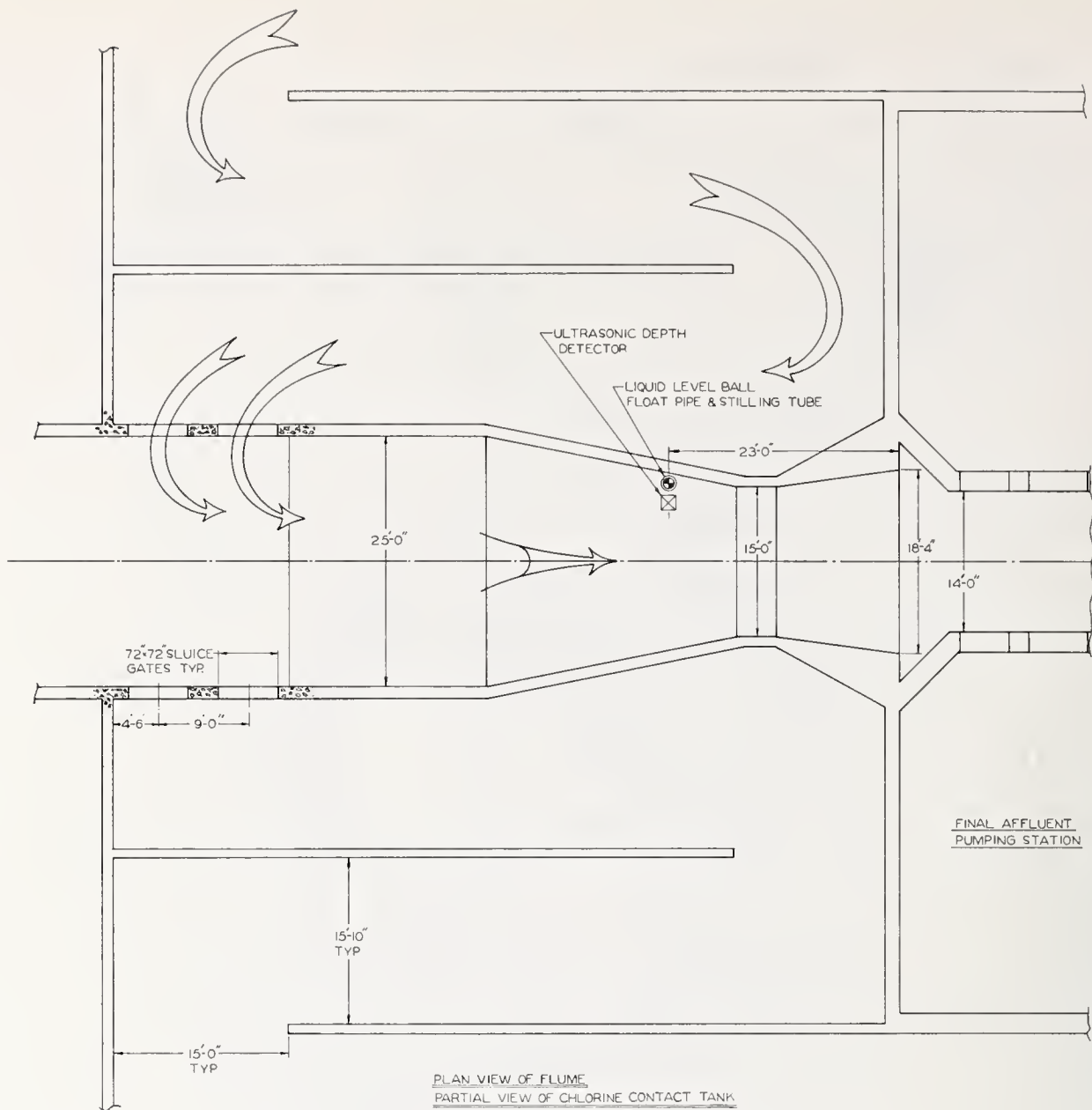
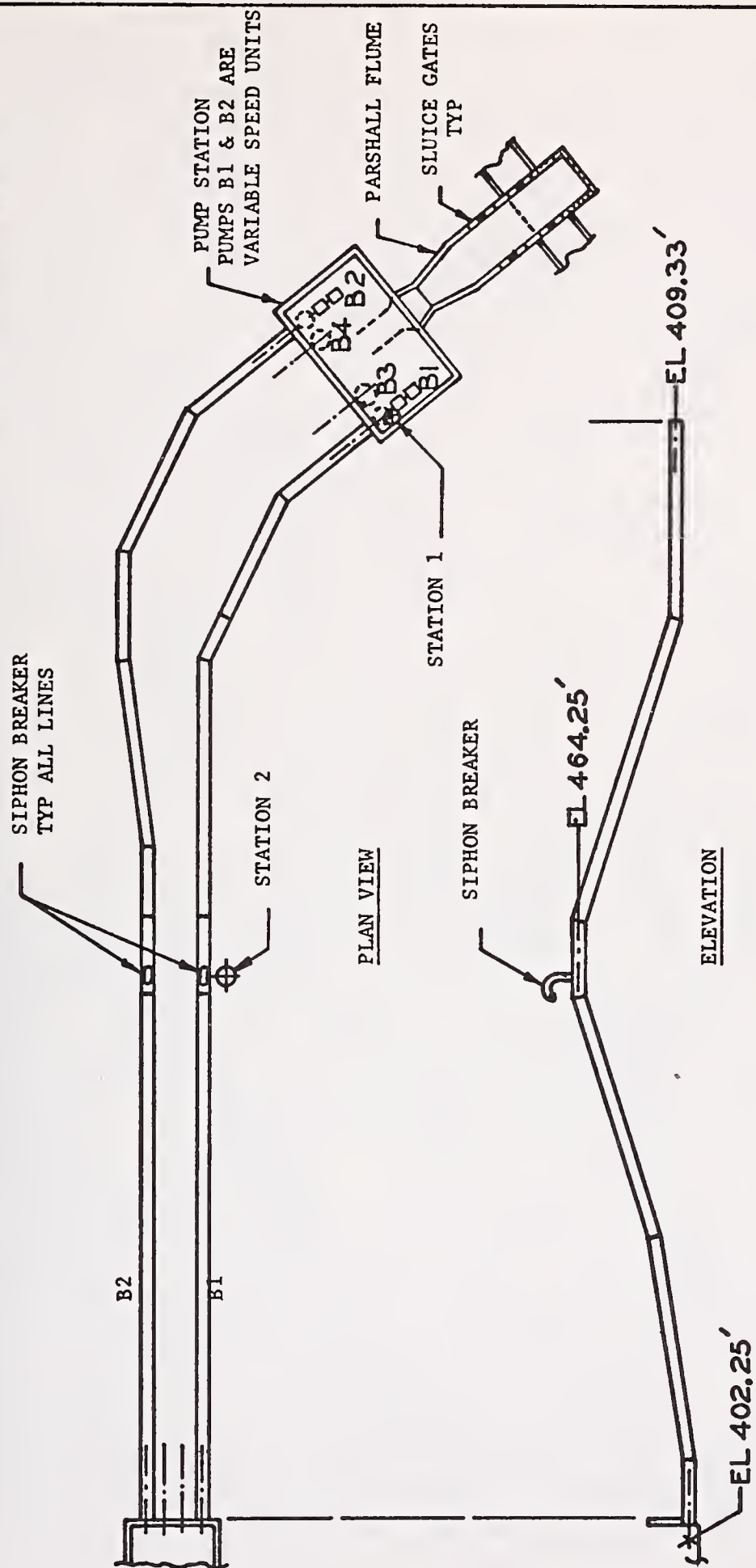


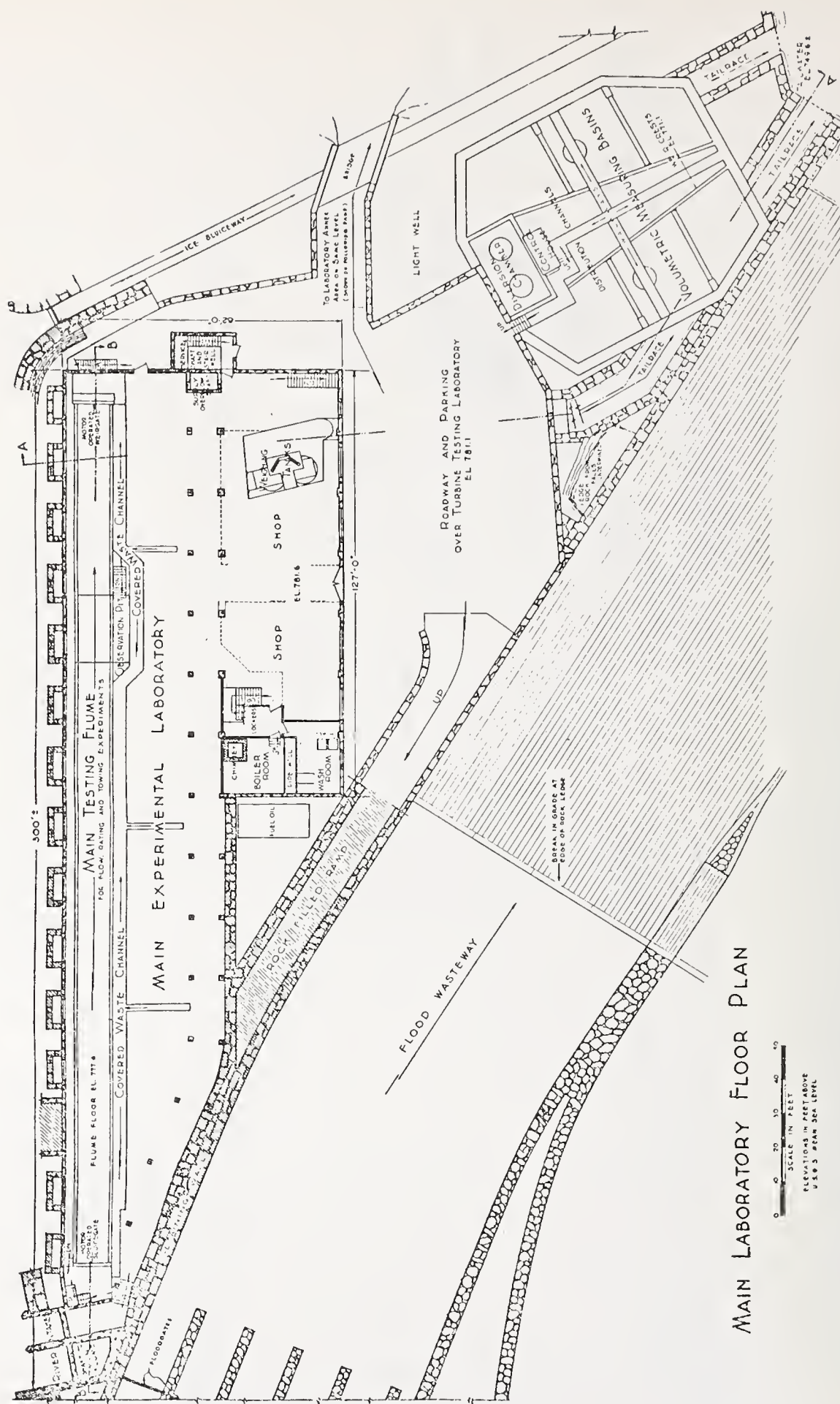
FIG. 4

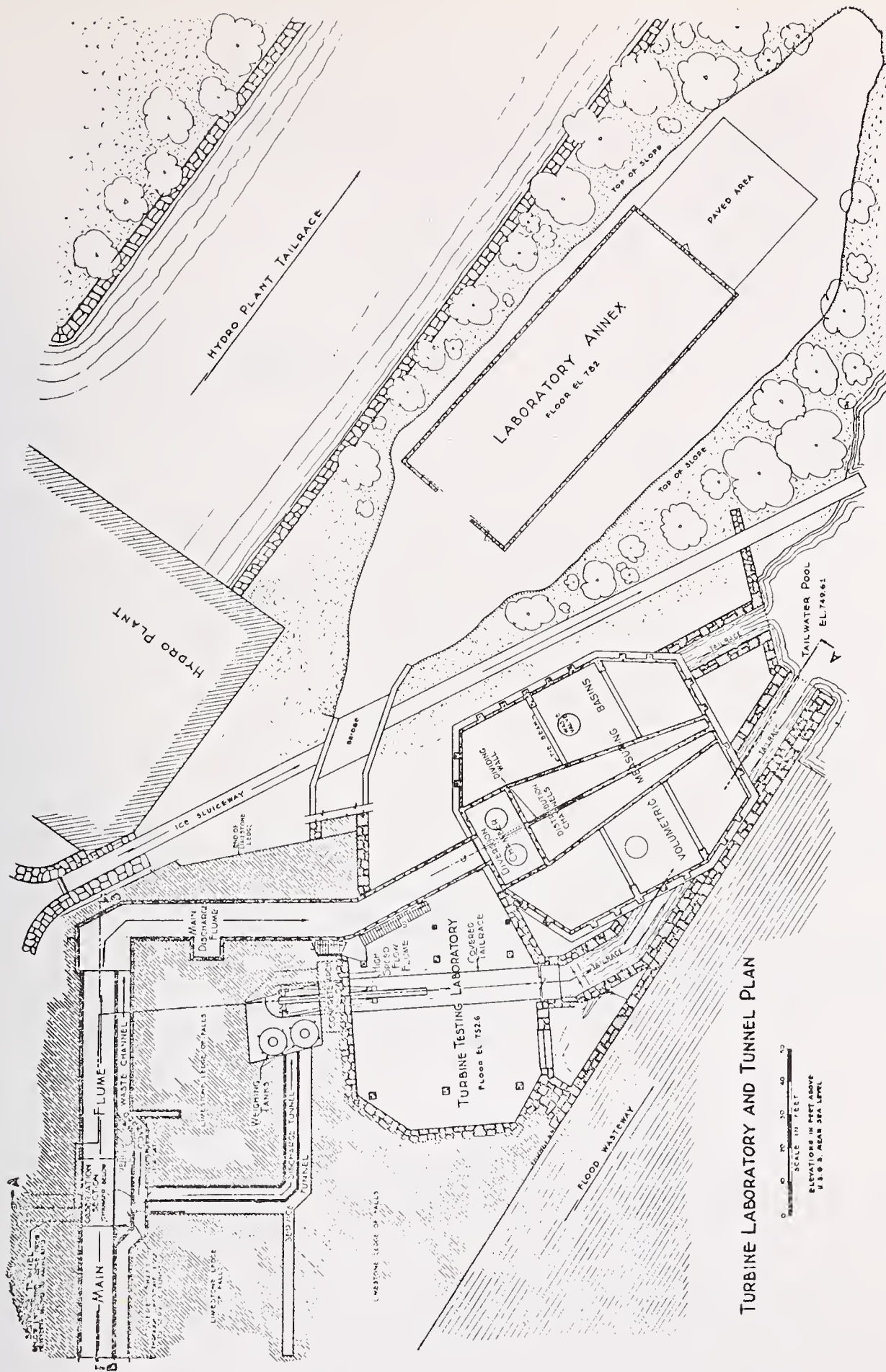
B₁ TO STATION #2 = 363 FT.
 B₂ TO STATION #2 = 418 FT.



VERIFICATION TESTS
 LOCATION OF DATA COLLECTION STATIONS
 FOR
 FLOW DETERMINATION BY DYE-DILUTION METHOD

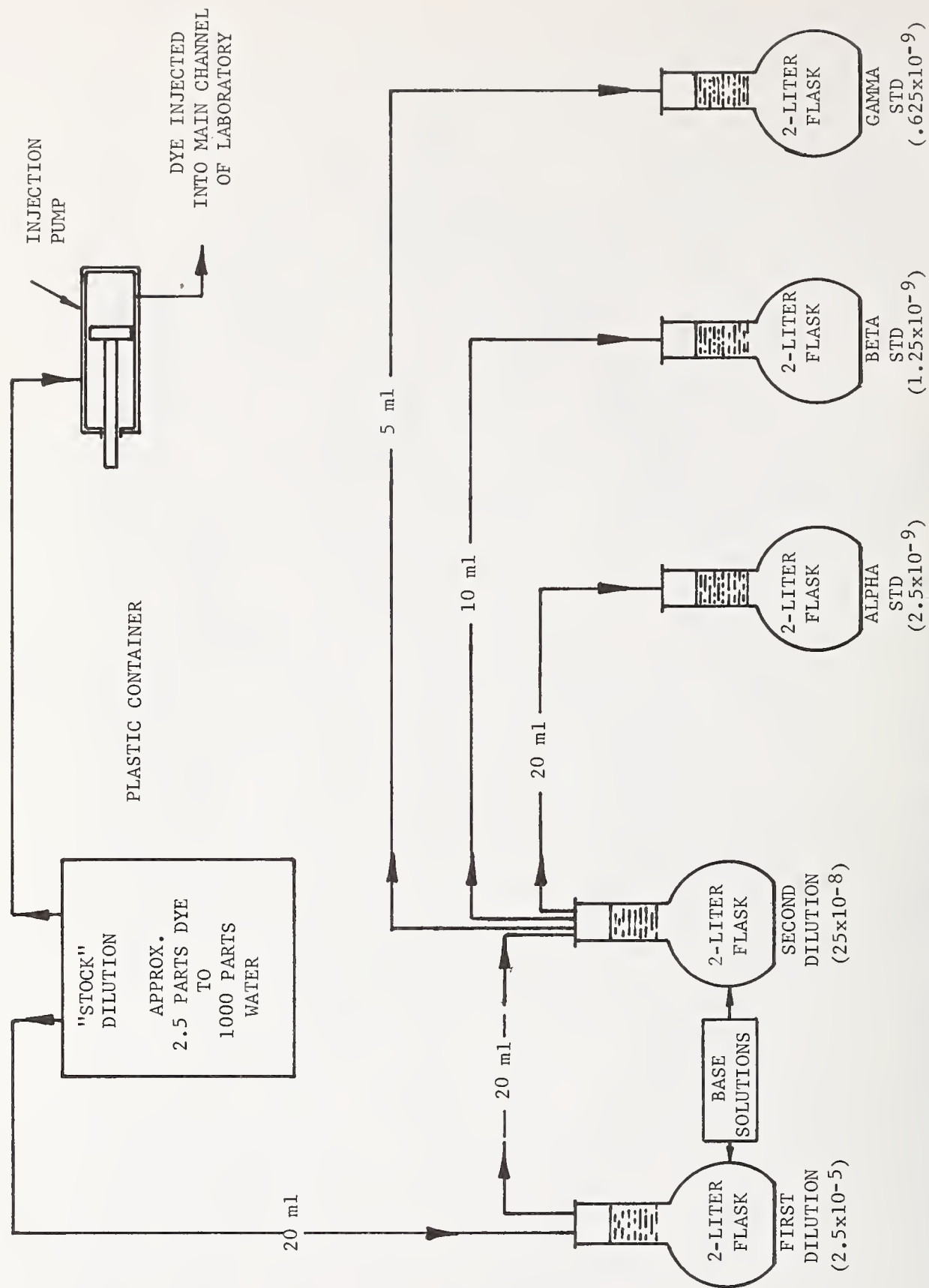
FIG. 5





TURBINE LABORATORY AND TUNNEL PLAN

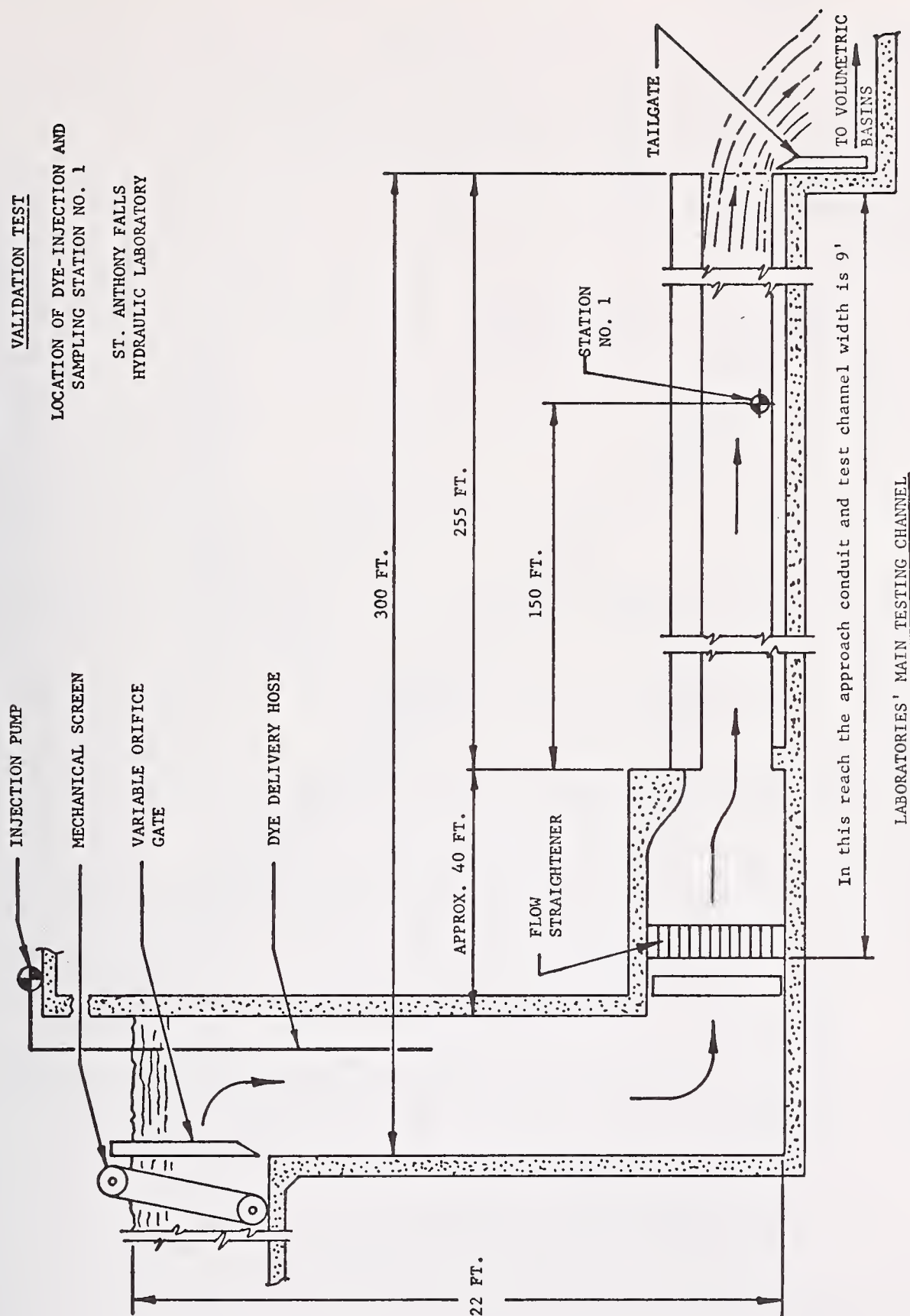
FIG. 7



VALIDATION TEST - PREPARATION OF STANDARDS
EACH FLASK CONTAINS 2-LITERS OF RIVER WATER PRIOR TO DILUTION
NOTE: VALUE IN PARENTHESIS IS DYE CONCENTRATION RELATIVE TO STOCK SOLUTION

FIG. 8

VALIDATION TEST
 LOCATION OF DYE-INJECTION AND
 SAMPLING STATION NO. 1
 ST. ANTHONY FALLS
 HYDRAULIC LABORATORY



LABORATORIES' MAIN TESTING CHANNEL

FIG. 9

DETERMINED BY VOLUMETRIC MEASUREMENTS
 SAINT ANTHONY FALLS HYDRAULIC LABORATORY
 UNIVERSITY OF MINNESOTA

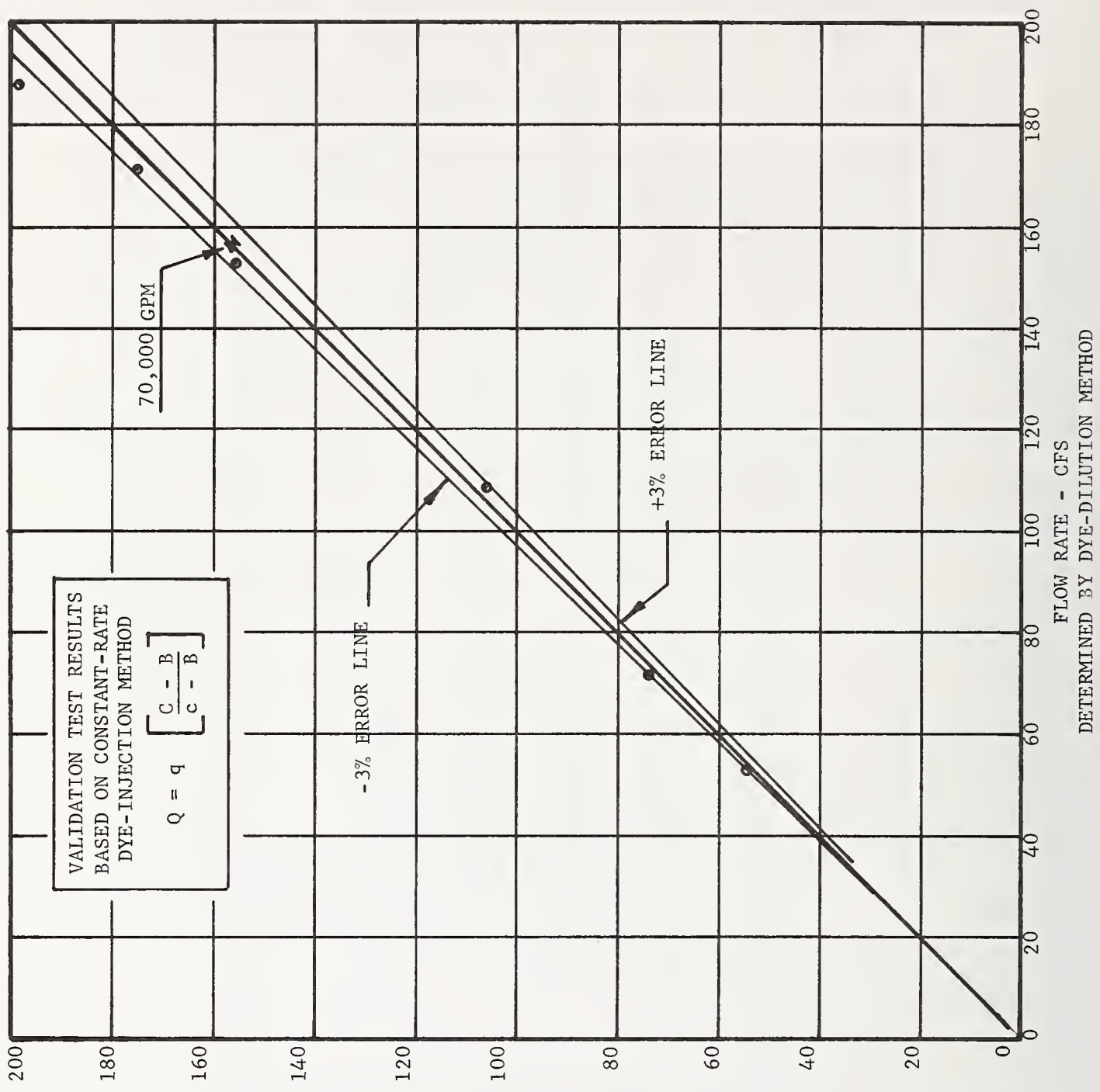


FIG.10

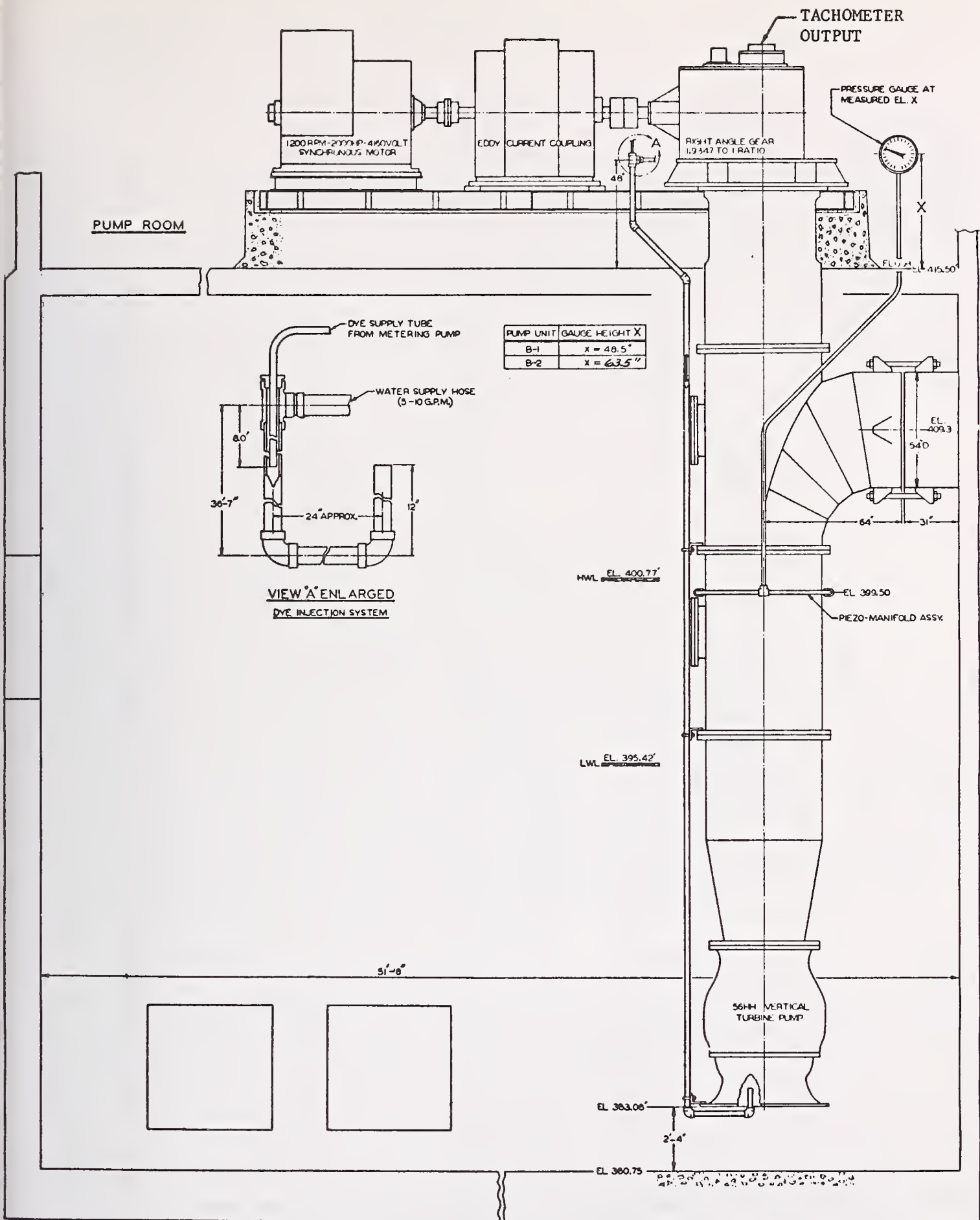


FIG. II

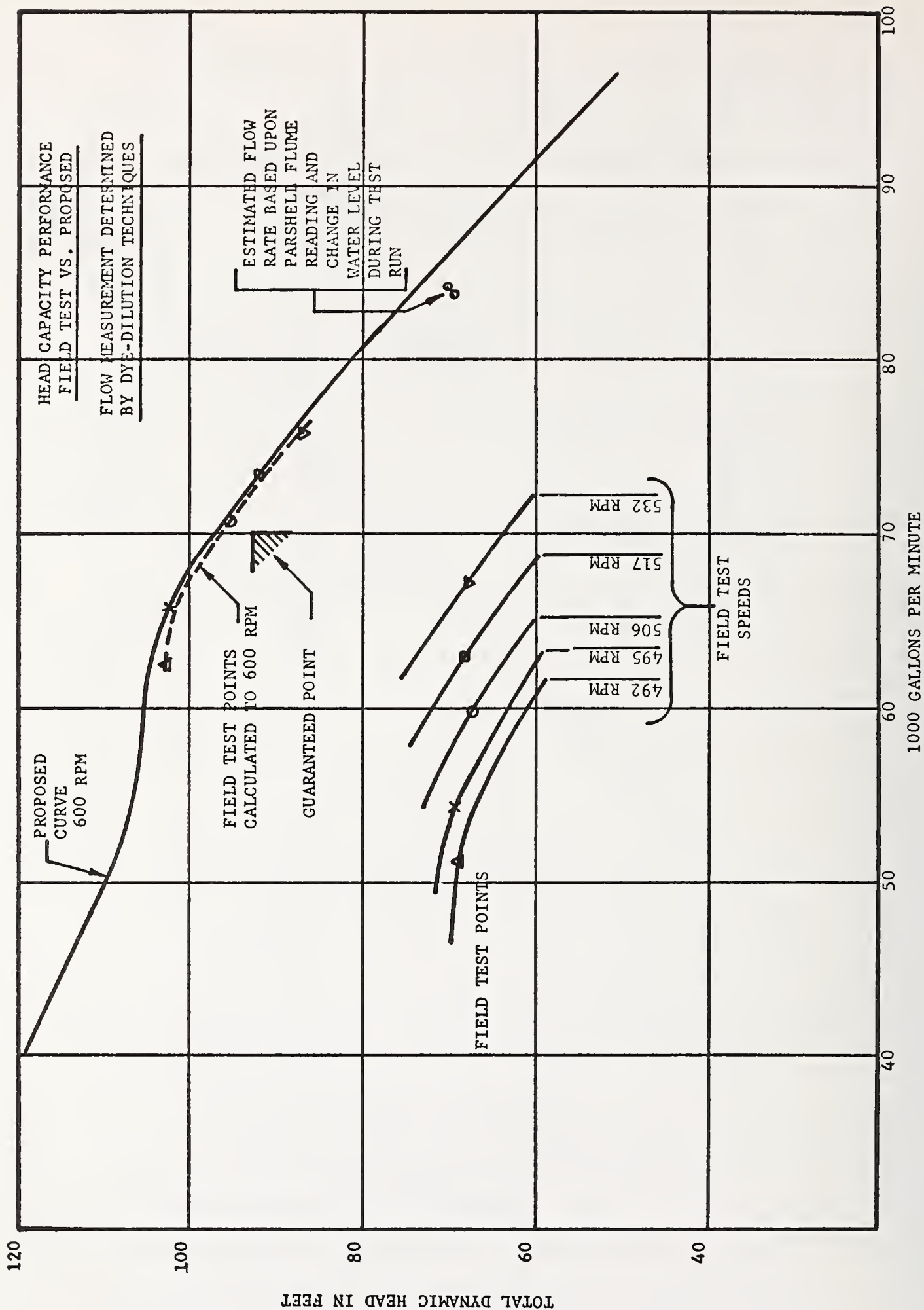


FIG. 12

DILUTION METHOD OF DISCHARGE MEASUREMENT IN PIPES

E. R. Holley

Department of Civil Engineering
University of Illinois at Urbana-Champaign
Urbana, Illinois 61801

The dilution method, or the method of mixtures, is a tracer technique for discharge measurement in steady flow. The method is based on the mass balance of a tracer injected at a steady rate into the pipe flow and depends on measuring the concentration at one or more points downstream of the injector in order to evaluate the average concentration of the tracer. The accuracy of the method depends on the tracer, on the injection and measurement equipment, and on the locations of the sampling ports since these locations determine the accuracy with which the concentration measurements represent the actual average concentration.

Minimizing the errors associated with the locations of the sampling ports depends on being able to predict the rates at which mixing takes place for the applicable injection and pipe flow conditions. The mixing can be viewed as being either initial mixing associated with the injection or ambient mixing associated with the pipe flow. Both analytical work and experimental work on ambient mixing are presented with attention being focused on injection and sampling at the pipe wall. If the available mixing distance is restricted, multiple-point injection or multiple-point sampling can be used. However, analytical work and the limited available data indicate that the inherent asymmetry of the flow may have a strong influence on the rates of mixing for multiple-point systems.

Relatively little definitive information is available on initial mixing. Analytical and experimental work on one type of jet injection is reviewed.

Equipment errors can be analyzed if a sufficient number of experiments are done in advance of the discharge measurement. Based on data from the literature, an error analysis is presented for a situation where a radioactive tracer was used. The total error in the calculated discharge was determined to be approximately 0.5% at the 95% confidence level.

Some possible areas for additional research are presented.

1. Introduction

1.1. Basic Concepts

The dilution method, which is also called the method of mixtures, is a tracer technique for discharge measurement. The method is based on the

mass balance of a tracer which is injected into the flow. For a steady mass rate of injection and for steady flow, the mass balance of a conservative tracer gives

$$c_i q + c_b Q = \int_A c u dA = \bar{c}_Q (Q+q) \quad (1)$$

where c_i is the injection concentration of the tracer, q is the volumetric injection rate, c_b is the background concentration, Q is the pipe discharge, c and u are the concentration and velocity distributions at a downstream cross section, A is the area of the pipe, and \bar{c}_Q is the average concentration. From eq. (1),

$$Q = \left(\frac{c_i - \bar{c}_Q}{\bar{c}_Q - c_b} \right) q \quad (2)$$

By knowing the injection conditions (c_i and q) and by measuring the background concentration and the concentration downstream of the injector in order to determine \bar{c}_Q , the pipe discharge Q can be calculated using eq. (2). If $c_i \gg \bar{c}_Q \gg c_b$, eq. (2) can be simplified to

$$Q = \frac{c_i}{\bar{c}_Q} q \quad (3)$$

which gives the pipe discharge in terms of the dilution of the injected tracer after thorough mixing with the flow. As implied by eq. (1), \bar{c}_Q is defined as

$$\bar{c}_Q = \frac{1}{Q_T} \int_A c u dA \quad (4)$$

with $Q_T = Q + q$. If $Q \gg q$, then $Q_T \approx Q$ in eq. (4). An area-average concentration may also be defined as

$$\bar{c}_A = \frac{1}{A} \int_A c dA \quad (5)$$

1.2. Modus Operandi

There are many possibilities for types and locations of injection and subsequent measurement of concentration in the pipe, and these in turn affect the accuracy with which \bar{c}_Q can be approximated at a specified

distance downstream of the injector. The simplest injection is normally a single injection at the pipe wall. If enough flow length is allowed or is available for the tracer to become thoroughly mixed with the flow, any single measured value of c will be representative of \bar{c}_Q and the accuracy will depend primarily on the random errors.

In situations where the flow length available for mixing is restricted so that uniformity of the concentration distribution can not be obtained by mixing associated with the pipe flow, there are at least two possible alternatives for evaluating \bar{c}_Q . One alternative is to accelerate the mixing. This may be done by injecting the tracer at more than one point at a particular cross section and/or by using high velocity injection. In some cases, mixing vanes or other types of mixing devices downstream of the injection location might also be practical. Essentially any desired degree of mixing can be obtained with properly designed mixing devices, but devices which produce a high degree of mixing may also cause an unacceptably large head loss.

A second alternative is to use multiple-point sampling. In many cases, this alternative is less expensive than multiple injection or mixing devices. The ASME Research Committee on Fluid Meters [1] recommended that thorough mixing should take place between the injection and sampling locations. This recommendation apparently assumes that only one sampling port will be used and therefore may be overly restrictive if multiple-point sampling is used. However, even if sampling points are distributed throughout the pipe cross section, multiple-point sampling may not be desirable at very short flow distances where the concentration distribution is highly non-uniform within a cross section because multiple-point sampling leads to an evaluation of \bar{c}_A , which may be a poor approximation to \bar{c}_Q for highly non-uniform distributions. This distinction is normally important only near the injection location. See the end of section 2.1.2.

In this paper, attention will be directed primarily toward circular pipes where both injection and sampling are done at the pipe wall and where no mixing devices are used. This type of application is often the most convenient because it requires no access to the interior of the pipe and sometimes it can be implemented without interrupting flow in the pipe.

1.3. Some Advantages and Disadvantages

Some of the potential advantages of the dilution method are that (a) it can be used to obtain either intermittent or continuous measurement of Q , (b) it can be applied to a range of discharges differing by a factor of as much as 10^9 using essentially the same equipment [2], (c) in most cases it causes negligible head loss, (d) in many cases it does not require interruption of flow in the pipe, (e) it can be used for either liquids or gases, (f) it is independent of the size or degree of uniformity of the pipe, and (g) it does not require full pipe flow. Some of the potential

Figures in brackets indicate the literature references at the end of this paper.

disadvantages are that (a) it requires the addition of a foreign substance (the tracer) into the flow, (b) the tracer must be conservative or must have a well-defined or measurable behavior in the flowing fluid, (c) a significant length of pipe may be required between the injection and measurement stations, (d) the method has only been investigated for steady flows, and (e) it would appear to have restricted applicability in entrance sections (e.g. penstocks) which are too short for complete development of the turbulent boundary layer. The dilution method apparently could be applied to some types of unsteady flows; however, this possibility has apparently not been investigated in detail and will not be considered further in this paper.

1.4. General Accuracy Considerations

The accuracy of the dilution method is affected by several factors. For example, it is essential that the sampling downstream from the injector location provide an accurate representation of \bar{c}_0 . The selection of the appropriate sampling location(s) depends on being able to analyze and predict the mixing of the injected tracer. These factors are considered in section 2. In addition, the accuracy of the method depends on the random errors associated with the injection equipment, the measurement instruments and the procedures which are used. These factors are considered in an example in section 3.

2. Analysis of Mixing

Errors can be introduced into the determination of Q if the sampling does not provide for an accurate evaluation of \bar{c}_0 . The accuracy with which \bar{c}_0 can be obtained with a particular set of sampling points will depend on the concentration distribution at the sampling cross section. If no mixing devices are used, the concentration distribution or the degree of mixing at any cross section can be viewed as being a result of initial mixing associated with the injection system and ambient mixing associated with the flow in the pipe.

Some analytical solutions for concentration distributions will be presented to gain insight into the ambient mixing problem, then some data related to ambient mixing will be presented. The degree of initial mixing which can be obtained for various types of injectors is not well defined. Some analytical and numerical work and some data which are available for one particular type of injection will be presented after the discussion of ambient mixing.

2.1. Ambient Mixing

2.1.1. Analytical Representation

An analytical representation of ambient mixing in an idealized steady, uniform, turbulent pipe flow can be obtained by assuming that the velocity, radial diffusivity, and circumferential diffusivity are each constant and equal to their cross sectional averages which are respectively \bar{u} , \bar{e}_r , and

\bar{e}_θ . These assumptions are supported by the work of Evans [3] who investigated the effects of variable diffusion coefficients on concentration distributions, by the agreement of the calculated results with numerical simulations using variable u , e_r , and e_θ [4], and by the agreement between the analytical results and the data, as discussed in section 2.1.2. The assumption of a constant velocity implies that $\bar{c}_A = \bar{c}_Q$. Thus, the subscript will be dropped and \bar{c} will be used in this section. In obtaining the analytical solution, let r = radial coordinate, R = pipe radius, D = pipe diameter, x = longitudinal coordinate, θ = circumferential coordinate, c = concentration, f = Darcy-Weisbach friction factor, Sc_t = turbulent Schmidt number and $\bar{}$ = cross sectional average. Define the dimensionless variables

$$\begin{aligned}\eta &= \bar{e}_\theta / \bar{e}_r \\ \rho &= r/R \\ X &= \bar{e}_r x / \bar{u} R^2 \approx 0.0480 \sqrt{f} (x/D) / Sc_t \quad [5] \\ C &= c / \bar{c}\end{aligned}\tag{6}$$

The concentration distribution for a conservative tracer released at a constant rate from a point source located at $X = 0$, $\rho = \rho'$, and $\theta = \theta'$ can then be written [5] for $\rho' \neq 0$ and $X > 0$ as

$$C = 1 + \sum_{n=0}^{\infty} W_n \cos n(\theta - \theta') \sum_{m=1}^{\infty} \exp(-\lambda_{nm}^2 X) \frac{J_\nu(\lambda_{nm} \rho') J_\nu(\lambda_{nm} \rho)}{(1 - \frac{\nu^2}{2}) J_\nu^2(\lambda_{nm})} \tag{7}$$

in which $W_n = 1$ for $n = 0$, $W_n = 2$ for $n > 0$, $\nu = n\sqrt{\eta}$, λ_{nm} = the m th positive root of $J'_\nu(\lambda) = 0$, and J_ν is a Bessel function of the first kind of order ν . For an undisturbed source at the pipe centerline ($\rho' = 0$), the analogous solution is

$$C = 1 + \sum_{m=1}^{\infty} \exp(-\lambda_{0m}^2 X) \frac{J_0(\lambda_{0m} \rho)}{J_0^2(\lambda_{0m})} \tag{8}$$

For multiple sources, the principle of superposition can be used to obtain the concentration distribution. If there are k sources and the j -th source is located at ρ'_j, θ'_j and has a strength or mass injection rate of M_j , then the normalized concentration distribution is

$$C = \frac{\sum_{j=1}^k M_j C_j}{\sum_{j=1}^k M_j} \quad (9)$$

with C_j being given by eq. (7) for each ρ'_j, θ'_j or eq. (8) if $\rho'_j = 0$. Similarly, if as a result of injection and initial mixing, a concentration distribution given by

$$C_o = C_o(\rho', \theta') \quad (10)$$

exists at $X = X_o$, then the mass flux through each incremental area ($\rho' d\rho' d\theta'$) at X_o can be considered to be a source with a mass injection rate of $\bar{u} C_o(\rho', \theta') \rho' d\rho' d\theta'$. Again, the principle of superposition can be applied and the concentration resulting from all of the incremental sources or from eq. (10) can be obtained by integrating over the cross section at X_o to give

$$C = \frac{\int_0^{2\pi} \int_0^1 \bar{u} C_o(\rho', \theta') C(X-X_o, \rho, \theta, \rho', \theta') \rho' d\rho' d\theta'}{\int_0^{2\pi} \int_0^1 \bar{u} C_o(\rho', \theta') \rho' d\rho' d\theta'} \quad (11)$$

where $C(X-X_o, \rho, \theta, \rho', \theta')$ is the concentration distribution given in eq. (7) or eq. (8) if $\rho' = 0$. In both eq. (9) and eq. (11), the denominator is included to normalize the calculated concentration so that the average value will be unity.

For the assumed flow conditions, these analytical expressions can be used to obtain the concentration distributions, the coefficient of variation (C_v) of the concentration distribution, and the maximum variation of the concentration within a cross section. In order to perform these calculations, it is necessary to specify the value of η , and in order to relate the calculations to actual distance in a pipe, it is necessary to specify the value of Sc_t . Both η and Sc_t are defined in eq. (6). Holley and Ger [5] have shown that a good representation of data from various investigators is obtained for $\eta = 1.8$ and $Sc_t = 1.0$, so these values will be used in the following computations. All of the results will be presented in terms of dimensionless variables and parameters. For reference, $X = 1.0$ corresponds to $x/D = 170$ for $f = 0.015$ and as shown in eq. (6), x/D for a given X varies inversely with the square root of f . It was also shown [5] that the value assumed for Sc_t affects the value calculated for η when analyzing data on mixing in pipes. Thus, one of these values can not be changed independent of the other. For example, the value Sc_t can not be changed in the definition of X without also changing the value of η . In all of the calculations, it is assumed as mentioned previously that both injection and sampling are at the pipe wall.

The coefficient of variation is frequently used as a statistical measure of the degree of mixing and is defined by

$$C_v = \left[\frac{1}{\pi} \int_0^{2\pi} \int_0^1 (C-1)^2 \rho d\rho d\theta \right]^{1/2} \quad (12)$$

with $C = c/\bar{c}$. Calculated values of C are shown in figure 1 for three injection conditions, namely a single wall source, two sources of equal strengths spaced 180° apart at $X = 0$, and three sources of equal strengths spaced 120° apart. By definition, a mathematical source has no initial mixing associated with it. Corresponding curves for $N_+ \geq 4$ (where N_+ is the number of equally spaced sources at $X = 0$) give curves of C_v vs. X which are essentially the same as for $N_+ = 3$. Figure 1 shows a large decrease in the mixing distance required to obtain a given value of C_v when the two sources are used instead of just one. However, mixing distances as short as those indicated in figure 1 for $N_+ \geq 2$ can not be obtained in the laboratory without extreme experimental care and certainly would never be obtained under normal operating conditions. The reason is that the steeper slope of the $C_v - X$ curves for $N_+ \geq 2$ is a characteristic of the analytical evaluation of C_v for mathematical symmetry with respect to the centerline of the pipe. Symmetry in this case means symmetry of both the flow and the concentration distributions as represented by symmetrical (or uniform) distributions of velocity and diffusion coefficients and by $\sum_{j=1}^k M_j \cos(\theta - \theta'_j)$ identically zero for all θ , where k is the number of sources as in eq. (9). For $k \geq 2$, this expression is identically zero for any number of equally spaced sources of equal strengths. This type of mathematical symmetry will never actually exist in either the velocity distribution or the injection of the tracer into the pipe. The flatter slope for $N_+ = 1$ is a characteristic of the asymptotic slope for increasing X for all asymmetrical conditions [5].

A qualitative indication of the effect of asymmetry on the rates of mixing can be obtained from the analytical solution. The nature of the solution is such that it would be extremely difficult to obtain an analytical solution analogous to eq. (7) for a variable velocity and diffusivity. However, using eq. (9), it is rather straightforward to introduce asymmetry into the mixing by varying the strengths of the sources. Figure 2 shows the results of this type of computation for two sources where the strengths of the sources differed from the average strength by $\pm P$, with P varying from 0% to 20% as indicated on the figure. The figure also shows the curve for $N_+ = 1$ for comparison. It should be emphasized that variation of source strengths is being used to indicate the general effect of asymmetry which would be present for any of a number of reasons and not because it is felt that variations of 20% in source strengths are likely to actually occur. Figure 2 shows that the $C_v - X$ curves break away from a common curve at values of X which depend on the amount of asymmetry (i.e. on P) and that each curve approaches or attains the asymptotic slope for asymmetrical conditions. It will be seen in figure 5 (section 2.1.2) that this is the type of behavior found in measured concentration distributions.

If the behavior shown in figure 2 does indeed represent the effects of asymmetry of any type, then this behavior would have definite implications both on analyzing laboratory data to study mixing rates and on trying to predict mixing distances for discharge measurements with multiple-point injection. If the asymmetry of the flow and mixing (rather than the mean flow characteristics or the injection condition) has a dominant influence on the $C_v - X$ behavior, it will be difficult to find consistency in data collected by different investigators and it will be equally difficult to predict mixing distances with any degree of assurance.

These comments above refer only to multiple-point injections. As mentioned again in section 4, research is needed to define the effects of multiple-point injections and multiple-point sampling on the accuracy of the dilution method. For a single injector, the inherent asymmetry of the injection is apparently more dominant than any flow asymmetry, at least for laboratory flows. This matter is considered further in the discussion of the experimental data in section 2.1.2 (figures 5 and 6).

While C_v is indicative of the degree of mixing or the uniformity of the concentration distribution at a cross section, it does not give a direct indication of the maximum possible error using a specific set of concentration measurements to approximate \bar{c} . This maximum error can be evaluated for the analytical solutions. It will be assumed that samples are taken from S ports spaced equally around the pipe wall and that c_s is the average of the S measurements of c . Then, by letting the sampling ports be in the "worst" position relative to the concentration distribution so that the difference between c_s and \bar{c} is a maximum, it is possible to evaluate ΔC_s where

$$\Delta C_s = \left| \frac{c_s - \bar{c}}{\bar{c}} \right|_{\max} \quad (13)$$

ΔC_s is a direct indication of the maximum possible error in calculating \bar{c} and Q from concentration measurements obtained at the pipe wall.

Figure 3 shows values calculated for ΔC_1 and $\Delta C_1/C_v$ for $N_+ = 1$ and 2, including the effects of asymmetry. The general appearance of the ΔC_1 curves is similar to the corresponding C_v curves. The characteristic slopes on figure 2 are the same as those on figure 1. However, the values of ΔC_1 are larger than the corresponding C_v values, with the ratio of ΔC_1 to C_v being shown at the top of figure 3. For $X > 0.13$, $\Delta C_1/C_v$ varies between 1.76 and 2.90 depending on the injection conditions and on X . For large X , $\Delta C_1/C_v$ for all asymmetrical conditions approaches 1.76. As the figure shows, if enough pipe length is available to provide a mixing distance of $X = 1.25$ ($x/D = 220$ for $f = 0.015$), then any concentration measured at the pipe wall will be within a maximum of 0.5% of \bar{c} (except for random measurement errors). It is only for situations where the available mixing distance is limited that multiple-point sampling or multiple-point injection needs to be considered. As shown in figure 3, the mixing distance required to obtain a given value of ΔC can be reduced significantly by using two sources, but the amount of reduction again depends on the asymmetry of the mixing.

Since the principle of superposition applies to the calculated concentration distributions, it can be shown that ΔC_1 for $N_+ = 2$ is the same as ΔC_2 for $N_+ = 1$. Thus, the curves in figure 3 for ΔC_1 for two asymmetric sources can also be viewed as indicating the behavior to be expected when two samples are taken from an asymmetrical flow with one source. This fact will be useful in the discussion of some of the data in section 2.1.2 and particularly in conjunction with figure 6.

2.1.2. Analysis of Data

Data from three sources as presented in Table 1 were analyzed for comparison with the material presented in section 2.1.1.

Table 1. Sources of Data on Ambient Mixing

Source	Pipe Diam- eter inches	Reynolds Number Range	Pipe Material	Fluid	Tracer	Sampling Points per Cross Section
Clayton, Ball, and Spackman [6]	4	5×10^3 - 5×10^5	Smooth	Water	Radioactive	10
Ger and Holley [4,7]	6	7.7×10^4 - 1×10^5	Galvanized Iron	Water	Dilute NaCl	37
Filmer and Yevdjovich [8]	36	5.8×10^4 - 4.5×10^5	Steel	Water	Rhodamin WT	28

Clayton et al [6] performed experiments at four Reynolds numbers (Re). For $Re = 5 \times 10^3$, 1×10^4 , and 7.7×10^4 , they used four injection conditions, namely a single wall injector ($N_+ = 1$), a single center injector, four wall injectors ($N_+ = 4$), and four injectors at $\rho' = 0.63$. For $Re = 5 \times 10^5$, they used a single edge injector and a single center injector. A radioactive tracer was used. Concentration measurements were made at several cross sections on 3 radii spaced 90° apart. The sampling ports were at $\rho = 0, 0.31, 0.63$, and 0.98 , giving a total of 10 samples. The radioactivity measurements were analyzed by calculating χ^2 (relative to well-mixed conditions) for each group of ten results from a given cross section. The χ^2 values were apparently obtained by giving the same weight to each of the 10 samples, while eq. (12) for calculating C_v would imply the use of weighting factors proportional to the pipe subarea represented by each sampling point. Nevertheless, it was assumed that this area-weighting was negligible, as is usually the case except very near the injection location. Then C_v could be calculated directly from the given χ^2 values just by comparing the definitions of χ^2 and C_v . The individual concentration measurements were not reported, so it was not possible to obtain ΔC for this data.

Ger and Holley [4,7] reported two experiments at $Re = 7.7 \times 10^4$ and 1×10^5 with one wall source (as well as data on jet injections to be considered in section 2.2). A NaCl tracer was used with concentration measurements being made at 37 points within each measurement cross section. The 37 points were distributed to sample the center of 37 approximately equal subareas of the pipe. C_v values were reported.

Filmer and Yevdjovich [8] performed five experiments with an injection tube on the pipe centerline. Although these experiments do not conform to the specified condition of having wall injection, they do provide data which can be used to gain insight into the ambient mixing process since by definition ambient mixing is associated with the flow in the pipe and not with the injection conditions. The Reynolds numbers for the experiments were 5.8×10^4 , 25×10^4 , 32×10^4 , 39×10^4 , and 45×10^4 . Even though the injector was on the pipe centerline, the mixing was asymmetrical primarily because part of the tracer is normally drawn into the wake of the arm supporting an injection tube. A fluorescent tracer was used. Concentration measurements were made on 4 radii spaced 90° apart. One set of measurements was made using 12 radii spaced 30° apart, but the authors concluded that the 4 radii provided sufficient accuracy. There were 7 sampling tubes placed on a rotatable radial arm so that each sampling tube was at the center of equal subareas of the pipe cross section. Thus, C_v in eq. (12) could be calculated directly as the coefficient of variation of the concentration measurements. These measurements were tabulated by Filmer and Yevdjovich [8] and provide what is apparently one of the largest sets of available data for a single injection condition.

The values of C_v calculated from measured concentration distributions are influenced both by the degree of non-uniformity of the concentration distributions and by the accuracy with which the individual values of c are measured. For the smaller values of X , the dominant influence is the concentration distribution within the pipe and the empirical values of C_v and ΔC should be expected to agree closely with the analytical work presented in section 2.1.1. However, for the larger values of X where the concentration is relatively uniform within each cross section, empirical C_v values do not approach zero; rather they approach an approximately constant value which is indicative of the random errors in the individual concentration measurements. Similarly, for the smaller distances, the values of ΔC for multiple-point sampling are indicative of averaging of unequal concentrations from non-uniform distributions within the pipe. Therefore ΔC_2 should be significantly less than ΔC_1 . However, as X increases and ΔC_2 decreases, a point is reached where the magnitude of ΔC_2 relative to ΔC_1 is indicative simply of sampling statistics. The "critical" value of X at which the values of C_v and ΔC cease to represent the mixing and begin to represent random errors depends on the injection conditions, the number of samples, and the random errors in the measurement of c . (See figures 4, 5, and 6, which are discussed below.)

Figure 4 shows empirical values of C_v for $N_t = 1$. The solid points are from the four applicable experiments of Clayton et al [6] and the open points are from the two experiments of Ger and Holley [4,7]. There is good agreement between experiments of the different investigators and between the experiments and the analytical curve for $N_t = 1$ which is also shown on figure 4. The results for Clayton et al also indicate the approximately

constant value of C_v for large X . For the radioactive counting used by Clayton et al, they indicated a 90% confidence interval for random errors in their values of χ^2 . The corresponding 90% confidence interval for random errors in C_v is $1.7 \times 10^{-3} \leq C_v \leq 4.6 \times 10^{-3}$. In figure 4 (and in figure 5 to be considered later), the values of C_v for large X do fall within this confidence interval. The dashed lines which are shown in figures 4 and 5 to separate the regions of the influence of mixing in the pipe from the regions of random errors correspond to $C_v = 4.6 \times 10^{-3}$.

Clayton et al [6] also reported three experiments with four equally spaced wall injectors ($N_+ = 4$). The C_v values for these experiments are shown in figure 5 which also includes some calculated curves analogous to those shown in figure 2 for $N_+ = 2$. The curve for $N_+ = 1$ is also shown for comparison. The values of P_+ shown in figure 5 indicate the range of injector strengths relative to the mean. Around the pipe circumference the injector strengths were equal to the mean value plus P , plus $P/2$, minus $P/2$, and minus P . There is general agreement between the calculated curves and the data, especially if it is assumed that the degree of asymmetry in the flow may have not been the same for all of the experiments. It must be emphasized that the comparison shown in figure 5 is not intended to imply that the strength of the injectors actually varied by 10% or 20%. Rather, the major part of the asymmetry undoubtedly was inherent in the flow, but as mentioned earlier it is easier to obtain asymmetry of mixing in the analytical solution by varying the source strengths than by varying the flow characteristics. In figure 5, as in figure 4, the C_v values for large X fall within the previously given confidence interval for random errors.

Figure 6 shows several types of information from Filmer and Yevdjovich's [8] experiments with a (disturbed) centerline injector. Specifically, the figure shows C_v values and ΔC_1 , ΔC_2 , and ΔC_4 . The ΔC values are based on the four concentration measurements obtained nearest the wall ($\rho = 0.96$). ΔC_1 is the one of the four values with the greatest deviation from \bar{c} . ΔC_2 is based on the "worse" one of the two averages of the diametrically opposed samples, and ΔC_4 is the average of the four values. First, consider the values of C_v , as indicated by the open symbols. There is good agreement between the five sets of data as long as the C_v values are large enough not to be significantly influenced by random errors. (The dividing line of $C_v = 0.035$ between the effects of mixing and random errors was obtained by a visual injection of the data in figure 6.) The line drawn through the data points for C_v is the visual best-fit line having a slope corresponding to the asymptotic slope for asymmetric conditions shown in the previous figures.

The solid points above the C_v line are for ΔC_1 . The line drawn through these points is based on the line drawn for C_v and corresponds to the previously cited value of $\Delta C_1/C_v = 1.8$. Having drawn these two lines, it was possible to see that the data were the same as if a point source injection had been used at a virtual origin of $X = -0.08$. Assuming this condition, it was possible to use figure 3 and the equivalence between ΔC_1 for $N_+ = 2$ and ΔC_2 for $N_+ = 1$ to draw the curve for ΔC_2 on figure 6. The value of $P = 5\%$ was chosen as the one providing the best envelop curve for the ΔC_2 values in the mixing region on the figure. Considering that only

four values were available at each cross section for evaluating ΔC_1 and ΔC_2 , the data show excellent agreement with the characteristics obtained from the analytical solution.

The values of ΔC_4 at a given X are naturally smaller than the corresponding values of ΔC_2 , but a mixing distance based on ΔC_4 would not be very much shorter than that based on ΔC_2 . Thus, the installation of more than two ports for sampling might not be justified, but this statement is based on very limited data and needs more study, as mentioned in section 4. Certainly, both the data and the analytical work indicate that the accuracy of evaluating \bar{c} based on the mixing characteristics does not continue to increase as the number of sampling ports increase. Thus, the use of 10 sampling ports at the wall does not give any better average of the mixing characteristics than say 3 wall ports. Of course, multiple samples from the 3 ports would reduce the random errors.

The data of Filmer and Yevdjovich [8] were also used to compare values of \bar{c}_A and \bar{c}_Q by assuming a power law velocity distribution and using eqs. (4) and (5). For $X > 0.3$, it was found that there was less than 0.1% difference in the two values of \bar{c} .

2.2. Initial Mixing

For any number of injection ports and any number of sampling ports, the mixing distance required to obtain a specified C_y or ΔC value can be reduced compared to those considered above by using initial mixing. If attention continues to be restricted to injection at the pipe wall with no mixing devices mounted inside the pipe, then initial mixing can still be achieved by having jet injection instead of the source-type injection considered throughout section 2.1.

With jet injection, there are a number of parameters which can be varied to control the amount of initial mixing. Among the significant parameters are the number of jets, the angle of injection relative to the flow in the pipe, and the initial jet diameter and velocity relative to the pipe diameter and flow velocity in the pipe. There are some indications [4,7,9] that the diameters and velocities can all be combined and replaced by the ratio (M) of the initial momentum in the jet to the momentum in the pipe flow.

There are many publications on topics such as jets in cross flows and other similar topics which have some relation to jet injections into pipes. However, there are relative few publications that directly address the topic of the mixing of a tracer with a jet injection at the pipe wall. Ger and Holley [4,7] performed both analytical and experimental studies of a single jet injected perpendicular to the pipe wall. The analytical work led to a numerical model to simulate both the initial jet mixing and the subsequent ambient mixing. It was found that there was an optimum momentum ratio (M) which produced the shortest mixing distance. The optimum corresponds to the penetration of the bent-over jet to approximately the pipe centerline, as shown in figure 7. For smaller M , the jet does not reach the centerline and a larger mixing distance results. For larger M , there is an overpenetration with an associated increase in the

mixing distance. The experiments indicated that the optimum value of M is approximately 0.016. The two experiments conducted with this value of M and the corresponding results of the numerical model are shown in figure 8. (After completion of the previous publications [4,7], a slight error was found in the value of η which was used in the numerical model. As a result, the curve shown in figure 8 is slightly different from the similar curves shown in the previous publications.) Figure 8 shows excellent agreement between the calculations and the data and also shows a significant reduction in the mixing distance compared to that for a single source as shown in figure 1. However, if mixing distances on the order of that shown in figure 8 are needed, in some cases it might be more practical to use multiple-point, low-velocity or source injection (figure 2) or multiple-point sampling (figure 6). If even shorter mixing distances are required, it still remains to be determined how much initial mixing can be obtained by using multiple jets. This topic is currently being investigated by the author.

3. Random Errors

In the previous section, it was shown that some general conclusions could be obtained about the magnitude of possible errors resulting from the selection of a particular set of sampling points to approximate \bar{c}_0 . After a high degree of mixing has been obtained in the pipe so that no errors are expected because of inappropriate sampling locations, random errors will still be present. It is usually not possible to draw general conclusions about the magnitude of random errors since these errors depend on the particular tracer, procedures, equipment and instrumentation being used. Therefore, in this section, an example is presented to demonstrate the evaluation of random errors when using a particular tracer, namely a radioactive tracer, and to show that the errors can be kept within generally acceptable limits if sufficient care is used. The example is based on measurements reported by Clayton and Evans [2], who also presented an error analysis and discussed a number of other aspects of radioactive tracer techniques. The present error analysis has the same general purpose as that of Clayton and Evans and therefore has some similarities to their analysis. However, most of the presentation and discussion given here is different from that of Clayton and Evans since a different approach is used.

3.1. Experimental Procedure

Clayton and Evans [2] used a radioactive tracer (sodium-24) to measure a discharge of approximately 11 m³/s (388 cfs) of water. A unidirectional piston pump which was driven by a synchronous motor was used to inject the tracer into a secondary injection circuit which withdrew water from the pipe and then flowed back into the pipe through a single port. The volumetric flow rate (q) from the injection pump was determined from previous calibrations. Downstream of the distance required for mixing, nine samples from the pipe (after a steady state concentration distribution developed) were used for evaluation of \bar{c}_0 . Also, five diluted samples of the injection solution were used to determine c_i . All of the instruments were calibrated before and after (and sometimes during) the testing to

eliminate systematic errors. The background concentrations were determined. The densities of the injection solution of the water in the pipe and of the samples were also measured.

3.2. Error Analysis

The purpose of this error analysis is to evaluate the confidence interval for the calculated mean discharge Q . In doing this type of analysis for an expression such as eq. (2), normally some assumptions must be made. The assumptions which are made in this analysis are different from the assumptions made or implied by Clayton and Evans [2] in their error analysis; this difference is the reason that this analysis is different from theirs. In their analysis, Clayton and Evans apparently used several approximations and methods that had been presented in earlier reports [10, 11] which they cited, but the author did not have access to those reports while preparing this paper.

The present error analysis generally follows the method presented by Ang and Tang [12] and is based on standard techniques for the analysis of propagation of errors when the mean value (indicated by an overbar) of x is a function of the mean values of other variables such that

$$\bar{x} = \phi(\bar{u}, \bar{v}, \bar{w}, \dots) \quad (14)$$

Assuming that the errors in $\bar{u}, \bar{v}, \bar{w}, \dots$ are small relative to the mean values and are independent of each other, then

$$\text{var}(\bar{x}) = \text{var}(\bar{u}) \left(\frac{\partial \bar{x}}{\partial \bar{u}} \right)^2 + \text{var}(\bar{v}) \left(\frac{\partial \bar{x}}{\partial \bar{v}} \right)^2 + \text{var}(\bar{w}) \left(\frac{\partial \bar{x}}{\partial \bar{w}} \right)^2 + \dots \quad (15)$$

where $\text{var}(\)$ is the variance of the variable indicated. The square root of the variance is the standard deviation which will be indicated as $s(\)$. If the variable is a mean value (indicated by an overbar) then $s(\)$ is the standard deviation of the mean or the standard error. If the function ϕ in eq. (14) involves only products and quotients (no sums, exponentials, etc.), then dividing eq. (15) by the square of eq. (14) gives

$$\frac{\text{var}(\bar{x})}{\bar{x}^2} = \frac{\text{var}(\bar{u})}{\bar{u}^2} + \frac{\text{var}(\bar{v})}{\bar{v}^2} + \frac{\text{var}(\bar{w})}{\bar{w}^2} + \dots \quad (16)$$

The standard error for any of the variables (for example, \bar{u}) is

$$s(\bar{u}) = \frac{s(u)}{\sqrt{n}} \quad (17)$$

where $s(u)$ is the estimated or known standard deviation of the sample and n is the sample size. If the standard deviations are known or can be evaluated for samples of u, v, w, \dots , then the standard error for \bar{x} can be calculated from eq. (15).

The analysis of the propagation of errors will be applied to eq. (2) for \bar{Q} written in the form

$$\bar{Q} = \bar{q} \frac{\bar{c}_i}{\bar{d}} \quad (18)$$

where it has been assumed that $\bar{c}_Q \ll \bar{c}_i$ and \bar{d} is defined as

$$\bar{d} = \bar{c}_Q - \bar{c}_o \quad (19)$$

The overbar on c_Q previously indicated an integration over the pipe cross section as shown in eq. (4). However, throughout section 3, the overbar on c_Q indicates the mean value of the measured values used to evaluate the average concentration in the pipe. From eqs. (14) and (18), the standard error in \bar{Q} can be expressed as

$$\frac{\text{var}(\bar{Q})}{\bar{Q}^2} = \frac{\text{var}(\bar{q})}{\bar{q}^2} + \frac{\text{var}(\bar{c}_i)}{\bar{c}_i^2} + \frac{\text{var}(\bar{d})}{\bar{d}^2} \quad (20)$$

Each of the three terms on the right-hand side of eq. (20) will be evaluated and the results combined to determine the standard error in \bar{Q} . Throughout the evaluation of the errors, the standard errors will be divided by the mean values and presented as percentages of the mean values.

One of the major assumptions in the analysis will come in the specification of a confidence interval for \bar{Q} from the standard error in \bar{Q} . If the distribution of \bar{Q} were known, then the relation between $s(\bar{Q})$ and a confidence interval would be known or could be calculated. Knowledge of the distributions of all of the variables included explicitly or implicitly on the right-hand side of eq. (18) does not give a direct indication of the distribution of \bar{Q} , although it would allow the determination of the distribution of \bar{Q} (for example, by a Monte Carlo analysis). In the present error analysis, it will simply be assumed that \bar{Q} is normally distributed. Then the confidence interval for the calculated value of \bar{Q} is $\lambda s(\bar{Q})$ where $\lambda_{0.95}$ for the 95% (two-sided) confidence interval is 1.96 and $\lambda_{0.99}$ for the 99% confidence interval is 2.58.

3.2.1. Standard Error in \bar{q}

The pump was calibrated to determine \bar{q}_{50} at a line frequency (in the United Kingdom) of 50 Hz. In order to correct for variations in line frequency (f), the actual discharge was given by

$$\bar{q} = \frac{\bar{f}}{50} \bar{q}_{50} \quad (21)$$

Application of eq. (16) gives

$$\frac{\text{var}(\bar{q})}{\bar{q}^2} = \frac{\text{var}(\bar{f})}{\bar{f}^2} + \frac{\text{var}(\bar{q}_{50})}{\bar{q}_{50}^2} \quad (22)$$

From the calibration of the pump, it was known that $q_{50} = 2.0996 \text{ cm}^3/\text{s}$ and $s(\bar{q}_{50})/\bar{q}_{50} = 0.05\%$. It was determined that $f = 49.96 \text{ Hz}$ during the discharge measurement, and the electric utility company quoted $s(\bar{f})/\bar{f} = 0.04\%$. Substituting these values into eq. (22) and taking the square root gives

$$\frac{s(\bar{q})}{\bar{q}} = 0.06\% \quad (23)$$

3.2.2. Standard Error in \bar{d}

Each of the concentrations in d was determined from counting the radioactive emissions from collected samples over a given time interval. In order to compensate for the radioactive decay of the samples being used to determine \bar{c}_0 , an adjustment factor was applied to determine the equivalent count rate at a base time. The adjustment factor involves integration of the exponential decay term over the counting period. However, in order to provide some simplification in the presentation of the error analysis, it will be assumed following Clayton and Evans that just for the error analysis the adjustment factor can be represented by a single exponential decay term based on the mean time of counting the samples. This assumption seems justified since the error in the adjustment factor does not make a large contribution to the total error.

If \bar{K} is the equivalent count rate at the base time, and \bar{k} is the measured count rate, then

$$\bar{k} = \bar{K} \exp(-\alpha \frac{\bar{t}}{\bar{T}_{1/2}}) \quad (24)$$

where $\alpha = 0.693$, \bar{t} is mean time measured from the base time and $\bar{T}_{1/2}$ is the half-life. The concentration is

$$\bar{c} = \bar{K} \frac{\bar{\rho}_1}{\bar{\rho}_2} = \bar{k} \exp(\alpha \frac{\bar{t}}{\bar{T}_{1/2}}) \frac{\bar{\rho}_1}{\bar{\rho}_2} \quad (25)$$

where $\bar{\rho}_1$ is the density of the water under the conditions (temperature and pressure) for which the concentration is desired (e.g. in the pipe) and $\bar{\rho}_2$ is the density of the water during counting. Equation (25) applies to both \bar{c}_0 and \bar{c}_1 (as well as to \bar{c}_1 to be considered later, when $\bar{\rho}_1$ must be the density in the injection pump). It will be assumed that the relative standard errors were the same in all density measurements. The use of eq. (19) for the definition of \bar{d} , eq. (15) for the standard error and eq. (25) for both \bar{c}_0 and \bar{c}_1 with subscripts on K and k corresponding to the subscripts on c gives

$$\frac{\text{var}(\bar{d})}{\bar{d}^2} = \frac{\bar{K}_Q^2}{(\bar{K}_Q - \bar{K}_O)^2} \left[\frac{\text{var}(\bar{k}_Q)}{\bar{k}_Q^2} + \left(\alpha \frac{\bar{t}_Q}{\bar{T}_{1/2}} \right)^2 \frac{\text{var}(\bar{T}_{1/2})}{\bar{T}_{1/2}^2} + 2 \frac{\text{var}(\bar{\rho})}{\bar{\rho}^2} \right] \quad (26)$$

$$+ \frac{\bar{K}_O^2}{(\bar{K}_Q - \bar{K}_O)^2} \left[\frac{\text{var}(\bar{K}_O)}{\bar{K}_O^2} + 2 \frac{\text{var}(\bar{\rho})}{\bar{\rho}^2} \right]$$

after dividing by \bar{d}^2 and cancelling the $\bar{\rho}_1/\bar{\rho}_2$ terms since the densities multiplying \bar{K}_Q and \bar{K}_O are equal in this case. In eq. (26), the first set of bracketed terms comes from \bar{c}_Q . The second set of terms comes from \bar{c}_O . It has been assumed that there is no error in the measurement of time and that the background measurement is not subject to a decay adjustment.

The following data were given by Clayton and Evans:

$$\bar{N}_Q = 80488 \text{ counts (average of nine 4-min unadjusted counts)}$$

$$\bar{K}_Q = 20150 \text{ counts/min (adjusted for decay)}$$

$$\bar{t}_Q = 25.8 \text{ min.}$$

$$\bar{K}_O = 396 \text{ counts/min (average of two 10-min counts)}$$

$$\frac{s(\bar{\rho})}{\bar{\rho}} = 0.1\%$$

$$\bar{T}_{1/2} = 15.0 \text{ hr} = 900 \text{ min}$$

$$s(\bar{T}_{1/2}) = 0.1 \text{ hr} = 6 \text{ min}$$

$$\bar{\rho}_1 = 1.002 \text{ g/cm}^3 \text{ (for both } \bar{c}_Q \text{ and } c_O)$$

$$\bar{\rho}_2 = 0.9982 \text{ g/cm}^3 \text{ (for both } \bar{c}_Q \text{ and } c_O)$$

Based on the Poisson distribution for counting radioactive emissions, the dimensionless standard deviation of the count rate for determining \bar{c}_Q is

$$\frac{s(k_Q)}{\bar{k}_Q} = \frac{100\%}{\sqrt{\bar{N}_Q}} = 0.35\% \quad (27)$$

Eq. (17) for $n = 9$ gives the standard error as

$$\frac{s(\bar{k}_Q)}{\bar{k}_Q} = 0.12\% \quad (28)$$

In conjunction with the sampling to obtain \bar{c}_0 , one background count was obtained immediately before taking the samples and another one about 4½ hours later. The actual counting of the samples to determine k_0 took about one hour. The two background count rates differed by about 3% over the 4½ hour period. In the calculation of Q , \bar{K}_0 was assumed to be constant. In conjunction with taking water from the pipe for diluting the samples of the injected solution (see section 3.2.3), five 16.67-minute background counts were taken over a period of 11 hours. For these samples, $s(K_0)/\bar{K}_0 = 2.49\%$. An F test showed at a confidence level greater than 99% that this value of $s(K_0)$ was not due just to counting statistics and therefore that the background concentration was varying. The use of $s(K_0)/\bar{K}_0 = 2.49\%$ and eq. (17) for $n = 5$ gives

$$\frac{s(\bar{K}_0)}{\bar{K}_0} = 1.11\% \quad (29)$$

Because of the 11-hour time interval and the tendency for background concentrations to vary slowly in many cases, the value in eq. (29) do doubt over-estimates the error in \bar{K}_0 during the actual one-hour sampling period.

Substitution of the appropriate values into eq. (26) and taking the square root gives

$$\frac{s(\bar{d})}{\bar{d}} = 0.19\% \quad (30)$$

Even with the apparent over-estimation of the error in the background count, the error associated with the determination of \bar{c}_Q accounts for 99% of the value given in eq. (30).

3.2.3. Standard Error in \bar{c}_i

The injection concentration was determined from counting five dilutions of the injection solution. The dilution was done to reduce the concentration so that the counting could be done on the same equipment used to count the samples from the pipe. If D is the dilution ratio, then

$$\bar{c}_i = \bar{K}_i \frac{\bar{\rho}_1}{\bar{\rho}_2} = \bar{K}_D D \frac{\bar{\rho}_1}{\bar{\rho}_2} \quad (31)$$

where K_i is the count rate of the undiluted injection solution, K_D is the count rate of the diluted solution and ρ_1 and ρ_2 are as defined for eq. (25). It was not practical to dilute all of the samples by the same ratio. The five dilution ratios varied from 2.676×10^6 to 4.265×10^6 . The dilutions were counted for 16.67 min with the adjusted count rates varying from 29392.3 to 46847.5 counts/min. The products of K_D and D for the five samples were approximately equal (as they should be) with the mean value of K_i being

$$\bar{K}_i = 1.25206 \times 10^{11} \text{ counts/min} \quad (32)$$

The standard deviation of the 5 values of K_D or K_i was

$$\frac{s(K_i)}{\bar{K}_i} = 0.13\% \quad (33)$$

From eq. (17) with $n = 5$,

$$\frac{s(\bar{K}_i)}{\bar{K}_i} = 0.06\% \quad (34)$$

From eqs. (16) and (31),

$$\frac{\text{var}(\bar{c}_i)}{\bar{c}_i^2} = \frac{\text{var}(\bar{K}_i)}{\bar{K}_i^2} + 2 \frac{\text{var}(\bar{\rho})}{\bar{\rho}^2} \quad (35)$$

As previously, it is assumed that both ρ values ($\rho_1 = 1.016 \text{ g/cm}^3$ and $\rho_2 = 0.9982 \text{ g/cm}^3$) were subject to the same relative error as given in section 3.2.2. Substitution of the appropriate values in eq. (35) and taking the square root yields

$$\frac{s(\bar{c}_i)}{\bar{c}_i} = 0.15\% \quad (36)$$

3.2.4. Confidence Interval

From eq. (18) and the experimental values given in the above sections, the discharge \bar{Q} was calculated to be $11.02 \text{ m}^3/\text{s}$ (389.2 cfs). Eqs. (20), (23), (30), and (36) give the standard error in \bar{Q} as

$$\frac{s(\bar{Q})}{\bar{Q}} = 0.25\% \quad (37)$$

Defining μ_Q as the true mean discharge and utilizing the previously stated assumption that \bar{Q} is normally distributed, it can be estimated from eq. (37) and the previously cited values of λ that

$$\left| \frac{\mu_Q}{\bar{Q}} - 1 \right| \leq 0.49\% \text{ at } 95\% \text{ confidence level} \quad (38)$$

$$\left| \frac{\mu_Q}{\bar{Q}} - 1 \right| \leq 0.64\% \text{ at } 99\% \text{ confidence level} \quad (39)$$

It should be noted that the magnitude of error represented in eqs. (38) and (39) normally can not be obtained by casual application of the experimental procedures and techniques presented by Clayton and Evans. Nevertheless, they indicated that this accuracy can be obtained routinely through well planned and carefully executed measurements with radioactive tracers.

Any errors associated with possible unsteady flow in the secondary injection circuit (section 3.1) were not included in the error analysis since the effects of this unsteadiness on the concentrations within the pipe will normally be damped out in the pipe "if the transit time of the tracer in the secondary circuit is short compared with the transit time" in the main pipe [2]. In addition, if any of the errors in q or c_i produce an unsteadiness in the mass injection rate, these may be damped out during flow in the pipe. Thomann [13,14] has presented an analytical method based on the Fourier frequency response function to allow a quantitative evaluation of the damping of temporal variations in rates of injection into fluid flows. Although his analysis was presented in terms of open channel flows, it is equally applicable to pipe flow with the proper selection of parameters.

4. Possible Research Areas

The potential and accuracy of the dilution method for discharge measurement can be increased by additional research in several areas. A few such areas for possible further work are indicated by the following comments:

- 1) While the available data for steady uniform flow provide some indication of the advantages of multiple-point sampling, the results are sparse and research is needed in this area since multiple-point sampling can greatly reduce the flow distance required to achieve a given accuracy and thereby increase the potential applicability of the method.
- 2) Data are available on mixing in uniform flows (with single-point injections), but study is needed on the effects of non-uniformities (elbows, contractions, valves, swirl in the flow, etc.) and on the effects of the associated flow asymmetry on mixing. This is especially needed for multiple-point injection and sampling systems.
- 3) There are some unpublished results indicating that pumps may provide essentially complete mixing even for tracers injected at the suction port. However, there needs to be a definitive investigation of the mixing efficiency of various types and sizes of pumps.
- 4) It is apparent that high velocity injection even at the pipe wall can increase the initial mixing and thereby reduce the required mixing distance as compared to a low velocity or source-type injection. Research is needed on various types of high velocity injection in order to evaluate the amount of initial mixing which can be obtained and to define the orientation and other characteristics of the injection which will provide the highest degree of mixing under a given set of conditions. The benefits of injection systems with high-initial mixing need to be compared with the benefits of multiple-point sampling. This comparison needs to consider the

power requirements of the injection system and the possibility of the injection system causing a head loss in the pipe.

5) Both analytical and experimental work is needed to evaluate the potential applicability of the dilution method to unsteady, full-pipe flows.

6) The dilution method is applicable to determining the discharge for steady, partially-full pipe flows in sewers [15]. The characteristics of various types of tracers when used in both storm and sanitary sewers needs to be established. Information similar to that for full pipe flow is needed on rates of mixing, effects of multiple-point injection and sampling, and means of accelerating mixing when the sewer length between manholes is not sufficient to obtain the desired degree of mixing. Applicability of the dilution method to unsteady, partially-full pipe flow as exists in sewers needs to be investigated.

7) For other situations besides sewer flow, the stability, reliability, accuracy and potential application of various tracers need to be established.

8) Similarly, the random errors for various types of equipment and instruments need to be evaluated.

9) The available information, including information on cost and power requirements for injection systems needs to be made available in readily usable form.

10) Standards for use of the dilution method need to be developed based on recent and on-going research results in order to recognize and utilize the potential of the method.

5. Conclusions

Errors in the use of the dilution method to measure discharge in a pipe may come from the use of inappropriate sampling points to determine the average concentration or from random errors in the equipment, instruments, and procedures being used.

It is customary to represent the completeness of mixing by using the coefficient of variation (C_v) of the concentration distribution or by using some other closely related parameter. However, C_v does not give a direct indication of the accuracy with which a given set of measured concentrations will represent the average concentration. ΔC was introduced for this purpose, where ΔC was defined as the maximum difference between the average of a set of measured values and the true average concentration (\bar{c}), with the difference being normalized with respect to \bar{c} . For a single injection port at the pipe wall and a single measurement port at the pipe wall, it is possible to predict the mixing distance which must be allowed in order to obtain a specified value of ΔC . For example, for distances greater than about 220 pipe diameters, any measured concentration is within a maximum of 0.5% of the average concentration (except for random measurement errors). When the available mixing distance is restricted, the use of either multiple-point injection or multiple-point sampling can reduce the

required distance by as much as 70%, but the amount of reduction apparently depends on the amount of asymmetry in the flow and is therefore difficult to predict accurately.

The use of a jet injection perpendicular to the pipe wall can provide initial mixing and significantly reduce the required mixing distance. However, the amount of reduction depends on the ratio of the initial momentum of the injected jet to the momentum of the pipe flow. For the optimum momentum ratio of about 0.016, the mixing distance with a jet injection can be reduced by about 35% compared to a single wall source. Study is needed to define the initial mixing that can be obtained with other types of high velocity injections.

Based on data from the literature, it was shown that at the 95% confidence level a discharge calculated using the dilution method with a radioactive tracer was within 0.5% of the actual discharge when the concentration measurements were made after a sufficient mixing distance.

Several areas for possible additional research were presented.

6. References

- [1] ASME Research Committee on Fluid Meters (H.S. Bean, ed.), *Fluid Meters - Their Theory and Application*, ASME, 6th ed. (1971).
- [2] Clayton, C. G. and Evans, G. V., The constant-rate-injection and velocity methods of flow measurement for testing hydraulic machines, Report AERE-R-5872, Wantage Research Laboratory, Berkshire, U.K., 50 p. (1968).
- [3] Evans, G. V., A study of diffusion in turbulent pipe flow, *J. Basic Engrg.* ASME, 89D, 624-632 (1967).
- [4] Ger, A. M. and Holley, E. R., Turbulent jets in crossing pipe flow, *Hydr. Engrg. Ser. 30*, Univ. of Ill., 197 p. (1974).
- [5] Holley, E. R. and Ger, A. M., Circumferential mass diffusivity in pipes, *J. Hydr. Div. ASCE*, in preparation.
- [6] Clayton, C. G., Ball, A. M., and Spackman, R., Dispersion and mixing during turbulent flow of water in a circular pipe, Report AERE-R-5569, Wantage Research Laboratory, Berkshire, U.K., 31 p. (1968).
- [7] Ger, A. M. and Holley, E. R., Comparison of Single-Point Injections in Pipe Flow, *J. Hydr. Div. Am. Soc. Civil Engr.* 102, 731 (1976).
- [8] Filmer, R. W. and Yevdjovich, V. M., The use of tracers in making accurate discharge measurements in pipelines, Report CER66RWF-VMY 38, Colorado State Univ., Fort Collins, 90 p. (1966). See also: Experimental results of dye diffusion in large pipelines, *Proc. Twelfth Congress, Intern. Assn. Hydr. Res.*, Fort Collins, 4, 115 (1967).

- [9] Beltaos, S. and Rajaratnam, N., Circular turbulent jet in an opposing infinite stream, Dept. of Civ. Engrg., Univ. of Alberta, Canada, 18 p. (1973).
- [10] Clayton, C. G., Spackman, R., and Ball, A. M., The accuracy and precision of flow measurements by radioactive isotopes, *Symp. on Radioactive Tracers in Industry and Geophysics*, IAEA, Prague (1967).
- [11] Smith, D. B., Wearn, P. L., and Parsons, T. V., Accuracy of Open-Channel Flow Measurement using Radioactive Tracers, Report AERE-R-5676, Wantage Research Laboratory, Berkshire, U.K. (1968).
- [12] Ang, A. H-S. and Tang, W. H., *Probability Concepts in Engineering Planning and Design*, (John Wiley and Sons, Inc., New York, 1975).
- [13] Thomann, R. V., *Systems Analysis and Water Quality Management*, (Environmental Research and Applications, Inc., New York, 1972).
- [14] Thomann, R. V., Effect of longitudinal dispersion on dynamic water quality response of streams and rivers, *Water Resources Research*, 9, 355 (1973).
- [15] Shelley, P. E. and Kirkpatrick, G. A., Sewer flow measurement - A state-of-the-art assessment, Report EPA-600/2-75-027, EPA Municipal Environmental Research Laboratory, Cincinnati, Ohio (1975).

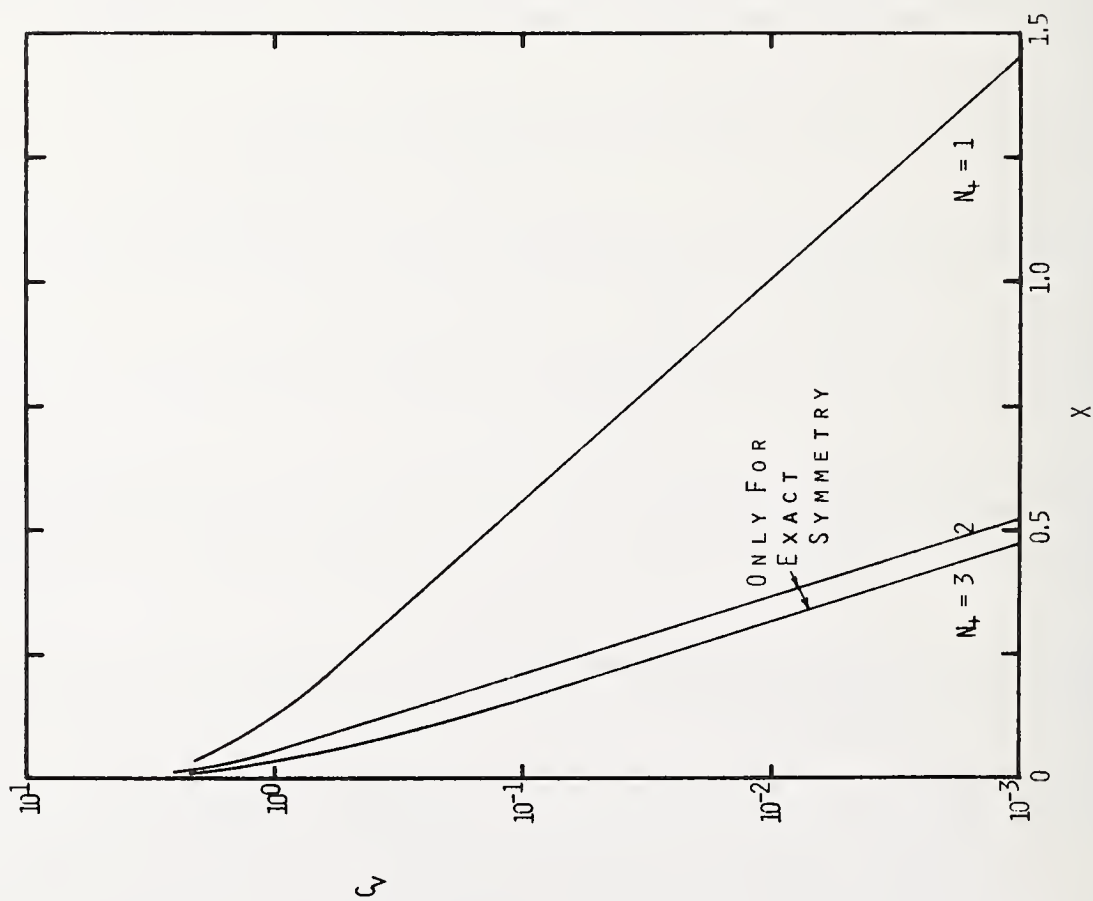


FIGURE 1. - COEFFICIENT OF VARIATION FOR WALL SOURCES OF EQUAL STRENGTHS

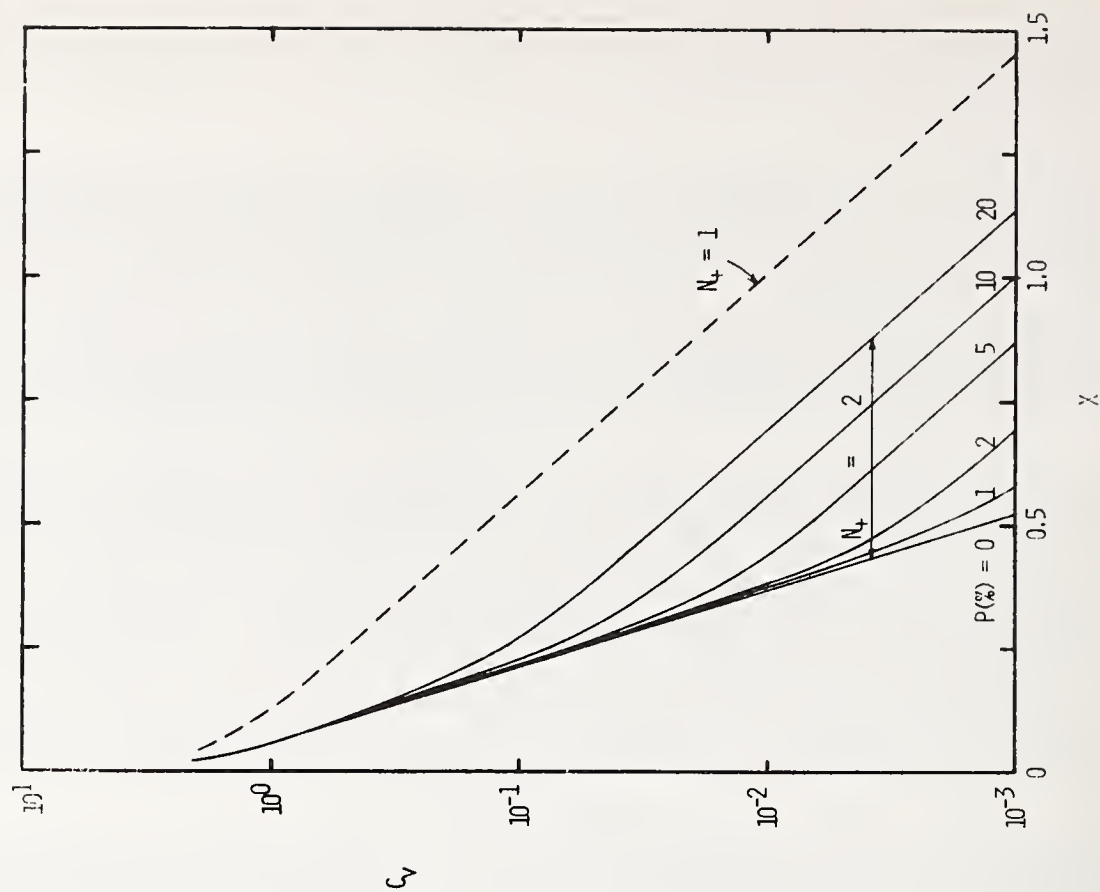


FIGURE 2. - EFFECT OF ASYMMETRY ON THE COEFFICIENT OF VARIATION

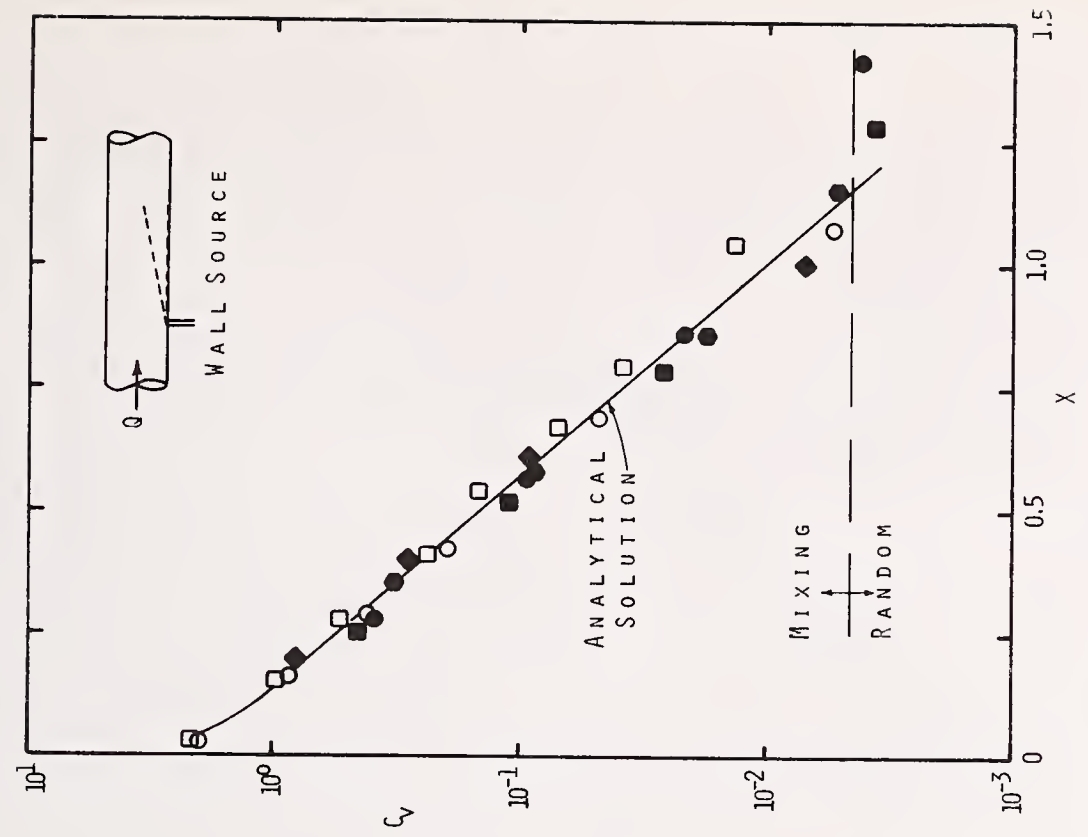


FIGURE 4. - COEFFICIENT OF VARIATION FOR ONE WALL SOURCE

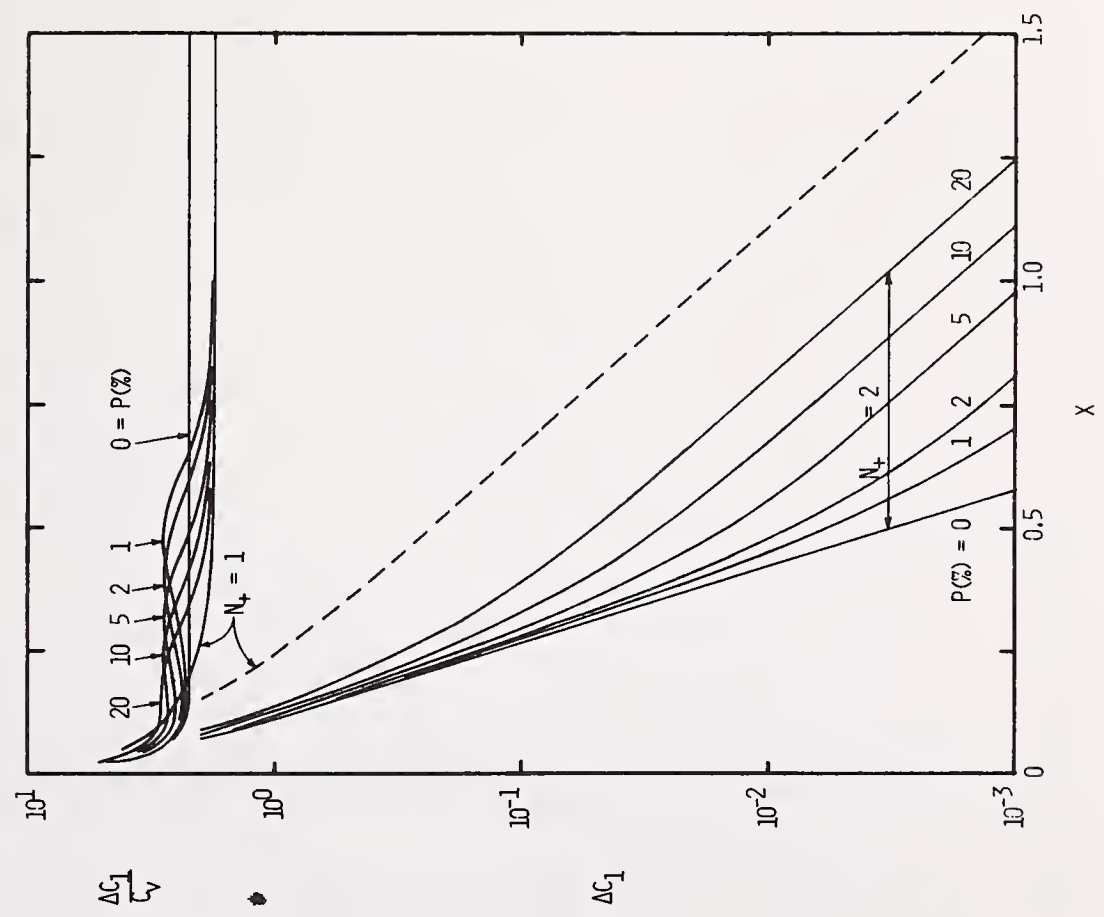


FIGURE 3. - MAXIMUM ERROR IN \bar{C} FROM ONE CONCENTRATION MEASUREMENT AT THE WALL

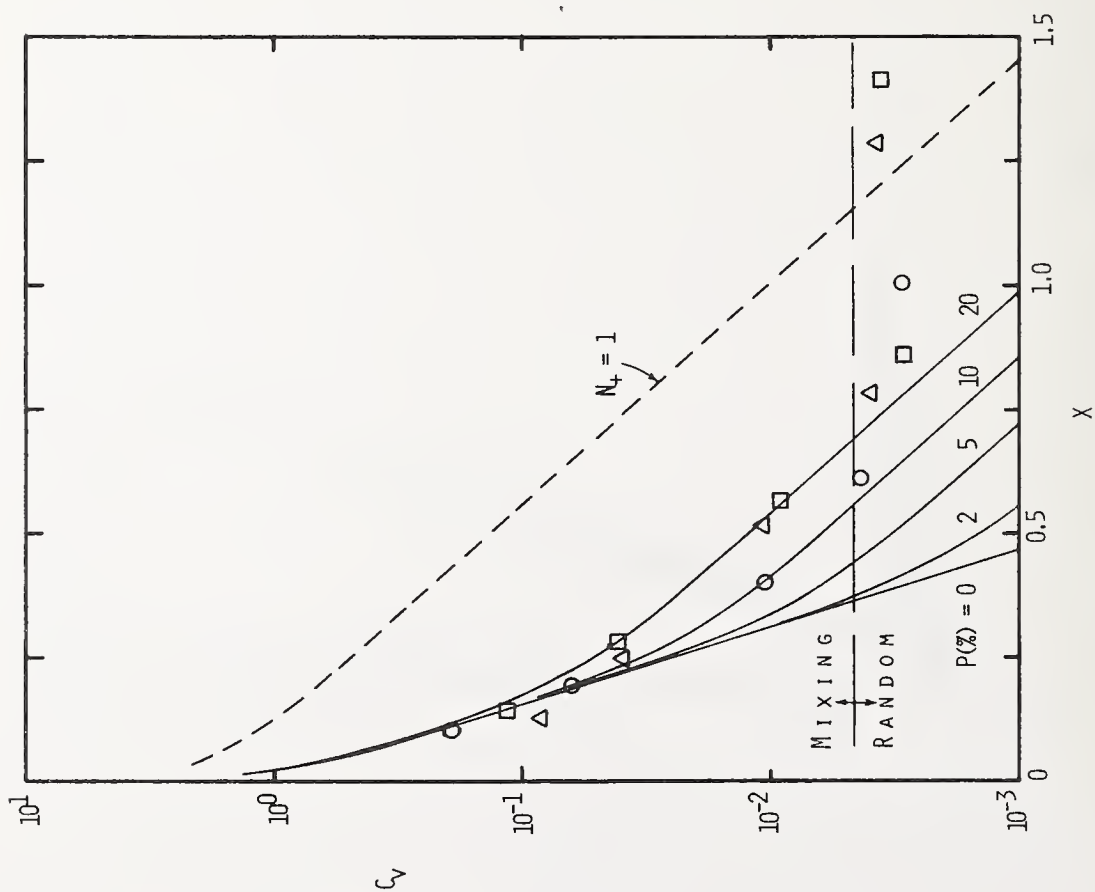


FIGURE 5. - COEFFICIENT OF VARIATION FOR FOUR WALL SOURCES

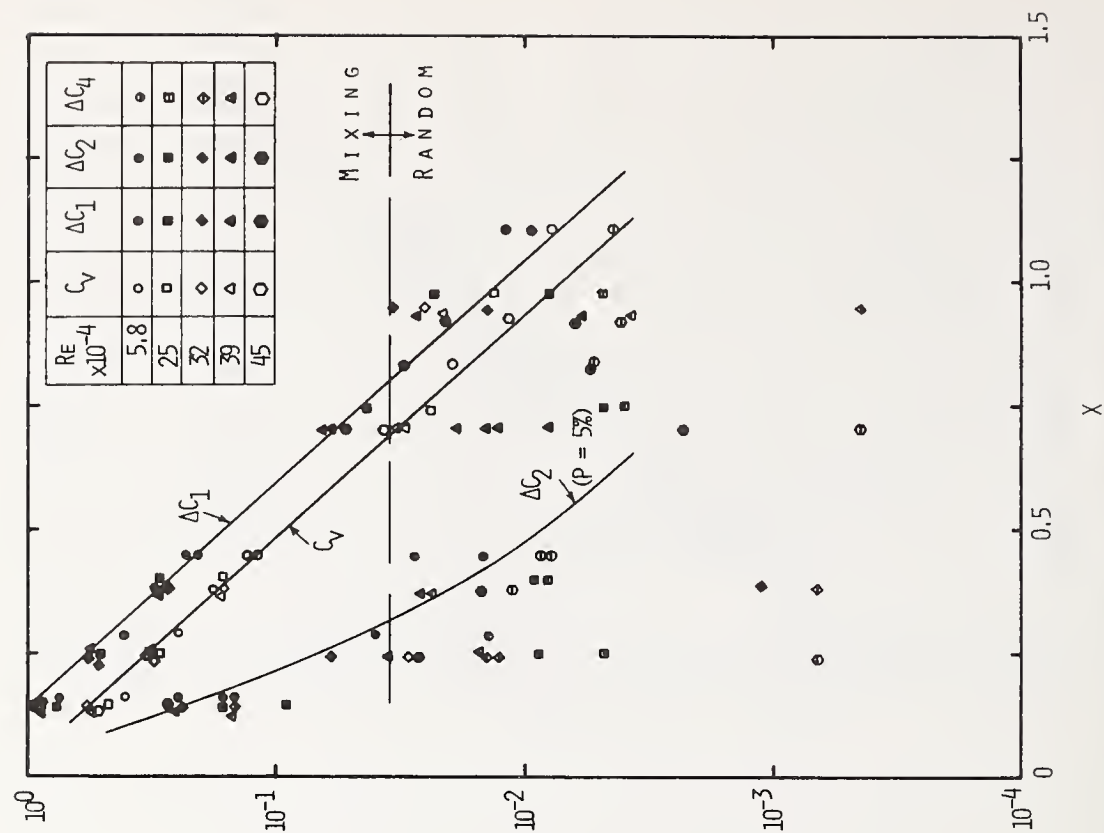


FIGURE 6. - EFFECT OF MULTIPLE-POINT SAMPLING ON MAXIMUM ERROR IN \bar{c}

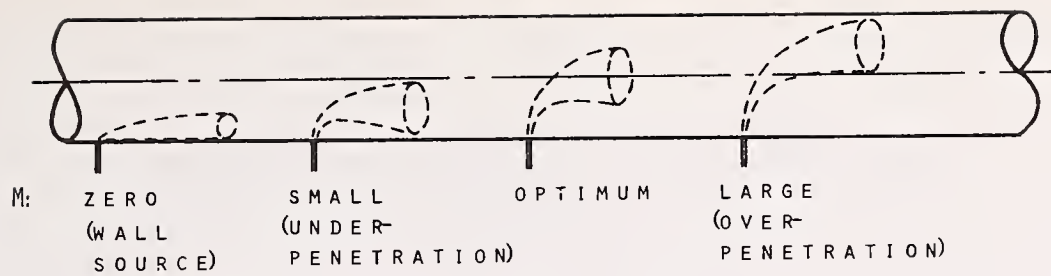


FIGURE 7. - PENETRATION OF JET PERPENDICULAR TO PIPE WALL

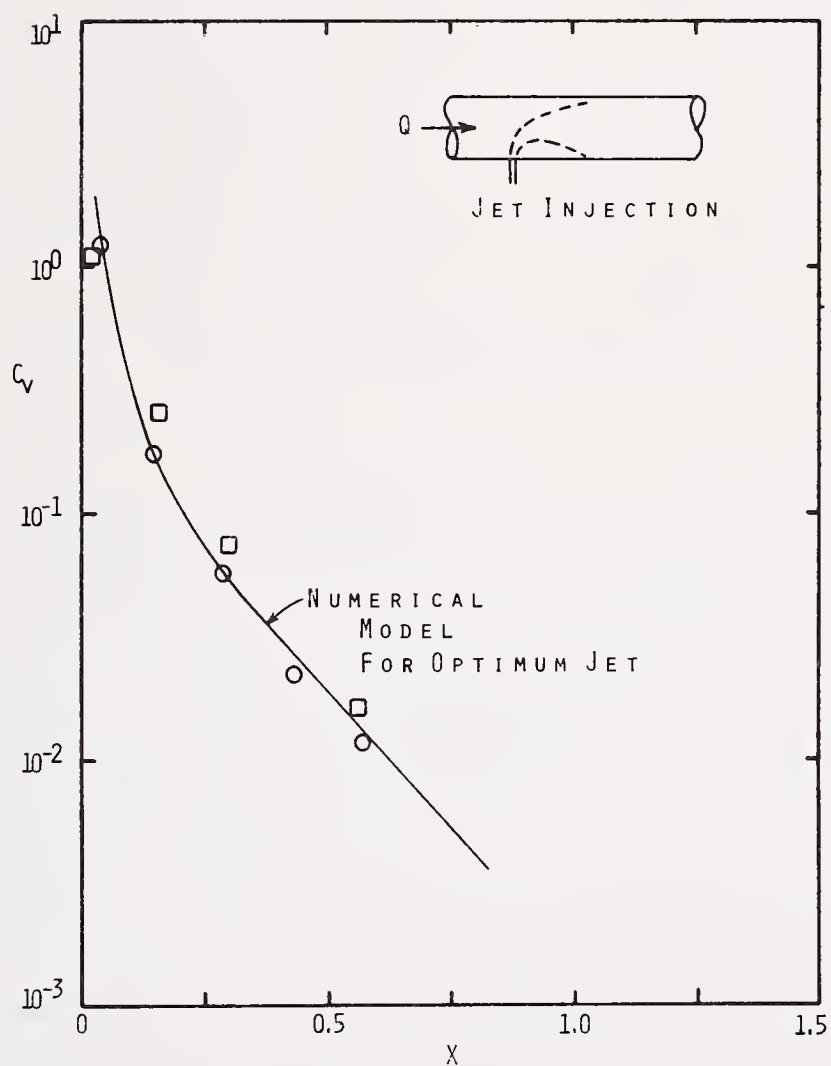
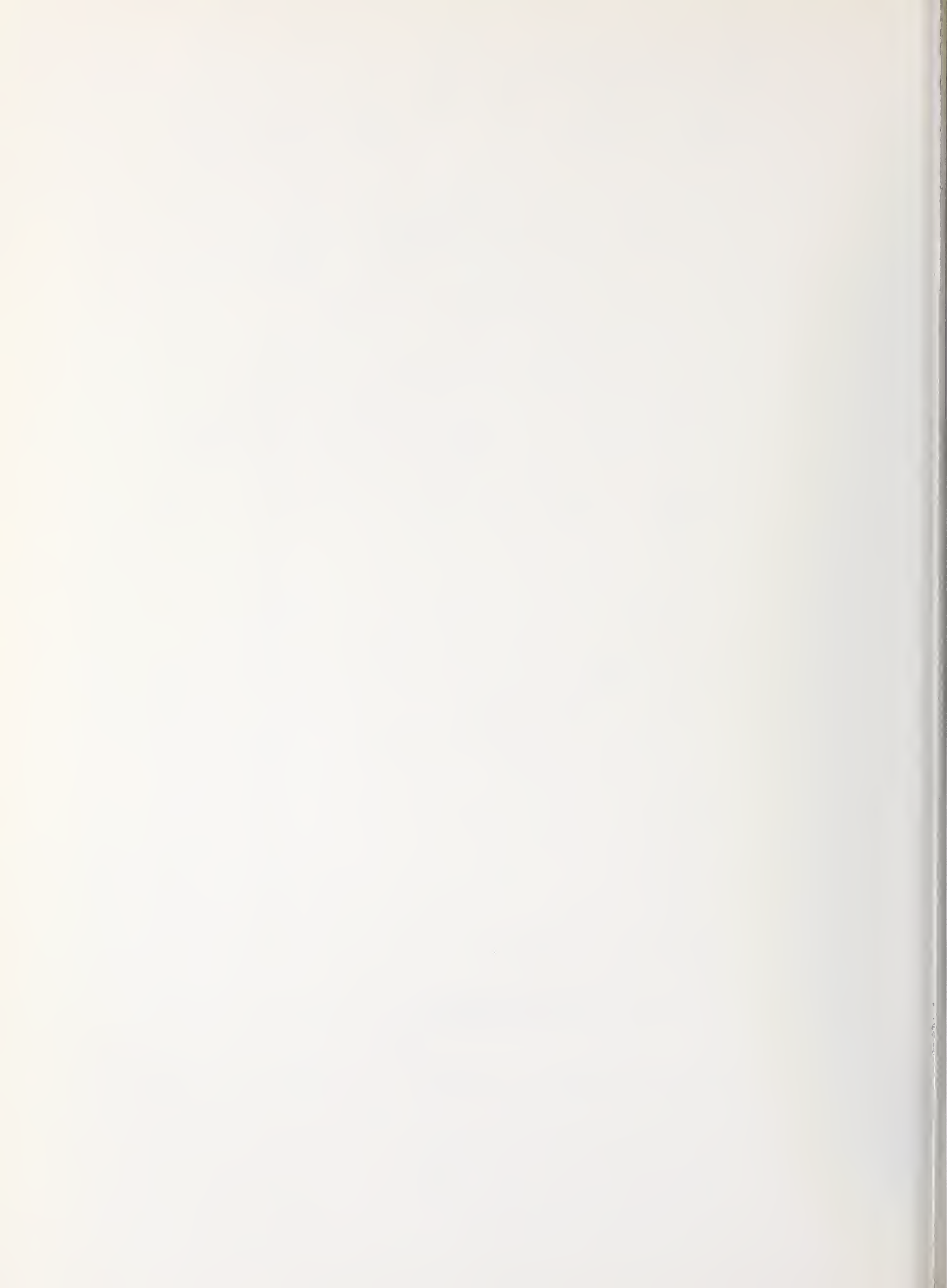


FIGURE 8. - COEFFICIENT OF VARIATION FOR OPTIMUM JET INJECTION PERPENDICULAR TO PIPE WALL



APPLICATION OF A FLUORESCENCE TECHNIQUE TO DYE-CONCENTRATION
MEASUREMENTS IN A TURBULENT JET

Hsien-Ta Liu, Jung-Tai Lin, Donald P. Delisi, and Frank A. Robben

Flow Research Company
A Division of Flow Industries, Inc.
Kent, Washington 98031

A laser dye-fluorescence technique for measuring the concentration of Rhodamine-6G dye in a turbulent water jet is presented. The measurement device consists of a 1-watt argon laser, which was used to excite the fluorescent dye, and an optics assembly, which was used to detect the radiated energy from the dye.

The dye-fluorescence technique is a remote-sensing method, which does not interfere with the flow field. Thus, a unique feature of this technique is that it provides the ability to conduct simultaneous measurements at many positions, which are as close as desired, parallel to the jet axis. Measurements show that the detecting device has an extremely high frequency response and that the sensing volume can be as small as 0.1 mm^3 . This technique can measure a wide range of concentrations with ratios larger than 10^4 . In the concentration range from 10^{-3} to 10^{-7} g/l , the calibration of the photomultiplier tube output to the dye concentration is linear.

Measurements of the mean and fluctuating dye concentrations in a round, turbulent water jet are reported. The Reynolds number of the jet was approximately 1600. The jet was tripped inside the nozzle to ensure a turbulent jet. Results show that the mean and rms concentrations on the jet axis decrease with the distance from the nozzle as x^{-1} . The profile of the axial mean concentration agrees very well with the profiles other investigators have measured in an air jet traced by oil smoke. The axial rms concentration, however, tends to have a relatively high value in the case reported here. Spectra of the concentration fluctuations are also discussed.

Simultaneous measurements of mean and fluctuating concentrations parallel to the jet axis were conducted to demonstrate the unique features of this technique. The results for tests made with two sensors focused at the same point show that the two sensors indeed measured the same signal. Both on- and off-axis measurements were conducted at $x/D = 30$, with three sensors separated by 0.3 and 0.7 cm. Cross-correlations and the convective velocity estimated from the cross-correlation are presented.

Key Words: Auto-correlation; convective velocity; cross-correlation; exit concentration; exit velocity; flow visualization; fluorescence; fluorescent dye; laser; laser dye-fluorescence technique; mean concentration; mean velocity; measuring volume; remote sensing; root-mean-square concentration; simultaneous measurements; Schmidt number; spectra; water jet.

1. Introduction

A laser dye-fluorescence (LDF) technique for measuring concentration fluctuations of dye in liquids has been developed [1].* The measurement device uses a 1-watt argon laser as the light source to excite fluorescent dye, which is the tracer. An optical assembly detects the radiated energy or fluorescence from the dye. The LDF technique is remote-sensing and, therefore, does not interfere with the flow field. The optical detector has an extremely high frequency response, which is limited only by the electronic circuitry. In the concentration range from 10^{-3} to 10^{-7} g/l, the calibration curve of the detector output to the dye concentration is linear [1]. In our investigation, we applied the LDF technique to measure mean and turbulent dye concentrations in a turbulent water jet.

Previous investigators have used various techniques to measure concentrations of scalar quantities. For example, Corrsin and Uberoi [2] used thin-wire probes to measure the temperature in a heated air jet. Kiser [3] used conductivity cells to measure the salinity concentration in a water jet. Rosensweig, et al. [4] was the first to use a light-scatter technique to measure the material transport of oil smoke in a turbulent air jet. The light-scatter technique was further developed by Becker, et al. [5], Liu and Karaki [6], Yang and Meroney [7], and Gad-el-Hak, et al. [8] for measuring concentrations in various turbulent flows.

Using the principle of light absorption, Lee and Brodkey [9] developed a light probe to study turbulent mixing in a pipe flow, where water was the working fluid. Nye and Brodkey [10] refined the light probe to improve its spatial resolution and frequency response.

In this paper we first describe the experimental setup and the LDF technique in section 2. In section 3 we present the results of our experiments and compare them with results obtained with other techniques. Finally, concluding remarks are given in section 4.

2. Experimental Setup

Figure 1 is a schematic of the experimental setup. The system consists of a water jet with a diluted solution of a fluorescent dye as the effluent, an argon-ion laser beam, and a photomultiplier detector assembly. The photomultiplier detector, which is focused onto a small volume of the laser beam, measures the dye fluorescence excited by the laser. Since the intensity of the fluorescence is proportional to the dye concentration, we can measure the dye concentration accordingly. Figures 1a and 1b show the orientation of the laser beam for measurements taken perpendicular and parallel to the jet axis.

2.1 The Water Jet

For the experiments, a submerged water jet was injected through a 0.32-cm-I.D. stainless-steel tube into a water tank. The tank was 7.5 m long, 20 cm wide, and 80 cm deep and had glass side walls to permit flow visualization. The effluent of the water jet was a dilute solution of Rhodamine-6G dye, manufactured by Kodak, and its concentration was 30

* Figures in brackets indicate the literature references at the end of this paper.

$\mu\text{g}/\ell$. The exit velocity of the effluent was 51 cm/s, and the corresponding Reynolds number was 1620. To ensure a turbulent jet, we tripped the water jet with a small nozzle, 0.8 mm in diameter, installed about 2 cm upstream of the jet exit. The effluent was stored in a chamber in which the pressure was regulated. The flow rate was regulated to within 2 ~ 3% with a needle valve and was measured with a flowmeter-valve assembly (Gilmont Model F7360).

For simultaneous measurements perpendicular to the jet axis, the jet was oriented downward (fig. 1a). To reduce reentrainment into the jet, we added NaCl solution to the effluent to increase its specific gravity to 1.001. The resulting Froude number $\bar{U}_0 / (1/2\pi \sqrt{g \Delta\rho/\rho} D)$ was 17,000, where g is the acceleration of gravity, $\Delta\rho$ is the density difference between the effluent and the ambient fluid, ρ is the density of the ambient fluid, and D is the diameter of the jet. The buoyancy of the effluent was negligible compared to the inertia of the jet at such a high Froude number.

For simultaneous measurements parallel to the jet axis, the water jet was oriented horizontally (fig. 1b). In this case, the effluent was neutrally buoyant, and we closely monitored the ambient dye concentration. The water in the tank was drained and refilled after every few measurements.

2.2 The Laser

The laser used in the experiment was a 1-watt argon-ion laser manufactured by Lexel (Model 85). The spectrum of the laser light was composed of two major lines at wavelengths 514.5 and 488 nm, and several other minor lines.

In the experiment, the laser was operated in a single-line mode (488 nm at 500 mW) with the use of a prism wavelength selector. The laser beam was projected horizontally through the glass side walls and onto a mirror inside the tank. The laser beam and the water jet were aligned by adjusting the angle between the incident and reflected beams on the mirror. An achromatic lens (approximately 0.6-m focal length) was used to reduce the diameter of the laser beam at the measuring points to about 1 mm.

2.3 The Photomultiplier Detector

The photomultiplier detector assembly consists of an achromatic lens (48-mm effective aperture and 193-mm focal length), a filter, a pinhole, and an RCA 931A photomultiplier. For the experiments the lens was mounted in one end of an aluminum tube. The pinhole, which had a diameter of 0.6 mm, was mounted in the other end, and it was imaged on the laser beam. Therefore, the measuring volume was formed by a cylinder with a diameter of 1 mm, which crossed the 1-mm-diameter laser beam at a right angle. The geometry gave an effective measuring volume of about 1 mm^3 .

2.4 Optical Characteristics of the System

Upon excitement by the laser light, the molecules of the Rhodamine-6G dye absorb photons of radiation (peaked at 530 nm), and, subsequently, some of the energy absorbed is reradiated (peaked at 560 nm). Figure 2a gives the absorption and stimulated emission characteristics of Rhodamine-6G, as published by Kodak. A Corning glass filter, stock no. CS 3-67, is installed in the detector assembly to block the laser light scattered

by particulates or air bubbles in the water jet. The filter transmits very little light with wavelengths shorter than 550 nm, and the RCA 931A photomultiplier, which has an S4 response, determines the high end cutoff (approximately 600 nm). Figure 2b shows the window that results from this system. We also measured the attenuation of the laser along the path of the Rhodamine-6G solution. For a concentration of 30 $\mu\text{g}/\ell$, the attenuation was as low as 0.1%/cm.

2.5 Calibration

For calibration, we prepared dye solutions of known concentrations in 15-ml pyrex beakers. The beakers were positioned, one at a time, at the measuring point in the tank, and the fluorescence intensity was measured for various dye concentrations. The output from the photomultiplier was first amplified and fed into a Nova 800 minicomputer (see section 2.6). Figure 3 shows a typical calibration curve, which is linear for dye concentrations, between 10^{-7} and 10^{-3} gm/ ℓ .

2.6 Data Acquisition and Analysis System

The outputs of the photomultiplier detectors were recorded with a Nova 800 minicomputer (Data General). This system can handle multiple channels (up to 32 channels) for direct on-line data acquisition and processing. For the experiment each channel was equipped with a signal conditioner, which has the functions of D.C. offset, differential amplification, and low-pass filtering.

In our experiment, we chose a cutoff frequency of 400 Hz. The filtered signals were digitized with an Analogic A/D converter at a sampling rate of 800 Hz for each channel. The signal was first recorded on an IOMEC magnetic disk and then stored on digital tapes for future processing. A set of computer programs is available for calculating statistics, such as mean and rms values, auto- and cross-correlations, skewness and flatness factors, and auto- and cross-spectra.

3. Experimental Results

In this section, we present the results of flow visualizations and concentration measurements made in a turbulent, round water jet and compare our results with those obtained by other investigators with other techniques.

3.1 Flow Visualization

The experimental setup described in section 2 was slightly modified to permit flow visualization of the turbulent water jet. With a glass rod 2 mm in diameter placed in front of the laser beam, the beam spreads into a sheet of light. We used the sheet of light to observe the interior structure of the jet. Figure 4 shows two cross-sectional views of the jet, one along and the other perpendicular to the jet axis. These two-dimensional cuts reveal the turbulent structure of the jet, such as the eddy sizes and the entrainment through the jet boundary. These results also provide useful information for designing quantitative measurements.

3.2 Mean and Root-Mean-Square Concentrations

Figures 5 and 6 are, respectively, the profiles of mean and root-mean-square (rms) concentrations measured at four stations, $x/D = 25, 50, 100$, and 160 downstream of the jet exit. The measurements were made with three photomultiplier detectors, separated by 0.3 and 0.7 cm. At each station, we made six to ten sets of measurements, with a total of about 20 or 30 data points. Figures 5 and 6 show that the maximum mean concentration occurs on the jet axis, while the maximum rms concentration occurs off the axis. These findings are consistent with those of similar measurements [2,11]. Figure 7 shows the decay of the mean concentration along the jet axis, along with two other sets of data measured in an air jet with heat and oil smoke as the tracers [2,11]. All three sets of data indicated an x^{-1} decay law. There was excellent agreement between our data and those of Becker, et al. [11], and the decay of the mean concentration along the jet axis can be approximated by

$$\frac{\bar{C}_{\max}}{\bar{C}_0} = 6.2 \left(\frac{x}{D}\right)^{-1} \quad \text{for } 25 < \frac{x}{D} < 160 . \quad (1)$$

Because of the relatively high sensitivity of the LDF technique, we were able to measure dye concentrations at a distance about four times greater than that reported by Becker, et al. [11]. The advantage becomes apparent when we examine the self-preserving state of the jet later in this section.

In view of the excellent agreement of the results, we compare the half-radius of the same two sets of data in figure 8. Although both sets of data show that the half-radius increases as x , the virtual origins were different. The negative virtual origins of our data may be attributed to the tripping nozzle, which is installed 2 cm upstream of the jet exit. Taking this into account, we can approximate our data by

$$\frac{R_{1/2}}{D} = 0.1 \left(\frac{x}{D} - 10\right) \quad \text{for } 25 < \frac{x}{D} < 100 . \quad (2)$$

The decay of the rms concentration along the jet axis of the same three sets of data are shown in figure 9. Our data can be approximated by

$$\frac{\sqrt{c_c^2}}{\bar{C}_0} = 3 \left(\frac{x}{D}\right)^{-1} \quad \text{for } 50 < \frac{x}{D} < 160 . \quad (3)$$

No agreement was observed between any two sets of the data. Notice that the tracers used in these experiments were altogether different. Corrsin and Uberoi [2] used heat that had a Prandtl number of 0.74 as a tracer. Becker, et al. [11] used oil smoke as the tracer. The oil smoke had an "equivalent" Schmidt number estimated to be 6×10^5 [4]. Here, we used Rhodamine-6G dye, which has a Schmidt number of the order of 10^3 as the tracer. The effect of the Schmidt number may be one of the major reasons accounting for the differences among the three sets of data. More research is required, however, to resolve these differences.

To examine whether the jet has reached the self-preserving state, we plotted, in figure 10, the ratio of $\sqrt{c_c^2}$ to \bar{C}_{\max} as a function of x/D .

The data of Becker, et al. [11] and that of Corrsin and Uberoi [2] are also shown in that figure. When the self-preserving state is reached, the value of $\sqrt{c^2/\bar{c}_{\max}}$ should reach an equilibrium value. The data of Becker, et al. [11] shows an equilibrium $\sqrt{\gamma_c^2/\bar{\gamma}_{\max}}$ at about 0.22, and the data of Corrsin and Uberoi [2] shows a value of about 0.18. Our data show that the self-preserving state is reached at $x/D \approx 60$ and that the equivalent value is about $\sqrt{c_c^2/\bar{c}_{\max}} = 0.44$. Again, we speculate that the effect of the Schmidt number could have a significant effect on the self-preserving state of the concentration field in a turbulent jet. More research is required to clarify this point.

3.3 Simultaneous Measurements Along the Jet Axis

Because the LDF technique is remote-sensing and does not interfere with the flow field, we can conduct simultaneous measurements at many positions along the jet axis. These measurements cannot be performed with a non-remote-sensing technique because the presence of the upstream sensor would interfere with the measurements of the downstream sensor. To demonstrate this capability, we conducted two series of experiments. In the first series, we carefully aligned two photomultipliers so they were focused, as close as possible, at the same measuring volume. Measurements were made at $x/D = 20, 50, \text{ and } 100$, along the centerline of the jet. In the second series, we measured the centerline concentrations simultaneously with three photomultipliers at $x/D = 30$ and at 50 . The measuring volumes, parallel to the jet axis, were separated by 0.3 and 0.7 cm.

In figure 11a, we show the auto- and cross-correlations of the concentration fluctuations measured with the two photomultipliers focused at the same measuring volume ($x/D = 50$). As shown, they are practically identical to each other. The coefficient of cross-correlation $\sqrt{c_1 c_2} / \sqrt{c_1^2} \sqrt{c_2^2}$ is as high as 0.998 . In addition, examination of the individual spectra shows that there is no noticeable difference. Up to 100 Hz, the data measured by the two photomultipliers show high coherence and little phase shift (figure 11b). Beyond 100 Hz, the coherence begins to decrease, and the phase shift increases, probably because of the imperfect matching of the measuring volumes.

The cross-correlations,

$$R_{12}(\tau) = \frac{1}{T \sqrt{c_1^2} \sqrt{c_2^2}} \int_0^T c_1(t) c_2(t - \tau) dt, \quad (4)$$

with three photomultipliers focused at measuring volumes separated along the jet axis by 0.3 and 0.7 cm, are shown in figure 12. Here the upstream measuring volume was at $x/D = 30$. In figure 12, we see that, as the separation between the measuring volumes increases, the maximum $R_{12}(\tau)$ decreases, and the time at which it occurs increases. The envelope of the cross-correlations defines the space-time correlation, which is represented by the heavy line in figure 12. Furthermore, from the spatial separation Δx between the sampling volumes and from the corresponding time separation $\Delta \tau$ between the times at which the maximum $R_{12}(\tau)$ occurs, we can estimate the convective velocity $\bar{U}_c = \Delta x / \Delta \tau$. This convective velocity should be very close to the mean velocity of the jet, except in the region near the edge of the jet. In figure 13 we plot the convective velocity, normalized by the exit velocity, as a function of x/D . Also plotted are the results measured in an air jet [2] and in a water jet [12]. It should be noted

that the convective velocity is evaluated indirectly from the cross-correlations of the concentration fluctuations, and, yet, there is excellent agreement among the three sets of data.

3.4 Spectra

Spectra of concentration fluctuations were calculated by transforming the auto-correlations with an FFT algorithm [13]. There were a total of 2^{13} points, with a maximum sampling rate of $\Delta t = 0.0013$ second. The statistical error was about 30 percent.

According to Batchelor [14], the spectrum of concentration fluctuations in the viscous-convective subrange follows

$$E_Y(k) = A \left(\frac{\nu}{\epsilon} \right)^{1/2} \frac{\epsilon_Y}{k} \exp \left(-A \frac{k^2}{k_c^2} \right) \quad (5)$$

for a scalar quantity of large Schmidt number, where $k_c = (\epsilon/\nu\kappa^2)^{1/4}$ and ϵ is the dissipation rate of the turbulent energy, ν is the kinematic viscosity, κ is the diffusivity, and ϵ_Y is the dissipation rate of the concentration fluctuations. According to Batchelor [14], the constant A has a value of 2, but experimental data show that the value of A varies from 0.72 to 13.2 [15]. Since our measurement was made for a dye solution with a large Schmidt number ($\sim 10^3$), we decided to test the theory Batchelor expressed in eq. (5).

In figure 14, we plot the spectra measured at $x/D = 20, 50$, and 100 . The frequency is given in Hz, and it can be related to the wave number by Taylor's hypothesis $k = 2\pi f/\bar{U}$. For the station at $x/D = 50$, we show two spectra calculated from two ensembles to indicate the statistical error. In this figure, we see that, in the low-frequency range, all three spectra contain a f^{-1} region over about one decade of frequency. This range tends to increase with the distance. In figure 15 we replot the spectra presented in figure 14 as $\log fS(f)$ versus f^2 . For the f^{-1} range, the data should present a constant of $fS(f)$. Also, if equation (5) is valid, the plot should show a linear region. In figure 15, we see that linear regions occur for all three spectra. For each spectrum, we indicate a cutoff frequency f_o , which is estimated by $f_o = k_o \bar{U}/2\pi$, where k_o is the cutoff wave number corresponding to the dimension of the measuring volume (~ 1 mm) and has a value of about 6.28 mm^{-1} and the convective velocity \bar{U} is estimated from the results shown in figure 13. The spectral measurement beyond this cutoff frequency will therefore be invalid. These results support the theory of Batchelor expressed in eq. (5) although we cannot estimate the value of the constant A for lack of information concerning the measurement of the dissipation rate ϵ .

4. Concluding Remarks

In this paper, we have successfully demonstrated the usefulness of the LDF technique for measuring dye concentrations in a turbulent water jet. The present system, however, is by no means optimized; there is still considerable room for improvement. For example, by suitably collimating the laser beam and using a smaller diameter pinhole, the measuring volume could be reduced to as small as 0.1 mm^3 with some sacrifice of the intensity of the fluorescence signals. The reduction of the fluorescence intensity

could be compensated by optimizing the optical characteristics of the system. Perhaps one optimization would be the use of the 514.5-nm line instead of the 488-nm line of the laser, if we could find a filter that would efficiently block the laser light from the fluorescent light.

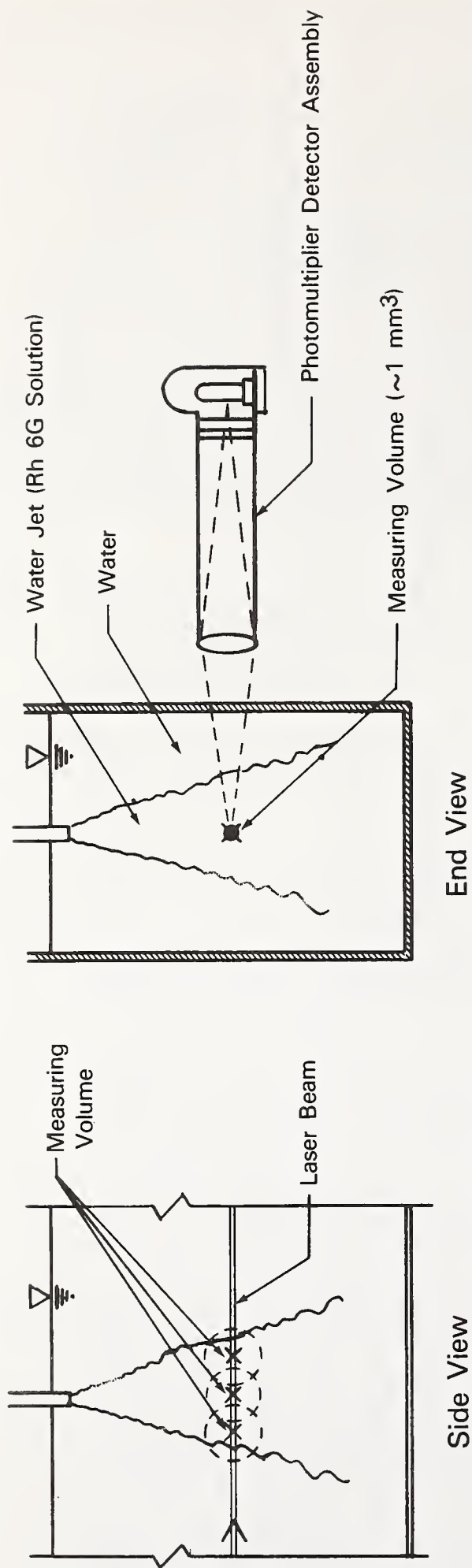
By comparing our results with those obtained from heat and oil-smoke transport [2,11], we see various degrees of agreement. The centerline mean concentration, which varies as x^{-1} , agrees excellently with that of the oil-smoke transport [11] and has a higher value than that of the heat transport [2]. The centerline root-mean-square concentration, which also varies as x^{-1} , is, however, consistently higher than those of the other two [2,11]. The differences could likely indicate the significance of the Schmidt-number effect.

We also show that, with the LDF technique, we can make simultaneous measurements along the jet axis or at the same point. This result demonstrates the system's remote-sensing capability. Finally, our spectral measurements validate Batchelor's theory on the spectrum of concentration fluctuations for a scalar quantity of large Schmidt number.

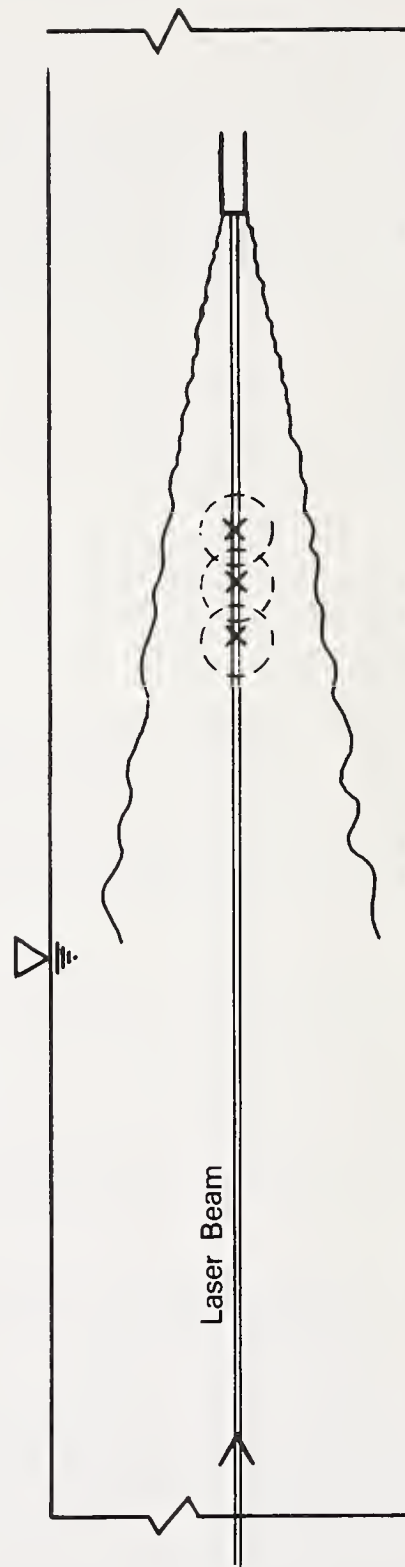
5. References

- [1] Robben, F.A., Lin, J. T., Delisi, D. P., and Liu, H. T., Feasibility study of a dye-fluorescence technique for measuring concentrations in fluids, Flow Research Note No. 91, Flow Research Company, Kent, Washington (1976).
- [2] Corrsin, S. and Uberoi, M. S., Further experiments in the flow and heat transfer in a heated air jet, Natl. Advisory Comm. Aeronaut. Tech. Notes No. 998 (1950).
- [3] Kiser, K. M., Material and momentum transport in axisymmetric turbulent jet of water, AI.Ch.E. Journal 9, 386 (1963).
- [4] Rosensweig, R. E., Hottel, H. C., and Williams, G. C., Smoke-scattered light measurements of turbulent concentration fluctuations, Ch. Eng. Sci. 15, 111 (1961).
- [5] Becker, H. A., Hottel, H. C., and Williams, G. C., On the light-scatter technique for the study of turbulence and mixing, J. Fluid Mech. 30, part 2, 259 (1967).
- [6] Liu, H. T. and Karaki, S., An optical system for measurement of mean and fluctuating concentrations in a turbulent air stream, J. of Physics E: Scientific Instruments 5, 1165 (1972).
- [7] Yang, B. T. and Meroney, R. N., A portable laser light-scattering probe for turbulent diffusion studies, Rev. Sci. Instrum. 45, no. 2, 210 (1974).
- [8] Gad-el-Hak, M., Morton, J. B., and Humphris, R. R., An investigation of turbulent diffusion, Tech. Rept. No. ESS-3837-102-75, Univ. of Virginia (1975).
- [9] Lee, J. and Brodkey, R. S., Light probe for the measurements of turbulent concentration fluctuations, Rev. Sci. Instrum. 34, 1086 (1963).

- [10] Nye, J. O. and Brodkey, R. S., The scalar spectrum in the viscous-convective subrange, J. Fluid Mech. 29, 151 (1967).
- [11] Becker, H. A., Hottel, H. C., and Williams, G. C., The nozzle-fluid concentrations field of the round turbulent free jet, J. Fluid Mech. 30, 285 (1967).
- [12] Albertson, M. L., Dai, Y. B., Jensen, R. A., and Hunter Rouse, M., Diffusion of submerged jets, Trans. ASCE 115, 639 (1950).
- [13] Bendat, J. S. and Piersol, A. G., Random Data (John Wiley & Sons, Inc., New York, 1971).
- [14] Batchelor, G. K., Small-scale variations of convected quantities like temperature in turbulent fluid, J. Fluid Mech. 5, 113 (1959).
- [15] Hinze, J. O., Turbulence - An Introduction to Its Mechanism and Theory (second edition, McGraw-Hill Book Co., Inc., New York, 1975).

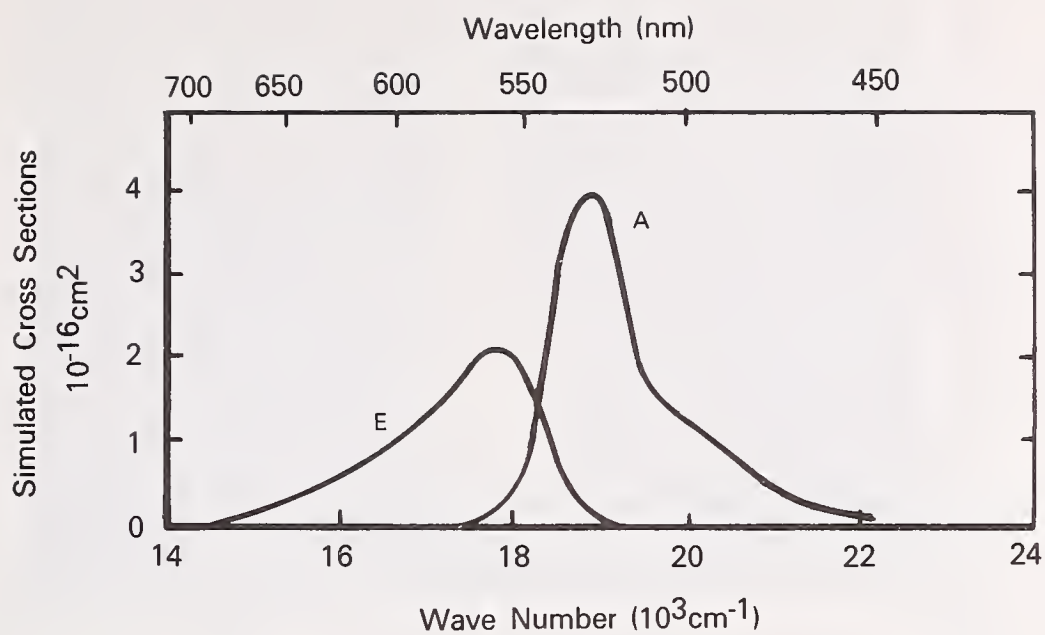


(a) Measurement Perpendicular to Jet Axis

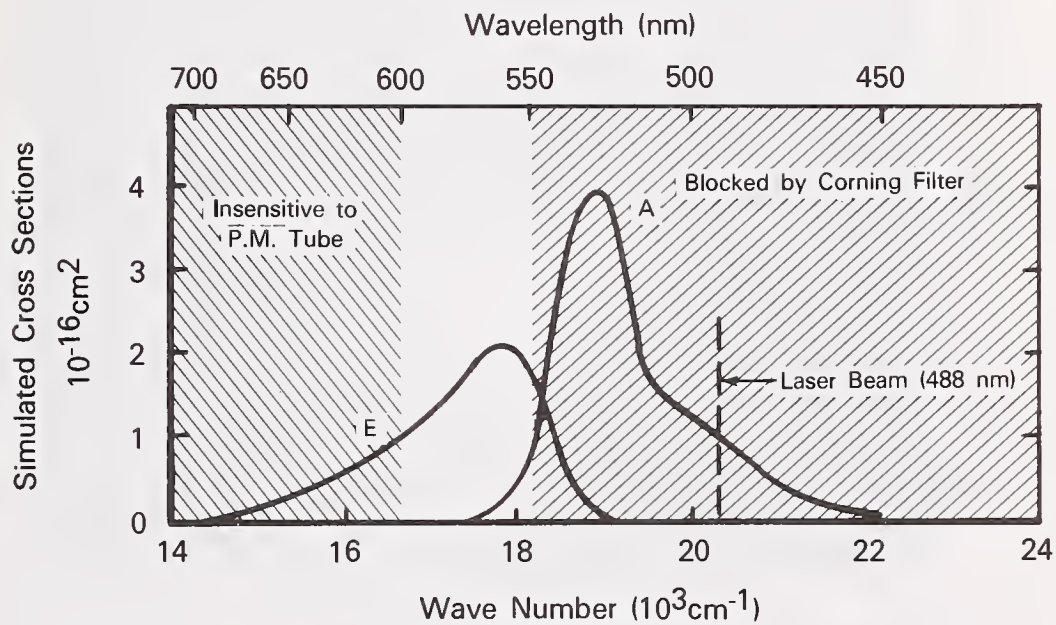


(b) Measurement Parallel to Jet Axis

Fig. 1 Schematic of the Experimental Setup



(a) Absorption (A) and Stimulated Emission (E) for Rhodamine 6G Dye (Eastman Number 10724).



(b) Effective Window for the Receiving Optics

Fig. 2 Optical Characteristics of the Laser Dye-Fluorescence System

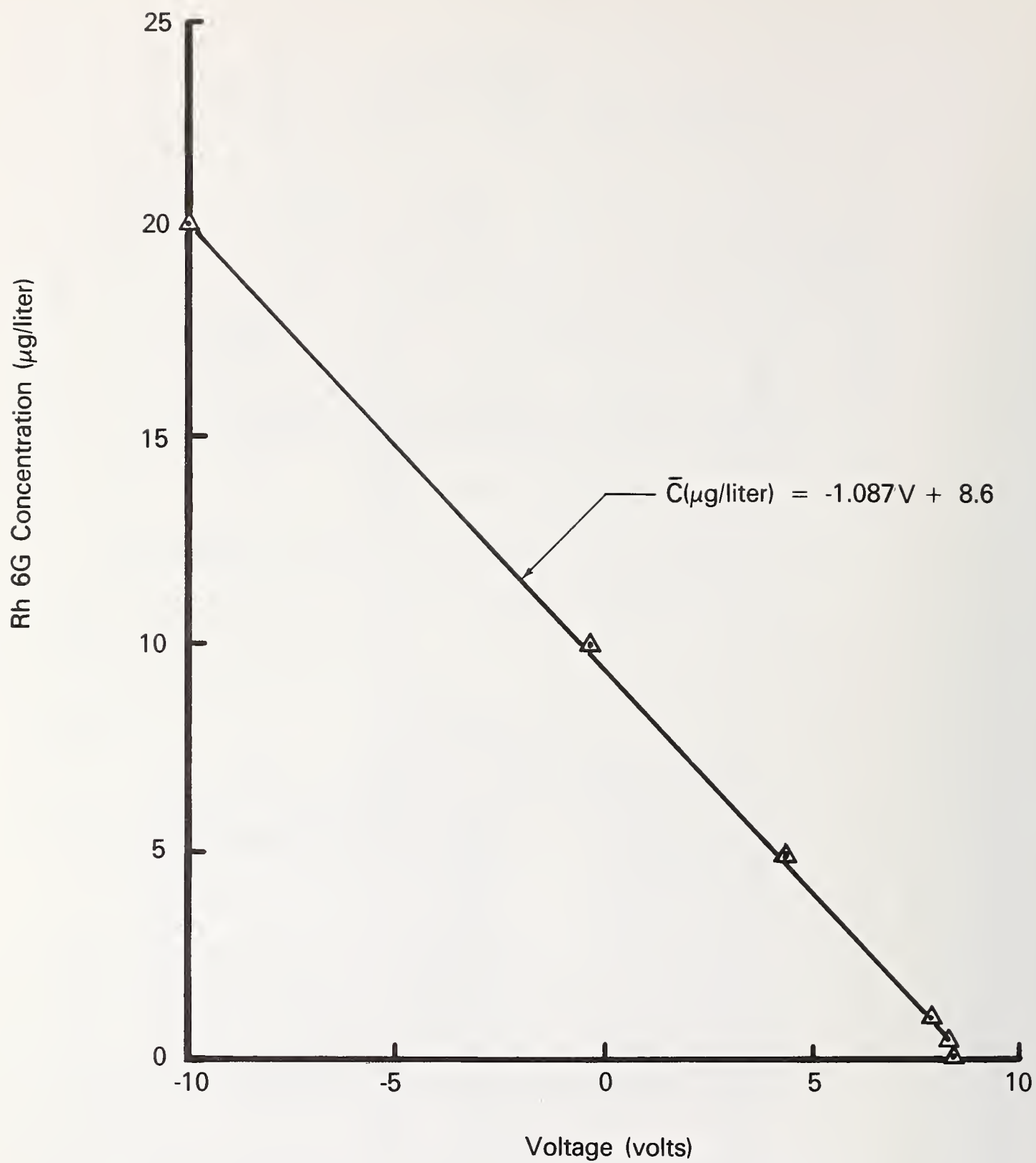


Fig. 3 A Calibration of LDF System



(a) Cross-Sectional View Along the Jet Axis



(b) Cross-Sectional View Perpendicular to the Jet Axis

Fig. 4 Flow Visualization of the Turbulent Water Jet With a Sheet of Laser Light

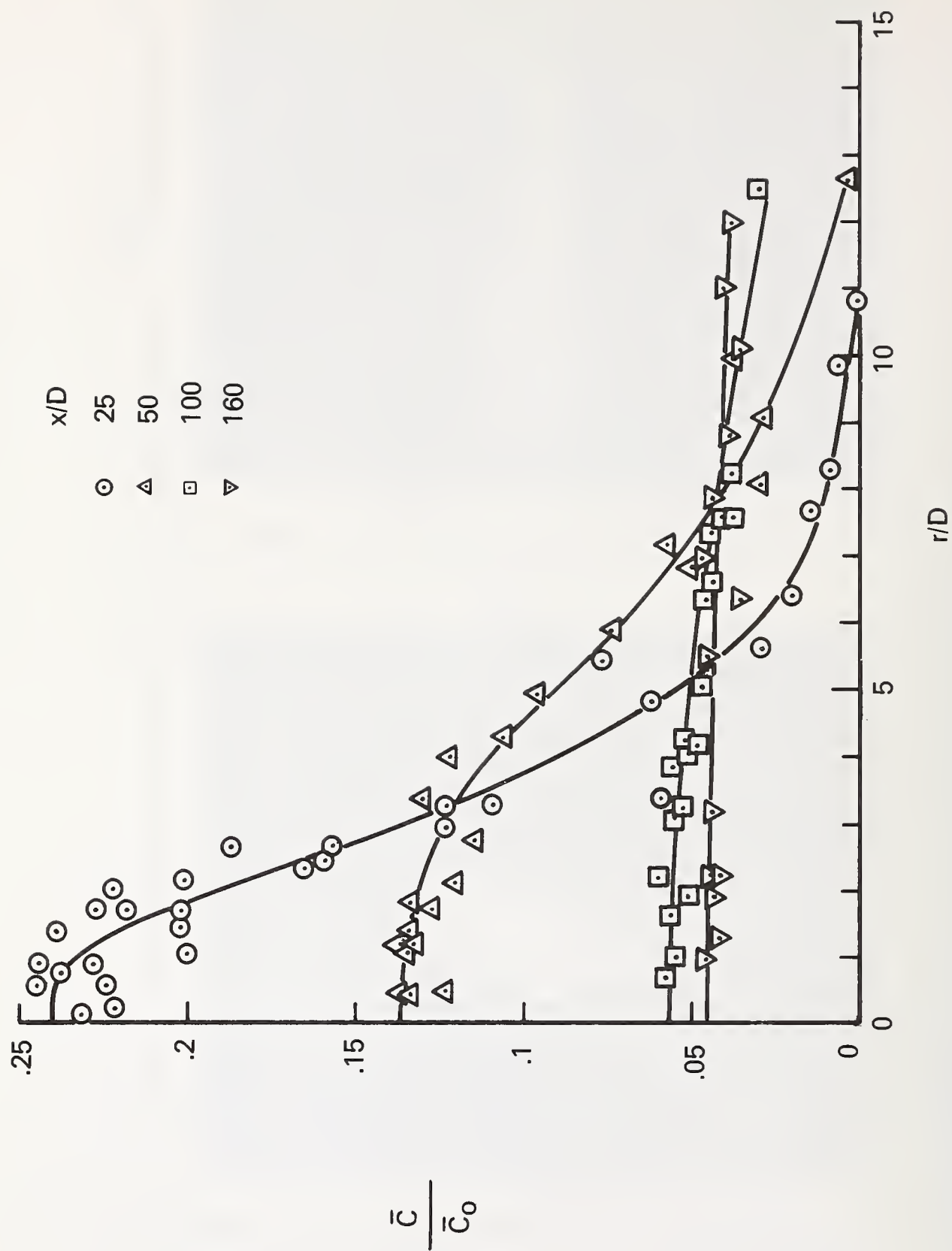


Fig. 5 Profiles of Mean Concentrations

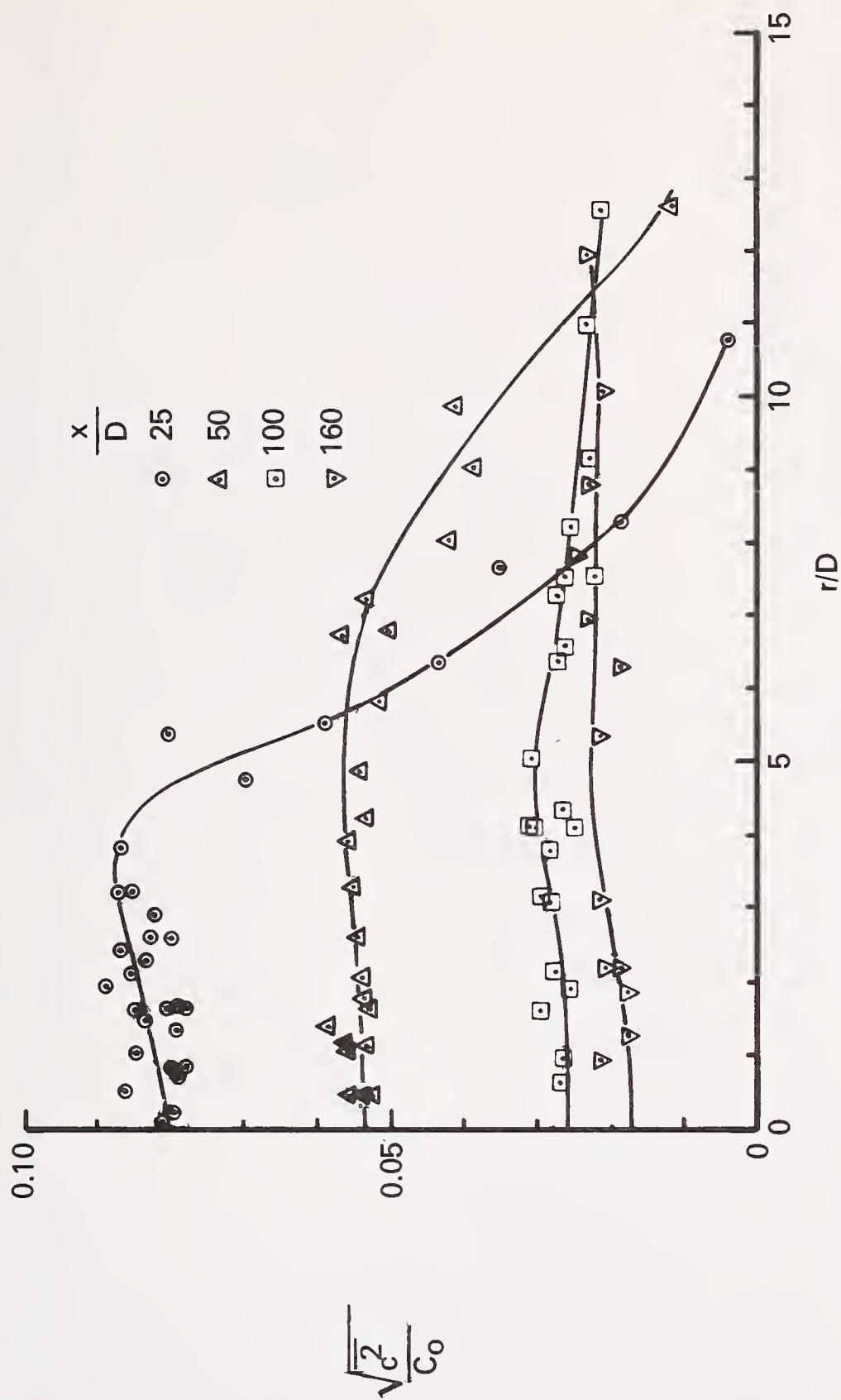


Fig. 6 Profiles of Root-Mean-Square Concentrations

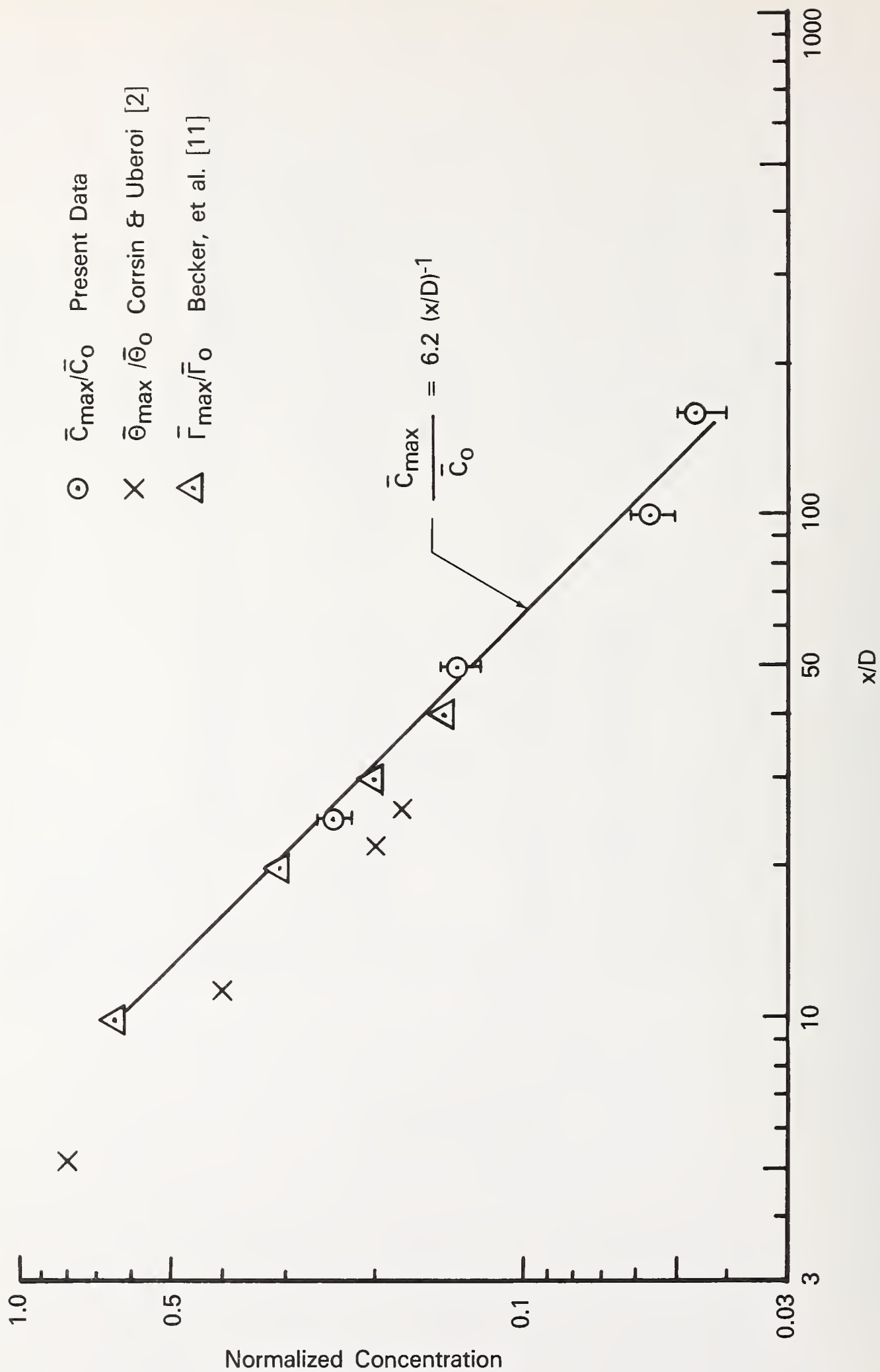


Fig. 7 On-Axis Mean Concentration as a Function of Distance Downstream

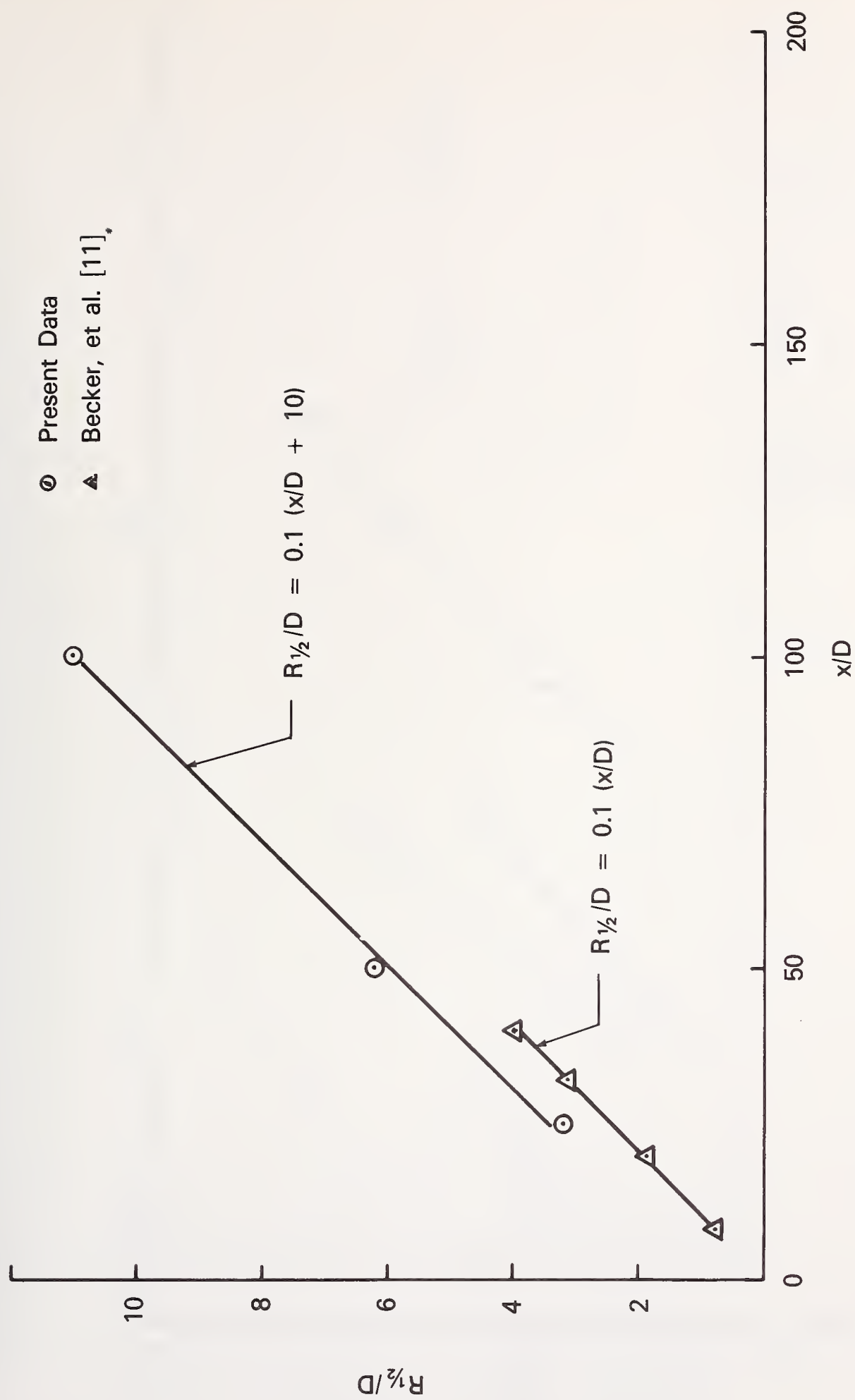


Fig. 8 Half-Radii of Turbulent Jets as a Function of Distance Downstream

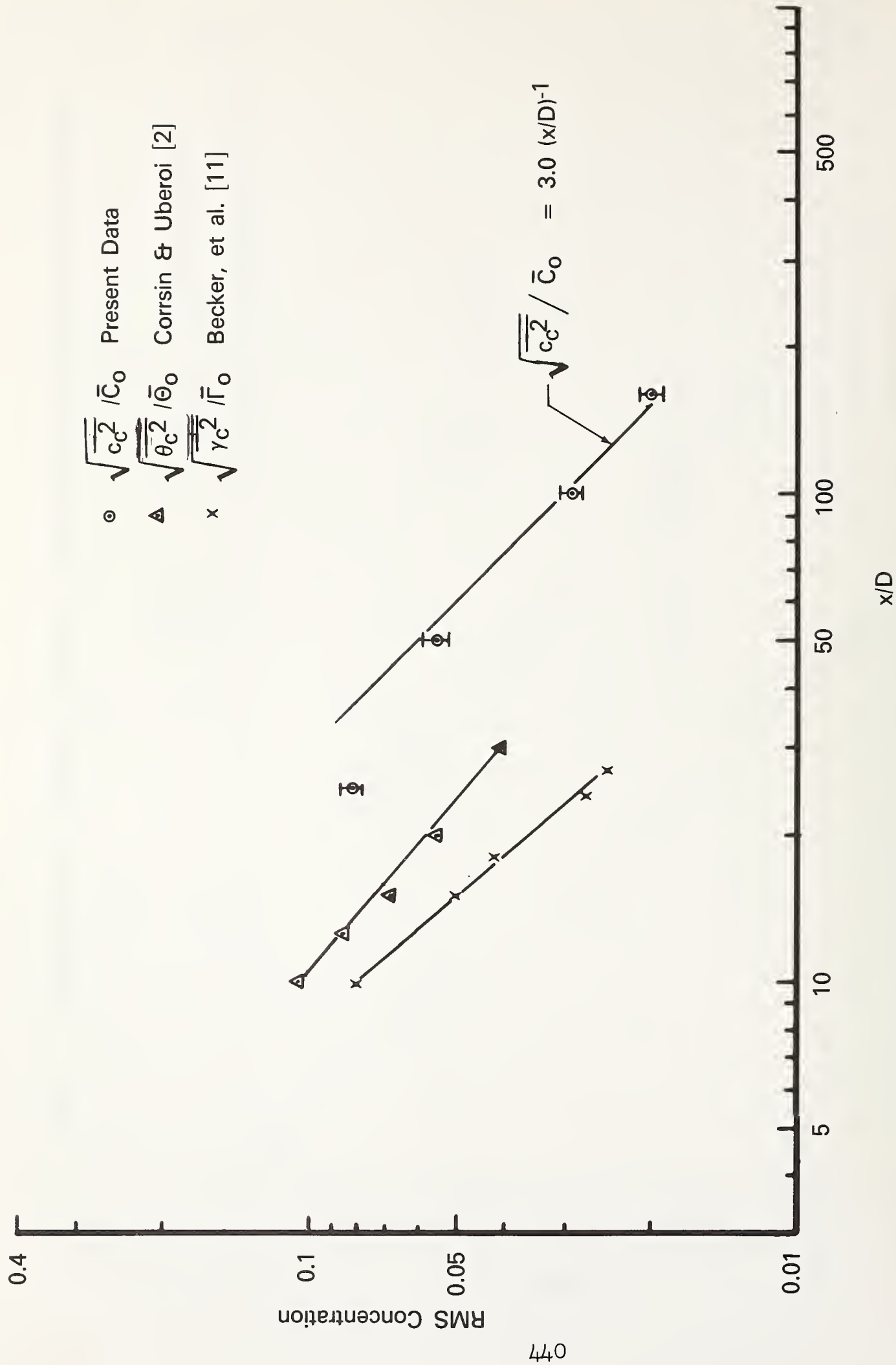


Fig. 9 On-Axis Root-Mean-Square Concentration as a Function of Distance Downstream

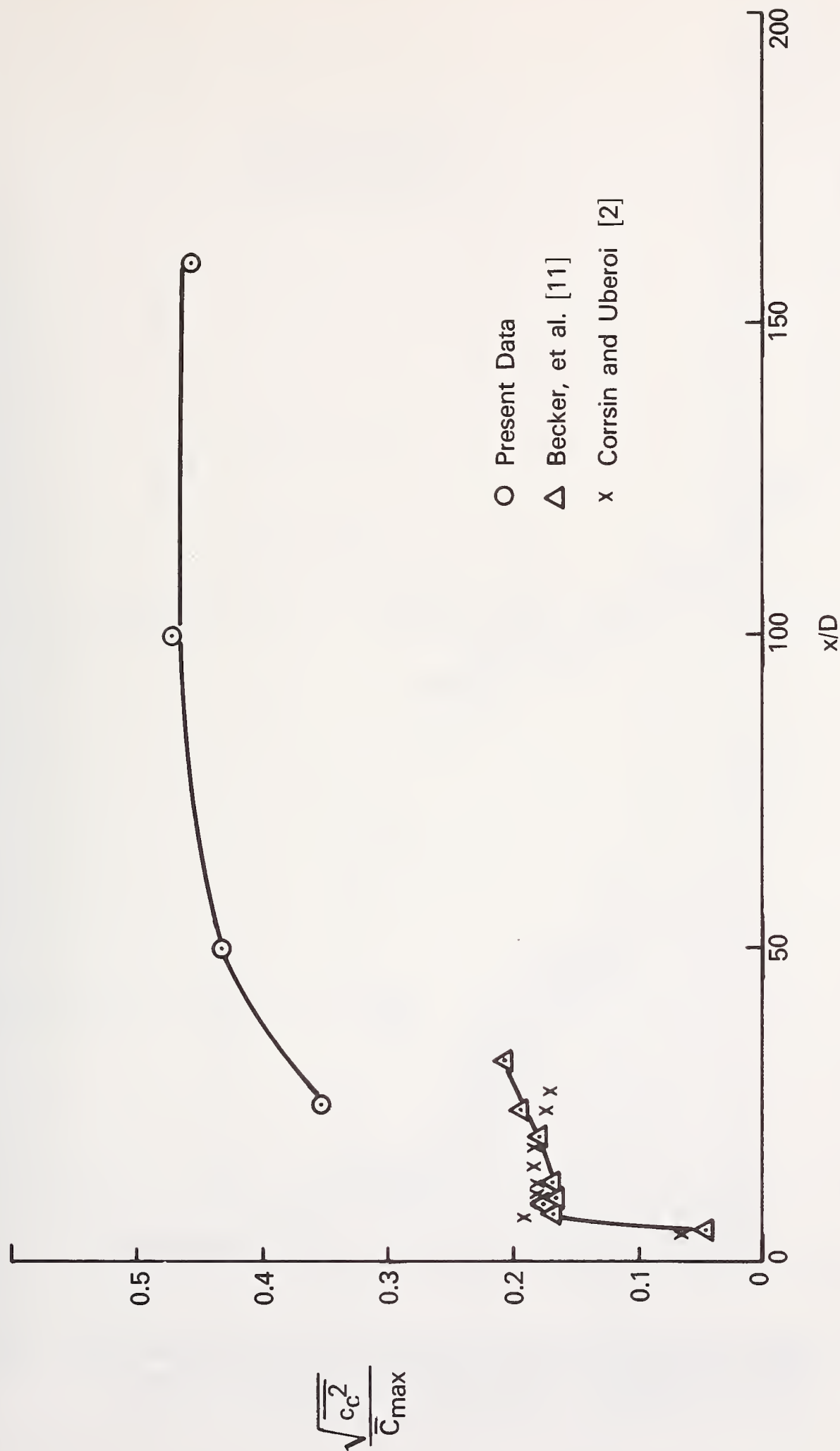
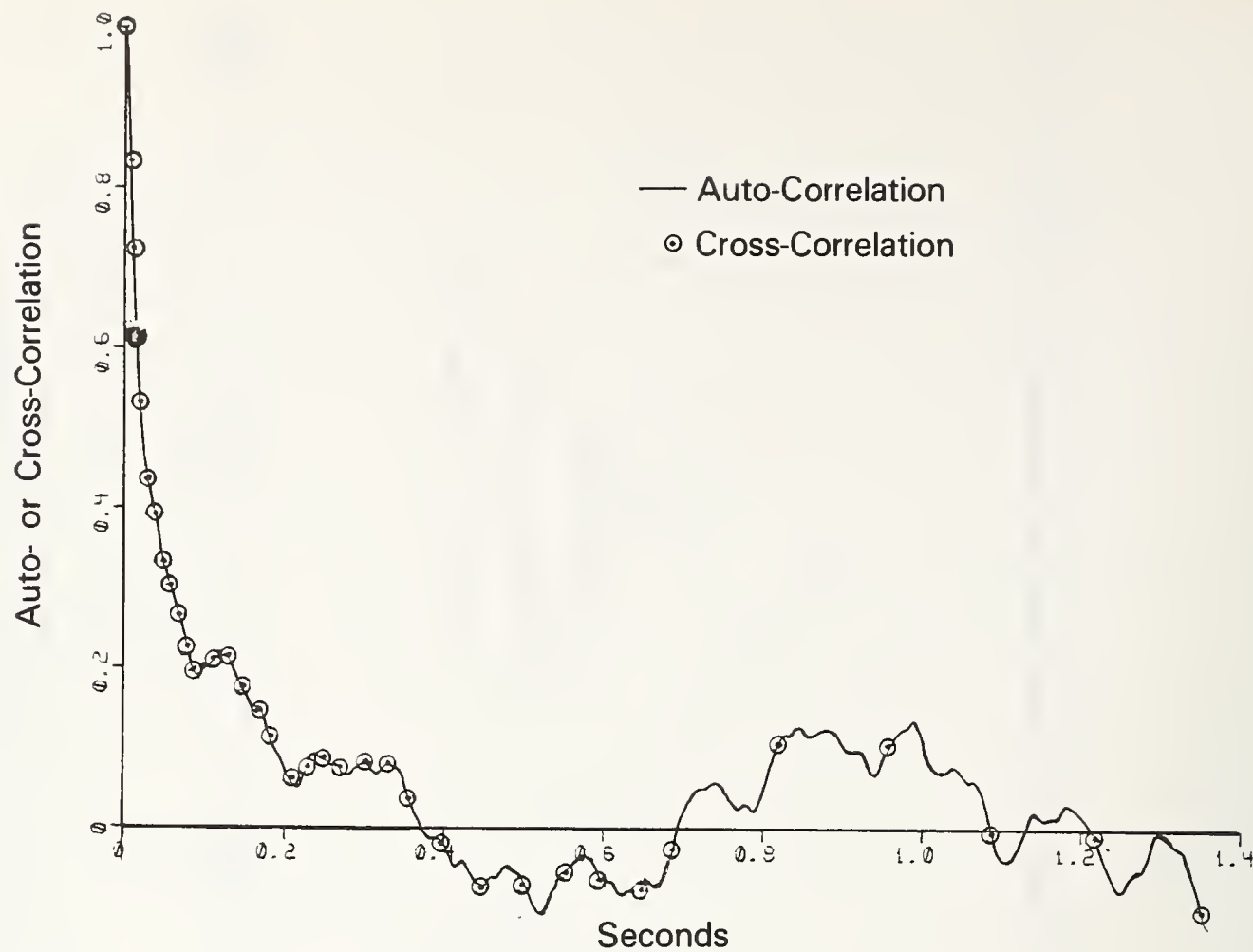
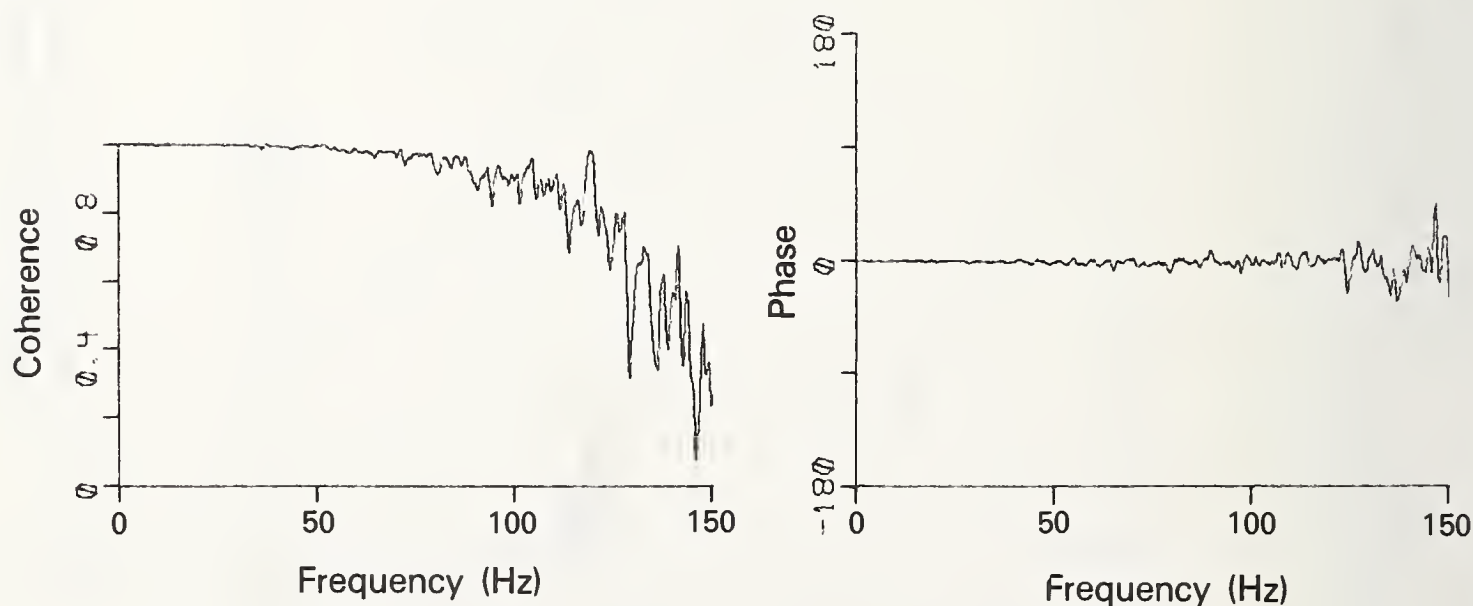


Fig. 10 On-Axis Root-Mean-Square Concentration Normalized by the Local Mean Concentration as a Function of Distance Downstream



(a)



(b)

Fig. 11 Measurements of Concentration Fluctuations With Two Photomultipliers Focused at the Same Volume

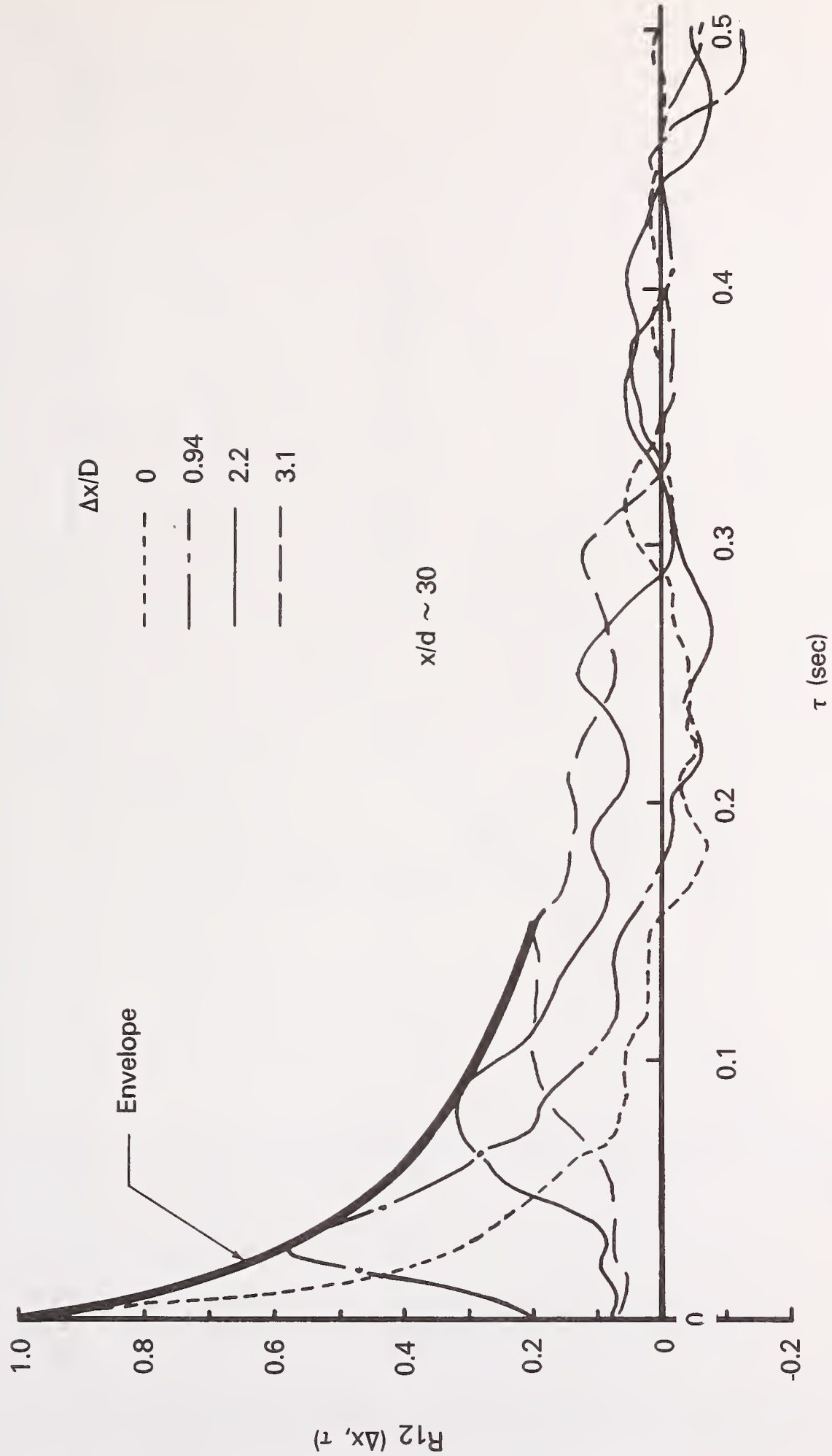


Fig. 12 Cross-Correlations of Concentration Fluctuations

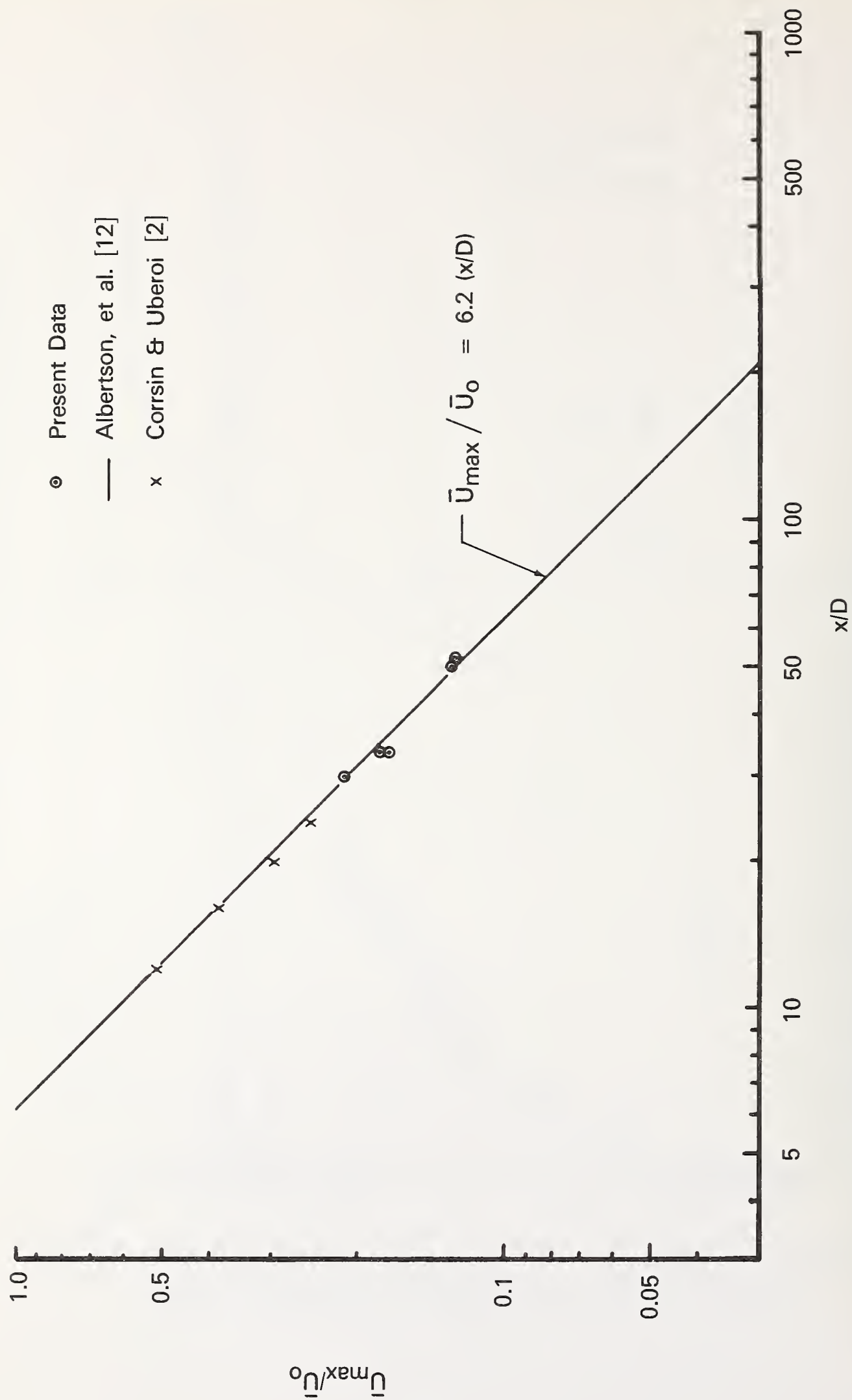


Fig. 13 Comparison of the Convective Velocity With the Mean Velocity of Air and Water Jets

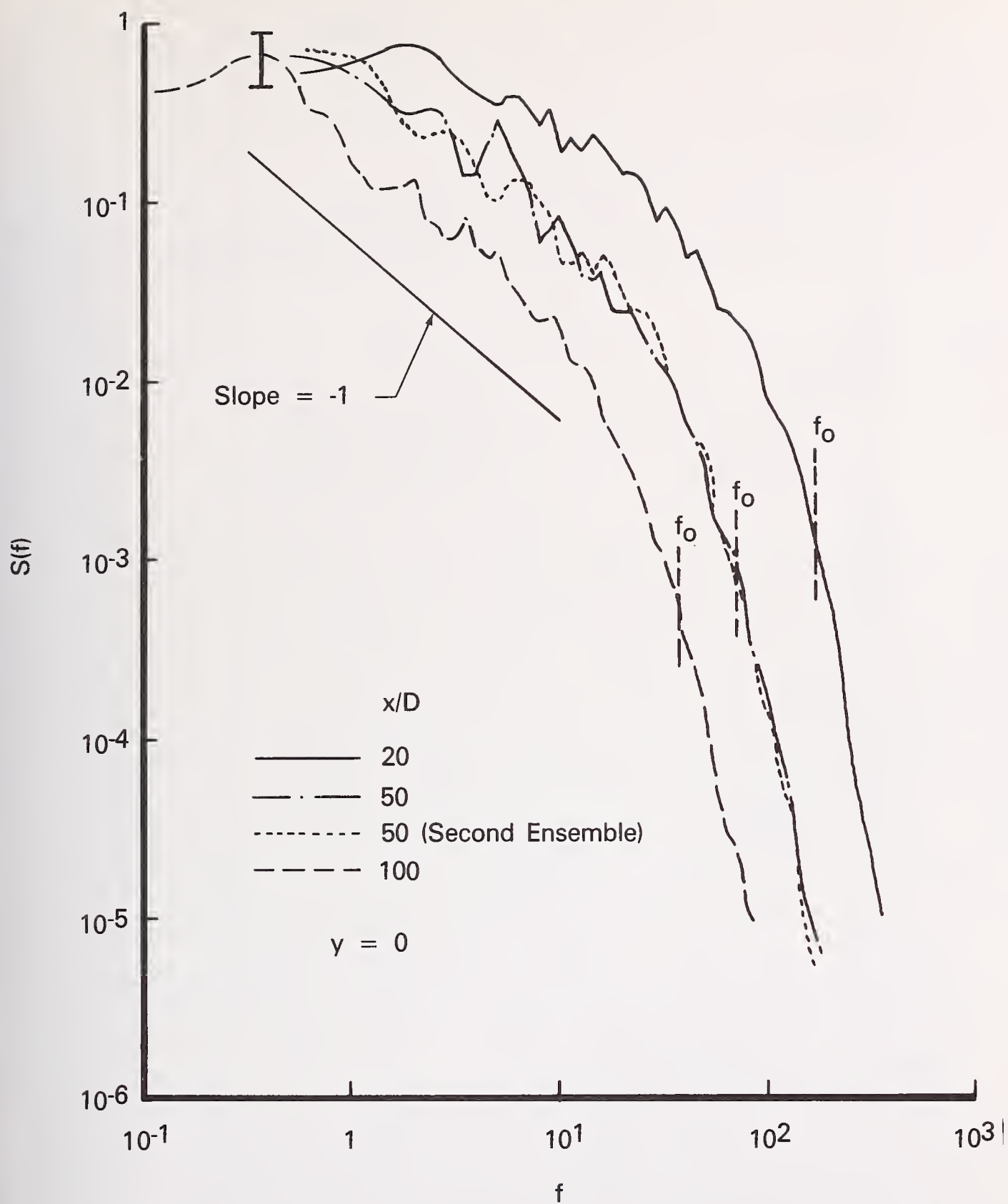


Fig. 14 Spectra of Concentration Fluctuations

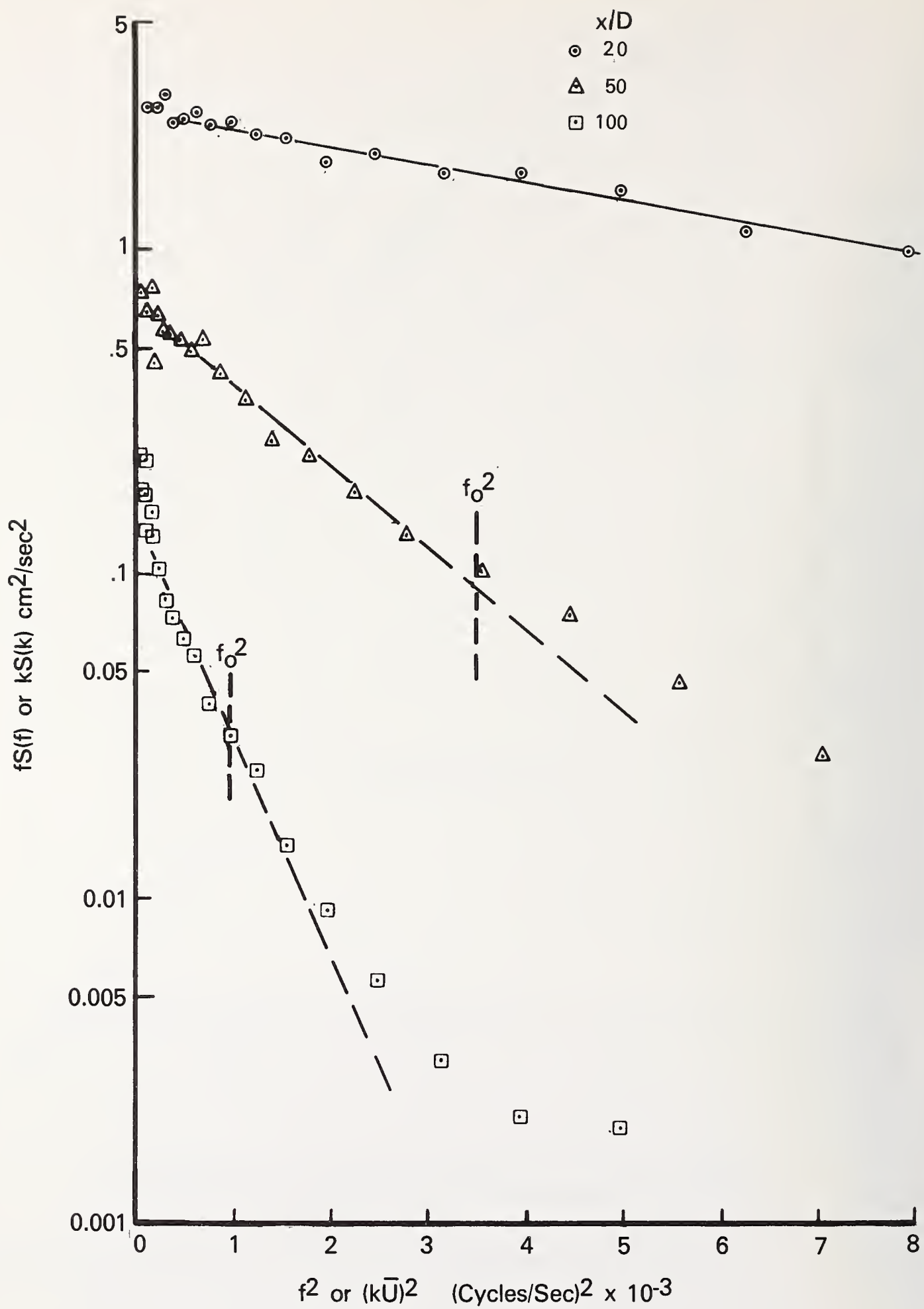


Fig. 15 Region of $E(k) \sim k^{-1}e^{-2(k/kc)^2}$

THE APPLICATION OF MONTE CARLO AND BAYESIAN PROBABILITY TECHNIQUES TO FLOW PREDICTION AND DETERMINATION

Dr. Frank J. Berte'

Reactor Thermal Design and Analysis

COMBUSTION ENGINEERING POWER SYSTEMS, INC.

Windsor, Connecticut

06095

The prediction of flow rate through a flow network, which is in the design stage, requires a detailed analysis of component resistance and pump performance uncertainties. In order to evaluate the predicted best estimate flow rate and its associated probability distribution, a combination of the Monte Carlo and Stratified Sampling techniques can be utilized. The use of these techniques permits the required results to be obtained even when non-gaussian probability distributions are associated with network flow resistances and/or pump performance parameters. The calculations necessary to produce the best estimate predicted flow rate and its associated probability distribution, are performed using a computer code, which embodies the Monte Carlo and Stratified Sampling techniques. After the flow network has been constructed, and flow measurements have been made, the problem becomes one of determining the best estimate true flow rate and its associated probability distribution. Ordinarily if a number of different techniques were available for measuring the flow in the network, the one with the smallest uncertainty would be utilized to determine the true flow rate. An alternate technique exists whereby the predicted flow as well as the flows measured by the available techniques are combined to produce one best estimate flow rate and its associated probability distribution. The statistical technique which can be used to accomplish this combination is Bayes' rule. This combination of predicted and measured flow rates and their associated uncertainties is performed by a computer code which embodies Bayes' Rule as well as the Monte Carlo and Stratified Sampling techniques.

Key Words: Flow prediction, flow determination, Monte Carlo; Stratified Sampling; Bayes' Rule; statistics

1. Summary

The evaluation of both flow prediction and flow determination uncertainties require the generation and manipulation of probability distributions. The generation of these probability distributions has been accomplished by using a combination of Monte Carlo and Stratified Sampling techniques[2][3]¹. A detailed discussion of the methodology employed to generate these probability distributions is presented in section 2. The use of the probability distribution generation methodology in the calculation of predicted flow rate and its associated probability distribution is presented in section 3. This section also contains an example of the application of the discussed analysis techniques to a sample problem. In section 4, the analysis technique for the combination of flow prediction and measurement values according to Bayes' Rule is discussed, again a sample problem is presented.

2. Probability Distribution Generation

Before probability distribution generation is discussed per se, a brief discussion of how these distributions are used is in order. Let us assume that we are dealing with a problem in flow prediction. The flow prediction code input is made up of various parameters related to the flow network characteristics. Each of these parameters is assumed to have a known probability distribution associated with it. In order to utilize the Monte Carlo technique, a set of data for each of these parameters must be generated, such that the set conforms to the input specification of its probability distribution. Once the sets have been generated, (we will discuss this generation in detail shortly) one value for each parameter is chosen at random, for the respective data set for that parameter, and put into the functional relationship equations relating these input parameters to the predicted flow rate. This process is repeated "N" times, where "N" is the number of data points in each data set, and "N" values of the resulting predicted flow rate are generated. From this set of predicted flow rates the probability histogram for the predicted flow rate is generated.

It is obvious that the larger the number "N" the more computer time is used by the code performing the calculation. The objective of the probability distribution generation scheme presented here is to minimize "N", while still achieving the most accurate and precise results for the predicted flow rate probability distribution.

The Monte Carlo-Stratified Sampling technique employed in both the flow prediction and determination methodology requires the division of a probability distribution into a finite number of intervals. If one wishes to generate a probability distribution for a variable X, that is, if one wants a set of X_i values having a specified probability distribution, the following steps would be required. It is assumed

¹Figures in brackets refer to the numbered references at the end of this paper.

that the values of X_i are bounded by a lower limit "a", and an upper limit "b". First, the range from "a" to "b" is divided into a finite number of intervals of equal width.* The probability that a value of X falls within each interval is then used to find the number of X values required in the interval, given a fixed total number of X values required in the complete set of X values. The interval probabilities can be supplied from analytical algorithms for standard probability distributions, such as the gaussian, or they can be supplied specifically, on an interval by interval basis, in the code input. Non-symmetrical or discontinuous probability distributions can thus be readily accommodated. However, most problems encountered have only required a gaussian or a uniform probability distribution for code input variables.

For gaussian probability distributions the code utilizes the following analytical expression for cumulative probability as a function of the normal deviate [5].

$$P(x) = 1 - 1/2 (1 + d_1 x + d_2 x^2 + d_3 x^3 + d_4 x^4 + d_5 x^5 + d_6 x^6)^{-16} + \epsilon(x) \quad (1)$$

where $\epsilon(x)$ is the error associated with the result, and is bounded by $|\epsilon(x)| \leq 1.5 \times 10^{-7}$

$$d_1 = 0.04986 \quad 73470$$

$$d_2 = 0.02114 \quad 10061$$

$$d_3 = 0.00327 \quad 76263$$

$$d_4 = 0.00003 \quad 80036$$

$$d_5 = 0.00004 \quad 88906$$

$$d_6 = 0.00000 \quad 53830$$

x is the normal deviate, or

$x = \{\text{deviation/standard deviation of the gaussian distribution}\}$

Once the number of data points in each interval has been determined for the variable of interest, a pseudo random number generation scheme [1] incorporated into the computer software is utilized to generate the required number of data points in each interval. This process is repeated until all intervals are filled. The data set for the variable X now has the properties of the input probability distribution specified. Only one more step remains, that is to randomize the order in which the data points appear in line matrix; Data

*Note, in the generation of data sets having gaussian distributions, which theoretically should span the region from minus to plus infinity, it has been found, for our purposes, that a range from minus to plus five (5) standard deviations about the mean value was satisfactory.

Point 1, Data Point 2....Data Point "N". This is necessary because the code generates the data for each interval starting at the lowest and working to the highest numbered one. Therefore, although the data is random within each interval, on an interval to interval basis it is not. After the randomization of the whole data set has been completed, one has a set of randomly ordered X_i data with the statistical properties specified in the code input.

The scheme for generating a set of data with the required statistical properties has been presented. The question now becomes, how do you decide on the optimum number of intervals and data points to generate a set of data whose statistical properties are in good correspondence with the specified input properties, and yet assure the minimum use of computer time to accomplish the task? One needs an optimization procedure for determining the number of intervals, and number of data points to be used. This procedure has been devised for gaussian distributions and is based on the optimization parameter given in equation (2).

$$\begin{array}{lcl} \text{Optimization} & & \text{standard deviations} \\ \text{Parameter} & = & \text{of code generated data set} \\ \text{for Gaussians} & & \frac{\text{specified input}}{\text{standard deviation}} \quad (2) \end{array}$$

The object then becomes to achieve an optimization parameter with a value close to unity, while still minimizing the number of data points and hence computer running time used.

A number of test cases were run to determine the number of intervals and the number of data points required to achieve an optimization parameter approximately equal to unity. Two sets of test cases were run, first the number of intervals was held constant and the number of data points was varied, and second, the number of data points was held constant and the number of intervals was varied. For each of these cases the optimization parameter was plotted vs. the varied parameter. These two plots are shown in Figure 1 and 2, respectively. Figure 3 illustrates the combination of the results from Figures 1 and 2, which is an optimization parameter surface. A number of deductions can be drawn from these figures, they are as follows.

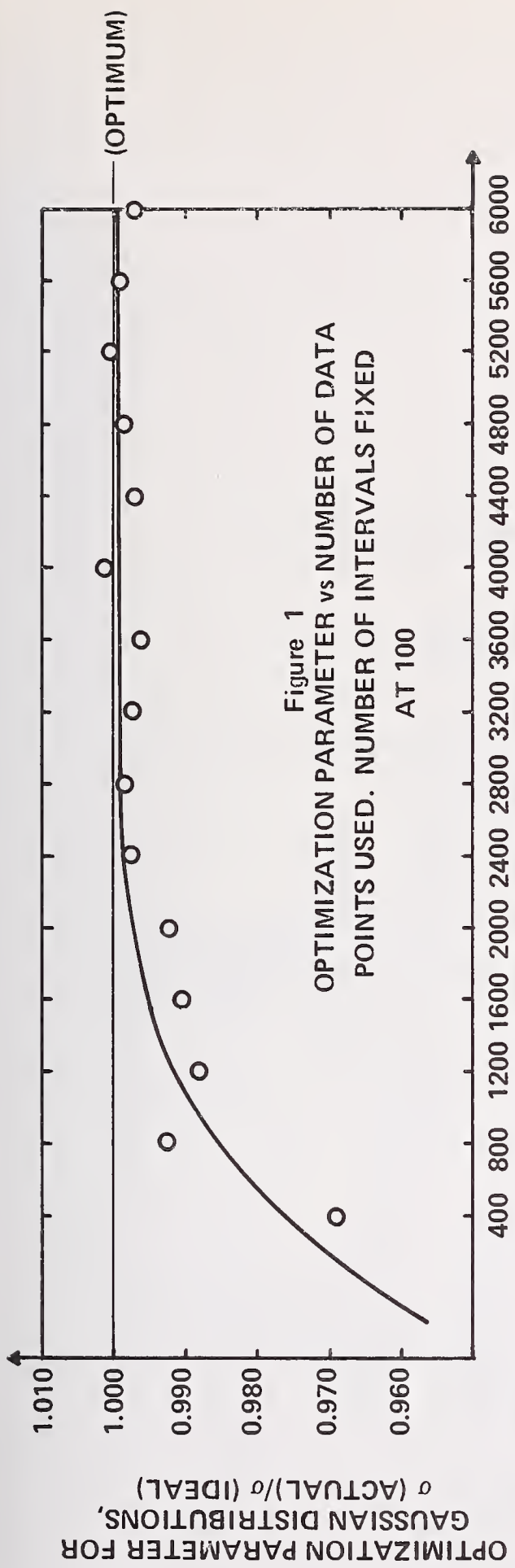
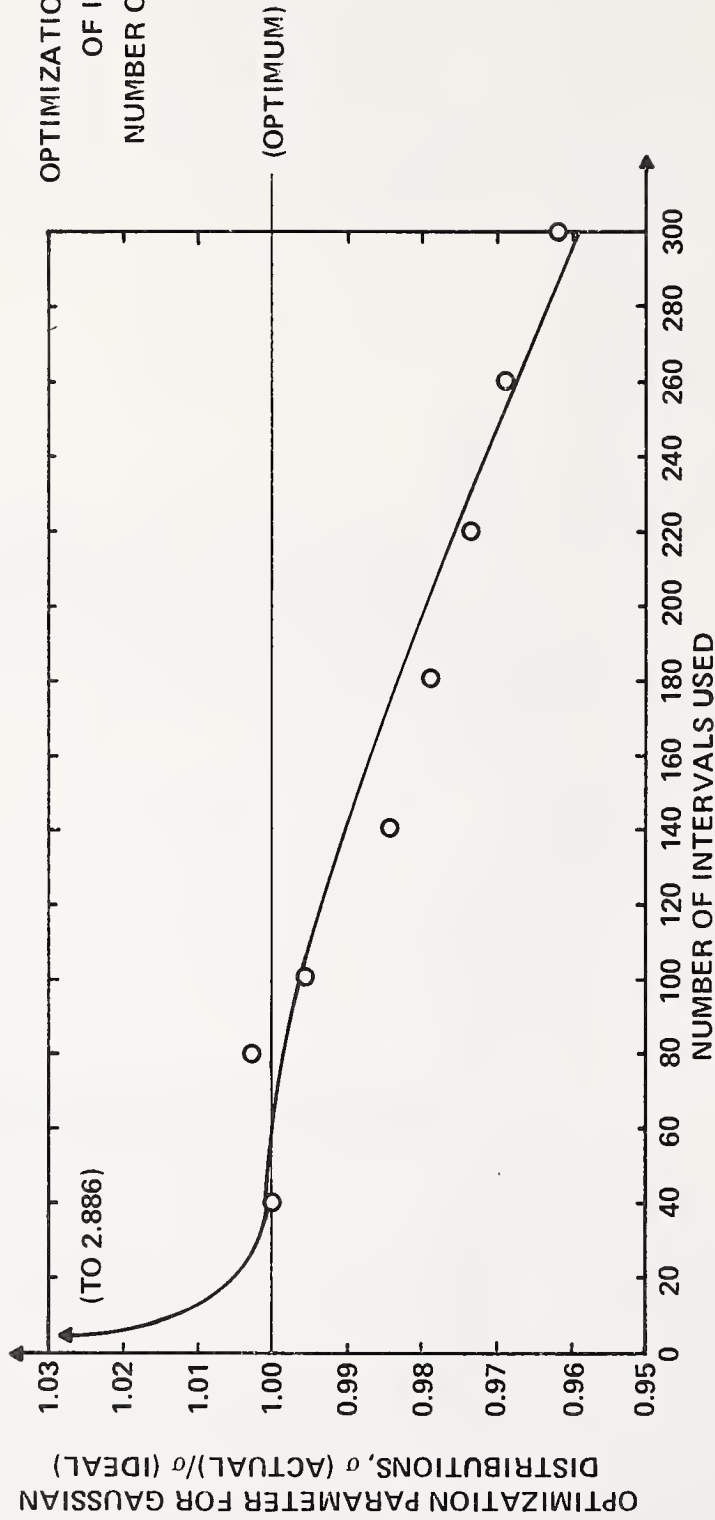


Figure 1
OPTIMIZATION PARAMETER vs NUMBER OF DATA
POINTS USED. NUMBER OF INTERVALS FIXED
AT 100

TABULATED VALUES OF PLOTTED DATA	
NUMBER OF DATA POINTS USED	σ (ACTUAL)/ σ (IDEAL)
400	0.969438
800	0.993760
1200	0.988840
1600	0.990141
2000	0.992007
2400	0.997768
2800	0.998012
3200	0.997014
3600	0.995819
4000	1.001213
4400	0.996859
4800	0.998038
5200	0.999340
5600	0.998608
6000	0.996840

Figure 2
OPTIMIZATION PARAMETER vs NUMBER
OF INTERVALS USED
NUMBER OF DATA POINTS FIXED
AT 800

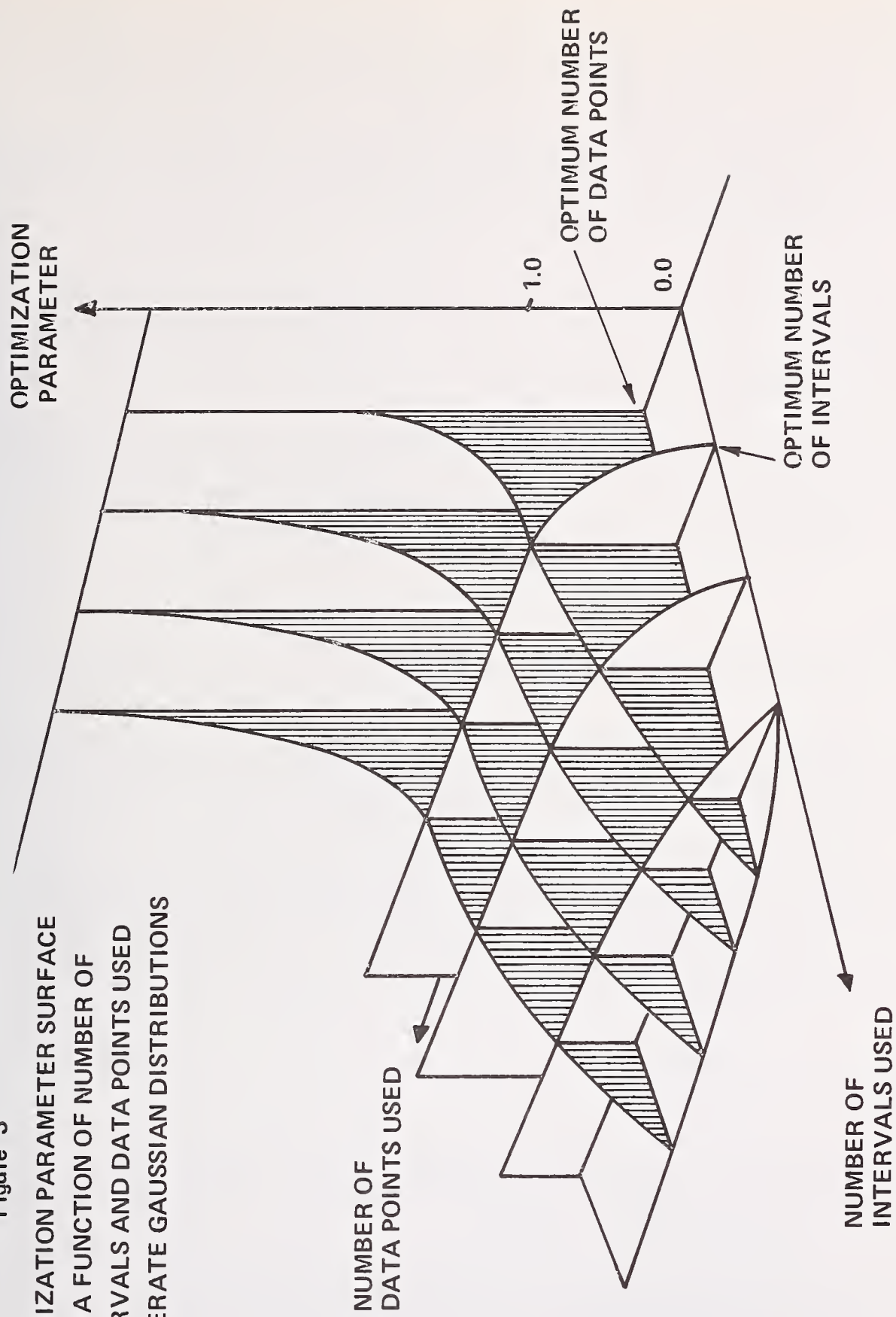


TABULATION VALUES OF PLOTTED DATA	
INTERVALS USED	σ (ACTUAL)/ σ (IDEAL)
2	2.886000
40	1.000860
80	1.003180
100	0.995416
140	0.984692
180	0.979632
220	0.973861
260	0.969160
300	0.961755

CODE RESULTS

Figure 3

OPTIMIZATION PARAMETER SURFACE
AS A FUNCTION OF NUMBER OF
INTERVALS AND DATA POINTS USED
TO GENERATE GAUSSIAN DISTRIBUTIONS



From Figure 1

1. As the number of data points increases the optimization parameter approaches unity as expected.
2. The curve is expected to lie beneath the optimization parameter equals unity line, since one would need an infinite number of points and intervals to get the gaussian tails completely filled.
3. The optimization parameter is sufficiently close to unity when the number of data points used is greater than about 2000. The variation observed beyond this number of data points is believed due to slight random fluctuations in the data distributions within each interval of the generated probability distribution.
4. The optimum number of data points for 100 intervals is therefore about 2000, this gives an optimization parameter close to unity (error in generated standard deviation is less than one percent) with the minimum required computer running time. Note that the optimum number of data points per interval is approximately 20.

From Figure 2

1. The optimum number of intervals is approximately 40, for 800 data points utilized.
2. As the number of intervals gets too small relative to the optimum 40, the gaussian distribution changes, until a uniform distribution is achieved, when the lower limit of two intervals is reached.
3. As the number of intervals increases beyond the optimum 40 value, the generated data set standard deviation falls off until at a large enough number of intervals one expects a zero value for it. This is due to the fact that the probability that a data point falls in any interval must decrease as the number of intervals increases, assuming that the total number of data points is fixed.
4. The optimum ratio of the number of data points to number of intervals again appears to be about 20.

For uniform distributions it is obvious that the optimum number of intervals must equal the number of data points required. It is usually sufficient though, to make the number of data points divisible by the number of intervals used, an integral number of times.

If other probability distributions are required, which are not gaussian or uniform, the same procedure can be utilized, except that higher moments may have to be considered in devising the optimization parameter.

Another method of generating a set of data with a given probability distribution, involves the use of the Monte Carlo technique in conjunction with the cumulative distribution function. This method, which does not rely on Stratified Sampling is deficient in two respects, relative to the combination of Monte Carlo and Stratified Sampling techniques. First, when one generates a probability distribution, one has no assurance that the tails, say for a gaussian distribution, will be adequately represented by the data. Second, for the same number of points one can expect a wider variation in statistical properties of the resultant data set.

These deductions were verified by a brief study whose results are presented in Table I. In order to generate a set of data having a normal distribution using the cumulative distribution function technique, the following calculation is required. First, a random number is generated between 0 and 1. This value, considered to represent a probability, is then utilized to determine the corresponding value of the normal deviate. This process is carried out "N" times in the computer code by using a rational approximation [5] given in equation (3).

$$xp = t - \left\{ \frac{c_0 + c_1 t + c_2 t^2}{1 + d_1 t + d_2 t^2 + d_3 t^3} \right\} + \epsilon(p) \quad (3)$$

$$\text{where } t = \sqrt{\ln\left(\frac{1}{p^2}\right)}$$

p is the input cumulative probability, this value must be between 0 and 0.5 in magnitude.

xp is the normal deviate for a gaussian distribution with a standard deviation of unity

$$c_0 = 2.515517$$

$$c_1 = 0.802853$$

$$c_2 = 0.010328$$

$$d_1 = 1.432788$$

$$d_2 = 0.189269$$

$$d_3 = 0.001308$$

$\epsilon(p)$ is the error in the approximation $|\epsilon(p)| < 4.5 \times 10^{-4}$

TABLE I

Comparison of the Standard Deviation of a Gaussian Distribution as Generated by the Combined Monte Carlo-Stratified Sampling (MCSS) Techniques and by the Monte Carlo Technique Using the Cumulative Distribution Function (MCCDF)

Note

Seven runs were made using each technique, for MCSS runs, 26 intervals and 500 data points were used; for the MCCDF runs, 500 data points were used. In both cases the specified input was a gaussian distribution with a standard deviation of unity.

<u>Technique</u>	<u>Mean Standard Deviation of the Seven Runs</u>	<u>Standard Deviation of the Seven Standard Deviations</u>
MCSS	0.987981	0.003955
MCCDF	0.955134	0.027560

3. Calculation of the Predicted Flow Rate and Its Associated Probability Distribution

Prediction of flow rate, in a flow network with parallel loops, requires the solution of simultaneous equations. It is the author's opinion that it is difficult, if not impossible, to analytically determine predicted flow uncertainties, under these conditions, without resorting to some type of Monte Carlo or finite difference approach.

The calculation of the predicted flow rate and its associated uncertainty distribution for a flow network in the design stage, is usually based on the following information.

1. A complete description of the flow network geometry,
2. The uncertainty distribution and best estimate predicted values for each network component flow resistance,
3. The best estimate values, and the uncertainty distributions, for the coefficients of each pump head vs. flow characteristic equation,
4. The network flow equations relating pump head to flow head losses.

The calculation sequence is as follows, first the data sets for each flow resistance and pump characteristic equation coefficient are generated according to the input probability specifications. Second, the first random value of each resistance and pump characteristic equation coefficient is inserted into the network equations. These equations are then solved for one possible value of the predicted flow rate. This step is repeated until all values, in each data set, have been utilized once. The final step is the printout of the probability histogram for the predicted flow rate and the relevant associated statistics. The nature of the Monte Carlo-Stratified Sampling technique is such that functional relationship between the input uncertainties and the predicted flow uncertainty can be accounted for accurately.

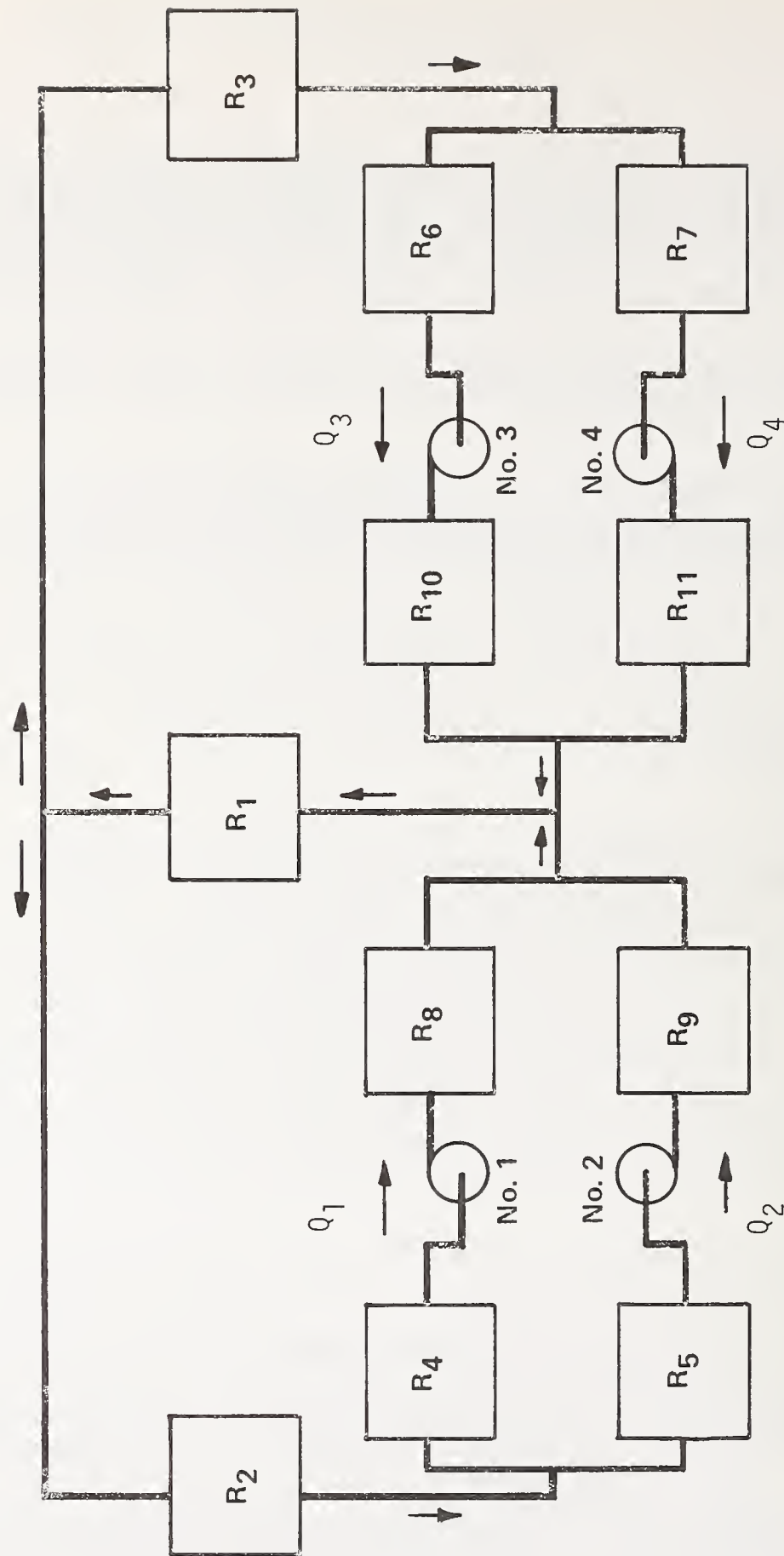
An illustrative example of the application of the above procedure is presented below.

Flow Prediction Uncertainty Analysis; Illustrative Example

Objective: Find the best estimate predicted flow rate and its associated probability distribution, in the flow network.

Given: 1. Flow network schematic diagram, see Figure (4).

Figure 4
FLOW NETWORK SCHEMATIC DIAGRAM



LEGEND

SQUARES ARE LUMPED COMPONENT FLOW RESISTANCES

CIRCLES ARE CENTRIFUGAL PUMPS

ARROWS INDICATE FLOW DIRECTION

2. Flow network simultaneous equations

$$\begin{aligned}A_1 Q_1^2 + B_1 Q_1 + C_1 &= R_1 [Q_1 + Q_2 + Q_3 + Q_4]^2 + R_2 [Q_1 + Q_2]^2 + [R_4 + R_8] [Q_1]^2 \\A_2 Q_2^2 + B_2 Q_2 + C_2 &= R_1 [Q_1 + Q_2 + Q_3 + Q_4]^2 + R_2 [Q_1 + Q_2]^2 + [R_5 + R_9] [Q_2]^2 \\A_3 Q_3^2 + B_3 Q_3 + C_3 &= R_1 [Q_1 + Q_2 + Q_3 + Q_4]^2 + R_3 [Q_3 + Q_4]^2 + [R_6 + R_{10}] [Q_3]^2 \\A_4 Q_4^2 + B_4 Q_4 + C_4 &= R_1 [Q_1 + Q_2 + Q_3 + Q_4]^2 + R_3 [Q_3 + Q_4]^2 + [R_7 + R_{11}] [Q_4]^2\end{aligned}\tag{4}$$

where A_1, B_1, C_1 are the coefficients of the number one pump head vs flow characteristic equation.

A_2, B_2, C_2 , etc are the same coefficients for the number two pump, etc.

$R_1, R_2 \dots R_{11}$ are the network component flow resistances.

Q_1 is the flow through number one pump, Q_2 through number two pump, etc.

3. The best estimate and standard deviation values for the coefficients of each pump head vs flow characteristic equation, see Table 2 below.

TABLE 2

Pump Characteristic Equation Coefficient Uncertainties

<u>Pump Number</u>	<u>Coefficient</u>	<u>Mean Value</u>	<u>Standard Deviation</u>
1	A_1	-1.700	1.213×10^{-1}
	B_1	5.977	1.360
	C_1	106.8	3.621
2	A_2	-1.448	0.8572×10^{-1}
	B_2	3.280	0.9995
	C_2	113.7	2.788
3	A_3	-1.398	1.625×10^{-1}
	B_3	3.355	1.885
	C_3	112.3	5.200
4	A_4	-1.672	0.8707×10^{-1}
	B_4	6.028	0.9918
	C_4	106.4	2.690

Note (1) all uncertainty distributions are assumed to be gaussians

(2) the dimensional units of " A_i " are $[M/(M^3/sec)^2]$

the dimensional units of " B_i " are $[M/(M^3/sec)]$

the dimensional units of " C_i " are $[M]$

(3) See Figure (4) for locations of each pump in the flow network.

(4) All gaussian distributions were generated using 2000 data points and 100 intervals.

4. The network loop component flow resistances best estimate and standard deviation values, see Table 3 below.

TABLE 3

<u>Component Number</u>	<u>Mean Value</u>	<u>Standard Deviation</u>
1	3.381×10^{-2}	1.690×10^{-3}
2	3.047×10^{-1}	1.524×10^{-2}
3	3.046×10^{-1}	1.523×10^{-2}
4	1.015×10^{-1}	5.075×10^{-3}
5	1.015×10^{-1}	5.076×10^{-3}
6	1.015×10^{-1}	5.075×10^{-3}
7	1.015×10^{-1}	5.076×10^{-3}
8	2.292×10^{-1}	1.146×10^{-2}
9	2.292×10^{-1}	1.146×10^{-2}
10	2.292×10^{-1}	1.146×10^{-2}
11	2.292×10^{-1}	1.146×10^{-2}

- Note: (1) the dimensional units of each " R_i " are $[M/(M^3/sec)^2]$
- (2) see Figure (4) for locations of each network component flow resistance
- (3) All resistance probability distributions were assumed to be gaussian and each was generated using 2000 points and 100 intervals.

Code Results

1. Best estimate predicted flow rate is 24.6627 (M³/sec) or 120.4 percent of the reference flow rate.*
2. Standard deviation of the predicted flow rate probability distribution is 0.5469 (M³/sec), or 2.67 percent of the reference flow rate.

The probability histogram for the predicted flow rate is shown in Figure 5, also shown in this figure is an ideal gaussian having the same standard deviation and mean value as the code result.

The correspondence of these two curves indicates that the predicted flow probability distribution is indeed a gaussian. In order to qualify the correspondence level of the code generated histogram and an ideal gaussian histogram, a chi-squared statistic was used, which compared the actual to the ideal data point population in each interval. This statistic has the property that when the correspondence is ideal, its value is zero. As the level of confidence decreases the value of this statistic increases. This single index of the degree of correspondence has been found useful. Equation (5) defines this statistical index mathematically [4].

$$\chi^2 = \sum_{i=1}^n \left\{ \frac{[\text{Pop}_i(\text{actual}) - \text{Pop}_i(\text{ideal})]^2}{\text{Pop}_i(\text{ideal})} \right\} \quad (5)$$

where, n is the number of intervals into which the predicted probability distribution is divided

$n-1$ is the degrees of freedom of this chi-squared distribution

$\text{Pop}_i(\text{actual})$ is the number of data points which fall within the i th interval.

$\text{Pop}_i(\text{ideal})$ is the ideal number of data points expected in the i th interval, if the distribution is a gaussian.

There are two requirements for using this statistic correctly, first none of the $\text{Pop}_i(\text{ideal})$ must be less than 1, and not more than 20 percent of these values should be less than 5.

The code results for the predicted flow rate probability distribution are shown in Figure 5, note that 100 intervals were used for the print-out of the result distribution. In order to apply the chi-square test of this resultant the 100 intervals were reduced to 20, this was done in order to fulfill the first requirement for the use of this test.

*For simplicity, flow rates will be expressed as a percentage of the reference flow rate of 20.4839 (M³/sec), in the remainder of this paper.

TABLE 4

Actual and Ideal Interval Populations for
the Predicted Flow Probability Distribution

<u>Interval</u>	<u>Actual Population</u>	<u>Ideal Gaussian Population</u>
1	2	1
2	2	5
3	7	12
4	24	26
5	42	50
6	100	86
7	120	135
8	158	188
9	211	235
10	289	262
11	256	262
12	255	235
13	195	188
14	137	135
15	94	86
16	52	50
17	28	26
18	13	12
19	9	5
20	3	1

The confidence limits for the chi-square can be found from the following approximation, for a large number of degrees of freedom [5].

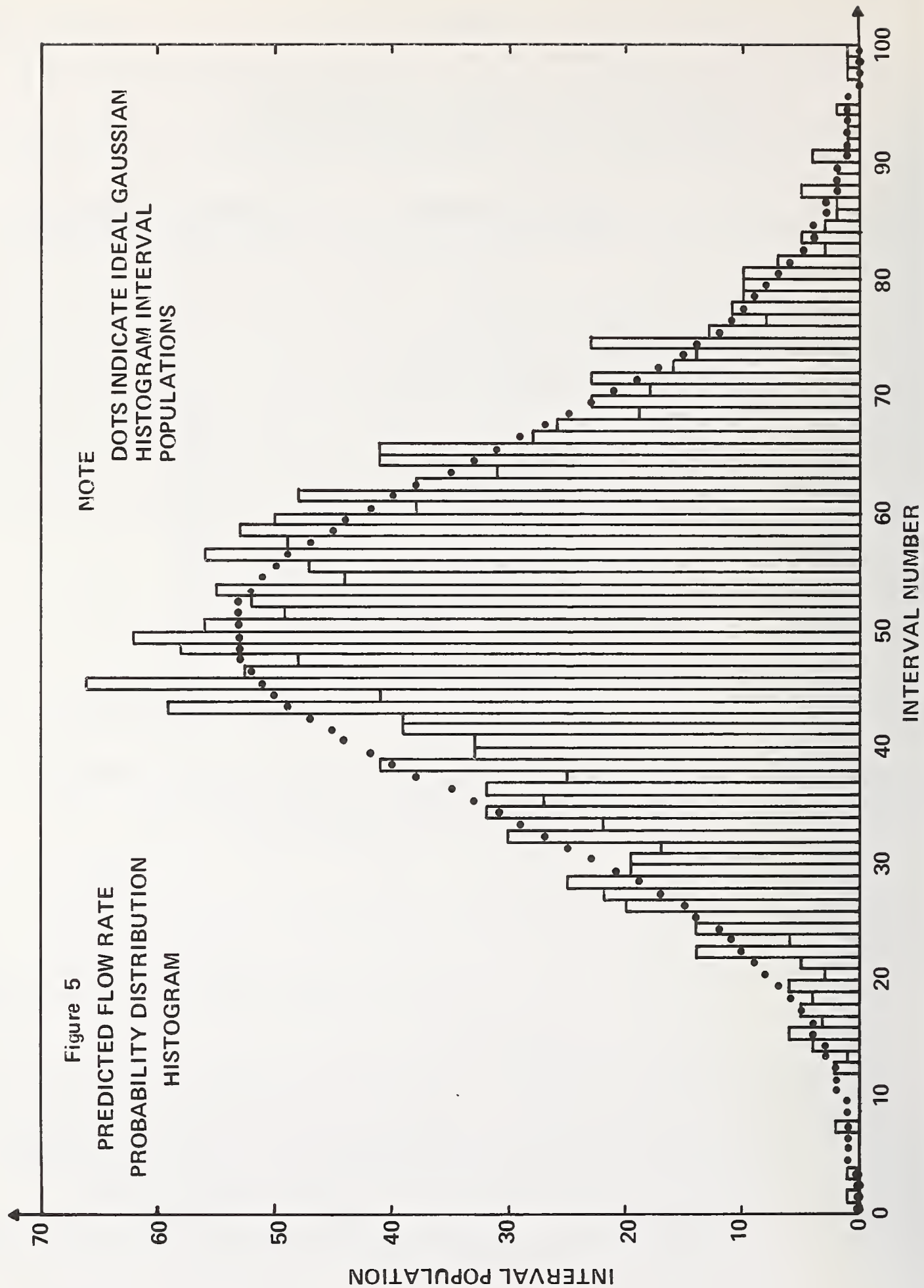
$$\chi^2_{\alpha} = v \left[1 - \frac{2}{9v} + z_{\alpha} \sqrt{\frac{2}{9v}} \right]^3 \quad (6)$$

where α , is the probability level associated with the confidence limit calculated.

v is the degrees of freedom of the chi-square statistic, which is the number of intervals minus 1.

z_{α} is the normal deviate corresponding to the " α " probability level.

For $\alpha = .99$, and $v = 19$, χ^2 is 36.21, from equation (6). From equation (5), the predicted flow rate probability distribution chi-square value is 30.66. This value falls below the confidence limit, and the hypothesis, that the predicted flow probability distribution is a gaussian, is confirmed.



4. Determination of the True Flow Rate and its Associated Probability Distribution

When flow measurements are made on the actual flow network, these measurements can be combined with the predicted flow using Bayes' Rule. The resulting true flow rate probability distribution thus reflects all available flow data. The following information is required to apply the analysis technique.

1. The predicted flow rate uncertainty distribution and best estimate value
2. "J" independent flow measurements", uncertainty distributions and best estimate values.

The calculation of the true flow rate uncertainty distribution involves the following sequence of events. First, the data sets for the predicted and measured flow rates, according to the input probability specifications, are generated. Second for each flow rate interval, Bayes' rule as shown in equation (7), is applied [2].

$$P(T_i | M_1 \& M_2 \& \dots M_J) = \frac{P(M_1 \& M_2 \& \dots M_J | T_i) \cdot P(T_i)}{\sum_{i=1}^I \{P(M_1 \& M_2 \& \dots M_J | T_i) \cdot P(T_i)\}} \quad (7)$$

where

$P(T_i)$

i

I

$P(T_i | M_1 \& M_2 \& \dots M_J)$

$P(M_1 \& M_2 \& \dots M_J | T_i)$

and
$$P(M_1 \& M_2 \& \dots M_J | T_i) = \prod_{j=1}^J P(M_j | T_i)$$

J

is the predicted probability that T_i
is the true flow rate,
is the flow interval index,
is the total number of flow intervals used,
is the probability that T_i is the true flow
rate given that the independent measurements
 $M_1 \& M_2 \& \dots M_J$ have been made.
is the probability of measuring the $M_1 \& M_2$
& $\dots M_J$ flow rates given that the true
flow is T_i .

is the number of independent flow measurements
made.

The true flow rate probability histogram is found by plotting $P(T_i | M_1 \& M_2 \& \dots M_J)$, for each possible true flow rate T_i . Further development of this method is planned to associate a confidence level with the true flow rate probability distribution calculated.

*Independent flow measurement refers to the method, for example, heat balance, and venturi Δp flow measurements, are independent methods.

An illustrative example of the above procedure for evaluation of the true flow best estimate value, and associated probability distribution, is presented below.

True Flow Probability Distribution Determination; Illustrative Example

Objective: Find the best estimate true flow rate and its associated probability distribution given the predicted and measured flow rate information required.

Given:

TABLE 5

Flow Prediction and Measurement Probability Distributions

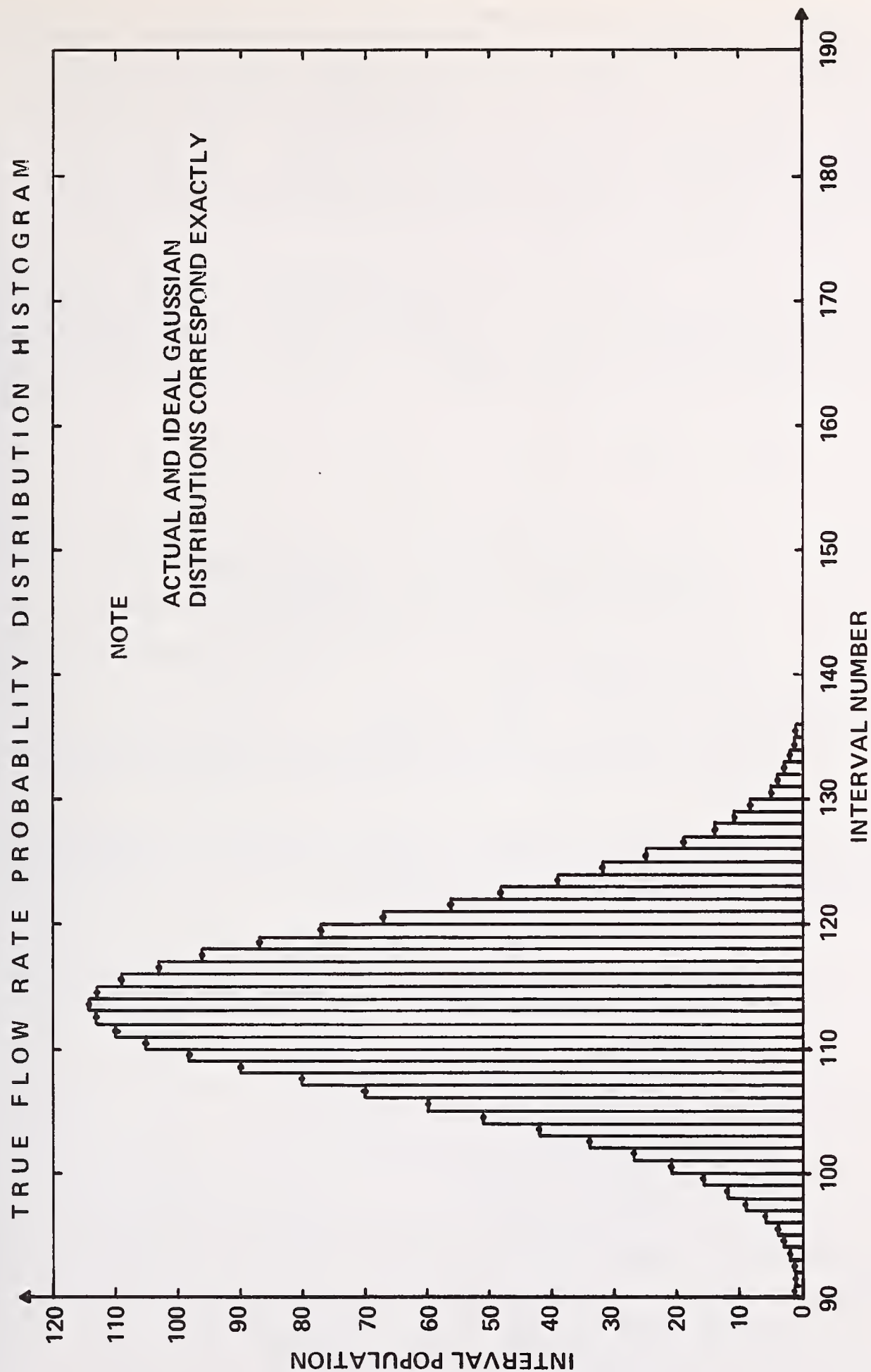
<u>Source of Flow</u> <u>Rate Data</u>	<u>Best Estimate Value</u>	<u>Standard Deviations*</u>
Predicted	120.4%	2.67%
Measured, Method 1	123.1	1.81
Measured, Method 2	125.3	3.75

*All probability distributions were assumed to be gaussian in form, 2000 data points and 200 intervals between 100 and 140 percent design flow were used.

Code Results:

1. Best Estimate True Flow Rate is 122.6 percent of the reference flow rate.
2. Standard Deviation of True Flow Rate Probability Distribution is 1.389 percent of the reference flow rate.
3. The true flow rate probability distribution is a perfect gaussian as can be seen from the coincidence of the actual and ideal gaussian distributions presented in Figure 6.

Figure 6



One interesting result of the application of Bayes' Rule to continuous probability distributions, is that if all the distributions involved are gaussian in form, the result can also be found without recourse to a computer code by the application of the method called minimization of the chi-squared. In this analysis the flow prediction is treated as another independent measurement of the flow rate. The derivation of the standard deviation and the mean value of the true flow rate probability distribution by this method are presented below, and the code and analytical results are compared in Table 6.

If one is given a number of independent variables which are measures of the same parameter and each of the variables has a gaussian probability distribution associated with it, the most likely value of this parameter can be found by the following technique. First a chi-squared variable [2] can be generated using equation (8)

$$\chi^2 = \sum_{i=1}^n \left\{ \frac{x_i - \bar{X}}{\sigma_i} \right\}^2 \quad (8)$$

where, n is the no. of independent measures of the parameter in question

x_i is the mean value of the i th independent measurement

σ_i is the standard deviation of the i th independent measurement about its mean value.

\bar{X} is the unknown value of the measured parameter which will minimize the magnitude of the chi-square statistic.

One can find the value of \bar{X} which minimizes the value of the chi-square statistic by differentiating χ^2 with respect to \bar{X} and setting the resulting expression equal to zero, as in equation (9).

$$\frac{d\chi^2}{d\bar{X}} = 0 = -2 \left(\frac{1}{\sigma_1} \right)^2 (x_1 - \bar{X}) - 2 \left(\frac{1}{\sigma_2} \right)^2 (x_2 - \bar{X}) - 2 \left(\frac{1}{\sigma_3} \right)^2 (x_3 - \bar{X}) \quad (9)$$

$$\text{or, } \bar{X} = \frac{x_1 \left(\frac{1}{\sigma_1} \right)^2 + x_2 \left(\frac{1}{\sigma_2} \right)^2 + x_3 \left(\frac{1}{\sigma_3} \right)^2}{\left(\frac{1}{\sigma_1} \right)^2 + \left(\frac{1}{\sigma_2} \right)^2 + \left(\frac{1}{\sigma_3} \right)^2} \quad (10)$$

The standard deviation of \bar{X} can be found by utilizing expressions (10) and (11).

$$\sigma^2(\bar{X}) = \left(\frac{\partial \bar{X}}{\partial x_1} \right)^2 \sigma_1^2 + \left(\frac{\partial \bar{X}}{\partial x_2} \right)^2 \sigma_2^2 + \left(\frac{\partial \bar{X}}{\partial x_3} \right)^2 \sigma_3^2 \quad (11)$$

$$\text{Thus, } \sigma(\bar{X}) = \sqrt{\frac{1}{\left(\frac{1}{\sigma_1}\right)^2 + \left(\frac{1}{\sigma_2}\right)^2 + \left(\frac{1}{\sigma_3}\right)^2}} \quad (12)$$

\bar{X} analytical value
using equation (10),
and data from
Table 5. = 112.56 percent of volumetric
reference flow

$\sigma(\bar{X})$ analytical value
using equation (12),
and data from
Table 5. = 1.391 percent of volumetric
reference flow

TABLE 6

Comparison of Bayes' Rule Result and
Minimization of the Chi-Square Statistic
Analytical Technique

	<u>Bayes' Rule</u>	<u>Chi-Square Minimization</u>
Best Estimate True Flow Rate	122.67	122.56
True Flow Rate Standard Deviation	1.389	1.391

REFERENCES

- [1] Knuth, D.E., The Art of Computer Programming Vol. 2, Semi-Numerical Algorithms (Addison-Wesley 1969).
- [2] Meyer, S.L., Data Analysis for Scientists and Engineers, (John Wiley and Sons, New York, 1975).
- [3] Clark, Jr., M. and Handson, K.F., Numerical Methods of Reactor Analysis (Academic Press, New York, 1964).
- [4] Dixon, W. J., and Massey, Jr., F.J., Introduction to Statistical Analysis, (McGraw Hill Inc., 1969).
- [5] Abramowitz, M., and Stegun, I.A., Ed. Handbook of Mathematical Functions, (National Bureau of Standards Applied Mathematic Series 55, Ninth Printing, November 1970).

AUTHOR INDEX

- Abernathy, F. H. 957
 Allion, H. 33
 Annett, John 145
 Appell, Gerald 109

 Bajura, R. A. 523
 Baker, Milton 803
 Ball, John M. 847
 Baumoel, J. 267
 Berte', Frank J. 447
 Bradshaw, J. E. 293
 Brennan, J. A. 881
 Brower, W. B. Jr. 719
 Bruner, Ronald F. 277

 Clark, M. E. 479
 Cullen, J. T. 549

 Dang, Clement 187
 Davis, L. M. 55
 Davis, R. W. 219, 491
 DeCarlo, J. P. 549
 Delisi, Donald P. 423, 783
 Dijstelbergen, H. H. 935
 Durgin, William W. 471
 Dussauge, J. P. 649

 Edgerly, D. E. 921

 Fabris, Gracio 659
 Flandro, G. 335
 Flemons, R. S. 319

 Gad-el-Hak, Mohamed 571
 Gaviglio, J. 649
 Gold, D. S. 621
 Grant, D. M. 91
 Greenleaf, J. F. 335
 Guthrie, D. L. 173

 Halmi, Dezsoe 61
 Haney, Robert A. 755
 Hayward, A. T. J. 1
 Holley, E. R. 395

 Irwin, L. K. 895

 Jennings, Roger 821
 Johnson, S. A. 335

 Kempf, D. 361
 Kirchhoff, Robert H. 783
 Koenig, H. L. 145
 Kondic, N. N. 765
 Kulin, G. 123
 Kullman, C. G. 25

 LaNasa, Paul J. 871
 Lin, Jung-Tai 423
 Liu, Hsien-Ta 423
 Lowell, Francis C. Jr. 243
 Lynnworth, L. C. 293

 Mann, D. B. 881
 Martig, Kenneth W. Jr. 83
 Mattingly, G. E. 33, 491
 McQuivey, S. 109
 Meagher, Thomas F. V. 687
 Mero, Thomas 109
 Miller, R. W. 549
 Moore, E. 33
 Morel, P. R. 293
 Morgan, W. H. 361

 Neale, Lawrence C. 471

 O'Brien, Joseph F. 145

 Peckham, Vernon D. 687
 Pedersen, N. E. 293
 Pellegrin, M. T. 523
 Phillips, R. E. 361
 Pierce, F. J. 621
 Pontius, P. 33

 Replogle, John A. 201
 Robben, Frank A. 423
 Robertson, J. M. 479
 Rudland, R. S. 705
 Ruff, James F. 187

Sachs, Donald C. 687
Saxton, Keith 187
Scotttron, V. E. 737
Servoz, Alan 719
Seward, Wallace N. 929
Singley, G. Wayne 145
Skridulis, James 145
Spencer, E. A. 947
Suhoke, Robert B. 597

Tabler, J. H. 25
Tanaka, M. 335

Vincenty, C. 173

Washington, D. R. 173
West, James A. 945

U.S. DEPT. OF COMM. BIBLIOGRAPHIC DATA SHEET	1. PUBLICATION OR REPORT NO. SP 484 -- Volume 1	2. Gov't Accession No.	3. Recipient's Accession No.
4. TITLE AND SUBTITLE Flow Measurement in Open Channels and Closed Conduits Volume 1		5. Publication Date October 1977	
		6. Performing Organization Code	
7. AUTHOR(S) Lafayette K. Irwin, Editor		8. Performing Organ. Report No.	
9. PERFORMING ORGANIZATION NAME AND ADDRESS NATIONAL BUREAU OF STANDARDS DEPARTMENT OF COMMERCE WASHINGTON, D.C. 20234		10. Project/Task/Work Unit No.	
		11. Contract/Grant No.	
12. Sponsoring Organization Name and Complete Address (Street, City, State, ZIP) National Bureau of Standards		13. Type of Report & Period Covered Final	
		14. Sponsoring Agency Code	
15. SUPPLEMENTARY NOTES Library of Congress Catalog Card Number: 77-14243			
16. ABSTRACT (A 200-word or less factual summary of most significant information. If document includes a significant bibliography or literature survey, mention it here.) The wide range and complexity of problems and potential solutions that must be considered for useful flow measurements are emphasized by the papers contained in these proceedings. Fifty-three presentations cover: characteristics of new and improved instruments; applications of traditional and new measuring devices in field environments; procedures for identifying and analyzing errors or uncertainties in data under specific conditions; uses of physical and numerical models; politico-economic changes that affect international standards for flow measurement; and philosophical bases for making measurements. The fluids of most interest are water and waste water, petroleum and related refined products, air, natural gas and stack gas. Experimental and analytical investigations on instrument performance and interpretation of results include innovative applications of traditional and new flow measurement techniques to fluid flows in open channels and closed conduits. The traditional devices or techniques include weirs, flumes, current meters, orifice plates, turbines, hot-wires, pitot-static tubes, velocity traverses, dye-dilution, and others. More recent instrumentation developments and procedures such as laser doppler anemometry, acoustic and thermal imaging, acoustic pulse velocity and doppler anemometry, numerical modeling, vortex shedding and digital computation are covered for particular measurement purposes. The most significant trend reflected in these presentations is the general awareness that uncertainties in measured quantities at the lowest point in the measurement chain, i.e., in the field or plant, are more important than accuracy statements derived from controlled laboratory studies. Other trends in evidence are the rising importance of turbine meters for use as transfer standards and in-line measurements of liquids and gases in filled pipes and the increasing number of applications for acoustics and laser technology for flow measurements in both open channels and closed conduits.			
17. KEY WORDS (six to twelve entries; alphabetical order; capitalize only the first letter of the first key word unless a proper name; separated by semicolons) Acoustic flow meters; closed conduit flows; current meters; dye-dilution methods; errors in flow measurement; flow measurement; fluid flow modeling; fluid velocity; flumes; gas flow standard; hot-wire anemometry; international flow standards; laser anemometry; open channel flows; orifice meters; pitot-static meters; turbine meters; weirs.			
18. AVAILABILITY <input type="checkbox"/> Unlimited <input type="checkbox"/> For Official Distribution. Do Not Release to NTIS <input checked="" type="checkbox"/> Order From Sup. of Doc., U.S. Government Printing Office Washington, D.C. 20402, SD Cat. No. C13.10:484/Vol. 1 <input type="checkbox"/> Order From National Technical Information Service (NTIS) Springfield, Virginia 22151		19. SECURITY CLASS (THIS REPORT) UNCLASSIFIED	21. NO. OF PAGES 479
		20. SECURITY CLASS (THIS PAGE) UNCLASSIFIED	22. Price \$12.25 Per 2 Part Set

There's
a new
look
to...

DIMENSIONS



... the monthly magazine of the National Bureau of Standards. Still featured are special articles of general interest on current topics such as consumer product safety and building technology. In addition, new sections are designed to . . . PROVIDE SCIENTISTS with illustrated discussions of recent technical developments and work in progress . . . INFORM INDUSTRIAL MANAGERS of technology transfer activities in Federal and private labs. . . DESCRIBE TO MANUFACTURERS advances in the field of voluntary and mandatory standards. The new DIMENSIONS/NBS also carries complete listings of upcoming conferences to be held at NBS and reports on all the latest NBS publications, with information on how to order. Finally, each issue carries a page of News Briefs, aimed at keeping scientist and consumer alike up to date on major developments at the Nation's physical sciences and measurement laboratory.

(please detach here)

SUBSCRIPTION ORDER FORM

Enter my Subscription To DIMENSIONS/NBS at \$12.50. Add \$3.15 for foreign mailing. No additional postage is required for mailing within the United States or its possessions. Domestic remittances should be made either by postal money order, express money order, or check. Foreign remittances should be made either by international money order, draft on an American bank, or by UNESCO coupons.

Send Subscription to:

NAME-FIRST, LAST

COMPANY NAME OR ADDITIONAL ADDRESS LINE

STREET ADDRESS

CITY

STATE

ZIP CODE

PLEASE PRINT

☐ Remittance Enclosed
(Make checks payable
to Superintendent of
Documents)

☐ Charge to my Deposit
Account No.

MAIL ORDER FORM TO:
Superintendent of Documents
Government Printing Office
Washington, D.C. 20402

NBS TECHNICAL PUBLICATIONS

PERIODICALS

JOURNAL OF RESEARCH reports National Bureau of Standards research and development in physics, mathematics, and chemistry. It is published in two sections, available separately:

• **Physics and Chemistry (Section A)**

Papers of interest primarily to scientists working in these fields. This section covers a broad range of physical and chemical research, with particular emphasis on standards of physical measurement, fundamental constants, and properties of matter. Issued six times a year. Annual subscription: Domestic, \$17.00; Foreign, \$21.25.

• **Mathematical Sciences (Section B)**

Studies and communications designed mainly for the mathematician and theoretical physicist. Topics in mathematical statistics, theory of experiment design, numerical analysis, theoretical physics and chemistry, logical design, programming of computers and computer systems, and short numerical tables. Issued quarterly. Annual subscription: Domestic, \$9.00; Foreign, \$11.25.

DIMENSIONS/NBS (formerly Technical News Bulletin)—This monthly magazine is published to inform scientists, engineers, businessmen, industry, teachers, students, and consumers of the latest advances in science and technology, with primary emphasis on the work at NBS. The magazine highlights and reviews such issues as energy research, fire protection, building technology, metric conversion, pollution abatement, health and safety, and consumer product performance. In addition, it reports the results of Bureau programs in measurement standards and techniques, properties of matter and materials, engineering standards and services, instrumentation, and automatic data processing.

Annual subscription: Domestic, \$12.50; Foreign, \$15.65.

NONPERIODICALS

Monographs—Major contributions to the technical literature on various subjects related to the Bureau's scientific and technical activities.

Handbooks—Recommended codes of engineering and industrial practice (including safety codes) developed in cooperation with interested industries, professional organizations, and regulatory bodies.

Special Publications—Include proceedings of conferences sponsored by NBS, NBS annual reports, and other special publications appropriate to this grouping such as wall charts, pocket cards, and bibliographies.

Applied Mathematics Series—Mathematical tables, manuals, and studies of special interest to physicists, engineers, chemists, biologists, mathematicians, computer programmers, and others engaged in scientific and technical work.

National Standard Reference Data Series—Provides quantitative data on the physical and chemical properties of materials, compiled from the world's literature and critically evaluated. Developed under a world-wide program coordinated by NBS. Program under authority of National Standard Data Act (Public Law 90-396).

BIBLIOGRAPHIC SUBSCRIPTION SERVICES

The following current-awareness and literature-survey bibliographies are issued periodically by the Bureau:

Cryogenic Data Center Current Awareness Service. A literature survey issued biweekly. Annual subscription: Domestic, \$25.00; Foreign, \$30.00.

Liquified Natural Gas. A literature survey issued quarterly. Annual subscription: \$20.00.

NOTE: At present the principal publication outlet for these data is the Journal of Physical and Chemical Reference Data (JPCRD) published quarterly for NBS by the American Chemical Society (ACS) and the American Institute of Physics (AIP). Subscriptions, reprints, and supplements available from ACS, 1155 Sixteenth St. N.W., Wash. D. C. 20056.

Building Science Series—Disseminates technical information developed at the Bureau on building materials, components, systems, and whole structures. The series presents research results, test methods, and performance criteria related to the structural and environmental functions and the durability and safety characteristics of building elements and systems.

Technical Notes—Studies or reports which are complete in themselves but restrictive in their treatment of a subject. Analogous to monographs but not so comprehensive in scope or definitive in treatment of the subject area. Often serve as a vehicle for final reports of work performed at NBS under the sponsorship of other government agencies.

Voluntary Product Standards—Developed under procedures published by the Department of Commerce in Part 10, Title 15, of the Code of Federal Regulations. The purpose of the standards is to establish nationally recognized requirements for products, and to provide all concerned interests with a basis for common understanding of the characteristics of the products. NBS administers this program as a supplement to the activities of the private sector standardizing organizations.

Consumer Information Series—Practical information, based on NBS research and experience, covering areas of interest to the consumer. Easily understandable language and illustrations provide useful background knowledge for shopping in today's technological marketplace.

Order above NBS publications from: Superintendent of Documents, Government Printing Office, Washington, D.C. 20402.

Order following NBS publications—NBSIR's and FIPS from the National Technical Information Services, Springfield, Va. 22161.

Federal Information Processing Standards Publications (FIPS PUBS)—Publications in this series collectively constitute the Federal Information Processing Standards Register. Register serves as the official source of information in the Federal Government regarding standards issued by NBS pursuant to the Federal Property and Administrative Services Act of 1949 as amended, Public Law 89-306 (79 Stat. 1127), and as implemented by Executive Order 11717 (38 FR 12315, dated May 11, 1973) and Part 6 of Title 15 CFR (Code of Federal Regulations).

NBS Interagency Reports (NBSIR)—A special series of interim or final reports on work performed by NBS for outside sponsors (both government and non-government). In general, initial distribution is handled by the sponsor; public distribution is by the National Technical Information Services (Springfield, Va. 22161) in paper copy or microfiche form.

Superconducting Devices and Materials. A literature survey issued quarterly. Annual subscription: \$30.00. Send subscription orders and remittances for the preceding bibliographic services to National Bureau of Standards, Cryogenic Data Center (275.02) Boulder, Colorado 80302.

U.S. DEPARTMENT OF COMMERCE
National Bureau of Standards
Washington, O.C. 20234

OFFICIAL BUSINESS

Penalty for Private Use, \$300

POSTAGE AND FEES PAID
U.S. DEPARTMENT OF COMMERCE
COM-215



SPECIAL FOURTH-CLASS RATE
BOOK
